Petrogenesis and Evolution of Alkalic Basaltic Magmas in a Continental Intraplate Setting: The South Auckland Volcanic Field, New Zealand

---

A thesis submitted in fulfilment of the requirements
for the Degree of
Doctor of Philosophy in Earth Sciences
in the
University of Waikato

by

Craig Cook

University of Waikato

October 2002

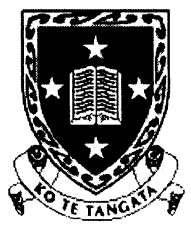

The University of Waikato
Te Whare Wānanga o Waikato

Abstract

The South Auckland volcanic field (SAVF) is situated in a continental intraplate tectonic setting and consists of silica-undersaturated alkalic basalts that erupted from about 100 centres between 1.59 and 0.51 Ma. The basalts range in composition from basanites to quartz tholeiites. Two basalt groups are distinguished based on their contrasting mineralogical and geochemical characteristics: group A, a less silica-undersaturated transitional basalt to quartz tholeiite suite; and group B, a strongly silica-undersaturated basanite to nepheline hawaiite suite. The petrogenesis and evolution of the SAVF basalts is examined using new data from 200 samples on mineral chemistry from electron microprobe analyses, major and trace elements from XRF, incompatible trace elements and REE from ICP-MS, and Sr, Nd, and Pb isotopic data from TIMS analyses.

Forsteritic olivine is the dominant phenocryst phase in each rock group (group A: Fo_{61} - Fo_{82}; group B: Fo_{64} - Fo_{92}). Clinopyroxene is abundant and ranges from augite (Wo_{35-47} En_{36-50} Fs_{11-23}) in group A to diopside (Wo_{42-52} En_{32-46} Fs_{10-20}) in group B basalts. Plagioclase (An_{40-70}) is found as a phenocryst only in group A basalts. The group A basalts are distinguished by their low total alkalis (3.0 - 4.8 wt.%), Nb (9 – 29 ppm) and Zr (97 - 210 ppm) abundances, and low $(La/Yb)_N$ (3.4 - 7.6), which contrast with group B that have large total alkalis (3.3 - 7.9 wt.%), Nb (35 - 102 ppm) and Zr (194 - 491 ppm), and $(La/Yb)_N$ (12 - 47).

The incompatible trace elements of group A lavas have characteristics indicating derivation from an enriched upper mantle source but relatively depleted in Th, K, Nb, Ta, and LREE with small LREE/HREE values, whereas those in group B exhibit strong trace element affinities (i.e., large Th, Nb, Ta, and LREE abundances) with an OIB-like source. Petrogenetic modelling suggests that the group A and B lavas evolved as discrete lineages that do not appear to be related to a common parental magma or source. Partial melting models indicate that < 8 % melting of a garnet-peridotite source is required to produce primary group B magmas, whereas primary group A magmas are generated from < 11 % melting of a spinel-peridotite source. Differentiation of basalts from each group is dominated by olivine and clinopyroxene fractionation, and only minor plagioclase in group A.

Both rock groups fall within a narrow range of Sr and Nd isotopic compositions ($^{87}Sr/^{86}Sr$ = 0.70273±19 – 0.70330±17 and ε_{Nd} = + 5.97 to + 6.89) similar to the composition of HIMU-OIB, whereas Pb isotopic compositions are unradiogenic relative to HIMU-OIB (i.e., $^{206}Pb/^{204}Pb$ = 18.95 - 19.33; $^{207}Pb/^{204}Pb$ = 15.586 - 15.589; $^{208}Pb/^{204}Pb$ = 38.731 - 38.906) and range between Atlantic MORB and EMII. The group A lavas have slightly higher $^{87}Sr/^{86}Sr$ and $^{207}Pb/^{204}Pb$, lower $^{206}Pb/^{204}Pb$ and $^{208}Pb/^{204}Pb$, and similar ε_{Nd} values compared to those in group B, but there is no isotopic or geochemical evidence to suggest that any of the lavas have been contaminated by continental crust. Therefore, the relatively small but distinct differences in Sr and Pb isotopic compositions and similar ε_{Nd} values are considered to be source-related.

Variations in incompatible element ratios such as K/Nb and Zr/Nb indicate that the SAVF basalts were derived from two distinct sources. Group B basalts show incompatible trace element signatures characteristic of a LREE-enriched HIMU-OIB-like source, which can be accounted for by recycling of subducted oceanic crust at mantle depths. In contrast, the group A basalts have incompatible trace element affinities that are intermediate between a HIMU and an EMII-type component that could have resulted from subduction-related metasomatism of the subcontinental lithosphere modified by a HIMU plume. These events may have been connected with the subduction of the Phoenix plate and plume-related magmatism when New Zealand was at the eastern margin of the Gondwanaland supercontinent.

Acknowledgements

I am truly grateful to the great number of people who have assisted me during the development of this thesis.

Dr. Roger Briggs (University of Waikato) provided his expertise to guide me through this process. Many discussions with Dr. Richard Price, Dr. Peter Hodder, Dr. Richard Smith, Dr. Barbara Hobden, Debra Bowyer (all from the University of Waikato), Mike Rosenberg (Institute of Geological and Nuclear Research), Dr. Ian Smith (University of Auckland), Dr. John Gamble (Victoria University), Dr. Gordon Goles (University of Oregon), and Dr. Keith Piturka (University of Indiana, Pennsylvania) provided thought-provoking suggestions and much encouragement. Dr. Piturka also provided his expertise and a generous amount of time with the clinopyroxene analyses and pressure and temperature calculations.

Renat Radosinsky assisted with thin section preparation, Frank Bailey helped with artwork, Arne Pallentin provided his expertise in the production of the photomicrographs, and Stu Pilling assisted in the MATLAB programme development.

I would also like to thank Dr. Roger Briggs and Karen Denyer for their help in editing the manuscript and their critical remarks.

Ritchie Simms (University of Auckland) provided technical assistance on electron microprobe analyses. John Wilmshurst (University of Auckland) analysed my XRF samples and instructed me on sample preparation.

At the Institute of Geological and Nuclear Research, Nick Mortimer provided useful data on the Waipapa and Murihiku Terranes.

Overseas, Dr. Roland Maas (La Trobe University, Melbourne) provided instruction on sample preparation for Sr, Nd, and Pb isotope and REE analyses, and the use of their TIMS. Dr. Louise Frick (Monash University, Melbourne) conducted the ICP-MS analyses.

I am thankful to the many generous South Auckland farmers and landowners who welcomed me to wander around on their property to collect samples, especially Ross Eyer for his enthusiasm. I am also grateful to Winstone Aggregates' Smeed's Quarry (Pat Tunny, manager) and Milburn's Bombay Quarry (Les Ashton, manager) who allowed me onto their property to collect samples.

Table of Contents

List of Figures

Chapter Two

Chapter Four

Chapter Six

List of Tables

Chapter Five

Chapter Six

Chapter Seven

Chapter One: Introduction

Chapter One

Introduction

1.1 Continental intraplate volcanism

Throughout the Cenozoic Era, a wide range of alkalic basaltic magmas erupted within continental intraplate provinces worldwide. These provinces are commonly associated with continental rifting (e.g., Paslick *et al.*, 1995) or lithospheric extension (e.g., Fitton *et al.*, 1991). The diversity of lava compositions commonly observed within these provinces often evokes a complex petrogenetic history. Petrographic mapping, together with whole-rock and K-Ar age data of eruptive products, and the compositions of mantle xenoliths in the alkalic basalts, may be used to qualitatively constrain the history and evolution of magma compositions, and to some extent the compositional characteristics of their mantle sources. Integrated petrologic studies of primitive intraplate alkalic basalts, utilising major and trace element and radiogenic isotope systematics, can provide a quantitative insight into the nature of magmas parental to suites of basaltic lavas observed in continental intraplate volcanic provinces, and the mantle source regions from which these magmas were derived.

Generally, intraplate volcanism occurs in regions "remote" from continental or oceanic plate boundaries and, therefore, intraplate magma petrogenesis cannot be attributed to processes associated with either convergent or divergent margins. However, the South Auckland volcanic field (SAVF), North Island, New Zealand, developed in a continental setting, near an active convergent margin[1]. The implication of processes associated with slab subduction and interaction with the lithospheric mantle on the compositions of magma erupted in the SAVF has not been previously addressed.

Previous petrographic and geochemical observations, and K-Ar age data indicate that a wide range of alkalic basaltic magmas, having contrasting compositions, erupted closely in time and space in the SAVF (Rafferty and Heming, 1979; Briggs *et al.*, 1994). Such diversity strongly suggests that a variety of parental magmas generated the range of lava compositions observed in the SAVF, rather than derivation from a discrete parental magma (e.g., Kempton *et al.*, 1987). This study investigates the diverse geochemical, mineralogical, and radiogenic isotopic characteristics of these lavas, identifying

[1] Refer to Figs. 2.1 and 2.2 (pp. 8 and 9) for tectonic setting of New Zealand and location of SAVF and other intraplate volcanic fields in the North Island, New Zealand.

similarities and differences between the lavas of the SAVF with those from other continental intraplate provinces and fields. These data can provide insight into (i) the composition and evolution of the mantle source (or sources) for the SAVF basalts, (ii) possible source modification by subduction-related components, (iii) the nature of the primary magmas parental to the suite of SAVF basalts, and (iv) the extent to which magmatic processes (i.e., partial melting, fractional crystallisation, assimilation/fractional crystallisation), and post-differentiation processes (i.e., crustal contamination) have affected the compositions of the SAVF basalts.

1.2 General background

The compositions of eruptive products in continental intraplate volcanic provinces worldwide are predominantly alkalic basalts. Compositions may range from leucitite to nephelinite to hawaiite to quartz-tholeiitic basalts. In addition, lavas and tephra of phonolitic, trachytic, and peralkaline rhyolitic compositions have also been documented together with those of alkaline association in some provinces (e.g., Coombs *et al.*, 1986, 1996; Ewart *et al.*, 1988). Numerous petrological studies (Table 1.1) of the mafic magmas

Table 1.1 Representative continental intraplate volcanic provinces.

East Eifel, Germany	Wörner and Schmincke (1984b); Bednarz and Schmincke (1990)
Hessian Depression, Germany	Wedepohl (1985, 1987)
Vogelsberg, Germany	Wedepohl (1987); Jung and Masberg (1998)
Calatrava Volcanic Province, Spain Garrotxa Volcanic Province, Spain	Cebriá and Lopez-Ruiz (1995) Cebriá *et al.* (2000)
Eastern China	Zhi *et al.* (1990); Song *et al.* (1990); Basu *et al.* (1991); Liu *et al.* (1994), Zou *et al.* (2000)
Khorat Plateau, Thailand	Zhou and Mukasa (1997)
Vietnam	Hoang *et al.* (1996); Hoang and Flower (1998)
Taiwan	Chung *et al.* (1994; 1995)
Eastern Australia volcanic provinces	Frey *et al.* (1978); McDonough *et al.* (1985); Ewart *et al.* (1988); Ewart, (1989); O'Reilly and Zang (1995); Price *et al.* (1997)
Northland Volcanic Province, New Zealand	Heming (1980a,b); Huang *et al.* (2000)
Auckland Volcanic Province, New Zealand (which includes the South Auckland volcanic field)	Rafferty and Heming (1979); Briggs and Goles (1984); Heming and Barnet (1986); Briggs *et al.* (1990); Briggs and McDonough (1990); Briggs *et al.* (1994); Huang *et al.* (1997)

from these regions provide evidence that demonstrates that despite their geographic isolation they commonly have ocean island basalt (OIB)-like geochemical characteristics, which suggest they are products of closely related petrogenetic processes. These studies

however, also demonstrate that the mantle sources for these magmas typically vary on a regional scale, and that these variations represent the mixing of two or more of the mantle reservoir end-members; DM, HIMU, EMI, or EMII[2] of Zindler and Hart (1986).

In the South Auckland region of North Island, New Zealand, the South Auckland volcanic field developed in a continental setting, near an active convergent margin (see Figs. 2.1 and 2.2, pp. 8 and 9). The eruptive products throughout the field are interpreted as intraplate in origin (Rafferty and Heming, 1979; Smith, 1989; Briggs *et al.*, 1994). Volcanism in the SAVF was comparatively short lived. The field developed between 1.59 and 0.51 Ma (Briggs *et al.*, 1994) and consists predominantly of monogenetic volcanoes. Eruptions were either effusive or explosive (Rafferty, 1977; Rafferty and Heming, 1979; Rosenberg, 1991) producing lavas and magmatic pyroclasts having (i) silica-undersaturated basanite and nephelinite, and (ii) less silica-undersaturated alkali olivine-basalt, transitional basalt, hawaiite, nepheline-hawaiite, and olivine- and quartz-tholeiitic basalt compositions (Briggs *et al.*, 1994).

The most comprehensive geochemical investigation of the South Auckland volcanic field was conducted by Rafferty (1977) and is summarised in Rafferty and Heming (1979). Rafferty and Heming (1979) divided the South Auckland volcanic field basalts into two broad groups based on their distinct petrographic, mineralogical, and geochemical differences: an alkalic group, which consists of basanites and nephelinites, and a subalkalic group characterised by tholeiitic compositions. From their work, Rafferty (1977) and Rafferty and Heming (1979) reached several notable conclusions regarding the petrogenesis and evolution of the SAVF lavas:

1. Lavas from each group are not petrogenetically linked. They based this interpretation on the variations in major and trace element abundances within and between the two groups and from the presence of ultramafic xenoliths and megacrysts observed only in the alkalic lavas.

2. The lavas that represent the alkalic and subalkalic groups were generated from different upper mantle source regions in the low velocity zone, between 75 and 125 km depth.

3. The subalkalic lavas are derived from magmas that fractionated, in part, within a crustal magma chamber.

4. Overall, the SAVF developed in stages, e.g., the earliest volcanoes erupted alkalic basalts while later volcanoes erupted subalkalic compositions. This interpretation is similar to that proposed by Heming (1980a) for the Whangarei-Puhipuhi and Auckland volcanic fields of the North Island, New Zealand, where the initial eruptions are characterised by small volumes of alkalic basalts (i.e.,

[2] Mantle reservoirs: DM = depleted mantle, HIMU = mantle with high U/Pb ratio, EM = enriched mantle.

alkali olivine basalts) followed by voluminous subalkalic (i.e., tholeiitic) compositions.

Since Rafferty (1977) and Rafferty and Heming (1979) reported their findings, a number of important studies have been conducted in the SAVF (i.e., Rosenberg, 1991; Middleton, 1993; Sanders, 1994; Briggs *et al.*, 1994).

Rosenberg (1991) described the petrographic characteristics of magmatic pyroclasts from tuff deposits at five explosive volcanic centres within the SAVF. He identified a range of distinct rock types that characterise the pyroclasts, i.e., nephelinite, basanite, nepheline-hawaiite, transitional basalt, hawaiite, and olivine-tholeiitic basalt, and showed that populations of juvenile pyroclasts at individual centres may be characterised by a discrete rock type. Based on these observations, Rosenberg (1991) concluded that the explosive (phreatomagmatic) centres were the result of the interaction of discrete magma batches, of unique compositions, with aquifer-bearing strata near the surface. Rosenberg's study demonstrated that phreatomagmatic volcanism in the SAVF may be associated with magmas having either alkalic or subalkalic compositions such as those described by Rafferty and Heming (1979). However, Rosenberg's findings contrast with those of Rafferty and Heming who concluded that explosive volcanism in the SAVF was restricted to magmas with alkalic compositions (e.g., basanites). In addition, he determined that in the tuff ring of a small explosive monogenetic volcano (Barriball volcano), there are two distinct populations of juvenile magmatic pyroclasts, (1) olivine-tholeiitic basalt, and (2) basanite. He concluded that these clasts were derived from the sequential eruption of distinct magma batches at separate vents within the same tuff ring.

Middleton (1993) conducted a comprehensive study on the Murihiku Terrane (the basement rocks underlying much of the SAVF) in which he described their petrographical and geochemical characteristics. The results of this study suggest that SAVF magmas ascended primarily through arc-derived volcanic epiclastic sediments and metasediments.

Sanders (1994) described petrographic and mineralogical characteristics of ultramafic mantle xenoliths found in some SAVF lavas: harzburgites, lherzolites, and wehrlites in the ne-hawaiite lavas at Stevenson's Quarry, and dunite, harzburgite, and lherzolite xenoliths in the basanite lavas at Brewsters/Wilkins Quarry and Davies Quarry (see Appendix 1 for locations). His study suggests that such xenoliths may be restricted to lavas with alkalic compositions (e.g., basanites). Sanders (1994) concluded that the ultramafic xenoliths in these lavas are not cognate but are accidental fragments from either an undepleted upper mantle source or refractory residues. He also determined that

they were derived from a metasomatised, strongly heterogeneous mantle source at estimated P-T conditions of 15-17 kbar and 1180-1230°C, respectively.

Based on the classification scheme described in Johnson and Duggan (1989), Briggs *et al.* (1994) identified nine distinct rock types in the SAVF[3,4] (see Table 3.1, p. 31). They provided general petrographic descriptions for each rock type, identifying contrasting petrographic and mineralogical differences between fine-grained rocks; basanites, nephelinites, and nepheline hawaiites, and those with coarse-grained textures; mugearites transitional basalts, hawaiites, and olivine- and quartz-tholeiitic basalts. Briggs *et al.* (1994) observed that contrasting major and trace element geochemical characteristics also match the contrasts in petrography and mineralogy between the rock types.

Briggs *et al.* (1994) reported major and trace element data for 14 samples representative of the range of lava types observed in the SAVF. They also determined 43 new K-Ar ages of lavas from 33 selected volcanic centres throughout the field. Their reported ages are consistent with the K-Ar ages determined by Stipp (1968), suggesting that the field developed between 1.59 and 0.51 Ma, although one of their ages indicates that activity may have begun as early as 2.09 Ma. Briggs *et al.* (1994) concluded that volcanism was intermittent during the million-year period with two peaks of activity at 1.3 and 0.6 Ma, and that there is no apparent systematic spatial or temporal trends in lava compositions.

1.3 Objective of study

Many models of magma petrogenesis in continental intraplate tectonic settings share two common components: (1) the generation of partial melts of a peridotite source, and (2) subsequent melt modification, principally by fractional crystallisation processes (e.g., Briggs *et al.*, 1990; Wedepohl, 1995). While useful for showing a possible genetic link between parent-daughter pairs along a liquid line of descent, such models do not adequately explain the relatively small but distinct variations in the abundances of the incompatible elements (e.g., Ba, Rb, and K), moderately incompatible elements (e.g., Nb, Zr, Sr, Ti, and Ta), and the rare-earth elements (REE), commonly observed between provinces. Such variations in the incompatible trace element and REE abundances are commonly attributed to source heterogeneity (e.g., Hodder, 1988; Zhi *et al.*, 1990), or

[3] Briggs *et al.* (1994) collected 94 lava and magmatic pyroclast samples throughout the SAVF. Each sample was made available for this investigation. These samples contain the prefix "SA" whereas new samples are labeled "SAB" (see Appendix 2 for details).

[4] In addition to the six rock types reported in Rosenberg (1991), Briggs *et al.* (1994) identified alkali olivine basalt, quartz tholeiitic basalt, and mugearite lavas.

variable degrees of partial melting (e.g., Frey *et al.*, 1978; Takahashi and Kushiro, 1983; McKenzie and Bickle, 1988; Takahshi *et al.*, 1993; Zou and Zindler, 1996), or both. Incompatible trace element enrichment due to mantle metasomatism (e.g., McDonough *et al.*, 1985; Nielson and Noller, 1987; O'Reilly and Griffin, 1988; O'Reilly and Zhang, 1995; McBride, 1998; Norman, 1998) or geochemical processes in the crust-mantle system (e.g., Green, 1995; Nakada *et al.*, 1997) may also explain these variations. Some magma may also be modified by assimilation/fractional-crystallisation processes (e.g., Thompson *et al.*, 1986) or by a slab-derived flux mixing with the mantle (e.g., Ringwood, 1990).

The distinct diversity in the compositions of the South Auckland volcanic field basalts, together with their close time-space relationships, and proximity to a convergent margin, raises some key questions regarding their origin. The focus of this investigation is on the petrogenesis and evolution of the alkalic basaltic lavas that erupted throughout the South Auckland volcanic field. Therefore, the aims of this study are to determine;

1. The petrographic, mineralogy, and geochemical characteristics of the South Auckland volcanic field basalts.
2. The nature of the mantle source (or sources) of the SAVF basalts.
3. To what extent the compositions of the SAVF basalts are source- or process-dependent.
4. If there is a genetic link between the ranges of magma compositions erupted throughout the field.
5. What magmatic processes are involved in their genesis and evolution?

The detailed mineralogical and major and trace element analyses presented in this investigation document the variations in compositions between the lavas from individual, predominantly monogenetic volcanoes, thus providing important constraints on models of magma generation, and processes involved in their differentiation. The results of these models are integrated with radiogenic isotope data to evaluate mantle source characteristics and the extent to which primary magmas may have been modified by processes associated with mantle metasomatism and interaction with the sub-continental lithosphere and continental crust.

Chapter Two: Geologic Background

Chapter Two

Geologic Background

2.1 Introduction

Cenozoic volcanism has been a dominant feature in the geological development of northern North Island, New Zealand. The North Island is located toward the eastern margin of the continental Indo-Australian plate, the boundary of which is marked by the convergence and associated subduction of the Pacific plate (Fig. 2.1). The complex volcanic successions observed in this region are attributed principally to processes associated with convergent margin arc-trench systems. Since the early Miocene, the evolution of the plate boundary has resulted in subduction-related volcanism in Northland Peninsula and the Coromandel and Taupo Volcanic Zones (Ballance, 1976; Ballance *et al.*, 1982; Cole, 1986; Malpas *et al.*, 1992) (Fig. 2.2). The geologic record from this time however, contains distinct volcanic deposits with petrologic characteristics commonly associated with magma generation in regions "remote" from plate margins. These intraplate deposits[5] temporally overlap those derived from subduction-related processes, but are generally spatially separate.

Most continental intraplate volcanism is associated with extensional tectonics (Turcotte and Oxburgh, 1978). Tensional fractures in continental lithosphere provide pathways for magma to the surface, and act as important tectonic constraints regarding the location of intraplate volcanism (e.g., Calatrava Volcanic Province, central Spain, Cebriá and López-Ruiz, 1995; Laacher See, West Eifel, Germany, Wörner and Schmincke, 1984a,b; Newer Volcanic Province, eastern Australia, Price *et al.*, 1997). Volcanism in the intraplate fields of North Island may be characterised by the eruption of basaltic magmas from numerous central vents commonly distributed over a wide area. Evaluation of the continental crust suggests that the location of the fields and many of the vents within them is structurally controlled. In addition, the nature of eruptions (i.e., effusive or explosive) may be closely associated with the hydrological properties of the formations that underlie the intraplate fields.

The South Auckland volcanic field represents one of a number of geographically isolated and geochemically distinct fields in northern North Island that do not appear to be

[5] Because all intraplate volcanic fields in the North Island developed within 200 km of the Indo-Australian/Pacific plate boundary, the term "intraplate", used in this and subsequent chapters, refers principally to petrological and geochemical features of the deposits rather than a strict tectonic characterisation.

directly linked to convergent margin processes (Fig. 2.2). Previous work on the tectonic history of North Island, and the composition and structural evolution of the continental lithosphere upon which the SAVF developed, is discussed with the aim of a better understanding of (i) the temporal and spatial association of the SAVF with other volcanic areas in North Island, (ii) the nature and location of volcanism in the field, and (iii) the distinct geochemical characteristics of the eruptive products in the SAVF.

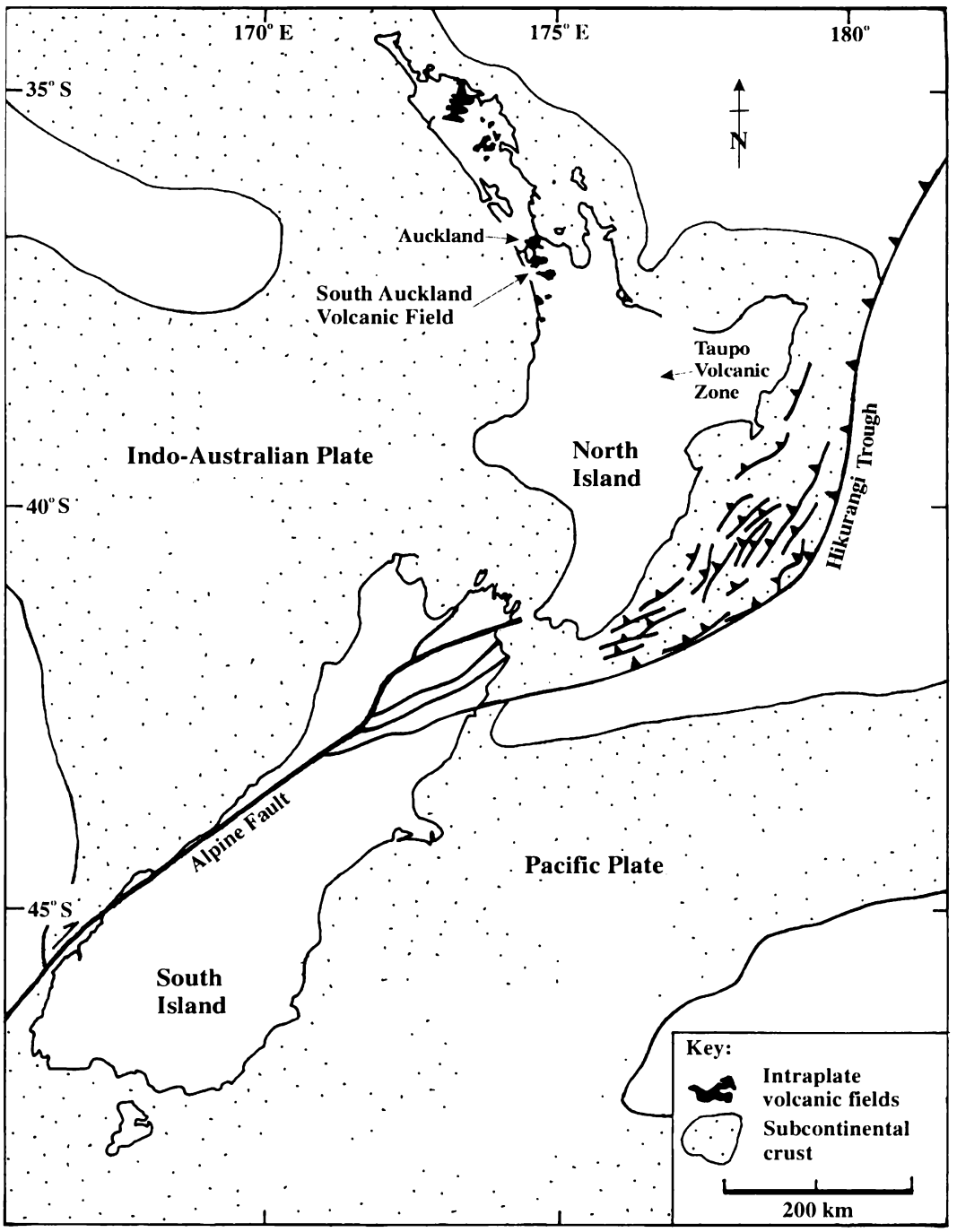

Fig. 2.1 Regional tectonic setting of New Zealand relative to the Indo-Australian and Pacific plates. The stippled area represents subcontinental crust (after Price *et al.*, 1999). Subduction of the Pacific plate beneath North Island takes place along the Hikurangi Trough. The black areas illustrate the location of the South Auckland volcanic field relative to other North Island intraplate fields and the Taupo Volcanic Zone (shaded in grey).

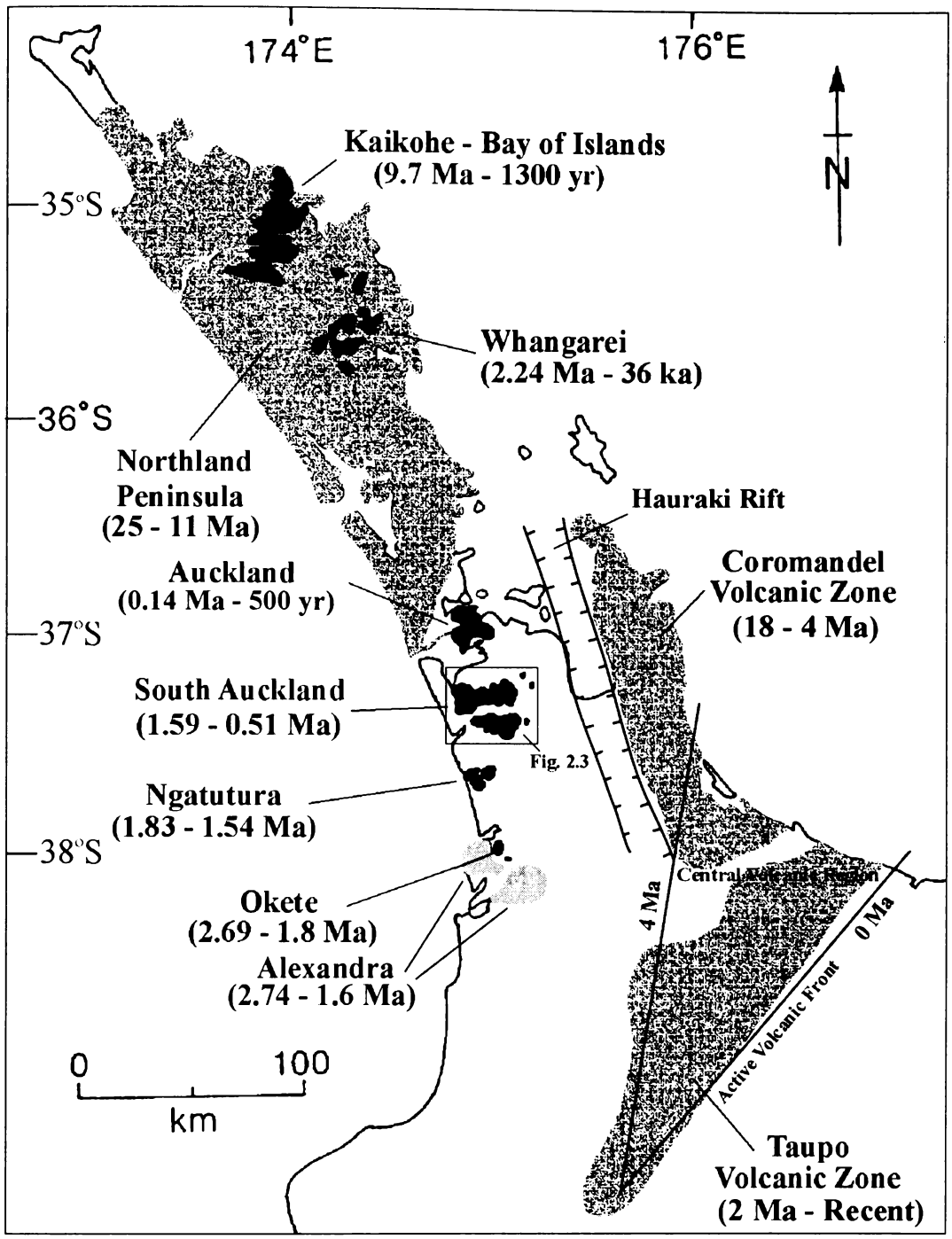

Fig. 2.2 Distribution and age-range of the intraplate volcanic fields of northern North Island (black areas) relative to the subduction-related Northland Peninsula (Herzer, 1995, Hayward *et al.*, 2001), the Coromandel (Adams *et al.*, 1994) and Taupo Volcanic Zones (Wilson *et al.*, 1995), and the Hauraki Rift (Black *et al.*, 1992). The stippled areas represent onshore regions containing subduction-related volcanic deposits. The grey-shaded areas represent the back-arc, subduction-related, calcalkaline basaltic magma series of the Alexandra Volcanics (Briggs *et al.*, 1989; Briggs and McDonough, 1990), which erupted contemporaneously with the intraplate Okete Volcanics. The boundaries and ages for the Central Volcanic Region are from Stern (1987). The Northland province (referred to in the text) contains the Kaikohe-Bay of Islands and the Whangarei fields. The Auckland province consists of the Auckland, South Auckland, Ngatutura, and Okete fields. Note that in contrast to the southward trend of decreasing age of subduction-related volcanism, there is a progressive increase in age of the Auckland, South Auckland, Ngatutura, and Okete intraplate volcanic fields. Some data adapted from Briggs *et al.* (1989; Fig.1).

2.2 General Background

Much of the volcanism in North Island is attributed to subduction-related processes – associated predominantly with the convergence between the Indo-Australian and Pacific plates. Since the early Miocene, large volumes of eruptive products with calc-alkaline basaltic-andesitic-rhyolitic association were produced along the Northland Peninsula and later in the Coromandel and Taupo Volcanic Zones[6] (Fig. 2.2). Currently, the boundary of these plates is dominated by the oblique westward subduction of the Pacific plate beneath the North Island at the Hikurangi margin, forming the Taupo-Hikurangi arc-trench system (Cole and Lewis, 1981; Cole, 1990; Kelsey *et al.*, 1995).

In contrast to subduction-related volcanism, volumetrically minor amounts of lava and tephra were produced in a number of distinct, geographically isolated, intraplate volcanic fields that comprise the Northland and Auckland intraplate volcanic provinces (Fig. 2.2). These provinces characterise the only known intraplate volcanism in the North Island. The Northland and Auckland provinces are located west of the Hauraki Rift (Hochstein and Nixon, 1979; Hochstein and Ballance, 1993) behind the active volcanic front of the Taupo Volcanic Zone and are interpreted as being situated in a back-arc continental intraplate setting (Cole, 1986).

The Northland Volcanic Province (9.7 Ma – 1300 yr; Stipp and Thompson, 1971, Smith *et al.*, 1993) consists of the Kaikohe-Bay of Islands and Whangarei volcanic fields (Heming, 1980a,b; Ashcroft, 1986). The Auckland Volcanic Province (2.69 Ma – 500 yr; Briggs *et al.*, 1989; Wood, 1991; Briggs *et al.*, 1994) consists of the Okete Volcanics[7] (Briggs and Goles, 1984; Briggs and McDonough, 1990); Ngatutura Volcanics (Briggs *et al.*, 1990); South Auckland volcanic field (Rafferty, 1977; Rafferty and Heming, 1979; Briggs *et al.*, 1994); and the Auckland volcanic field (Heming and Barnet, 1986; Huang *et al.*, 1997, 2000). Each field contains numerous relatively small-volume, predominantly monogenetic volcanoes that produced lava flows, scoria cones, tuff rings, and maars[8]. Geochemical investigations show that eruptive products in each field have predominantly alkalic to tholeiitic compositions typical of continental intraplate volcanism[9].

---

[6] The Taupo Volcanic Zone lies within the larger Central Volcanic Region (*cf.* Stern, 1985, 1987).

[7] The Okete Volcanics is excluded in the Smith (1989) description of the Auckland province. However, Briggs *et al.* (1994) argued that based on petrologic characteristics similar to those of the other fields, the Okete Volcanics should be included as a fourth field in the province.

[8] In the Northland fields, volcanic landforms are mainly scoria cones (Heming, 1980b).

[9] Huang *et al.* (2000) argued that some of the volcanics in discrete fields (e.g., Whangarei field) exhibit geochemical features that suggest derivation from mantle source regions modified by subduction-related processes. See chapter 6 for a discussion of the nature of the mantle source(s) for the South Auckland volcanic magmas.

Volcanic activity in the Auckland Volcanic Province began during the mid-Pliocene. The four volcanic fields in the province display an age trend with increasing distance away from the active volcanic front of the TVZ (see Fig. 2.2). Ages range from the 2.69 - 1.80 Ma for the Okete Volcanics (Briggs *et al.*, 1989) in the south, to 1.83 - 1.54 Ma for the Ngatutura Volcanics (Briggs *et al.*, 1989), 1.59 - 0.51 Ma[10] for the South Auckland volcanic field (Briggs *et al.*, 1994), and 0.14 Ma - 500 yr for the Auckland volcanic field (Wood, 1991) in the north. Based on their ages and spatial distribution, Briggs *et al.* (1994) noted that as activity waned in an individual field, the development of a new field commenced approximately 35 to 38 km to its north. The linear nature of these fields is similar to the intraplate fields in the South Island, New Zealand, and eastern Australia, which are interpreted to be a response, in part, to intraplate extensional forces (Shaw, 1980; Coblentz *et al.*, 1995). On this interpretation it could be inferred that the localisation of volcanism in the Auckland Volcanic Province is controlled, to some extent, by fractures in the subcontinental lithosphere. Spörli and Eastwood (1997) argued that tensional stresses not only control the location of individual intraplate fields but also could facilitate decompressional melting and thus the onset of volcanism. In the case of the Auckland Volcanic Province, Spörli and Eastwood (1997) argued that the youngest field could represent the tip of a northward-propagating lithospheric fracture. However, in an alternative hypothesis, they proposed that each field could be the result of a northward-propagating source along a lithosphere fracture induced during Mesozoic tectonism.

2.3 Geological Setting of the South Auckland volcanic field

The South Auckland volcanic field is located in the Auckland Volcanic Province 175 km behind the active volcanic front of the Taupo Volcanic Zone (TVZ; Fig. 2.2). Depth contours of the Wadati-Benioff zone, outlined by earthquake foci, show a progressive steepening dip of the Pacific plate from the southeast to the northwest that strikes N 45° E and dips 50° to the northwest (Adams and Ware, 1977). The SAVF lies within 50 km of "the limit of plunging seismic activity" of the subducting Pacific plate (Briggs *et al.*, 1997) with the Wadati-Benioff zone projecting approximately 300 km beneath the SAVF.

The SAVF covers an area of approximately 300 km^2 and principally occupies the lowlands of the lower Waikato Valley and the Manukau Lowlands south of Auckland

[10] Briggs *et al.* (1994) reported K/Ar ages of 2.24 ± 0.37 and 2.09 ± 0.37 Ma for a quartz tholeiitic basalt sample. They noted however, that this sample contains quartz xenocrysts and argued that the excess Ar due to these contaminants may result in anomalously older ages. This sample therefore, may not be representative of a maximum age for the SAVF. Nevertheless, Jukic (1995) reported rocks of "basaltic" composition stratigraphically older than the sedimentary Pliocene Kaawa Formation. This suggests that volcanism in the SAVF may have begun earlier than hypothesised by Briggs *et al.* (1994) with activity in the SAVF possibly coeval with volcanism in the Ngatutura and Okete volcanic fields.

City. Volcanic deposits cover widespread areas located mainly west of the Drury Fault and State Highway 1 (SH1)(Fig. 2.3). East of the Drury Fault, exposed volcanic deposits cover relatively small, isolated areas (< 3 km^2 in total) with volcanic centres located at irregular intervals from Hunua Falls in the northeast to Kellyville in the south (Schofield, 1976; Rafferty, 1977; Waterhouse, 1978). The region is divided by the north-trending Junction (Stoke's) Magnetic Anomaly (Hunt, 1978; Hatherton *et al.*, 1979).

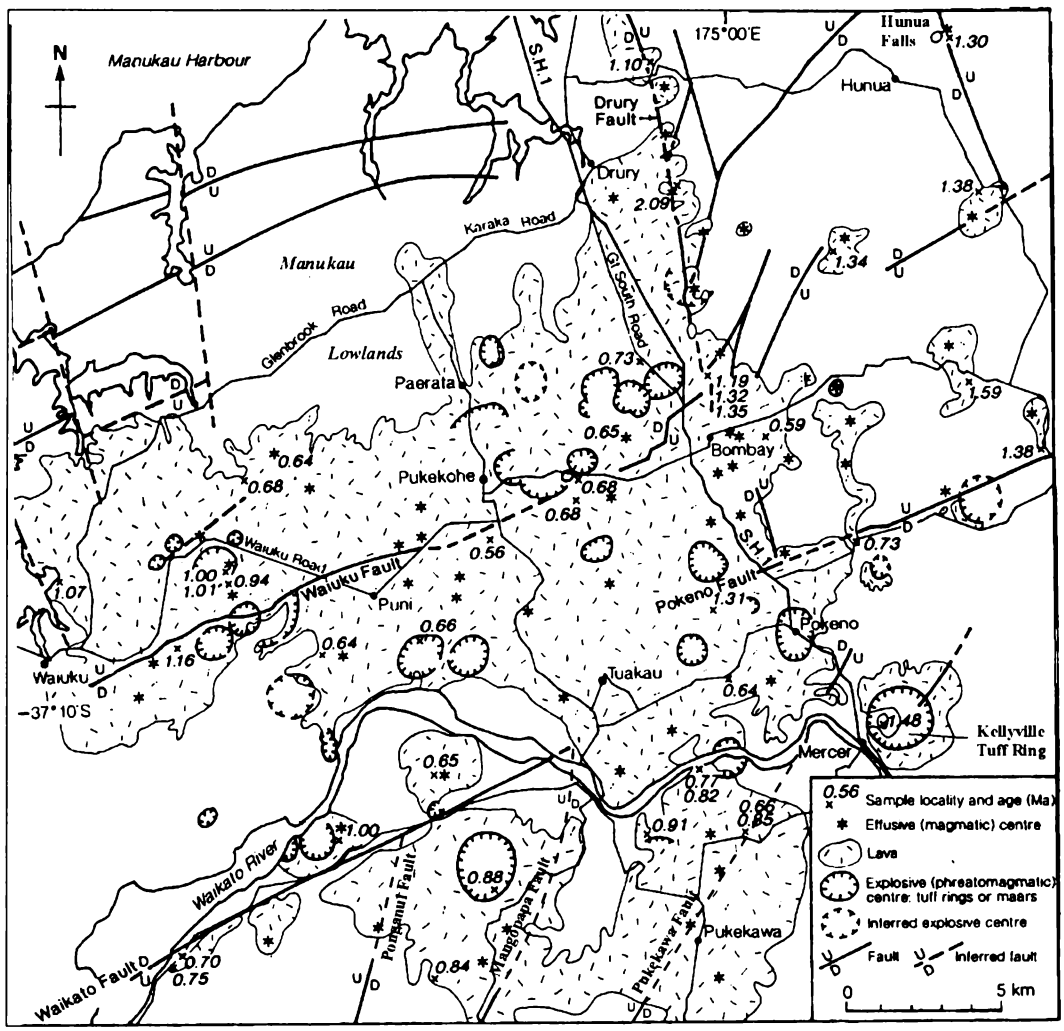

Fig. 2.3 The main structural features, K-Ar ages, and distribution of explosive and effusive centres in the South Auckland volcanic field (after Briggs *et al.*, 1994). Refer to Fig. 2.2 for the general location of the SAVF.

The SAVF consists of approximately 100 predominantly monogenetic volcanic centres (Briggs *et al.*, 1994). The monogenetic nature and the diverse geochemical characteristics of the magmas erupted at these vents precludes the presence of a long-lived shallow magma reservoir beneath the field.

Forty-three K/Ar ages from 33 volcanic centres (Briggs *et al.*, 1994) indicate two peaks of activity at 1.3 and 0.6 Ma, with volcanism occurring intermittently throughout this

period. The location of each of these centres together with their corresponding age is shown in Fig. 2.3 and the age range for each rock type identified in the SAVF, except mugearite, is illustrated in Fig. 2.4. Based on these data, Briggs *et al.* (1994) concluded that there is no temporal or spatial relationship among the volcanic centres. However, further examination of these data suggests that the majority of the "oldest" centres (i.e., those greater than 1.0 Ma) occur in the northeast corner of the field, principally in the area bounded on the west by the Drury Fault and the Pokeno Fault to the south (Fig. 2.3). Additionally, the composition of the lavas sampled in this area is predominantly nepheline-hawaiite. These lavas exhibit distinct geochemical features unlike those from volcanoes at other locations in the SAVF. In contrast to the "nepheline-hawaiite" volcanoes, these later volcanoes exhibit no apparent spatial relationship relative to their compositions.

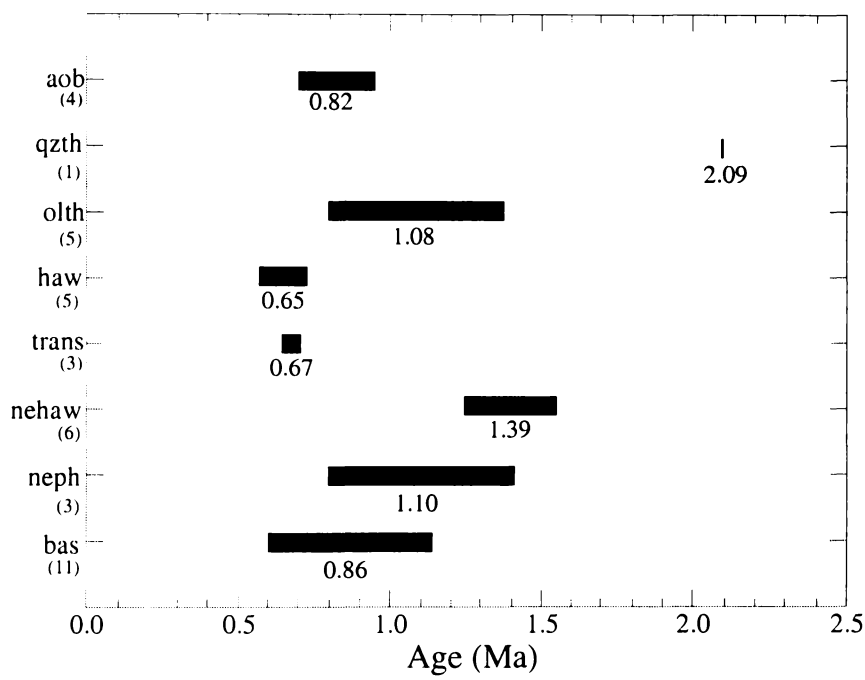

Fig. 2.4 Age range for each rock type erupted in the South Auckland volcanic field compiled from the K/Ar age data of Briggs *et al.* (1994). bas = basanite, neph = nephelinite, nehaw = nepheline hawaiite, trans = transitional basalt, haw = hawaiite, olth = olivine tholeiitic basalt, qzth = quartz tholeiitic basalt, aob = alkali olivine basalt. The number below each bar represents the average age for each rock type. The number in parentheses below each rock type represents the number of K/Ar age analyses.

Kear (1964) hypothesised that (i) volcanic centre alignment in North Island is often closely associated with pre-existing faults, and (ii) volcanism occurs as the result of fault dilation. This sympathetic association is best illustrated in the SAVF. Field observations supported by air photo analysis indicate that there is a close association between the locations of the volcanic centres throughout the field and crustal structure. Many of the volcanic centres are located either along or adjacent to faults, or inferred extensions of

faults, which can provide pathways for magma ascending through the upper crust. Additionally, the linear distribution of many of the centres suggests the existence of unmapped faults obscured by subsequent volcanic deposits.

Eruptions were either explosive or effusive (Rafferty, 1977; Rafferty and Heming, 1979; Rosenberg, 1991). The deposits at 38 centres exhibit depositional characteristics typical of explosive events. The explosive eruptions were principally phreatomagmatic. Evidence for this exists in tuff deposits where clasts from aquifer-bearing Tertiary formations occur together with juvenile magmatic pyroclasts throughout the deposit. These explosive events probably occurred when relatively small magma batches exploited fault-induced crustal fractures, forming feeder dykes that propagated along the faults until the magma encountered and mixed with groundwater near the surface (e.g., Spence and Turcotte, 1985). The phreatomagmatic eruptions produced tuff rings, maars, and associated craters that range in diameter from 0.5 to 2.6 km (Rosenberg, 1991). Craters are commonly clustered or nested, and occasionally contain a nested scoria cone. A number of the craters were partially filled by subsequent lava flows resulting in small lava lakes.

Sixty-two centres are characterised principally by effusive (i.e., magmatic) activity. The effusive volcanoes generally formed small, relatively low relief shield volcanoes indicative of Hawaiian-style volcanism. Many of the shields are characterised by uniform slopes of less than 10° and rounded summits without a distinguishable crater. In contrast, other shields contain steep-sided scoria cones that typically are less than 200 m in height and 500 m in diameter, possibly the result of late-stage Strombolian activity. Field observations supported by bore log data (Bell *et al.*, 1991; Petch *et al.*, 1991; Jukic, 1995) indicate that lava flows are relatively thin, ranging from a few metres to several tens of metres. These observations and data suggest that the thicker flows represent partially filled paleovalleys and that lava rarely traveled more than several kilometres from their source. Additionally, lava from effusive centres occasionally ponded in topographic lows creating inactive lava lakes (Swanson *et al.*, 1979) similar to those in Kilauea Iki, Alae, and Makaopuhi craters on Kilauea volcano, Hawaii (Richter *et al.*, 1970; Swanson *et al.*, 1972; Wright and Okamura, 1977; Peck, 1978). Some of these "lakes" in the SAVF, which may exceed 70 m in thickness, have been quarried.

Exposure of the deposits from most of the centres is generally poor, and most of the volcanic features and associated deposits have been severely eroded. The morphology of the maars, craters, tuff rings, and scoria cones has been modified by weathering, erosion, mass wasting, and infilling of lacustrine deposits or pyroclastic material derived from nearby centres. However, abundant bore log data (Bell *et al.*, 1991; Petch *et al.*, 1991;

Jukic, 1995) indicate a range of stratigraphic variations throughout the field that may be attributed to eruptive products derived from one or more volcanic centres. These variations include:

1. Continuous volcanic successions that may include intercalated lava, scoria, and tuff. The thickness of these sequences is variable, ranging from < 20 to ~ 200 m.
2. Two or more distinct volcanic successions separated by discrete sedimentary horizons that may include units of sandstone, siltstone, clay, and peat.
3. Alternating sequences of relatively thin volcanic and sedimentary deposits.

Bore log data suggest that many volcanoes underwent alternating episodes of magmatic (i.e., Hawaiian) and Strombolian activity. At most centres, lava from magmatic episodes dominates the thickness of the deposit. Field observations supported by bore log data suggest that eruptions often occurred through older lava flows or tuff deposits. Evidence for this has been observed in a number of tuff deposits where lava clasts and reworked magmatic pyroclasts of contrasting whole-rock geochemical compositions occur together in the same stratigraphic horizon, often in contact with one another.

2.4 Tectonic history and crustal evolution of the South Auckland region

Since the Permian period, a number of depositional, erosional, and tectonic events occurred in New Zealand that markedly influenced the geological development of the South Auckland region. Four events in particular have affected the tectonic evolution, crustal structure, nature of volcanism, and possibly the compositions of the magmas erupted within the South Auckland volcanic field:

1. The mid Triassic to late Jurassic formation of the Murihiku and Waipapa Terranes, the basement rocks underlying the South Auckland region (Spörli, 1978; Ballance and Campbell, 1993; Middleton, 1993, Mortimer and Smith-Lyttle, 2001).
2. The Rangitata Orogeny during the late Jurassic – early Cretaceous (Waterhouse, 1978).
3. Extensional block faulting and sedimentation from late Cretaceous to the early Miocene (Schofield, 1976, 1988; Waterhouse, 1978; Spörli, 1980).
4. The Kaikoura Orogeny during the early Miocene to recent (Waterhouse, 1978).

During the Permian to Cretaceous period the geological history of New Zealand was marked by the deposition of predominantly terrestrial volcanic epiclastic sediments and tuff into the forearc basin, associated with an arc-trench system, at the eastern margin of

Gondwanaland super-continent where active subduction was taking place (Spörli and Ballance, 1989; Ballance and Campbell, 1993). The discrete geological units deposited during that time now comprise the distinct, fault-bounded terranes that make up much of the basement rock of New Zealand (e.g., Bradshaw, 1989).

2.4.1 Basement terranes of the South Auckland region

The South Auckland volcanic field developed upon Triassic to Tertiary period sedimentary rocks ubiquitous in the South Auckland region. The basement of the region comprises two distinct terranes that represent contrasting sedimentary lithofacies. The Murihiku Terrane is predominant west of the Drury Fault, and underlies most of the SAVF. The Waipapa Terrane extends from the eastern margin of the SAVF east to the Firth of Thames (Mortimer and Smith-Lyttle, 2001) (Fig 2.5).

The Murihiku Terrane

The Murihiku Terrane (MT) is a 9 to >15 km thick sequence of volcanic epiclastic detritus and tuffs (Ballance and Campbell, 1993). Lithologies of the MT are moderately fossiliferous and include predominant marine siltstones, sandstones, and mudstones with subordinate conglomerates and minor argillite, greywacke, and andesitic to rhyolitic vitric and crystal tuffs (Schofield, 1976, 1988; Middleton, 1993). The MT developed within a forearc basin at the eastern margin of Gondwanaland associated with a convergent arc-trench system (Spörli, 1978; Middleton, 1993). Ballance and Campbell (1993) determined that deposition began prior to mid Triassic time and the youngest rocks were deposited in the late Jurassic. However, based on fission track age data Kamp and Liddell (2000) concluded that deposition of volcaniclastic sequences continued into the Cretaceous (e.g., 100 Ma). The sediments have undergone low-grade metamorphism and subsequent deformation resulting in large, open, regional-scale anticlines and synclines (Bradshaw, 1989; Kamp and Liddell, 2000). Formations that comprise the MT crop out as a north-trending belt at the southwestern margin of the SAVF (Fig. 2.4).

The Dun Mountain Ophiolite Belt (Maitai Terrane) separates the MT from the Waipapa Terrane (Mortimer and Smith-Lyttle, 2001). Field evidence suggests that Maitai Terrane rocks are not exposed in the SAVF, although they have been detected geophysically in the subsurface as the Junction (Stoke's) Magnetic Anomaly (Hatherton and Sibson, 1970; Hunt, 1978; Hatherton *et al.*, 1979).

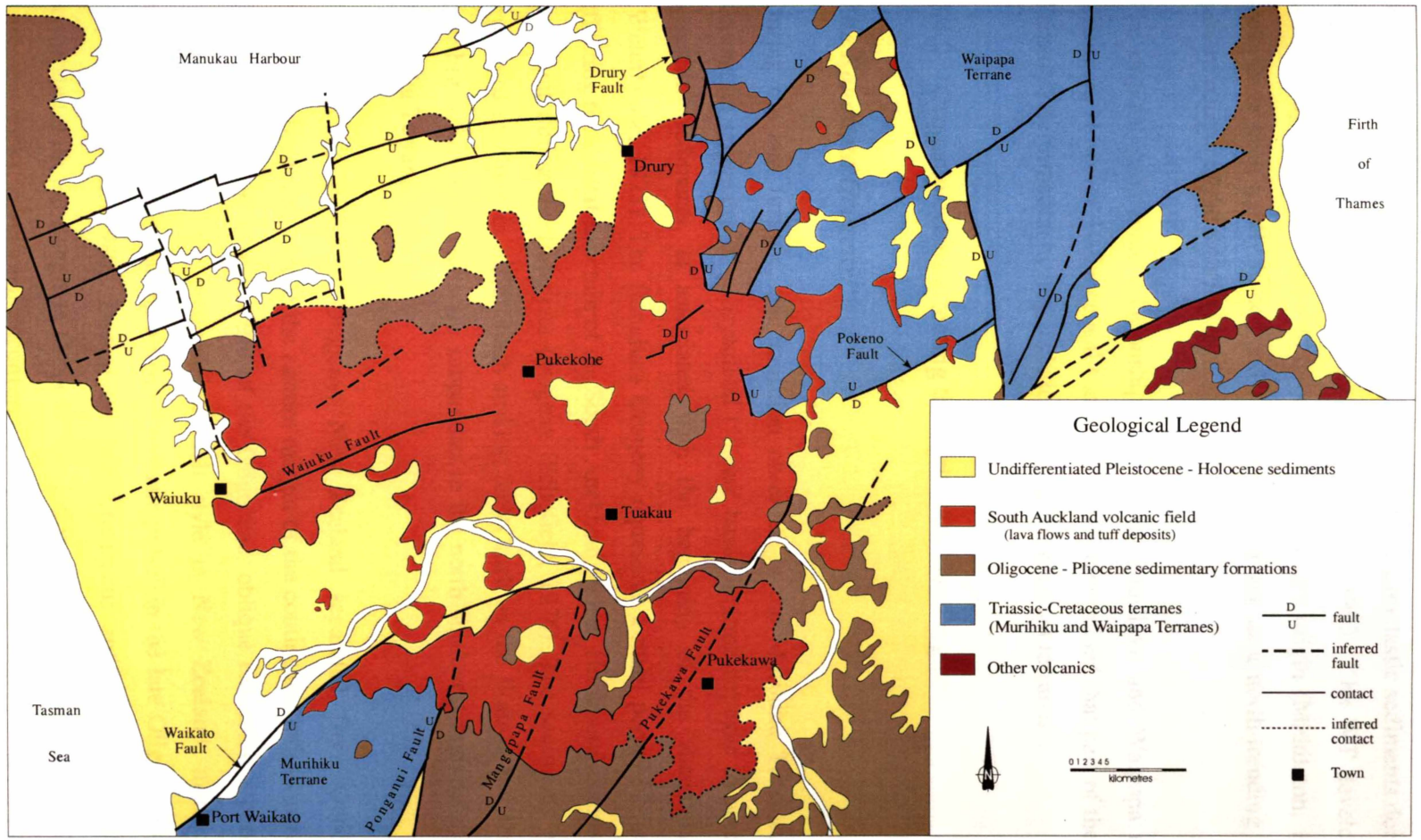

Fig. 2.5 Geological map of part of the South Auckland Region illustrating the Murihiku and Waipapa Terranes relative to the South Auckland volcanic field (adapted from Rosenberg, 1991). The Drury Fault separates the Murihiku Terrane, which crops out southwest of the SAVF, from the Waipapa Terrane located east of the Fault (see Mortimer and Smith-Lyttle, 2001, for the regional distribution of each Terrane). The faults in the southern part of the map (e.g., Pukekawa Fault) are adapted from Waterhouse (1978).

The Waipapa Terrane

The Waipapa Terrane (WT), with a minimum thickness of 6 km (Schofield, 1976), represents a sequence of Triassic-Jurassic, mainly volcaniclastic sediments dominated by abundant mudstones (Waterhouse, 1978; Middleton, 1993). The WT developed as an accretionary prism having an intra-oceanic volcanic-arc origin (Middleton, 1993). The rocks have been tightly folded and faulted and crop out as a north-trending belt at the eastern margin of the SAVF (Fig. 2.5).

The original geographic relationship between the Murihiku and Waipapa terranes is unknown. However, Ballance and Campbell (1993) determined that part of the Murihiku Terrane's deformation history includes suturing to "adjacent terranes".

2.4.2 Orogenic events affecting the South Auckland region

The Rangitata Orogeny

During the late Jurassic, the transition observed in the Murihiku Terrane, from the alternating sequences of geosynclinal (forearc basin) marine deposits to predominantly terrestrial sediments, is associated with the beginning of the Rangitata Orogeny (Waterhouse, 1978). The Rangitata Orogeny represents a main period of fault activity affecting the crustal structure of the South Auckland region. Horizontal compression was dominant during the Rangitata Orogeny (Schofield, 1976). The sediments were thrust westward resulting in major north-striking faults such as the Wairoa and Drury Faults (see Fig. 2.3). These faults are subparallel to the north-northwest regional strike of the Murihiku Terrane.

Following the Rangitata Orogeny, New Zealand separated from Gondwanaland, eventually becoming part of the eastern margin of the continental Indo-Australian plate. From late Cretaceous to the end of the Oligocene, oblique extension accompanied by block faulting was the predominant fault style in New Zealand, marked by fault reactivation and uplift during a major "tectonic pulse" in the late Oligocene (Weissel *et al.*, 1977; Spörli, 1980). During the late Cretaceous and Palaeocene, deformation associated with the Rangitata Orogeny was followed by intense erosion of the uplifted basement rocks. A regional unconformity separates the Murihiku and Waipapa terrane basement rocks from Tertiary sedimentary rocks, marking this period of erosion. The basal Te Pake Sandstone of the Murihiku's Newcastle Group is the erosional remnant

from this time and forms the basement of the region now occupied by the majority of the SAVF (Waterhouse, 1978). This period of erosion was followed by renewed sedimentation during the Tertiary Period, accompanied by continued extension-related block faulting.

The Kaikoura Orogeny

The Kaikoura Orogeny, a predominantly tensional tectonic event, is dominated by block-faulting, uplift, and fault reactivation (Brothers, 1975). The fault patterns observed in the South Auckland region today were developed primarily during the main phases of the Kaikoura Orogeny in the early-mid Miocene (Waterhouse, 1978).

During the Kaikoura Orogeny, Rangitata orogenic thrust faults were reactivated as high-angle normal faults. Additionally, two opposing stress fields developed; a NE-directed, principal horizontal stress believed to be a relic from the Rangitata Orogeny, and a NW-directed, principal horizontal stress that developed during the Kaikoura Orogeny (Schofield, 1978). Two distinct fault geometries developed in the South Auckland region (Fig. 2.3). The region north of the Waikato Fault is dominated by high angle normal faults (e.g., Waikato, Pokeno, and Waiuku Faults) that generally trend perpendicular to the NNW-striking Drury Fault, forming a rectangular grid pattern (Schofield, 1976, 1988; Spörli, 1980). In contrast, south of the Waikato Fault, NNE-striking high-angle normal faults (e.g., Ponganui and Pukekawa Faults) truncate numerous smaller scale normal faults at approximately 30° to 45° producing a distinct NNW- to ENE-striking rhombic block-fault pattern (Waterhouse, 1978; Spörli, 1980). The rhombic geometry, described by Spörli (1980), is interpreted to be the result of a "NNE directed transcurrent dextral shear applied to normal faults associated with block faulting" produced during sporadic Cretaceous deformation (Pilaar and Wakefield, 1978).

2.4.3 The influence of Tertiary deposits and water

The distribution of subsurface water throughout the SAVF had a major influence on the eruption style at many of the centres. Magma interaction with groundwater reservoirs resulted in phreatomagmatic eruptions and the subsequent formation of tuff rings and maars.

Tertiary deposits – marine and estuarine sandstones and siltstones, volcanic deposits, and unconsolidated terrestrial sediments – are widespread throughout SAVF and form a relatively thin veneer (i.e., < 500 m) upon the basement rocks. A number of Tertiary

formations have hydrogeological properties favourable for aquifer development (Bell *et al.*, 1991; Petch *et al.*, 1991). Most of the phreatomagmatic centres are located in the Manukau Lowlands, a down-faulted block north of the Waikato River, bounded on the east by the Drury Fault and the Waikato Fault to the south, and infilled with Tertiary sediments (Fig. 2.3). Rosenberg (1991) determined that some of the phreatomagmatic centres north of the Waikato Fault are the result of magma interaction with the aquifer-bearing Pliocene Kaawa Formation (Henderson and Grange, 1926), which occurs approximately 100 to 200 m below the surface. Additionally, field observations indicate that the Oligocene Ahirau Sandstone Member (Nelson pers. comm., 2000) of the Glen Massey Formation in the Te Kuiti Group (White and Waterhouse, 1993) is probably an aquifer-bearing strata. Evidence for this exists in the tuff deposit at Bombay Quarry where clasts of Ahirau Sandstone occur throughout the deposit.

2.4.4 Tectonics and intraplate magmatism

The linear nature of the four volcanic fields in the Auckland province suggests a correlation between intraplate magmatism and within-plate stress fields induced, to some extent, by the Rangitata and Kaikoura orogenies. In addition, the structure of the continental lithosphere and magmatic processes within the asthenosphere could act as important tectonic and geochemical constraints in the petrogenesis and evolution of magmas in tectonic environments such as the SAVF. For example, if faults originally under compression during the Rangitata Orogeny were subsequently opened and propagated as tensional faults during the Kaikoura Orogeny, as Schofield (1976) suggested, then this would allow fracturing through the subcontinental lithosphere, thus providing a triggering mechanism (e.g., decompression) required for mantle upwelling, partial melting, and subsequent magma generation in the asthenosphere. This suggests that intraplate stress fields and associated fault reactivation control the sites of alkalic volcanism in the subcontinental lithosphere, although it does not provide an explanation for the regular spacing of volcanic fields such as those observed in the Auckland province.

Weertman (1971) proposed that magma in the asthenosphere could nucleate cracks in the lithosphere provided that the lithosphere is in tension. Ascending magma could dilate and propagate pre-existing near-surface fractures provided that magma fluid pressure exceeds the least principal *in situ* stress component and the tensile strength of the country rock (e.g., Spence and Turcotte, 1985; Cas, 1989). Spence and Turcotte (1985) determined that magma-driven crack propagation through the lithosphere is limited by magma viscosity

and assuming a constant rate of injection, calculated that propagation rates of up to $0.25ms^{-1}$ for cracks up to 2 m in width are possible. In the case of the SAVF, the close association between volcanic centres and tensional, tectonic-related faults indicates a correlation between alkalic magmatism, tectonism, and the reactivation of lithospheric shear zones. This tectonic regime allows for the rapid ascent of magma through the lithosphere and upper crust to the surface without significant contamination, or interaction with the crust[11].

2.5 Spatial and temporal association of the North Island intraplate fields

Duncan and McDougall (1989) argued that since 43 Ma the Indo-Australian plate has moved northwards relative to a mantle-fixed reference frame. However, there is no spatial or temporal evidence to suggest that volcanism in each province or field of the North Island may be attributed to a stationary magma source (hot spot). Hot-spot volcanism of the style attributed to the development of island chains, e.g., the Hawaiian Islands (Duncan and Clague, 1985) or an age-progressive linear distribution of continental intraplate volcanic fields, e.g., eastern Australia (Duncan and McDougall, 1989), requires a progressive southward decrease in age of the individual volcanic fields of the North Island. Although the oldest intraplate-derived deposits are found in the Kaikohe – Bay of Islands field of the Northland province (~ 10 Ma), 150 - 250 km north of the Auckland province, during the last 2.24 m.y. volcanism in each province has been coeval. Furthermore, in the Auckland province the linear distribution of volcanism exhibits an increasing age trend southward from the Auckland volcanic field to the Okete Volcanics (see Fig. 2.2). This trend contrasts with the decreasing age trend that would be expected from the northerly movement of the Indo-Australian plate passing over a stationary mantle source.

Hodder (1984) proposed that the relationship between the linear nature and age trend of the four volcanic fields in the Auckland province and the apparent direction of rifting of the Hauraki Rift as evidence that these fields developed as a response to membrane stresses (e.g., Turcotte and Oxburgh, 1976) associated with development of the Hauraki Rift. Alternatively, Briggs *et al.* (1994) hypothesised that such an age trend may be a response to the beginning of subduction related to the southerly propagation of the converging Indo-Australian/Pacific plate boundary, southeast of the province.

[11] The role of the continental lithosphere and crust in magma composition is discussed in Chapter 6.

2.6 Models for North Island intraplate volcanism

A number of models have been proposed to explain: (i) the spatial distribution of the intraplate fields of northern North Island, New Zealand, (ii) the geochemical characteristics of the basaltic magmas that erupted within them, and (iii) the nature of the mantle source regions from which these magmas were derived. These models are summarised below to provide a context for comparison with the new model proposed in this investigation for the South Auckland volcanic field[12]. Each model generally has a number of common features:

1. Two distinct magma types erupted in each field; silica-undersaturated alkalic and less undersaturated subalkalic basalts[13].

2. Magmas were derived predominantly from an enriched OIB-like source region in the asthenospheric upper mantle within the low-velocity zone (LVZ) – located beneath North Island at depths between 75 and 125 km (Mooney, 1970) – rather than deep-seated mantle plumes. Available Pb isotopic data indicate that the magmas are significantly less radiogenic than HIMU OIB.

3. Magma was generated as discrete batches, the result of progressive melting of ascending mantle diapirs.

4. There is no geochemical evidence to suggest that crustal contamination occurred on a large scale, although quartz xenocrysts and xenoliths from sedimentary country rock have been identified in rocks from each field.

5. With the exception of the Whangarei-Puhipuhi field in the Northland Volcanic Province, there is no geochemical evidence that suggests the source regions for the intraplate basalts of North Island have been modified by convergent margin processes despite their relative close proximity to mantle regions modified by such processes. However, this has not been conclusively demonstrated for the SAVF basalts.

2.6.1 Northland Volcanic Province – Kaikohe-Bay of Islands and Whangarei-Puhipuhi fields

Heming (1980a) identified an overall temporal trend in basalt compositions in the Whangarei-Puhipuhi field (WHP) marked by the initial eruption of small volumes of alkalic basalts (i.e., alkali ol-basalts) followed by voluminous subalkalic (i.e., tholeiitic) compositions. He concluded that this trend could result from the progressive melting of a discrete mantle diapir beneath the field, rather than the fractional crystallisation of a common parent magma. In contrast to the WHP, there is no temporal correlation between

[12] Petrogenetic models for the SAVF are presented in Chapter 6.
[13] The Ngatutura Basalts, located ~ 35 km south of the SAVF (Fig. 2.2), consists entirely of alkalic compositions (Briggs *et al.*, 1990).

the alkalic and subalkalic basalts of the Kaikohe-Bay of Islands field (KBI). Based on (i) this observation, (ii) the large range in ages for the KBI alkalic basalts (i.e., ~ 10 m.y.; see also Smith *et al.*, 1993), and (iii) the relatively large volume of magma erupted in the KBI, i.e., ~ 15 – 20 km^3, compared with the ~ 6 – 10 km^3 erupted in the WHP, Heming (1980a, b) argued that there was probably more than one diapiric upwelling event beneath the KBI. Despite the temporal differences in magma evolution between fields, Heming (1980a) concluded that for each field the alkalic magmas represent relatively small degree melts, i.e., ~ 4 %, which segregated at ~ 60 km depth, and that the subalkalic magmas were derived by larger degrees of melting, i.e., 15 – 20%, which segregated at ~ 40 km depth.

Heming (1980b) argued that the diapirs formed as the result of convection within a mantle wedge behind an island arc and that the oldest volcanism in the Northland Volcanic Province (i.e., ~ 10 m.y.) was due to mantle convection behind the NNW-trending Coromandel Arc, in association with Pacific plate subduction beneath the Northland Peninsula during the Miocene. In addition, Heming (1980b) proposed that the relatively recent volcanism in the KBI, i.e., 1300 – 1800 years bp, is the consequence of convection within the mantle wedge associated with the NNE-trending Taupo-Hikurangi arc-trench system, adjacent to the Taupo Volcanic Zone approximately 400 km southeast of the KBI. In an alternative hypothesis, Hodder (1984) used major and trace element discrimination diagrams to argue that the KBI and WHP basalts have geochemical characteristics consistent with continental rift magmatism. He concluded that the "recent" lavas in these fields may be associated directly with the Hauraki Rift (see Fig. 2.2) and that the "older" basalts may be linked either to a Miocene analogue to the Hauraki Rift or a back-arc basin of a former island arc.

Huang *et al.* (2000) identified distinct, spatially separate mantle sources for the KBI and WHP fields, located at > 50 km and < 50 km depth respectively. They concluded that although each source has similar Sr and Nd isotopic compositions, LREE abundances, and relatively low LREE/HREE values, the KBI source was modified by "within-plate processes" producing basalts with OIB-like trace element characteristics and comparatively large LILE/HFSE values and Pb isotopic ratios relative to those of the WHP. In contrast, the WHP source was modified by processes associated with Pacific plate subduction beneath the Coromandel Arc prior to the onset of intraplate volcanism, i.e., 30 – 15 Ma. Lavas derived from this source have large negative Nb anomalies and Pb isotopic ratios similar to those of TVZ and Kermadec Island Arc basalts (see also Gamble *et al.*, 1990, 1993). Huang *et al.* (2000) argued that the comparable REE characteristics of

the KBI and WHP basalts suggest that each source had similar mineral assemblages during melting and that their relatively low LREE/HREE values, i.e., La/Yb ~ 2.8 – 8.4, indicate that melting took place at depths shallower than the garnet stability field (e.g., < 20 kbar; 60 km). Huang *et al.* (2000) estimated the degree of partial melting to be in the range ~ 5 – 20 %, presumably the lower values referring to the alkalic and the higher values to the subalkalic magmas, and at depths similar to those estimated by Heming (1980a).

2.6.2 Auckland volcanic field

The Auckland volcanic field basalts exhibit an overall temporal compositional trend comparable to that of the WHP (Heming, 1980a) marked by early eruptions of small volumes of silica-undersaturated alkalic compositions (e.g., basanites and alkali ol-basalts) followed by large volumes of less undersaturated subalkalic compositions (e.g., transitional and tholeiitic basalts). As with the WHP, Heming and Barnet (1986) concluded that the range of compositions of the Auckland basalts is a function of the degree of partial melting of a discrete ascending diapir and depth of melt segregation. Huang *et al.* (1997) cited the relatively large Ce/Pb, Nb/Ce, and U/Pb values of the alkalic magmas as evidence for a HIMU signature in their source. They suggested that this signature could be the result of dehydration processes associated with the subduction of oceanic crust into a relatively shallow region of the mantle (e.g., < 150 km), rather than the influence of a deep-seated mantle plume. In addition, they argued that the HIMU signature is relatively "young" and could evolve to HIMU OIB in 500 my. Huang *et al.* (2000) argued that the similarity in isotopic compositions and OIB-like trace element features exhibited by the KBI and Auckland rocks reflect similar enrichment processes, i.e., subducting oceanic crust into the LVZ (see Huang *et al.*, 1997).

As with the recent volcanism in the KBI field, Heming (1980b) argued that volcanism in the Auckland field is the result of convection within the mantle wedge associated with the NNE-trending Taupo-Hikurangi arc-trench system. However, noting the elliptical boundary defined by the outer-most centres in the Auckland field and the tectonic relationship between the ellipse and the Junction Magnetic Anomaly, Spörli and Eastwood (1997) argued that the source for these volcanoes may be either (i) a small elliptical mantle dome rising in the lithosphere where pressure release melting occurs in the upper parts of the dome, or (ii) a flat elliptical area within the upper mantle where decompression melting occurs due to extension-related tensional stresses.

Huang *et al.* (2000) noted that because Sm/Yb is sensitive to the presence or absence of residual garnet, the relatively large values of Sm/Yb (i.e., 3.4 – 6.5) in the Auckland rocks compared to those of the KBI (Sm/Yb = 1.1 – 2.4) is indicative that they were derived from a garnet-bearing source, and therefore were generated at depths greater than those of the KBI. Their model implies a spatial relationship between contrasting mantle source regions for the KBI, WHP, and Auckland fields that allows relatively deep mantle-derived intraplate magmas (e.g., the Auckland basalts) to rise to the surface unaffected by shallow level subduction-related processes.

Huang *et al.* (1997) estimated that the degree of partial melting of the alkalic magmas from the Auckland field ranged from 0.6 % – 4 %. They also determined that the melting rates were relatively low, i.e., 2 x 10^{-5} to 3 x 10^{-4} kg m^{-3} yr^{-1}, and suggested that the peridotite matrix remained in the melt zone for a relatively long period, i.e., 0.5 – 1.0 my. Heming (1986) argued that the progressive decrease in the incompatible trace elements (e.g., Ba, Rb, Sr, and Zr) with increasing degrees of silica undersaturation is the result of increasing degrees of partial melting of the mantle source rather than large-scale fractional crystallisation of a common parent magma. However, Heming (1986) and Huang *et al.* (1997) noted that some olivine fractionation must have occurred to account for some of the more silica-undersaturated compositions. The degree of partial melting for the subalkalic magmas in the Auckland field is not given in the studies mentioned here but based on the estimates of Heming (1980a) for similar rock types from the KBI and WHP, probably ranges up to 20%.

2.6.3 Okete Volcanics

The Okete volcanics are part of the Alexandra Volcanic Group (Briggs and Goles, 1984) and spatially and temporally overlap subduction-related volcanics within the Group. As with the other intraplate fields of northern North Island, Briggs and Goles (1984) recognised a temporal change in the composition of the magmas erupted throughout the field, from silica-undersaturated basanites and alkali ol-basalts to less undersaturated hawaiites. They concluded that the decrease in silica undersaturation could be the result of the progressive melting of ascending mantle diapirs. However, unlike the petrogenetic models discussed for the Northland and Auckland fields, they argued that the progressive depletion in compatible and incompatible trace elements concomitant with decreasing silica undersaturation was the result of a combination of variable degrees of partial melting, followed by fractional crystallisation, possibly under polybaric conditions.

Briggs and Goles (1984) determined that the degree of partial melting ranged from 5 % for the basanites to 15 % for the hawaiites, and the degree of fractional crystallisation ranged from 5 % for the basanites to 25 % for the hawaiites, with olivine and clinopyroxene the fractionating phases. Based on the relatively large values of $(Ce/Yb)_N$ of the basanites [$(Ce/Yb)_N$ = 9.0 – 11.0] compared to those of the hawaiites [$(Ce/Yb)_N$ = 2.8 – 4.8] they argued that partial melting took place in the presence of residual garnet at pressures > 20 kbar (e.g., > 60 km), the minimum pressure stability of garnet. The HREE enrichment exhibited by the hawaiites indicates that with increasing degrees of partial melting, garnet was completely consumed, within the limit of a garnet stability zone of the upper mantle.

Briggs and Goles (1984) also noted that the positive ε_{Nd} values of the Okete basalts indicate that their source region had been recently enriched. Although the nature of the enrichment process remains uncertain, Briggs and McDonough (1990) argued that the OIB-like isotopic compositions and distinct incompatible trace element ratios (i.e., Ta/Yb ~ 1.6, Th/Yb ~ 2.5, Ba/La ~ 11, Ba/Nb ~ 10; see Briggs and Goles (1984) for trace element data) ruled out subduction-related enrichment processes. Briggs and Goles (1984) proposed that diapiric upwelling was the result of a convecting mantle wedge, but that the distinct geochemical trends of the Okete basalts compared to those of the other fields could be due to the relatively close proximity of their source to the TVZ where mantle convection may be more vigorous than elsewhere. Briggs and McDonough (1990) argued that the generation of the Okete magmas could have occurred within the underlying continental lithospheric mantle at pressures > 20 kbar or at the base of the lithosphere previously enriched by low-degree melts percolating upwards from the LVZ.

2.6.4 Ngatutura Basalts

The Ngatutura Basalts (Briggs *et al.*, 1990) are characterised by their restricted range of alkalic compositions, and unlike the basalts from the other fields, there is no apparent time-related compositional trend. The Ngatutura Basalts consist of ne-hawaiite and hawaiite lavas, each of which has OIB-like trace element characteristics (e.g., enrichment in LILE, HFSE, and LREE). Although there is a strong overlap in major and trace element compositions, the ne-hawaiites are slightly more differentiated than the hawaiites. Collectively, there is a general trend of increasing incompatible trace element concentrations with decreasing MgO contents. Because of this, Briggs *et al.* (1990) argued that fractional crystallisation was the dominant magmatic process involved in the

evolution of these lavas as opposed to variable degrees of partial melting, which would result in the systematic decrease in incompatible element concentrations.

Briggs *et al.* (1990) argued that the relatively large $(Ce/Yb)_N$ values for the ne-hawaiites (i.e., 12.8 – 14.6) and hawaiites (i.e., 9.8 – 11.7) and similar REE patterns on chondrite-normalised plots indicated that garnet was a residual phase during the partial melting required to produce their parental magmas. They concluded that the magmas were derived from a LREE-enriched source in the LVZ. The nature of source enrichment for the Ngatutura Basalts remains poorly understood. Briggs *et al.* (1990) suggested that the enrichment could have involved a MORB source metasomatised by low-degree, silica-undersaturated melts ascending from the LVZ, a process similar to that inferred by Briggs and McDonough (1990) for the Okete Volcanics,

Although the Ngatutura field lies ~ 300 km above the subducting Pacific oceanic lithosphere, Briggs *et al.* (1990) found no geochemical evidence to suggest that the source for the magmas was modified by a slab-related component. They concluded that convection above the subducting slab probably carried slab-contaminated mantle down to deeper levels that were transferred beneath the alkalic magma source region (75 – 120 km). They further argued that (p. 68):

> "It is also unlikely that there was any upward migration of contaminated mantle rising as plumes above the slab that extended throughout the mantle wedge. Instead, the extent of slab-contaminated mantle must be confined to a more limited region immediately overlying the subducted slab".

2.6.5 South Auckland volcanic field

As with the petrogenetic models proposed for most of the other North Island intraplate fields, Rafferty and Heming (1979) argued that volcanism in the South Auckland volcanic field is characterised by the sequential eruption of relatively small volumes of alkalic magma followed by larger volumes of subalkalic magma. They proposed that each magma type could be derived from the progressive melting of a mantle peridotite diapir ascending within the LVZ, and that the subalkalic magmas are the product of larger degrees of partial melting than the alkalic magmas. Rafferty and Heming (1979) and Heming (1980b) cited the relative depletion in the incompatible elements Ba, Rb, Sr, and Zr in the subalkalic group lavas compared to those in the alkalic group as evidence for this, and concluded that the lavas from each group are not related by a common differentiation process.

Unlike the models proposed for the WHP in Northland and Auckland fields, Rafferty and Heming (1979) and Heming (1980b) concluded that the alkalic and subalkalic lavas represent deep- and shallow-level differentiates respectively, each derived from distinct parent magmas generated from discrete mantle diapirs. Alternatively, Hodder (1984) argued that the South Auckland basalts have geochemical characteristics representative of "contaminated" magmas having a rift association and proposed that this association is possibly due to the positioning of the Hauraki Rift on top of a mantle swell that initiated rifting and the onset of intraplate volcanism. However, Rafferty and Heming (1979) and Heming (1980b) argued that melting for the alkalic magmas occurred at approximately 80 km depth (27 kbar), and based on the presence of megacrysts of the high-pressure phases, olivine, clinopyroxene, and kaersutite, Rafferty and Heming (1979) concluded that the alkalic magmas differentiated near their source. Because Rafferty and Heming (1979) and Heming (1980b) considered the subalkalic magmas to be the result of relatively large degrees of partial melting, they argued that the diapirs from which they were derived originated lower in the LVZ. The onset of melting at such depths apparently provides the time required for larger degrees of melting to occur as the diapirs ascend through the mantle. The relative low density of such melts would allow them to rise further into the lower mantle, thus segregating at between 30 and 45 km depth.

2.7 Summary

The South Auckland volcanic field is one of a number of spatially and temporally distinct intraplate volcanic fields in northern North Island, New Zealand, that developed near a convergent margin in association with the subduction of the Pacific plate beneath the Indo-Australian plate. Intraplate volcanism commenced approximately 10 Ma in the Kaikohe-Bay of Islands field of the Northland province and continued intermittently until the recent eruptions in the Auckland volcanic field about 500 years ago. K-Ar age data suggest that volcanism in the SAVF occurred between 0.51 and 1.59 Ma, although bore-log data indicate that volcanic activity may have been coeval with the older fields (e.g., > 2 m.y.) to the south of the SAVF.

The geologic history of the South Auckland region dates to the mid Triassic to late Jurassic. During this time, the basement rocks of the region – the Murihiku and Waipapa Terranes – formed at the eastern margin of Gondwanaland. These terranes were subsequently folded and faulted during the Rangitata and Kaikoura orogenic events beginning in the late Jurassic. Although there is no good agreement as to the cause of the onset of volcanism in the SAVF, or the other intraplate fields in North Island, a plausible

scenario is that deep fractures in these terranes allow for the rapid ascent of mantle-derived melts to the surface in the SAVF without significant contamination. In addition, the fault geometry and distribution of the volcanic centres, either along or adjacent to faults, in the SAVF suggests that much of the volcanism is structurally controlled. Many of the faults in the region can be attributed to the main phases of the Kaikoura Orogeny in the early to mid Miocene.

The models for intraplate volcanism in North Island suggest that generally two distinct magma types, alkaline and subalkaline, erupted in each field. These magmas are derived principally from an OIB-like source region in the low-velocity zone between 75 and 125 km depth and were generated as small batches from an ascending mantle diapir. These batches ascended rapidly through the crust, erupting from numerous central vents that are distributed over a wide area. This scenario is apparent in the SAVF, where approximately 100 predominantly monogenetic volcanoes erupted over a 300 km^2 area. Most models infer that small volumes of alkalic magma erupted first, followed later by larger volumes of subalkalic magma. However, K-Ar age data from the SAVF basalts indicate that there is no temporal correlation among the various magma types erupted throughout the field.

The nature of volcanism in the SAVF (i.e., magmatic or phreatomagmatic) was influenced by the hydrogeological properties of the Tertiary sediments deposited throughout the South Auckland region, and by the localised fault style. Thirty-eight of the 100 centres are considered phreatomagmatic. The majority of the phreatomagmatic centres are located in the Manukau Lowlands, an area dominated by down-faulted block faults where aquifer-bearing Tertiary formations were preserved. The explosive eruptions most likely occurred when small magma batches exploited crustal fractures until the magma encountered and mixed with groundwater near the surface. Activity at the magmatic centres was dominated by Hawaiian-style eruptions that produced relatively thin lava flows and scoria cones.

Chapter Three: Petrography of the SAVF Basalts

Chapter Three

Petrography of the SAVF Basalts

3.1 Introduction

Numerous petrological studies of basaltic lavas from continental intraplate volcanic provinces (see Table 1.1; p.2) indicate that they are products of magmas that have undergone a complex crystallisation history. Thin section analyses reveal that such lavas have extremely variable petrography and show that complete, or near complete, crystallisation is a feature common to most continental intraplate basalts. The variety of phenocryst phases, e.g., olivine, pyroxene, feldspar, and relatively small quantities or absence of glass in these lavas suggests that they were derived from magmas that crystallised nearly continuously en route to the surface.

The data acquired from a petrographic investigation may contribute to a better understanding of processes involved in the evolution of basaltic magmas and help validate the results of models reliant on mineral chemical and geochemical data. Generally, phenocrysts represent crystallisation during an early period of magma evolution, whereas microphenocrysts, groundmass phases, and matrix material document the final stages of cooling and crystallisation (Shelley, 1993). The presence of xenoliths and xenocrysts not in equilibrium with their host rock suggest possible assimilation of exotic material and by inference, modification in the geochemistry and mineralogy of the host magma. Alternatively, the absence of this material may (i) be indicative of total assimilation and consequently, significant magma contamination, or (ii) indicate that no assimilation has occurred. Therefore, documentation of variations in the type and abundance of megacrysts, phenocrysts, xenoliths, xenocrysts, and the groundmass phases, together with their textural features is an important component of an integrated petrological study.

Petrographic and whole-rock geochemical analyses[14] indicate that a broad range of alkalic basaltic lavas erupted throughout the South Auckland volcanic field. Based on these differences the SAVF lavas can be divided into two groups. In this chapter, the lavas that comprise each group are classified and a general petrographic description for each group is given. Detailed petrographic descriptions of each lava type are given in Appendix 2,

[14] Whole-rock geochemistry is discussed in Chapter 5.

with emphasis on the petrographic differences between the various lava types within each group. These petrographic distinctions are supported by relevant modal mineralogy data.

3.2 Rock classification

The basalts of the SAVF examined in this investigation are classified based on their CIPW normative compositions according to the classification scheme described in Johnson and Duggan (1989). Normative composition criteria used for classification purposes are summarised in Table 3.1. Based on these criteria the SAVF lavas are alkali olivine-basalts (alkali ol-basalts), transitional basalts, hawaiites, olivine-tholeiitic basalts[15] (ol-tholeiitic basalts), quartz-tholeiitic basalts[15] (qz-tholeiitic basalts), nephelinites, basanites, nepheline-hawaiites (ne-hawaiites), and mugearites. CIPW normative compositions for selected SAVF samples are given in Appendix 4, Tables A4.1and A4.2.

Table 3.1 Summary of normative mineralogy criteria for SAVF basaltic rock classification (adapted from Johnson and Duggan, 1989). Normative values are in volume %.

Rock type	Normative mineral criteria
basanite	> 5% ne, > 5% Ab, An/(An + Ab) > 50
nephelinite	> 5% ne, <5% Ab, ne > lc, An/(An + Ab) > 50
ne-hawaiite	> 5% ne, <5% Ab, 30 - 50% An/(An + Ab)
mugearite	< 5% ne, 10 - 30% An/(An + Ab)
alkali ol-basalt	< 5% ne, An/(An + Ab) > 30
transitional basalt	< 10% hy, An/(An + Ab) > 50
hawaiite	< 10% hy, 30 - 50% An/(An + Ab)
ol-tholeiitic basalt	> 10% hy without normative qz
qz-tholeiitic basalt	> 10% hy with normative qz

ne, nepheline; hy, hypersthene, lc, leucite; An, anorthite; Ab, albite; qz, quartz

The Johnson and Duggan scheme was used because its classification provides distinct rock names for a range of mafic, intermediate, and felsic rock types, which reflects variations in their whole-rock geochemistry and avoids confusion with rock types from other tectonic associations. This contrasts with classification schemes such as IUGS (Le Bas *et al.*, 1986) and TAS (Le Maitre *et al.*, 1989), or the nomenclature of Cox *et al.* (1979), which group volcanic rocks into broad categories, e.g., basalt, trachybasalt, etc., based on their SiO_2 wt% vs. total alkalies (K_2O + Na_2O wt%) relationship. In addition, the Johnson and Duggan scheme allows direct comparison of the petrology, mineralogy, and major and trace element and isotope geochemistry between the SAVF basalts with those from other intraplate fields that have used this scheme, e.g., 700 samples from

[15] The ol-tholeiitic and qz-tholeiitic basalts from the SAVF contain Ca-rich clinopyroxene phenocrysts together with olivine in the groundmass. These features contrast those of the tholeiitic basalts defined by the TAS classification scheme (La Maitre *et al.*, 1989), which contain Ca-poor pyroxene phenocrysts and no olivine in the groundmass.

intraplate fields in the North Island, South Island, and the Sub-Antarctic and Chatham Islands, New Zealand, and 2700 samples from the intraplate provinces of eastern Australia (see Johnson, 1989, for a summary of these data).

3.3 SAVF rock groups

The SAVF basalts have been previously categorised by Rafferty and Heming (1979) as members of either an alkalic or subalkalic group. Rocks were assigned to their respective group based on their location in the SiO_2 vs. total alkalies plot, as defined by MacDonald and Katsura (1964) and Irvine and Baragar (1971).

In recognition of the notable differences in petrography, normative mineralogy, and geochemistry exhibited by the SAVF basalts, they may be divided into two new groups (A and B). Group A consists of alkali ol-basalts[16], transitional basalts, hawaiites, ol-tholeiitic basalts, and qz-tholeiitic basalts. They tend to be hypersthene normative (except for the alkali ol-basalts) and have subalkalic compositions and petrographic features similar to rocks in the subalkalic group of Rafferty and Heming (1979). Additionally, the group A rocks are distinguished from those in group B by their relatively small high field strength elements (HFSE) abundances, e.g., Nb (9 – 29 ppm) and Zr (97 – 219 ppm).

The group B rocks consist of alkali ol-basalts, nephelinites, basanites, ne-hawaiites, and mugearites. Group B rocks tend to be nepheline normative (except for the mugearites) and have alkalic compositions and petrographic features similar to rocks in the alkalic group of Rafferty and Heming (1979). Furthermore, the group B rocks have comparatively large HFSE abundances, e.g., Nb (35 – 102 ppm) and Zr (194 – 491 ppm). Normative mineralogy compositions and Nb and Zr abundances for groups A and B are summarised in Table 3.2. Generalised petrographic descriptions for each rock group are given in section 3.5.

Table 3.2. Summarised normative nepheline and hypersthene compositions and Nb and Zr abundances for each group A and B rock type, South Auckland volcanic field.

	Group A					Group B				
Rock type	trans	aob	haw	ol-th	qz-th	bas	neph	ne-haw	mug	aob
nepheline	-	0.2 - 3.2	-	-	-	5.1 - 17.6	14.1 – 23.0	2.4 - 20.7	-	0.2 - 4.7
hypersthene	2.5 - 9.8	-	0.1 - 9.6	10.1 - 21.6	4.8 - 24.2	-	-	-	1.1	-
trace elements (ppm)										
Nb	10 - 23	16 - 29	9 - 23	9 - 26	10 - 19	38 - 80	55 - 102	54 - 89	35	35 - 65
Zr	97 - 194	130 - 219	110 - 198	103 - 151	124 - 154	194 - 436	281 - 469	315 - 491	253	238 - 410

trans = transitional basalts; haw = hawaiites; ol-th = ol-tholeiitic basalts; qz-th = qz-tholeiitic basalts; bas = basanites; neph = nephelinites; ne-haw = ne-hawaiites; mug = mugearites; aob = alkali ol-basalts

[16] The alkali ol-basalts have been divided into each group based on their contrasting geochemical and petrographic characteristics.

3.4 Definition of terms

The terms megacryst, phenocryst, microphenocryst, and microlite are used to describe the relative size of the principal mineral phases and groundmass crystals in the SAVF basalts. Since megacryst, phenocryst, microphenocryst are not formally defined (Shelley, 1993), in this study megacrysts are > 1.5 mm, phenocrysts are 500 μm – 1.5 mm, and microphenocrysts are 100 μm – 500 μm in length along their longest axis when viewed in thin section. Microlites, primarily needle-like crystals of plagioclase and apatite in the SAVF rocks, generally range up to 100 μm. The terms lath and tabular (see MacKenzie *et al.*, 1982, p.20) generally apply to groundmass clinopyroxene and plagioclase. However, some group A lavas contain tabular plagioclase phenocrysts and microphenocrysts, and microphenocryst-sized laths of clinopyroxene occur in many group B lavas.

3.4.1 Megacrysts

Many group A and B lavas contain olivine and clinopyroxene megacrysts. Shelley (1993) suggested that most megacrysts are actually xenocrysts that are in disequilibrium, both geochemically and texturally, with their host magma. However, based on textural evidence that suggests crystal-host rock equilibrium and electron microprobe analyses, which often show similar compositions among megacryst and phenocryst populations within the same sample, many megacrysts in the SAVF basalts appear to be crystals that are merely larger versions of their phenocryst-sized counterparts.

3.4.2 Xenocrysts

The apparent state of equilibrium of a number of megacrysts in the SAVF samples suggests they had sufficient time to grow into large crystals, e.g., > 3 mm. Alternatively, these "megacrysts" could be cognate material (xenocrysts) related to the same cycle of magma generation as the erupted magma. It is, however, difficult to make this distinction in some SAVF samples. In contrast, Sanders (1994) cited the resorbed crystal margins (e.g., rounded sponge-like boundaries) in contact with the host magma as textural evidence for a xenocrystic origin for many of the larger olivine crystals observed in some ne-hawaiite and basanite lavas in the SAVF.

3.4.3 Xenoliths

The SAVF lavas often contain xenoliths (up to 7 mm) that may be completely exotic material (e.g., country rock) ripped off conduit walls, or restite material from a mantle source region. Rafferty (1977), Rafferty and Heming (1979), and Rosenberg (1991) observed quartzose and feldspathic xenoliths in most SAVF rock types. Sanders (1994) determined that the ultramafic xenoliths in SAVF lavas, observed principally in samples from the group B rocks, are derived from an upper mantle source. He cited the presence of orthopyroxene phenocrysts and olivine megacrysts that displayed metamorphic textures (e.g., kink-bands) as evidence for their mantle origin.

3.5 Petrography and modal mineralogy

General petrographic descriptions for the group A and B rocks and modal mineralogy are summarised in Table 3.3 and presented in sections 3.5.1 and 3.5.2 respectively. Detailed petrographic descriptions for each rock type from groups A and B, together with the modal abundance of each phenocryst phase[17], major groundmass phases, and vesicles of selected samples are given in Appendix 2 sections A2.1.1 to A2.1.5 for the group A rocks and A2.2.1 to A2.2.5 for those in group B. Modal mineralogy data for each sample from each rock type from groups A and B used in this investigation are given in Appendix 3, Tables A3.1 and A3.2 respectively.

3.5.1 General petrographic descriptions of the Group A lavas – alkali ol-basalts, transitional basalts, hawaiites, ol-tholeiitic basalts, and qz-tholeiitic basalts

Hand specimens of the group A lavas typically range from light to medium grey, tend to be relatively coarse-grained, and slightly to moderately vesicular. Generally, vesicles tend to be small, e.g., << 1 mm, although larger vesicles occur in some samples, but they are usually a minor component of the total rock volume. Olivine megacrysts and phenocrysts are conspicuous and range up to 3 mm. Feldspar and clinopyroxene phenocrysts are less apparent. Xenocrysts and xenoliths are rare.

In thin section, olivine megacrysts and phenocrysts are generally subhedral and frequently skeletal and embayed. Although large crystals may form at low rates of undercooling (Shelley, 1993), a large number of these crystals in the SAVF basalts have

[17] The term "phenocrysts" collectively includes megacrysts, phenocrysts, and microphenocrysts, when referring to the modal mineralogy of specific rock types or groups.

Table 3.3 Summarised petrographic characteristics and modal abundances of the main phenocryst and groundmass phases of each group A and B rock type, South Auckland volcanic field.

	Group A					Group B				
Rock type	Alkali ol-basalts (n = 8)	Transitional basalts (n = 14)	Hawaiites (n = 29)	Ol-tholeiitic basalts (n = 34)	Qz-tholeiitic basalts (n = 4)	Alkali ol-basalts (n = 4)	Basanites (n = 33)	Nephelinites (n = 13)	Ne-hawaiites (n = 9)	Mugearite (n = 1)
Texture	porph-glom holo	porph-glom-vitro hypo-holo	porph-glom holo	porph-holo	porph-holo	porph-hypo	porph-glom hypo-holo	porph-hyalo-hypo	porph-holo	porph-holo
Phenocrysts/ (modal abundance)	ol (< 1 – 15) cpx (< 1 – 8) plag (<1 – 12) mag (< 1 – 4) ilm (tr)	ol (2 – 15) cpx (tr – 2) plag (tr – 11) mag (tr – 5) ilm (tr)	ol (2 – 17) cpx (tr – 10) plag (tr – 21) mag (tr – 7) ilm (tr – 1)	ol (tr – 17) cpx (tr – 8) plag (tr – 21) mag (tr – 3) ilm (tr – 2)	ol (< 1 – 15) cpx (< 1 – 3) plag (tr – 2) mag (tr) ilm (tr)	ol (3 – 13) cpx (4 –11) plag (tr – 2) mag (tr) ilm (nil)	ol (5 – 21) cpx (2 – 20) plag (tr) mag (tr – 2) ilm (nil)	ol (6 – 16) cpx (< 1 – 5) plag (nil) mag (tr – 1) ilm (nil)	ol (2 – 12) cpx (tr – 10) plag (tr) mag (tr) ilm (nil)	ol (18) cpx (4) plag (3) mag (tr) ilm (nil)
Groundmass texture	coarse-grained intergranular	fine to coarse grained hyalopilitic-intergranular	fine to coarse grained intergranular	medium- coarse grained intersertal-intergranular	fine to coarse grained intergranular	coarse -grained intergranular	fine-grained hyalopilitic-intersertal-intergranular	coarse -grained hyalopilitic-intersertal-intergranular poikilitic	fine to medium grained intersertal-intergranular	course-grained intergranular
Groundmass phases/ (modal abundance)	ol (2 – 5) cpx (21 – 39) plag (49 – 69) mag (2 – 8) ilm (1 – 5) apatite (tr – 2) carbonate (nil) glass (nil)	ol (tr – 5) cpx (13 – 25) plag (53 – 69) mag (3 – 10) ilm (tr – 4) apatite (nil) carbonate (nil) glass (nil – 19)	ol (tr – 3) cpx (27 – 40) plag (51 – 63) mag (3 – 14) ilm (nil – 3) apatite (nil) carbonate (nil) glass (nil)	ol (2 – 9) cpx (10 – 25) plag (34 – 62) mag (2 – 31) ilm (tr – 7) apatite (nil) carbonate (nil – 7) glass (nil - 51)	ol (1 – 2) cpx (37 – 45) plag (48 – 53) mag (tr – 3) ilm (4 – 6) apatite (tr – 2) carbonate (nil – 2) glass (nil)	ol (6 – 10) cpx (24 – 34) plag (42 – 59) mag (7 – 16) ilm (nil) apatite (tr) carbonate (nil) glass (nil – tr)	ol (tr – 8) cpx (28 – 55) plag (9 – 52) mag (10 – 25) ilm (nil) apatite (tr) carbonate (nil) glass (nil - 35)	ol (tr – 4) cpx (39 – 61) plag (10 – 30) mag (10 – 19) ilm (nil) apatite (nil – tr) carbonate (nil) glass (tr – 33)	ol (nil – 2) cpx (14 – 38) plag (35 – 61) mag (7 – 24) ilm (nil) apatite (tr) carbonate (nil) glass (nil – 22)	ol (tr) cpx (16) plag (74) mag (3) ilm (5) apatite (tr) carbonate (nil) glass (nil)
Xenoliths	nil	nil	present	nil	nil	present	present	nil	present	nil

porph = porphyritic; glom = glomeroporphyritic; holo = holocrystalline; hypo = hypocrystalline; vitro = vitrophyric; ol = olivine; cpx = clinopyroxene; plag = plagioclase; mag = titanomagnetite; ilm = ilmenite; tr = trace amounts observed; n = number of samples analysed

textures that suggest a possible xenocrystic origin or derivation from disaggregated olivine-bearing xenoliths. Evidence for this includes: (i) crystals that exhibit disequilibrium textures, e.g., crystal margins partially sheathed with clinopyroxene grains and microphenocrysts (Helz, 1987; Aspen *et al.*, 1990), and (ii) crystals that indicate partial melting or partial dissolution has occurred, or a mantle origin, e.g., deeply incised, rounded embayments with severely corroded margins or kink-band metamorphic textures (Tsuchiyama, 1986; Shelley, 1993).

Some of the larger olivine crystals in the alkali ol-basalts and ol-tholeiitic basalts have relatively large angular cavities imparting a shattered appearance. Pearce *et al.* (1987) and Shelley (1993) suggested that olivine phenocrysts may "shatter" during an eruption due to rapidly expanding gas or magma trapped in the crystal. In addition, olivine from each rock type often exhibits iddingsite or bowlingite alteration depending on the state of oxidation. In some samples each form of alteration was observed, which varies from slight alteration along rims and fractures to completely altered crystals, especially microphenocrysts and groundmass crystals. Occasionally, phenocrysts occur with interiors extensively altered to iddingsite and unaltered rims suggesting that they have been overgrown by fresh olivine (Shelley, 1993). Some phenocrysts are compositionally zoned. These zones can be identified optically by abrupt changes in interference colours between the crystal's rim and adjacent core[18]. Crystals in many samples, especially those from the alkali ol-basalts, transitional basalts, and hawaiites contain, < 50 μm, blocky Cr-titanomagnetite inclusions[19].

Clinopyroxene is generally subhedral, colourless, pale green, or pale greenish brown to light brown. Some crystals in the alkali ol-basalts and transitional basalts have strong purple margins, indicative of relatively large Ti contents (Deer *et al.*, 1992). Margins such as these are commonly observed in the titaniferous clinopyroxenes in most group B rocks but are uncharacteristic for the majority of clinopyroxenes in the group A rocks. Occasionally, phenocrysts have irregular margins, some with rare aegerine-augite rims, and partially resorbed interiors, indicative of crystal-melt disequilibrium (Shelley, 1993). Many megacrysts and phenocrysts contain relatively small, e.g., < 50 μm, titanomagnetite inclusions, rare Cr-titanomagnetite inclusions, and other unidentified opaque and clear inclusions. In many crystals, the great abundance of these inclusions results in a sieve-textured core. Orthopyroxene was not observed in thin-section in any group A samples.

---

[18] Large numbers of olivine phenocrysts in the group A rocks are compositionally zoned. However, such zoning is not commonly observed in thin section and is detectable only by electron microprobe analyses (see section 4.4.2 for details).
[19] Cr-titanomagnetite, in the ulvöspinel-chromite series, was identified by electron microprobe analyses (see sections 4.3.1 and 4.3.2 for details).

Plagioclase typically occurs as relatively large prismatic phenocrysts and less frequently as tabular microphenocrysts. Megacrysts are rare. Variations in crystal size, shape, and density suggest variations in nucleation, growth, diffusion, and cooling rates (e.g., Marsh, 1988; Cashman and Marsh, 1988; Cashman, 1993). A minor number of phenocrysts and microphenocrysts, especially those in the alkali ol-basalts and hawaiites, have distinct marginal zones or oscillatory zoning, possibly the result of crystal recycling or magma mixing (e.g., Nixon and Pearce, 1987; Pearce *et al.*, 1987). Some phenocrysts have partially resorbed cores mantled with "fresh" plagioclase. These features are analogous to those described by O'Brien *et al.* (1988) for clinopyroxene xenocrysts, considered to be the result of magma mixing. Plagioclase in all samples contains small (e.g., < 20 μm) apatite inclusions.

Olivine, clinopyroxene, and plagioclase phenocrysts and microphenocrysts often occur in monomineralic and polymineralic glomeroporphyritic clusters up to 6 mm across. Olivine clusters are often composed of rounded subhedral or anhedral phenocrysts and microphenocrysts that may consist of as few as four crystals. Clinopyroxene clusters consist of assemblages of subhedral and anhedral phenocrysts and microphenocrysts that are typically interlocked or intergrown resulting in gabbroic texture. Many of these clusters have morphologies similar to those of non-euhedral olivine aggregates, documented by Helz (1987) in Kilauea Iki lava lake formed during the 1959 eruption. Helz (1987) attributed the formation of such aggregates to slow cooling during periods of quiescence between eruption episodes. In contrast, other clusters have corroded margins lined with opaque reaction products and crystals with partially resorbed interiors. These features indicate crystal-melt disequilibrium and suggest a possible exotic origin or derivation from a disaggregated, partially melted xenolith (Shelley, 1993). Plagioclase clusters often consist of aggregates of radiating prismatic crystals. Clusters of this nature are generally restricted to the group A lavas.

Groundmass textures range from relatively fine- to very coarse-grained, and vary from hyalopilitic to intersertal to intergranular. All phases that occur as phenocrysts and microphenocrysts occur in the groundmass. Plagioclase is ubiquitous in all samples with subordinate clinopyroxene and minor titanomagnetite and ilmenite. Olivine is generally present in minor amounts and is often completely altered to iddingsite. Granular and skeletal opaques, apatite microlites, and rare sulphide minerals, are additional groundmass phases.

Patchy areas, veins, and amygdales of secondary minerals such as zeolites, chlorite, and carbonate occur in many samples. In addition, a large number of samples have areas

containing clots of granular clinopyroxene, interpreted as partially or completely resorbed quartzose xenoliths (or xenocrysts). Partially resorbed quartz, feldspar, olivine, and clinopyroxene xenoliths (or xenocrysts) commonly with reaction rims of granular clinopyroxene occur in minor amounts. Fresh glass is rare.

3.5.2 General petrographic descriptions of the Group B lavas – basanites, nephelinites, ne-hawaiites, alkali ol-basalts, and mugearites

Hand specimens of the group B rocks range from dark grey to black, are typically slightly vesicular, and have textures that range from very fine-grained to relatively coarse-grained. All group B rocks are finer-grained than those in group A. Vesicles tend to be small, e.g., << 1 mm in diameter. Some larger vesicles are filled with zeolite or carbonate. Olivine megacrysts and phenocrysts are conspicuous and often range up to 3 mm across. In some samples, olivine is altered to iddingsite. Pyroxene phenocrysts are identifiable in some of the coarser-grained samples. Xenocrysts and xenoliths are rare, observed only in basanite and ne-hawaiite samples.

In thin section, the group B lavas are porphyritic and generally contain few vesicles. Crystallinity ranges from hyalocrystalline to hypocrystalline to holocrystalline. The main mineral phases are olivine and titaniferous clinopyroxene. Plagioclase and the Fe-Ti-oxides are generally restricted to the groundmass.

Olivine is the predominant phenocryst phase in each group B rock type, commonly occurring with subordinate clinopyroxene. Phenocrysts are typically euhedral or subhedral 6-sided crystals that are often embayed. Olivine megacrysts occur less frequently than in the group A lavas, and are either subhedral or elongate, typically embayed, and often skeletal. In most samples, a large number of phenocrysts have textures indicative of crystal-melt disequilibrium similar to those observed in the group A rocks. In addition, the group B olivines may also have partially resorbed interiors and deeply incised corroded margins mantled by relatively thin, e.g., < 10 μm, assemblages that may include black devitrified glass, opaque granular crystals, and clinopyroxene grains. As with the group A rocks, these features suggest a possible exotic origin.

Olivine phenocrysts are commonly compositionally zoned, identifiable in thin section by contrasts in core-rim interference colours. However, most zones are identifiable only by electron microprobe analyses (see section 4.4.2 for details). Iddingsite and bowlingite alteration tends to be less extensive than in the group A olivines.

Clinopyroxene is purplish-brown and titaniferous. Megacrysts and phenocrysts are rare. Ti-clinopyroxene crystals are typically 6- and 8-sided microphenocrysts that often have strong purple margins, indicative of comparatively large Ti contents in the rim relative to the adjacent core (Deer *et al.*, 1992). Occasionally, these crystals have complex compositional zones, a feature that may be indicative of magma mixing (Clarke *et al.*, 1986; Helz, 1987; O'Brien *et al.*, 1988). Prismatic phenocrysts and microphenocrysts occur in some samples and are often the dominant crystal habit. These crystals are often twinned and have distinct sector zones. Titanomagnetite inclusions[20] are common.

Many samples in each rock type, except mugearite, contain populations of clinopyroxene crystals that have partially resorbed interiors with numerous opaque and clear inclusions and groundmass-filled cavities resulting in sieve-textured cores surrounded by distinct marginal zones. In addition, some samples contain bimodal populations of crystals with partially resorbed interiors together with unaltered crystals, suggesting variable crystallisation conditions. Orthopyroxene was not observed in thin-section in any group B samples.

Plagioclase phenocrysts are rare and generally restricted to the alkali ol-basalts and the mugearite sample (SA88). In other rock types, plagioclase is generally restricted to the groundmass. Titanomagnetite occurs as rare, relatively small microphenocrysts.

All group B rock types contain either olivine and Ti-clinopyroxene monomineralic clusters or polymineralic clusters of these minerals. All cluster types are less common and typically much smaller than those in the group A rocks and generally occur in quantities insufficient for the sample to be considered glomeroporphyritic. However, as with the group A clusters, those in the group B rocks commonly have disequilibrium textures, e.g., corroded margins and occasionally kink-band metamorphic textures, which suggests possibly exotic origin.

Olivine clusters generally occur as relatively open or skeletal aggregates that generally consist of less than five crystals. In contrast to those in group A, olivine clusters in the group B rocks typically consist of euhedral or subhedral 6-sided phenocrysts and microphenocrysts often with glass trapped between crystals. These crystals often appear to have parallel crystallographic axes, inferred from similar interference colours. Schwindinger *et al.* (1983) and Schwindinger and Anderson (1989) suggested that aggregates such as these form by synneusis – "the swimming together of crystals" in a

[20] Subsequent electron microprobe analyses indicated that some titanomagnetite inclusions are Cr-titanomagnetite (see section 4.7.2 for details).

liquid-rich magma[21]. Helz (1987) documented similar morphologies for olivine aggregates in the Kilauea Iki lava lake. She argued that the aggregates formed in the presence of abundant melt in Kilauea's summit reservoir. Clinopyroxene clusters are relatively small, e.g., < 2 mm across, and generally consist of fewer than six euhedral to subhedral microphenocrysts.

Groundmass textures range from very fine-grained to relatively coarse-grained and vary from hyalopilitic to intersertal to intergranular. A number of samples show a combination of these textures. All phases present as phenocrysts and microphenocrysts occur in the groundmass. In many samples, these minerals occur in a devitrified glassy matrix. Plagioclase is often abundant and the dominant phase in most basanites and alkali ol-basalts, occurring as relatively thin laths, microlites, and interstitial pools. In contrast, plagioclase is often absent or rare in some nephelinites and ne-hawaiites. Nepheline[22] occurs as small, untwinned laths, and interstitial pools in each rock type except mugearite. Potassium feldspar[23] occurs in a minor number of samples, primarily in the basanites, ne-hawaiites, and the mugearite, either as short laths or interstitial pools.

Titaniferous clinopyroxene is abundant and the dominant groundmass phase in a number of samples, especially those from the nephelinites and ne-hawaiites. It typically occurs as 6-sided euhedral and subhedral crystals and also as relatively short laths often with titanomagnetite inclusions.

Titanomagnetite is relatively abundant and ubiquitous in all lava types. Skeletal opaques are less common but are abundant in some samples and commonly occur in areas containing devitrified glass. Apatite and rare pyrrhotite are additional groundmass phases. Patchy areas, veins, and amygdales of chlorite, carbonate, and smectite occur as secondary phases. Some samples of each rock type contain patchy areas of dark brown devitrified glass.

3.6 Discussion and summary

The South Auckland volcanic field lavas are divided into two broad groups (A and B) based on differences in petrography and mineralogy that are marked by distinct geochemical features. The group A lavas are predominantly subalkalic, hypersthene

[21] The concept of synneusis suggests that two or more crystals, suspended in magma, become annealed to each other - with parallel crystallographic axes. They subsequently continue to grow as a distinct crystal unit.
[22] In thin section, nepheline is commonly indistinguishable from plagioclase and is identifiable only by electron microprobe analyses. Therefore its relative abundance in the groundmass is uncertain.
[23] In thin section, potassium feldspar is commonly indistinguishable from plagioclase and is identifiable only by electron microprobe analyses. Therefore its relative abundance in the groundmass is uncertain.

normative, and have relatively small Nb and Zr abundances. Rock types in group A include; alkali ol-basalts, transitional basalts, hawaiites, ol-tholeiitic basalts, and qz-tholeiitic basalts. In contrast, the group B lavas are typically alkalic, nepheline normative, and have comparatively large Nb and Zr abundances. Rock types in group B include; nephelinites, basanites, ne-hawaiites, alkali ol-basalts, and mugearite.

The group A lavas are typically coarse-grained and consist predominantly of the mineral assemblage: olivine + clinopyroxene + plagioclase ± titanomagnetite ± ilmenite. The group B lavas are comparatively fine-grained and consist of olivine + titaniferous clinopyroxene. In addition to these distinctions, the lavas in each group exhibit variations in the type, abundance, and textures of the main phenocryst phases (i) among the lavas within each group, (ii) between samples of the same rock type, and (iii) frequently between individual mineral phases within the same sample.

Perhaps one of the most important features of the SAVF rocks is the disequilibrium texture exhibited by many olivine and clinopyroxene megacrysts, phenocrysts, and microphenocrysts in samples from each rock type. Olivine, the dominant phenocryst phase in each rock type, and clinopyroxene crystals often display textural evidence of reaction with their host magma. Olivine may have rounded or corroded crystal margins. These margins are often lined with opaque reaction products or mantled with clinopyroxene crystals, indicative of olivine – melt disequilibrium.

Clinopyroxene phenocrysts and microphenocrysts, especially those in the group B rocks, commonly exhibit resorption textures. In the group B rocks, many of these crystals have distinct zones at their margins. These features may be indicative of magma mixing (e.g., O' Brien *et al*, 1988), although complex compositional zoning was not readily observed in thin section in the clinopyroxenes from the SAVF rocks. In addition, some samples contain a bimodal population of clinopyroxene – those with and those without resorbed interiors. Mixed populations such as these may be indicative of disequilibrium crystallisation conditions and that clinopyroxenes crystallised near continuously as magma ascended to the surface (Shelley, 1993).

The diverse textures of group A and B rocks represent crystallisation conditions that may include disequilibrium crystallisation and varying degrees of undercooling, which in turn affect variations in nucleation, diffusion and crystal growth rates. The minimum amount of glass, common intergranular groundmass textures, and the absence of quench textures, such as swallow-tailed plagioclase, indicates that the SAVF lavas probably ascended to the surface at rates sufficient for near complete crystallisation to occur. However, the

partially resorbed cores and distinct marginal zones in many clinopyroxenes from the group B rocks suggest that complete equilibrium was not reached during crystallisation. Shelley (1993) noted that this occurs most frequently during rapid crystallisation. Additionally, the occurrence of skeletal olivine in a large number of samples suggests higher degrees of undercooling for some magmas from each rock group.

The documentation of the type and nature of crystal clusters, xenocrysts, and xenoliths in the group A and B rocks is important to the development of a practical petrogenetic model for the SAVF magmas. Monomineralic and polymineralic clusters of olivine, clinopyroxene, and plagioclase phenocrysts and microphenocrysts are common in many samples from each rock type. The mechanism by which these clusters occur is uncertain. However, many olivine clusters in the group B rocks are similar to those in Hawaiian lavas considered by Helz (1987) to have formed by synneusis in liquid-rich reservoirs. Alternatively, many glomeroporphyritic clusters may be cognate xenoliths. Their textures often suggest crystal-melt equilibrium. Therefore, they may represent crystal cumulates derived from the same or closely related magma. In contrast, some olivine and clinopyroxene clusters exhibit textures indicative of a mantle origin, e.g., corroded margins with reaction products and kink-band metamorphic textures. Although the presence of xenoliths in some of the SAVF samples suggest that processes such as fractional crystallisation may have played a limited role in their evolution, their occurrence does not preclude fractionation prior to xenolith entrainment (Kempton *et al.*, 1987). Some phenocrysts with disequilibrium textures may have been derived from disaggregated xenoliths. This suggests that xenolith melting or dissolution occurred and by inference, partial xenolith assimilation (e.g., Tsuchiyama, 1986). Alternatively, the absence of xenoliths in some samples suggest either total assimilation of all xenoliths or that no xenoliths were incorporated into the magma during its ascent to the surface.

Some xenoliths are clearly exotic material. They commonly have quartz or quartzofeldspathic compositions and have margins sheathed with reaction products such as pyroxene. Clots of clinopyroxene grains are also observed in many samples, especially those from the group B rocks. Although these xenoliths and clots are not apparently abundant, their occurrence indicates that material of high silica content has been completely or nearly completely incorporated into the melt.

Chapter Four:
Mineralogy and Mineral Chemistry

Chapter Four

Mineralogy and Mineral Chemistry

4.1 Introduction

The petrology of the South Auckland volcanic field consists of silica-undersaturated basaltic lavas with compositions that range from basanite to qz-tholeiitic basalt. The main phenocryst phases contained within these rocks include olivine, clinopyroxene, and plagioclase feldspar. The main accessory minerals include nepheline, K-feldspar, titanomagnetite, and ilmenite – occurring primarily as groundmass phases, and chromian titanomagnetite – found predominantly as inclusions in olivine.

Rafferty and Heming (1979) described the mineral chemistry of a variety of the alkalic and subalkalic rocks found in the SAVF and documented their diverse mineral chemical characteristics. Rafferty and Heming (1979) also used plagioclase geothermometry to constrain the range of temperatures over which the subalkalic lavas crystallised.

Building on the work of Rafferty and Heming (1979), new mineral chemical data from over 1800 electron microprobe analyses are reported in this chapter. These data provide quantitative mineral chemical information, which characterise the petrologic relationships between group A and B lavas. The data are also used to characterise and constrain pre-eruptive crystallisation conditions such as temperature, pressure, oxygen fugacity, and mineral-liquid equilibria of the discrete magma batches that erupted throughout the SAVF.

Volcanic fields in other continental intraplate tectonic environments commonly contain a range of basaltic rock types similar to those erupted in the SAVF (e.g., Coombs and Wilkinson, 1969; Duda and Schmincke, 1978; Frey *et al.*, 1978; Briggs and Goles, 1984; Ewart *et al.*, 1988; Ewart, 1989; Weaver and Smith, 1989; Briggs *et al.*, 1990; Zhi *et al.*, 1990). The distinctive geochemical features of these lavas are commonly attributed to one or more of a range of magmatic processes combined with variable source characteristics. As a component of an integrated petrogenetic model, precise analyses of mineral compositions may be used to constrain the extent to which magmatic processes, such as fractional crystallisation, may have been factors in the genesis and evolution of the diverse range of magmas that erupted throughout the SAVF. This chapter presents an

extensive mineral chemical database for each rock type from groups A and B that may be used in petrogenetic models (see Chapter 6).

4.2 Methodology

Chemical compositions of phenocryst[24], microphenocryst, and groundmass crystals from 26 group A and 26 group B rock samples were obtained using the University of Auckland's electron microprobe (see Appendix 5 for analytical procedures, operating conditions, and precision estimates). All analyses are presented in Appendix 6, Tables A6.1 to A6.39. Sample selection was based on the following criteria:

1. A minimum of three representative samples were chosen from each rock type in groups A and B. Where possible, samples were chosen from a range of geochemical compositions for each rock type, based on whole-rock geochemistry, e.g., variation in $100Mg/(Mg + Fe^{2+})_{(whole\text{-}rock)}$ values, spatial distribution, and age.

2. Each sample must contain relatively large modal abundances of phenocrysts and microphenocrysts (modal analyses for each sample are summarised in Appendix 3). Because one of the objectives of this chapter is to characterise the crystallisation conditions of the mineral phases, only unaltered euhedral and subhedral phenocrysts and microphenocrysts were probed. These crystals are considered to have core compositions that most likely represent equilibrium crystallisation conditions.

4.3 Summary of mineral assemblages

4.3.1 Group A rocks

Forsteritic olivine, clinopyroxene, and plagioclase occur as phenocrysts in each group A rock type; transitional basalt, hawaiite, ol-tholeiitic basalt, qz-tholeiitic basalt, and alkali ol-basalt. A summary of the mineral assemblages and groundmass phases that occur in each rock type is presented in Table 4.1. Generally, olivine ($Fo_{82\text{-}59}$) is the principal mineral phase in all rock types from group A. Plagioclase ($An_{71\text{-}35}$) is dominant in a small number of alkali ol-basalt, transitional basalt, hawaiite, and ol-tholeiitic basalt samples, but is uncommon or absent in other samples of these rock types. The plagioclase in all

[24]As the relative size of megacrysts, phenocrysts, microphenocrysts, and groundmass crystals have not been formally defined (e.g., Shelley, 1993), in this and subsequent chapters, the term "phenocryst" is used to refer to crystals that range in size from megacryst (i.e., > 1.5 mm) to phenocryst (i.e., 500 μm to 1.5 mm) unless specified otherwise (see section 3.4 for details).

rock types contains small (e.g., < 20 μm) apatite inclusions. Clinopyroxene ($Wo_{47-36}En_{51-36}Fs_{37-11}$) is often subordinate to plagioclase, and is occasionally absent as a phenocryst phase in a number of transitional basalt and ol-tholeiitic basalt samples. Titanomagnetite and ilmenite are found principally as groundmass phases in the group A rocks, although rare microphenocrysts of these minerals have been identified in samples from each group A rock type.

Groundmass mineralogy is similar to that of the phenocryst assemblages – dominated by either olivine (Fo_{76-21}) or plagioclase (An_{72-17}). Clinopyroxene is often abundant but is typically subordinate to olivine and plagioclase. Clinopyroxene compositions are principally augite but range to pigeonite in some ol-tholeiitic and qz-tholeiitic basalt samples. Titanomagnetite is present in the groundmass of all rock types. Ilmenite is less common and occurs primarily in the hawaiites and ol-tholeiitic basalts. Apatite is an additional groundmass phase occurring as small, needle-like crystals.

True chromian spinel (Cr-spinel), in the magnesiochromite-chromite series (Deer *et al.*, 1992, p. 560), such as those described by Allan *et al.* (1988) for MORB-type lavas, Dungan (1987) for hybrid tholeiitic basaltic lavas, Ewart (1989) for alkalic basaltic lavas, and Clynne and Borg (1997) for primitive tholeiitic and calc-alkaline lavas, was not identified in thin-section or by electron microprobe analyses in any of the group A rocks. However, chromian titanomagnetite (Cr-titanomagnetite; in the ulvöspinel-chromite series) is relatively common in some of the transitional basalt, hawaiite, ol-tholeiitic basalt, and alkali ol-basalt samples occurring principally as small (e.g., < 50 μm) inclusions within the cores of olivine phenocrysts.

Table 4.1 Summary of phenocryst assemblages and groundmass phases of group A rock types, South Auckland volcanic field. Ph = phenocryst, Gm = groundmass, n = number of samples

Rock type	n	Olivine	Clinopyroxene	Feldspars	Titano-magnetite	Ilmenite	Minor phases	Inclusions
transitional basalt	3	Ph: Fo_{80-76} Gm: Fo_{76-43}	Ph: augite Gm: augite	Ph: An_{71-61} Gm: An_{72-45}	Gm	Gm	Gm: apatite	Cr-titano-magnetite; apatite
hawaiite	4	Ph: Fo_{82-61} Gm: Fo_{58-21}	Ph: augite Gm: augite	Ph: An_{71-50} Gm: An_{60-17} Gm: rare anorthoclase	Gm	Gm	Gm: apatite	Cr-titano-magnetite; apatite
ol-tholeiitic basalt	11	Ph: Fo_{81-59} Gm: Fo_{76-31}	Ph: augite Gm: augite to pigeonite	Ph: An_{67-35} Gm: An_{71-27} Gm: rare anorthoclase, sanidine	Gm	Gm	Gm: apatite	apatite
qz-tholeiitic basalt	3	Ph: Fo_{82-74} Gm:Fo_{61}	Ph: augite Gm: augite to pigeonite	Ph: An_{68-46} Gm: An_{66-31}	Gm	Gm	Gm: apatite	apatite
alkali ol-basalt	5	Ph: Fo_{80-63} Gm: Fo_{68-47}	Ph: augite Gm: augite	Ph: An_{71-47} Gm: An_{69-18}	Gm	Gm	Gm: apatite	Cr-titano-magnetite; apatite

4.3.2 Group B rocks

Olivine and titaniferous, Ca-rich clinopyroxene are the dominant phenocryst phases in each group B rock type: basanite, nephelinite, ne-hawaiite, mugearite, and alkali ol-basalt. All olivine is forsteritic (Fo_{92-60}) and is the principal phenocryst phase in the nephelinites, ne-hawaiites, and the only mugearite sample, SA88. Olivine is occasionally subordinate to clinopyroxene ($Wo_{52-42}En_{46-33}Fs_{20-10}$) in the basanites and alkali ol-basalts. Plagioclase (An_{73-40}) occurs as rare microphenocrysts, primarily in the alkali ol-basalts and mugearite. The phenocryst assemblages and groundmass phases that occur in each rock type in group B are summarised in Table 4.2.

Table 4.2 Summary of phenocryst assemblages and groundmass phases of group B rock types, South Auckland volcanic field.
Ph = phenocryst, Gm = groundmass, n = number of samples. Ol = olivine, Cpx = clinopyroxene, Ti-mag = titanomagnetite, Ilm = ilmenite.

Rock type	n	Ol	Cpx	Feldspar	Felds-pathoid	Ti-mag	Ilm	Minor phases	Inclusions
basanite	13	Ph: Fo_{85-64}	Ph: diopside Gm: diopside	Ph: An_{68-60} Gm: An_{96-26} Or_{79-27}	Gm: nepheline	Gm		Gm: apatite	Cr-titano-magnetite
nephelinite	5	Ph: Fo_{83-70}	Ph: diopside Gm: diopside	Ph: rare Gm: An_{62-47} Or_{20-14}	Gm: nepheline	Gm		Gm: apatite	Cr-titano-magnetite
ne-hawaiite	4	Ph: Fo_{78-66}	Ph: diopside Gm: diopside	Ph: rare Gm: An_{60-25} Or_{58-17}	Gm: nepheline	Gm		Gm: apatite	
mugearite	1	Ph: Fo_{81-60}	Ph: diopside Gm: diopside	Ph: An_{73-40} Gm: An_{65-38} Or_{38-19}		Gm	Gm	Gm: apatite	apatite
alkali ol-basalt	3	Ph: Fo_{92-65}	Ph: diopside Gm: diopside	Ph: An_{62-57} Gm: An_{63-22}	Gm: nepheline	Gm		Gm: apatite	Cr-titano-magnetite; apatite

Groundmass minerals are predominantly feldspar and clinopyroxene. A variety of plagioclase species (An_{96-26}) is common in all rock types, though labradorite tends to be the predominant composition. Some basanites, nephelinites, and ne-hawaiites and the mugearite contain a broad range of feldspar compositions, from calcic plagioclase to alkali feldspar compositions (Or_{79-14}) in the series anorthoclase - high potassium sanidine. Clinopyroxene crystals commonly have a restricted range of diopside compositions. Apatite is an additional groundmass phase occurring as small needle-like crystals.

Nepheline occurs in samples from each rock type in group B except mugearite. However, it is identifiable only by the use of the electron microprobe and therefore its relative abundance in the groundmass is uncertain. Titanomagnetite is ubiquitous and abundant in the groundmass of all group B rocks, and occasionally occurs as small (e.g., < 50 μm),

blocky inclusions in clinopyroxene and olivine. Ilmenite is notably absent in all group B rock types, except mugearite.

As with the group A rocks, true Cr-spinel was not identified in any of the samples from the group B rocks. However, Cr-titanomagnetite is relatively common occurring typically as small (e.g., < 50 μm) inclusions in the cores of olivine phenocrysts and to a lesser extent, in the cores and along rims of titaniferous clinopyroxene phenocrysts and microphenocrysts. Cr-bearing titanomagnetite (defined in this study as containing less than 1 wt. % Cr_2O_3) occurs as discrete groundmass grains in some samples from each group B rock type, except mugearite.

4.4 Olivine

Olivine is commonly the dominant phenocryst phase in all SAVF lava samples (see Appendix 3, Tables A3.1 and A3.2 for complete modal analyses of all SAVF samples). The abundance of olivine phenocrysts typically varies considerably between samples of the same rock type (Table 4.3). Olivine crystals in each rock type within groups A and B display a range of morphologies with individual samples generally containing a variety of crystal forms and sizes that may reflect crystallisation at different degrees of subcooling (e.g., Donaldson, 1976; Maaløe, 1982; Helz, 1987). Generally, olivine occurs as rare subhedral megacrysts, abundant subhedral phenocrysts and microphenocrysts, and anhedral groundmass crystals in the group A rocks. In the group B rocks, olivine occurs as rare subhedral megacrysts, abundant euhedral and subhedral phenocrysts and microphenocrysts, and rare anhedral groundmass grains. In the most primitive group A rock types (e.g., transitional basalts, hawaiite, and alkali ol-basalts) and all group B rocks, except mugearite, some olivine megacrysts and phenocrysts contain inclusions of Cr-titanomagnetite and rare granular titanomagnetite. Groundmass olivine is present in all rock types, although it is more common in group A rocks, including the qz-tholeiitic basalts.

Olivine phenocryst core compositions[25] span a relatively broad, continuous range that varies from $Fo_{82.1}$ to $Fo_{58.6}$ in group A, and $Fo_{91.8}$ to $Fo_{59.6}$ in group B rocks (see Tables 4.1

[25] Olivine is generally very susceptible to alteration. Olivine crystals with iddingsite alteration along rims and crystal margins are common in all SAVF rock types. Many rock samples contain crystals with cores that have iddingsite overgrowth. Iddingsite can form at the vapour-rich top of a magma column prior to eruption, during post-eruptive deuteric alteration, and possibly during post-deposition weathering (Shelley, 1993). However, samples selected for this study generally contain large populations of unaltered-olivine. Therefore, only these crystals were selected for mineral chemistry analysis.

and 4.2). Rims and groundmass crystals range from $Fo_{78.4}$ to $Fo_{21.3}$ in group A, and rims in group B[26] from $Fo_{79.8}$ to $Fo_{42.9}$. Representative analyses of olivine from each rock type in groups A and B are given in Tables 4.4 and 4.5 respectively (see Appendix 6, Tables A6.1 to A6.5 and A6.20 to A6.24 for complete analyses). A histogram of 102 group A and 122 group B olivine phenocryst and microphenocryst core analyses (Fig. 4.1) illustrates the extensive overlap in the range of compositions between each rock group.

Table 4.3 Summary of the modal abundance of olivine phenocrysts and microphenocrysts in selected South Auckland volcanic field basalts sampled from each rock type within group A and B lavas. Modal abundances based on 1000 point counts. n = number of samples counted

Group A					Group B				
Rock type	modal abundance				Rock type	modal abundance			
	max	min	mean	n		max	min	mean	n
transitional basalt	14.8	2.0	5.4	15	basanite	21.2	5.2	12.9	34
hawaiite	17.2	1.6	8.4	29	nephelinite	16.0	6.0	9.4	14
ol-tholeiitic basalt	16.6	0.2	8.8	35	ne-hawaiite	12.0	2.4	5.6	11
qz-tholeiitic basalt	14.8	0.8	8.9	4	alkali ol-basalt	13.0	0.8	6.9	4
alkali ol-basalt	14.8	0.8	7.6	7	mugearite	18.0	-	-	1

Table 4.4 Representative electron microprobe analyses of group A olivines, South Auckland volcanic field. n.d. = not detected. C = core, R = rim.

Rock type	alkali ol-basalt			transitional basalt			hawaiite			ol-tholeiitic basalt			qz-tholeiitic basalt		
Sample	SA17		SA33	SA07		SA13	SAB151		SA20	SA36		SAB181	SA76		
Analysis	140	141	1711	1904	1906	571	197	198	1879	800	801	183	124	125	132
	C	R	C	C	R	C	C	R	C	C	R	C	C	R	C
SiO_2	38.75	35.74	36.70	38.74	35.17	39.27	39.31	34.89	39.70	39.27	36.34	36.12	39.53	38.34	38.50
Al_2O_3	0.28	-	-	-	-	-	-	0.43	0.53	-	0.30	-	-	0.29	-
Cr_2O_3	n.d	n.d	n.d	-	3.45	n.d	n.d	n.d	-	n.d	n.d	n.d	n.d	n.d	n.d
FeO	23.46	37.22	32.42	18.60	40.42	21.04	20.07	36.56	30.93	18.35	38.12	33.36	17.27	22.18	23.50
MnO	-	0.42	0.50	0.26	0.22	-	0.32	0.52	0.27	0.26	0.31	0.42	0.26	0.27	0.32
MgO	37.98	26.18	30.77	41.25	18.75	38.47	40.48	25.27	26.96	42.11	23.52	28.90	42.34	39.09	38.11
CaO	0.28	0.45	0.38	0.23	0.58	0.24	0.24	0.38	0.24	0.16	0.35	0.28	0.21	0.20	0.27
Total	100.75	100.01	100.77	99.08	98.99	99.02	100.42	98.05	98.63	100.15	98.94	99.08	99.61	100.37	100.70
Number of ions on the basis of 4 oxygen															
Si	0.997	0.997	0.992	0.994	1.072	1.035	1.000	0.994	1.130	1.000	1.040	0.998	1.001	0.974	0.994
Al	0.008	-	-	-	-	-	-	0.014	-	-	0.010	-	-	0.009	-
Cr	-	-	-	-	0.138	-	-	-		-	-	-	-	-	-
Fe^{2+}	0.505	0.869	0.733	0.399	1.030	0.464	0.427	0.871	0.736	0.391	0.912	0.771	0.366	0.471	0.507
Mn	-	0.010	0.012	0.006	0.006	-	0.007	0.012	0.006	0.006	0.008	0.010	0.006	0.006	0.007
Mg	1.457	1.089	1.240	1.577	0.852	1.512	1.535	1.072	1.144	1.599	1.004	1.191	1.598	1.481	1.466
Ca	0.008	0.014	0.011	0.006	0.019	0.007	0.007	0.012	0.007	0.004	0.011	0.008	0.006	0.006	0.008
End-member composition															
Fo	74.3	55.3	62.5	79.6	45.1	76.5	78.0	54.8	60.6	80.1	52.2	60.4	81.1	75.6	74.0

[26] Groundmass olivine was not analysed in the group B samples because these crystals occur predominantly in the devitrified glassy matrix, characteristic of most group B samples. Electron microprobe analyses yielded spurious results as glass composition was commonly incorporated into the results of the olivine analyses.

Table 4.5 Representative electron microprobe analyses of group B olivines, South Auckland volcanic field. n.d. = not detected. C = core, R = rim.

Rock type	alkali ol-basalt			basanite			nephelinite			ne-hawaiite			mugearite		
Sample	SAB207		SA54	SAB179		SA27	SA28		SAB113	SA29		SA65	SA88		
Analysis	1602 C	1603 R	1695 C	217 C	218 R	1336 C	1435 C	1436 R	238 C	154 C	155 R	1536 C	492 C	493 R	57 C
SiO_2	39.46	37.58	36.27	39.89	36.11	36.46	37.69	35.72	37.99	38.15	35.30	37.17	39.68	39.51	36.40
Al_2O_3	-	-	-	-	-	0.40	-	-	-	-	-	-	0.28	0.60	-
Cr_2O_3	n.d.	n.d.	n.d.	n.d.	n.d.	n.d.	n.d.	n.d.	n.d.	n.d.	n.d.	n.d.	n.d.	n.d.	n.d.
FeO	14.94	30.72	30.07	15.78	34.42	30.09	24.54	32.32	25.49	26.16	37.17	29.65	17.61	18.99	34.36
MnO	-	0.62	0.49	0.22	0.58	0.82	0.32	0.94	0.43	0.46	0.98	0.43	-	-	0.48
MgO	44.09	28.70	31.77	43.80	28.03	30.76	36.35	29.32	35.29	35.47	25.71	32.88	42.11	40.89	28.76
CaO	0.19	1.20	0.40	0.24	0.57	0.43	0.40	0.61	0.52	0.38	0.57	0.32	0.24	0.24	0.41
Total	98.68	98.82	99.00	99.93	99.71	98.96	99.30	98.91	99.72	100.62	99.73	100.45	99.92	100.23	100.41
Number of ions on the basis of 4 oxygen															
Si	1.004	1.057	0.988	0.999	0.998	1.007	0.995	0.990	1.002	0.999	0.992	0.994	1.007	1.006	0.996
Al	-	-	-	-	-	0.013	-	-	-	-	-	-	0.008	0.018	-
Cr	-	-	-	-	-	-	-	-	-	-	-	-	-	-	-
Fe^{2+}	0.318	0.723	0.685	0.330	0.795	0.695	0.542	0.749	0.562	0.573	0.874	0.663	0.374	0.404	0.786
Mn	0.000	0.015	0.011	0.005	0.014	0.019	0.007	0.022	0.010	0.010	0.023	0.010	-	-	0.011
Mg	1.672	1.204	1.290	1.636	1.154	1.267	1.430	1.211	1.387	1.384	1.078	1.311	1.593	1.551	1.174
Ca	0.005	0.036	0.012	0.006	0.017	0.013	0.011	0.018	0.015	0.011	0.017	0.009	0.006	0.006	0.012
End-member composition															
Fo	84.0	62.0	64.9	83.0	58.8	63.9	72.3	61.1	70.8	70.4	54.6	66.1	81.0	79.3	59.5

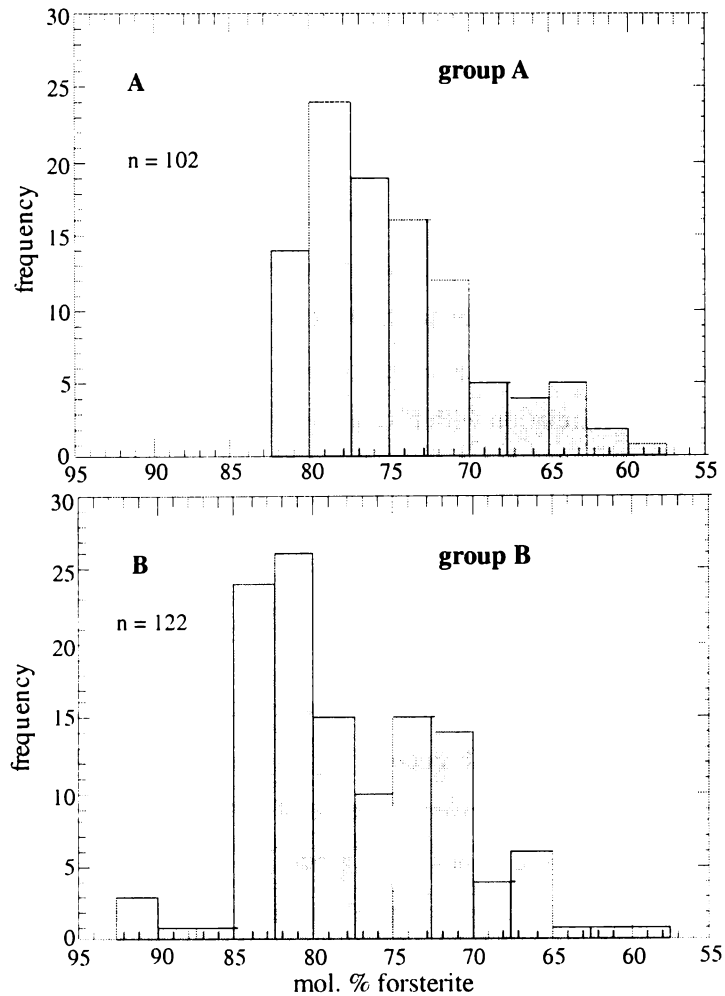

Fig 4.1 Range of forsterite content of olivine phenocryst and microphenocryst cores from selected (A) group A and (B) group B lavas in the SAVF.
n = number of olivine cores analysed.

Individual rock types within each group exhibit a diverse range of olivine phenocryst and microphenocryst core compositions (Fig. 4.2). There is a noticeable difference in the relative distribution of Fo contents between many of the different rock types. For example, the ol-tholeiitic basalts (group A) and basanites (group B) have a larger proportion of Fo-rich (e.g., > Fo_{75}) crystals than other rock types in their respective groups. Additionally, some basanite and ol-tholeiitic basalt samples have populations of comparatively small phenocrysts and microphenocrysts that tend to have relatively lower forsteritic cores (e.g., < Fo_{75}). In contrast to the basanites and ol-tholeiitic basalts, the ne-hawaiites have phenocrysts with core compositions that are predominantly less forsteritic (e.g., < Fo_{75}) than those of the other group A and B lavas.

Olivine phenocryst compositions in the hawaiites (group A) span a similar range to those in the ne-hawaiites (group B). This feature is analogous to the olivine compositions in the hawaiite and ne-hawaiite lavas of the Ngatutura Basalts, New Zealand (Briggs *et al.* 1990). In contrast, the majority of olivine phenocrysts in the hawaiites and basanites have notably dissimilar ranges of compositions, a feature comparable to olivine phenocrysts from similar rocks in the Okete Volcanics, New Zealand (Briggs and Goles, 1984).

4.4.1 Minor elements MnO and CaO

Concentrations of the minor elements MnO and CaO in olivine cores from each rock type in groups A and B generally show a negative correlation with forsterite content (Figs. 4.3 and 4.4). In group A, MnO increases to 0.50 wt. % as forsterite content decreases from Fo_{82} to Fo_{58}, with all rock types showing considerable scatter (Fig 4.3A). In group B, MnO shows a stronger correlation with Fo content increasing to 0.82 wt. % over the same range of decreasing Fo content (Fig 4.3B). In a large number of olivines in basanites, MnO increases weakly from 0.21 to 0.30 wt. % as forsterite contents vary from Fo_{84} to Fo_{79}. In contrast, CaO increases markedly from 0.22 to 0.41 wt. % (Fig. 4.4B) for the same change in Fo content.

Overall, the CaO concentration in olivine cores is highly variable, although there is a crude trend of increasing CaO with decreasing Fo content (Fig 4.4). All rock types in group A show considerable scatter over the range of CaO content 0.16 to 0.42 wt. % (Fig. 4.4A). CaO concentrations in olivines from group B rocks are scattered over the range 0.17 to 0.52 wt. % (Fig. 4.4B). Some nephelinite samples contain olivines that show a negative correlation with Fo content along a trend subparallel to that of many phenocryst cores in basanites.

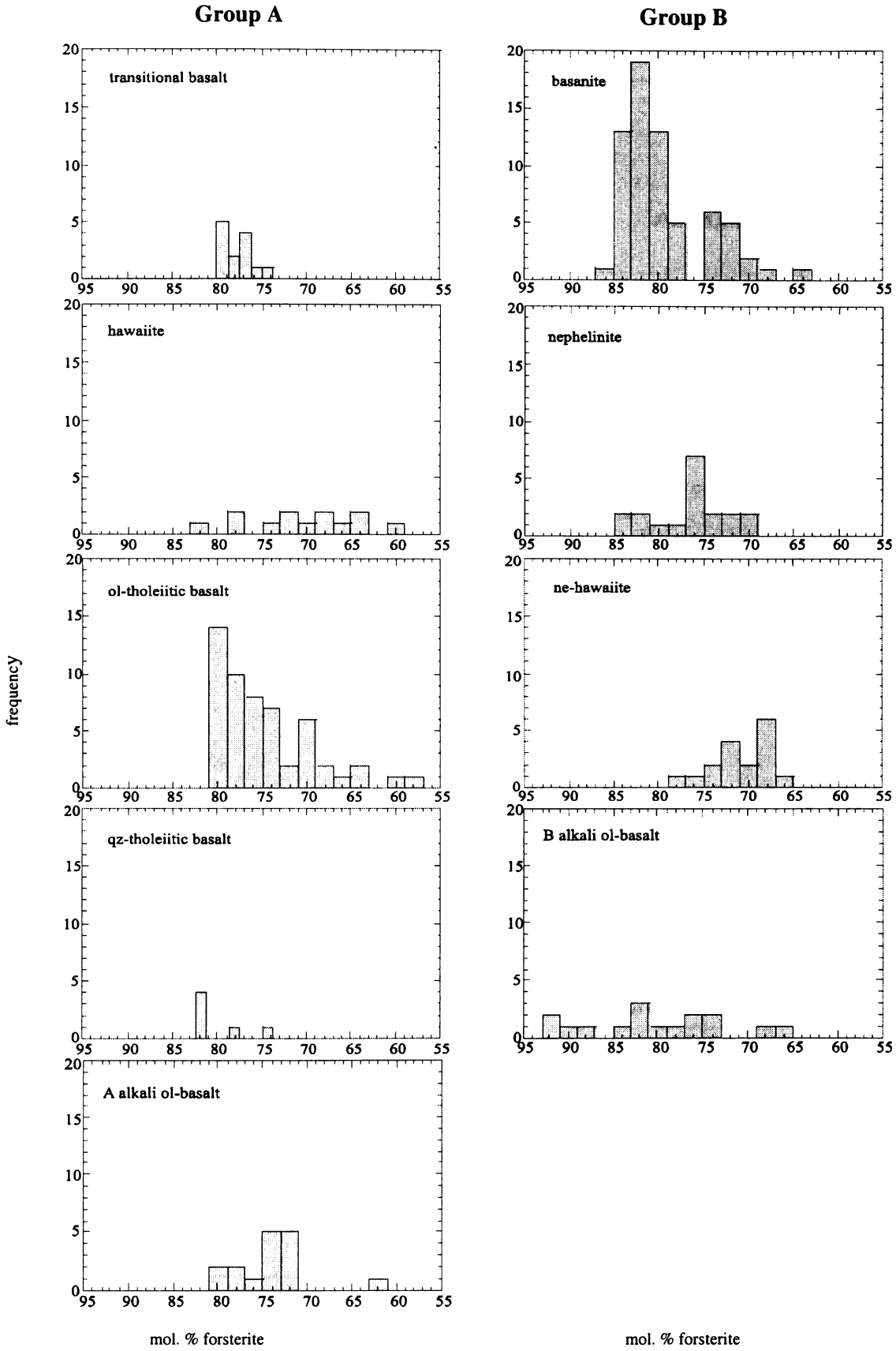

Fig. 4.2 Range of forsterite contents in olivine phenocryst cores from the different rock types within groups A and B.

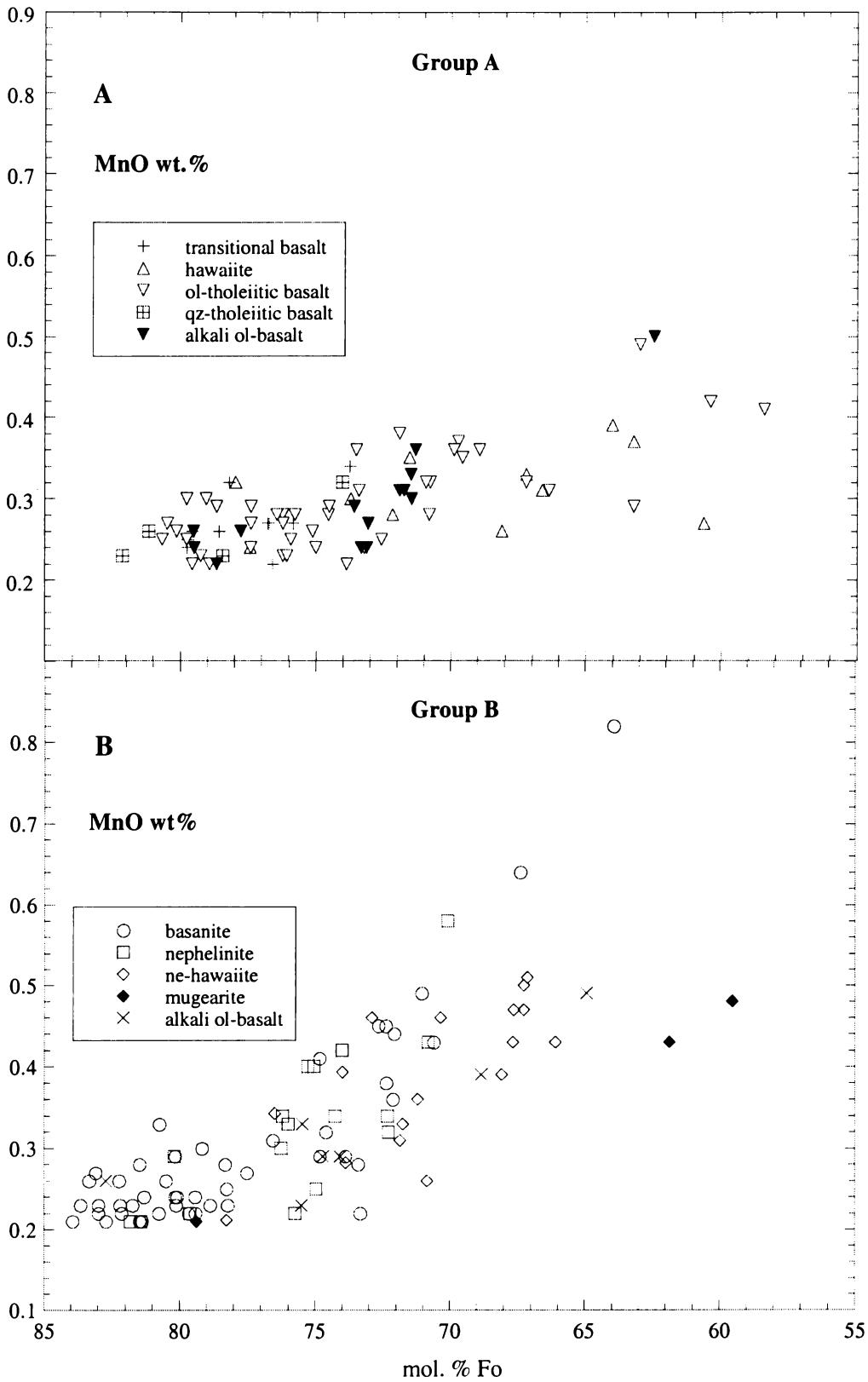

Fig. 4.3 Plots of the minor element MnO (in wt. %) against Fo content for olivine cores in selected (A) group A and (B) group B samples.

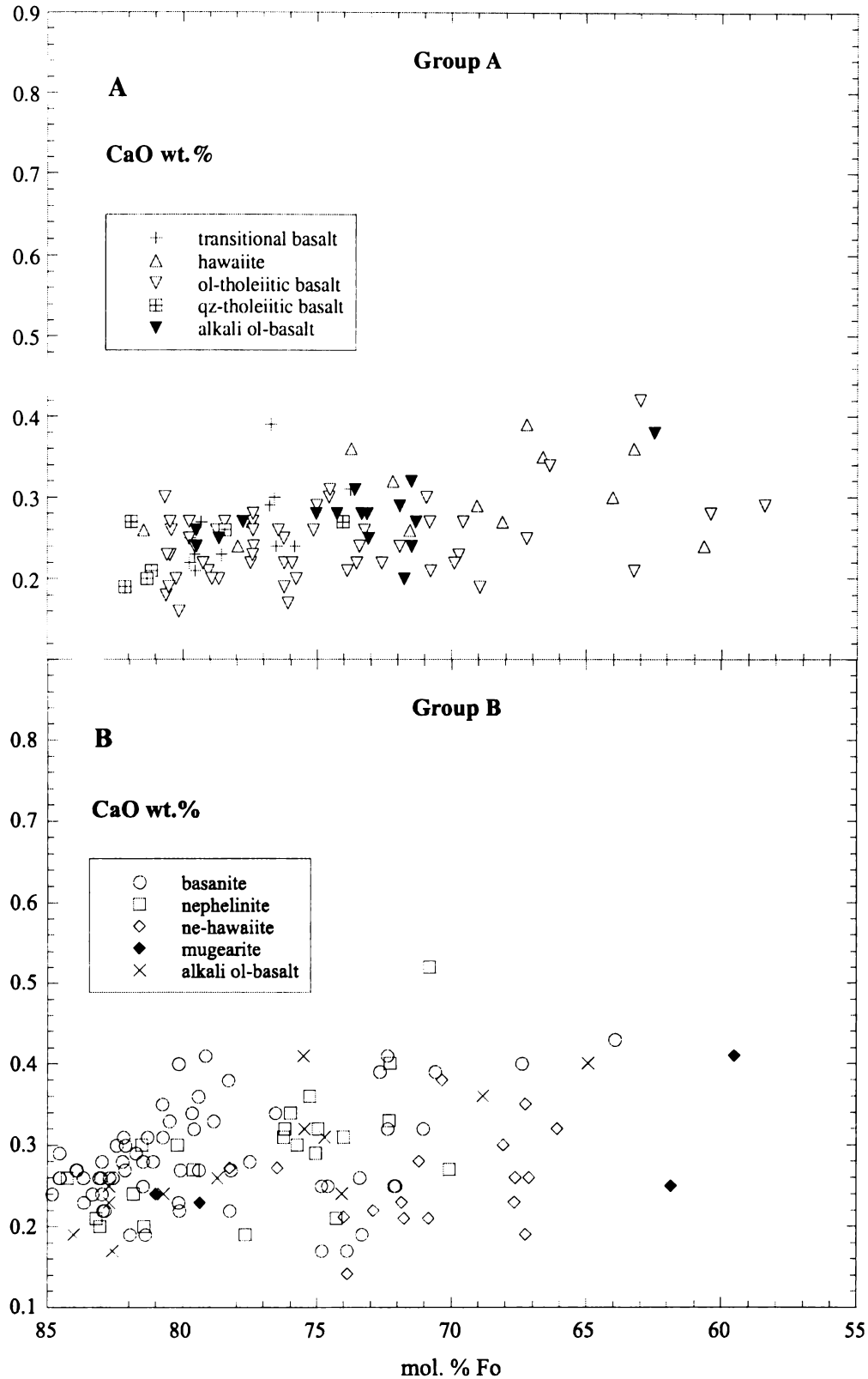

Fig. 4.4 Plots of the minor element CaO (in wt. %) against Fo content for olivine cores in selected (A) group A and (B) group B samples. All group A cores contained CaO. In group B, only the megacrysts of the alkali ol-basalts with > Fo_{88} did not contain detectable CaO. These analyses are not included in the plots.

4.4.2 Olivine phenocryst zoning patterns

Olivine found in natural volcanic systems is generally compositionally zoned. Zoned olivine crystals may be the result of either (1) temporal changes in magma composition (i.e., crystallisation at decreasing temperatures, e.g., subcooling; Corrigan, 1982; Helz, 1987), or (2) the diffusive cation exchange of Fe^{2+}, Mg, Ca, and Mn ions between olivine phenocrysts and basaltic melts (e.g., Watson, 1977; Maaløe and Hansen, 1982; Jurewicz and Watson; 1988b; Kohn and Schofield, 1994).

Normal compositional zoning is characteristic of most olivine megacrysts and relatively large phenocrysts in all SAVF rock types. Generally, these crystals consist of comparatively large, Mg-rich cores, and relatively thin, (e.g., < 150 μm) Fe-rich rims. The rims are rarely prominent in thin-section, usually identifiable only by an abrupt change in rim interference colour. Furthermore, in thin-section, phenocrysts do not exhibit apparent textural features, such as distinctive alternating bands, that would suggest they have complex compositional zoning such as those described by Clark *et al.* (1986) for magmatic olivines.

Clark *et al.* (1986) demonstrated that fine oscillatory zones in olivine, indiscernible in normal polished thin-sections, could be detected and subsequently analysed by using the Nomarski imaging technique with HCl-etched surfaces of olivines in polished thin-sections. Their study details relatively small changes in MgO (e.g., ~ 1 wt. %) and FeO (e.g., > 2 wt. %) content over comparatively small distances (e.g., < 200 μm) within a crystal's interior. Zones such as these may exist in the cores of phenocrysts of the selected SAVF rock samples. Changes in Fo content of up to 4 mol. % Fo over several hundred microns within phenocrysts cores were observed in a number of randomly selected crystals.

Intricate compositional zones such as those described by Clark *et al.* (1986) may provide important insights into an individual phenocryst's complex crystallisation history. However, such fine zoning in SAVF olivines is not the focus of this investigation. The important observation in the SAVF olivines is the zoning defined by contrasts between core and rim compositions. In each rock type, except the qz-tholeiitic basalts, the decrease in rim Fo content, relative to adjacent cores, is often large, resulting in strong compositional zones that are commonly the same width around the entire crystal. The measured decrease in Fo content of phenocryst rims, relative to cores, typically exceeds 10% with averages between 5.5 ± 0.9 and 14.0 ± 4.3% Fo in group A and 7.3 ± 4.4 to 15.6 ± 8.8% in the group B samples, except for mugearite SA88 (Table 4.6). However,

decreases as large as 43.1% Fo occur, with the strongest zoned phenocryst ($Fo^{core}_{79.7} - Fo^{rim}_{45.3}$) observed in transitional basalt sample SA07.

Table 4.6 Range of percent decrease of Fo content in rims relative to cores of normally zoned phenocrysts in group A and B lavas. Max and min values were excluded from mean calculations to reduce bias potentially caused by extreme values. n = number of core-rim pairs analysed. Mean values = ± 1 standard deviation.

Group A					Group B				
Rock type	% Fo decrease				Rock type	% Fo decrease			
	n	max	min	mean		n	max	min	mean
transitional basalt	10	43.1	2.1	10.1 ± 7.3	basanite	47	29.0	0.4	11.0 ± 5.9
hawaiite	11	29.5	8.4	14.0 ± 4.3	nephelinite	17	15.0	1.5	7.3 ± 4.4
ol-tholeiitic basalt	34	34.7	2.1	13.6 ± 8.4	ne-hawaiite	8	22.4	3.1	10.9 ± 2.5
qz-tholeiitic basalt	6	6.5	4.6	5.5 ± 0.9	alkali ol-basalt	11	26.5	0.9	15.6 ± 8.8
alkali ol-basalt	12	25.4	4.7	12.0 ± 4.5	mugearite	3	30.9	2.2	2.4 ± 0

Most rock types contain populations of relatively large phenocrysts that have strong, normal compositional zoning, though some samples contain large phenocrysts that are unzoned or weakly zoned (e.g., alkali ol-basalt; SAB188). In addition to these, small unzoned to weak normally zoned crystals are widespread in all rock types and commonly occur together with normally zoned crystals in individual samples. Reversed zoned crystals occur in a number of samples, although they are rare and their zoning is always weak, with rims typically < 2 mol. % Fo greater than the adjacent cores.

Some samples contain olivine phenocrysts with core compositions that vary only slightly from crystal to crystal, and have similar core and rim compositions. These features are indicative of olivine-liquid equilibrium (Helz, 1987). In contrast, other samples may contain populations of olivine phenocrysts that have core-rim pairs that span a wide range of Fo content, and similar core Fo contents but very different rim compositions. Each of these features is characteristic of olivine-liquid disequilibrium, which may suggest that for each magma batch erupted in the SAVF, olivine crystallised under a range of P-T-fO_2 conditions (e.g., Maaløe and Hansen, 1982). Alternatively, olivine-liquid disequilibrium may be the result of magma mixing either prior to or during an eruption (e.g., Dungan, 1987; Helz, 1987).

Compositions of selected phenocryst cores and core-rim pairs for each rock type in groups A and B are shown in Fig. 4.5. Phenocryst compositions are mainly between Fo_{85} and Fo_{65} for all samples (see also Fig. 4.2). Although not statistically proven in this study, visual observations of probed crystals suggest that there is an apparent correlation between crystal size and core composition. Crystals having Fo contents less than Fo_{65} tend to be comparatively small unzoned or weakly zoned phenocrysts or microphenocrysts. These crystals generally have relatively homogeneous cores with smaller Fo content than those of the larger phenocrysts that may occur in the same sample.

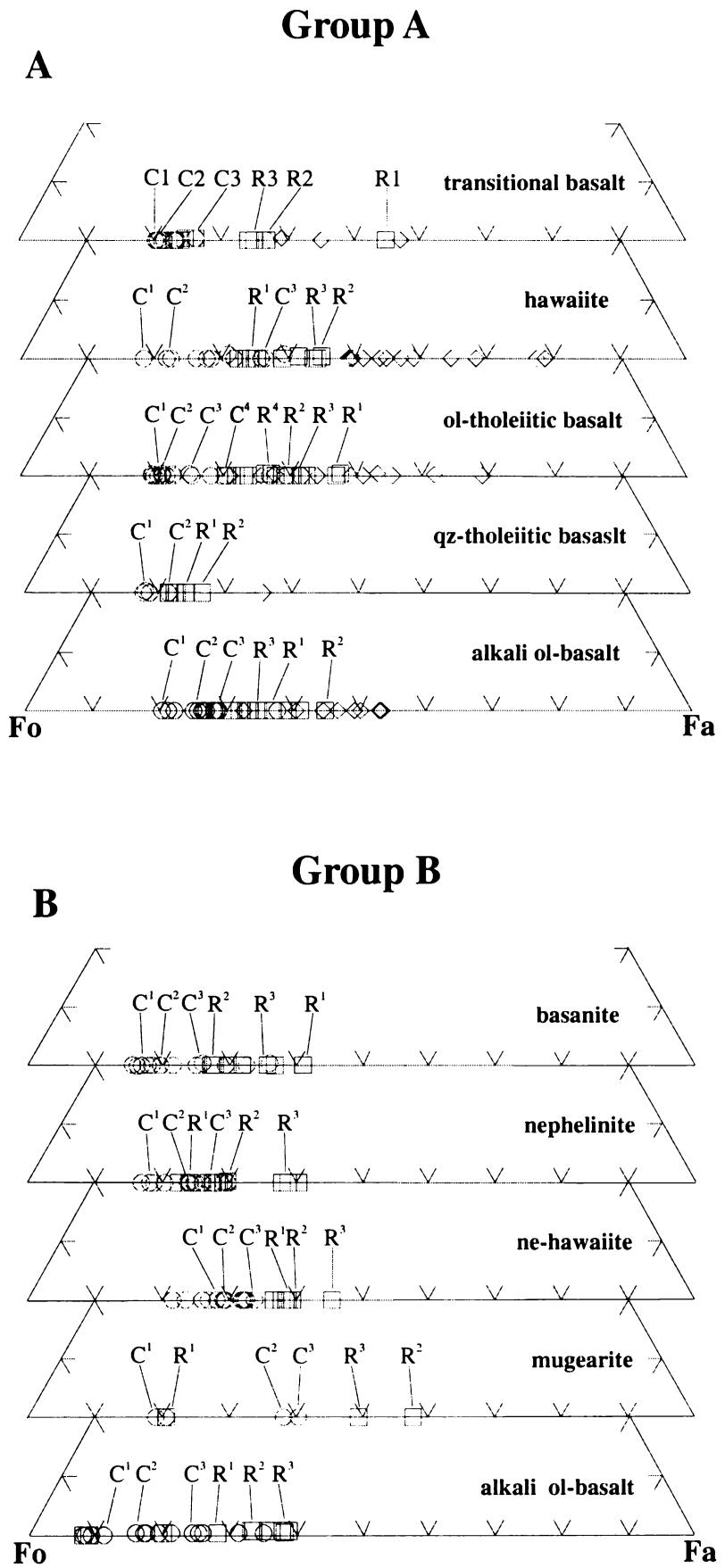

Fig. 4.5 Representative olivine compositions in mol.% for South Auckland volcanic field lavas, (A) group A and (B) group B. ○ = cores, □ = rims, and ◊ = groundmass crystals. Selected phenocryst core-rim pairs (C = core, R = rim), identified by their corresponding superscript numbers, are representative of the range of core-rim compositions within each rock type.

MnO and CaO zoning

A majority of olivine phenocrysts in the lavas from both rock groups are compositionally zoned in the minor elements, MnO and CaO. Such zoning may provide information regarding the evolution of magma systems during olivine crystallisation, especially the importance of melt composition in controlling the partitioning of these elements between olivine and its host magma (Watson, 1977; Jurewicz and Watson, 1988a; Kohn and Schofield, 1994; Libourel, 1999). In both rock groups, most phenocrysts are reversely zoned with rims richer in MnO and CaO than their cores. However, there is no obvious correlation between core-rim MnO and CaO concentrations and the extent to which the same crystals may be zoned relative to Fo content. Some crystals (predominantly in group A lavas) are either unzoned or have relatively weak MnO and CaO normal zoning. Additionally, the distribution of MnO and CaO between cores and rims is often complex from crystal to crystal in a number of group A samples. For example, phenocrysts with MnO-rich rims may have CaO-rich cores. Other phenocrysts may have MnO-rich cores and CaO-rich rims (see Appendix 6, Tables A6.1 to A6.5 for these and other core-rim combinations).

In contrast to group A olivines, olivine phenocrysts in most group B rock samples are predominantly reversely zoned in MnO and CaO. Additionally, olivines in group B samples tend to have larger contrasts between cores and rims in each of these elements than their group A counterparts, with strong MnO and CaO core to rim enrichment trends up to 0.62 wt. % MnO and 0.84 wt. % CaO in individual phenocrysts. The comparatively large CaO enrichment in the group B phenocryst rims relative to those in group A rocks is consistent with the observations of Stormer (1973) for olivines in highly alkaline, undersaturated nephelinites and more siliceous Hawaiian tholeiites.

4.4.3 Olivine phenocryst – host rock relations

The rock samples used for mineral chemistry investigations in this study have whole-rock compositions with $100Mg/(Mg + Fe^{2+})$ values that range from 47 to 68, although the majority of samples in both rock groups have values > 60 (Tables 4.7 and 4.8; p.59). Generally, samples with values of $100Mg/(Mg + Fe^{2+}) > 60$ tend to contain olivine phenocrysts with core compositions in the range Fo_{92} to Fo_{73}. In contrast, rock samples with smaller $100Mg/(Mg + Fe^{2+})$ values, especially those in group B, commonly contain olivine phenocrysts that are relatively less forsteritic (e.g., < Fo_{73}) than their larger $100Mg/(Mg + Fe^{2+})$ value counterparts. Overall, olivine phenocryst core compositions in

group A and B rocks generally show a positive correlation with the whole-rock 100Mg/(Mg + Fe^{2+}) values of their respective host rock (Fig. 4.6).

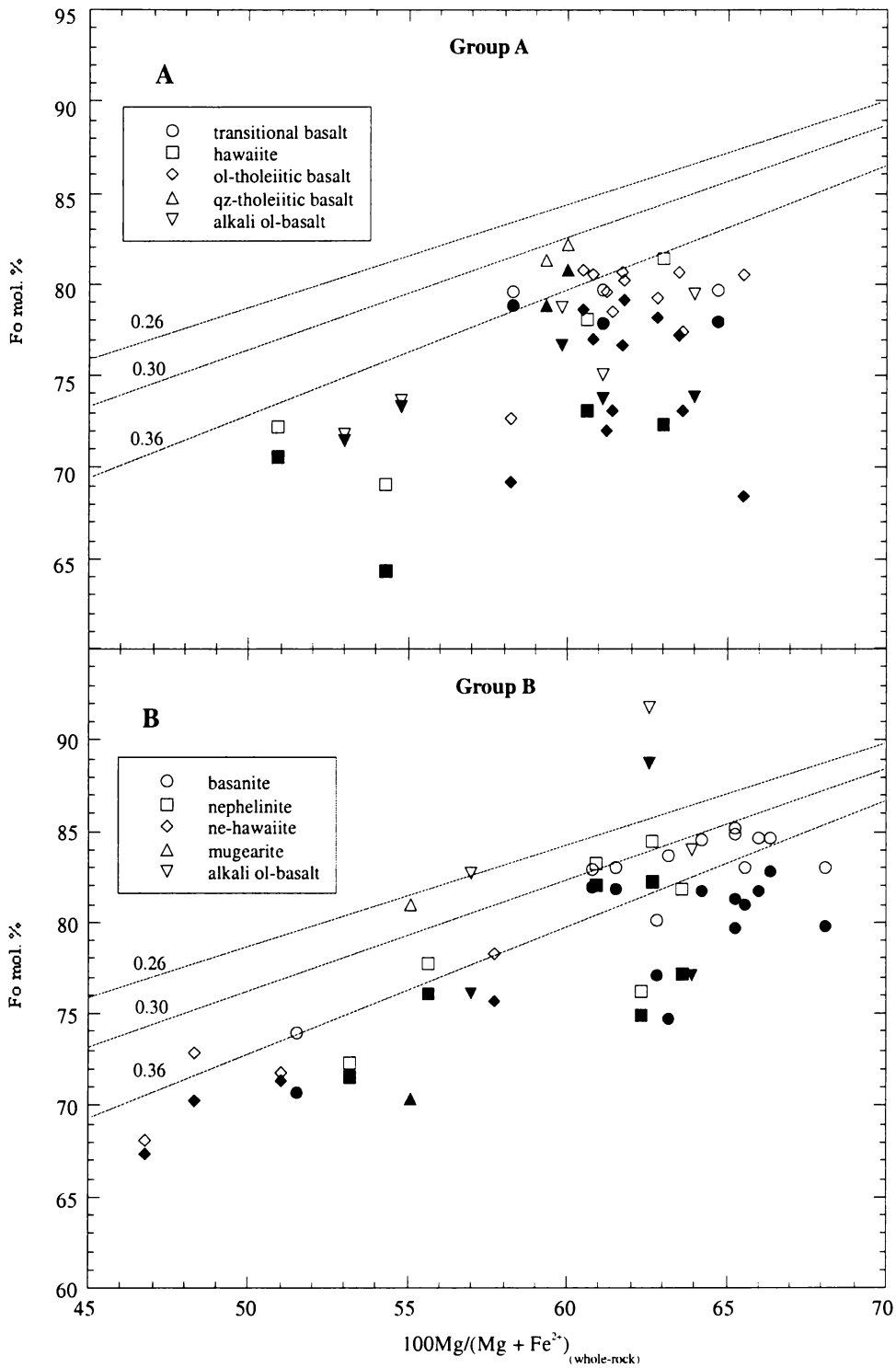

Fig. 4.6 Forsterite contents of olivine phenocryst cores vs. whole-rock 100Mg/(Mg + Fe^{2+}) values in host rock samples from (A) group A and (B) group B. Open symbols are the maximum Fo content recorded for phenocryst cores in each sample (Fo_{max}; Tables 4.7 and 4.8). Filled symbols are the average compositions of phenocryst cores from the same sample (Fo_{mean}; Tables 4.7 and 4.8). Curves for $K_{d_{Fe-Mg}}^{ol-melt}$ values 0.26, 0.30, and 0.36 are derived from the distribution coefficient equation of Roeder and Emslie (1970), described in the text. Note: symbols for the group A rocks and group B alkali ol-basalt and mugearite are different to those in Figs. 4.7 and 4.8.

Table 4.7 Maximum and mean forsterite content for olivine cores in selected samples from each group A rock type, and the corresponding host rock 100Mg/(Mg + Fe^{2+}) values. Partition coefficients, K_d for Fe^{2+} and Mg are derived from Eq. 1 in Roeder and Emslie (1970) and Ca from Eq. 13 in Libourel (1999), described in the text. n = number of core analyses per sample. Mean values = ± 1 standard deviation.

Group A							
Rock type	Sample	n	Fo_{max}	Fo_{mean}	host rock $\frac{100Mg}{(Mg + Fe^{2+})}$	$K_{d_{Fe-Mg}}^{ol-melt}$ range	$K_{d_{Ca}}^{ol-melt}$ range
alkali ol-basalt	SA17	3	75.1	73.7 ± 1.6	61	0.52 – 0.61	0.113-0.123
	SA18	3	78.7	76.6 ± 2.8	60	0.40 – 0.54	0.094-0.116
	SA19	3	73.6	73.3 ± 0.2	55	0.43 – 0.44	0.097-0.120
	SA33	3	79.6	73.8 ± 9.8	64	0.46 – 1.06	0.094-0.199
	SAB162	4	71.9	71.5 ± 0.2	53	0.44 – 0.45	0.078-0.124
transitional basalt	SA07	3	79.6	78.8 ± 0.7	58	0.36 – 0.39	0.088-0.120
	SA10	5	79.7	77.8 ± 1.5	61	0.40 – 0.48	0.101-0.164
	SA13	5	79.7	77.9 ± 2.5	64	0.45 – 0.63	0.088-0.143
hawaiite	SA20	3	69.1	64.3 ± 4.4	54	0.53 – 0.78	0.146-0.189
	SA32	4	73.8	72.3 ± 6.9	63	0.60 – 0.85	0.120-0.227
	SAB151	3	78.1	73.1 ± 7.8	61	0.43 – 0.86	0.097-0.157
	SAB163	3	72.2	70.6 ± 2.2	51	0.40 – 0.48	0.105-0.128
ol-tholeiitic basalt	SA36	7	80.5	77.0 ± 4.2	61	0.38 – 0.68	0.071-0.142
	SA80	3	80.7	77.2 ± 3.5	64	0.42 – 0.62	0.077-0.121
	SAB152	3	79.4	78.2 ± 1.7	63	0.44 – 0.52	0.095-0.105
	SAB169	5	72.6	69.2 ± 5.7	58	0.52 – 0.81	0.089-0.207
	SAB170	6	80.3	79.1 ± 1.0	62	0.40 – 0.47	0.089-0.131
	SAB171	7	78.5	73.1 ± 3.6	61	0.44 – 0.78	0.122-0.142
	SAB172	3	80.7	78.6 ± 3.5	60	0.37 – 0.52	0.085-0.148
	SAB173	5	79.6	72 ± 6.7	62	0.41 – 0.94	0.106-0.158
	SAB174	7	80.6	76.6 ± 2.2	62	0.39 – 0.57	0.091-0.155
	SAB181	4	77.6	73.1 ± 7.1	64	0.51 – 1.14	0.100-0.185
	SAB187	3	80.5	68.4 ± 11.1	65	0.46 – 1.34	0.109-0.202
qz-tholeiitic basalt	SA76	3	81.3	78.8 ± 4.1	59	0.33 – 0.51	0.087-0.131
	SA77	3	82.1	80.8 ± 2.1	60	0.32 – 0.41	0.081-0.117

Table 4.8 Maximum and mean forsterite content for olivine cores in selected samples from each group B rock type, and the corresponding host rock 100Mg/(Mg + Fe^{2+}) values. Partition coefficients, K_d for Fe^{2+} and Mg are derived from Eq. 1 in Roeder and Emslie (1970) and Ca from Eq. 13 in Libourel (1999), described in the text. n = number of core analyses per sample. Mean values = ± 1 standard deviation.

Group B							
Rock type	Sample	n	Fo_{max}	Fo_{mean}	host rock $\frac{100Mg}{(Mg + Fe^{2+})}$	$K_{d_{Fe-Mg}}^{ol-melt}$ range	$K_{d_{Ca}}^{ol-melt}$ range
nephelinite	SA21	4	76.2	74.9 ± 1.0	62	0.51– 0.58	0.064-0.107
	SA28	3	72.3	71.7 ± 1.3	53	0.43 – 0.48	0.095-0.115
	SA51	5	77.7	76.1 ± 0.9	56	0.36 – 0.42	0.049-0.088
	SAB113	4	81.8	77.2 ± 5.3	64	0.39 – 0.71	0.055-0.169
	SAB135	3	83.2	82.0 ± 2.0	61	0.31 – 0.40	0.049-0.069
	SAB178	3	84.3	82.0 ± 2.1	63	0.31 – 0.42	0.065-0.079
ne-hawaiite	SA02	4	78.3	75.7 ± 2.1	58	0.38 – 0.49	0.052-0.096
	SA25	4	71.8	71.4 ± 0.5	51	0.41 – 0.43	0.085-0.113
	SA29	3	72.9	70.3 ± 2.6	48	0.35 – 0.44	0.072-0.128
	SA65	6	68.1	67.3 ± 0.7	47	0.41 – 0.45	0.077-0.141
basanite	SA12	4	82.9	81.9 ± 0.7	61	0.32 – 0.36	0.051-0.076
	SA27	7	73.9	70.7 ± 3.7	52	0.38 – 0.60	0.066-0.153
	SA37	8	84.6	81.7 ± 2.4	66	0.36 – 0.54	0.061-0.112
	SAB102	4	83.0	81.8 ± 1.2	62	0.33 – 0.39	0.055-0.077
	SAB111	5	83.7	74.7 ± 5.2	63	0.33 – 0.71	0.072-0.106
	SAB128	4	80.1	77.1 ± 3.2	63	0.42 – 0.63	0.064-0.124
	SAB175	7	85.2	79.7 ± 4.9	65	0.32 – 0.71	0.052-0.130
	SAB176	5	83.0	81.0 ± 1.8	66	0.39 – 0.53	0.071-0.099
	SAB177	7	84.5	81.7 ± 2.2	64	0.32 – 0.47	0.066-0.093
	SAB179	4	83.0	79.8 ± 3.7	68	0.43 – 0.71	0.072-0.130
	SAB180	3	84.6	82.8 ± 1.6	66	0.36 – 0.45	0.083-0.084
	SAB204	5	84.8	81.3 ± 2.3	65	0.34 – 0.49	0.071-0.093
mugearite	SA88	4	81.0	70.4 ±11.3	55	0.29 – 0.83	0.118-0.302
alkali ol-basalt	SA54	4	82.7	76.1 ± 8.5	57	0.28 – 0.71	0.084-0.200
	SAB188	5	91.8	88.7 ± 9.6	63	0.15 – 0.40	0.000-0.090
	SAB207	7	84.0	77.1 ± 5.1	64	0.34 – 0.80	0.062-0.156

4.4.4 Olivine – liquid equilibrium

Magnesium and iron partitioning between olivine and host rock

Experimental studies by Roeder and Emslie (1970) show that the distribution coefficient (K_d), relating the partitioning of Mg and Fe^{2+} between olivine and a basaltic liquid, can be estimated from the empirical equation

$$K_{d_{Fe-Mg}}^{ol-melt} = \frac{(X_{FeO}^{Ol})(X_{MgO}^{Liq})}{(X_{FeO}^{Liq})(X_{MgO}^{Ol})}$$

where X represents the mole fraction of FeO and MgO[27]. From their olivine-liquid equilibrium experiments, Roeder and Emslie (1970) demonstrated that the distribution coefficient that best represents the partitioning of Mg and Fe^{2+} between olivine in equilibrium with most basaltic liquid compositions is $K_{d_{Fe-Mg}}^{ol-melt} = 0.30$. Their studies however, also show that K_d values for which olivine and liquid may coexist in equilibrium range from $K_{d_{Fe-Mg}}^{ol-melt} = 0.26$ to 0.36. These values have been reproduced in subsequent experimental studies for a variety of natural and synthetic source compositions (e.g., C1 chondrite, Sp-lherzolite, MORB-Pyrolite), e.g., Takahashi and Kushiro (1983), Gee and Sack (1988), Kinzler and Grove (1992), Trønnes *et al.* (1992), Herzberg and Zhang (1996), Robinson *et al.* (1998). Collectively, these studies show that $K_{d_{Fe-Mg}}^{ol-melt}$ values principally range from 0.26 to 0.36 for pressures between 1 atm and 14 GPa. This pressure range encompasses that estimated by Heming (1980b) at which melting occurred beneath the SAVF within the low velocity zone (i.e., 1.4 to 2.5 GPa). Therefore, by comparing calculated $K_{d_{Fe-Mg}}^{ol-melt}$ values for phenocryst core compositions in the SAVF samples with the "best fit" $K_{d_{Fe-Mg}}^{ol-melt} = 0.30$ curve of Roeder and Emslie (1970), phenocryst–host-rock pairs can be tested for equilibration with respect to Mg and Fe^{2+} partitioning.

Calculated distribution coefficients, $K_{d_{Fe-Mg}}^{ol-melt}$, for selected SAVF samples range from 0.32 to 1.34 for group A (Table 4.7) and 0.15 to 0.83 for group B samples (Table 4.8). In the

---

[27] $K_{d_{Fe-Mg}}^{ol-melt}$ can also be expressed in terms of the Mg/(Mg + Fe^{2+}) value of the liquid ($Mg^{\#}$) and Fo content of olivine crystallising in the liquid where $K_{d_{Fe-Mg}}^{ol-melt} = \frac{Mg_{liq}^{\#}(1 - Fo)}{Fo(1 - Mg_{liq}^{\#})}$.

group A rocks, the majority of samples contain olivine phenocrysts with Fo content smaller than may be expected from their host rock 100Mg/(Mg + Fe^{2+}) value, inferred from crystal populations where maximum Fo contents (Fo_{max}) and average core compositions (Fo_{mean}) are smaller than those predicted by the $K_{d_{Fe-Mg}}^{ol-melt} = 0.36$ curve (Fig. 4.6A). This suggests that the analysed phenocrysts, and by inference possibly most phenocrysts in the sample, are poorly equilibrated. These olivines are comparable to those from similar rock types (e.g., quartz and olivine + hypersthene normative basalts) from eastern Australia (see Ewart, 1989; Fig. 5.3.1A; p. 198). Ewart (1989) proposed that the occurrence of olivine insufficiently magnesian for their host rock 100Mg/(Mg + Fe^{2+}) value could be due to the resorption of more forsteritic olivine that formed during early crystallisation, olivine accumulation, or non-equilibrium crystallisation under subcooling conditions. Only five samples contain olivines that plot within the range of equilibrium $K_{d_{Fe-Mg}}^{ol-melt}$ values (0.26 to 0.36). Of these, only transitional basalt SA07 and qz-tholeiitic basalt SA77 contain olivine populations that have Fo_{mean} compositions within the range of equilibrium $K_{d_{Fe-Mg}}^{ol-melt}$ values, suggesting phenocryst–host-rock equilibrium for the majority of olivines in the sample.

Figure 4.6A shows that in a number of group A host rocks with values of 100Mg/(Mg + Fe^{2+}) in the range 59 to 66, the Fo_{max} values for olivine phenocryst cores remain relatively constant. Over this range, phenocrysts from host rocks with smaller100Mg/(Mg + Fe^{2+}) values (e.g., < 62) tend to plot near the high-value $K_{d_{Fe-Mg}}^{ol-melt}$ curve (i.e., $K_{d_{Fe-Mg}}^{ol-melt} = 0.36$). Conversely, phenocrysts from host rocks that have values of 100Mg/(Mg + Fe^{2+}) > 62 tend to have values of $K_{d_{Fe-Mg}}^{ol-melt} > 0.36$. These trends are comparable to those observed by Dungan (1987) for the tholeiitic lavas of the Servilleta Basalts in the Taos Plateau volcanic field, New Mexico. Dungan (1987) concluded that such trends might be indicative of populations of phenocrysts in hybrid lavas, the result of the mixing of mafic parent magmas.

The majority of group B samples contain olivines with core compositions in equilibrium with their host rock over a range of 100Mg/(Mg + Fe^{2+}) values. However, these crystals commonly occur together with populations of "non-equilibrium" phenocrysts (Fig. 4.6B), a feature comparable to that of the nepheline normative basalts from eastern Australia (see Ewart, 1989; Fig. 5.3.1B; p. 198). In the case of SAVF olivines, this observation most likely reflects: (1) the presence of unzoned or weakly zoned phenocrysts and microphenocrysts in these samples, which typically have smaller Fo contents than their

larger, normally zoned phenocryst counterparts, and (2) the presence of olivines of very different core compositions in the same sample. Heltz (1987) emphasised the importance of mixed populations of normally zoned, reversely zoned, and unzoned phenocrysts as an indicator of crystal disequilibrium in the 1959 Kilauea Iki, Hawaii, lavas.

Phenocryst–host-rock equilibrium for the majority of olivines in basanites SA12 and SAB102 and nephelinites SAB135 and SAB178 is inferred based on Fo_{mean} compositions within the range of equilibrium $K_{d_{Fe-Mg}}^{ol-melt}$ values shown in Fig. 4.6B. In addition, a number of group B samples (predominantly basanites) plot either along or near the "best fit" equilibrium curve $K_{d_{Fe-Mg}}^{ol-melt} = 0.30$ (Fig. 4.6B), suggesting that these phenocrysts formed as equilibrium near-liquidus phases in magmas having their host rock compositions.

In contrast, alkali ol-basalt SAB188 contains olivine phenocrysts more magnesian (Fo_{mean} = 89) than may be expected for the $100Mg/(Mg + Fe^{2+})$ value of their host rock (63) indicated by values of $K_{d_{Fe-Mg}}^{ol-melt} < 0.26$. Gee and Sack (1988) reported similar $K_{d_{Fe-Mg}}^{ol-melt}$ values (i.e., 0.17 – 0.25) in their experimental study of natural melilite nephelinite lavas. They concluded that $K_{d_{Fe-Mg}}^{ol-melt}$ is a function of the silica activity of the host rock where $K_{d_{Fe-Mg}}^{ol-melt}$ increases with decreasing degrees of Si-undersaturation. Later experiments (e.g., Herzberg and Zhang, 1996) however, demonstrate that there is little correlation between $K_{d_{Fe-Mg}}^{ol-melt}$ and highly Si-undersaturated to less Si-undersaturated compositions. Ewart (1989) argued that crystals with $K_{d_{Fe-Mg}}^{ol-melt} < 0.26$ might be relict olivines initially in equilibrium with their peridotite source in the region of melt segregation, or disaggregated olivine-bearing xenoliths.

Ca partitioning between olivine and host rock

Ca is an important minor element in magmatic olivines because:

1. Ca partitioning coefficients may be used to determine whether olivines are equilibrated with their host magma.
2. Experimental studies have determined that below 20kbar, temperature, pressure, and oxygen fugacity (fo_2) have no direct influences on Ca partitioning (e.g., Simkin and Smith, 1970; Ferguson, 1978; Watson, 1979; Jurewicz and Watson, 1988a; Libourel, 1999). Therefore, for most basaltic magma compositions, Ca systematics are useful for interpreting the environment of olivine crystallisation and equilibration.

3. The CaO concentration in olivine is highly dependent on (i) the Fo content of olivine, (ii) the CaO content in the host melt, and (iii) the amount of Al, Na, K, and Fe^{2+} present in the coexisting melt (Libourel, 1999). Therefore, CaO concentrations in equilibrated olivines may provide important information about melt compositions during progressive olivine crystallisation and subsequent magma differentiation.

The dependence of CaO concentration on forsterite content in olivine is well documented (e.g., Watson, 1979; Jurewicz and Watson, 1988a; Libourel, 1999). The overall trend, albeit weak, of increasing CaO with decreasing Fo shown in Fig. 4.4 (p.53) indicates that the CaO concentration in olivine from each rock type is dependent, in part, on the Fo content of the olivine. However, the large scatter of CaO in olivine relative to Fo content suggests that factors other than Fe^{2+} and Mg activity must have influenced Ca solubility. The results of equilibrium experiments of Libourel (1999) for Ca partitioning in olivine-liquid pairs can be used to test naturally occurring SAVF olivine—host-rock pairs for equilibration.

Partition coefficients of Ca between olivines and their host rock were obtained by using the empirical equation (Eq.13) of Libourel (1999):

$$D^{*\,ol-melt}_{CaO} = X^{Ol-melt}_{CaO} / a^{*melt}_{CaO}$$

which accounts for the effect of melt composition on the observed Ca variations in olivine.

The calculated $D^{*\,ol-melt}_{CaO}$ values for olivine cores obtained by this equation range from 0.071 to 0.227 for group A (Table 4.7) and 0.049 to 0.301 for group B (Table 4.8). The range of $D^{*\,ol-melt}_{CaO}$ values for both groups overlap the Ca partitioning equilibrium values determined by Libourel (1999) for iron-poor (Type I) and iron-rich (Type II) chondrites (Fig. 4.7). A large number of group A olivine cores correlate with Type II equilibrium values. In contrast, many group B olivine cores have equilibrium values similar to those of Type I chondrites, suggesting possible source differences for group A and B melts.

Values of $D^{*\,ol-melt}_{CaO}$ positively correlate with $K^{ol-melt}_{d_{Fe-Mg}}$ for group A and B olivines, with a majority of group A and a large number of group B cores falling outside the fields of equilibrium for Fe^{2+}-Mg and Ca (Fig. 4.7). This suggests that olivine—host-rock disequilibrium conditions occur for many olivines from each group, not only with respect to Fe^{2+}-Mg partitioning (see Fig. 4.6), but also with Ca partitioning. The data illustrated in Fig. 4.7 also show that the extent of disequilibrium varies not only between the two rock

groups but also between samples of the same rock type and, by inference, from phenocryst to phenocryst within the same sample. This observation together with those illustrated in Fig. 4.6 suggests that most of the SAVF host rocks are too magnesian to be in equilibrium with the majority of their olivine phenocrysts.

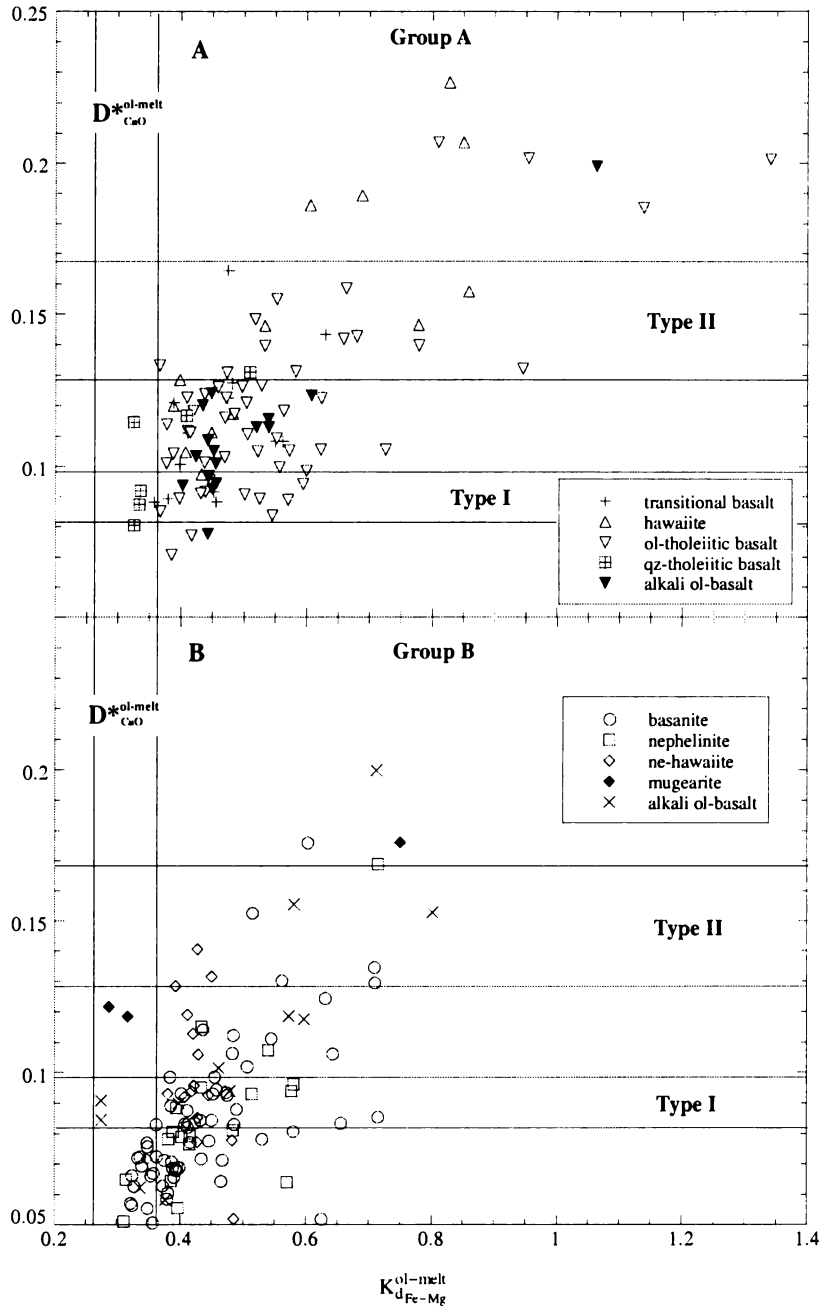

Fig. 4.7 $K_{d_{Fe-Mg}}^{ol-melt}$ *vs.* $D^{*}_{CaO}{}^{ol-melt}$ diagram for olivine phenocryst cores in (A) group A and (B) group B rock samples[28]. Horizontal fields represents the range of $D^{*}_{CaO}{}^{ol-melt}$ for equilibrated olivines in Type I and II chondrites (from Libourel, 1999). The vertical field represents the range of $K_{d_{Fe-Mg}}^{ol-melt}$ for olivine-liquid equilibrium in basaltic melts (from Roeder and Emslie, 1970).

[28] The CaO content of four olivine crystals analysed in group B alkali ol-basalt sample SAB188 was below the detection limits of the electron microprobe and therefore were excluded from the sample set used in Fig. 4.7. These crystals have notably large Fo content (e.g., > Fo_{88}).

Crystallisation temperature estimates

Crystallisation temperatures for olivine can be estimated based on the amount of Ca in olivine normalised to Fo_{90} (Jurewicz and Watson, 1988a). Most olivine phenocrysts in the group A and B rock types crystallised between 1250 and 1350°C (Fig. 4.8). These temperatures are comparable to those calculated by Ewart (1989) for olivine in similar rock types from eastern Australia (see Ewart, 1989, Fig. 5.3.31B, p. 218).

Ewart (1989) noted that olivine temperatures generally correlate positively with the degree of silica undersaturation of their host rock. Olivines with the highest crystallisation temperature tend to occur in the more Si-undersaturated basalts (e.g., basanites and nephelinites) whereas, those with lower crystallisation temperatures were from less Si-undersaturated host rocks (e.g., qz-tholeiitic basalts), which generally have more evolved compositions inferred by their relatively small $100Mg/(Mg + Fe^{2+})$ values.

Although some of the less undersaturated samples in groups A and B shown in Fig.4.8 contain olivine with among the lowest crystallisation temperatures (i.e., group A alkali ol-basalt SAB162, SiO_2 = 48.38 wt.%; group B ne-hawaiite SA02, SiO_2 = 46.33 wt.%) of their respective groups, the temperature–host-rock correlation described by Ewart (1989) is not apparent in the SAVF basalts.

Some samples from each group A rock type with $100Mg/(Mg + Fe^{2+}) \leq 60$ contain olivine with among the lowest crystallisation temperatures (~ 1250°C or less; Fig. 4.8A) whereas SAB188 [$100Mg/(Mg + Fe^{2+}) = 63$] from group B also contains olivine with low crystallisation temperatures (Fig. 4.8B). The $K_{d_{Fe-Mg}}^{ol-melt}$ values for these samples however, indicate olivine/melt disequilibrium (see section 4.4.4.), which suggests incorporation of olivine of exotic origin, e.g., xenocrysts or disaggregated olivine-bearing xenoliths, or possibly magma mixing. In contrast, SA02, SA29, and SA54 [$100Mg/(Mg + Fe^{2+}) = 48$, 58, and 57 respectively] from group B each contain low-temperature olivine ($T \leq$ 1250°C). Their $K_{d_{Fe-Mg}}^{ol-melt}$ values indicate crystal/melt equilibrium for at least some olivine in these samples, which suggests a possible low-temperature, low-pressure crystallisation environment. In addition, SAB175 [$100Mg/(Mg + Fe^{2+}) = 65$] also contains low-temperature olivine in equilibrium. This may be due to crystal formation in a low-temperature, high-pressure environment.

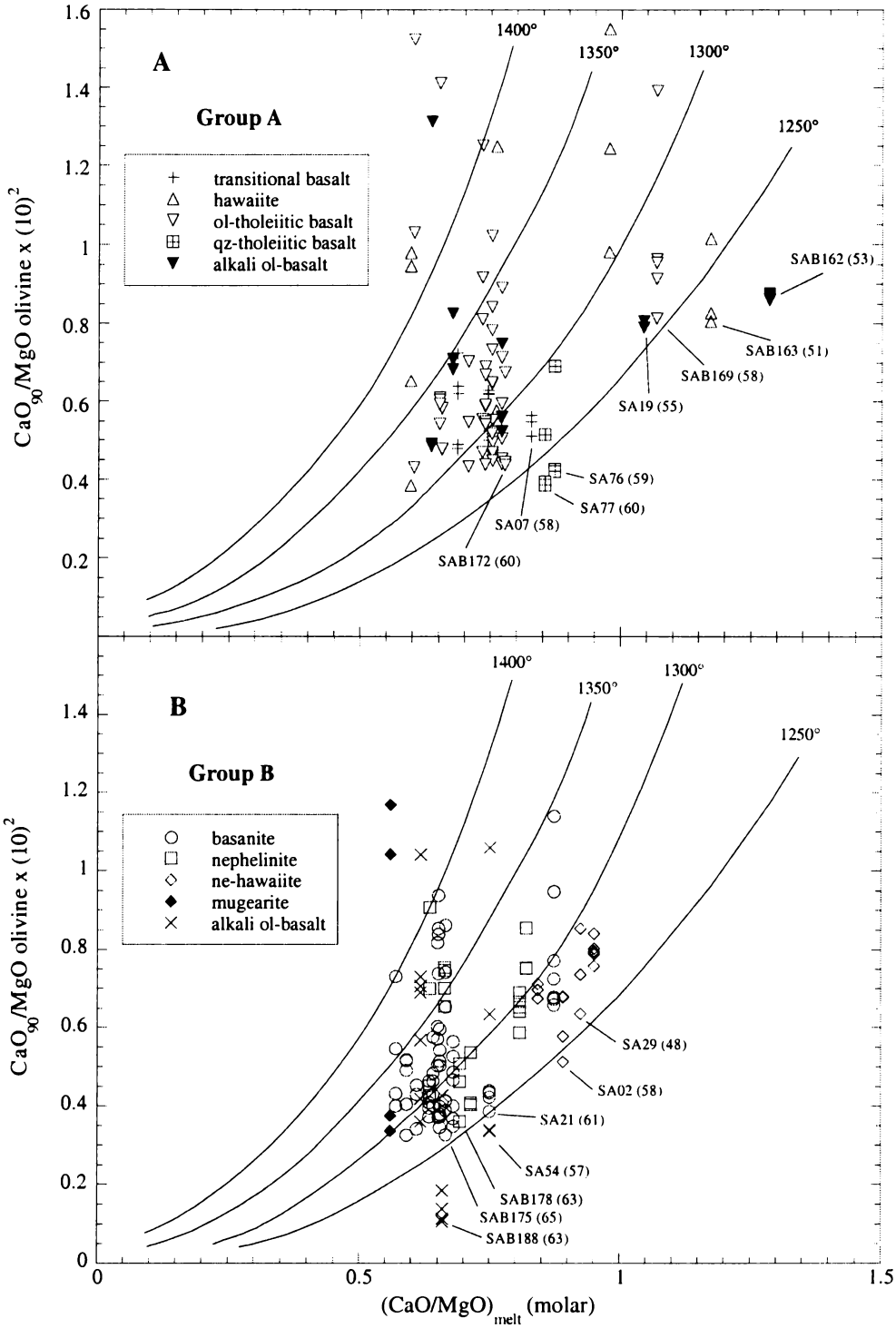

Fig. 4.8 Diagram of CaO_{90}/MgO x (10^2) for olivine vs. molar CaO/MgO for coexisting melt (host rock) referred to in the text. CaO_{90} represents the CaO content of olivine cores normalised to Fo_{90} (after Jurewicz and Watson, 1988a). The isotherms are from Jurewicz and Watson (1988a) and contain an original error estimated to be ± 10°C. Clynne and Borg (1997) estimated that the average error attributed to transcribing the isotherms onto a similar graph to be ± 25°C. Selected samples and their corresponding $100Mg/(Mg + Fe^{2+})$ values (in parentheses) illustrated the relationship between crystallisation temperatures and $100Mg/(Mg + Fe^{2+})$ values, referred to in the text.

4.5 Clinopyroxene

Clinopyroxene is widespread in all South Auckland volcanic field lavas. Occasionally, clinopyroxene is more abundant than olivine in individual samples, primarily in basanites. The abundance of clinopyroxene in all SAVF rock types varies considerably. The modal abundance data given in Table 4.9 for selected samples of each rock type shows that clinopyroxene phenocrysts and microphenocrysts are rare in some samples, most notably the transitional basalts, hawaiites, ol-tholeiitic basalts, and ne-hawaiites, and relatively abundant in other samples of the same rock type. This variation indicates that the modal abundance of clinopyroxene in individual samples is independent of host rock composition and therefore, does not appear to be related to the degree of differentiation of the host rock.

Table 4.9 Summary of modal abundance analyses for clinopyroxene phenocrysts and microphenocrysts in selected South Auckland volcanic field basalts sampled from each rock type within group A and B lavas. Modal abundance based on 1000 point counts. Values for max, min, and mean are given as percentage of total phenocryst phases. n = number of samples counted. Mean = ± 1 standard deviaton.

Group A					Group B				
Rock type	modal abundance				Rock type	modal abundance			
	max	min	mean	n		max	min	mean	n
transitional basalt	2.2	< 0.2	0.8 ± 0.7	15	basanite	20.2	2.0	8.3 ± 4.5	34
hawaiite	10.0	< 0.2	3.7 ± 2.7	29	nephelinite	4.8	0.8	2.9 ± 1.4	14
ol-tholeiitic basalt	8.0	< 0.2	3.2 ± 2.4	35	ne-hawaiite	10.4	< 0.2	4.2 ± 3.8	11
qz-tholeiitic basalt	3.4	0.8	2.5 ± 1.2	4	alkali ol-basalt	11.2	1.2	5.2 ± 1.2	4
alkali ol-basalt	7.8	0.4	3.1 ± 2.5	7	mugearite	4.0	-	-	1

As with olivine, clinopyroxene phenocrysts in individual samples are often petrographically heterogeneous. In thin-section, they display a range of crystal morphologies and sizes suggesting that crystallisation may have occurred over a range of P-T-fO_2 conditions. Additionally, there are marked contrasts in the mineral chemistry between the clinopyroxenes from group A and B rocks, a feature noted by Rafferty and Heming (1979) for most of the alkaline and subalkaline lavas from the SAVF. The diverse mineral chemistry together with variations in non-quadrilateral components[29] such as jadeite (Jd; $NaAlSi_2O_6$), Ca-Tschermak's (CaTs; $CaAl^{VI}Al^{IV}SiO_6$), and Ti-

[29] Non-quadrilateral end-member components e.g., Jd, Ac, CaTs, and CaTi were determined from the procedures given in Lindsley (1983) and Putirka *et al.* (1996).

pyroxene (CaTi; $CaTiAl_2O_6$) in the clinopyroxene of the SAVF rocks suggests a complex crystallisation history and by inference, magma evolution.

Fifteen analyses of the 207 group A and fourteen of the 286 group B clinopyroxene phenocryst core-rim pairs, and groundmass crystals are presented in Tables 4.10 and 4.11 respectively. These analyses were chosen to illustrate (i) the range of compositions within each rock group and (ii) the contrasts in phenocryst compositions between the two rock groups. All clinopyroxene analyses for each rock sample from group A are given in Appendix 6, Tables A6.6 to A6.10 and for group B, Tables A6.25 to A6.29. A summary of mineral chemical data and end-member clinopyroxene compositions for each rock type from groups A and B is presented in Tables 4.12 and 4.13 respectively.

Table 4.10 Electron microprobe analyses of clinopyroxene phenocryst cores, rims, and groundmass from selected group A rock types. Cations are normalised to total four cations per formula unit. End-member compositions are based on normalised cation proportions. Aluminium ($Al_{(total)}$) has been recalculated into tetrahedral (Al^{IV}) and octahedral (Al^{VI}) Al where Al^{IV} is taken as 2-Si and $Al^{VI} = Al_{(total)} - Al^{IV}$. Fe^{3+} is calculated from the charge-balance equation given in Lindsley (1983). *C* = core, R = rim, and G = groundmass.

Rock type	alkali ol-basalt			transitional basalt			hawaiite			ol-tholeiitic basalt			qz-tholeiitic basalt		
Sample	SA33			SA07		SA13	SA20			SAB172		SAB173	SAB198		SA77
Analysis	1728C	1729R	1723G	1907C	1908R	46G	1854C	1855R	1852G	97C	98R	1012G	1582C	1583R	633G
SiO_2	49.87	46.96	49.73	49.44	47.40	51.10	48.19	50.10	49.71	50.67	49.44	51.71	50.61	50.96	51.86
TiO_2	1.31	1.62	0.92	0.77	1.99	1.15	1.80	1.27	1.52	1.40	1.85	0.58	0.91	1.07	0.64
Al_2O_3	3.43	2.70	0.84	5.30	4.81	2.56	6.02	1.67	2.24	2.95	2.16	0.55	2.53	2.11	0.93
Cr_2O_3	0.79	-	-	1.05	0.26	-	0.43	-	-	-	-	-	0.65	-	-
FeO*	7.68	18.64	20.43	6.61	10.16	10.81	8.40	12.69	14.98	11.93	18.23	22.44	8.41	9.81	22.10
MnO	-	0.26	0.41	-	-	0.30	-	0.22	0.34	0.39	0.26	0.51	-	0.22	0.42
MgO	14.48	10.29	8.13	15.67	13.29	15.19	13.53	12.97	11.02	14.92	11.29	19.04	15.85	14.53	17.63
CaO	21.35	18.72	19.76	18.91	20.10	18.75	21.53	19.72	19.78	17.56	17.30	4.28	19.45	20.23	5.89
Na_2O	0.52	0.90	0.68	0.90	0.89	-	1.03	0.75	0.80	-	-	-	0.58	0.72	0.00
Total	99.43	100.09	100.90	98.65	98.90	99.86	100.93	99.39	100.39	99.82	100.53	99.11	98.99	99.65	99.47
Cations on basis of 6 oxygens															
Si	1.857	1.804	1.922	1.831	1.783	1.910	1.765	1.895	1.855	1.901	1.898	1.971	1.885	1.898	1.978
Ti	0.037	0.047	0.027	0.021	0.056	0.033	0.050	0.036	0.043	0.039	0.053	0.017	0.026	0.030	0.019
$Al_{(total)}$	0.150	0.121	0.038	0.231	0.214	0.113	0.260	0.074	0.101	0.131	0.098	0.025	0.111	0.093	0.042
Al^{IV}	0.131	0.121	0.038	0.169	0.214	0.90	0.235	0.074	0.099	0.099	0.098	0.025	0.111	0.093	0.022
Al^{VI}	0.020	-	-	0.062	-	0.023	0.025	-	-	0.032	-	-	-	-	0.020
Cr	0.023	-	-	0.031	0.008	-	0.012	-	-	-	-	-	0.019	-	-
Fe^{3+}	0.077	0.221	0.115	0.098	0.166	0.002	0.173	0.057	0.074	-	-	-	0.082	0.086	-
Fe^{2+}	0.162	0.371	0.546	0.107	0.153	0.336	0.085	0.345	0.402	0.375	0.585	0.715	0.180	0.220	0.705
Mn	-	0.008	0.014	-	-	0.01	-	0.007	0.011	0.013	0.008	0.016	-	0.007	0.013
Mg	0.804	0.583	0.469	0.865	0.745	0.846	0.739	0.731	0.623	0.835	0.646	1.082	0.880	0.806	1.002
Ca	0.852	0.763	0.818	0.750	0.810	0.751	0.844	0.800	0.804	0.706	0.712	0.175	0.776	0.808	0.241
Na	0.038	0.066	0.051	0.065	0.065	-	0.073	0.055	0.059	-	-	-	0.042	0.052	-
Al^{IV}/Al^{VI}	20.4	-	-	2.7	-	3.9	9.7	-	-	3.1	-	-	-	-	1.1
$\frac{100Mg}{(Mg+\Sigma Fe)}$	0.77	0.50	0.42	0.81	0.7	0.71	0.74	0.65	0.57	0.69	0.52	0.60	0.77	0.73	0.59
Fe^{3+}/Fe^{2+}	0.47	0.19	0.06	0.91	1.08	0.01	2.04	0.16	0.18	-	-	-	0.46	0.39	-
End-member compositions															
Wo	45.0	39.2	41.7	41.2	43.2	38.6	45.9	41.2	42.0	36.6	36.5	8.8	40.5	41.9	12.3
En	42.4	30.0	23.9	47.5	39.8	43.5	40.1	37.7	32.6	43.3	33.1	54.4	45.9	41.9	51.1
Fs	12.6	30.9	34.4	11.2	17.0	17.9	14.0	21.1	25.4	20.1	30.4	36.8	13.7	16.2	36.6

* Total Fe reported as FeO

Table 4.11 Electron microprobe analyses of clinopyroxene phenocryst cores and rims and groundmass from selected group B rock types. Cations are normalised to total four cations per formula unit. End-member compositions are based on normalised cation proportions. Aluminium ($Al_{(total)}$) has been recalculated into tetrahedral (Al^{IV}) and octahedral (Al^{VI}) Al where Al^{IV} is taken as 2-Si and $Al^{VI} = Al_{(total)} - Al^{IV}$. Fe^{3+} is calculated from the charge-balance equation given in Lindsley (1983). C = core, R = rim, and G = groundmass.

Rock type	alkali ol-basalt			basanite			nephelinite			ne-hawaiite			mugearite	
Sample	SAB207		SA54	SAB180		SAB175	SAB113		SA51	SA65		SA29	SA88	
Analysis	1613C	1614R	1690G	1309C	1310R	1057G	239C	240R	1468G	1544C	1545R	156G	50C	51R
SiO_2	46.83	40.89	50.27	46.60	48.29	45.57	49.35	45.41	42.35	49.09	45.35	47.15	51.11	51.18
TiO_2	2.26	5.38	1.41	2.20	1.87	3.16	1.61	3.37	4.71	1.57	3.04	2.75	1.15	1.37
Al_2O_3	6.33	11.22	1.85	7.08	4.08	7.93	4.60	7.55	8.94	3.34	6.96	5.93	2.62	2.26
Cr_2O_3	0.40	-	-	0.45	-	0.62	-	-	-	-	-	-	-	-
FeO*	7.28	8.89	10.79	6.86	9.07	7.24	6.78	7.80	9.11	8.86	9.51	8.98	8.42	8.83
MnO	-	-	0.26	-	0.23	-	0.23	-	-	0.25	-	-	0.21	0.24
MgO	13.19	10.42	11.96	12.62	12.07	12.42	13.70	11.31	10.44	13.14	11.26	11.49	14.77	14.20
CaO	22.35	22.98	22.09	22.25	22.58	23.04	22.69	22.69	22.53	22.22	22.18	22.56	20.81	21.42
Na_2O	0.83	0.86	1.08	0.54	0.44	-	-	0.50	0.96	0.86	1.05	0.39	-	-
Total	99.47	100.64	99.71	98.60	98.63	99.98	98.96	98.63	99.04	99.33	99.35	99.25	99.09	99.50
Cations on basis of 6 oxygen														
Si	1.740	1.534	1.891	1.730	1.834	1.703	1.852	1.722	1.593	1.837	1.705	1.783	1.918	1.920
Ti	0.063	0.15	0.04	0.063	0.054	0.088	0.045	0.096	0.135	0.044	0.086	0.078	0.033	0.039
$Al_{(total)}$	0.278	0.490	0.082	0.317	0.182	0.349	0.204	0.337	0.401	0.148	0.308	0.264	0.116	0.100
Al^{IV}	0.260	0.466	0.082	0.270	0.166	0.297	0.148	0.278	0.401	0.148	0.295	0.217	0.082	0.080
Al^{VI}	0.018	0.024	-	0.047	0.016	0.052	0.056	0.059	-	-	0.013	0.047	0.034	0.020
Cr	0.012	-	-	0.014	-	0.019	-	-	-	-	-	-	-	-
Fe^{3+}	0.163	0.203	0.082	0.123	0.076	0.049	0.002	0.062	0.202	0.124	0.185	0.042	-	0.277
Fe^{2+}	0.063	0.073	0.258	0.095	0.212	0.177	0.211	0.184	0.088	0.154	0.114	0.243	0.265	0.008
Mn	-	-	0.008	-	0.007	-	0.007	-	-	0.008	-	-	0.007	0.008
Mg	0.731	0.576	0.671	0.714	0.683	0.692	0.766	0.639	0.592	0.733	0.631	0.648	0.826	0.794
Ca	0.890	0.913	0.890	0.905	0.919	0.923	0.913	0.922	0.919	0.891	0.894	0.914	0.837	0.862
Na	0.060	0.061	0.079	0.04	0.033	-	-	0.037	0.071	0.063	0.076	0.028	-	-
Al^{IV}/Al^{VI}	14.6	19.0	-	5.7	10.3	5.7	2.7	4.7	-	-	21.7	4.6	2.4	3.9
Fe^{3+}/Fe^{2+}	2.6	2.8	0.3	1.3	0.4	0.3	-	0.3	2.3	0.8	1.6	0.2	-	-
$\frac{100Mg}{(Mg + \Sigma Fe)}$	0.76	0.68	0.66	0.77	0.70	0.75	0.78	0.72	0.67	0.73	0.68	0.70	0.76	0.74
End-member compositions														
Wo	48.2	51.8	46.6	49.3	48.4	50.1	48.1	51.0	51.0	46.7	49.0	49.5	43.3	44.4
En	39.6	32.6	35.1	38.9	36.0	37.6	40.4	35.3	32.9	38.4	34.6	35.1	42.7	40.9
Fs	12.3	15.6	18.2	11.9	15.6	12.3	11.6	13.7	16.1	14.9	16.4	15.4	14.0	14.7

*Total Fe reported as FeO

Table 4.12 Summary of clinopyroxene core, rim, and groundmass compositions (min-max) from selected samples from the group A type rocks in the SAVF. Values for Cr_2O_3 and Na_2O preceded by "<" indicate that these oxides were below the detection limits of the electron microprobe in some of the crystals in individual samples. Values for Al^{VI} preceded by "<" indicate that insufficient Al occurred in the crystal to go into the octahedral site for some of the analysed crystals. Values for Fe^{3+} preceded by "<" indicate that, based on Fe recalculations, only Fe^{2+} is present in some of the analysed crystals. n.d. = not detected. n = number of analyses.

Rock type	alkali ol-basalt			transitional basalt			hawaiite		
	Core n=14	Rim n=6	Groundmass n=14	Core n=5	Rim n=4	Groundmass n=11	Core n=14	Rim n=10	Groundmass n=15
SiO_2	45.99 - 50.47	46.59 - 49.53	48.08 - 50.83	49.44 - 51.52	47.40 - 51.13	45.24 - 51.10	47.87 - 51.86	47.98 - 50.82	48.53 - 50.84
TiO_2	0.78 - 2.30	1.62 - 2.42	0.92 - 2.25	0.71 - 1.28	1.03 - 1.99	1.15 - 2.32	0.79 - 2.12	1.15 - 2.27	1.18 - 2.09
Al_2O_3	1.63 - 7.91	2.70 - 5.52	0.84 - 4.63	2.73 - 5.30	2.44 - 4.81	2.43 - 4.62	1.99 - 6.12	1.67 - 5.73	1.52 - 4.04
Cr_2O_3	<0.91	<0.77	n.d.	<1.10	<0.36	<0.34	<1.04	<0.88	<0.97
FeO*	6.81 - 13.69	7.57 - 18.64	9.51 - 20.43	6.61 - 9.91	7.63 - 10.16	9.56 - 12.29	7.18 - 10.22	7.50 - 12.69	7.29 – 14.98
MgO	11.96 - 15.47	10.29 - 13.27	8.13 - 13.41	14.25 - 16.43	13.29 - 15.68	13.03 - 18.58	13.21 - 15.88	12.31 - 14.23	11.02 - 14.67
CaO	19.38 - 21.89	18.72 - 21.94	19.76 - 21.79	18.06 - 20.02	19.43 - 21.35	15.40 - 20.16	19.88 - 21.94	19.72 – 22.04	19.78 - 21.83
Na_2O	<1.09	0.70 - 1.01	<1.91	<0.98	<0.89	<1.03	<1.07	<0.89	<1.00
Cations on basis of 6 oxygen									
Si	1.714 - 1.904	1.759 - 1.857	1.808 - 1.922	1.831 - 1.917	1.783 - 1.898	1.679 - 1.910	1.764 - 1.939	1.776 - 1.943	1.815 - 1.935
Ti	0.022 - 0.065	0.047 - 0.069	0.027 - 0.065	0.020 - 0.036	0.029 - 0.056	0.033 - 0.065	0.021 - 0.059	0.033 - 0.065	0.033 - 0.059
Al_{total}	0.073 - 0.348	0.121 - 0.244	0.038 - 0.208	0.120 - 0.231	0.107 - 0.214	0.108 - 0.207	0.088 - 0.266	0.074 - 0.250	0.068 - 0.176
Al^{IV}	0.073 - 0.286	0.121 - 0.233	0.038 - 0.167	0.083 - 0.169	0.102 - 0.217	0.090 - 0.207	0.061 - 0.236	0.057 - 0.224	0.065 - 0.176
Al^{VI}	<0.007 - 0.081	<0.001 - 0.014	<0.004 - 0.057	0.037 - 0.062	<0.001 - 0.059	<0.001 - 0.023	<0.001 - 0.065	<0.001 - 0.037	<0.001 - 0.019
Cr	<0.011 - 0.027	<0.001 - 0.022	n.d.	<0.001 - 0.032	<0.001 - 0.011	<0.001 - 0.010	<0.001 - 0.031	<0.001 - 0.026	<0.001 - 0.028
Fe^{3+}	<0.039 - 0.166	0.082 - 0.169	<0.027 - 0.156	<0.001 - 0.124	<0.001 - 0.166	0.002 - 0.159	<0.001 - 0.176	<0.001 - 0.153	<0.001 - 0.110
Fe^{2+}	0.070 - 0.380	0.068 - 0.499	0.164 - 0.625	0.084 - 0.315	0.160 - 0.355	0.160 - 0.355	0.074 - 0.289	0.098 - 0.397	0.126 - 0.416
Mg	0.675 - 0.860	0.583 - 0.741	0.469 - 0.751	0.807 - 0.903	0.745 - 0.868	0.732 - 1.028	0.737 - 0.856	0.697 - 0.800	0.623 - 0.809
Ca	0.766 - 0.888	0.763 - 0.883	0.807 - 0.880	0.717 - 0.798	0.773 - 0.849	0.613 - 0.821	0.771 - 0.877	0.800 - 0.877	0.797 - 0.867
Na	<0.038 - 0.080	0.051 - 0.074	<0.030 - 0.141	<0.001 - 0.070	<0.001 - 0.065	<0.001 - 0.074	<0.001 - 0.075	<0.001 - 0.065	<0.001 - 0.073
Al^{IV}/Al^{VI}	<1.8 – 25.6	<0.1 - 15.8	<1.9 - 24.5	2.1 - 4.0	<0.1 - 51.9	<0.1 - 43.5	<0.1 - 38.5	<0.1 - 8.6	<0.1 - 7.4
Fe^{3+}/Fe^{2+}	<0.1 - 2.3	0.2 - 2.5	<0.1 – 1.0	<0.1 - 1.5	<0.1 - 1.1	<0.1 - 1.0	<0.1 - 2.4	<0.1 - 1.6	<0.01 - 0.8
$\frac{100Mg}{(Mg+\Sigma Fe)}$	62 - 80			72 - 81			70 - 80		
$\frac{100Mg}{(Mg+Fe^{2+})}$	53 - 64			58 - 64			51 - 63		
Wo	41.5 - 46.8	39.2 - 47.0	41.4 - 46.7	39.1 - 41.2	39.9 - 44.4	30.1 - 43.5	41.7 - 46.9	41.2 - 47.0	40.9 - 45.6
En	35.7 - 46.0	29.9 - 40.1	23.9 – 39.0	42.1 - 49.3	39.8 - 44.8	38.6 - 50.5	38.5 - 46.3	36.4 - 41.4	32.4 - 42.6
Fs	11.4 - 22.7	12.8 - 30.9	15.9 - 34.4	11.2 - 16.8	12.8 - 17.0	15.6 - 19.6	11.8 - 17.1	12.4 - 21.1	11.9 - 25.4

*Total Fe reported as FeO

Table 4.12 Summary of clinopyroxene core, rim, and groundmass compositions for group A rocks continued.

Rock type	ol-tholeiitic basalt			qz-tholeiitic basalt		
	Core n=18	Rim n=10	Groundmass n=58	Core n=13	Rim n=7	Groundmass n=9
SiO_2	49.02 - 52.09	49.44 - 52.28	47.33 - 51.87	49.46 - 54.07	50.36 - 53.07	48.72 - 52.51
TiO_2	0.82 - 2.42	0.87 - 1.85	0.45 - 2.02	0.59 - 1.67	0.52 - 1.07	0.61 - 1.91
Al_2O_3	2.55 - 5.28	1.27 - 4.57	0.55 - 5.88	2.00 - 5.85	1.58 - 3.98	0.71 - 2.73
Cr_2O_3	n.d.	n.d.	<0.82	<0.86	<0.57	n.d.
FeO*	7.04 - 11.93	7.3 - 18.23	7.93 - 28.16	7.01 - 12.45	7.24 - 11.67	9.68 - 22.47
MgO	12.27 - 15.54	11.29 - 15.34	5.52 - 19.78	13.24 - 17.55	14.27 - 17.73	10.86 - 18.97
CaO	17.56 - 21.32	15.69 - 21.00	4.10 - 21.13	16.84 - 20.94	17.08 - 20.46	3.93 - 20.39
Na_2O	<0.49	<0.38	<1.07	<0.99	<0.78	<0.88
Cations on basis of 6 oxygen						
Si	1.859 - 1.952	1.853 - 1.966	1.864 - 1.971	1.830 - 2.009	1.873 - 1.965	1.863 - 1.982
Ti	0.022 - 0.070	0.025 - 0.053	0.013 - 0.059	0.016 - 0.047	0.014 - 0.030	0.017 - 0.055
Al_{total}	0.064 - 0.228	0.057 - 0.201	0.025 - 0.262	0.042 - 0.257	0.069 - 0.174	0.032 - 0.122
Al^{IV}	0.048 - 0.141	0.034 - 0.147	0.025 - 0.136	<0.001 - 0.170	0.035 - 0.127	0.018 - 0.122
Al^{VI}	0.013 - 0.095	<0.001 - 0.076	<0.001 - 0.188	<0.001 - 0.257	<0.001 - 0.047	<0.001 - 0.032
Cr	n.d.	n.d.	<0.001 - 0.025	<0.001 - 0.025	<0.001 - 0.017	n.d.
Fe^{3+}	<0.001 - 0.029	<0.001 - 0.054	<0.001 - 0.038	<0.001 - 0.127	<0.001 - 0.092	<0.001 - 0.087
Fe^{2+}	0.188 - 0.426	0.173 - 0.585	0.248 - 0.928	0.094 - 0.705	0.177 - 0.364	0.253 - 0.716
Mg	0.708 - 0.861	0.646 - 0.859	0.334 - 1.117	0.733 - 1.002	0.791 - 0.979	0.622 - 1.078
Ca	0.706 - 0.861	0.647 - 0.845	0.166 - 0.850	0.241 - 0.829	0.750 - 0.717	0.161 - 0.827
Na	<0.001 - 0.035	<0.001 - 0.028	<0.001 - 0.081	<0.001 - 0.071	<0.001 - 0.056	<0.001 - 0.065
Al^{IV}/Al^{VI}	1.4 - 8.8	<0.1 - 5.0	<0.1 - 51.7	<0.1 - 7.5	<0.1 - 3.6	<0.1 - 2.2
Fe^{3+}/Fe^{2+}	<0.01 - 0.2	<0.01 - 0.3	<0.01 - 0.1	<0.1 - 1.4	<0.01 - 0.5	<0.01 - 0.3
$\frac{100Mg}{(Mg+\Sigma Fe)}$	65 - 80			68 - 80		
$\frac{100Mg}{(Mg+Fe^{2+})}$	58 - 65			57 - 60		
Wo	36.6 - 44.9	33.4 - 44.3	8.3 - 43.9	35.5 - 44.1	34.9 – 44.0	8.2 - 43.3
En	37.5 - 45.9	33.1 - 44.7	16.8 - 55.9	42.1 - 50.2	41.8 - 50.2	31.9 - 54.8
Fs	11.6 - 20.6	12.5 - 30.4	13.1 - 48.9	11.7 - 20.6	12.0 - 19.3	15.9 - 37.1

*Total Fe reported as FeO.

Table 4.13 Summary of clinopyroxene core, rim, and groundmass compositions (min-max) from selected samples from the group B type rocks in the SAVF. Values for Cr_2O_3 and Na_2O preceded by "<" indicate that these oxides were below the detection limits of the electron microprobe in some of the crystals in individual samples. Values for Al^{VI} preceded by "<" indicate that insufficient Al occurred in the crystal to go into the octahedral site for some of the analysed crystals. Values for Fe^{3+} preceded by "<" indicate that, based on Fe recalculations, only Fe^{2+} is present in some of the analysed crystals. n.d. = not detected, n = number of analyses.

Rock type	alkali ol-basalt			basanite			nephelinite		
	Core n=11	Rim n=11	Groundmass n=13	Core n=54	Rim n=37	Groundmass n=56	Core n=17	Rim n=15	Groundmass n=20
SiO_2	43.37 - 49.92	40.89 - 49.34	44.18 - 51.57	42.40 - 50.76	40.90 - 49.95	39.38 - 49.92	40.74 - 49.42	40.31 - 47.23	40.95 - 51.42
TiO_2	0.99 - 3.30	1.52 - 5.38	0.89 - 4.74	1.21 - 4.60	1.71 - 5.23	1.14 - 6.51	1.61 - 5.19	2.63 - 6.50	0.74 - 4.83
Al_2O_3	3.58 - 8.97	4.07 - 11.22	1.85 - 7.95	4.19 - 10.26	4.08 - 11.85	2.51 - 11.81	3.14 - 10.38	5.43 - 14.04	3.30 - 23.94
Cr_2O_3	<0.70	<0.43	<0.31	<1.08	<0.36	<0.62	<0.41	<0.22	n.d.
FeO*	6.91 - 8.90	7.56 - 9.14	7.19 - 10.92	5.96 - 9.04	6.46 - 9.65	6.76 - 16.30	6.78 - 9.12	6.98 - 9.59	6.08 - 14.89
MgO	11.87 - 15.22	10.42 - 13.84	9.98 - 15.29	10.47 - 14.52	9.09 - 13.13	8.23 - 14.18	10.32 - 13.70	6.71 - 12.30	1.37 - 14.87
CaO	19.41 - 22.65	21.66 - 23.28	20.64 - 23.80	20.75 - 23.32	19.47 - 23.05	19.99 - 21.10	22.28 - 23.13	18.51 - 25.31	2.50 - 23.03
Na_2O	0.79 - 1.42	0.84 - 10.03	0.76 - 1.22	<0.77	<2.66	<1.23	<1.13	0.43 - 3.71	0.40 - 11.95
Cations on basis of 6 oxygen									
Si	1.623 - 1.832	1.534 - 1.822	1.652 - 1.896	1.589 - 1.883	1.603 - 1.880	1.510 - 1.893	1.533 - 1.852	1.548 - 1.767	1.533 - 1.919
Ti	0.027 - 0.093	0.042 - 0.150	0.024 - 0.137	0.034 - 0.132	0.049 - 0.137	0.033 - 0.188	0.045 - 0.147	0.074 - 0.188	0.021 - 0.138
Al_{total}	0.157 - 0.396	0.176 - 0.490	0.082 - 0.349	0.187 - 0.456	0.182 - 0.497	0.115 - 0.534	0.138 - 0.461	0.240 - 0.612	0.145 - 0.449
Al^{IV}	0.157 - 0.377	0.176 - 0.466	0.082 - 0.348	0.117 - 0.411	0.120 - 0.397	0.107 - 0.490	0.138 - 0.461	0.233 - 0.452	0.081 - 0.401
Al^{VI}	<0.001 - 0.067	<0.001 - 0.029	<0.001 - 0.017	<0.001 - 0.136	0.016 - 0.164	<0.001 - 0.083	<0.001 - 0.082	<0.001 - 0.219	<0.001 - 0.064
Cr	<0.001 - 0.020	<0.001 - 0.012	<0.001 - 0.009	<0.001 - 0.032	<0.001 - 0.011	<0.001 - 0.019	<0.001 - 0.019	<0.001 - 0.006	n.d.
Fe^{3+}	0.110 - 0.229	0.122 - 0.203	0.045 - 0.215	<0.001 - 0.159	<0.001 - 0.156	<0.001 - 0.188	<0.001 - 0.229	0.042 - 0.222	0.031 - 0.233
Fe^{2+}	0.045 - 0.167	0.073 - 0.161	0.047 - 0.302	0.089 - 0.254	0.090 - 0.289	0.089 - 0.406	0.044 - 0.246	0.037 - 0.235	0.055 - 0.320
Mg	0.662 - 0.830	0.576 - 0.761	0.572 - 0.830	0.598 - 0.809	0.514 - 0.735	0.478 - 0.788	0.578 - 0.766	0.370 - 0.679	0.554 - 0.840
Ca	0.761 - 0.903	0.857 - 0.930	0.850 - 0.946	0.838 - 0.941	0.770 - 0.935	0.834 - 0.933	0.898 - 0.937	0.734 - 1.034	0.699 - 0.928
Na	0.057 - 0.101	0.060 - 0.074	0.055 - 0.091	<0.001 - 0.058	<0.001 - 0.191	<0.001 - 0.093	<0.001 - 0.081	0.031 - 0.266	0.028 - 0.114
Al^{IV}/Al^{VI}	<0.1 - 19.7	<0.1 - 42.3	<0.1 - 15.9	<0.1 - 49.9	1.8 - 11.1	<0.1- 20.7	<0.1 - 22.8	<0.1 - 73.0	<0.1 - 37.7
Fe^{3+}/Fe^{2+}	0.7 - 5.1	0.8 - 2.8	0.2 - 4.6	<0.1 - 1.7	<0.1 - 1.7	<0.1 - 2.1	<0.1 - 5.1	0.2 - 5.7	0.1 - 4.2
$\frac{100Mg}{(Mg+\Sigma Fe)}$	71 - 80			68 - 81			45 - 78		
$\frac{100Mg}{(Mg+Fe^{2+})}$	57 -64			52 - 68			53 - 64		
Wo	42.1 - 49.5	46.2 - 51.8	45.0 - 50.9	46.0 - 51.3	48.0 - 52.8	44.8 - 53.0	47.8 - 52.2	49.1 - 55.6	27.3 - 52.7
En	36.8 - 45.9	32.6 - 41.1	32.1 - 43.5	33.5 - 43.1	29.8 - 40.0	25.7 - 41.1	32.2 - 40.4	27.1 - 36.6	20.7 - 41.6
Fs	11.4 - 15.2	11.4 - 15.2	11.4 - 15.2	9.9 - 16.3	11.8 - 19.7	11.0 - 29.4	11.6 - 16.1	11.9 - 19.1	12.7 - 51.9

*Total Fe reported as FeO.

Table 4.13 Summary of clinopyroxene core, rim, and groundmass compositions for group B rocks continued.

Rock type	ne-hawaiite			mugearite		
	Core n=15	Rim n=14	Groundmass n=15	Core n=4	Rim n=3	Groundmass n=0
SiO_2	44.69 - 50.52	44.93 - 49.86	45.68 - 51.05	50.14- -51.32	50.34 - 51.18	-
TiO_2	1.19 - 3.43	1.36 - 3.46	1.04 - 2.89	1.02 - 1.60	1.01 - 1.43	-
Al_2O_3	2.80 - 7.58	2.94 - 7.88	2.23 - 16.08	1.50 - 4.51	1.76 - 3.11	-
Cr_2O_3	<0.49	n.d.	<0.29	n.d.	n.d.	-
FeO*	7.36 - 10.10	7.93 - 9.74	5.77 - 14.18	7.03 - 12.00	8.35 - 11.78	-
MgO	11.04 - 13.72	10.70 - 13.39	5.96 - 13.48	12.98 - 14.82	13.19 - 14.20	-
CaO	20.26 - 22.62	21.13 - 23.20	13.26 - 22.63	20.71 - 21.84	20.49 - 21.49	-
Na_2O	<1.53	0.42 - 1.38	0.39 - 2.87	n.d.	n.d.	-
Cations on basis of 6 oxygen						
Si	1.675 - 1.904	1.677 - 1.856	1.721 - 1.891	1.869 - 1.941	1.896 - 1.935	-
Ti	0.033 - 0.097	0.038 - 0.099	0.030 - 0.082	0.028 - 0.045	0.029 - 0.040	-
Al_{total}	0.122 - 0.335	0.129 - 0.353	0.100 - 0.721	0.067 - 0.197	0.079 - 0.138	-
Al^{IV}	0.096 - 0.325	0.129 - 0.323	0.100 - 0.278	0.059 - 0.131	0.065 - 0.104	-
Al^{VI}	<0.001 - 0.091	<0.001 - 0.097	<0.001 - 0.587	0.008 - 0.065	0.014 - 0.034	-
Cr	<0.001 - 0.014	n.d.	<0.001 - 0.009	n.d.	n.d.	-
Fe^{3+}	<0.001 - 0.199	<0.001 - 0.186	<0.001 - 0.204	<0.001 - 0.010	-	-
Fe^{2+}	0.088 - 0.266	0.083 - 0.297	0.094 - 0.303	0.208 - 0.380	0.263 - 0.373	-
Mg	0.617 - 0.759	0.609 - 0.747	0.338 - 0.747	0.732 - 0.826	0.743 - 0.794	-
Ca	0.799 - 0.916	0.847 - 0.925	0.540 - 0.914	0.837 - 0.865	0.830 - 0.867	-
Na	<0.001 - 0.109	0.031 - 0.100	0.028 - 0.213	n.d.	n.d.	-
$Al^{IV}:Al^{VI}$	<0.1 - 33.4	<0.1 - 88.1	<0.1 - 63.2	2.0 - 7.5	3.0 - 4.8	-
Fe^{3+}/Fe^{2+}	<0.1 - 1.8	<0.1 - 2.2	<0.1 - 2.2	<0.01- 0.05	-	-
$\frac{100Mg}{(Mg+\Sigma Fe)}$	67 - 76			66 - 79		
$\frac{100Mg}{(Mg+Fe^{2+})}$	47 - 58			55		
Wo	45.1 - 49.3	46.8 - 50.1	45.2 - 50.9	42.9 - 45.4	42.4 - 45.0	-
En	33.9 - 40.9	33.9 - 39.4	28.4 - 39.0	37.4 - 42.9	37.9 - 40.9	-
Fs	12.8 - 17.4	13.6 - 16.7	13.7 - 24.7	11.8 - 19.7	14.1 - 19.6	-

*Total Fe reported as FeO

4.5.1 Group A clinopyroxene

Clinopyroxene in the group A rocks occurs principally as colourless to pale brown to pale greenish brown subhedral phenocrysts and subhedral and anhedral microphenocrysts, which are often observed only in glomeroporphyritic clots. Megacrysts are rare. Many of the megacrysts and phenocrysts contain relatively small (e.g., < 50 μm) titanomagnetite inclusions and other small, unidentified opaque and clear inclusions, often resulting in sieve-like textures. The clear (possibly glass) and opaque inclusions could not be analysed by electron microprobe due to their small size. In the groundmass, clinopyroxene occurs as abundant anhedral grains often in aggregates with other groundmass phases.

Many phenocrysts are compositionally zoned but in thin-section have optically continuous rims indistinguishable from adjacent cores. Electron microprobe analytical results indicate that unzoned crystals are relatively abundant and commonly occur together with zoned crystals in the same sample. Some alkali ol-basalt and transitional basalt samples also contain pale purplish brown phenocrysts that are slightly titaniferous.

Tables 4.12 and 4.13 show that, of the two rock groups, the clinopyroxene in the group A rocks have, overall, the most diverse range of phenocryst and groundmass compositions. Much of this diversity occurs between individual crystals from the same rock sample. In general, clinopyroxene phenocrysts, microphenocrysts, and groundmass crystals span a relatively broad range of compositions comparable to clinopyroxenes in similar basaltic rock types from the intraplate volcanic fields of eastern Australia (e.g., Ewart, 1989). The transitional basalts, hawaiites, and alkali ol-basalts have the most restricted range of phenocryst ($Wo_{46.9\text{-}39.1}En_{49.3\text{-}35.7}Fs_{22.7\text{-}11.3}$) and groundmass ($Wo_{46.7\text{-}30.1}En_{50.5\text{-}23.9}Fs_{34.4\text{-}11.9}$) compositions, predominantly calcic augite (Table 4.12; Figs. 4.9A,B, and E). A number of hawaiite and alkali ol-basalt samples contain Wo-enriched phenocrysts and groundmass crystals with compositions similar to those in the hawaiites from the Ngatutura Basalts (Briggs *et al.*, 1990). These crystals project predominantly in the diopside field of the (Wo; $Ca_2Si_2O_6$)-(En; $Mg_2Si_2O_6$)-(Fs; $Fe_2Si_2O_6$) ternary system, described in Morimoto *et al.* (1988) (Figs. 4.9B and E). Additionally, the alkali ol-basalt and hawaiite samples also contain populations of less calcic clinopyroxene similar to those in the hawaiites from the Okete Volcanics (Briggs and Goles, 1984). However, unlike the alkali ol-basalt, transitional basalt, or hawaiite rocks from the eastern Australia fields, sub-calcic augite phenocrysts were not observed in thin-section or detected by electron microprobe analyses in similar rocks from the SAVF.

Phenocrysts and microphenocrysts from the ol-tholeiitic and qz-tholeiitic basalts exhibit the widest range of clinopyroxene compositions. These crystals tend to be calcic augites that range from $Wo_{35.5}En_{45.9}Fs_{18.7}$ to the diopside-augite join (Figs. 4.9C and D). Additionally, in contrast to the other group A rock types, samples from the ol-tholeiitic and qz-tholeiitic basalts contain calcic and sub-calcic augite and pigeonite groundmass grains ($Wo_{43.9\text{-}8.2}En_{55.9\text{-}16.8}Fs_{48.9\text{-}13.2}$), considered by Ewart (1989) to represent high temperature quench groundmass phases.

Group A clinopyroxene compositions[30]

The clinopyroxene phenocrysts of the Group A rocks typically have heterogeneous compositions marked by relatively large SiO_2, MgO, FeO_{total} and small TiO_2, Al_2O_3, and Na_2O contents compared to those from the group B samples (Tables 4.12 and 4.13; pp. 70 - 73). The clinopyroxene of the Group A rocks have MgO contents in the range 11.9 – 17.5 wt. %. Values of 100Mg/(Mg + ΣFe) for phenocryst cores range from 62 to 81. Generally, there is no apparent correlation between Wo content of individual cores and their corresponding 100Mg/(Mg + ΣFe) values (Fig. 4.10), possibly reflecting a wide range of equilibrium crystallisation pressure conditions (Wass, 1979; Green, 1992). Furthermore, there is no apparent correlation between the composition of phenocryst cores and the composition of their host rock. This suggests that phenocryst compositions do not appear to be dependent upon the degree of differentiation of the host magma in which they crystallised. The whole-rock and phenocryst compositions shown in Table 4.14 are indicative of the lack of correlation between host rock major-element oxides and 100Mg/(Mg + ΣFe), and the phenocryst compositions, typical of most group A rocks.

Clinopyroxene cores in each rock type from group A generally have relatively large FeO_{total}, ranging from 6.61 to 13.69 wt. %. Most clinopyroxene phenocrysts in each rock type from group A, except those in the ol-tholeiitic basalt samples, are relatively rich in Fe^{3+} with contents[31] comparable to the green-core clinopyroxene from the foidites and basanites of the West Eifel, Germany (Duda and Schmincke, 1985) and the Cr-diopsides and titanaugites in the alkalic basalts from the Transdanubia and Nógrád County regions, Hungary (Dobosi, 1989). Only four of the 18 cores analysed in the ol-tholeiitic basalt samples were determined to contain Fe^{3+} with the largest Fe^{3+} content a comparatively

[30]See Appendix 6, Tables A6.6 to A6.10 for all mineral chemical data referred to in this section.
[31] Fe^{3+} contents were determined from the charge-balance equation of Lindsley (1983).

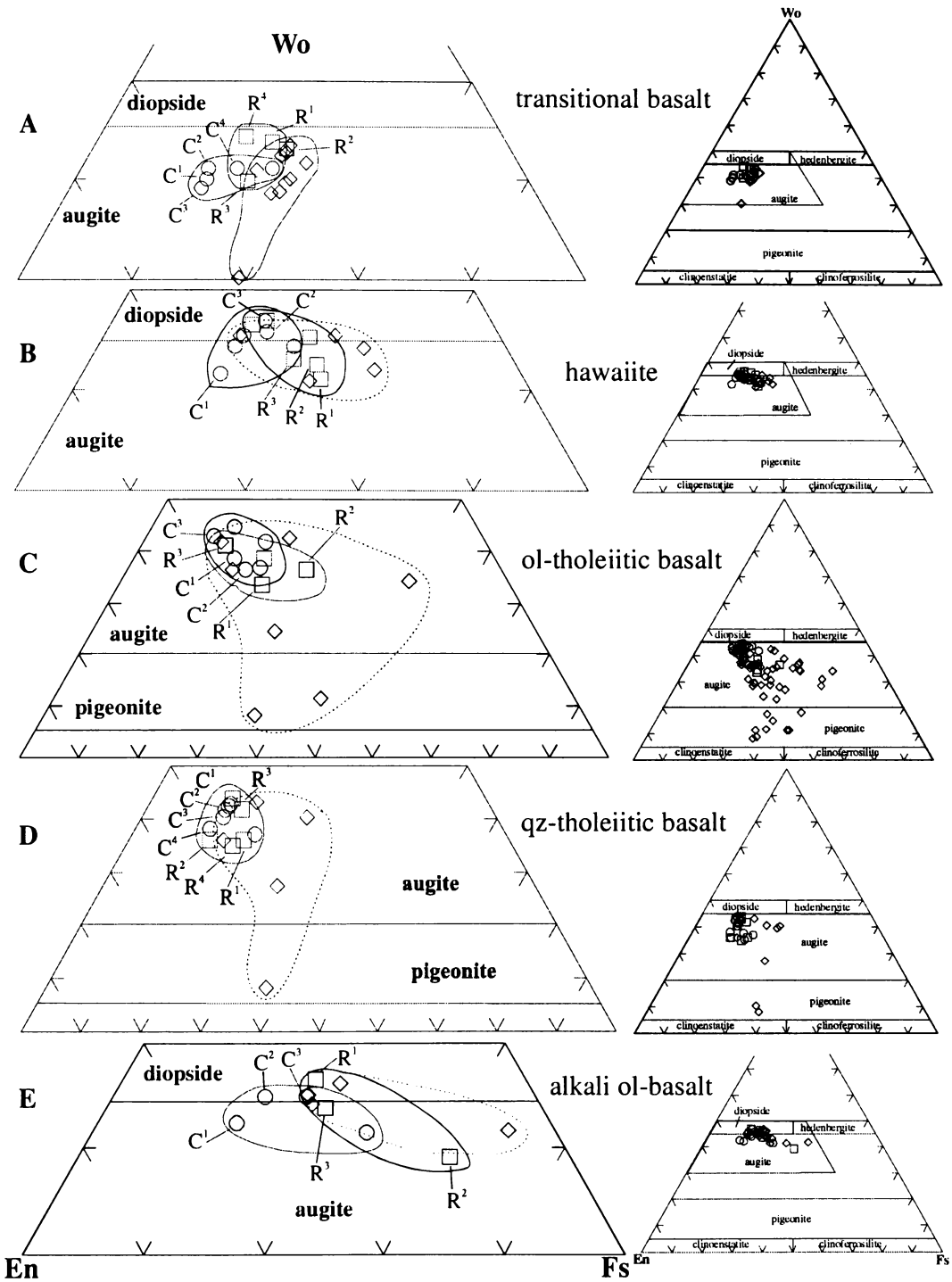

Fig. 4.9 Clinopyroxene compositions (mol. %) for selected samples from each rock type in group A; (A) transitional basalts, (B) hawaiites, (C) ol-tholeiitic basalts, (D) qz-tholeiitic basalts, and (E) alkali ol-basalts. The compositions of all analysed phenocrysts and groundmass crystals in these samples are shown in the wollastonite (Wo) – enstatite (En) – ferrosilite (Fs) ternary diagrams. The composition fields and mineral classification are from Morimoto *et al.* (1988). The shaded areas depict the dimensions of the enlarged composition field adjacent to the diagram. The fields enclosed by the solid and dashed curves define the approximate compositional range for phenocryst cores and rims, and for groundmass crystals, respectively. Selected phenocryst core-rim pairs, identified by their corresponding superscript numbers, are representative of the range of core-rim compositions within each rock type. ○ = cores, □ = rims, and ◊ = groundmass crystals. C = core and R = rim.

small 0.03 atoms per formula unit (afu). In contrast, crystal cores from the other rock types exhibit a broad range of Fe^{3+} contents (e.g., <0.001 – 0.176 afu) and small values of Fe^{3+}/Fe^{2+} (e.g., <0.1 – 2.4), which commonly occur between (i) crystals from different rock types, (ii) crystals from the same rock type, and (iii) populations of crystals within the same sample.

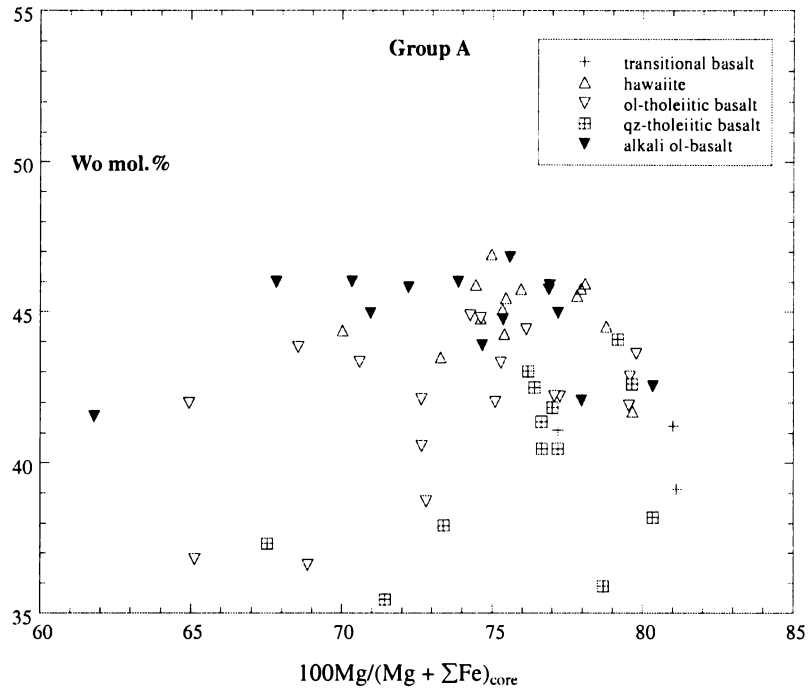

Fig. 4.10 Wollastonite (Wo) content vs. 100Mg/(Mg + ΣFe) values for clinopyroxene phenocryst cores from selected samples for each rock type in group A.

Table 4.14 Selected group A host rock compositions with representative clinopyroxene phenocryst analyses. n.d. = not determined

Sample	SA33		SA07		SA20		SAB172		SAB198	
Type	alkali ol-basalt		transitional basalt		hawaiite		ol-tholeiitic basalt		qz-tholeiitic basalt	
Analysis	host rock	1728-C	host rock	1907-C	host rock	1854-C	host rock	97-C	host rock	1582-C
SiO_2	47.28	49.87	45.83	49.44	48.94	48.19	50.15	50.67	52.77	50.61
TiO_2	2.13	1.31	2.19	.077	2.17	1.80	1.76	1.40	2.47	0.91
Al_2O_3	13.38	3.43	15.13	5.30	15.01	6.02	14.55	2.95	17.67	2.53
Cr_2O_3	n.d.	0.79	n.d.	1.05	n.d.	0.43	n.d.	-	n.d.	0.65
Fe_2O_3	2.12	-	2.20	-	2.04	-	1.99	-	1.04	-
FeO*	10.58	7.68	10.98	6.61	10.20	8.40	9.93	11.93	5.20	8.41
MnO	0.18	-	0.20	-	0.16	-	0.18	0.39	0.10	-
MgO	10.55	14.48	8.63	15.67	6.81	13.53	8.53	14.92	3.89	15.85
CaO	9.35	21.35	9.93	18.91	9.26	21.53	9.23	17.56	11.23	19.45
Na_2O	3.02	0.52	2.67	0.9	3.23	1.03	2.73	-	3.80	0.58
K_2O	0.74	-	0.27	-	0.76	-	0.43	-	0.80	-
P_2O_5	0.33	-	0.15	-	0.29	-	0.22	-	0.35	-
LOI	0.39	-	2.15	-	1.30	-	1.05	-	0.79	-
TOTAL	100.04	99.43	100.33	98.65	100.17	100.93	100.74	99.82	100.11	98.99
$\frac{100Mg}{(Mg + Fe^{2+})}$	64		58		54		60		57	
$\frac{100Mg}{(Mg + \Sigma Fe)}$		77		81		74		69		77

*In clinopyroxene, total Fe reported as FeO.

Concentrations of TiO_2, Na_2O, and Al_2O_3 are normally variable with notable differences between crystals from samples of the same rock type and between crystals from the same sample. Concentrations of TiO_2 for clinopyroxene cores range from 0.6 – 2.4 wt. % and are typically at or smaller than the TiO_2 contents of their host rock. The TiO_2 contents in cores generally decrease with increasing 100Mg/(Mg + ΣFe) values, with crystals from the hawaiites showing the strongest negative correlation (Fig. 4.11). A number of crystals from each rock type have TiO_2 contents and 100Mg/(Mg + ΣFe) values similar to those of the "high-pressure" augite series xenoliths and megacrysts in the alkalic basalts from the Massif Central, France and the Southern Highlands, Australia (Wass, 1979).

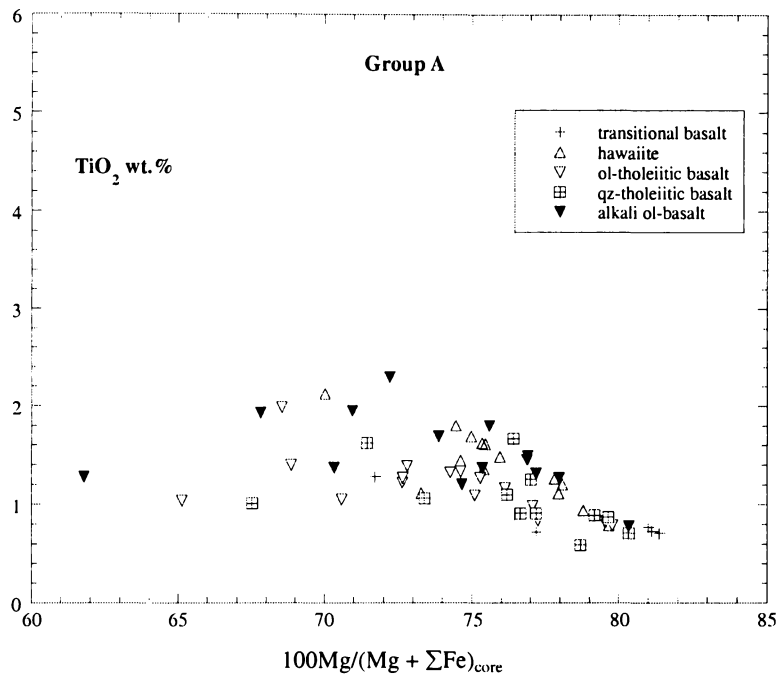

Fig. 4.11 Concentrations of TiO_2 vs. 100Mg/(Mg + ΣFe) values for clinopyroxene phenocryst cores from selected samples for each rock type in group A.

Phenocryst cores have Al_2O_3 contents that range from 1.4 to 7.9 wt. %. In contrast to the TiO_2 trends, Al_2O_3 shows an overall positive correlation with increasing core 100Mg/(Mg + ΣFe) values, although Al_2O_3 in crystals for each rock type poorly correlates with 100Mg/(Mg + ΣFe) values over the range of 65 to 82 (Fig. 4.12). Additionally, concentrations of Al_2O_3 generally have an antipathetic relationship with core SiO_2 content.

Recalculation of Al_2O_3 into non-quadrilateral end-members using the method of Putirka *et al.* (1996) indicates that Al_2O_3 is apportioned predominantly into the Ti-pyroxene molecule (CaTi) in the majority of clinopyroxenes in the transitional basalt, alkali ol-basalt, and hawaiite samples, and qz-tholeiitic basalt SAB198. The large excess of Al

relative to Ti in the clinopyroxenes in samples from these rock types is illustrated in Fig. 4.13.

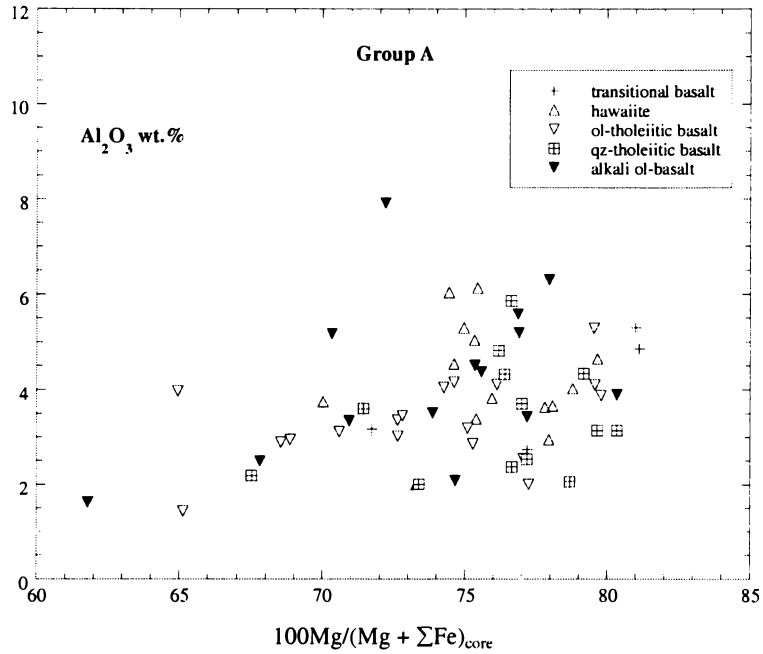

Fig. 4.12 Concentrations of Al_2O_3 vs. 100Mg/(Mg + ΣFe) values for clinopyroxene phenocryst cores from selected samples for each rock type in group A.

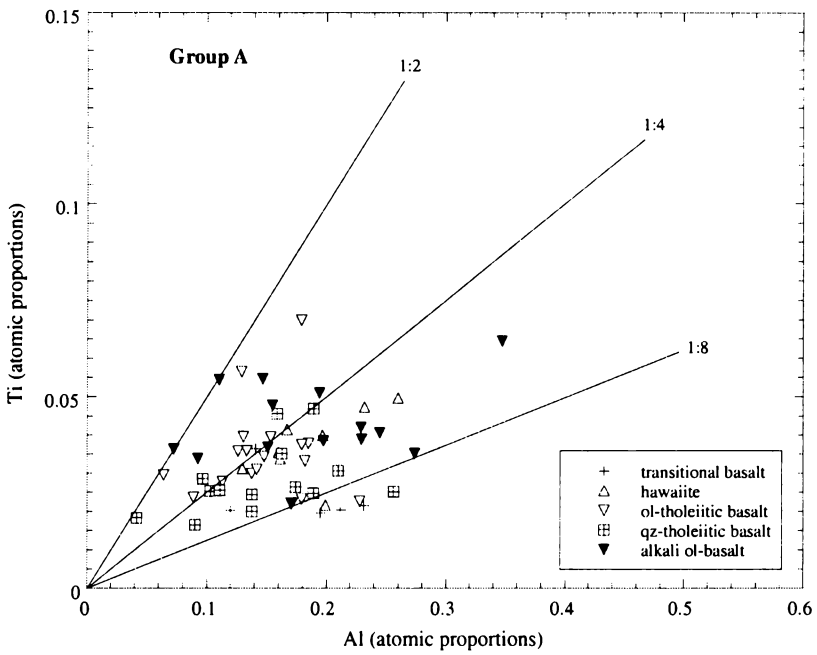

Fig. 4.13 Relationship between the number of total Al and Ti atoms per four cation formula in the group A clinopyroxenes. Lines of specific Ti:Al ratios are given.

Most phenocryst cores have Ti:Al ratios[32] between 1:4 and 1:8, similar to those of the clinopyroxenes from West Eifel, Germany (Duda and Schmincke, 1985), the

[32] Cameron and Papike (1980) determined that stoichiometric constraints of a $TiAl_2$ component in clinopyroxene limits the maximum Ti:Al ratio to 1:2.

Transdanubian and Nógrád basalts of Hungary (Dobosi, 1989), and the ol-tholeiitic basalts, hawaiites, and alkali ol-basalts from eastern Australia (Ewart, 1989). Small Ti:Al ratios such as these have been attributed to clinopyroxene crystallisation during "low-pressure" experiments (Forsythe *et al.*, 1994). In contrast, Al_2O_3 in the crystals in all ol-tholeiitic basalt samples and qz-tholeiitic basalts SA76 and SA77 is accommodated primarily in the Ca-Tschermak's (CaTs) molecule, and to a lesser extent the CaTi molecule. These crystals tend to have Ti:Al ratios between 1:2 and 1:4 (Fig. 4.13) indicating that they may have crystallised at pressures greater than those from the other group A rock types. Since CaTs is generally considered to be more sensitive to the pressure of crystal formation (e.g., Nimis, 1995), the comparatively large CaTs contents of these crystals may also be indicative of crystallisation at higher pressures. However, experimental studies of the exchange reactions between non-quadrilateral clinopyroxene components and silicate melts suggest that CaTs may also be influenced by bulk chemistry (e.g., Sack and Carmichael, 1984; Sack and Ghiorso, 1994).

An important feature of all group A clinopyroxenes is the relatively small proportion of Al required to fill the Si-deficient tetrahedral sites (see Table 4.12; pp.70 – 71). This is because the relatively large SiO_2 content in most crystals from the group A samples (45.1 – 52.1 wt. %) requires that the tetrahedral site be filled almost entirely by Si (e.g., most clinopyroxene crystals have Si > 1.85 afu). Only the hawaiite samples have a majority of clinopyroxenes with smaller Si contents that are typically between 1.75 and 1.85 afu. Concentrations of Al^{IV} and Al^{VI} vary irregularly between crystals from the same rock type. Generally, Al^{IV} contents range up to 0.150 afu. However, since most group A clinopyroxenes have characteristically small Al_2O_3 contents, the largest value for Al^{VI} is also small (e.g., < 0.06 afu). Values of Al^{IV}/Al^{VI} range from < 0.2 to 15.4 but most values are between 1.1 and 4.7. Crystals with relatively small Al^{IV}/Al^{VI} values (e.g., < 3.0) are comparable to those considered by Wass (1979), Wörner and Schmincke (1984a), Duda and Schmincke (1985), Dobosi (1989), and Green (1992) to be representative of "high-pressure" clinopyroxenes.

The Na_2O content in a large number of phenocrysts from each group A rock type is often below the detection limits of the electron microprobe, most notably those from the majority of ol-tholeiitic basalt samples, transitional basalt SA10, hawaiite SAB151, and qz-tholeiitic basalts SA76 and SA77. Most samples however, contain clinopyroxene with cores that have Na_2O contents that range from < 0.49 to 1.09 wt. %. Crystal populations in individual samples commonly have comparatively small but distinct variation in Na_2O contents, typically up to 0.5 wt. %. Non-quadrilateral end-member calculations indicate

that a number of Al-rich crystals contain the jadeite (Jd) molecule. However, there is no apparent correlation between Jd, CaTs, or CaTi content in individual crystals. In contrast, Al-poor crystals typically have comparable Na and Fe^{3+} concentrations to those of the Al-rich crystals thus favouring formation of the aegirine (Ac; $NaFe^{3+}Si_2O_6$) molecule.

The Jd and CaTs components of clinopyroxene are generally considered the most sensitive to pressure (e.g., Nimis, 1995; Putirka *et al.*, 1996). By inference, the presence of these molecules may be indicative of a relatively high-pressure origin. However, if high-pressure Na favours the formation of Jd over Ac (Putirka, pers. comm., 2000) then the occurrence of Ac in some crystals may be indicative of crystal formation at comparably lower pressures.

Group A clinopyroxene phenocrysts zoning patterns

As with olivine phenocrysts, some group A rock samples contain populations of clinopyroxene phenocrysts that exhibit a range of zoning features that may vary from strong compositional zones to weak or reverse zoned, to unzoned crystals. Such variations within individual samples may be indicative of a complex crystallisation history that may include crystallisation over a range of P-T conditions or possible incomplete magma mixing (e.g., Shimizu and LeRoex, 1986; Helz and Wright, 1992; Putirka *et al.*, 1996). Alternatively, the lack of zoning may indicate that the crystals are derived from magmas that have undergone little differentiation since melt segregation, which suggests that the differences in clinopyroxene compositions observed between rock types is a function of differences in composition between parental magmas (Mitropoulos and Tarney, 1992).

Zoned clinopyroxene phenocrysts in the group A rocks typically have rims enriched in FeO_{total} and depleted in MgO and Al_2O_3 relative to adjacent cores. Most of these crystals however, exhibit relatively weak compositional zoning in these oxides. Generally, the majority of phenocrysts have rims that are typically within 1 wt. % MgO of the adjacent cores, although core to rim differences up to 3.0 wt. % MgO were observed in alkali ol-basalt SA33 and ol-tholeiitic basalt SAB172. The strongest compositional zones observed in some crystals have rims with up to 6.0 wt. % greater FeO_{total} than cores, with one sample (alkali ol-basalt; SA33) containing a crystal with a rim ~11 wt. % greater in FeO_{total} than its core. Core to rim contrasts in Al_2O_3 are typically < 2.5 wt. %, although strong normal zones were noted in crystals from alkali ol-basalt (SA18) and hawaiite (SA20) with core to rim differences of 4.7 and 4.3 wt. % respectively. There is little

variation in the concentrations of TiO_2 and Na_2O between cores and rims, typically < 1wt. % for normal and reversed-zoned crystals.

4.5.2 Group B clinopyroxene

In contrast to clinopyroxene in the group A rocks, the group B rocks contain purplish brown titaniferous clinopyroxene that typically occurs as euhedral and subhedral microphenocrysts that are frequently twinned and zoned. Megacrysts and large phenocrysts are rare in most samples. However, where present, these crystals comprise a minor volume proportion of total clinopyroxene content. Microphenocrysts generally consist of a relatively large, often sieved or partially resorbed, central core surrounded by a relatively narrow, strong concentrically zoned rim of dark, purplish pink, high-Ca augite or diopside. The resorbed areas are commonly filled with matrix material. Prismatic crystals are common, primarily in those samples with low modal clinopyroxene, and often have hourglass zoning. The compositions of these crystals are similar to that of the euhedral and subhedral microphenocrysts. Many crystals contain abundant, up to 40 μm, titanomagnetite and rare Cr-titanomagnetite inclusions. Groundmass clinopyroxene is abundant, and commonly occurs in aggregates in the devitrified glassy matrix characteristic of most group B rocks. Most groundmass crystals are petrographically similar to the microphenocrysts – occurring as euhedral, subhedral, and prismatic crystals, many with distinct marginal zones, and small titanomagnetite or Cr-titanomagnetite inclusions.

The clinopyroxene in the group B rocks is generally very calcic. Crystals exhibit Wo-enrichment similar to the clinopyroxene in the basanites and alkali ol-basalts of the Okete Volcanics (Briggs and Goles, 1984), the ankaramites and transitional olivine basalts of the Alexandra Volcanics, New Zealand (Briggs and McDonough, 1990), the ne-hawaiites of the Ngatutura Basalts (Briggs *et al.*, 1990), and the basanites and ne-hawaiites from the intraplate volcanic fields throughout eastern Australia (e.g., Ewart, 1989). A majority of cores, rims, and groundmass crystals from each group B rock type show a relative homogeneity in their mineral chemical compositions. The majority of phenocryst core and groundmass compositions are within a very restricted range ($Wo_{52.2\text{-}45.1}En_{45.9\text{-}32.2}Fs_{19.8\text{-}9.9}$) and ($Wo_{53.0\text{-}44.8}En_{43.5\text{-}25.7}Fs_{29.5\text{-}11.0}$) respectively, which plot predominantly in the diopside field of the Wo-En-Fs ternary system of Morimoto *et al.* (1988). Selected core-rim pairs and groundmass compositions for each rock type are plotted in Fig. 4.14 (see Table 4.13, pp.72 – 73, for summary of end-member compositions).

The values of 100Mg/(Mg + ∑Fe) for phenocryst cores are similar to those of group A, ranging from 66 to 81, although cores from two nephelinite samples (SA21 and SA51) have notably smaller 100Mg/(Mg + ∑Fe) values, 45 and 48 respectively. Unlike their group A counterparts however, the clinopyroxene in group B rocks have cores with Wo contents that collectively exhibit an overall negative correlation (albeit weak) with their corresponding core 100Mg/(Mg + ∑Fe) values (Fig. 4.15; p.85), possibly the result of Ca-enrichment concomitant with clinopyroxene fractionation. Furthermore, in contrast to group A, core compositions tend to correlate well with host rock compositions, although the comparatively large MgO content in phenocryst cores 1544-C and 50-C from ne-hawaiite (SA65) and mugearite (SA88) respectively, illustrate that there may be notable exceptions (see Table 4.15; p.85).

Group B clinopyroxene compositions[33]

Much of the compositional variations exhibited by group B clinopyroxenes occurs between crystals from samples of the same rock type and between crystals in the same sample. Generally, core compositions are characterised by relatively small SiO_2 contents that range from 40.7 to 51.3 wt. % with the largest contents occurring in cores from the mugearite sample. Most SiO_2 contents are between 46.1 and 50.8 wt. % and average 48.1 ± 2.3 wt. %, similar to the average SiO_2 content of 50.1 ± 1.4 wt. % for clinopyroxene in the group A rocks.

Unlike the clinopyroxene from group A, TiO_2 contents in the majority of clinopyroxene phenocrysts in the group B rocks are larger than the TiO_2 content of their host rock. Concentrations of TiO_2 in phenocryst cores range from 1.0 to 5.2 wt. % and show a stronger negative correlation with core 100Mg/(Mg + ∑Fe) values, between 70 and 80 (Fig. 4.16; p.86), than group A clinopyroxene over the same range of 100Mg/(Mg + ∑Fe) values (see Fig. 4.11; p.78). With the exception of the ne-hawaiite clinopyroxene, most phenocryst cores have TiO_2 contents and 100Mg/(Mg + ∑Fe) values similar to those of the Al-augite series xenoliths and megacrysts described by Wass (1979), possibly reflecting a "high-pressure" origin for at least some of these crystals. The clinopyroxene in the ne-hawaiites form a discrete population that have relatively small but distinct compositional differences from those in other group B rock types (Fig. 4.16). Such differences are also observed in the whole-rock geochemistry between the ne-hawaiites and other group B rock types.

[33] See Appendix 6, Tables A6.24 to A6.29 for all mineral chemical data referred to in this section.

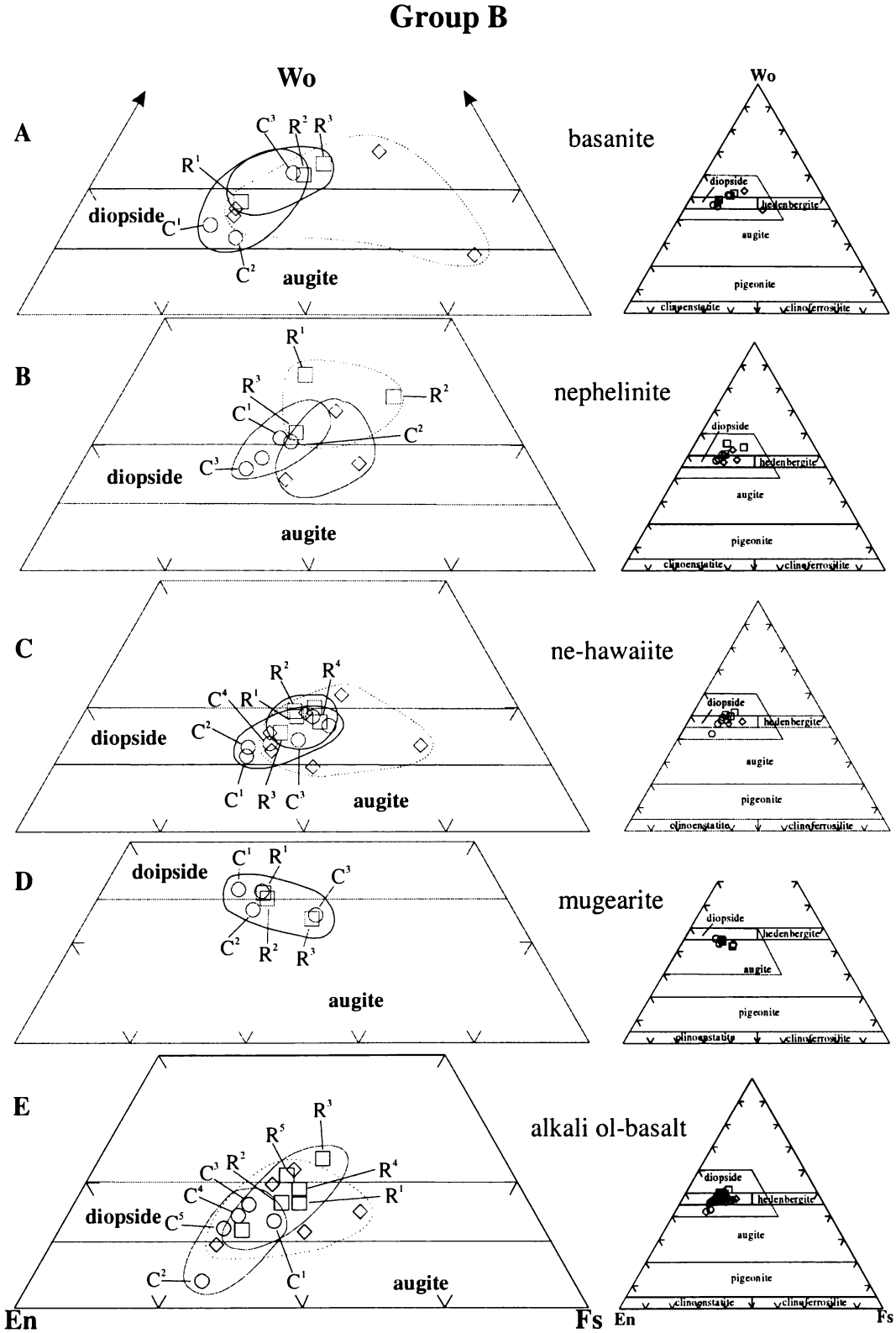

Fig. 4.14 Clinopyroxene compositions (mol. %) for selected samples from each rock type in group B; (A) basanites, (B) nephelinites, (C) ne-hawaiites, (D) mugearite, and (E) alkali ol-basalts. The compositions of all analysed phenocrysts and groundmass crystals in these samples are shown in the wollastonite (Wo) – enstatite (En) – ferrosilite (Fs) ternary diagrams. The composition fields and mineral classification are from Morimoto *et al.* (1988). The shaded areas depict the dimensions of the enlarged composition field adjacent to the diagram. The fields enclosed by the solid and dashed curves define the approximate compositional range for phenocryst cores and rims, and for groundmass crystals, respectively. Selected phenocryst core-rim pairs, identified by their corresponding superscript numbers, are representative of the range of core-rim compositions within each rock type. ○ = cores, □ = rims, and ◊ = groundmass crystals. C = core and R = rim.

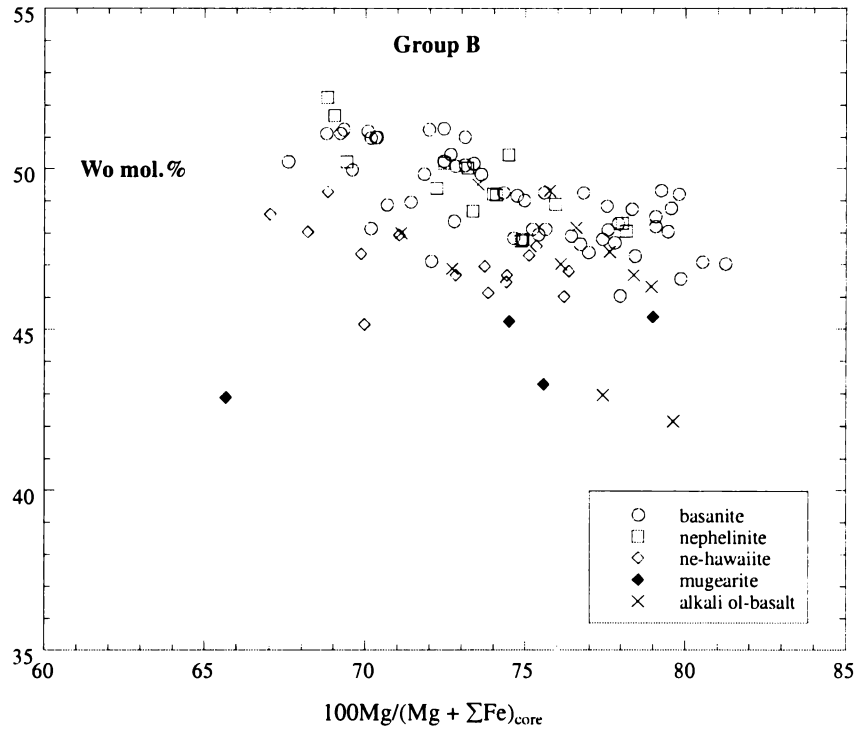

Fig. 4.15 Wollastonite (Wo) content vs. 100Mg/(Mg + ΣFe) values for clinopyroxene phenocryst cores from selected samples for each rock type in group B.

Table 4.15 Selected group B host rock compositions with representative clinopyroxene phenocryst analyses. n.d. = not determined

Sample	SAB207		SAB180		SAB113		SA65		SA88	
Rock type	alkali ol-basalt		basanite		nephelinite		ne-hawaiite		mugearite	
Analysis	host-rock	1613-C	host-rock	1309-C	host-rock	239-C	host-rock	1544-C	host-rock	50-C
SiO_2	42.78	46.83	43.86	46.60	42.26	49.35	46.44	49.09	47.14	51.11
TiO_2	3.20	2.26	2.76	2.20	3.20	1.61	2.40	1.57	2.96	1.15
Al_2O_3	12.60	6.33	12.54	7.08	12.48	4.60	14.79	3.34	11.01	2.62
Cr_2O_3	n.d.	0.40	n.d.	0.45	n.d.	n.d.	n.d.	n.d.	n.d.	n.d.
Fe_2O_3	2.36	-	2.15	-	2.27	-	2.21	-	2.68	-
FeO*	11.82	7.28	10.74	6.86	11.35	6.78	11.03	8.86	13.38	8.42
MnO	0.20	n.d.	.020	n.d.	0.20	0.23	0.27	0.25	0.22	0.21
MgO	11.74	13.19	11.93	12.62	11.13	13.70	5.45	13.14	9.21	14.77
CaO	10.07	22.35	10.13	22.25	9.85	22.69	7.21	22.22	7.18	20.81
Na_2O	2.50	0.83	3.02	0.54	3.81	n.d.	5.61	0.86	3.32	n.d.
K_2O	0.73	n.d.	1.33	n.d.	1.48	n.d.	2.21	n.d.	1.33	n.d.
P_2O_5	0.73	n.d.	0.60	n.d.	0.86	n.d.	1.03	n.d.	0.64	n.d.
LOI	0.50	-	0.79	-	0.66	-	1.22	-	1.03	-
TOTAL	99.24	99.43	100.06	98.60	99.56	98.96	99.86	99.33	100.09	99.09
$\frac{100Mg}{(Mg + Fe^{2+})}$	63.9		66.4		63.6		46.8		55.1	
$\frac{100Mg}{(Mg + \Sigma Fe)}$		76.6		76.8		78.1		72.8		75.6

*In clinopyroxene, total Fe reported as FeO

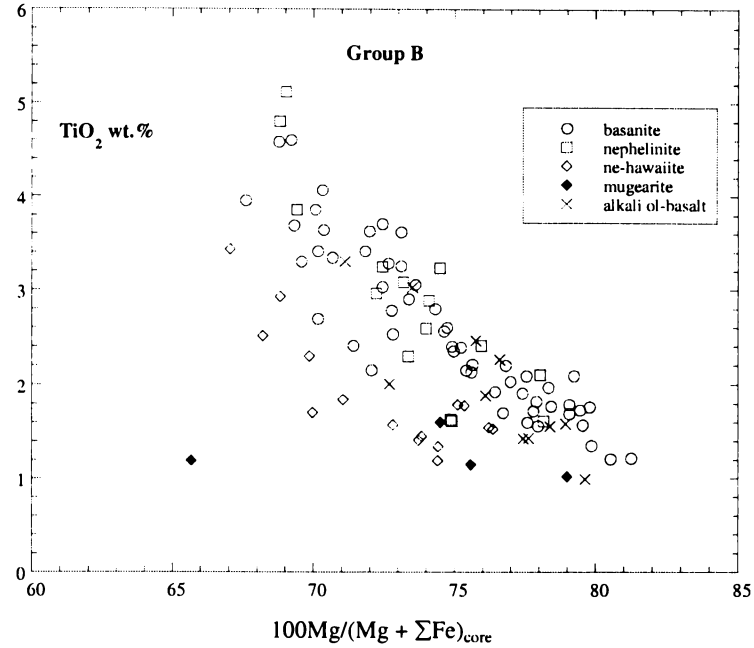

Fig. 4.16 Concentrations of TiO_2 vs. 100Mg/(Mg + ΣFe) values for clinopyroxene phenocryst cores from selected samples for each group B rock type.

Concentrations of Al_2O_3 in phenocryst cores range between 1.5 and 10.4 wt. %, with most contents between 3.0 and 9.0 wt. %. In contrast to the clinopyroxenes from group A, the range of Al_2O_3 content in the cores of clinopyroxenes from group B rocks decreases with increasing core 100Mg/(Mg + ΣFe) values (Fig. 4.17 and *cf.* Fig. 4.12; p.79). In addition, concentrations of Al_2O_3 in crystals from each rock type have a marked negative correlation with SiO_2, a feature that may be associated with clinopyroxene fractionation.

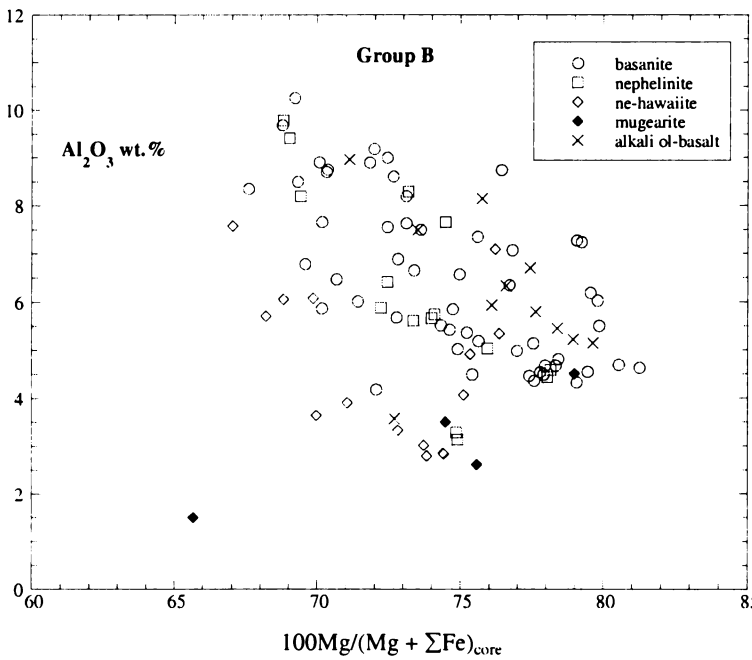

Fig. 4.17 Concentrations of Al_2O_3 vs. 100Mg/(Mg + ΣFe) values for representative clinopyroxene phenocryst cores from selected samples for each rock type in group B.

Calculation of non-quadrilateral end-members indicates that Al_2O_3 is accommodated in the CaTi molecule in the clinopyroxenes in all samples except nephelinite SA28. In addition to a CaTi component, the majority of crystals in the basanites and nephelinites, and the mugearite sample contain a CaTs component. In contrast, CaTs does not occur in most clinopyroxenes in ne-hawaiite and alkali ol-basalt samples.

In contrast to most of the clinopyroxenes from the group A rocks, the majority of phenocryst cores from the group B rocks have Ti:Al ratios that plot above the Ti:Al = 1:4 line (Fig. 4.18 and *cf.* Fig. 4.13; p.79), similar to some of the titanaugites from the Transdanubian and Nógrád basalts of Hungary (Dobosi, 1989) and basanites, alkali ol-basalts, and transitional basalts from eastern Australia (Ewart, 1989). These larger Ti:Al ratios in the group B phenocrysts may be indicative of relatively higher pressures of crystal formation (e.g., Forsythe *et al.*, 1994). There is a distinct population of clinopyroxene crystals, from some basanite samples and alkali ol-basalt SAB207, with smaller Ti:Al ratios between 1:4 and 1:8. Such increases in total Al have been associated with increasing silica undersaturation of the host rocks (e.g., Ewart, 1989), a feature characteristic of the basanites and SAB207 in the SAVF (Table 4.15).

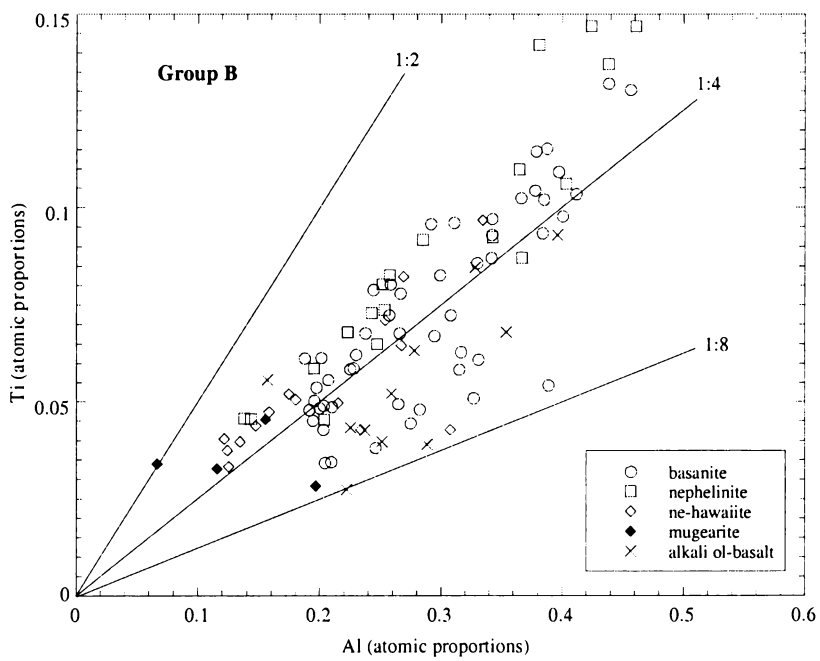

Fig. 4.18 Relationship between the number of total Al and Ti atoms per four cation formula in the group B clinopyroxenes. Lines of specific Ti:Al ratios are given.

Because a large number of crystals have generally small SiO_2 contents compared to those from group A, an important characteristic of the group B clinopyroxenes is the large proportion of Al required to fill the Si-deficient tetrahedral sites. Concentrations of Al^{IV}

relative to Al^{VI} generally vary irregularly between crystals from the same rock type (e.g., Al^{IV} ranges from 0.096 to 0.461 afu and Al^{VI} from < 0.001 to 0.136 afu, see Table 4.13; pp 72 – 73). Values of Al^{IV}/Al^{VI} range from ~1.0 to 41.9, although most values are typically between 2.0 and 6.8. Crystals with relatively large Al^{IV}/Al^{VI} values (e.g., > 3.0) are comparable to those considered by Wass (1979), Wörner and Schmincke (1984a), Duda and Schmincke (1985), Dobosi (1989), and Green (1992) to be representative of "low-pressure" clinopyroxenes.

Clinopyroxenes from the group B rocks also have large Na_2O contents compared to the majority of clinopyroxenes from group A (see Tables 4.12 and 4.13, pp.70 – 73). The Na_2O contents in phenocryst cores range from < 0.4 to 1.5 wt. %. With the exception of the mugearite sample[34], clinopyroxenes in the basanite samples generally have smaller Na_2O contents (e.g., < 0.77 wt. %) than those from the other group B rock types as well as the clinopyroxenes that contain Na_2O from the group A samples. The largest values for Na_2O are predominantly in crystals from the alkali ol-basalt samples SA54, SAB188, and SAB207, up to 1.42, 1.19, and 1.00 wt% respectively, although the ne-hawaiite samples SA02, SA25, and SA65 contain cores with Na_2O between 1.1 and 1.5 wt. %. Most samples from the other group B rock types contain clinopyroxenes with cores that show little variation in Na_2O content between individual crystals, typically << 1.0 wt. %.

The FeO_{total} contents in clinopyroxene cores from the group B samples tend to be slightly smaller than those from the group A samples, ranging from ~ 6.0 – 12.0 wt. % (see Tables 4.12 and 4.13, pp.70 – 73). However, most clinopyroxenes from the group B rocks, except mugearite, have larger Fe^{3+} contents (up to 0.254 afu) and values of Fe^{3+}/Fe^{2+} (up to 5.1) than their group A counterparts. Additionally, Fe^{3+} contents may be up to four times greater than Na in the same crystal. As with the group A clinopyroxenes, Fe^{3+} contents and Fe^{3+}/Fe^{2+} values are variable, with some crystals in each rock type, except mugearite, having little or no Fe^{3+}, whereas other crystals in the same rock type or sample have relatively large Fe^{3+} contents.

The occurrence of large Na_2O together with large Fe^{3+} contents suggests a possible incorporation of the aegirine (Ac) molecule. However, in the case of the relatively large-Al_2O_3 group B clinopyroxenes, Na could be charge-balanced by excess Al (Al^{VI}), rather than Fe^{3+} (Putirka, pers. comm. 2000), thus favouring formation of a jadeite (Jd) molecule. Non-quadrilateral end-member calculations indicate that the majority of clinopyroxene crystals in all group B rock types, except mugearite, contain a Jd

[34] In each of the core and rim analyses for mugearite sample, SA88, Na_2O content was below the detection limit.

component. Large Na and Al^{VI} contents, such as those exhibited by most group B clinopyroxenes, are considered by Nimis (1995) as typical of "high-pressure" clinopyroxene. Additionally, Adam and Green (1994) argued that trends of increasing Na and Al^{VI} contents are indicative of clinopyroxene formation in association with increasing pressure. The Jd and CaTs components of clinopyroxene are generally considered the most sensitive to pressure (Nimis, 1995; Putirka *et al.*, 1996). By inference, the presence of these molecules in most group B clinopyroxenes, together with comparatively large Na and Al^{VI} contents, may be indicative of crystal formation at relatively high pressures.

Group B clinopyroxene phenocrysts zoning patterns

The majority of phenocrysts and microphenocrysts in the group B rocks are compositionally zoned. For all group B rock types the magnitude of compositional zoning is variable, with rim compositions overlapping those of cores (see Fig. 4.14, p.84). However, in individual core-rim pairs, rims tend to be enriched in Al_2O_3, TiO_2, FeO_{total}, and Na_2O, and depleted in MgO contents.

In contrast to clinopyroxene phenocrysts in the group A rocks, most group B phenocrysts and microphenocrysts have small rim to core differences in FeO_{total} (typically < 2.0 wt. %, with approximately half of the analysed rims within 1 wt. % of the core FeO_{total} content). These crystals also tend to exhibit larger contrasts in MgO content from core to rim than their group A counterparts, although in a number of crystals MgO zoning is relatively weak. The basanites tend to exhibit the strongest MgO zoning, with MgO content in some cores up to 4.0 wt. % greater than adjacent rims.

Some phenocrysts and microphenocrysts in alkali ol-basalts, basanites, and nephelinites have relatively strong TiO_2 zones with rims up to 3.7 wt. % greater than cores. Other crystals in the same sample however, may be weakly or normally zoned in TiO_2. Clinopyroxene in the ne-hawaiites and the mugearite tend to have smaller TiO_2 rim contents (< 3.46 and 1.43 wt. % respectively) and less distinct core-rim contrasts (e.g., < 1.6 and 0.6 wt. % TiO_2 respectively). The comparatively small TiO_2 rim contents suggest that these crystals may be closer to equilibrium with their host magma than those with larger rim TiO_2 contents. The experimental studies of Hart and Dunn (1993) on trace element partitioning between clinopyroxene and silicate melts demonstrated that crystals with Ti-enriched rims are indicative of phenocryst-host magma disequilibrium. They concluded that rims with the largest Ti contents, relative to adjacent cores, might be furthest from equilibrium.

Variations in Al_2O_3 zoning are similar to that of TiO_2. In all samples, many crystals exhibit strong compositional zoning with Al_2O_3 in rims up to 6.9 wt. % greater than adjacent cores. For many clinopyroxenes from group B, $(Al^{IV}/Al^{VI})^{core} < (Al^{IV}/Al^{VI})^{rim}$ implying that cores equilibrated at a pressure greater than adjacent rims (e.g., Wass, 1979; Adam and Green, 1994). Conversely, a number of basanite (e.g., SA37, SAB128), nephelinite (e.g., SA28, SAB135), and ne-hawaiite (e.g., SA25, SA65) samples contain zoned crystals where $(Al^{IV}/Al^{VI})^{core} > (Al^{IV}/Al^{VI})^{rim}$ indicating a more complex crystallisation history that may involve magma mixing at mantle depths (e.g., Duda and Schmincke, 1985).

Generally, in all group B rock types, except mugearite, there is little variation in Na_2O content between cores and rims, typically < 1 wt. %. Rims tend to have slightly larger Na_2O contents than adjacent cores, although some samples also contain crystals with cores that have larger Na_2O content than adjacent rims. Microphenocrysts in nephelinite samples SA21 and SA28 and ne-hawaiite samples SA02, SA25, and SA65 have the largest rim Na_2O contents (0.54 – 1.38 wt. %). The cores of these crystals however, also have comparatively large Na_2O contents (0.63 – 1.53 wt. %) and therefore exhibit weak compositional zoning similar to those core-rim pairs in other samples that have smaller Na_2O contents. In a number of samples from each rock type, except mugearite, microphenocryst core content is below the detection limit while the adjacent core is slightly Na_2O-enriched (e.g., < 1 wt. % Na_2O).

4.5.3 Clinopyroxene crystallisation

The composition of minerals segregated from melts crystallising at depth is a function of pressure, temperature, and magma bulk composition (Nimis and Ulmer, 1998). Because clinopyroxene plays an important role in controlling the fractionation of many trace elements during mantle melting (e.g., Hart and Dunn, 1993; Adam and Green, 1994; Forsythe *et al.*, 1994; Skulski *et al.*, 1994; Blundy, *et al.*, 1995; Lindstrom *et al.*, 1998; Putirka, 1999), the common occurrence of clinopyroxene in all SAVF rock types is indicative of its importance to the evolution of the magmas from which the SAVF lavas were derived. The textural characteristics and mineral chemical diversity of the clinopyroxenes from each SAVF rock type are suggestive of diverse and complex crystallisation conditions. Because clinopyroxene compositions are sensitive to the pressure and temperature of formation, the correlation between clinopyroxene and equilibrium conditions may provide important information regarding:

1. The depths and temperature of melt segregation.
2. Relative transport time to the surface.
3. The relative location of magma reservoirs and whether or not the magmas that erupted in the SAVF stalled at the base of the crust prior to eruption. This information may in turn help constrain crustal thickness.

Qualitative pressure and temperature estimates

The relative pressure of crystal formation for the clinopyroxenes from the group A and B rocks can be compared based on their Al^{IV}/Al^{VI} values. Studies by Thompson (1974), Velde and Kushiro (1978), Wass (1979), and Adam and Green (1994) of high-pressure clinopyroxenes in alkalic basalts demonstrate that Al^{IV}/Al^{VI} variability within a crystal population may be used to identify relative crystallisation pressures. Collectively these studies show that with increasing pressure of formation, Al^{IV} content decreases, whereas Al^{VI} increases. The results of these studies suggest that small Al^{IV}/Al^{VI} values are indicative of crystal formation at relatively high pressures. Additionally, the experiments of Adam and Green (1994) showed that there is a positive correlation between Al^{IV}/Al^{VI} and temperature.

Although the clinopyroxenes from the group A and B rocks have overlapping Al^{IV}/Al^{VI} values (see Tables 4.12 and 4.13, pp.70 – 73), the majority of crystals from the group A samples have predominantly small Al^{IV}/Al^{VI} values (e.g., < 3.0) compared to those from the group B samples (e.g., > 5.0). These differences suggest contrasting temperatures and pressures of crystal formation, and by inference, depths of crystallisation: i.e., a large number of clinopyroxenes in group A rocks crystallised in comparatively high-pressure environments, but at lower temperatures, relative to those from group B.

Quantitative pressure and temperature estimates

Crystallisation pressures and temperatures for clinopyroxenes from mafic volcanic rocks can be estimated from geothermobarometer models such as those constructed by Putirka *et al.* (1996) for temperatures > 1100°C and pressures from 0 to 30 kbar. The geothermobarometers of Putirka *et al.* (1996) are thermodynamic rather than empirical (e.g., Wass, 1979). They are based on the exchange of jadeite (Jd) and Ca-Tschermak's (CaTs) components between clinopyroxene and melt over a wide range of mafic igneous rock bulk-compositions. Crystallisation P-T conditions of individual crystals are calculated from expressions using clinopyroxene-liquid equilibrium constants known to be sensitive to pressure and temperature. For example, the experiments of Putirka *et al.*

(1996) show that the jadeite (Jd)-diopside/hedenbergite (DiHd) clinopyroxene-liquid exchange equilibrium is temperature sensitive. Clinopyroxene crystallisation temperatures can therefore be estimated from their geothermometer model T1:

$$T = 10^4\left[6.73-0.26\ln\left(\frac{Jd^{cpx}Ca^{liq}Fm^{liq}}{DiHd^{cpx}Na^{liq}Al^{liq}}\right)-0.68\ln\left(\frac{Mg^{liq}}{Mg^{liq}+Fe^{liq}}\right)+0.52\ln\left(Ca^{liq}\right)\right]^{-1}$$

For those crystals that do not contain a Jd component but have sufficient Al to form a CaTs component, crystallisation temperatures may be estimated from the geothermometer model T3 of Putirka *et al.* (1996):

$$T = 10^4\left[6.92-0.18\ln\left(\frac{CaTs^{cpx}Si^{liq}Fm^{liq}}{DiHd^{cpx}\left(Al^{liq}\right)^2}\right)-0.84\ln\left(\frac{Mg^{liq}}{Mg^{liq}+Fe^{liq}}\right)-0.29\ln\left(\frac{1}{\left(Al^{liq}\right)^2}\right)\right]^{-1}$$

where T is in Kelvin and estimated to $\pm$ 27 K.

Putirka *et al.* (1996) also determined that there is a large pressure dependency for Jd formation[35]. The pressure of crystal formation can be estimated from their geothermobarometer model P1:

$$P = -54.3 + 299\frac{T}{10^4} + 36.4\frac{T}{10^4}\ln\left[\frac{Jd^{cpx}}{\left(Si^{liq}\right)^2 Na^{liq} Al^{liq}}\right] + 367\left(Na^{liq} Al^{liq}\right)$$

where P is in kbar and estimated to $\pm$ 1.4 kbar.

Each model assumes clinopyroxene-liquid equilibrium. The quantities; Si^{liq}, Al^{liq}, Fe^{liq}, Mg^{liq}, Ca^{liq}, and Na^{liq} represent the cation fraction of the related oxide. Fm^{liq} = $(MgO + FeO)_{whole\text{-}rock}$. The clinopyroxene components Jd ($NaAlSi_2O_6$) and DiHd [$Ca(Mg,Fe)Si_2O_6$] were calculated using the procedure in Putirka *et al.* (1996).

P-T modeling results

The estimated crystallisation pressures (P) and temperatures (T) for selected clinopyroxene cores and core-rim pairs from 11 group A and 20 group B samples are

[35] In the case of the SAVF rocks, the distinct disadvantage of these models is that relatively few samples from the group A rocks and the mugearite from group B have clinopyroxene that contain the Jd component necessary for estimating pressure. Putirka *et al.* (1996) did not provided an alternative model for estimating P for those crystals without a Jd component.

presented in Tables 4.16 and 4.17 respectively. Tables 4.16 and 4.17 show that the P-T estimates for crystals from samples of the same rock type and for crystals within the same sample are often variable. Pressure and temperature estimates for all analysed clinopyroxene phenocryst cores in samples from group A and B are summarised in Tables 4.18 and 4.19 respectively. Estimated P's for cores in the group A rocks range from 6.4 to 19.5 kbar while T-estimates range from 1214 to 1539°C. Estimated P for cores in the group B rocks range from 3.5 to 21.4 kbar and T from 1196 to 1534°C.

Table 4.16 Temperature and pressure estimates, using the geothermobarometer models of Putirka *et al.* (1996), for clinopyroxene from selected group A samples[36]. Partition coefficient $K_{Na}^{cpx\text{-}melt}$ is derived from Eq. 4 in (Putirka, 1999). Errors for P and T are ± 1.4 kbar and ± 27° C respectively.

Sample	Rock Type	Location	Temp °C	P (kbar)	Depth (km) at 3.3 km/kbar	Al^{IV}/Al^{VI}	Fe^{3+}/Fe^{2+}	$K_{Na}^{cpx\text{-}melt}$ (Putirka, 1999)	$K_{Fe\text{-}Mg}^{cpx\text{-}melt}$
SA18	alkali ol-basalt	CORE 1	1437	11.1	37	4.6	1.0	0.165	0.183
SA18		CORE 3	1512	19.5	65	1.8	0.2	0.251	0.517
SA19		CORE	1440	14.3	48	4.6	1.6	0.198	0.135
SAB162		CORE 1	1347	7.9	26	9.6	2.4	0.140	0.103
SAB162		RIM 1	1314	4.3	14	15.8	2.5	0.112	0.104
SAB162		CORE	1350	8.3	28	8.2	1.3	0.144	0.148
SA20	hawaiite	CORE 1	1386	8.2	27	9.6	2.0	0.141	0.139
SA20		CORE 2	1415	11.1	37	4.7	1.7	0.167	0.114
SA20		CORE 3	1368	6.4	21	10.5	1.3	0.127	0.175
SAB163		CORE 1	1372	9.6	32	8.0	2.4	0.155	0.102
SAB163		RIM 1	1361	8.5	28	8.5	1.6	0.145	0.140
SAB163		CORE	1357	7.9	26	8.0	1.0	0.140	0.173
SA80	ol-tholeiitic basalt	CORE 1	1443	9.0	30	1.7	0.1	0.145	0.392
SA80		RIM 1	1449	9.7	32	2.7	0.3	0.151	0.372
SAB169		CORE	1419	10.8	36	1.4	0.2	0.163	0.311
SAB187		CORE 2	1486	11.6	39	1.6	0.1	0.166	0.441
SA77	qz-tholeiitic basalt	CORE	1539	18.2	61	0.1	-	0.231	0.453
SAB198		CORE 1	1353	11.4	38	4.3	0.8	0.174	0.240
SAB198		RIM 1	1361	12.5	42	2.7	0.4	0.185	0.308
SAB198		CORE 2	1312	6.9	23	7.4	1.3	0.133	0.154
SA07	transitional basalt	CORE 1	1464	13.4	45	3.9	1.5	0.186	0.134
SA07		CORE 3	1480	15.0	50	3.6	1.2	0.201	0.150

[36] Pressures and temperatures could not be estimated for the majority of clinopyroxenes in the group A samples using the Putirka *et al.* (1996) models because these crystals do not contain a Jd component.

Table 4.17 Temperature and pressure estimates, using the geothermobarometer models of Putirka *et al.* (1996), for clinopyroxene from selected group B samples. Partition coefficient $K_{Na}^{cpx/liq}$ is derived from Eq. 4 in (Putirka, 1999). Errors for P and T are ± 1.4 kbar and ± 27° C respectively.

Sample	Rock Type	Location	Temp °C	P (kbar)	Depth (km) at 3.3 km/kbar	Al^{IV}/Al^{VI}	Fe^{3+}/Fe^{2+}	$K_{Na}^{cpx\text{-}melt}$ (Putirka, 1999)	$K_{Fe\text{-}Mg}^{cpx\text{-}melt}$
SA54	alkali ol-basalt	CORE 4	1478	16.2	54	3.5	2.1	0.215	0.114
SA54		RIM 4	1412	9.4	31	10.5	1.1	0.151	0.252
SAB188		CORE 1	1481	14.1	47	5.5	3.1	0.192	0.121
SAB188		CORE 2	1433	8.2	27	20.2	5.1	0.139	0.114
SAB207		CORE 2	1547	19.2	64	5.1	2.4	0.242	0.174
SAB207		RIM 2	1401	3.3	11	25.5	1.9	0.104	0.218
SA12	basanite	CORE 3	1422	12.8	43	2.7	0.2	0.138	0.413
SA12		RIM3	1440	14.9	50	9.9	1.2	0.205	0.307
SA27		CORE	1409	13.4	45	9.2	0.8	0.191	0.292
SA27		CORE	1400	12.6	42	6.6	0.4	0.183	0.353
SA37		CORE 1	1462	11.9	40	2.6	0.1	0.171	0.680
SA37		RIM 1	1474	13.3	44	5.8	0.2	0.184	0.820
SAB102		CORE1	1467	14.4	48	4.6	0.5	0.196	0.393
SAB102		RIM1	1461	13.4	45	6.9	0.5	0.186	0.509
SAB128		CORE 1	1480	15.0	50	4.2	0.6	0.202	0.405
SAB128		RIM1	1467	13.7	46	4.0	0.3	0.188	0.531
SAB128		CORE 3	1445	11.7	39	3.3	0.2	0.170	0.414
SAB175		CORE2	1456	11.8	39	6.6	0.6	0.170	0.331
SAB175		RIM2	1489	14.6	49	10.3	1.3	0.197	0.343
SAB177		CORE3	1449	11.6	39	4.1	0.5	0.169	0.299
SAB177		RIM3	1468	13.3	44	4.7	0.5	0.184	0.512
SAB179		CORE 1	1533	16.9	56	2.3	0.5	0.217	0.359
SAB179		RIM 1	1496	12.8	43	6.0	0.4	0.177	0.576
SAB180		CORE 2	1534	17.5	58	1.9	0.3	0.223	0.484
SAB180		RIM 2	1447	9.1	30	9.1	0.4	0.146	0.543
SA02	ne-hawaiite	CORE 1	1496	21.4	71	2.3	1.4	0.279	0.189
SA02		RIM 1	1386	9.4	31	13.9	2.2	0.152	0.183
SA02		CORE 4	1415	13.0	43	5.5	1.7	0.185	0.167
SA02		RIM 4	1416	12.8	43	8.9	1.8	0.184	0.207
SA25		CORE 4	1387	11.7	39	7.9	1.1	0.174	0.222
SA29		CORE 1	1349	13.4	45	6.1	0.3	0.197	0.343
SA29		RIM 1	1363	15.2	51	6.2	0.4	0.216	0.331
SA65		CORE 2	1285	7.3	24	18.6	1.2	0.138	0.196
SA21	nephelinite	CORE 3	1411	8.6	29	18.2	2.7	0.143	0.158
SA21		CORE 4	1396	6.3	21	34.0	2.8	0.126	0.159
SA51		CORE	1360	7.9	26	22.1	2.2	0.140	0.178
SAB113		CORE2	1470	14.5	48	3.5	0.4	0.197	0.474
SAB113		RIM2	1469	14.5	48	5.2	0.7	0.197	0.384
SAB135		CORE 1	1412	9.9	33	8.9	0.4	0.155	0.351
SAB135		RIM 1	1469	15.8	53	5.4	0.5	0.212	0.457

Table 4.18 Temperature and pressure estimates, using the geothermobarometer models of Putirka *et al.* (1996), for clinopyroxene cores from selected group A samples[37]. Partition coefficient $K_{Na}^{cpx\text{-}melt}$ is derived from Eq. 16 in Blundy *et al.* 1995) and Eq. 4 in (Putirka, 1999) described in text. Errors for P and T are ± 1.4 kbar and ± 27° C respectively (Putirka *et al.*, 1996). n = number of cores per sample suitable for P-T modeling. Note: samples with a single P estimate indicates that only one of the analysed crystals contained a Jd component (necessary for modeling P). n.d. = not determined

Rock Type	Sample	n	Temp °C	P (kbar)	Depth (km) at 3.3 km/kbar	Al^{IV}/Al^{VI}	Fe^{3+}/Fe^{2+}	$K_{Na}^{cpx\text{-}melt}$ (Blundy *et al.*, 1995)	$K_{Na}^{cpx\text{-}melt}$ (Putirka, 1999)	$K_{Fe\text{-}Mg}^{cpx\text{-}melt}$	Host-rock Fe^{2+}/Mg
alkali ol-basalt	SA17	2	1251-1280	n.d.	n.d.	2.9-62.9	0.0-0.1	n.d.	n.d.	0.508-0.664	0.64
	SA18	3	1437-1512	11.1-19.5	37-65	1.8-4.6	0.2-1.2	0.075-0.152	0.165-0.251	0.183-0.517	0.67
	SA19	1	1440	14.3	48	4.6	1.6	0.112	0.198	0.135	0.82
	SAB162	2	1347-1366	8.3-7.9	26-28	8.6-9.2	1.4-2.4	0.071-0.074	0.140-0.144	0.103-0.148	0.88
transitional basalt	SA07	3	1464-1480	13.4-17.5	45-50	2.7-3.9	0.9-1.5	0.091-0.126	0.186-0.277	0.134-0.179	0.70
	SA13	2	1264-1270	n.d.	n.d.	2.3-2.4	0.0-0.2	n.d.	n.d.	0.520-0.701	0.56
hawaiite	SA20	3	1368-1415	6.4-11.1	21-37	4.7-10.5	1.3-2.3	0.052-0.083	0.127-0.167	0.114-0.175	0.83
	SAB151	3	1238-1285	n.d.	n.d.	1.8-2.9	-	n.d.	n.d.	0.419-0.563	0.64
	SAB163	2	1357-1372	7.9-9.6	26-32	8.0	1.0-2.4	0.068-0.082	0.140-0.155	0.102-0.173	0.96
ol-tholeiitic basalt	SA80	3	1220-1443	9.0	30	1.7-4.4	0.0-0.1	0.55	0.145	0.392-0.938	0.57
	SAB152	3	1214-1274	n.d.	n.d.	1.9-10.1	-	n.d.	n.d.	0.555-0.778	0.59
	SAB169	4	1245-1419	10.8	36	1.4-4.5	0.0-0.2	0.077	0.163	0.311-0.748	0.72
	SAB172	4	1259-1275	n.d.	n.d.	2.0-3.3	-	n.d.	n.d.	0.574-0.690	0.65
	SAB187	3	1275-1486	11.6	39	1.6-1.9	0.0-0.1	0.065	0.166	0.441-0.628	0.52
qz-tholeiitic basalt	SA76	3	1280-1293	n.d.	n.d.	1.7-2.8	-	n.d.	n.d.	0.398-0.458	0.67
	SA77	7	1250-1539	18.2	61	0.1-3.0	-	0.117	0.231	0.372-1.073	0.66
	SAB198	2	1312-1353	6.9-11.4	23-38	4.3-7.4	0.8-1.3	0.073-0.115	0.133-0.174	0.154-0.240	0.74

[37] P-T estimates were reported only for those crystals that met all crystal-structure modeling criteria. Pressure could not be estimated for crystals that do not contain a Jd component. Samples for which the pressure of all crystals could not be determined are indicated by "n.d." in the P(kbar) column.

Table 4.19 Temperature and pressure estimates, using the geothermobarometer models of Putirka *et al.* (1996), for clinopyroxene from selected group B samples[37]. Partition coefficient $K_{Na}^{cpx\text{-}melt}$ is derived from Eq. 16 in Blundy *et al.* (1995) and Eq. 4 in (Putirka, 1999) described in text. Errors for P and T are ± 1.4 kbar and ± 27° C respectively (Putirka *et al.*, 1996). n = number of cores per sample suitable for P-T modeling. Note: samples with a single P estimate indicates that only one of the analysed crystals contained a Jd component (necessary for modeling P). n.d. = not determined

Rock type	Sample	n	Temp °C	P (kbar)	Depth (km) at 3.3 km/kbar	Al^{IV}/Al^{VI}	Fe^{3+}/Fe^{2+}	$K_{Na}^{cpx\text{-}melt}$ (Blundy *et al.*, 1995)	$K_{Na}^{cpx\text{-}melt}$ (Putirka, 1999)	$K_{Fe-Mg}^{cpx-melt}$	Host-rock Fe^{2+}/Mg
nephelinite	SA21	2	1396-1411	6.3-8.6	21-29	18.2-34.0	2.7-2.8	0.046-0.059	0.126-0.143	0.159-0.210	0.59
	SA51	1	1360	7.9	26	22.1	2.2	0.067	0.140	0.178	0.78
	SAB113	4	1290-1470	7.6-14.5	25-48	2.7-14.4	0.0-0.6	0.054-0.101	0.136-0.197	0.395-0.618	0.56
	SAB135	3	1281-1433	9.9-11.6	33-39	8.9-9.0	0.4-0.6	0.071-0.082	0.155-0.170	0.351-0.574	0.64
	SAB178	3	1219-1286	n.d.	n.d.	7.5-19.9	0.3-0.5	n.d.	n.d.	0.424-0.455	0.59
ne-hawaiite	SA02	3	1344-1496	5.0-21.4	17-71	2.3-14.6	1.4-1.7	0.047-0.200	0.117-0.279	0.167-0.189	0.72
	SA25	1	1387	11.7	39	7.9	1.1	0.101	0.174	0.222	0.93
	SA29	3	1237-1349	13.4	44	2.9-6.1	0.0-0.3	0.153	0.197	0.338-0.359	1.05
	SA65	2	1271-1285	5.5-7.3	18-24	18.6-33.3	1.2-1.8	0.07-0.088	0.122-0.138	0.158-0.196	1.12
basanite	SA12	3	1362-1422	6.7-13.2	22-45	2.7-12.3	0.2-0.9	0.056-0.105	0.130-0.187	0.250-0.413	0.64
	SA27	3	1400-1409	12.6-13.4	42-45	5.2-9.2	0.3-0.8	0.108-0.115	0.183-0.190	0.292-0.391	0.90
	SA37	5	1281-1462	3.5-13.7	12-46	2.6-34.6	0.1-1.7	0.031-0.087	0.105-0.188	0.273-0.680	0.50
	SAB102	3	1283-1495	14.4-17.4	48-58	4.6-6.4	0.3-0.5	0.101-0.129	0.196-0.227	0.393-0.544	0.62
	SAB111	5	1266-1459	12.1	40	2.5-6.8	0.0-0.2	0.078	0.174	0.395-0.655	0.58
	SAB128	4	1276-1484	11.7-15.2	39-51	3.3-6.3	0.1-0.7	0.078-0.103	0.174-0.203	0.405-0.502	0.59
	SAB175	6	1257-1494	4.3-15.4	14-51	4.4-19.2	0.2-0.9	0.034-0.102	0.110-0.204	0.278-0.605	0.53
	SAB176	4	1276-1407	13.0	43	3.5-5.8	0.0-0.4	0.084	0.182	0.481-0.603	0.52
	SAB177	5	1266-1474	11.6-13.9	39-46	4.1-8.2	0.1-0.6	0.076-0.092	0.169-0.190	0.299-0.453	0.56
	SAB179	3	1313-1533	16.9	56	1.5-2.3	0.0-0.5	0.103	0.217	0.359-0.515	0.47
	SAB180	4	1321-1534	14.0-17.5	47-58	1.9-5.7	0.0-1.3	0.085-0.110	0.189-0.233	0.267-0.484	0.50
	SAB204	5	1196-1504	12.4-14.0	41-47	5.8-47.8	0.2-1.3	0.071-0.083	0.173-0.189	0.269-0.489	0.53
mugearite	SA88	4	1207-1315	n.d.	n.d.	2.0-11.5	-	n.d.	n.d.	0.316-0.644	0.81
alkali ol-basalt	SA54	3	1455-1506	14.1-19.0	47-63	3.3-5.4	1.5-2.2	0.103-0.147	0.194-0.246	0.114-0.171	0.74
	SAB188	4	1433-1481	8.2-14.1	37-47	5.5-20.2	1.8-5.1	0.051-0.092	0.139-0.192	0.114-0.222	0.59
	SAB207	3	1449-1574	8.5-19.2	28-64	5.1-14.3	1.4-2.6	0.050-0.126	0.141-0.242	0.156-0.199	0.56

In the group A rocks, alkali ol-basalt (SA18) and qz-tholeiitic basalt (SA77) contain crystals with the highest P-estimates, 19.4 and 18.2 kbar respectively and T-estimates, 1512 and 1539°C respectively (see Table 4.16; p.93). Additionally, SA18 and qz-tholeiitic basalt (SAB198) contain clinopyroxenes that exhibit the broadest range of crystallisation pressures, 11.1 to 19.5 kbar and 6.9 to 11.4 kbar respectively (Fig. 4.19), whereas SA77 contains crystals that crystallised over the broadest range of temperatures, 1250 to 1539°C, (see Table 4.18; p.95). Crystals from the ol-tholeiitic basalt and hawaiites samples show the least variation in P, Δ1.5 and Δ3.6 kbar respectively, and T, Δ65 and Δ60°C respectively. Pressure and temperature data for core-rim pairs exist for only four crystals in the group A rocks (see Table 4.16) and only one of these crystals (in alkali ol-basalt SAB162) have P-T estimates greater than the estimated error for these parameters. The lower P-T estimates for this crystal's rim suggests that at least some crystals from the group A rocks may have rims that crystallised at depths shallower than adjacent cores.

Clinopyroxenes in each group B rock type generally have overlapping P-T estimates, although crystal cores from some basanites e.g., SAB102, SAB128, SAB179, and SAB180, alkali ol-basalts e.g., SA54 and SAB207, and ne-hawaiite SA02, tend to have the highest P, e.g., > 15 kbar (see Table 4.17; p.94). Crystals in these samples also tend to have the highest estimated crystallisation temperatures, commonly > 1467°C. Each rock type in group B has samples with crystal populations that show little variations in P and T (e.g., $\Delta P < 2$ kbar and $\Delta T < 60$°C). However, as with the group A rocks, a number of samples from each rock type in group B contain crystals with relatively large variations in estimated P and T. Crystals in these samples generally have $\Delta P > 6$ kbar and $\Delta T > 125$°C (see Table 4.19; p. 133). Crystals in ne-hawaiite (SA02) exhibit the broadest range of P, 5.0 to 21.4 kbar. Basanites (SA37) and (SAB175) and alkali ol-basalt (SAB207) each contain crystal populations with $\Delta P > 10.0$ kbar, while nephelinite (SAB113) contains clinopyroxenes that crystallised over the range 7.6 to 14.5 kbar (Fig. 4.19). Crystals from the basanite samples generally have the greatest variations in T, e.g., ΔT up to 308°C.

Table 4.17 shows that P-T estimates for core-rim pairs in many crystals in the group B rocks are within the estimated error of the models, implying similar depths of crystallisation. A number of crystals however, show distinct differences in P and T between their core and rim where P-T values for rims are commonly less than those for adjacent cores, notably $\Delta P = 15.9$ kbar for core2-rim2 in alkali ol-basalt (SAB207) and $\Delta P = 12.0$ kbar for core1-rim1 in ne-hawaiite (SA02). Differences such as these possibly indicate continued crystallisation during magma ascent. Additionally, most of these

crystals have rims that are Ti enriched relative to their adjacent cores, a feature considered by Hart and Dunn (1993) to be indicative of crystal disequilibrium at lower pressure. In contrast, a number of crystals have rims with estimated P and T greater than their cores (e.g., SAB135 core1-rim1 and SAB175 core2-rim2; Table 4.17; p.94) suggesting a more complex crystallisation history.

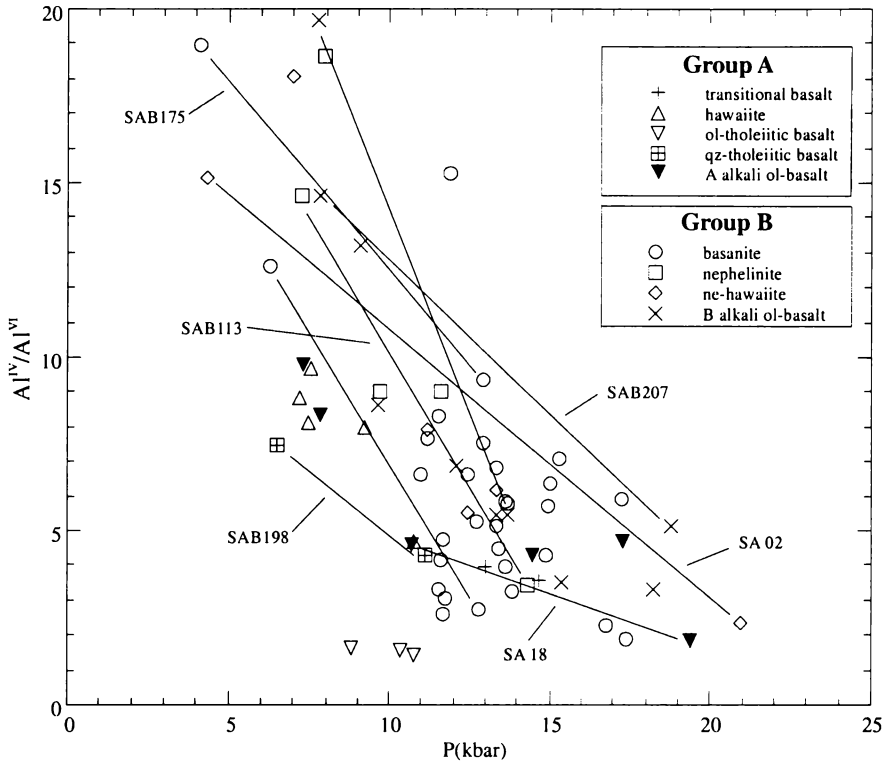

Fig. 4.19 Estimated pressure P(kbar) plotted against Al^{IV}/Al^{VI} for clinopyroxene phenocryst cores in selected samples from group A and B. The tie-lines join some of the high- and low-pressure clinopyroxene phenocrysts from the same sample.

The data in Tables 4.16 and 4.17 indicate that there is no apparent correlation between Fe^{3+}/Fe^{2+} and P for clinopyroxene cores from most samples of each rock type, except the alkali ol-basalts in group A and the basanites in group B. Values of Fe^{3+}/Fe^{2+} have been used to predict the relative oxygen fugacity (fo_2) in alkalic basalts (e.g., Dobosi, 1989). However, this lack of correlation suggests that, in the case of the SAVF clinopyroxenes, Fe^{3+}/Fe^{2+} may not be a good indicator of the fo_2 of the melt in which clinopyroxene crystallised.

Evaluation of the data in Tables 4.16 – 4.19 suggests that there is no apparent correlation between T and Al^{IV}/Al^{VI} for clinopyroxene in samples from either rock group. This feature is inconsistent with the findings of Adam and Green (1994) who showed that, in basanitic melts, T positively correlates with Al^{IV}/Al^{VI}. However, there is an overall

negative correlation between Al^{IV}/Al^{VI} and P (Fig. 4.19), which is consistent with the trends considered by Wass (1979), Wörner and Schmincke (1984a), Duda and Schmincke (1985), Dobosi (1989), and Green (1992) to be characteristic of clinopyroxene crystallisation at increasing pressure. Crystals from most group B samples generally exhibit the strongest correlation. However, when considering the relatively small sample size of crystals from group A, it is difficult to estimate the abundance of crystals from each group A rock type (or sample of a specific rock type) that may have crystallised under specific P-T conditions. On the other hand, the trends inferred from the existing data for the group A crystals (see Fig. 4.19) suggest that most crystals from this group may have Al^{IV}/Al^{VI}: P ratios similar to those of group B. Therefore, in the absence of numerical estimates for P based on models such as those of Putirka *et al.* (1996), Al^{IV}/Al^{VI} may be a useful indicator of relative crystallisation pressures.

4.5.4 Clinopyroxene – liquid equilibrium

Fe and Mg partitioning

The partitioning of Fe^{2+} and Mg between clinopyroxene and the host magma in which it crystallised can be estimated from an $(Fe\text{-}Mg)^{cpx}$ exchange equilibrium relationship similar to that used by Roeder and Emslie (1970) for olivines where:

$$K_{Fe-Mg}^{cpx-melt} = \frac{Fe^{cpx}Mg^{liq}}{Mg^{cpx}Fe^{liq}}$$

The calculated distribution coefficient, $K_{Fe-Mg}^{cpx-melt}$, for individual clinopyroxene cores and core-rim pairs from selected group A and B samples, are presented in Tables 4.16 and 4.17 respectively (see pp. 93 and 94). The range of $K_{Fe-Mg}^{cpx-melt}$ values for populations of clinopyroxene phenocryst cores in each sample from groups A and B are summarised in Tables 4.18 and 4.19 respectively (see pp. 95 and 96). Values for $K_{Fe-Mg}^{cpx-melt}$ range from 0.102 to 1.073 for phenocryst cores from the group A samples and 0.114 to 0.680 for those in the group B samples.

In group A the range of $K_{Fe-Mg}^{cpx-melt}$ values for crystal populations in individual samples commonly varies between samples of the same rock type as well as between samples from different rock types. For example, phenocrysts in hawaiites SA20 and SAB163 have $K_{Fe-Mg}^{cpx-melt}$ values < 0.175, whereas crystals in hawaiite SAB151 are in the range 0.419 -

0.563. Crystal populations in samples from the other rock types, except those from the ol-tholeiitic basalts, exhibit similar variations. Each ol-tholeiitic basalt sample has crystals with $K_{Fe-Mg}^{cpx-melt}$ values > 0.311 with the broadest range occurring in SA80 (0.392-0.938).

In the group B rocks, similar variations occur in the nephelinite and ne-hawaiite samples. In contrast, the clinopyroxene phenocrysts in the alkali ol-basalt samples have relatively small $K_{Fe-Mg}^{cpx-melt}$ values (e.g., 0.114 - 0.222), which are in marked contrast to those from the basanites, all of which have $K_{Fe-Mg}^{cpx-melt}$ values > 0.250.

Studies by Irving and Frey (1984) and Liotard *et al.* (1988) of natural clinopyroxene megacrysts from alkalic basalts suggest that crystals with $K_{Fe-Mg}^{cpx-melt}$ values between 0.20 and 0.40 may be in equilibrium with their host rock under "high-pressure" conditions. An important observation of the data given in Tables 4.18 and 4.19 is that the majority of samples from group B contain crystals with $K_{Fe-Mg}^{cpx-melt}$ values between 0.20 and 0.40. In contrast, only 5 samples from group A contain crystals that fall within this range. Additionally, evaluation of these data indicates that in 12 samples from group A and 8 from group B all analysed crystals have $K_{Fe-Mg}^{cpx-melt}$ values that fall outside the range of crystal-host equilibrium.

Crystals that fall outside this range may have an exotic origin. Alternatively, the small $K_{Fe-Mg}^{cpx-melt}$ values, e.g., < 0.20, may be a response to a comparatively large Fe^{2+}/Mg of the host rock. Evaluation of the data in Table 4.18 suggests that $K_{Fe-Mg}^{cpx-melt}$ and Fe^{2+}/Mg negatively correlate in the group A rocks. However, a similar correlation does not appear to occur in the group B rocks (see Table 4.19).

Liotard *et al.* (1988) suggested that $K_{Fe-Mg}^{cpx-melt}$ values exceeding the accepted equilibrium maximum, e.g., > 0.4, may be due to the occurrence of small mafic xenoliths or olivine xenocrysts in the host rock, which will modify the whole-rock MgO content. This is a plausible explanation for the SAVF rocks given that many of the samples contain populations of "non-equilibrium" olivine crystals (see Fig. 4.6, p. 95), many of which are megacrysts, possibly of exotic origin. Alternatively, the experimental studies of Sack and Carmichael (1984) involving the exchange reactions of Fe^{2+}, Mg, and Ti between clinopyroxene and silicate melts show that Ti substitution in clinopyroxene significantly affects the partitioning of Fe^{2+} and Mg between clinopyroxene and its host magma.

Na partitioning between clinopyroxene and host-rock

Na is an important minor element in the SAVF clinopyroxenes because:

1. The abundance of Na in mantle melts is sensitive to the degree of partial melting of the source mantle peridotite. When considering that the majority of the Na budget of a plagioclase-free peridotite is restricted to clinopyroxene (e.g., McKenzie and O'Nions, 1991; Blundy *et al.*, 1995), Na partition coefficients are useful in the study of mantle melting.

2. Experimental studies have shown that Na partitioning is sensitive to P (e.g., Blundy *et al.*, 1995; Putirka, 1999). Therefore, partial-melting depths of individual magma batches may be inferred from Na partition coefficients derived from clinopyroxene compositions.

Partition coefficients for Na between clinopyroxenes and their host rocks were obtained by using Eq. 4 of Putirka (1999). This model was constructed from least-squares regression analyses of synthetic clinopyroxene-liquid pairs under experimental conditions that range from 0 to 100 kbar and 1350 to 2500 K. The partition coefficient $K_{Na}^{cpx\text{-}melt}$ is given as:

$$K_{Na}^{cpx\text{-}melt} = \exp\left[-2.48 + 0.11\left(\frac{P(bars)}{T(K)}\right) - 5x10^{-7}\left(\frac{P(bars)^2}{T(K)}\right)\right]$$

where P is in kbars and T in Kelvin. The values for P and T are given in Tables 4.16 and 4.17 (pp. 93 and 94) for individual clinopyroxene phenocrysts.

For comparison purposes, $K_{Na}^{cpx\text{-}melt}$ for each crystal was also calculated from the empirical equation Eq. 16 of Blundy *et al.* (1995):

$$K_{Na}^{cpx\text{-}melt} = \exp\left(\frac{10367 + 2100P - 165P^2}{T} - 10.27 + 0.358P - 0.0184P^2\right)$$

where values for P given in Tables 4.16 and 4.17 are converted to gigapascals. Temperature (T) is in Kelvin. This model was derived from experimental studies of synthetic clinopyroxene under conditions that range from ~ 0 to 60 kbar and ~1000 to 2000 K.

Calculated distribution coefficients $K_{Na}^{cpx\text{-}melt}$ for clinopyroxene from selected group A and B samples are summarised in Tables 4.18 and 4.19 (pp. 95 and 96). Based on the Putirka *et al.* (1999) model, values for $K_{Na}^{cpx\text{-}melt}$ range from 0.127 to 0.277 for phenocryst cores from the group A samples and 0.105 to 0.279 for those in the group B samples. The

values of $K_{Na}^{cpx\text{-}melt}$ for the same crystals derived by the Blundy *et al.* (1995) equation are considerably less, typically by a factor of two.

The relationship between $K_{Na}^{cpx\text{-}melt}$ and estimated P is illustrated in Fig. 4.20, which indicates that $K_{Na}^{cpx\text{-}melt}$ and P values for crystal populations in each rock type are variable. The most important feature of Fig. 4.20 is that for the clinopyroxenes in the SAVF rocks, $K_{Na}^{cpx\text{-}melt}$ strongly correlates with P irrespective of rock type or group. This is consistent with the findings of the experimental study of Blundy *et al.* (1995) on Na partitioning between synthetic clinopyroxene and silicate melts, which clearly demonstrated a positive correlation between $K_{Na}^{cpx\text{-}melt}$ and pressure for clinopyroxene-liquid pairs.

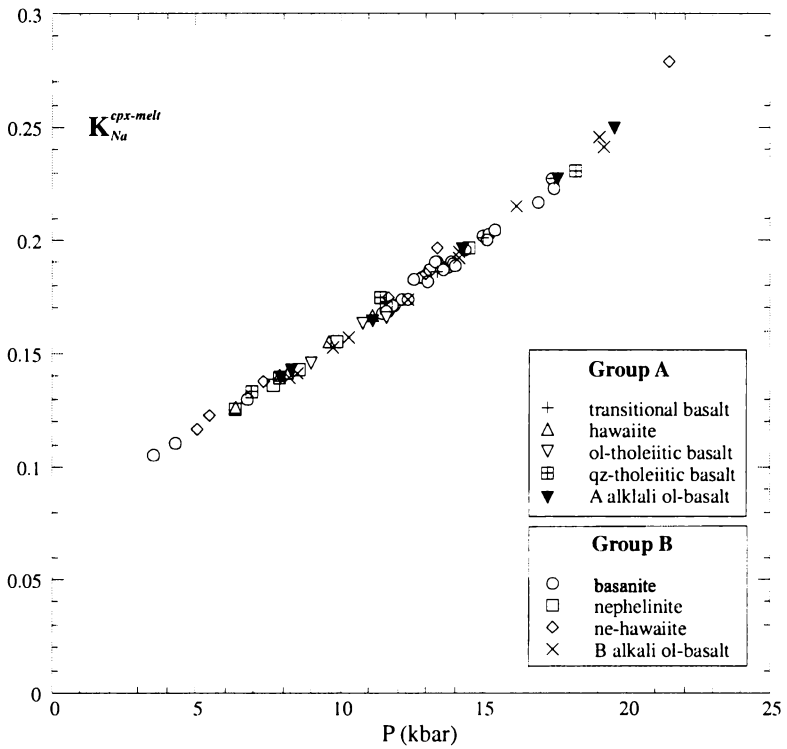

Fig. 4.20. Calculated partition coefficients $K_{Na}^{cpx\text{-}melt}$, derived from Eq. 4 of Putirka (1999), plotted against estimated pressure (P kbar), for clinopyroxene phenocryst cores in selected samples from group A and B rocks.

4.6 Feldspars and feldspathoids

Plagioclase is the only feldspar present as a phenocryst phase in the South Auckland volcanic field lavas and is generally restricted to the group A rocks. Additionally, plagioclase is the dominant groundmass phase in each group A rock type. Feldspathoid minerals (e.g., nepheline, kalsilite, and leucite) were not observed in thin-section or detected by electron microprobe analyses in any of the group A samples, which is

consistent with their absence in whole-rock CIPW normative mineralogy. In the group B rocks, plagioclase is generally limited to the groundmass and is the dominant phase in all samples. However, rare microphenocrysts were observed in a small number of samples, primarily from the alkali ol-basalts and the mugearite. Potassium feldspar (K-feldspar) is an additional groundmass phase in some group A alkali ol-basalts, hawaiites, and ol-tholeiitic basalts, whereas nepheline and K-feldspar occur in many group B rocks. These minerals however, are identifiable only by electron microprobe analysis, therefore their relative abundance is uncertain.

4.6.1 Group A feldspars

Plagioclase commonly occurs as relatively large (up to 1.5 mm) tabular phenocrysts and less frequently as tabular microphenocrysts that exhibit a range of morphologies (e.g., euhedral, subhedral, and irregularly shaped crystals). Phenocrysts and microphenocrysts infrequently have partially resorbed or sieve-textured cores. Zoned crystals were observed in some thin-sections but they are typically not abundant. In the groundmass in all rock types, plagioclase occurs as abundant tabular laths and in interstitial pools. Most phenocrysts, microphenocrysts, and groundmass crystals contain small (e.g., < 20 μm) apatite inclusions.

The abundance of plagioclase phenocrysts typically varies between rock types and within individual samples of the same rock type (Table 4.20). Additionally, plagioclase is the dominant phenocryst phase in a number of samples from each rock type, except the qz-tholeiitic basalts, ranging from < 1.0 to 20.0 modal percent greater than olivine and clinopyroxene (see Appendix 3, Table A3.1 to A3.5, for complete modal abundance data set for all group A samples). There does not appear to be an overall correlation between plagioclase and olivine or clinopyroxene abundance. The largest modal variation occurs in ol-tholeiitic basalt sample SA93 where plagioclase exceeds olivine by a ratio of 100:1. High-modal plagioclase samples tend to be from the more differentiated host rocks, which have $100Mg/(Mg + Fe^{2+})$ values ranging between 50.4 and 54.3, possibly indicative of olivine removal during fractional crystallisation processes. However, SA93 is a notable exception to this trend with a $100Mg/(Mg + Fe^{2+})$ value of 60.4.

Nineteen representative analyses selected from 300 group A plagioclase core-rim pairs, and groundmass crystals are presented in Table 4.21. All plagioclase analyses for each group A rock sample are given in Appendix 6, Tables A6.11 to A6.15. The range of core and rim compositions for all group A rock types and some of the extreme compositions of

core-rim pairs are shown in Fig. 4.21. Plagioclase phenocrysts and microphenocrysts in all group A rock types have similar core compositions – predominantly labradorite and rare high-Ca andesine ($An_{35.2-46.7}$). Phenocrysts of labradorite compositions typically have a small orthoclase component. However, orthoclase content in cores generally increases as they become more sodic, which correlates well with the relatively small K_2O content of their host rock.

Table 4.20 Plagioclase phenocryst and microphenocryst modal abundance for selected group A rocks. Mode based on 1000 point counts. n = number of samples counted. Mean = ± 1 standard deviation.

	modal abundance			
Rock type	Max	Min	Mean	n
transitional basalt	10.8	<0.2	2.8 ± 3.3	15
hawaiite	21.0	0.2	4.3 ± 4.4	29
ol-tholeiitic basalt	20.8	< 0.2	3.0 ± 3.9	34
qz-tholeiitic basalt	2.0	0.4	1.2 ± 0.7	4
alkali ol-basalts	12.4	0.8	5.8 ± 4.3	5

Most phenocrysts in each group A rock type have weak normal zoning. Phenocrysts commonly have relatively narrow rims (many indistinguishable in thin-section), although some crystals display complex oscillatory patterns. Typically, rims have comparatively sodic compositions relative to adjacent cores. A small number of phenocrysts have rare, reverse zoning. These crystals generally have cores $<An_{60}$ and rims with An contents up to 5 mol. % greater than adjacent cores.

Although most phenocryst zoning is relatively weak (typically core-rim pairs are within the range of labradorite compositions) some alkali ol-basalt, hawaiite, and ol-tholeiitic basalt samples contain phenocrysts that are strongly zoned. These crystals typically have labradorite cores with rims that range from high-Na bytownite ($An_{71.7}$) to oligoclase ($An_{29.9-19.0}$) compositions (Fig. 4.21). Samples of these rock types often have populations of crystals with rims that exhibit a systematic increase of orthoclase content, up to 8.3 mol. %, with decreasing An content.

In contrast to the other group A rock types, zoned phenocrysts are rare in the transitional basalts. Cores and rims generally have a narrow range of labradorite compositions ($An_{56.2-57.6}$).

Groundmass compositions in each group A rock type overlap those of cores and rims (Fig 4.21). In each rock type, especially the transitional basalts and qz-tholeiitic basalts, most groundmass crystals range from labradorite to high-Na andesine ($An_{69.9-40.6}$). Groundmass crystals in the alkali ol-basalts, hawaiites, and ol-tholeiitic basalts however, exhibit a relatively continuous range of compositions, from high-Na bytownite to calcic

Table 4.21 Representative electron microprobe analyses of feldspars in selected group A lavas, South Auckland volcanic field. C = core, R = rim, G = groundmass

Rock type	transitional basalt			hawaiite				ol-tholeiitic basalt				qz-tholeiitic basalt				alkali ol-basalt			
Sample	SA13		SA17	SA20		SA32	SAB151	SAB169		SAB173	SA36	SA76		SA77	SAB198	SA33		SA17	
Analysis	40-C2	41-R2	1914-G	1867-C3	1868-R3	1954-G	677-G	411-C3	412-R3	989-G	810-G	460-C3	461-R3	627-G	1592-G	1707-C1	1708-R1	142-G	427-G
SiO_2	51.14	54.28	52.97	50.86	54.52	51.82	63.36	52.99	57.02	59.37	59.72	51.62	53.91	52.79	58.92	51.70	60.34	51.47	62.96
TiO_2	-	-	0.30	-	0.37	-	-	-	0.33	0.21	0.27	-	-	-	-	-	-	-	-
Al_2O_3	30.88	28.44	26.73	30.36	28.45	29.49	21.47	29.59	26.20	24.60	23.73	30.35	29.09	29.66	24.61	30.18	23.30	30.36	23.02
FeO	0.72	0.90	1.75	0.56	1.84	1.08	0.82	0.47	0.99	0.73	1.01	0.55	0.66	0.90	0.59	0.48	1.20	0.56	0.58
MgO	-	-	0.74	0.29	0.30	-	-	-	-	-	-	-	-	-	-	0.38	0.45	-	-
CaO	14.32	11.46	11.40	13.46	9.87	12.06	3.48	12.30	8.83	6.65	7.78	13.77	12.16	12.56	6.45	12.84	5.43	13.42	3.89
Na_2O	3.48	4.81	4.45	4.01	4.96	4.38	7.94	4.42	6.05	7.04	5.00	3.74	4.63	4.40	7.45	4.43	7.77	3.56	7.83
K_2O	-	0.20	0.27	0.15	0.37	0.27	2.15	0.12	0.51	0.59	1.52	-	0.22	0.18	0.84	0.19	1.07	0.23	2.49
Total	100.54	100.09	98.61	99.69	100.68	99.10	99.22	99.89	99.93	99.19	99.03	100.03	100.67	100.49	98.86	100.20	99.56	99.60	100.77
Number of ions on the basis of 32 oxygen																			
Si	9.226	9.760	9.975	9.315	9.827	9.530	11.379	9.622	10.288	10.826	10.932	9.398	9.722	9.565	10.744	9.405	10.874	9.341	11.165
Ti	-	-	0.008	-	0.051	-	-	-	0.045	0.029	0.038	-	-	-	-	-	-	-	-
Al	6.566	6.029	5.933	6.554	6.045	6.390	4.544	6.333	5.571	5.286	5.120	6.515	6.182	6.336	5.290	6.474	4.947	6.496	4.810
Fe^{2+}	0.109	0.134	0.275	0.086	0.278	0.166	0.125	0.070	0.150	0.112	0.157	0.083	0.099	0.138	0.090	0.074	0.179	0.083	0.086
Mg	-	-	0.208	0.077	0.080	-	-	-	-	-	-	-	-	-	-	0.102	0.122	-	-
Ca	2.768	2.208	2.301	2.643	1.907	2.378	0.669	2.394	1.709	1.299	1.526	2.688	2.349	2.438	1.261	2.502	1.050	2.611	0.739
Na	1.216	1.677	1.626	1.424	1.734	1.565	2.765	1.555	2.118	2.490	1.773	1.322	1.619	1.549	2.634	1.565	2.717	1.251	2.691
K	-	0.045	0.064	0.035	0.086	0.064	0.493	0.026	0.118	0.138	0.355	-	0.051	0.042	0.195	0.045	0.246	0.054	0.563
End-member compositions																			
An	69.5	56.2	57.7	64.4	51.2	59.3	17.0	60.2	43.3	33.1	41.8	67.0	58.4	60.5	30.8	60.9	26.2	66.7	18.5
Ab	30.5	42.7	40.7	34.7	46.5	39.1	70.4	39.1	53.7	63.4	48.5	33.0	40.3	38.4	64.4	38.1	67.7	31.9	67.4
Or	-	1.1	1.6	0.9	2.3	1.6	12.6	0.6	3.0	3.5	9.7	-	1.3	1.0	4.8	1.1	6.1	1.4	14.1

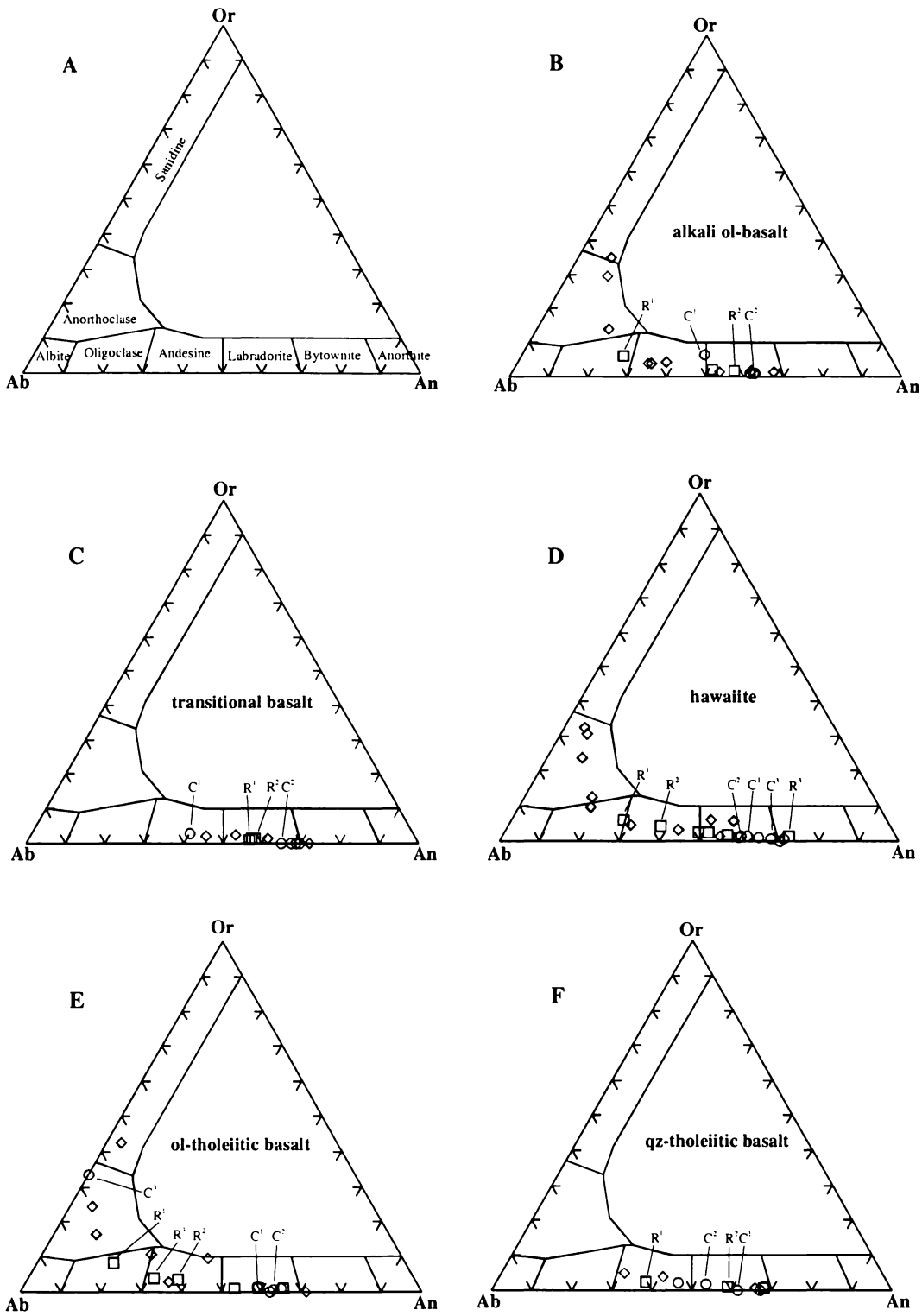

Fig. 4.21 Representative feldspar phenocryst and groundmass compositions (mol. %) for each rock type. ○ = phenocryst core, □ = rim, and ◊ = groundmass crystal. The composition fields and mineral classification for each diagram are as in the template shown in figure (A). Selected phenocryst core-rim pairs (C = core, R = rim) are identified by their corresponding superscript numbers.

anorthoclase in the hawaiites, to rare high-Na sanidine in the alkali ol-basalt and ol-tholeiitic basalts (see Appendix 6, Table A6.16 for K-feldspar compositions in the group A rocks). There is no apparent distinction in composition between the tabular laths and crystals that from the interstitial pools.

4.6.2 Group B feldspars and feldspathoids

Plagioclase

Plagioclase occurs as rare microphenocrysts in a minor number of samples in each group B rock type. However, with the exception of the mugearite sample, plagioclase in the group B rocks is generally limited to the groundmass. Eighteen representative analyses selected from 156 group B plagioclase core-rim pairs, and groundmass crystals are presented in Table 4.22. Complete plagioclase analyses for group B rock samples are given in Appendix 6, Tables A6.30 to A6.34.

The mugearite sample is atypical of the group B rock types. It contains compositionally zoned plagioclase phenocrysts that span a broad range of compositions from labradorite ($An_{58.6}$) to oligoclase ($An_{16.3}$), as shown in Fig. 4.22F. As with the group A phenocryst cores and rims, orthoclase content increases with decreasing An content reaching 10.3 mol. % Or in the most sodic oligoclase crystal. In contrast to most zoned group A phenocrysts, a number of the mugearite phenocrysts exhibit relatively strong reverse zoning trends, indicative of disequilibrium crystallisation conditions. Rim compositions are comparable to those in the group A alkali ol-basalts, hawaiites, and ol-tholeiitic basalts but adjacent cores are generally more sodic than their group A counterparts.

In the other group B rocks, microphenocryst compositions range from labradorite to moderately calcic andesine ($An_{69.6\text{-}37.8}$), although most of these crystals have compositions $< An_{50}$ (Figs. 4.22B -E).

Plagioclase is the dominant groundmass phase in all group B rock types. It occurs as laths, microlites, and small crystals in interstitial pools. The pools are generally much larger than the other groundmass crystals. However, there is no apparent correlation between crystal habit or size and plagioclase composition. The groundmass crystals in all group B rock samples have plagioclase compositions, which overlap those of the group A rocks. Compositions span a continuous range from labradorite through to calcic oligoclase, although most compositions are labradorite to moderately sodic andesine (Fig.

Table 4.22 Representative electron microprobe analyses of feldspars from selected group B lavas, South Auckland volcanic field. C = core, R = rim, G = groundmass.

Rock type	basanite				nephelinite			ne-hawaiite			mugearite				alkali ol-basalt			
Sample	SAB128	SA12	SA37	SAB175	SAB113		SA21	SA02	SA25	SA65	SA88				SA54		SAB188	SAB207
Analysis	730-C	1257-G	903-G	1064-G	231-C	746-G	1410-G	1497-C	1531-G	1565-G	489-C3	491-R3	499-G	500-G	1673-C1	1674-R1	1664-C	1630-C
SiO_2	52.82	58.72	50.65	57.65	49.23	52.69	51.28	51.45	58.94	56.39	57.47	53.65	57.73	51.98	51.76	52.16	59.40	51.72
TiO_2	-	0.39	-	0.39	1.66	0.19	0.27	0.22	-	-	-	-	0.26	-	-	-	0.28	-
Al_2O_3	29.56	23.93	30.83	24.94	23.74	29.69	29.02	29.15	25.74	26.88	26.71	28.78	25.33	30.62	29.93	29.02	23.90	31.00
FeO	0.67	0.60	0.64	1.14	3.31	0.60	0.79	0.92	0.71	0.54	0.52	0.92	0.91	0.64	0.39	0.49	1.10	0.74
MgO	-	-	-	-	2.13	-	0.56	0.38	-	0.29	-	-	-	-	-	0.28	0.71	0.27
CaO	12.14	5.22	13.07	6.35	13.07	11.88	12.53	11.98	6.42	8.35	8.73	11.71	7.46	13.42	12.59	11.86	4.60	12.93
Na_2O	4.27	4.78	3.72	6.45	4.30	4.32	4.04	4.21	7.49	6.45	6.21	4.88	6.06	3.96	4.12	4.51	6.77	4.00
K_2O	0.29	5.00	0.29	2.07	1.22	0.42	0.30	0.35	0.68	0.56	0.58	0.30	1.11	0.20	0.31	0.29	3.12	0.25
Total	99.75	98.64	99.20	98.99	98.66	99.79	98.79	98.66	99.98	99.46	100.22	100.24	98.86	100.82	99.10	98.61	99.88	100.91
Number of ions on the basis of 32 oxygen																		
Si	9.616	10.844	9.309	10.525	9.270	9.587	9.579	9.585	10.563	10.211	10.310	9.731	10.559	9.398	9.494	9.664	10.742	9.341
Ti	-	0.054	-	0.054	0.237	0.026	0.038	0.032	-	-	-	-	0.035	-	-	-	0.038	-
Al	6.342	5.210	6.678	5.366	5.270	6.368	6.390	6.400	5.437	5.734	5.648	6.154	5.459	6.525	6.470	6.339	5.094	6.598
Fe^{2+}	0.102	0.093	0.099	0.176	0.522	0.093	0.125	0.142	0.106	0.080	0.080	0.141	0.138	0.096	0.061	0.077	0.166	0.112
Mg	-	-	-	-	0.598	-	0.157	0.106	-	0.080	-	-	-	-	-	0.077	0.192	0.070
Ca	2.368	1.034	2.573	1.242	2.637	2.317	2.509	2.391	1.232	1.619	1.680	2.275	1.462	2.602	2.474	2.355	0.893	2.502
Na	1.507	1.712	1.325	2.282	1.571	1.523	1.462	1.520	2.602	2.262	2.160	1.715	2.147	1.389	1.466	1.619	2.374	1.402
K	0.067	1.178	0.067	0.483	0.294	0.099	0.074	0.084	0.157	0.128	0.131	0.067	0.259	0.045	0.074	0.070	0.720	0.058
End-member compositions																		
An	60.1	26.3	64.9	31.0	58.6	58.8	62.0	59.9	30.9	40.4	42.3	56.1	37.8	64.5	61.6	58.2	22.4	63.2
Ab	38.2	43.6	33.4	56.9	34.9	38.7	36.2	38.0	65.2	56.4	54.4	42.3	55.5	34.4	36.5	40.0	59.6	35.4
Or	1.7	30.0	1.7	12.1	6.5	2.5	1.8	2.1	3.9	3.2	3.3	1.7	6.7	1.1	1.8	1.7	18.1	1.5

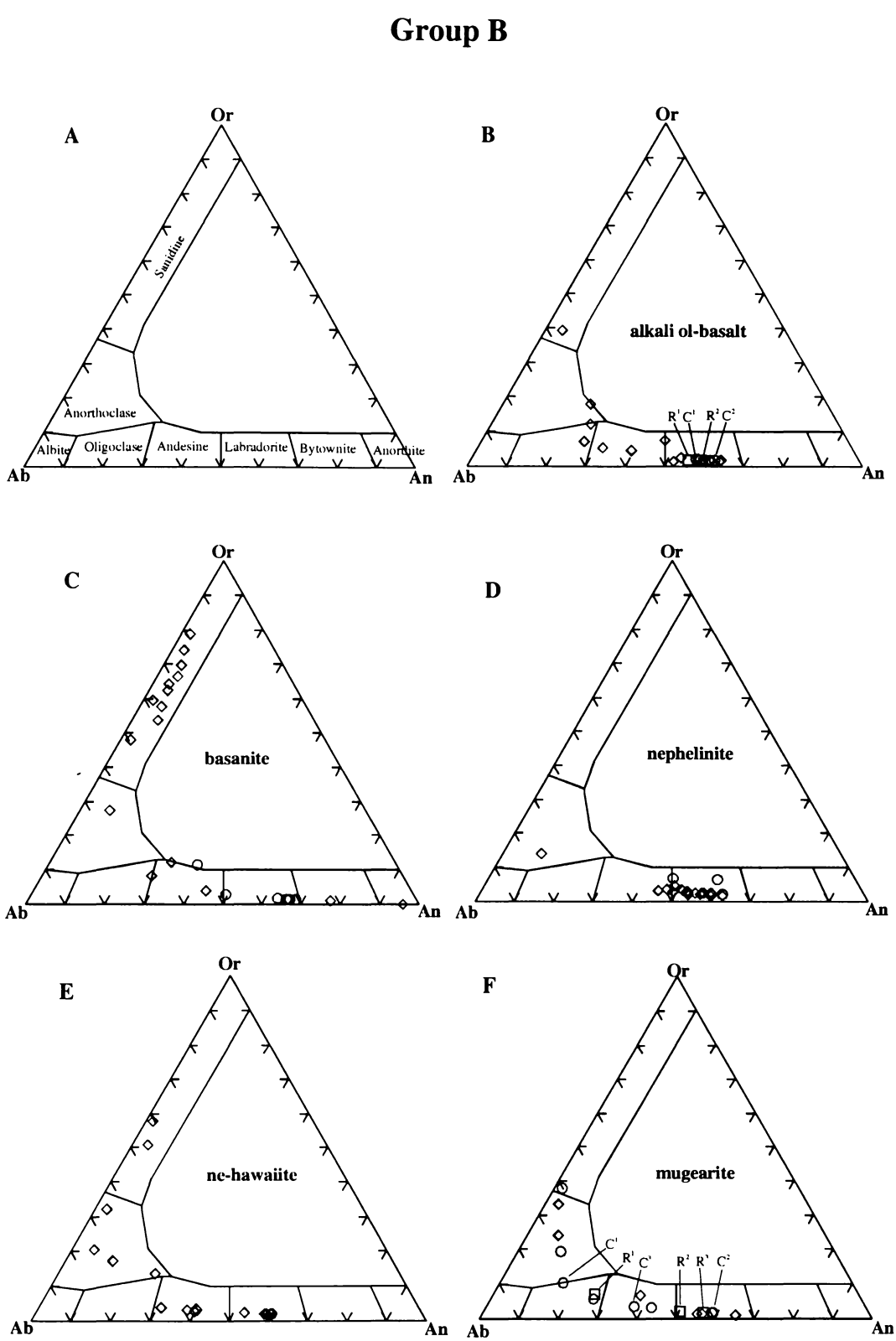

Fig. 4.22 Representative feldspar phenocryst and groundmass compositions (mol. %) for each group B rock type. ○ = phenocryst and microphenocryst core, □ = rim, and ◊ = groundmass crystal. The composition fields and mineral classification for each diagram are as in the template shown in figure (A). Selected phenocryst core-rim pairs (C = core, R = rim) are identified by their corresponding superscript numbers.

4.22). Crystals in the group B rocks tend to have larger Or-content at smaller An-contents than those in group A rocks, which probably reflects the larger K_2O contents of the group B host rocks.

Potassium feldspar and nepheline

In contrast to group A samples, each group B rock type, except mugearite, contains samples with distinct populations of potassium feldspar and nepheline. Although these crystals could not be positively identified optically, results of electron microprobe analyses suggest that these minerals occur only as groundmass phases as short, stubby twinned or untwinned laths, small, thin microlites, and interstitial pools. While the relative abundance of potassium feldspar and nepheline is uncertain, the comparatively small number detected using the electron microprobe suggests that these minerals are minor groundmass phases in all group B rock types.

Basanite samples tend to contain the greatest abundance of crystals having sanidine compositions ($Or_{47.9\text{-}78.9}$) with rare anorthoclase (Fig. 4.22C). Complete analyses of potassium feldspar are given in Appendix 6, Table A6.35. The large amount of sanidine attributed to basanite rocks however, may be due to sample bias (i.e., more basanites were analysed than any other rock type). Nevertheless, samples from the other rock types tend to contain crystals having predominantly anorthoclase compositions ($Or_{14.0\text{-}38.0}$) and rare sanidine (Figs. 4.22B, D, E, and F).

The relative abundance of K-feldspar may be attributed generally to the more potassic nature of the silica-undersaturated group B host rocks. However, the comparatively large amount of K-feldspar observed in the SAVF basanites contrasts with the relatively small abundance in the basanites from the volcanic provinces in eastern Australia. There, the greatest amount of K-feldspar is reported to occur in the hawaiites and ol-tholeiitic basalts (Ewart, 1989).

Nepheline crystals occur in samples from each group B rock type, except mugearite, and commonly occur together with groundmass K-feldspar. Representative nepheline analyses are presented in Table 4.23. Complete analyses of nepheline in all group B rock types are given in Appendix 6, Table A6.36.

Nepheline in each rock type has overlapping compositions similar to those from the alkaline basic rocks described in Henderson and Gibb (1983). The compositions for most of the nepheline in all samples show that the silica component (Q) generally correlates

negatively with the nepheline (Ne) and positively with the kalsilite (Ks) components (Fig. 4.23). For each rock type, nepheline shows small but distinct differences in composition, which may be related to the crystallisation history of their host rock (Henderson and Gibb, 1983). Nepheline in nephelinites ($Ne_{49.9\text{-}75.4}Ks_{8.2\text{-}16.7}Q_{5.5\text{-}22.0}$) and basanites ($Ne_{52.2\text{-}76.5}Ks_{4.8\text{-}20.1}Q_{12.0\text{-}27.7}$) exhibit the broadest range of compositions. In contrast, nepheline in the alkali ol-basalts ($Ne_{73.6\text{-}75.9}Ks_{5.8\text{-}8.3}Q_{15.7\text{-}20.6}$) has a narrow range of composition, which overlaps those of several of the nephelinite and basanite samples. In the ne-hawaiites, nepheline has a broad range of compositions ($Ne_{66.6\text{-}79.2}Ks_{6.1\text{-}18.8}Q_{13.9\text{-}32.8}$), some of which overlap those of the other rock types. However, a number of crystals, particularly those from ne-hawaiite SA65, are distinct from those of the other rock types. These crystals tend to be the most Q-rich nepheline and have Ks components that increase with increasing Q, a feature that correlates well with the comparatively large SiO_2 content of their host rocks.

Table 4.23 Representative electron microprobe analyses of nepheline in the groundmass of group B rocks, South Auckland volcanic field.

Rock Type	basanite				nephelinite			ne-hawaiite				alkali ol-basalt	
Sample	SA12	SAB176	SAB179	SAB180	SA21	SA28	SA51	SA29		SA65		SA54	SAB207
Analysis	1271-G	658-G	598-G	1297-G	1411-G	1446-G	1466-G	448-G	450-G	1555-G	1564-G	1696-G	1628-G
SiO_2	49.76	51.59	55.61	49.16	50.84	43.78	50.93	48.96	56.35	55.97	55.74	51.62	50.50
TiO_2	-	-	0.23	-	0.26	-	-	-	-	-	-	-	-
Al_2O_3	29.89	26.51	25.52	29.04	28.83	33.05	29.20	30.45	25.22	24.08	26.10	27.86	30.34
FeO	0.67	2.68	0.79	1.72	1.27	1.12	1.05	1.32	0.86	2.31	1.01	1.43	0.62
MgO	-	0.40	-	-	0.45	-	-	-	-	0.37	-	0.34	0.30
CaO	0.43	0.52	0.66	0.22	1.15	-	0.34	0.14	0.70	0.58	0.68	0.48	0.41
Na_2O	16.07	12.63	11.68	14.63	13.51	16.85	15.86	16.12	10.29	11.04	13.93	15.34	16.37
K_2O	2.33	4.35	5.48	3.91	2.59	4.46	2.56	3.13	5.29	5.30	2.20	1.64	2.45
Total	99.15	98.68	99.97	98.68	98.90	99.26	99.94	100.12	98.71	99.65	99.66	98.71	100.99
Number of ions on the basis of 32 oxygen													
Si	9.341	9.859	10.294	9.363	9.673	8.435	9.488	9.181	10.661	10.679	10.246	9.914	9.210
Ti	-	-	0.032	-	0.038	-	-	-	-	-	-	-	-
Al	6.614	5.971	5.568	6.518	6.464	7.504	6.413	6.730	5.626	5.418	5.654	6.307	6.522
Fe^{2+}	0.106	0.429	0.122	0.275	0.202	0.182	0.163	0.208	0.134	0.368	0.154	0.230	0.093
Mg	-	0.115	-	-	0.128	-	-	-	-	0.106	-	0.096	0.080
Ca	0.086	0.106	0.131	0.045	0.237	-	0.067	0.029	0.141	0.118	0.134	0.099	0.080
Na	5.850	4.682	4.195	5.402	4.986	6.294	5.731	5.862	3.776	4.083	4.966	5.712	5.786
K	0.557	1.062	1.296	0.950	0.630	1.098	0.608	0.749	1.277	1.290	0.515	0.400	0.570
End-member compositions													
Ne ($NaAlSiO_2$)	75.9	61.6	54.7	69.9	67.4	79.2	74.1	75.4	49.9	52.7	65.8	73.6	75.9
Ks ($KAlSiO_2$)	8.1	15.5	18.8	13.7	9.5	15.3	8.7	10.7	18.8	18.5	7.6	5.8	8.3
Q (SiO_2)	16.0	22.9	26.5	16.4	23.1	5.5	17.2	13.9	31.3	28.8	26.6	20.6	15.7

The nepheline in the group B rocks exhibits compositional trends similar to those studied by Henderson and Gibb (1983; Fig. 2), although most group B crystals plot notably above

the 1068°C isotherm of Hamilton (1961) (Fig. 4.23). Henderson and Gibb (1983) attributed trends such as these to nepheline crystallisation during different stages of the crystallisation history of their host magma where early-crystallised nepheline has relatively small Q content. In contrast, nepheline that crystallises late in the fractionation process is relatively Q enriched. Based on these findings, the data plotted in Fig. 4.23 suggest that most of the nepheline in the nephelinites represent "early" crystallisation while those in the ne-hawaiites crystallised "late" in the fractionation process. Those crystals with intermediate Q contents (e.g., basanites and alkali ol-basalts) crystallised under "intermediate" conditions.

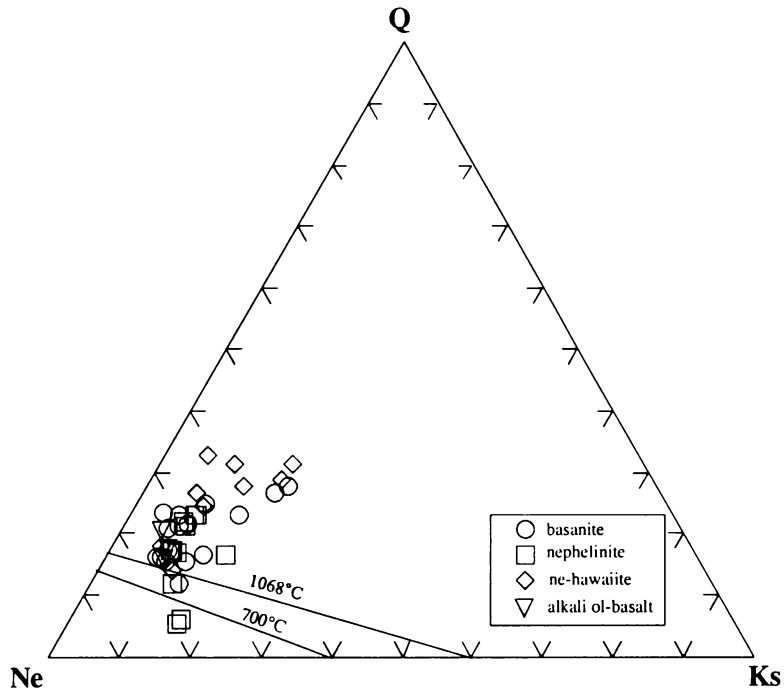

Fig. 4.23 Compositions of groundmass nepheline in the group B rocks. The 1068° C isotherm represents the maximum temperature for feldspar solid solution in nepheline at 1 atm (from Henderson and Gibb, 1983). The 700° C isotherm represents the limit of feldspar solid solution in nepheline at 1 kbar, P_{H_2O} (after Hamilton, 1961). Q = SiO_2, Ne = $NaAlSiO_2$, and Ks = $KalSiO_2$.

4.7 Fe-Ti-Cr oxides

4.7.1 Titanomagnetite and ilmenite

Titanomagnetite and ilmenite occur predominantly as groundmass grains in all group A rock types and the mugearite sample from group B. Titanomagnetite also occurs as rare microphenocrysts in a small number of group A and B samples.

In the group A rocks and mugearite, titanomagnetite typically occurs as equant or irregularly shaped grains with both crystal habits often occurring in the same sample. Ilmenite crystal morphology is variable, occurring as prismatic or slender anhedral crystals, or as small needle-like interstitial grains. Titanomagnetite and ilmenite commonly coexist in all group A rock types, although there are a few samples where each mineral occurs independently. Although each mineral is generally widespread, their relative abundance varies between rock types, and samples of the same rock type. Collectively titanomagnetite and ilmenite are comparatively minor components in groundmass assemblages. Only olivine has a smaller modal abundance than each of these minerals in most group A samples, although olivine may exceed ilmenite in some samples. Generally, the abundance of titanomagnetite exceeds ilmenite, often markedly, in the majority of samples from each rock type. Only in the qz-tholeiitic basalt samples is ilmenite the dominant Fe-Ti oxide phase.

The group B rocks are characterised by abundant titanomagnetite and the notable absence of ilmenite in the groundmass. Ewart (1989) suggested that the absence of ilmenite in rock types such as those of group B might be the result of the reduced silica activity, characteristic of alkaline magmas, and the partitioning of Ti between titaniferous clinopyroxene and ulvöspinel. In group B rocks titanomagnetite occurs predominantly as small, blocky, euhedral grains (i) in the groundmass, (ii) as inclusions in the Fe-rich rims of olivine phenocrysts, (iii) in the cores and rims of titaniferous clinopyroxene microphenocryst, and (iv) occasionally in olivine and titaniferous clinopyroxene groundmass crystals.

Selected titanomagnetite and ilmenite analyses for the group A rocks are presented in Tables 4.24 and 4.25[38] respectively and complete analyses of each mineral are given in Appendix 6, Tables A6.18 and Table A6.19 respectively. Analyses for representative titanomagnetite in the group B rocks are presented in Table 4.26 and complete analyses are given in Appendix 6, Table A6.38.

The compositions of titanomagnetite between each rock type are variable, with the greatest variations occurring in the concentrations of TiO_2, Al_2O_3, and MgO. Titanomagnetites in the group A rocks have compositions that contrast with those from the group B rocks[39]. Titanomagnetites from group A rocks generally have smaller Al_2O_3,

[38] Table 4.25 also includes representative ilmenite analyses for the mugearite sample from group B.

[39] The titanomagnetite and ilmenite crystals in all group A rock types appear to be petrographically homogeneous when viewed in thin section. Electron microprobe analyses of TiO_2 concentrations for rims of randomly selected titanomagnetites indicate that ilmenite lamellae have not formed along the margins of these crystals, suggesting, by inference, that subsolidus oxidation is minimal for most samples.

MgO, and MnO and slightly larger FeO_{total} than those in the group B rocks, except ne-hawaiite. Additionally, there are marked differences in the ulvöspinel–solid-solution abundance of the titanomagnetite from each rock type in both rock groups.

Generally, the ulvöspinel (Usp) contents of titanomagnetites in group A rocks range from 26 to 87 mol.% Usp, although the majority of crystals for all group A rock types are within the range Usp_{60-80}. Crystals from transitional basalt sample SA07 have ulvöspinel contents that are notably smaller (Usp_{26-58}) than those in the other group A rock types. In contrast, the largest ulvöspinel contents in the group A rocks were recorded in crystals from alkali ol-basalt (SA17; Usp_{82-83}) and hawaiite (SAB163; Usp_{85-86}). Although titanomagnetite compositions within individual samples may vary (e.g., hawaiite SAB151; Usp_{65-81}), each rock type tends to have distinct Usp composition characteristics.

Titanomagnetite in the group B rocks range from 55 to 83 mol.% Usp with the majority of crystals within the range Usp_{60-80}. Titanomagnetite in the basanites exhibits the broadest range of Usp contents (Usp_{55-83}), which includes samples with the largest (e.g., SAB180; ~Usp_{82}) and smallest (e.g., SA27; ~Usp_{58}) Usp contents for all group B rock types. In contrast, the ne-hawaiites show the least variation (Usp_{61-68}).

The compositional differences between titanomagnetites from each rock type in group A and B with respect to the ulvöspinel-magnetite solid-solution series, are illustrated in Figs. 4.24 and 4.25 respectively (see pp.118 and 119). The titanomagnetites in most rock types exhibit a relatively broad range of compositions along trends sub-parallel to the ulvöspinel-magnetite join, indicative of dissimilar oxidation states for individual samples. The titanomagnetites of some transitional basalt, hawaiites, and ol-tholeiitic basalt (Figs. 4.24B, C, and D) and basanite (Fig. 4.25B) samples are scattered along these trends, whereas titanomagnetites in the ne-hawaiites and mugearite (Figs. 4.25D and E) show little variation. Mitropoulos and Tarney (1992) proposed that trends such as these indicate that the temperatures and fo_2 conditions in individual magmas during titanomagnetite crystallisation, and by inference at distinct volcanic centres, are different.

Ilmenites from each rock type in group A and the mugearite exhibit a relatively restricted range of compositions and show less variation than the titanomagnetites from the same samples as seen in Figs. 4.24A-E and Fig. 4.25E respectively. Overall, ilmenites contain 0.3 to 10.1 mol. % hematite in solid solution (Table 4.25), with ilmenites from the transitional basalts and ol-tholeiitic and qz-tholeiitic basalts exhibiting the most oxidation. Concentrations of TiO_2 range from 45.2 to 53.4 wt. % with crystals from the alkali ol-basalts and hawaiites tending to have slightly larger TiO_2 than those

Table 4.24 Electron microprobe analyses for titanomagnetite in selected group A rocks, South Auckland volcanic field.

Rock Type	transitional basalt			hawaiite			ol-tholeiitic basalt				qz-tholeiitic basalt		alkali ol-basalt		
Sample	SA07	SA10	SA13	SA20	SA32	SAB163	SAB152	SAB181	SAB187	SAB173	SA77	SA77	SA17	SA18	SA33
Analysis	1917-G	1822-G	573-G	1845-G	1929-G	1962-G	257-G	188-G	276-G	1009-G	642-G	645-G	437-G	1787-G	1718-G
SiO_2	0.46	0.93	0.46	0.47	0.67	0.41	0.58	0.94	0.60	0.53	0.64	0.78	0.39	0.72	0.45
TiO_2	12.48	17.56	25.46	25.42	22.87	30.03	24.70	18.16	20.49	22.23	19.27	22.06	27.59	25.27	25.55
Al_2O_3	3.85	3.39	0.94	1.07	0.63	1.26	0.63	1.60	0.83	1.19	0.82	1.34	1.58	1.47	0.72
FeO_{total}	73.97	69.35	66.67	70.00	70.17	65.75	67.70	74.08	72.75	70.62	72.96	69.63	64.90	65.43	70.13
MnO	-	0.26	0.61	0.48	0.51	0.54	0.60	0.40	0.43	0.39	0.41	-	0.53	0.51	0.54
MgO	3.46	2.14	1.64	0.98	0.74	1.70	0.41	0.31	1.00	0.51	0.70	0.60	2.14	1.55	0.50
CaO	0.20	0.31	0.00	-	0.16	-	-	0.58	0.23	0.14	-	0.39	0.18	0.27	-
Total	94.42	93.94	95.78	98.42	95.75	99.69	94.62	96.07	96.33	95.61	95.80	94.82	97.31	95.22	97.89
Number of ions on the basis of 32 oxygen															
Si	0.157	0.310	0.150	0.147	0.221	0.125	0.189	0.317	0.198	0.176	0.214	0.256	0.122	0.230	0.144
Ti	3.190	4.400	6.150	6.006	5.661	6.803	6.118	4.579	5.110	5.520	4.835	5.491	6.435	6.093	6.122
Al	-	1.331	0.355	-	-	-	0.243	0.634	0.323	0.461	0.717	0.522	0.576	0.554	0.269
Fe^{2+}	21.034	19.331	17.914	18.397	19.312	16.570	18.646	20.771	20.189	19.507	20.362	19.277	16.832	17.546	18.685
Mn	-	0.074	0.166	0.128	0.141	0.138	0.166	0.115	0.122	0.109	0.115	-	0.141	0.138	0.147
Mg	1.757	1.066	0.787	0.461	0.365	0.765	0.202	0.157	0.493	0.250	0.346	0.304	0.989	0.739	0.240
Ca	0.074	0.109	-	-	0.058	-	-	0.208	0.080	0.048	-	0.138	0.061	0.093	-
Recalculated Fe ions and Fe oxides															
Fe^{2+}	13.860	11.127	13.025	14.663	13.630	15.249	13.588	11.969	12.203	12.875	12.148	12.909	13.120	13.075	13.498
Fe^{3+}	5.399	6.301	3.819	2.900	4.365	1.049	3.917	6.645	6.091	5.083	6.231	4.894	2.939	3.509	4.015
FeO	53.23	44.28	51.55	58.44	53.15	61.52	52.55	47.63	48.58	50.63	48.22	50.49	53.02	51.59	54.05
Fe_2O_3	23.04	27.86	16.80	12.85	18.92	4.70	16.84	29.39	26.86	22.21	27.49	21.27	13.20	15.38	17.87
Usp (mol.%)	38.0	57.6	75.5	74.5	68.1	87.2	75.1	56.4	60.2	67.8	59.9	68.8	82.0	77.8	74.8

Table 4.25 Electron microprobe analyses for ilmenite in selected group A rocks and mugearite, South Auckland volcanic field.

Rock Type	transitional basalt		hawaiite				ol-tholeiitic basalt				qz-tholeiitic basalt		alkali ol-basalt			mugearite	
Sample	SA13		SA20	SAB151	SAB163	SA32	SAB152	SAB187	SAB181	SAB172	SA76	SA77	SA17	SA33	SAB162	SA88	
Analysis	577-G	578-G	1870-G	201-G	1985-G	1949-G	707-G	278-G	186-G	933-G	130-G	649-G	144-G	1721-G	1751-G	480-G	481-G
SiO_2	0.46	0.76	0.45	0.52	0.25	0.39	0.74	0.41	0.58	0.78	0.61	0.58	0.44	0.40	0.54	0.47	0.62
TiO_2	48.72	48.17	51.09	48.76	52.93	51.32	50.11	49.13	48.6	45.42	49.93	48.42	51.70	51.22	51.31	51.35	50.27
Al_2O_3	-	0.25	-	-	-	-	-	-	0.62	0.26	-	-	0.25	-	0.21	-	-
FeO_{total}	45.64	46.18	47.12	46.63	44.58	45.46	46.90	47.21	47.79	48.72	47.06	48.52	44.24	48.32	45.23	45.38	44.17
MnO	0.60	0.50	0.44	0.44	0.63	0.55	0.55	0.39	0.45	0.56	0.44	0.38	0.67	0.58	0.78	0.60	0.61
MgO	2.04	1.64	0.99	0.84	1.66	1.78	1.01	1.62	0.89	0.87	0.76	0.86	2.70	0.67	0.70	2.28	2.40
CaO	.35	0.67	0.16	0.21	-	0.29	-	-	-	-	0.23	0.15	0.19	-	-	0.13	0.54
Total	97.81	98.17	100.25	97.4	100.05	99.79	99.31	98.76	98.93	96.61	99.03	98.91	100.19	101.19	98.77	100.21	98.61
Number of ions on the basis of 6 oxygen																	
Si	0.023	0.039	0.023	0.027	0.013	0.019	0.038	0.021	0.029	0.041	0.031	0.030	0.022	0.020	0.028	0.023	0.031
Ti	1.891	1.864	1.934	1.909	1.984	1.939	1.915	1.895	1.873	1.816	1.918	1.879	1.930	1.930	1.960	1.928	1.915
Al	0.000	0.016	-	-	-	-	-	-	0.037	0.016	-	-	0.014	-	0.012	-	-
Fe^{2+}	1.969	1.987	1.984	2.030	1.858	1.910	1.993	2.026	2.049	2.167	2.011	2.093	1.837	2.025	1.921	1.895	1.871
Mn	0.026	0.022	0.019	0.019	0.026	0.023	0.024	0.017	0.019	0.025	0.019	0.016	0.028	0.025	0.034	0.025	0.026
Mg	0.157	0.126	0.074	0.065	0.124	0.133	0.076	0.124	0.068	0.069	0.058	0.067	0.200	0.050	0.053	0.170	0.181
Ca	0.019	0.037	-	0.012	-	0.016	-	-	-	-	0.013	0.088	0.010	-	-	0.007	0.029
Recalculated Fe ions and Fe oxides																	
Fe^{2+}	1.677	1.680	1.836	1.814	1.844	1.769	1.833	1.739	1.786	1.705	1.838	1.776	1.696	1.852	1.897	1.727	1.687
Fe^{3+}	0.251	0.263	0.127	0.185	0.011	0.122	0.138	0.246	0.225	0.391	0.148	0.270	0.122	0.148	0.020	0.145	0.159
FeO	39.70	39.93	44.07	42.32	44.31	42.53	43.62	41.37	42.44	39.64	43.55	42.12	41.28	44.74	44.75	41.87	40.37
Fe_2O_3	6.60	6.94	3.39	4.79	0.30	3.25	3.64	6.49	5.94	10.91	3.90	7.11	3.29	3.98	0.53	3.90	4.22
Ilm (mol.%)	93.3	93.0	96.7	95.2	99.7	96.8	96.4	93.6	94.1	89.9	n.d.	93.1	96.7	96.2	n.d	96.2	95.7
Hem (mol.%)	6.7	7.0	3.3	4.8	0.3	3.2	3.6	6.4	5.9	10.1	n.d.	6.9	3.3	3.8	n.d	3.8	4.3

Table 4.26 Electron microprobe analyses for titanomagnetite in selected group B rocks, South Auckland volcanic field.

Rock Type	basanite			nephelinite				ne-hawaiite				mugearite		alkali ol-basalt		
Sample	SA12	SA27	SAB102	SAB175	SA51	SA113	SAB135	SA02	SA25	SA29	SA65	SA88		SA54	SAB188	SAB207
Analysis	1262-G	1331-G	85-G	1195-G	1476-G	244-G	7-G	1489-G	1518-G	164-G	1548-G	61-G	62-G	1684-G	1649-G	1621-G
SiO_2	0.55	0.43	0.47	0.55	0.61	0.49	0.42	0.49	0.50	0.60	0.37	0.47	0.44	0.59	0.46	0.49
TiO_2	21.85	18.67	23.73	24.28	21.64	20.42	18.72	20.77	22.17	19.79	20.36	26.46	26.63	26.34	26.84	24.34
Al_2O_3	4.37	3.62	1.71	4.06	4.18	6.20	6.55	3.98	1.24	1.82	3.52	0.36	0.75	1.35	1.23	2.52
FeO_{total}	66.85	68.29	69.73	66.19	67.16	65.23	62.31	66.47	71.83	72.18	69.70	69.92	68.07	65.59	67.50	68.35
MnO	0.68	0.64	0.68	0.79	0.74	0.58	0.68	0.55	0.67	0.72	0.70	0.64	0.66	0.81	0.66	0.67
MgO	1.52	3.40	1.74	1.05	0.90	3.88	5.30	3.84	0.63	0.72	1.92	1.05	1.37	0.98	1.79	2.12
CaO	0.23	0.12	0.16	0.18	0.24	-	-	0.16	0.15	0.28	0.45	-	-	0.17	0.13	0.30
Total	96.05	95.17	98.22	97.04	95.47	96.80	93.98	96.27	97.19	96.11	97.02	98.90	97.92	95.83	98.61	98.79
Number of ions on the basis of 32 oxygen																
Si	0.176	0.141	0.147	0.173	0.198	0.150	0.134	0.158	0.163	0.198	0.118	0.147	0.138	0.189	0.141	0.150
Ti	5.222	4.576	5.635	5.702	5.232	4.749	4.451	4.980	5.430	4.931	4.886	6.243	6.294	6.317	6.253	5.674
Al	1.635	1.392	0.637	1.472	1.584	2.259	2.442	1.494	0.477	0.710	1.325	0.134	0.278	0.506	0.451	0.918
Fe^{2+}	17.766	18.611	18.413	17.286	18.054	16.864	16.480	17.724	19.562	20.006	18.595	18.349	17.894	17.488	17.488	17.715
Mn	0.186	0.176	0.182	0.208	0.202	0.150	0.182	0.148	0.186	0.202	0.189	0.170	0.176	0.218	0.173	0.176
Mg	0.723	1.651	0.819	0.409	0.432	1.789	2.496	1.827	0.304	0.358	0.912	0.493	0.643	0.467	0.826	0.982
Ca	0.080	0.042	0.054	0.058	0.083	-	-	0.055	0.051	0.099	0.154	-	-	0.058	0.045	0.099
Recalculated Fe ions and Fe oxides																
Fe^{2+}	12.095	10.568	12.402	12.840	12.372	10.754	9.763	10.335	12.625	12.065	11.720	13.395	13.307	13.480	13.069	12.265
Fe^{3+}	4.439	6.231	4.667	3.501	4.432	4.836	5.342	5.786	5.313	6.050	5.327	3.850	3.585	3.148	3.470	4.269
FeO	48.90	42.96	50.66	52.01	49.45	45.00	40.27	42.61	50.55	48.07	47.92	54.31	53.63	53.17	53.34	50.70
Fe_2O_3	19.95	28.15	21.19	15.76	19.68	22.49	24.49	26.51	23.64	26.79	24.21	17.35	16.05	13.80	15.74	19.61
Usp (mol.%)	73.3	57.9	69.9	80.3	73.6	68.9	63.3	64.8	66.1	60.8	63.8	75.2	77.0	80.7	78.0	73.1

Group A

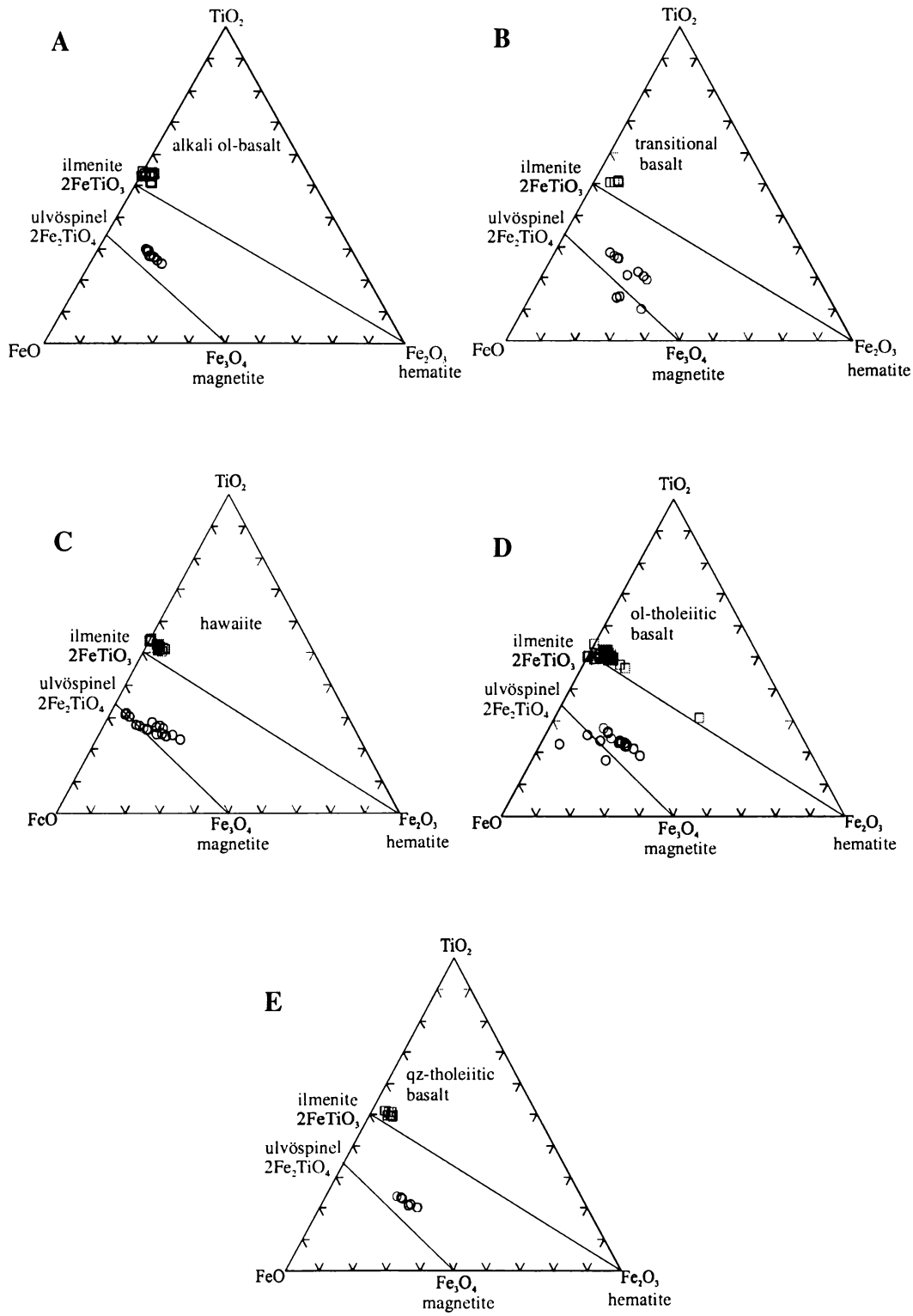

Fig. 4.24 Titanomagnetite (open circles) and ilmenite (open squares) compositions of South Auckland volcanic field group A rock types plotted relative to the ulvöspinel-magnetite and ilmenite-hematite solid-solution series.

Group B

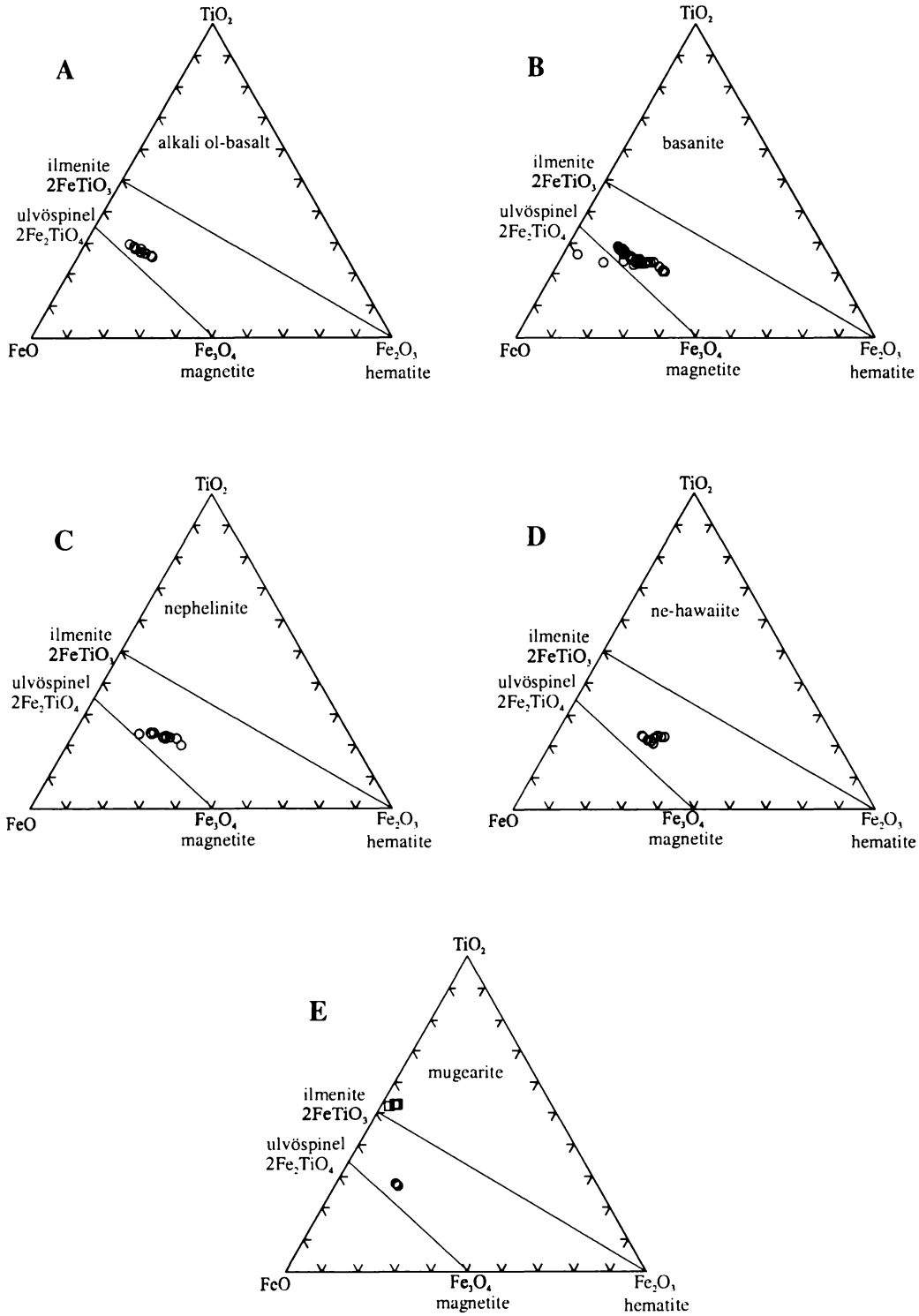

Fig. 4.25 Titanomagnetite (open circles) and ilmenite (open squares) compositions of South Auckland volcanic field group B rock types plotted relative to the ulvöspinel-magnetite and ilmenite-hematite solid-solution series curves.

from the other rock types (see Appendix 6, Table A6.19). The Al_2O_3 content in the majority of crystals in all samples is below the detection limit. When present however, Al_2O_3 contents are typically < 0.30 wt. %. The MnO contents are smaller than 0.79 wt. % for all analysed crystals. The MgO content of ilmenite is variable for all rock types ranging from 0.36 to 2.77 wt. % for all samples, with the alkali ol-basalts and hawaiites tending to have the largest concentrations.

Titanomagnetite and ilmenite–host-rock equilibrium

The relative concentration of the minor elements, MgO, MnO, and Al_2O_3, in coexisting titanomagnetite and ilmenite may be used as an indicator of crystallisation equilibrium conditions (Ewart, 1989). The titanomagnetites in the group A rocks and mugearite are Al_2O_3-enriched relative to ilmenite. Although the MgO concentration of ilmenites and titanomagnetites is variable between individual samples of the same rock type, ilmenites in the same sample generally have larger MgO contents than titanomagnetites (see Appendix 6, Tables A6.18, A6.19, A6.38, and A6.39). Crystals that are relatively MgO-enriched tend to occur in the more silica-undersaturated samples, especially those from the alkali ol-basalts and transitional basalts.

Titanomagnetite and ilmenite crystals tend to have similar MnO contents. Those crystals with the largest MnO content tend to occur in the samples with relatively large whole-rock SiO_2 contents, e.g., hawaiites and ol-tholeiitic and qz-tholeiitic basalts, a feature considered by Bacon and Hirschmann (1988) to be characteristic of "lower-temperature" titanomagnetite-ilmenite pairs.

The correlation between MgO, MnO, and Al_2O_3 for coexisting ilmenite and titanomagnetite in each of the group A rock types is illustrated in Fig. 4.26. Most of the coexisting magnetite-ilmenite pairs in each rock type have similar tie-line slopes indicative of crystal-host rock equilibrium. Generally, these pairs have similar values of Mg/Mn, which suggests similar crystallisation temperatures (Spencer and Lindsley, 1981). In contrast, a number of crystal pairs, especially those from hawaiites SA20 and SAB151, have compositions that are inconsistent with the general tie-line trends exhibited in the other rock types (see Fig. 4.26). These pairs commonly have dissimilar Mg/Mn values suggestive of disequilibrium coexisting compositions.

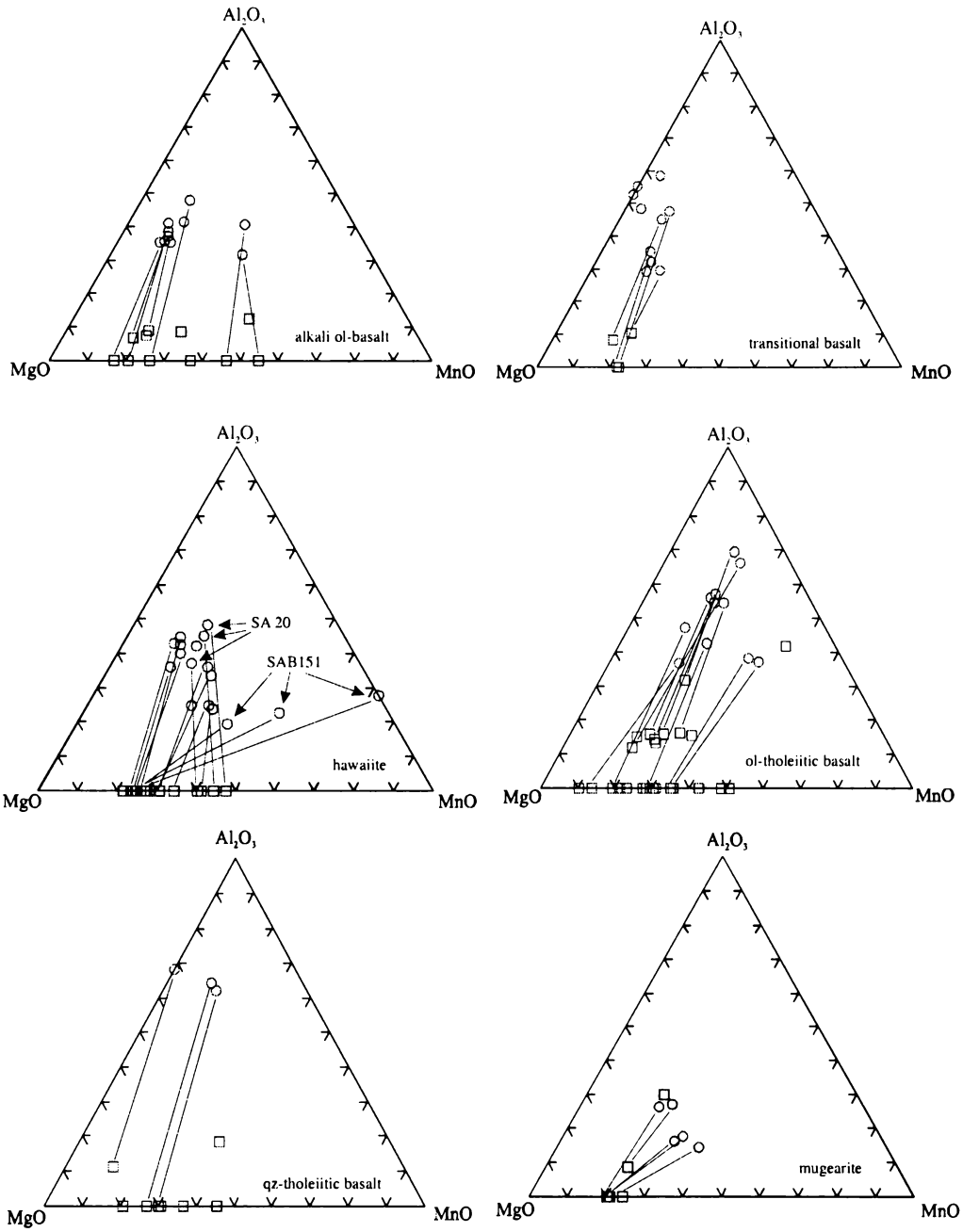

Fig. 4.26 Minor-element compositions (in wt. %) in coexisting Cr-bearing titanomagnetite (open circles) and ilmenite (open squares) in the South Auckland volcanic field group A rock types. Tie lines join co-existing minerals. Labelled samples are referred to in the text.

Titanomagnetite and ilmenite geothermometry and oxygen fugacity

Coexisting titanomagnetite-ilmenite pairs such as those shown in Fig. 4.26 can be utilised to estimate the temperature and oxygen fugacity conditions for many of the group A lavas using the geothermometer model of Spencer and Lindsley (1981)[40]. However, because only one titanomagnetite-ilmenite pair showed petrographic evidence of crystal

[40] Because ilmenite occurs predominantly in the group A rocks (the mugearite sample is the only exception from group B), it is not possible to obtain Fe-Ti oxide-derived T and fO_2 estimates for the group B samples using this model.

equilibrium, i.e., direct contact with each other, the Mg/Mn partitioning test for equilibrium between coexisting Fe-Ti oxides of Bacon and Hirschmann (1988) was first used to identify possible equilibrated pairs. The test results, illustrated in Fig. 4.27, show that the majority of titanomagnetite-ilmenite pairs plot outside the region of mineral–host-rock equilibrium. This may be due to (i) a small dependence on temperature variations or host magma composition on Mg-Mn partitioning, (ii) electron microprobe analytical precision, (iii) post-equilibration alteration, or (iv) crystal disequilibrium (Bacon and Hirschmann, 1988).

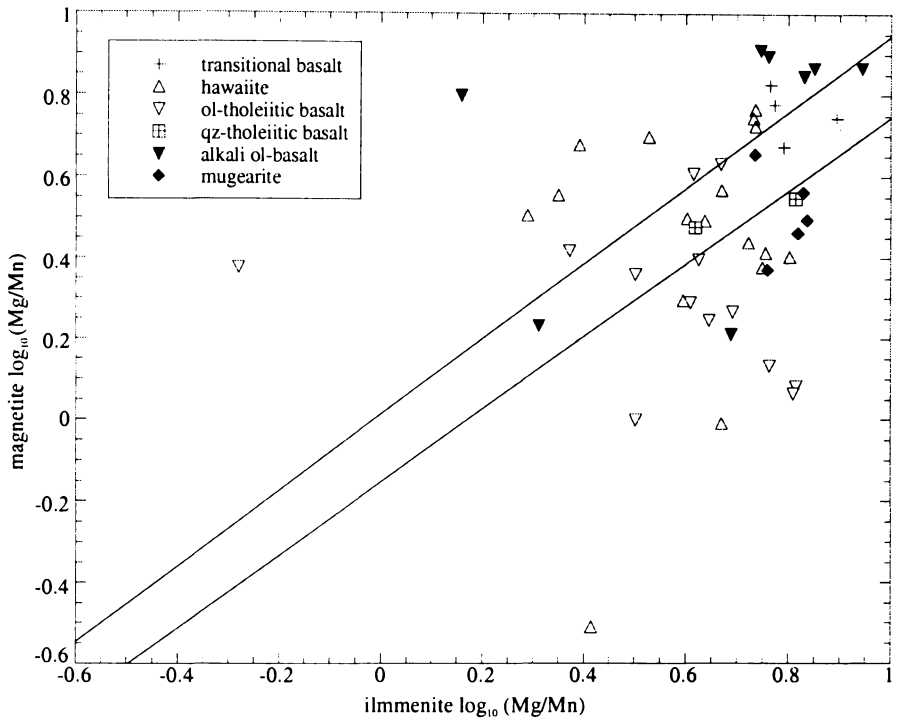

Fig. 4.27 Plot of log (Mg/Mn) for titanomagnetite-ilmenite pairs from group A rocks of the South Auckland volcanic field. Equilibrated minerals fall within the region enclosed by the solid lines. The estimated error for this region is ± 2σ based on electron microprobe precision as determined by Bacon and Hirschmann, (1988).

Temperature and fO_2 estimates (T-fO_2) derived from the geothermometer model of Spencer and Lindsley (1981) for "equilibrated" titanomagnetite-ilmenite pairs are presented in Table 4.27 and shown in Fig. 4.28[41]. Overall, the estimated temperatures of the titanomagnetite-ilmenite pairs range from 864 to 1119°C. Coexisting titanomagnetite and ilmenite crystals in transitional basalt SA13 and hawaiite SAB151 have estimated temperatures that probably reflect pre-eruptive magmatic conditions (1119 and 1150°C respectively). In contrast, estimated temperatures for crystals in samples from the other

[41] Due to potential errors associated with transcribing the region of mineral-host rock equilibrium shown in Fig. 4.27, the temperature and oxygen fugacity for titanomagnetite-ilmenite pairs that plotted close to this region were also estimated and are included in Table 4.27 and the -logfO_2 vs. T plot shown in Fig. 4.28.

rock types most likely represent lower, post-eruptive crystallisation conditions. The wide range of equilibration temperatures suggests that individual samples and by inference, magma batches, had distinct crystallisation and cooling histories.

Table 4.27 Temperature (T) and oxygen fugacity (fO_2) calculations for coexisting titanomagnetite and ilmenite from selected SAVF rocks

Rock type	Sample	Magnetite (analysis)	Ilmenite (analysis)	T (°C)	$-\log_{10} fO_2$
transitional basalt	SA13	573	578	1119	11.09
		39	580	1053	11.90
hawaiite	SA32	1928	1949	864	16.00
	SAB151	682	681	1150	11.51
		200	201	1000	13.19
ol-tholeiitic basalt	SAB152	704	707	896	15.22
	SAB172	932	933	1087	10.53
		936	925	910	13.96
	SAB181	196	186	898	13.81
	SAB187	276	278	876	13.87
qz-tholeiitic basalt	SA77	642	649	892	13.45
		644	648	874	13.45
alkali ol-basalt	SA17	436	151	975	14.55
		441	439	865	16.54
		149	144	947	14.80
	SA33	1718	1721	881	15.27
mugearite	SA88	482	481	970	13.18
		476	485	877	15.48
		62	483	896	15.22

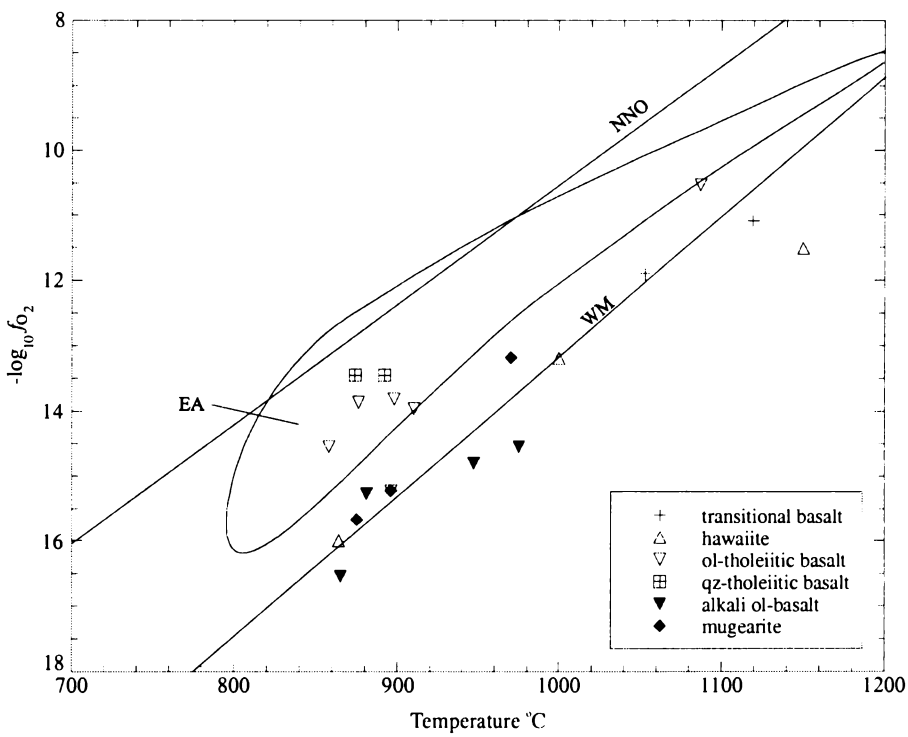

Fig. 4.28 Estimated equilibration temperatures vs. oxygen fugacities (fO_2) for coexisting groundmass titanomagnetite-ilmenite pairs in the mugearite from group B and each of the group A rock types in the SAVF. The curves for the NNO (Ni-NiO) and WM (wüstite-magnetite) fO_2 buffers are approximated from Huebner and Sato (1970) and Sato and Velenza (1980) respectively. The enclosed area, EA, represents coexisting Fe-Ti oxides from similar rock types from the mafic volcanic suites in eastern Australia (Ewart, 1989).

An important feature of the SAVF Fe-Ti oxides is that the T-fo_2 data for all analysed titanomagnetite-ilmenite pairs plot below the Ni-NiO (NNO) fo_2 buffer curve, with some of the coexisting Fe-Ti oxides below the WM (wüstite-magnetite) fo_2 buffer curve, as seen in Fig. 4.28. By way of comparison, coexisting oxides from similar rock types from eastern Australia plot entirely within the NNO-WM fo_2 buffer region, primarily near the NNO curve (Ewart, 1989) suggesting that Fe-Ti oxides in mafic volcanic rocks from continental intraplate tectonic settings commonly crystallise under reducing conditions.

4.7.2 Chromian titanomagnetite and Cr-bearing titanomagnetite

Chromian titanomagnetite (Cr-titanomagnetite) occurs primarily as inclusions in olivine megacrysts and phenocrysts, and as rare inclusions in titaniferous clinopyroxene in all group B rock types. Olivine megacrysts and phenocrysts, in a number of alkali ol-basalt, transitional basalt, and hawaiite samples from group A, also contain Cr-titanomagnetite inclusions. Typically, Cr-titanomagnetite inclusions occur in olivine cores that range in composition from Fo_{68} in the ne-hawaiites to Fo_{85} in the basanites. Cr-bearing titanomagnetite is found principally as small, euhedral grains (e.g., < 50 μm) in the groundmass of a number of group B rocks and in the alkali ol-basalts and transitional basalts from group A.

The abundance of Cr-titanomagnetite inclusions in individual samples is variable. Furthermore, there are some samples with large forsteritic phenocrysts (e.g., > Fo_{80}), which do not contain Cr-titanomagnetite inclusions, suggesting that there is no apparent correlation between the occurrence of Cr-titanomagnetite inclusions, crystal size, or Fo content. The absolute abundance of Cr-titanomagnetite in each sample is difficult to quantify but point counts of numerous thin sections indicate that its modal abundance in all samples is << 1.0 percent. As a groundmass phase, Cr-bearing titanomagnetite is indistinguishable from titanomagnetite and therefore its relative abundance could not be determined. However, the relatively large quantity of these crystals identified in the alkali ol-basalts and transitional basalts during electron microprobe analyses suggest that these rock types contain a larger quantity of Cr-bearing titanomagnetite than their group B counterparts.

The Cr-titanomagnetite inclusions and groundmass in all rock types span a broad range of overlapping compositions. Analyses of representative Cr-titanomagnetite inclusions in olivine phenocryst cores and groundmass grains from each rock type are given in Table 4.28. The forsterite content of the host olivine phenocryst of Cr-titanomagnetite

inclusions is also given in Table 4.28. These compositions were determined for olivine directly adjacent to the Cr-titanomagnetite. Complete analyses for all Cr-titanomagnetite are given in Appendix 6, Tables A6.17 and A6.37 for the group A and B rocks respectively.

Table 4.28 Representative electron microprobe analyses of Cr-titanomagnetite inclusions and Cr-bearing titanomagnetite groundmass crystals and Fo content for host olivine phenocryst. In the analyses number I = inclusion and G = groundmass grain. Table 4.28 continues on the next page.

	Group B								
Rock Type	alkali ol-basalt			basanite			nephelinite		
Sample	SAB207		SA54	SAB176	SA12	SAB178	SA21	SA28	SA51
Analysis	1600-I	1608-I	1694-G	1222-I	1268-I	1165-G	1399-I	1433-I	1460-G
SiO_2	0.52	0.37	0.86	0.49	0.47	0.51	0.51	0.57	0.55
TiO_2	17.07	6.65	26.87	2.04	23.41	19.76	4.75	11.59	20.11
Al_2O_3	7.49	19.92	2.51	31.59	4.62	6.59	23.31	7.89	5.18
Cr_2O_3	7.31	15.16	0.52	22.90	3.96	0.80	18.50	12.29	1.89
FeO_{total}	58.50	45.67	64.87	29.04	61.33	66.00	40.75	59.00	66.03
MnO	0.38	0.30	0.59	-	0.64	0.60	-	0.31	0.70
MgO	5.75	7.96	2.20	12.40	2.48	3.17	8.90	4.93	1.69
CaO	-	-	-	-	-	0.15	-	-	0.24
Total	97.02	96.03	98.42	98.46	96.91	97.58	96.72	96.58	96.39
Number of ions on the basis of 32 oxygen									
Si	0.157	0.102	0.259	0.122	0.144	0.157	0.138	0.176	0.176
Ti	3.859	1.395	6.147	0.378	5.389	4.576	0.960	2.669	4.774
Al	2.656	6.557	0.899	9.178	1.667	2.394	7.382	2.845	1.930
Cr	1.738	3.347	0.125	4.461	0.957	0.192	3.926	2.973	0.474
Fe^{2+}	14.707	10.666	16.499	5.987	15.702	16.992	9.155	15.104	17.434
Mn	0.096	0.070	0.150	-	0.166	0.157	-	0.080	0.189
Mg	2.579	3.315	0.998	4.557	1.130	1.456	3.565	2.250	0.794
Ca	-	-	-	-	-	0.051	-	-	0.080
Recalculated Fe ions and Fe oxides									
Fe^{2+}	9.239	6.404	13.038	4.054	12.042	10.836	5.876	8.750	11.607
Fe^{3+}	4.447	3.653	2.752	1.767	2.939	4.865	2.869	5.140	4.579
FeO	39.49	29.08	53.56	20.22	49.30	45.55	27.38	37.17	47.35
Fe_2O_3	21.12	18.44	12.56	9.80	13.37	22.73	14.86	24.26	20.76
host olivine Fo	74.7	78.7		81.1	81.7		74.0	72.3	
Atomic percentages									
$\frac{100Cr}{(Al + Cr)}$	39.5	33.8	12.2	32.7	36.5	7.4	34.7	51.1	19.7
$\frac{100Mg}{(Mg + Fe^{2+})}$	20.6	32.8	6.8	52.2	8.2	11.0	36.7	19.1	6.0
$\frac{100Fe^{3+}}{(Fe^{3+} + Cr + Al)}$	52.1	28.1	73.7	11.8	54.0	67.1	21.0	49.0	67.2
$\frac{Ti}{(Ti + Cr + Al)}$	46.8	12.3	85.7	2.7	67.3	63.9	7.8	31.4	66.5

(continued on next page)

Table 4.28 continued.

	Group B			Group A					
Rock Type	ne-hawaiite			alkali ol-basalt			transitional basalt		
Sample	SA65			SA19	SAB162	SA18	SA10	SA07	
Analysis	1561-I	1541-I	1568-G	2000-I	1741-I	1799-G	1816-I	1892-G	1915-G
SiO_2	0.54	0.50	0.50	0.33	0.30	0.41	0.68	0.96	0.64
TiO_2	14.39	20.18	20.66	2.12	24.09	24.38	4.56	3.27	12.35
Al_2O_3	5.81	3.62	2.83	19.90	4.26	2.02	17.01	6.67	4.22
Cr_2O_3	7.47	1.12	0.29	29.08	1.74	1.08	27.40	23.66	0.34
FeO_{total}	64.73	67.86	71.31	40.07	62.49	67.05	40.95	53.58	74.68
MnO	0.36	0.67	0.74	-	0.37	0.52	-	-	-
MgO	4.40	2.75	0.97	7.88	4.65	1.62	8.28	6.81	2.78
CaO	-	-	0.22	-	-	-	-	-	0.33
Total	97.70	96.70	97.52	99.38	97.90	97.08	98.88	94.95	95.34
Number of ions on the basis of 32 oxygen									
Si	0.166	0.160	0.160	0.090	0.090	0.128	0.182	0.301	0.218
Ti	3.366	4.832	5.005	0.426	5.456	5.792	0.931	0.771	3.126
Al	2.131	1.360	1.072	6.173	1.510	0.752	5.446	5.869	0.090
Cr	1.837	0.282	0.074	6.298	0.413	0.272	5.885	2.467	1.674
Fe^{2+}	16.842	18.067	19.210	8.998	15.731	17.718	9.302	14.054	21.037
Mn	0.096	0.179	0.202	-	0.096	0.138	-	-	-
Mg	2.042	1.306	0.467	3.152	2.090	0.765	3.350	3.187	1.395
Ca	-	-	0.077	-	-	-	-	-	0.118
Recalculated Fe ions and Fe oxides									
Fe^{2+}	9.270	11.217	12.032	5.699	11.379	12.716	6.097	6.294	9.791
Fe^{3+}	5.994	5.342	5.520	2.892	3.493	3.917	2.799	6.363	8.464
FeO	39.31	45.97	48.88	26.58	47.81	51.26	28.07	26.64	40.06
Fe_2O_3	28.25	24.33	24.92	14.99	16.31	17.55	14.32	29.93	38.48
host olivine Fo	68.1	67.3		73.6	71.8		76.8	78.6	
Atomic percentages									
$\frac{100Cr}{(Al + Cr)}$	46.3	17.2	6.4	50.5	21.5	26.6	51.9	29.6	94.9
$\frac{100Mg}{(Mg + Fe^{2+})}$	16.6	9.6	3.4	34.6	14.8	5.3	34.4	31.3	11.0
$\frac{100Fe^{3+}}{(Fe^{3+} + Cr + Al)}$	62.5	78.0	84.1	19.5	65.8	80.3	20.5	45.9	84.7
$\frac{Ti}{(Ti + Cr + Al)}$	45.9	74.6	81.4	3.3	73.9	85.0	7.6	8.5	63.9

All Cr-titanomagnetite inclusions are titaniferous, with TiO_2 ranging from 1.83 to 24.55 wt. %. Additionally, they contain very large FeO_{total} contents (27.2 – 67.9 wt. %) together with comparatively small MgO contents (2.5 – 13.3 wt. %) with most inclusions showing TiO_2-enrichment with increasing FeO_{total}. Concentrations of Al_2O_3 and Cr_2O_3 are highly variable, ranging from 3.6 to 34.3 wt. % and 0.3 to 29.1 wt. % respectively. In contrast to the Cr-titanomagnetite inclusions, the Cr-bearing titanomagnetite groundmass grains in the group B rocks are characterised by their notably small concentrations of Cr_2O_3

(typically << 1.0 wt. %), Al_2O_3 (0.6 to 7.3 wt. %), and MgO (1.0 to 5.5 wt. %), and large TiO_2 contents (17.0 to 28.4 wt. %). The FeO contents are large, ranging between 61.4 to 71.3 wt.% and are generally more Fe-enriched than inclusions in the same sample. In contrast to group B groundmass however, the transitional basalts have Cr-bearing titanomagnetites in the groundmass with compositions similar to those of the Cr-titanomagnetite inclusions of many group B samples. The Cr-titanomagnetite inclusions and groundmass Cr-bearing titanomagnetite have broad ranges of $Mg/(Mg + Fe^{2+})$, $Cr/(Al + Cr)$, $Fe^{3+}/(Fe^{3+} + Cr + Al)$, and $Ti/(Ti + Cr + Al)$ values (Table 4.28), which are comparable to those of the Cr-bearing titanomagnetite inclusions from East-Australian basaltic rocks (Ewart, 1989).

Concentrations of Al_2O_3 and Cr_2O_3 in the inclusions show an antipathetic relationship with FeO_{total} and TiO_2 and a positive correlation with MgO, indicative of the trend between the magnetite and ulvöspinel components of their compositions. Figure 4.29 illustrates these trends and shows that for each rock type there is an overall systematic increase in Al and Cr abundances with Mg-enrichment. An important observation in Fig. 4.29 is the relative primitive nature of a majority of the basanite Cr-titanomagnetites compared to those from the other rock types. The most magnesian and Al-rich Cr-titanomagnetites occur predominantly in basanites, considered to be some of the least differentiated rocks in the SAVF. These crystals tend to have the largest Cr_2O_3 contents (19.8 to 23.6 wt. %), which correlate well with the large Cr (288 – 376 ppm Cr) and MgO (11.73 to 12.99 wt. %) contents of their relatively primitive basanite host rocks. However, the compositions of these inclusions are not comparable to those of residual, upper-mantle lherzolite spinel (see Ewart, 1989, p.214) suggesting that their host olivines probably do not represent xenocrystic compositions. Additionally, Ewart (1989) argued that Cr-depleted and Ti-enriched Cr-bearing titanomagnetite groundmass crystals, such as those observed in the SAVF rocks, are indicative of small residual liquid Cr abundances which implies a lower T-fo_2 origin than that of the Cr-titanomagnetite inclusions.

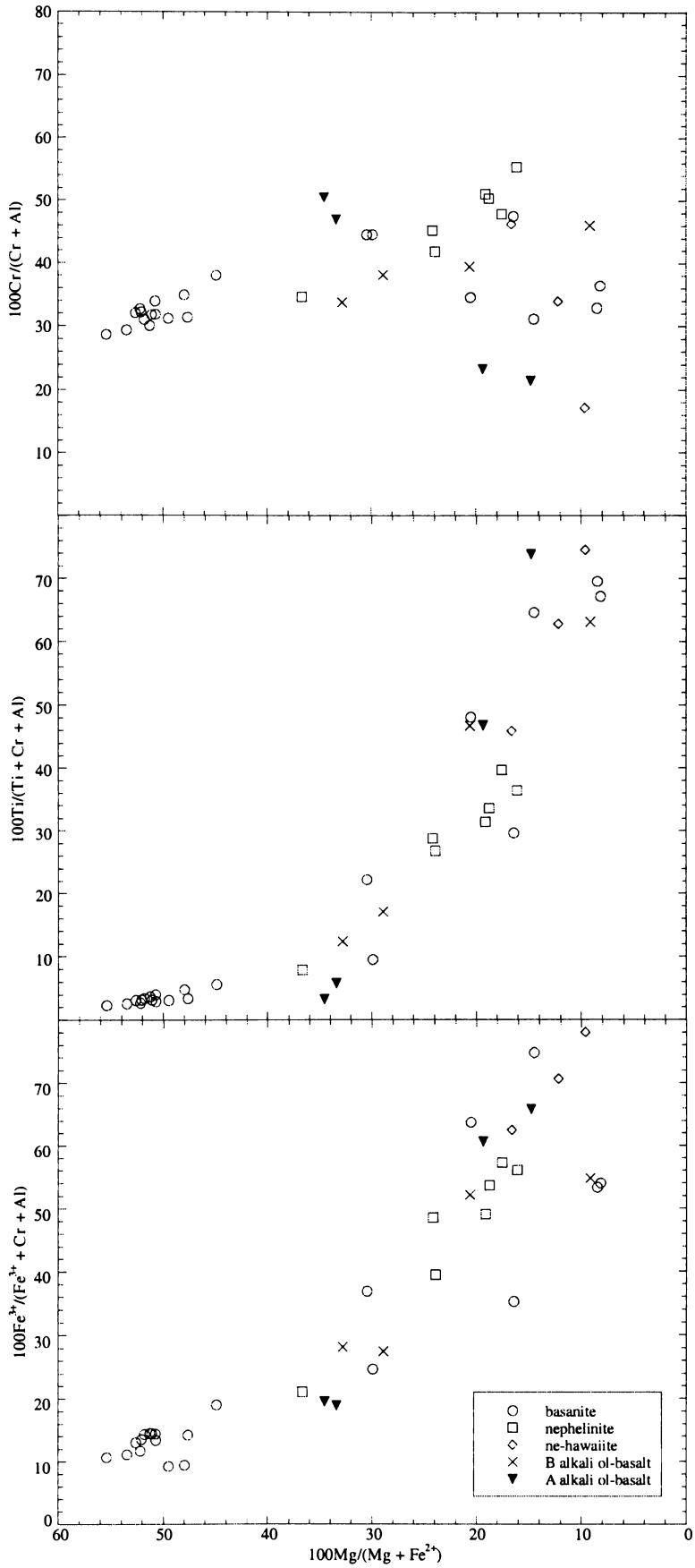

Fig. 4.29 Compositions of Cr-titanomagnetite and Cr-bearing titanomagnetite inclusions and groundmass grains (atomic percent) for South Auckland volcanic field rocks. Fe^{2+} and Fe^{3+} are recalculated values derived from the original concentrations of FeO_{total} using the method of Carmichael (1967) for ulvöspinel-magnetite solid-solution.

4.8 Summary

This chapter documents the diverse mineralogy and mineral chemistry of the phenocryst and groundmass phases in each rock type erupted throughout the South Auckland volcanic field. Variations in the composition of specific mineral phases (i) commonly occur between samples from the two rock groups (A and B), (ii) often occur between samples from the same rock type, and (iii) frequently occur between crystals within the same sample.

Olivine is the dominant phenocryst phase in each rock type from groups A and B[42] although its abundance varies between samples from the same rock type. Olivines in both rock groups tend to be compositionally zoned and have overlapping forsteritic compositions. However, in terms of their Fo content, the olivines in each rock type exhibit a distinct range of compositions with the most Fo-rich crystals occurring in samples of the group B rock types, except the ne-hawaiites.

Most samples of each group B rock type, except the ne-hawaiites, contain megacrysts and phenocrysts with core compositions in equilibrium with their host rock. In contrast, equilibrated olivines in the group A rocks are restricted to a few samples from the alkali ol-basalts and ol-tholeiitic and qz-tholeiitic basalts. Equilibrated olivines commonly occur together with populations of olivine that exhibit disequilibrium features such as (1) the presence of reversely zoned, unzoned, and (or) normally zoned crystals in the same sample, (2) crystals with very different compositions in the same sample, and (3) the presence of crystals with different rim compositions in the same sample. Additionally, evidence based on experimental studies indicates that most host rocks are too magnesian to be in equilibrium with the majority of their olivine phenocrysts. Compositions of a large number of olivines from the group B rocks however, correlate well with equilibrated olivines from Fe-poor Type I chondrites, whereas many olivines from the group A rocks are similar to those from Fe-rich Type II chondrites. These distinctions suggest possible source differences for group A and B magmas.

Olivine megacrysts and phenocrysts in each group B rock type, except mugearite, and in the alkali ol-basalts and transitional basalts from group A contain Cr-titanomagnetite inclusions. The most magnesian and Al- and Cr-rich inclusions occur in the basanites.

[42] Group A consists of alkali ol-basalts, transitional basalts, hawaiites, ol-tholeiitic basalts, and qz-tholeiitic basalts. Group B consists of alkali ol-basalts, basanites, nephelinites, ne-hawaiites, and mugearite.

Based on comparisons with Cr-spinel inclusions in olivines in lherzolite xenoliths, the host olivines in the SAVF rocks do not appear to have xenocrystic origins.

Clinopyroxenes in the group A and B rocks are characterised by their contrasting compositions. Phenocrysts in the group A rocks typically have calcic augite compositions, whereas those from group B are predominantly diopside. The majority of samples from group B contain crystals in equilibrium with their host rock. In contrast, relatively few group A samples contain equilibrated crystals, primarily those from the ol-tholeiitic and qz-tholeiitic basalts.

The values of Al^{IV}/Al^{VI} suggest that clinopyroxenes in the group A rocks generally crystallised at relatively greater pressures than those in the group B rocks. However, pressure and temperature estimates, derived from geothermobarometer models, appear to be more reliable. The results of these models indicate that clinopyroxenes from both rock groups crystallised over a broad range of P-T conditions. Estimated pressures and temperatures for cores in group A rocks range from 6.4 to 19.5 kbar and 1214 to 1539° C, whereas P-T estimates for cores in group B rocks range from 3.5 to 21.4 kbar and 1196 to 1534° C. Distinct differences in P-T estimates of core-rim pairs in some samples suggest that crystallisation continued during magma ascent. Additionally, some samples in each rock group contain crystals with very different P-T estimates implying polybaric crystallisation of distinct magma batches. Furthermore, calculated $K_{Na}^{cpx\text{-}melt}$ strongly correlates with P regardless of rock type or group suggesting that partial melting may have occurred over a range of depths.

Phenocrysts of feldspar are restricted to the group A rocks and the mugearite from group B. Core compositions are predominantly labradorite with rims in some samples ranging to andesine. Feldspar is the dominant groundmass phase in all rock types. Compositions are predominantly labradorite in all samples and range to sanidine in some samples, especially basanites. Nepheline is restricted to the group B rocks, occurring only as a groundmass phase.

Titanomagnetite occurs predominantly as groundmass grains in all rock types. Ilmenite is restricted to the groundmass of the group A rocks and the mugearite. Titanomagnetite compositions are variable with crystals from each rock type exhibiting a distinct range of Usp contents. In contrast, ilmenite shows little variation between rock types. Temperature and oxygen fugacity estimates, based on titanomagnetite-ilmenite pairs, indicate that crystallisation commonly occurred at post-eruptive temperatures and that these minerals commonly crystallised under reducing conditions.

Chapter Five:
Geochemical Compositions of the SAVF Basalts

Chapter Five

Geochemical compositions of the SAVF basalts

5.1 Introduction

The contrasting petrographic and mineral chemical characteristics between the group A and B rocks are also reflected in their geochemical compositions. The relationship between groups A and B and the various rock types within each group is discussed with emphasis on the variations in their major and trace element, rare earth element, and radiogenic isotopic compositions, and the contrasting geochemical trends that characterise each group.

5.2 Analytical techniques

Analyses for major and trace elements, rare earth elements, and radiogenic isotopes obtained from newly collected samples are combined with whole-rock analyses obtained previously by Briggs *et al.* (unpublished)[43]. In total, 203 SAVF samples were analysed by X-ray fluorescence (XRF) for abundances of the major elements (Si, Ti, Al, Fe, Mn, Mg, Ca, Na, K, and P) and selected trace elements. Thirty-four samples were analysed for trace elements and REE either by spark source mass spectrometry (SSMS) or inductively coupled plasma mass spectrometry (ICP-MS) techniques. Ratios for the radiogenic isotopes Sr and Nd for 36 samples, and Sm and Pb for a subset of 18 of these samples, were measured by thermal ionisation mass spectrometry (TIMS) techniques.

Analytical procedures are summarised in Appendix 5. All geochemical data obtained for this investigation and referred to in the text are presented in Appendix 7: major and trace element analyses by XRF for group A and B samples are given in Tables A7.1 and A7.2 respectively; trace element and REE analyses by SSMS and ICP-MS, and Sr, Nd, Sm, and Pb radiogenic isotope analyses for selected group A and B samples are given in Tables A7.3 and A7.4 respectively.

[43] All analytical data obtained for these samples were made available for use in this investigation.

5.3 General geochemical characteristics

5.3.1 Relative frequency of analysed group A and B rock types

The composition of the South Auckland volcanic field lavas range from silica-undersaturated nephelinites and basanites to less undersaturated ol-tholeiitic and qz-tholeiitic basalts[44]. The frequency distribution of each rock type in the SAVF is summarised in Table 5.1 and illustrated in Fig. 5.1[45]. Basanites are the dominant magma type erupted, followed by hawaiites and ol-tholeiitic basalts. Briggs *et al.* (1994) have demonstrated that there is no apparent correlation between rock type and age in the SAVF, which suggests that despite the predominance of basanites, overall group A- and B-type magmas erupted with similar frequency (∑frequency = 49% and 51% respectively) during the one million year life of the field.

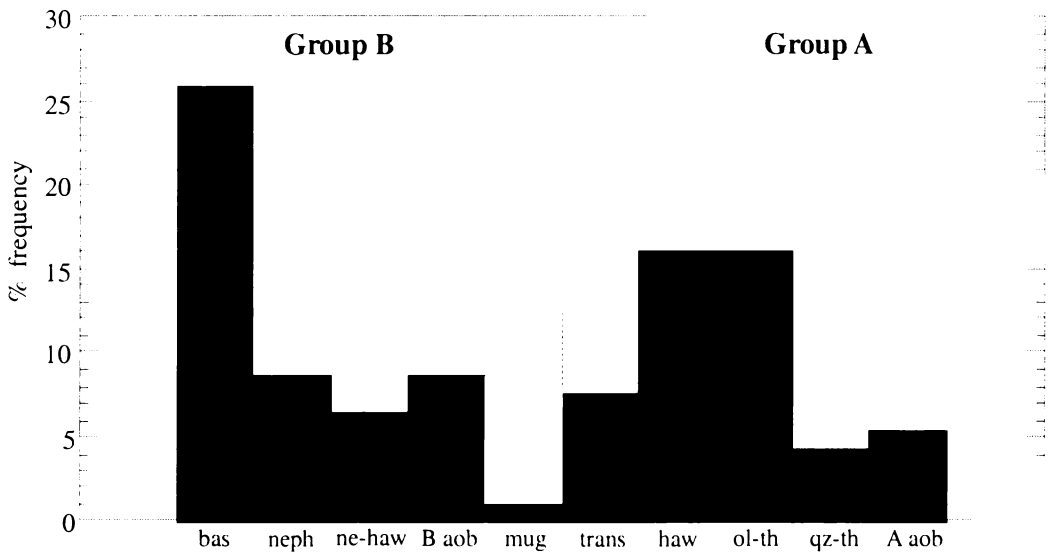

Fig. 5.1 Frequency distribution of each rock type in the group A and B lavas of the South Auckland volcanic field as a percentage of analysed samples, collected at 61 centres. Sample size = 93 (based on the presence of each rock type per volcanic centre). bas = basanite, neph = nephelinite, ne-haw = ne-hawaiite, B aob = group B alkali ol-basalt, mug = mugearite, trans = transitional basalt, haw = hawaiite, ol-th = ol-tholeiitic basalt, qz-th = qz-tholeiitic basalt, A aob = group A alkali ol-basalt.

Table 5.1 also contains the relative abundance of various rock types from other intraplate volcanic provinces and fields in New Zealand and eastern Australia. Evaluation of these data suggests that the predominance of basanite in the SAVF is a feature uncommon in

[44] The SAVF lavas have been classified according to the classification scheme outlined in Johnson and Duggan (1989). The criteria used in this scheme are summarised in Chapter 3 (section 3.3).

[45] The number of rocks analysed is unlikely to provide a precise estimate of the abundance of each rock type. However, because of the wide distribution of the 61 centres sampled, and lack of spatial or temporal correlation between rock types (Briggs *et al.*, 1994), the data presented in Table 5.1 are considered to provide a reasonable estimate of relative abundances.

New Zealand and eastern Australia. Hawaiite is the most common mafic magma type erupted in these regions, whereas basanite is predominant in only 4 of the 12 provinces and fields; the SAVF, Chatham Islands, New South Wales, and Tasmania.

Table 5.1 Frequency percentage distribution of analysed alkalic basalts from the South Auckland volcanic field (this study) and the mafic compositions of the Northland Volcanic Province and some of the volcanic provinces in South Island, New Zealand (adapted from Weaver *et al.*, 1989), and eastern Australia Cainozoic volcanic provinces (from Ewart *et al.*, 1988; Ewart, 1989). Values given for the Northland Volcanic Province and the volcanic provinces in the South Island have been normalised to 100% to reflect frequency percentages of mafic compositions only. The original percentages given in Weaver *et al.* (1989) included intermediate compositions. Rock classification based on Johnson and Duggan (1989).
n = number of analyses. n.d. = not determined. n.a. = not available.

	North Island, New Zealand		South Island, New Zealand			
Rock type	South Auckland volcanic field	Northland Volcanic Province	Canterbury and North Otago	Banks Peninsula	Dunedin Volcanic Group	Chatham Islands
melilitites, nephelinites, analcimites	9 (nephelinites only)	-	3 (nephelinites only)	2	19	53
basanites	26	2	8	14	29	40
alkali olivine basalts	Group A = 5 Group B = 6	10	5	14	10	-
ne-hawaiites	9	n.d.	n.d.	n.d.	n.d.	n.d.
mugearite	< 1	1	n.a.	n.a.	n.a.	n.a.
hawaiite	16	52	53	61	42	5
transitional basalts and ol-tholeiitic basalts	transitional basalts = 8 ol-tholeiitic basalts = 16	25	15	9	-	2
qz-tholeiitic basalts	4	10	15	-	-	-
n	93	n.a.	n.a.	n.a.	n.a.	n.a.

Table 5.1 continued.

	Eastern Australia					
Rock type	South and Central Queensland	New South Wales	Victoria and South Austrralia	Tasmania	North Queensland	Central complexes
melilitites, nephelinites, analcimites	2	6	< 1	28	7	< 1
basanites	7	31	5	19	12	< 1
alkali olivine basalts	4	18	4	11	2	3
ne-hawaiites	10	7	16	15	38	2
mugearite	n.a.	n.a.	n.a.	n.a.	n.a.	n.a.
hawaiite	30	16	40	10	39	45
transitional basalts and ol-tholeiitic basalts	26	7	25	9	2	26
qz-tholeiitic basalts	22	5	10	8	-	22
n	n.a.	n.a.	n.a.	174	202	240

5.3.2 Normative Ne-Ol-Di-Hy-Qz associations

Representative CIPW normative compositions for each rock type from groups A and B are presented in Tables 5.2 and 5.3 respectively (CIPW norms for selected SAVF samples are given in Appendix 4). These data reveal that the suite of SAVF lavas represent a diverse and heterogeneous group of basaltic magmas, which forms the basis for the distinction between the two rock groups identified – the predominantly hy-normative group A and the ne-normative group B rocks. Distinct geochemical features, discussed in later sections, mark each rock type within groups A and B.

Geochemical analyses for group A and B rocks in terms of their CIPW normative mineralogy[46] are shown in Fig. 5.2. With the exception of four qz-normative samples (SA31, SA76, SA77, and SAB198), the SAVF rocks are ol-normative. In addition, the continuous range of compositions from silica-undersaturated rocks with up to 23% normative nepheline through to less undersaturated rocks with up to 24% normative hypersthene (Tables 5.2 and 5.3) is similar to the mafic lavas from the Northland Volcanic Province, New Zealand, and volcanic provinces in eastern Australia (Weaver *et al.*, 1989; Ewart *et al.*, 1988; Ewart, 1989).

Important features of Fig. 5.2 are: (i) the distinct, high concentration of ne-normative samples over a relatively narrow range in the Ol-Ne field, and (ii) the relatively broad range of compositions from the transitional Ol-Di region, through the Ol-Hy field to qz-normative compositions. This range of compositions contrasts those of the other volcanic fields in the Auckland Volcanic Province (e.g., Okete, Briggs and Goles, 1984; Ngatutura, Briggs *et al.*, 1990; and Auckland, Heming and Barnet, 1986, Huang *et al.*, 1997).

[46] CIPW norms were calculated using volatile-free whole-rock analyses with major element oxides normalised to total 100% (e.g., Cox *et al.*, 1979) and an adjusted $Fe_2O_3/FeO = 0.20$ (Middlemost, 1989).

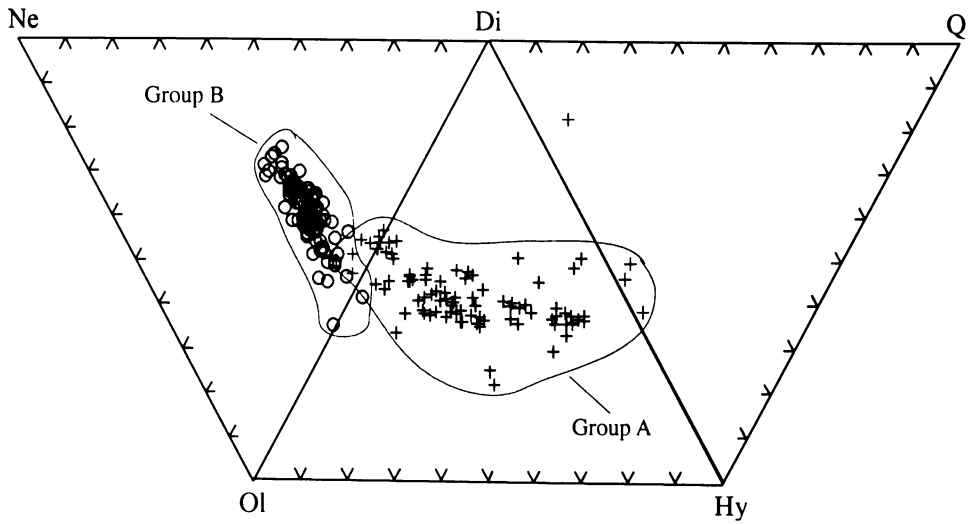

Fig. 5.2 CIPW normative mineralogy compositions for the group A and B lavas of the South Auckland volcanic field projected in the Ne-Ol-Di-Hy-Q system.
Ne = nepheline, Di = diopside, Q = quartz, Ol = olivine, Hy = hypersthene. + = group A, o = group B.

Table 5.2 CIPW normative compositions for representative group A rocks, South Auckland volcanic field.

	transitional basalt			hawaiite			ol-tholeiitic basalt			qz-tholeiitic basalt		alkali ol-basalt	
	SA07	SA48	SAB150	SA11	SA14	SA69	SA15	SAB174	SAB187	SA76	SAB198	SA19	SAB162
q	-	-	-	-	-	-	-	-	-	1.27	1.85	-	-
or	1.63	5.86	3.28	4.37	2.43	4.97	3.04	2.20	3.63	3.26	4.76	4.87	6.44
ab	22.98	26.14	23.75	28.45	24.98	26.53	25.94	23.32	22.39	23.35	32.34	26.85	29.23
an	28.99	26.22	24.91	25.98	24.66	22.27	24.68	26.18	22.40	22.55	28.95	24.96	26.50
ne	-	-	-	-	-	-	-	-	-	-	-	0.27	0.18
lc	-	-	-	-	-	-	-	-	-	-	-	-	-
di	16.60	14.32	15.15	16.22	16.98	16.04	18.88	14.86	16.38	19.21	20.29	18.83	16.51
hy	2.45	3.46	9.80	1.57	9.36	7.46	17.18	20.93	16.18	23.38	4.79	-	-
ol	19.53	14.18	15.34	14.70	15.09	14.50	2.93	5.97	11.82	-	-	15.47	11.55
mt	3.25	3.21	3.07	3.05	2.95	3.07	2.92	2.86	2.91	2.78	1.52	2.96	2.56
il	4.24	5.61	4.10	4.76	3.14	4.45	3.90	3.19	3.66	3.72	4.73	5.00	5.92
ap	0.33	1.00	0.62	0.90	0.42	0.71	0.55	0.48	0.64	0.49	0.77	0.79	1.12
D.I.	24.61	32.00	27.03	32.82	27.41	31.51	28.97	25.52	26.02	27.88	38.95	31.99	35.84

CIPW normative phases: q = quartz, or = orthoclase, ab = albite, an = anorthite, ne = nepheline, lc = leucite, di = diopside, hy = hypersthene, ol = olivine, mt = magnetite, il = ilmenite, ap = apatite, D.I. = differentiation index

Table 5.3 CIPW normative compositions for representative group B rocks, South Auckland volcanic field.

	basanite				nephelinite			ne-hawaiite			mugearite	alkali ol-basalt		
	SA05	SA56	SA60	SAB179	SA28	SA51	SAB135	SA24	SA65	SAB218	SA88	SAB188	SAB224	SAB227
q	-	-	-	-	-	-	-	-	-	-	-	-	-	-
or	6.94	7.69	6.92	6.85	13.00	10.39	10.07	10.88	13.25	11.24	7.94	8.28	10.65	9.17
ab	7.08	6.98	9.53	8.18	4.79	3.15	1.79	20.68	20.09	21.03	28.32	19.46	25.04	18.37
an	11.84	17.19	17.70	17.23	5.43	8.46	12.10	13.72	8.74	13.12	11.29	21.56	17.40	21.66
ne	15.56	10.36	8.57	8.63	21.18	19.59	16.47	9.21	15.16	10.00	-	2.78	4.34	3.19
lc	-	-	-	-	-	-	-	-	-	-	-	-	-	-
di	26.26	24.66	25.33	24.66	26.46	27.45	26.84	16.51	17.76	18.38	17.12	15.69	15.19	19.34
hy	-	-	-	-	-	-	-	-	-	-	1.04	-	-	-
ol	20.69	22.78	22.57	24.96	17.28	18.37	20.65	17.96	14.86	16.90	23.28	22.40	17.88	17.38
mt	3.44	3.27	3.01	3.14	3.63	3.67	3.49	3.43	3.25	3.02	3.92	3.08	3.07	3.19
il	6.24	5.67	5.31	5.13	5.41	6.06	6.10	5.45	4.62	4.64	5.68	5.13	4.73	5.72
ap	1.94	1.42	1.06	1.21	2.82	2.88	2.51	2.16	2.28	1.68	1.41	1.63	1.70	1.99
D.I.	29.58	25.02	25.02	23.66	38.98	33.13	28.32	40.77	48.50	42.26	36.26	30.52	40.03	30.73

CIPW normative phases: q = quartz, or = orthoclase, ab = albite, an = anorthite, ne = nepheline, lc = leucite, di = diopside, hy = hypersthene, ol = olivine, mt = magnetite, il = ilmenite, ap = apatite, D.I. = differentiation index

5.3.3 SiO_2:total alkali ($Na_2O + K_2O$) associations

The lavas of the South Auckland volcanic field are characterised by their relative silica-undersaturation and alkalic basaltic nature. The compositions of the SAVF lavas range from subalkalic to mildly alkaline for the group A rocks and strongly alkalic to mildly alkaline for those in group B (Fig. 5.3).

Group A and group B rocks have contrasting SiO_2:(total alkali) characteristics. Overall, the group A rocks have a relatively restricted range of total alkali contents (2.9 to 4.6 wt. %) that do not correlate with SiO_2. The alkali ol-basalts and the majority of hawaiites tend to be more alkaline than the transitional basalts and the ol-tholeiitic and qz-tholeiitic basalts. The group B rocks have a relatively broad range of total alkalies (3.2 – 7.8 wt. %), which overall exhibit a positive trend with increasing SiO_2. However, total alkalies in the basanites show little correlation with SiO_2 contents, whereas total alkalies in the nephelinites and ne-hawaiites decrease markedly with relatively small increases in SiO_2 contents. Trends such as these may be indicative of the fractionation of parent magmas with high $Mg/(Mg + Fe^{2+})$ towards differentiates with lower $Mg/(Mg + Fe^{2+})$. Only the alkali ol-basalts span the entire range of SiO_2 contents of the group B rocks, exhibiting a relatively strong positive correlation with total alkali contents.

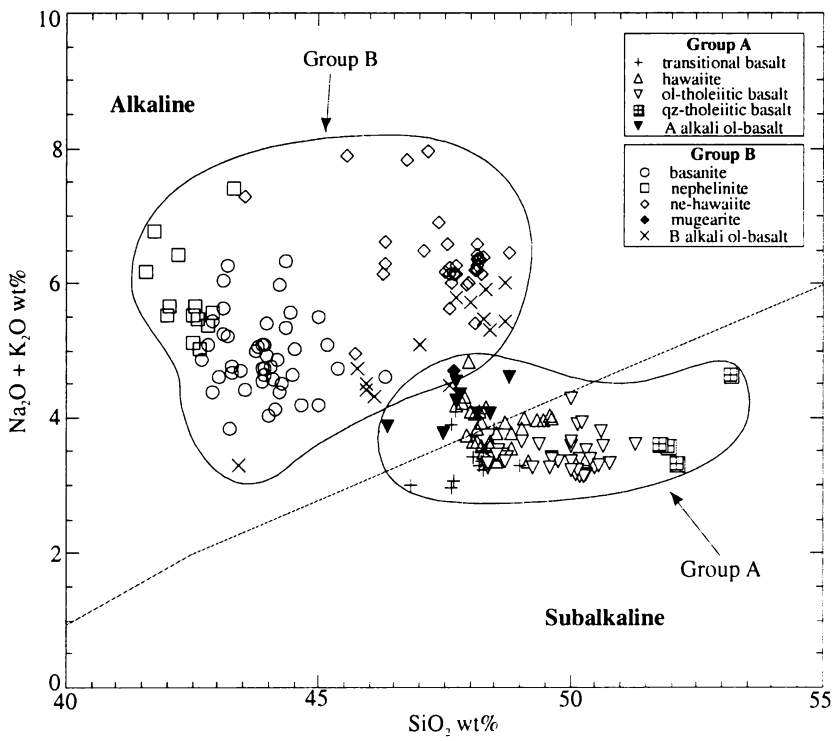

Fig 5.3 SiO_2:($Na_2O + K_2O$) relationships for the group A and B lavas of the South Auckland volcanic field. The boundary between the alkaline and subalkaline fields is from Miyashiro (1978).

5.3.4 Differentiation index:normative feldspar associations

In terms of the differentiation index (D.I.), the silica-undersaturated nature of the SAVF rocks and the contrasts in normative plagioclase compositions between groups A and B are illustrated in Fig. 5.4. Overall, the SAVF rocks have D.I. and normative plagioclase characteristics similar to those of the Okete Volcanics (Briggs and Goles, 1984), Ngatutura Basalts (Briggs *et al.*, 1990), and the Auckland volcanic field (Huang *et al.*, 1997), and the mafic lavas from the Northland Volcanic Province (Weaver *et al.*, 1989), the volcanic provinces in South Island, New Zealand (Weaver *et al.*, 1989), eastern Australia, and Tasmania (Ewart *et al.*, 1988; Ewart, 1989). The SAVF, however, lacks the felsic compositions found in the majority of the South Island and eastern Australia provinces (see Fig. 4.6.13 in Weaver *et al.*, 1989 and Fig. 5.2.5 in Ewart, 1989, respectively).

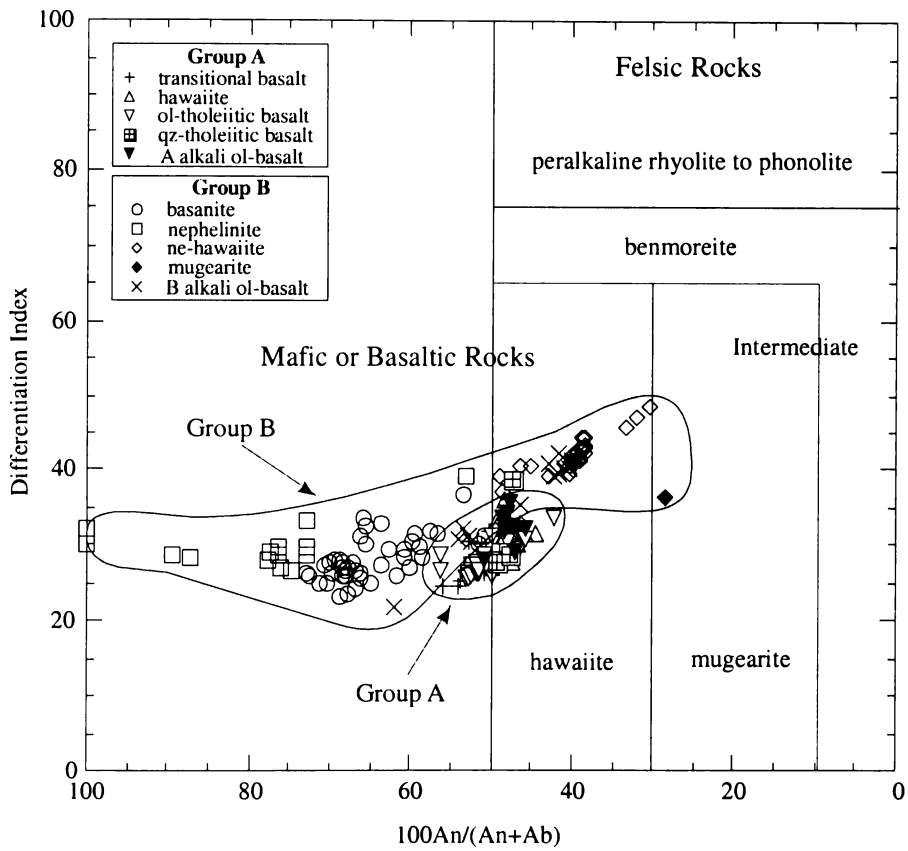

Fig. 5.4 Differentiation Index vs. normative plagioclase relationships for the group A and group B lavas of the South Auckland volcanic field. Field boundaries are after Coombs and Wilkinson (1969).

There is a distinct overlap in D.I. values between the rocks from groups A and B (Fig. 5.4). The group A rocks have a relatively restricted range of D.I. values (24 – 39) with each rock type spanning this range. Group B rocks, in contrast, have D.I. values that range from 22 to 48 with a majority of nephelinites, basanites, and alkali ol-basalts

having values similar to those from group A rocks. The ne-hawaiites generally have higher differentiation indices than other group A or B rock types. This distinction is also reflected in their geochemical compositions.

The group A rocks have a limited range of normative labradorite to andesine compositions, whereas those in group B exhibit a broad range of normative plagioclase compositions, from normative anorthite to oligoclase. The nephelinites, basanites, and ne-hawaiites plot in clearly defined fields over this range with each rock type having predominantly normative bytownite, labradorite, and andesine associations, respectively. Generally, there is a larger proportion of group B rocks with 100An/(An + Ab) > 60% than their mafic counterparts in the Northland Volcanic Province (Weaver *et al.*, 1989), Auckland volcanic field (Huang *et al.*, 1997) and most eastern Australia volcanic provinces (Ewart, 1989). In contrast, the group A rocks have normative plagioclase compositions comparable to the hy-normative mafic rocks in these regions.

5.4 Geochemical characteristics of the SAVF basalts

Major and trace element analyses for each rock type in groups A and B are summarised in Tables 5.4 and 5.5 respectively. Representative analyses of group A and B rocks are presented in Tables 5.6 and 5.7 respectively. Major element oxide data presented in the tables and discussed in the text are untreated XRF analyses unless specified otherwise. Oxide data used in plots are normalised free of volatiles to total 100%. Total Fe is reported as Fe_2O_3. Trace element data derived from SSMS and ICP-MS analyses are identified in Tables 5.6 and 5.7 and used in all plots rather than the XRF-derived analyses for these samples. The following discussion summarises the major and trace element characteristics of the SAVF lavas.

5.4.1 Mg-Fe relationships

The SAVF lavas exhibit a relatively broad range of 100Mg/(Mg + Fe^{2+}) values (47 to 68), with 107 of 203 samples > 60. In general, the distribution of 100Mg/(Mg + Fe^{2+}) for each rock type from groups A and B, illustrated in Fig. 5.5, suggests that basanites are the most primitive lavas in the SAVF, based on their consistent, relatively large 100Mg/(Mg + Fe^{2+}) values (e.g., 43 of 45 basanites are > 60 with 15 samples > 65). In contrast to the basanites, all ne-hawaiite samples have 100Mg/(Mg + Fe^{2+}) values < 58. The hawaiites display the largest range of 100Mg/(Mg + Fe^{2+}) values (47 – 64) and together with the ne-hawaiites contain samples with the smallest 100Mg/(Mg + Fe^{2+}) values.

Table 5.4 Summarised major and trace element analyses for group A rocks, South Auckland volcanic field. Mean = ± 1 standard deveation.

	Group A																	
	Group A (all analysed samples)			transitional basalt n = 15			hawaiite n = 29			ol-tholeiitic basalt n = 38			qz-tholeiitic basalt n = 4			alkali ol-basalt n = 8		
	max	min	mean	max	min	mean	max	min	mean	max	min	mean	max	min	mean	max	min	mean
SiO_2	52.57	44.71	48.34 ± 1.28	48.04	45.40	47.05 ± 0.68	49.39	44.71	47.87 ± 0.75	50.78	45.64	49.01 ± 0.97	52.57	50.45	51.25 ± 0.86	48.36	46.67	47.66 ± 0.65
TiO_2	3.09	1.60	2.12 ± 0.36	2.91	1.72	2.18 ± 0.40	3.01	1.66	2.27 ± 0.33	2.25	1.60	1.91 ± 0.20	2.46	1.90	2.13 ± 0.24	3.09	2.15	2.59 ± 0.37
Al_2O_3	17.60	12.94	14.48 ± 0.85	15.71	13.63	14.62 ± 0.55	16.04	12.94	14.55 ± 0.77	17.09	13.18	14.27 ± 0.74	17.60	13.02	14.44 ± 2.12	16.53	13.48	15.07 ± 1.14
Fe_2O_3	16.41	6.79	13.39 ± 1.06	14.41	13.42	13.94 ± 0.40	16.41	12.78	13.83 ± 0.74	14.59	11.31	13.10 ± 0.71	12.21	6.79	10.73 ± 2.66	15.10	11.49	13.57 ± 0.96
MnO	0.34	0.10	0.18 ± 0.03	0.23	0.15	0.19 ± 0.02	0.34	0.15	0.19 ± 0.03	0.23	0.15	0.18 ± 0.02	0.21	0.10	0.17 ± 0.05	0.19	0.16	0.18 ± 0.01
MgO	10.63	3.88	8.24 ± 1.29	10.11	6.17	8.39 ± 1.15	10.25	5.84	7.93 ± 1.33	10.59	6.68	8.65 ± 0.79	7.97	3.88	6.80 ± 1.96	10.63	5.56	7.56 ± 1.97
CaO	11.19	6.32	9.22 ± 0.56	10.15	8.69	9.33 ± 0.41	9.95	8.35	9.25 ± 0.47	10.01	6.32	9.00 ± 0.57	11.19	9.00	9.66 ± 1.03	10.19	9.42	9.73 ± 0.32
Na_2O	3.79	2.54	2.94 ± 0.22	3.00	2.65	2.83 ± 0.11	3.33	2.75	3.05 ± 0.15	3.20	2.54	2.81 ± 0.14	3.79	2.68	3.03 ± 0.51	3.47	3.04	3.30 ± 0.15
K_2O	1.08	0.26	0.65 ± 0.22	0.96	0.26	0.56 ± 0.23	1.02	0.41	0.74 ± 0.24	0.87	0.31	0.57 ± 0.14	0.79	0.53	0.68 ± 0.11	1.08	0.71	0.88 ± 0.15
P_2O_5	0.51	0.15	0.31 ± 0.09	0.48	0.15	0.28 ± 0.10	0.50	0.19	0.33 ± 0.11	0.38	0.19	0.28 ± 0.05	0.35	0.22	0.28 ± 0.05	0.51	0.33	0.43 ± 0.07
Total	101.10	96.99	100.04 ±	100.43	98.69	99.84 ± 0.52	100.95	97.48	100.11 ± 0.66	100.81	96.99	100.02 ±	100.01	99.15	99.66 ± 0.39	101.10	100.08	100.50 ± 0.34
LOI	2.08	-1.66	-0.06 ± 0.67	1.18	-1.25	0.00 ± 0.77	2.08	-0.69	-0.06 ± 0.61	1.98	-1.66	-0.06 ± 0.70	1.07	-0.09	0.46 ± 0.51	-0.19	-0.94	-0.54 ± 0.26
$\frac{100Mg}{(Mg+Fe^{2+})}$	66	47	59 ± 4	64	51	59 ± 4	64	47	57 ± 4	66	54	61 ± 2	61	57	60 ± 2	64	51	56 ± 5
trace elements (ppm)																		
Sc	30	17	24 ± 3	28	22	26 ± 2	28	19	24 ± 3	29	17	24 ± 2	30	23	26 ± 3	27	19	23 ± 3
V	310	184	224 ± 25	277	195	235 ± 29	280	185	229 ± 22	256	184	211 ± 16	274	196	221 ± 36	310	216	250 ± 29
Cr	368	55	271 ± 75	362	66	274 ± 95	357	62	261 ± 84	368	221	287 ± 33	316	291	307 ± 12	309	55	183 ± 101
Ni	434	38	176 ± 73	294	40	181 ± 73	244	41	151 ± 61	434	98	204 ± 58	403	38	196 ± 152	225	40	106 ± 74
Cu	106	38	62 ± 13	77	42	61 ± 12	92	38	59 ± 11	106	38	67 ± 13	78	41	57 ± 16	72	39	57 ± 12
Zn	170	86	104 ± 11	117	92	103 ± 7	117	87	100 ± 10	134	91	107 ± 8	170	104	123 ± 31	118	86	100 ± 11
Ga	32	20	24 ± 3	31	21	24 ± 3	31	20	24 ± 3	29	20	23 ± 2	30	21	24 ± 4	32	22	26 ± 4
As	4.3	0.4	1.6 ± 0.8	2.6	0.4	1.4 ± 0.7	2.4	0.4	1.5 ± 0.6	4.3	0.7	1.9 ± 0.9	1.6	1.1	1.4 ± 0.3	2.8	0.5	1.7 ± 0.9
Rb	17	2.4	9.8 ± 4	11	2.8	7.1 ± 3	17	5.9	11 ± 4.0	17	4.6	9.8 ± 3	15	10	13 ± 2	15	9.1	11 ± 2
Sr	620	251	362 ± 103	520	258	355 ± 78	592	271	400 ± 125	413	251	314 ± 43	445	283	342 ± 71	620	387	493 ± 89
Y	88	20	27 ± 10	47	20	28 ± 8	88	21	32 ± 14	45	20	25 ± 6	34	23	26 ± 5	30	21	24 ± 3
Zr	210	97	139 ± 34	194	97	140 ± 28	198	110	147 ± 46	151	103	127 ± 14	149	124	138 ± 10	210	130	174 ± 24
Nb	29	8.7	15 ± 6	23	10	16 ± 4	23	8.7	17 ± 9	26	8.7	13 ± 4	19	9.6	14 ± 4	29	16	21 ± 4
Ba	385	64	128 ± 57	205	65	111 ± 36	213	76	136 ± 49	236	64	116 ± 37	235	77	133 ± 70	385	99	193 ± 117
La	74	6.1	18 ± 10	30	9.8	17 ± 6	74	8.4	23 ± 12	32	6.1	15 ± 7	35	9.9	17 ± 12	30	15	20 ± 5
Pb	7.0	1.1	3.1 ± 1.2	4.7	1.1	2.7 ± 1.1	7.0	1.3	3.1 ± 1.5	5.2	1.3	3.0 ± 1.0	6.1	1.7	3.4 ± 2.0	5.0	2.5	3.4 ± 1.0
Ce	70	16	39 ± 12	44	24	37 ± 6	65	21	44 ± 13	59	16	34 ± 11	56	25	41 ± 13	70	44	51 ± 8
Th	4.9	0.6	2.4 ± 1.0	3.2	0.7	1.9 ± 0.7	4.1	1.1	2.3 ± 1.1	4.9	0.6	2.5 ± 1.0	3.4	1.2	2.3 ± 0.9	4.7	1.3	2.8 ± 1.0
U	2.3	-	0.6 ± 0.6	1.2	-	0.4 ± 0.4	2.3	-	0.6 ± 0.6	2.0	-	0.6 ± 0.1	1.7	0.4	0.8 ± 0.6	2.1	0.1	0.7 ± 0.8

LOI =Loss on ignition

Table 5.5 Summarised major and trace element analyses for group B rocks, South Auckland volcanic field. Mean = ± 1 standard deviation.

	Group B															
	Group B (all analysed samples)			basanite n = 45			nephelinite n = 13			ne-hawaiite n = 34			mugearite n = 1	alkali ol-basalt n = 16		
	max	min	mean	max	min	mean	max	min	mean	max	min	mean		max	min	mean
SiO_2	47.92	39.98	44.55 ± 2.15	45.23	41.55	43.33 ± 0.75	42.75	39.98	41.82 ± 0.63	47.92	42.97	46.54 ± 1.23	47.36	47.36	42.88	46.15 ± 1.47
TiO_2	3.29	2.06	2.73 ± 0.3	3.25	2.57	2.87 ± 0.19	3.29	2.80	3.15 ± 0.13	2.84	2.27	2.48 ± 0.14	2.97	3.21	2.06	2.58 ± 0.30
Al_2O_3	15.39	11.06	13.47 ± 1.06	14.72	12.17	12.73 ± 0.49	12.73	12.02	12.46 ± 0.17	15.39	12.41	14.47 ± 0.54	11.06	15.35	11.06	14.01 ± 0.73
Fe_2O_3	17.62	12.36	14.35 ± 0.86	15.62	13.27	14.53 ± 0.63	16.21	14.68	15.38 ± 0.48	16.04	12.36	13.91 ± 0.78	17.62	17.62	12.93	14.09 ± 0.58
MnO	0.30	0.17	0.20 ± 0.02	0.25	0.17	0.20 ± 0.02	0.25	0.19	0.22 ± 0.02	0.30	0.19	0.20 ± 0.03	0.22	0.22	0.18	0.20 ± 0.01
MgO	12.92	5.29	9.05 ± 2.08	12.92	7.03	10.83 ± 1.04	11.19	7.85	10.32 ± 1.00	7.51	5.29	6.78 ± 0.61	9.25	11.77	6.20	7.98 ± 1.69
CaO	10.59	7.21	9.14 ± 1.01	10.59	8.54	9.96 ± 0.38	10.39	8.96	9.96 ± 0.37	9.22	7.21	8.04 ± 0.45	7.21	10.10	7.21	8.44 ± 0.78
Na_2O	5.62	2.51	3.82 ± 0.63	4.49	2.58	3.49 ± 0.44	5.10	3.50	4.06 ± 0.48	5.62	2.91	4.34 ± 0.49	3.34	3.96	2.51	3.36 ± 0.47
K_2O	2.21	0.73	1.59 ± 0.31	2.04	0.97	1.35 ± 0.21	2.16	1.29	1.62 ± 0.21	2.21	1.40	1.87 ± 0.15	1.34	2.00	0.73	1.57 ± 0.33
P_2O_5	1.29	0.46	0.80 ± 0.18	1.12	0.46	0.73 ± 0.16	1.29	0.77	0.99 ± 0.17	1.28	0.55	0.85 ± 0.16	0.64	0.87	0.46	0.74 ± 0.11
Total	100.77	97.57	99.99 ± 0.58	100.77	97.57	100.11 ± 0.56	100.71	98.78	100.03 ± 0.60	100.51	97.76	99.83 ± 0.69	100.55	100.55	99.62	100.03 ± 0.26
LOI	2.20	-1.46	0.05 ± 0.62	1.96	-0.74	-0.11 ± 0.45	0.82	-0.75	-0.13 ± 0.46	1.93	-0.57	0.19 ± 0.62	-0.46	2.20	-1.46	0.33 ± 0.97
$\frac{100Mg}{(Mg + Fe^{2+})}$	68	47	59 ± 5	68	52	64 ± 3	64	54	61 ± 3	58	47	54 ± 3	55	64	52	57 ± 4
trace elements (ppm)																
Sc	30	12	19 ± 4	30	15	21 ± 3	28	13	20 ± 4	18	12	15 ± 2	18	26	12	18 ± 4
V	310	147	234 ± 42	310	190	266 ± 24	291	190	265 ± 27	227	147	191 ± 18	223	280	177	215 ± 27
Cr	404	61	248 ± 75	404	100	305 ± 57	312	160	239 ± 41	232	61	185 ± 55	293	346	159	242 ± 59
Ni	337	59	195 ± 70	337	89	249 ± 50	293	132	219 ± 45	173	59	126 ± 31	203	292	90	177 ± 54
Cu	86	36	63 ± 11	86	38	70 ± 8	81	55	66 ± 8	67	42	53 ± 7	67	67	36	59 ± 9
Zn	154	91	120 ± 13	135	91	113 ± 11	154	121	134 ± 10	148	101	123 ± 11	137	137	104	123 ± 11
Ga	30	21	25 ± 2	29	21	24 ± 2	29	24	27 ± 2	30	23	26 ± 1	26	28	21	26 ± 2
As	5.4	2.0	3.1 ± 0.8	4.7	2.0	2.9 ± 0.7	5.4	2.8	3.8 ± 0.9	4.9	2.1	3.4 ± 0.8	2.4	2.9	2.0	2.4 ± 0.6
Rb	45	14	27 ± 6	45	17	25 ± 7	45	21	30 ± 6	42	17	30 ± 4	25	33	14	24 ± 5
Sr	2193	547	905 ± 232	2193	547	823 ± 260	1411	869	1021 ± 157	1517	816	973 ± 185	317	1300	317	841 ± 158
Y	40	22	29 ± 4	35	22	26 ± 3	40	24	28 ± 5	40	27	32 ± 3	38	38	22	29 ± 3
Zr	491	194	321 ± 62	436	194	275 ± 48	453	281	330 ± 57	491	315	372 ± 40	253	410	238	322 ± 53
Nb	89	38	58 ± 11	80	38	54 ± 9	88	55	66 ± 11	89	54	62 ± 9	35	65	35	53 ± 7
Ba	1089	187	326 ± 112	593	197	284 ± 70	453	241	327 ± 66	528	283	358 ± 57	208	1089	187	363 ± 241
La	107	27	52 ± 15	76	27	46 ± 12	107	47	65 ± 20	100	44	57 ± 17	36	52	36	44 ± 5
Pb	9.5	2.0	5.0 ± 1.4	7.2	2.0	4.3 ± 1.3	8.4	3.3	5.3 ± 1.4	9.5	3.4	5.8 ± 1.3	4.5	6.6	2.3	4.5 ± 1.1
Ce	210	58	104 ± 31	160	58	95 ± 24	207	91	129 ± 41	210	86	112 ± 35	90	97	75	87 ± 6
Th	11.0	2.6	6.0 ± 1.6	8.8	2.6	5.5 ± 1.6	9.7	4.8	6.5 ± 1.8	11.0	4.4	6.7 ± 1.6	4.9	6.9	3.7	5.4 ± 0.9
U	4.4	-	1.5 ± 1.0	3.0	-	1.0 ± .07	2.8	-	1.4 ± 0.8	4.0	-	2.1 ± 1.0	0.1	4.4	-	1.8 ± 1.2

LOI = Loss on ignition

Table 5.6 Whole-rock analyses for representative samples of each group A rock type, South Auckland volcanic field.

	transitional basalt					hawaiite					ol-tholeiitic basalt				qz-tholeiitic basalt			alkali ol-basalt			
Sample #	SA07[2]	SA13	SA48[2]	SAB150[1]	SAB210	SA11[2]	SA14[2]	SA52[2]	SA69[2]	SAB163	SA15[1]	SA16[1]	SAB174[1]	SAB187[1]	SA31	SA76[2]	SAB198[1]	SA18	SA19[1]	SA33	SAB162[1]
SiO_2	45.83	48.63	46.59	47.98	47.95	47.74	49.05	47.59	48.36	47.53	50.30	49.70	49.90	49.17	51.34	51.00	52.77	47.33	47.87	47.28	48.38
TiO_2	2.19	1.69	2.89	2.14	2.65	2.48	1.65	2.64	2.31	3.00	2.04	1.90	1.67	1.91	2.09	1.92	2.47	2.29	2.62	2.13	3.09
Al_2O_3	15.13	14.34	15.46	14.26	15.27	15.70	14.33	15.45	14.07	16.02	14.57	14.31	14.45	13.15	13.70	13.16	17.67	14.02	15.30	13.38	16.53
Fe_2O_3	14.40	12.91	14.21	13.75	13.44	13.67	13.30	13.79	13.70	13.36	13.11	13.10	12.87	13.02	11.92	12.34	6.82	13.75	13.34	13.87	11.49
MnO	0.20	0.17	0.18	0.17	0.15	0.19	0.18	0.18	0.17	0.19	0.16	0.16	0.17	0.17	0.21	0.18	0.10	0.19	0.17	0.18	0.16
MgO	8.63	9.85	6.23	9.48	6.97	6.25	9.51	6.43	8.32	5.92	6.66	7.84	8.88	10.56	7.96	7.71	3.89	8.76	6.91	10.55	5.56
CaO	9.93	9.40	9.14	9.04	9.55	9.59	9.38	9.87	8.72	9.65	9.84	9.68	9.15	8.87	8.99	9.37	11.23	9.40	10.04	9.35	9.94
Na_2O	2.67	2.87	3.03	2.79	2.94	3.33	2.95	3.20	3.10	3.27	3.05	2.95	2.74	2.63	2.81	2.71	3.80	3.31	3.22	3.02	3.47
K_2O	0.27	0.39	0.97	0.55	0.84	0.78	0.41	0.84	0.83	1.02	0.51	0.42	0.37	0.61	0.72	0.54	0.80	0.91	0.82	0.74	1.08
P_2O_5	0.15	0.21	0.45	0.28	0.39	0.41	0.19	0.38	0.32	0.50	0.25	0.21	0.22	0.29	0.27	0.22	0.35	0.50	0.36	0.33	0.51
Total	99.40	100.46	99.15	100.43	100.15	100.14	100.95	100.37	99.90	100.45	100.49	100.27	100.42	100.40	100.01	99.15	99.90	100.46	100.65	100.83	100.22
LOI	0.93	-0.43	0.94	-0.39	-0.90	0.09	-0.69	-0.19	0.22	-0.49	-0.23	-0.01	-0.14	-0.50	-0.09	1.07	0.21	-0.31	-0.51	-0.79	-0.19
$\frac{100\,Mg}{(Mg + Fe^{2+})}$	58.9	64.2	51.2	61.9	55.1	51.9	62.6	52.4	59.0	51.1	54.5	58.5	61.9	65.6	61.2	59.9	57.4	60.0	54.9	64.1	53.3
trace elements (ppm)																					
Sc	27	25	23	25	27	27	27	24	24	23	26	26	25	24	25	23	32	24	25	23	24
Ti	-	-	-	12747	-	-	-	-	-	-	11536	11364	10175	11762	-	-	15052	-	15901	-	18510
V	200	209	277	227	253	238	201	255	220	280	215	218	192	198	210	196	259	254	250	216	279
Cr	336	329	81	325	190	205	322	203	296	67	260	301	263	385	316	305	333	210	218	309	89
Mn	-	-	-	1214	-	-	-	-	-	-	1253	1209	1230	1242	-	-	742	-	1283	-	1164
Co	-	-	-	77	-	-	-	-	-	-	90	70	64	75	-	-	29	-	78	-	63
Ni	294	196	40	245	79	68	183	65	183	42	127	156	216	297	161	403	40	66	80	225	51
Cu	77	51	44	65	57	48	48	56	66	52	45	67	74	60	49	78	42	39	44	72	49
Zn	117	93	92	112	103	93	96	94	96	96	109	106	104	110	108	111	169	97	112	101	121
Ga	24	21	25	26	28	26	21	25	24	29	-	-	-	-	22	21	-	23	-	22	-
As	2.5	1.2	1.3	-	-	1.7	1.8	1.2	0.4	-	-	-	-	-	1.4	1.1	-	2.8	-	1.4	-
Rb	5	6.2	11	6.7	11	10	7	11	14	10	6.6	6.5	7	11	15	10	16	11	12	11	14
Sr	332	290	495	314	444	400	271	463	366	592	280	270	255	315	321	283	469	450	460	409	621
Y	34	21	23	21	23	42	21	26	52	25	24	23	22	21	25	23	36	23	23	21	26
Zr	150	114	192	131	166	167	110	167	156	198	117	115	110	132	141	124	154	167	178	157	219
Nb	17	9.7	23	14	19	18	8.7	19	18	23	12	11	10	15	13	9.6	21	16	22	20	27
Mo	-	-	-	1.2	-	-	-	-	-	-	1.2	1.1	0.87	1.3	-	-	1.9	-	1.4	-	1.5
Sn	-	-	-	1.4	-	-	-	-	-	-	1.3	1.2	1.2	1.5	-	-	1.7	-	1.9	-	2.3
Cs	-	-	-	0.2	-	-	-	-	-	-	0.43	0.42	0.36	0.69	-	-	0.60	-	0.31	-	0.53
Ba	205	93	129	68	148	98	76	168	134	138	61	61	64	104	115	77	225	145	117	124	397
Hf	-	-	-	3.2	-	-	-	-	-	-	4.5	3.5	30	3.6	-	-	3.8	-	4.8	-	5.1
Ta	-	-	-	1.2	-	-	-	-	-	-	1.2	1.2	1.1	1.4	-	-	1.6	-	1.9	-	2.2
Pb	4.7	3.4	3.2	1.2	1.1	4.9	5.7	5.6	3.6	2.5	1.5	1.5	2.3	2.3	6.1	3.8	2.6	2.5	1.8	3.1	2.1
Th	1.8	2.6	1.5	0.69	1.2	1.3	1.1	1.2	1.9	1.6	0.82	0.79	1.1	1.3	2.4	1.2	1.9	3.0	1.1	2.7	1.3
U	0.37	0.60	0.49	0.29	1.1	0.31	0.25	0.35	0.35	0.70	0.29	0.28	0.34	0.42	0.40	0.40	0.66	0.10	0.53	0.10	0.54

LOI = loss on ignition; Total Fe expressed as Fe_2O_3.

[1] = trace element abundances determined by ICP-MS analyses.

[2] = trace element abundances determined by SSMS analyses.

Table 5.7 Whole-rock analyses for representative samples of each group B rock type, South Auckland volcanic field.

	basanite						nephelinite				ne-hawaiite						mugearite	alkali ol-basalt		
Sample #	SA03[2]	SA05[2]	SA55[2]	SA56[2]	SA60[2]	SAB179[1]	SA28[1]	SA51[2]	SAB113	SAB135[1]	SA02[1]	SA24[1]	SA25[1]	SA65[2]	SA66[2]	SAB218[1]	SA88	SAB188[1]	SAB224[1]	SAB227[1]
SiO_2	45.15	42.36	44.67	42.77	44.16	43.65	42.44	41.18	42.26	41.67	46.33	45.73	44.75	46.44	42.89	46.99	47.14	45.71	47.53	45.34
TiO_2	2.59	3.25	2.67	2.94	2.77	2.68	2.80	3.12	3.20	3.19	2.52	2.84	2.60	2.40	2.77	2.41	2.96	2.68	2.46	2.97
Al_2O_3	13.88	12.45	12.83	12.60	12.58	12.18	12.69	12.39	12.48	12.46	14.71	14.21	13.62	14.79	13.05	14.39	11.01	14.12	14.63	14.17
Fe_2O_3	13.34	15.42	13.73	14.53	13.48	14.12	16.11	16.25	14.88	15.67	12.50	15.35	15.37	14.46	15.99	13.63	17.54	13.81	13.89	14.40
MnO	0.19	0.20	0.19	0.19	0.17	0.20	0.25	0.24	0.20	0.22	0.22	0.19	0.23	0.27	0.25	0.19	0.22	0.21	0.19	0.19
MgO	9.56	10.47	11.65	11.50	12.07	12.88	7.84	8.72	11.13	10.44	7.31	6.82	6.86	5.45	7.48	7.30	9.21	9.87	7.12	7.73
CaO	9.10	9.85	10.21	10.22	10.38	10.22	8.95	9.81	9.85	10.38	9.07	7.89	8.05	7.21	9.19	7.99	7.18	9.06	8.08	10.08
Na_2O	3.32	4.19	3.00	3.04	2.97	2.83	5.10	4.55	3.81	3.78	3.77	4.41	4.20	5.61	5.24	4.61	3.32	2.89	3.87	2.83
K_2O	1.15	1.16	1.17	1.28	1.16	1.15	2.16	1.72	1.48	1.69	1.70	1.82	1.74	2.21	1.93	1.88	1.33	1.39	1.78	1.53
P_2O_5	0.62	0.88	0.46	0.64	0.48	0.55	1.27	1.29	0.86	1.14	0.56	0.98	1.07	1.03	1.28	0.76	0.64	0.74	0.77	0.90
Total	98.90	100.23	100.58	99.71	100.22	100.46	99.61	99.27	100.16	100.63	98.69	100.24	98.49	99.87	100.07	100.16	100.55	100.48	100.33	100.16
LOI	0.50	-0.07	-0.44	0.10	-0.29	-0.56	-0.08	0.27	-0.60	-0.14	1.13	-0.16	1.30	-0.01	-0.34	-0.45	-0.46	-1.46	0.36	2.20
$\frac{100Mg}{(Mg+Fe^{2+})}$	63.2	61.6	66.6	65.3	67.9	68.2	53.7	56.3	63.9	61.1	58.4	51.2	51.9	47.2	52.6	55.9	55.4	62.7	54.7	56.0
trace elements (ppm)																				
Sc	19	17	22	21	23	27	17	17	24	20	20	16	16	12	14	17	18	21	17	18
Ti	-	-	-	-	-	16241	16802	-	-	19005	15590	16613	15923	-	-	13965	-	16221	14302	16382
V	232	260	276	288	283	278	172	227	285	245	211	151	146	147	198	170	223	208	173	202
Cr	263	252	392	326	404	396	167	165	277	231	211	112	88	61	127	231	293	253	221	172
Mn	-	-	-	-	-	1465	1909	-	-	1567	1426	1430	1707	-	-	1447	-	1443	1431	1395
Co	-	-	-	-	-	79	62	-	-	74	81	71	56	-	-	56	-	60	56	62
Ni	289	205	263	240	283	324	149	142	251	225	157	111	102	61	115	153	203	217	159	140
Cu	64	63	69	67	70	67	57	55	72	64	59	48	53	44	53	63	67	61	54	57
Zn	98	122	91	104	95	111	163	146	131	146	125	146	154	140	148	128	137	115	127	121
Ga	24	25	22	23	23	-	-	25	28	-	-	-	-	29	28	-	26	-	-	-
As	3.1	2.6	2.2	2.6	2.0	-	-	3.9	-	-	-	-	-	3.8	3.1	-	2.4	-	-	-
Rb	24	24	20	20	19	20	37	36	21	38	33	26	31	38	33	32	25	23	29	23
Sr	746	932	547	666	568	581	1296	1161	869	937	783	822	1053	1253	1517	759	317	774	754	726
Y	26	27	23	25	23	22	37	36	24	27	27	28	34	39	40	25	38	26	26	25
Zr	311	311	194	231	199	215	469	428	287	309	354	352	438	491	404	346	253	289	339	310
Nb	55	56	38	43	38	45	102	88	57	73	61	68	87	89	78	62	35	54	61	57
Mo	-	-	-	-	-	2.3	9.0	-	-	5.1	6.1	4.7	5.6	-	-	5.1	-	4.4	4.7	4.1
Sn	-	-	-	-	-	1.9	3.8	-	-	2.7	2.8	3.0	3.6	-	-	2.8	-	2.5	2.8	2.5
Cs	-	-	-	-	-	0.34	1.4	-	-	0.95	0.81	0.31	0.47	-	-	0.51	-	0.51	0.52	0.54
Ba	260	263	200	214	206	200	429	420	268	364	270	280	355	425	478	281	208	241	277	260
Hf	-	-	-	-	-	4.9	8.8	-	-	6.1	7.5	7.7	8.4	-	-	6.8	-	5.9	6.5	6.5
Ta	-	-	-	-	-	3.4	7.2	-	-	5.4	4.9	4.6	6.5	-	-	4.4	-	4.1	4.3	3.9
Pb	5.7	3.8	3.4	4.1	3.4	2.3	5.3	5.3	5.0	4.0	4.4	3.3	5.1	6.4	7.4	4.1	4.5	3.4	3.9	4.0
Th	6.8	4.5	3.8	3.8	3.8	2.5	6.6	9.4	4.8	4.9	4.8	3.7	5.9	11	8.3	4.4	4.9	3.6	4.3	3.9
U	0.10	1.3	0.93	1.1	1.0	0.87	3.3	2.8	1.7	1.8	2.0	1.4	1.9	1.9	2.4	1.8	0.10	1.4	1.6	1.4

LOI = loss on ignition; Total Fe expressed as Fe_2O_3.

[1] = trace element abundances determined by ICP-MS analyses.

[2] = trace element abundances determined by SSMS analyses.

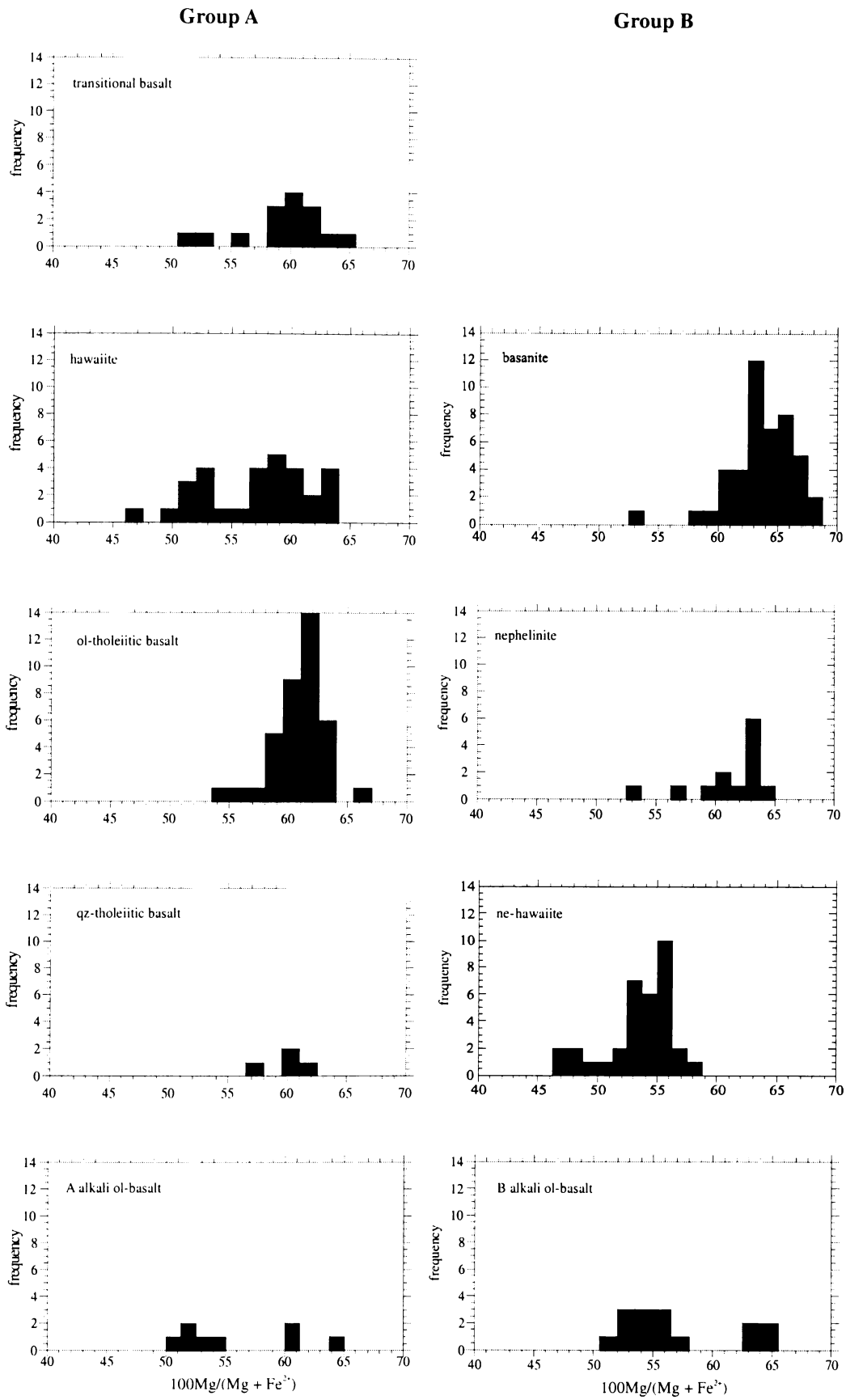

Fig. 5.5 Frequency distribution of $100Mg/(Mg + Fe^{2+})$ values for each rock type from groups A and B in the South Auckland volcanic field. The sample size for each rock type is given in Tables 5.4 and 5.5.

Although one third of the basanites have values of $100Mg/(Mg + Fe^{2+}) > 65$, they lack the low-CaO, high-magnesian olivine phenocrysts (e.g., CaO < 0.1 wt. %, Fo > 89), ultramafic mantle xenoliths, and high compatible trace element contents considered requisite to represent primary magmas[47]. In addition, there is a progressive general decrease in $100Mg/(Mg + Fe^{2+})$ in the basanite – nephelinite – ne-hawaiite sequence, indicating that these magmas have undergone olivine-dominated fractionation. Fractionation trends similar to those described by Ewart *et al.* (1988) and Ewart (1989; see Figure 5.2.3, p. 192 of Ewart, 1989) for alkali ol-basalts, transitional basalts, and ol-tholeiitic and qz-tholeiitic basalts from eastern Australia (e.g., values of $100Mg/(Mg + Fe^{2+})$ that positively correlate with decreasing degrees of silica undersaturation) are not apparent in the suite of similar rock types from the SAVF. However, the wide range of $100Mg/(Mg + Fe^{2+})$ that characterises the SAVF lavas suggests that the majority of them were derived from more Mg-rich parental magmas, the compositions of which were subsequently altered by differentiation processes that probably include fractional crystallisation.

5.4.2 Major element compositions

The group A and B rocks have distinctive major element compositions. The variation diagrams shown in Fig. 5.6 illustrate that large differences in major element oxide contents at a given MgO content are common. Collectively, the samples within each group define dissimilar trends that are best illustrated in plots of the more incompatible oxides K_2O, Na_2O, and P_2O_5, vs. MgO[48]. Correlation coefficients (r^2 values) for MgO vs. each oxide plotted in Fig. 5.6 are presented in Table 5.8.

Lavas in each rock group have a relatively broad range of MgO contents. The group A rocks have overlapping MgO contents that range from 3.9 to 10.6 wt. %[49] with the majority of samples > 8.0 wt. %. Rocks in group B have MgO in the range 5.3 – 12.9 wt.%. The group B alkali ol-basalts span a relatively broad range of MgO (6.3 – 11.8 wt.%), whereas the majority of basanites and nephelinites have MgO greater than the most magnesian group A rocks (e.g., > 10 wt.%). In contrast, the ne-hawaiites have MgO values (5.3 – 7.5 wt.%) that are lower than the majority of group A rocks.

---

[47]The geochemical characteristics used to categorise volcanic rocks as representative 'primary' upper mantle melts are not clearly defined. There is, however, generally good agreement among researchers that mantle-derived magmas considered primary melts should contain ultramafic mantle xenoliths, have $100Mg/(Mg + Fe^{2+}) > 65$, and relatively large abundances of the compatible trace elements (e.g., Ni ~ 320 ppm) (e.g., Green, 1973a, Frey *et al.*, 1978; Clague and Frey, 1982; Briggs and Goles, 1984; Clague and Dalrymple, 1988; Ewart *et al.*, 1988; Wilkinson, 1991; Kinzler and Grove, 1992).

[48] Since MgO content is sensitive to the decomposition of ferromagnesian phases such as olivine and clinopyroxene during partial melting or the removal of these phases during fractional crystallisation processes, the MgO variation diagrams best illustrate composition distinctions for suites of mafic rocks such as those in the SAVF.

[49] Note the one outlier, qz-tholeiitic basalt sample SAB198 (3.9 wt. % MgO), labelled in the SiO_2 vs. MgO plot (Fig. 5.6).

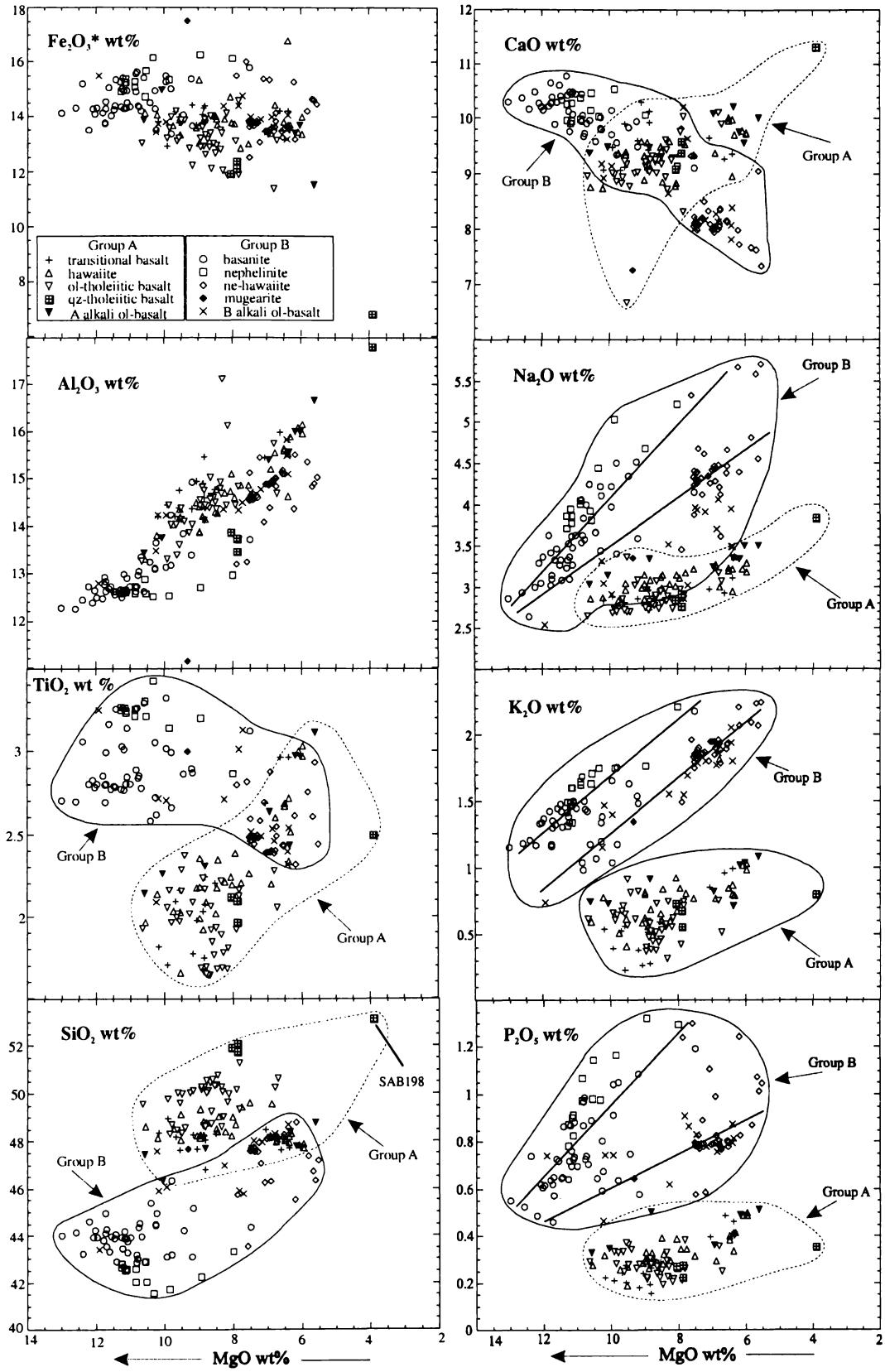

Fig 5.6 MgO variation diagrams for the whole-rock analyses of the South Auckland volcanic field lavas summarised in Tables 5.4 and 5.5. The analyses were recalculated to 100% without volatiles and all iron as Fe_2O_3 (Fe_2O_3*). The fields for the group A and B lavas in the Fe_2O_3* and Al_2O_3 vs. MgO diagrams have been omitted because they strongly overlap. The two major group B trends referred to in the text are illustrated in the Na_2O-, K_2O-, and P_2O_5-MgO diagrams.

Table 5.8 Correlation coefficients (r^2 values) for major element oxide data plotted in the MgO variation diagrams (Fig. 5.6) and referred to in the text. Negative values indicate negative MgO-oxide correlation. The strong correlation of the qz-tholeiitic basalt samples with most elements may be due to the small sample size and the outlying sample SAB198.

	Group A						Group B				
	All samples n = 94	trans n = 15	haw n = 29	ol-th n = 38	qz-th n = 4	Aaob n = 8	All samples n = 108	bas n = 45	neph n = 13	ne-haw n = 34	Baob n = 16
SiO_2	-0.09	0.29	0.27	-0.41	-0.98	-0.74	-0.81	-0.13	-0.13	-0.07	-0.82
TiO_2	-0.67	-0.91	-0.83	0.07	-0.95	-0.88	0.61	-0.20	0.71	-0.08	0.40
Al_2O_3	-0.79	-0.90	-0.92	-0.58	-0.99	-0.98	-0.92	-0.78	-0.56	-0.52	-0.91
$Fe_2O_3^*$	0.31	-0.23	-0.01	0.35	1.00	0.68	0.35	-0.28	-0.73	-0.09	0.39
CaO	-0.53	-0.02	-0.59	-0.49	-0.99	-0.71	0.91	0.72	0.52	0.44	0.70
Na_2O	-0.69	-0.66	-0.78	-0.44	-0.99	-0.86	-0.64	-0.77	-0.89	-0.56	-0.65
K_2O	-0.54	-0.81	-0.73	0.18	-0.67	-0.66	-0.84	-0.51	-0.88	-0.82	-0.94
P_2O_5	-0.57	-0.86	-0.76	0.22	-0.89	-0.64	-0.35	-0.63	-0.89	-0.22	-0.53

n = number of samples; trans = transitional basalt; haw = hawaiite; ol-th = ol-tholeiitic basalt; qz-th = qz-tholeiitic basalt; bas = basanite; neph = nephelinite ; ne-haw = ne-hawaiite; aob = alkali ol-basalt.

The SAVF lavas have SiO_2 contents that range from ~ 40.0 to 52.6 wt.%. Each group A rock type, except qz-tholeiitic basalts, has overlapping SiO_2 contents. However, the alkali ol-basalts, transitional basalts, and the majority of hawaiites tend to be the most silica-undersaturated group A rocks, with mean SiO_2 values of 47.7 ± 0.65, 47.1 ± 0.68, and 47.9 ± 0.75 wt.% respectively. The majority of ol-tholeiitic and the qz-tholeiitic basalts have the largest SiO_2 contents with mean values of 49.0 ± 0.97and 51.3 ± 0.86 wt.% respectively. In contrast, each group B rock type tends to span a distinct range of SiO_2 with only slight overlap between nephelinites (40.0 – 42.8 wt.%) and basanites (41.6 – 45.2 wt. %) with ne-hawaiites (43.0 – 47.9 wt.%) and alkali ol-basalts (42.9 – 47.4 wt.%).

Although relatively large variations in SiO_2 occur among hawaiites, ol-tholeiitic basalts, basanites, ne-hawaiites, and the group B alkali ol-basalts, there is a trend of decreasing silica-undersaturation from transitional basalt to qz-tholeiitic basalt and basanite to ne-hawaiite in groups A and B respectively. These trends are inferred on the basis of the mean SiO_2 contents for each rock type (see Tables 5.4 and 5.5) and the broad negative correlation of SiO_2 with MgO for each group, illustrated in Fig. 5.6. However, on an individual rock type basis, such correlations, albeit negative, are generally weak, with the exception of the group B alkali ol-basalts.

The majority of group A rocks have TiO_2 contents smaller (1.6 – 3.1 wt.%) than those in group B (2.1 – 3.3 wt.%), and although there are large variations in TiO_2 at a given MgO content each rock group exhibits a distinct trend. In the group A rocks, TiO_2 increases with decreasing MgO, whereas those in group B exhibit a weak trend of increasing TiO_2 with increasing MgO.

The group A lavas have overlapping Al_2O_3 contents (12.9 – 17.6 wt.%), larger than the nephelinites (12.0 – 12.7 wt.%) and most basanites (12.2 – 14.7 wt. %) and strongly

overlap the ne-hawaiites (12.4 – 15.4 wt.%) and group B alkali ol-basalts (11.1 – 15.4 wt.%). The mugearite (SA88) has the smallest, and qz-tholeiitic basalt (SAB198) the largest, Al_2O_3 contents of all rock types (11.1 and 17.6 wt. % respectively). Collectively, Al_2O_3 in the SAVF lavas negatively correlates with MgO (r^2 = 0.85). Al_2O_3-MgO correlation is strong in the transitional basalts, hawaiites, and group A and B alkali ol-basalts[50], moderate in the basanites, and weak in the ol-tholeiitic basalts, nephelinites, and ne-hawaiites.

Total Fe ($Fe_2O_3^*$) is variable (6.8 – 17.6 wt.%) although samples from each rock type, except qz-tholeiitic basalt, have overlapping $Fe_2O_3^*$ contents in the range 13 – 15 wt.% that show no apparent correlation with MgO. Basanites, nephelinites, ne-hawaiites, and mugearite tend to have the largest $Fe_2O_3^*$ contents (means ≥ 14 wt. %), whereas a large number of ol-tholeiitic basalts and the qz-tholeiitic basalts have the smallest (means ≤ 13 wt. %).

The group A rocks have smaller P_2O_5 contents (0.15 – 0.51 wt. %) than those in group B (0.46 – 1.3 wt. %), show little variation, and no apparent correlation with MgO. In contrast, each group B rock type exhibits a large variation in P_2O_5 at a given MgO content. Although P_2O_5 in the group B rocks overlap, the majority of basanites have the smallest P_2O_5 contents (means < 0.73 wt. %), whereas the nephelinites and ne-hawaiites tend to have the largest (means > 1.0 wt. %). Collectively, the group B rocks define a broad trend of increasing P_2O_5 with decreasing MgO, although the ne-hawaiites exhibit no apparent correlation with MgO.

Each group A rock type has similar Na_2O contents (2.5 – 3.8 wt. %) that are generally smaller than those in group B (2.5 – 5.6 wt. %), although a large number of basanites have Na_2O contents that overlap the group A rocks. In contrast, the nephelinites, group B alkali ol-basalts, and most ne-hawaiites have Na_2O greater than those in group A (i.e., > 3.5 wt. %). There is a marked increase in Na_2O with decreasing MgO in the group B rocks, whereas this trend in the group A rocks is generally weak. The nephelinites and group A alkali ol-basalts exhibit the strongest Na_2O-MgO correlation.

The group A and B rocks have distinctive K_2O-MgO relationships. Although a small number of samples in groups A and B have overlapping K_2O contents, each group exhibits discrete trends of increasing K_2O with decreasing MgO. The group A rocks have overlapping K_2O contents (0.26 – 1.1 wt. %) grouped mainly between 8.0 and 10.5 wt. %

[50] The strong correlation between some major element oxides and MgO in the qz-tholeiitic basalts may be due to the outlying sample SAB198 and the small sample size, n = 4.

MgO with relatively poor K_2O-MgO correlation for each rock type, except the transitional basalts. The group B rocks, in contrast, have a wide range of K_2O contents (0.73 – 2.2 wt. %). Although K_2O contents in the group B rocks overlap, the ne-hawaiites generally have the largest K_2O (1.4 – 2.2 wt. %) followed by nephelinites (1.3 – 2.2 wt. %) and the basanites (1.0 – 2.0 wt. %). The group B alkali ol-basalts have the widest range of K_2O (0.73 – 2.0 wt. %) of all rock types and strong negative K_2O-MgO correlation. The nephelinites and ne-hawaiites exhibit relatively good negative K_2O-MgO correlation, whereas K_2O in the basanites is generally scattered over their range of MgO contents.

Note that in addition to the overall trends of increasing P_2O_5, Na_2O, and K_2O with decreasing MgO exhibited by the suite of group B rocks, close examination of Fig. 5.6 indicates that at least two major trends may be defined within group B: (i) silica-undersaturated basanites to less silica-undersaturated basanites and nephelinites, and (ii) silica-undersaturated basanites to less silica-undersaturated ne-hawaiites and alkali ol-basalts. Trends such as these are also observed in incompatible trace element-MgO plots for the group B rocks, discussed in section 5.4.3.

The relationship between CaO and MgO is complex for all rock types. The majority of group A rocks have overlapping CaO contents (6.3 – 11.2 wt. %), which are smaller than most basanites (8.5 – 10.6 wt. %) and nephelinites (9.0 – 10.4 wt. %), larger than ne-hawaiites (7.2 – 9.2 wt. %), and overlap most group B alkali ol-basalts (7.2 – 10.1 wt. %). The group A rocks exhibit a weak trend of increasing CaO with decreasing MgO with relatively large variations of CaO at a given MgO content, especially between 8 and 10 wt. % MgO. In contrast, the group B rocks collectively show a strong positive CaO-MgO correlation, although CaO-MgO correlation for each rock type is generally poor.

The SAVF lavas exhibit large variations in values of Al_2O_3/CaO (Fig. 5.7). The majority of group A rock types have overlapping Al_2O_3/CaO values that are broadly scattered between 1.4 and 1.8 and show no apparent correlation with MgO. Only the alkali ol-basalts have values of Al_2O_3/CaO that increase (albeit weakly) with decreasing MgO contents. In contrast, values of Al_2O_3/CaO in the group B rocks increase with decreasing MgO. The majority of alkali ol-basalts and ne-hawaiites have comparatively large values of Al_2O_3/CaO, e.g., > 1.5 and > 1.8 respectively, whereas most basanites and nephelinites have smaller values, e.g., ~ 1.2 – 1.4 and 1.2 – 1.3 respectively, which are close to that of chondrites, i.e., ~ 1.2 (Frey *et al.*, 1978). Although the group B samples span a large range of Al_2O_3/CaO values, the majority of these plot outside the group A field, 1.4 to 1.8. Only the group B alkali ol-basalts have a near-continuous range of Al_2O_3/CaO

values, ~ 1.2 to 2.0 that negatively correlate with MgO. Frey *et al.* (1978) and Clague and Frey (1982) concluded that magmas with near-chondrite ratios have undergone sufficient melting such that olivine and orthopyroxene remain as the principal residual phases. Frey *et al.* (1978) and Clague and Frey (1982) also argued that those magmas with comparatively larger Al_2O_3/CaO values result, in part, from Ca-rich clinopyroxene fractionation over a range of pressure conditions.

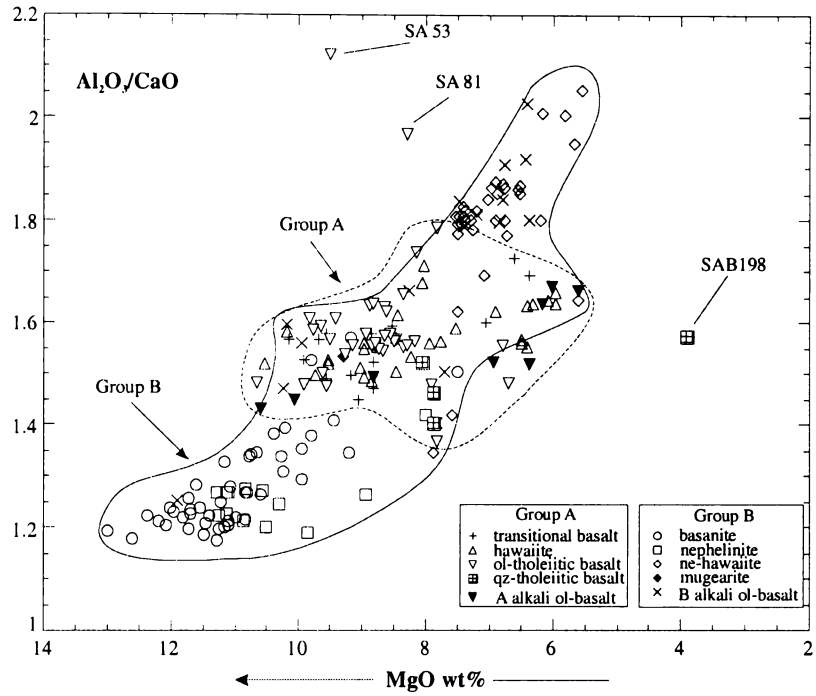

Fig 5.7 Al_2O_3/CaO values vs. MgO contents for the group A and B lavas. Note that values of Al_2O_3/CaO in a large number of basanites and nephelinites approaches the chondritic ratio of 1.2 indicating that their source(s) has near-chondritic Al_2O_3/CaO. Anomalous group A samples are labelled in the diagram (see Appendix 7, Table A7.1 and A7.2 for whole-rock analyses).

5.4.3 Trace element geochemistry

Evaluation of the major element geochemistry of the SAVF lavas showed that there are important geochemical differences between the group A and B rocks as well as among the various rock types within each group. The contrasts in major element geochemistry between the groups are also evident in their contrasting trace element geochemical characteristics as demonstrated in tectono-magmatic discrimination diagrams, which show clear division of the group A and B lavas into distinct tectonic affinities. In terms of the Wood (1980) Th-Hf-Ta and Meschede (1986) Zr-Nb-Y discrimination diagrams (Figs. 5.8A and B respectively), group B rocks have geochemical features typical of within-plate alkali basalts (Field C, Fig. 5.8A; Fields AI and AII, Fig. 5.8B). They exhibit

high field strength element (HFSE) characteristics comparable with those from other intraplate fields (e.g., the Ngatutura Basalts, Okete Volcanics, Auckland, and eastern Australia). In contrast, the group A rocks plot predominantly in fields that suggest they have either within-plate tholeiite or E-type mid-ocean ridge basalt (E-MORB) characteristics (Field B, Fig. 5.8A; Fields AIII and AIV, Fig. 5.8B). These features are shared by basalts from the Northland Volcanic Province (Smith *et al.*, 1993; Huang *et al.*, 2000), Okete hawaiites, and some East Australian tholeiitic basalts, but not by basalts from the Ngatutura or Auckland fields.

Unlike the Tertiary – Quaternary basalts from the intraplate fields in the Northland Volcanic Province, which have been grouped based on their time-space-tectonic association (see Smith *et al.*, 1993; Fig. 5), the contrasting geochemical features of the SAVF basalts are independent of temporal or spatial constraints. Furthermore, the presence in an intraplate field of two rock groups with dissimilar trends in major element contents, such as those shown in Fig. 5.6, is a distinctive geochemical feature of the SAVF. These features are also evident in their contrasting trace element concentrations, illustrated and discussed in the following sections. The correlation between MgO and each compatible and incompatible trace element for groups A and B and the various rock types within each group referred to in the text is summarised in Table 5.9.

Table 5.9 Correlation coefficients (r^2 values) for the compatible trace elements Ni, Cr, Sc, and V referred to in the text, and incompatible trace element data plotted in the MgO variation diagrams (Figs. 5.9 and 5.10). Negative values indicate negative MgO-trace element correlation. The strong correlation of the qz-tholeiitic basalt samples with most elements may be due to the small sample size and the outlying sample SAB198.

	Group A						Group B				
	All samples n = 94	trans n = 15	haw n = 29	ol-th n = 38	qz-th n = 4	Aaob n = 8	All samples n = 108	bas n = 45	neph n = 13	ne-haw n = 34	Baob n = 16
Ni	0.78	0.83	0.91	0.68	0.67	0.98	0.93	0.88	0.81	0.77	0.90
Cr	0.68	0.87	0.77	0.56	-0.80	0.85	0.83	0.83	0.91	0.60	0.83
Sc	-0.14	0.17	-0.02	-0.35	-0.97	-0.05	0.81	0.69	0.33	0.39	0.84
V	-0.58	-0.66	-0.67	-0.14	-0.97	-0.93	0.91	0.75	0.90	0.61	0.57
Rb	-0.26	-0.60	-0.20	0.13	-0.60	0.13	-0.45	-0.36	-0.56	-0.71	-0.83
Ba	-0.34	-0.48	-0.44	0.11	-0.96	-0.16	-0.44	-0.21	-0.83	-0.28	-0.48
Sr	-0.61	-0.88	-0.78	0.18	-0.97	-0.55	-0.40	-0.65	-0.92	-0.27	-0.22
Nb	-0.42	-0.77	-0.62	0.23	-0.94	-0.26	-0.72	-0.65	-0.99	-0.62	-0.86
Zr	-0.62	-0.86	-0.76	0.16	-0.76	-0.81	-0.83	-0.79	-0.96	-0.73	-0.91
Y	-0.17	0.09	-0.18	-0.03	-0.98	-0.58	-0.46	-0.64	-0.92	-0.40	-0.77
La	-0.21	-0.35	-0.18	0.19	-0.98	0.00	-0.37	-0.65	-0.89	-0.46	-0.72
Ce	-0.26	-0.38	-0.31	0.03	-0.66	0.24	-0.30	-0.72	-0.86	-0.39	-0.75

n = number of samples; trans = transitional basalt; haw = hawaiite; olth = ol-tholeiitic basalt; qz-th = qz-tholeiitic basalt; bas = basanite; neph = nephelinite ; ne-haw = ne-hawaiite; aob = alkali ol-basalt.

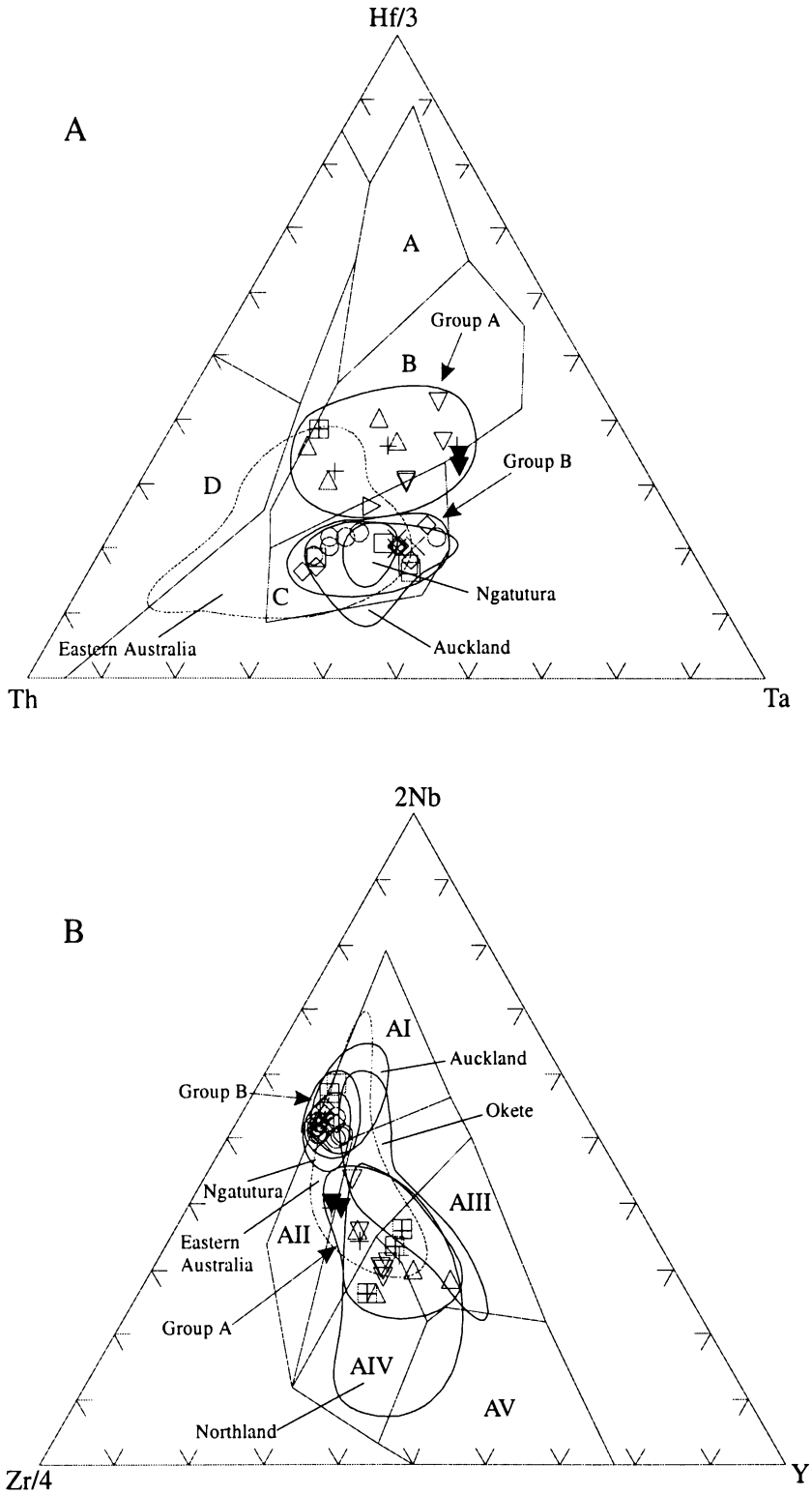

Fig. 5.8 **A** Th-Hf-Ta discrimination diagram (after Wood, 1980) showing the SAVF lavas, compared with the Ngatutura Basalts (from Briggs *et al.*, 1990), Auckland volcanic field (Huang *et al.*, 1997), and mafic lavas from eastern Australia (from Ewart, 1989; Price *et al.*, 1997; Zhang and O'Reilly, 1997). Field A = N-MORB, Field B = E-MORB and within-plate tholeiities. Field C = alkaline within-plate basalts, and Field D = destructive plate margin tholeiites. **B** Zr-Nb-Y discrimination diagram (after Meschede, 1986) showing the SAVF lavas compared with Ngatutura Basalts, Okete Volcanics (Briggs and Goles, 1984), Auckland volcanic field, basalts from Northland Volcanic Province (from Smith *et al.*, 1993; Huang *et al.*, 2000) and Eastern Australia (Price *et al.*, 1997; Zhang and O'Reilly, 1997. Field AI = within-plate alkali basalts, Field AII = within-plate alkali basalts and tholeiites, Field AIII = E-MORB, Field AIV = within-plate tholeiites and volcanic-arc basalts, Field AV = N-MORB and volcanic-arc basalts. Symbols as in Fig. 5.7.

Compatible trace elements (Ni, Cr, Sc, and V)

Each rock type in groups A and B has variable and overlapping Ni, Cr, Sc, and V abundances (Fig. 5.9). Each group A rock type has Ni and Cr in the range 38 – 434 ppm and 55 – 368 ppm respectively. Abundances of Ni and Cr in group B span similar ranges, 59 – 337 ppm and 61 – 404 ppm respectively, although the majority of basanites have among the largest Ni and Cr abundances (means = 249 ± 24 and 305 ± 57 ppm respectively) and most ne-hawaiites the smallest (means = 126 ± 31 and 185 ± 55 ppm respectively) of either group. Collectively, the group B rocks exhibit stronger positive MgO-Ni and Cr-MgO correlation than those in group A. The hawaiites, basanites, and the alkali ol-basalts from each group have the strongest Ni-MgO correlation, whereas Cr-MgO correlation is strongest in the nephelinites and transitional basalt (e.g., $r^2 > 0.87$).

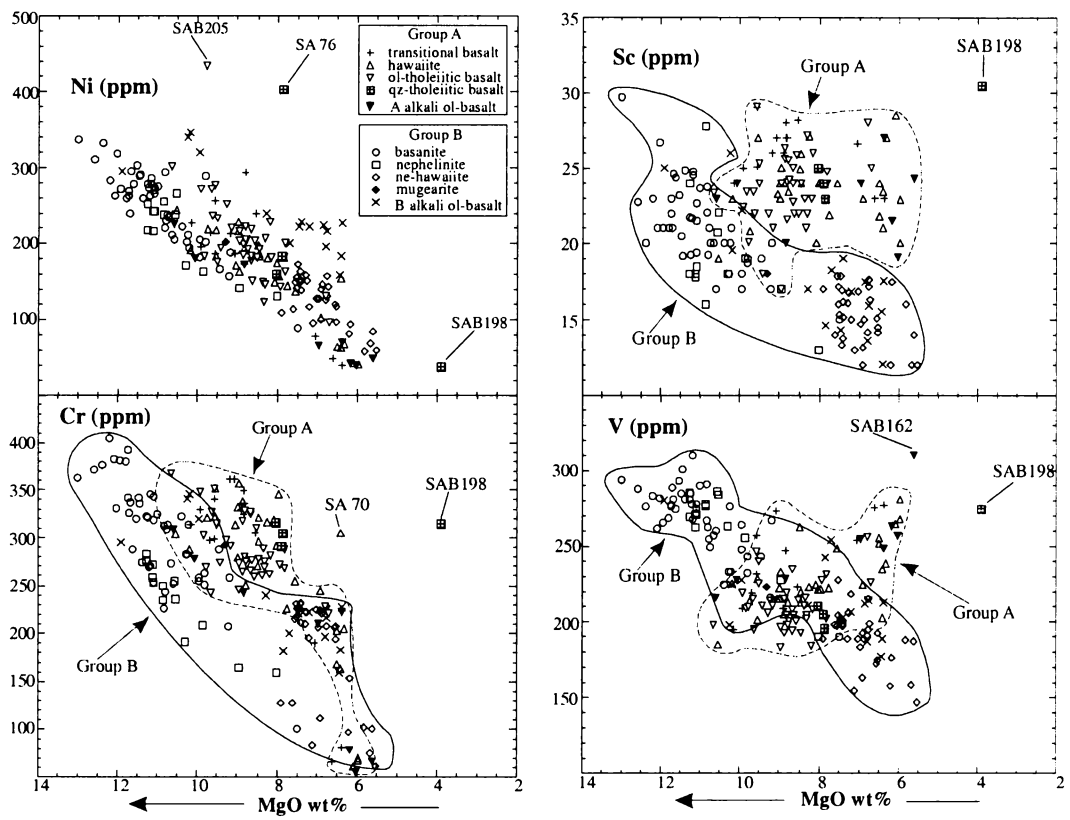

Fig. 5.9 MgO variation diagrams comparing the Ni, Cr, Sc, and V contents of the group A lavas with those of group B. The fields for the group A and B lavas in the Ni vs. MgO diagram have been omitted because they strongly overlap. Anomalous samples are labelled in each plot (see Appendix 7, Table A7.1 and A7.2 for whole-rock trace element analyses).

The relationships of Sc and V in the SAVF rocks are more complex than that of Ni or Cr. Each group A rock type has Sc and V abundances in the range 17 to 30 ppm and 184 to 310 ppm respectively. The group B rocks have Sc and V abundances that span similar ranges, 12 – 30 ppm and 147 – 310 ppm respectively, with basanites and nephelinites

containing the largest, and ne-hawaiites the smallest, Sc and V abundances. Many samples of each group A rock type have among the largest Sc contents of either group (e.g., Sc > 25 ppm), whereas the abundance of V in most group A rocks ranges between 180 and 240 ppm, which is typically smaller than the majority of basanites (190 – 310 ppm) and nephelinites (190 – 291 ppm), but larger than most ne-hawaiites (147 – 227 ppm). The group A rocks, however, are clearly distinguished by their poor Sc-MgO and V-MgO correlations. In contrast, Sc-MgO and V-MgO correlation in the group B rocks is relatively good.

Incompatible elements

The group A rocks are depleted in the large ion lithophile elements (LILE), e.g., Ba, Rb, and Sr, high field strength elements (HFSE), e.g., Zr and Nb, light rare earth elements (LREE), e.g., La and Ce, and also Y relative to the majority of group B rocks at similar MgO contents (see Tables 5.4 and 5.5; Fig. 5.10). Although there are large variations in incompatible trace element concentrations between the group A and B rocks, the majority of rocks tend to have similar LILE/LILE, e.g., Rb/Sr and K/Rb and LILE/LREE, e.g., Ba/La, Sr/Ce, and Sr/Nd values. In contrast, differences in K/Nb, Zr/Nb, Ti/Zr, and Zr/Y tend to be large (Table 5.10). As with their major element oxide-MgO trends, a distinctive geochemical feature of the SAVF lavas is the dissimilar trends of incompatible trace elements when plotted against MgO.

The group A rocks are characterised by a relatively narrow range of overlapping LILE, HFSE, and LREE abundances that show little variation with MgO contents, and there is no clear enrichment trend among the various group A rock types, a feature also exhibited by their major element chemistry (see Fig. 5.6, p.145). In this respect, the group A lavas are more similar to the hawaiites of the Ngatutura Basalts (Briggs *et al.*, 1990). In contrast, the group B rocks exhibit a relatively large range of incompatible trace element concentrations that exhibit increasing trends with decreasing MgO. Unlike the group A rocks, there is progressive enrichment from the most silica-undersaturated rocks, e.g., basanites, which tend to have the smallest incompatible trace element concentrations, to the least undersaturated rocks, e.g., ne-hawaiites, which predominantly have the largest concentrations. Trends such as these are similar to those observed in other intraplate fields e.g., the Okete Volcanics (Briggs and Goles, 1984) and eastern Australia (Ewart, 1989). However, as with the distinct trends defined in the P_2O_5-, Na_2O-, and K_2O-MgO plots (see Fig. 5.6), there are at least two discrete enrichment trends in the group B rocks, illustrated in the Sr-, Nb-, Zr-, La-, and Ce-MgO plots (Fig. 5.10) In each plot,

incompatible trace element concentrations vary along trends from: (i) silica-undersaturated basanites to less undersaturated basanites and nephelinites, and (ii) silica-undersaturated basanites to less undersaturated ne-hawaiites and alkali ol-basalts.

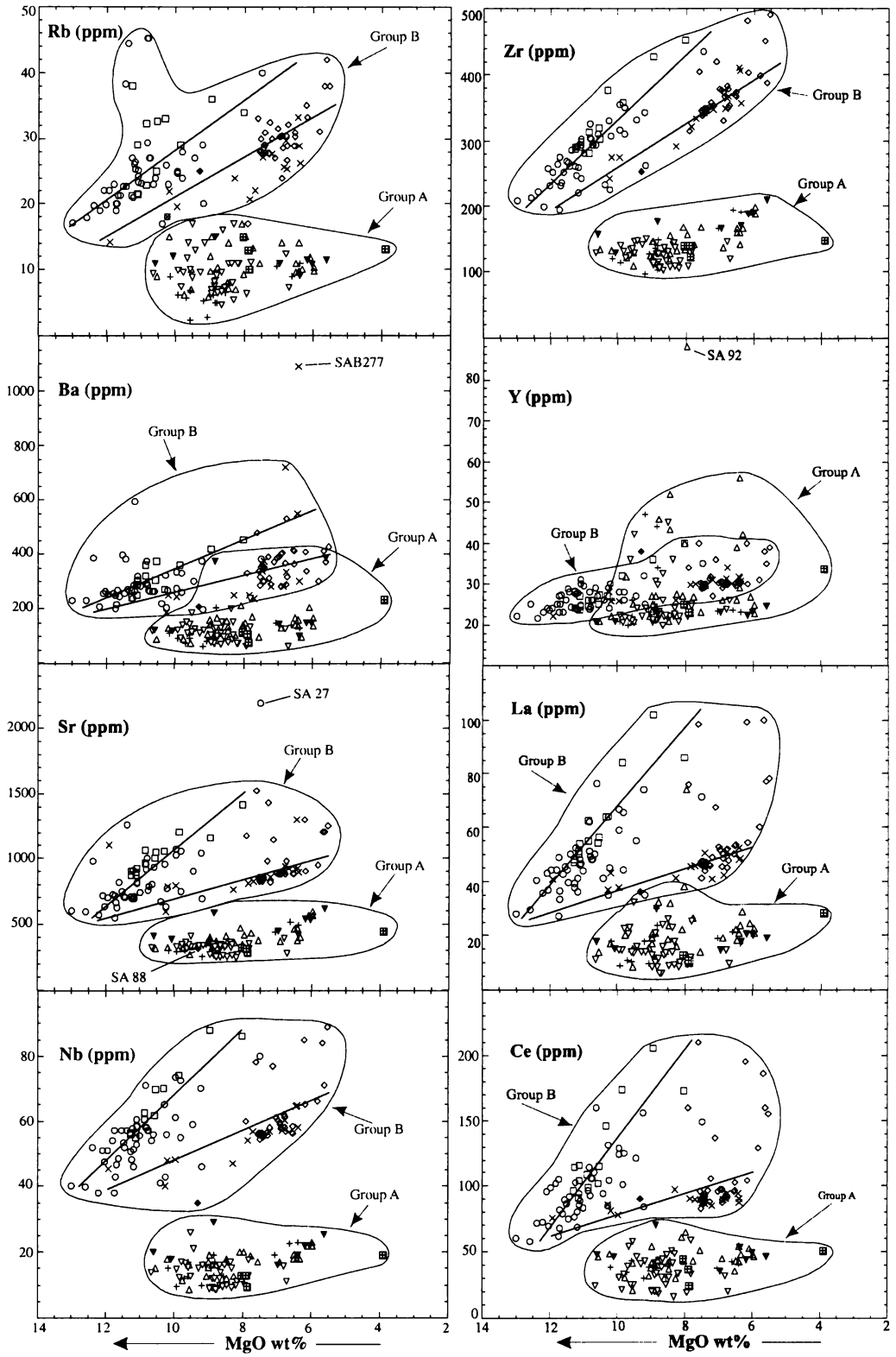

Fig 5.10 MgO variation diagrams for selected trace element analyses of the South Auckland volcanic field lavas summarised in Tables 5.4 and 5.5. The anomalous samples in the Ba-MgO, Sr-MgO, and Y-MgO plots are labelled (see Appendix 7 Tables A7.1 and A7.2 for whole-rock trace element analyses). The straight lines illustrate the possible enrichment trends of the group B rocks referred to in the text. Symbols as in Fig. 5.9.

Table 5.10 Range of values for selected incompatible trace element ratios for each group A rock type in the South Auckland volcanic field. Data are from XRF, ICP-MS, and SSMS analyses. trans = transitional basalt, haw = hawaiite, olth = ol-tholeiitic basalt, qzth = qz-tholeiitic basalt, aob = alkali ol-basalt

	Group A				
	trans	haw	olth	qzth	aob
Ba/La	2.5 -10.2	2.0 - 9.7	3.7 - 16.3	7.8 – 9.6	5.5 - 20.8
Ba/Nb	4.9 - 12.1	5.4 -11.8	5.1 - 13.3	8.0 – 10.7	5.2 - 14.7
Ba/Sr	0.22 - 0.62	0.23 - 0.45	0.22 - 0.67	0.27 – 0.48	0.24 - 0.64
Ba//Th	24 - 127	33 - 145	22 - 170	48 – 118	45 - 305
K/Ba	11 - 64	34 - 67	23 - 70	30 - 59	20 - 60
K/Rb	458 - 894	432 - 843	363 - 685	403 - 458	506 - 798
K/Nb	114 - 390	288 - 469	195 - 485	318 - 477	263 - 394
Rb/Ba	0.023 - 0.10	0.052 - 0.116	0.041 - 0.147	0.071 - 0.13	0.035 - 0.103
Rb/Sr	0.007 - 0.030	0.016 - 0.046	0.015 - 0.049	0.034 - 0.047	0.020 - 0.031
Rb/Nb	0.14 - 0.64	0.44 - 0.85	0.29 - 1.14	0.76 - 1.15	0.48 - 0.67
Rb/Zr	0.018 - 0.075	0.047 - 0.113	0.036 - 0.123	0.081 - 0.106	0.053 - 0.092
La/Ce	0.25 - 0.79	0.27 - 1.14	0.20 - 0.86	0.29 - 0.55	0.33 - 0.46
La/Nb	0.61 - 2.31	0.82 - 3.7	0.61 - 2.48	0.85 - 1.35	0.67 - 1.03
La/Yb[1]	6.5 - 10.8	5.7 - 11.0	5.1 - 7.2	5.7 - 11.4	8.8 - 10.7
Sr/Ce	6.8 - 12.5	6.4 - 13.1	5.9 - 16.2	7.1 - 11.4	7.8 - 13.5
Sr/Nd[1]	17 - 30	18 - 31	16 - 31	22 - 29	20 - 25
Ti/Zr	88 - 109	79 - 104	77 - 104	90 - 98	78 - 104
Ti/V	43 - 67	46 - 69	48 - 68	58 - 61	59 - 69
Zr/Nb	7.4 - 11.8	7.1 - 12.6	5.7 - 12.9	7.3 - 12.9	6.1 - 9.0
Zr/Hf[1]	37 - 41	34 - 41	26 - 37	36 - 41	37 - 43
Zr/Y	2.1 - 8.3	1.8 - 8.2	2.9 - 6.6	4.3 - 6.1	5.7 - 8.4
Ce/Pb[1]	8 - 21	4 - 12	9 - 14	7 - 20	20 - 22
Th/Yb[1]	0.43 - 0.95	0.51 - 0.72	0.51 - 0.84	0.71 - 0.77	0.66 - 0.73
Ta/Yb[1]	0.44 - 0.91	0.32 - 0.64	0.68 - 0.90	0.35 - 0.64	1.1 - 1.2

[1] Ratios based on ICP-MS and SSMS analyses only

Table 5.10 continued. bas = basanite, neph = nephelinite, nehaw = ne-hawaiite, mug = mugearite, aob = alkali ol-basalt

	Group B				
	bas	neph	nehaw	mug	aob
Ba/La	3.4 -16.5	4.1 - 6.5	4.1 - 10.2	5.8	5.1 - 22.6
Ba/Nb	4.3 - 11.6	3.9 - 5.7	4.1 - 8.6	5.9	4.2 - 16.8
Ba/Sr	0.17 - 0.85	0.25 - 0.41	0.22 - 0.57	0.66	0.23 - 1.17
Ba//Th	35 - 155	37 - 74	34 - 86	42	32 - 158
K/Ba	21 - 63	35 - 54	30 - 58	54	15 - 59
K/Rb	180 - 618	287 - 617	410 - 728	447	429 - 650
K/Nb	140 - 268	166 - 236	172 - 284	319	135 - 275
Rb/Ba	0.043 - 0.165	0.072 - 0.158	0.052 - 0.122	0.120	0.027 - 0.105
Rb/Sr	0.018 - 0.054	0.023 - 0.042	0.015 - 0.042	0.079	0.013 - 0.038
Rb/Nb	0.33 - 0.78	0.36 - 0.68	0.28 - 0.59	0.71	0.31 - 0.51
Rb/Zr	0.069 - 0.156	0.072 - 0.131	0.054 - 0.108	0.099	0.060 - 0.086
La/Ce	0.41 - 0.56	0.41 - 0.57	0.46 - 0.58	0.40	0.42 - 0.58
La/Nb	0.62 - 1.36	0.77 - 1.16	0.67 - 1.27	1.03	0.71 - 0.93
La/Yb[1]	17.3 - 57.9	39.0 - 60	21.7 - 69.6	-	20.3 - 25.7
Sr/Ce	5.8 - 14.7	5.7 - 9.9	6.5 - 16.2	3.5	6.9 - 14.6
Sr/Nd[1]	13 - 27	13 - 17	12 - 26	9	12 - 24
Ti/Zr	43 - 84	36 - 69	30 - 53	71	34 - 82
Ti/V	53 - 98	60 - 98	71 - 110	80	63 - 83
Zr/Nb	4.3 - 5.7	4.2 - 5.4	5.0 - 6.5	7.2	5.2 - 6.3
Zr/Hf[1]	38 - 45	42 - 53	46 - 52	-	48 - 52
Zr/Y	8.4 - 12.7	10.4 - 13.9	9.3 - 13.8	6.7	8.6 - 13.0
Ce/Pb[1]	18 - 42	29 - 39	19 - 29	-	21 - 23
Th/Yb[1]	1.7 - 4.6	3.1 - 5.6	2.2 - 5.9	-	1.9 - 2.4
Ta/Yb[1]	1.5 - 2.7	3.2 - 3.8	2.5 - 3.5	-	2.2 - 2.4

[1] Ratios based on ICP-MS and SSMS analyses only

In contrast to the distinct trends observed in some of the major and trace element vs. MgO plots (Figs. 5.6 and 5.10 respectively), incompatible elements such as Ba, Sr, Nb, Zr, La, and Ce form near continuous trends that positively correlate with P_2O_5 for all SAVF lavas (Fig. 5.11). Frey *et al.* (1990) concluded that trends such as these in some Mauna Kea lavas are indicative of the highly incompatible nature of these elements as opposed to the result of apatite fractionation.

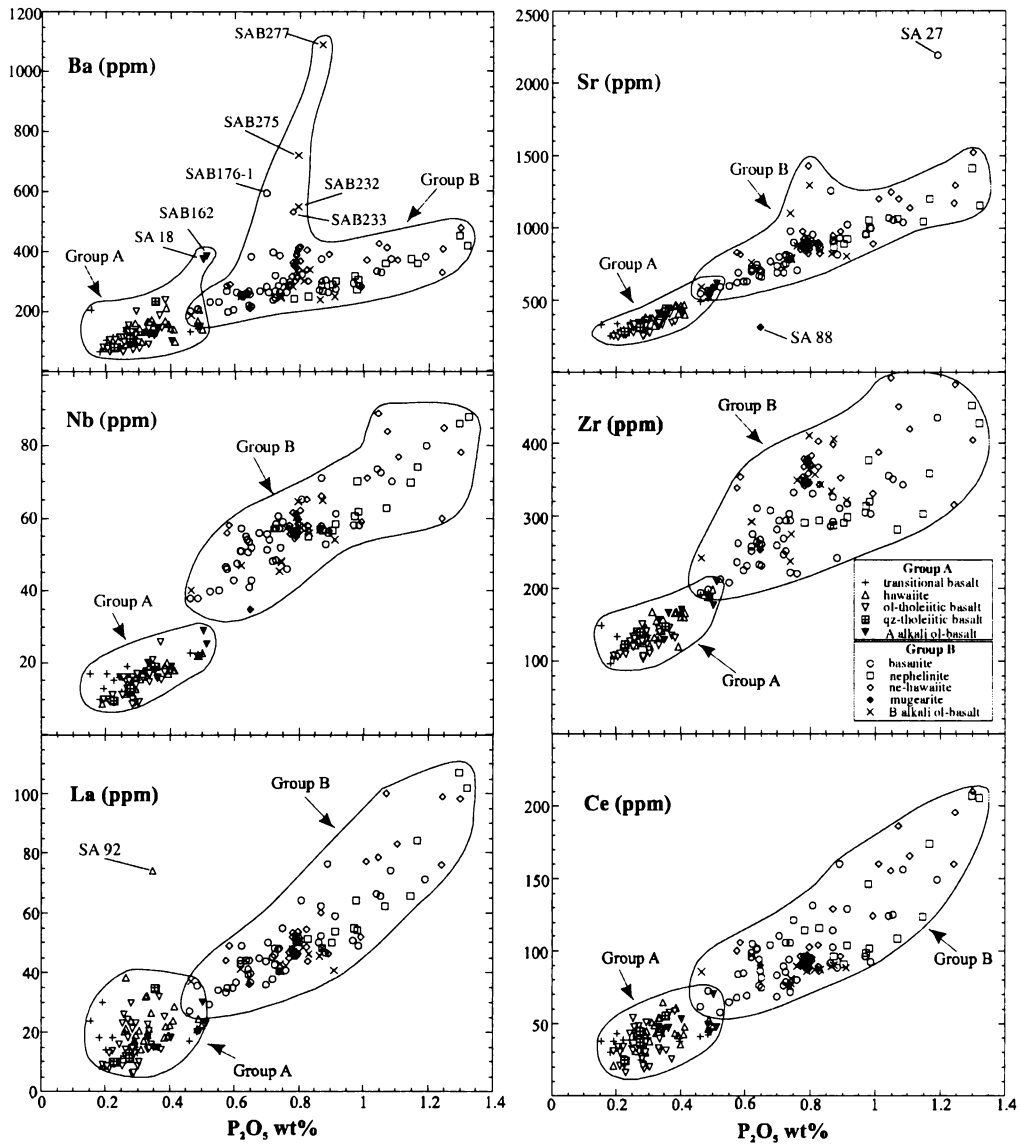

Fig. 5.11 Abundances of selected incompatible trace elements as a function of P_2O_5 for the South Auckland volcanic field lavas. The anomalous concentrations of Ba illustrated in the Ba-P_2O_5 plot may be due to incipient alteration accompanying weathering (see Price *et al.*, 1991; Cotton *et al.*, 1995). All anomalous samples identified in the group B field are magmatic pyroclasts collected from tuff deposits.

In contrast to the Mauna Kea lavas described by Frey *et al.* (1990), apatite in the SAVF is rare, although it does occur in minor amounts as inclusions in plagioclase in all rock types (Chapter 3). Because apatite fractionation will result in: (i) the depletion of La, Ce, and Sr

abundances (e.g., $K_{REE}^{apatite/melt} >> 1$; Paster *et al.*, 1974, $K_{Sr}^{apatite/melt} > 1$; Watson and Green, 1981); (ii) significant changes in La-,Ce-,Sr-P_2O_5 ratios; and (iii) contrasting P_2O_5-La,-Ce,-Sr slopes (e.g., Briggs and Goles; 1984; McDonough *et al.*, 1985; and Frey *et al.*, 1990), the comparatively strong La-,Ce-,Sr-P_2O_5 correlations shown in Fig. 5.11 (e.g., r^2 = 0.93 for the Sr-P_2O_5 trend) suggest that it is unlikely that apatite fractionation has affected the REE, and by inference, the LILE and HFSE characteristics of the group A and B rocks.

Near constant P_2O_5-REE ratios in suites of alkaline basalts are indicative of their mantle source characteristics. McDonough *et al.* (1985) argued that variations in P_2O_5-REE ratios might result from compositional heterogeneity in their mantle source region. Alternatively, Frey *et al.* (1978) concluded from their studies of southeastern Australia basalts, similar to those in the SAVF, that relatively large variation in P_2O_5 contents, such as those shown in Fig. 5.11, are indicative of variable degrees of partial melting. In the case of the SAVF basalts, although the REE and incompatible trace elements show relatively good correlations with P_2O_5, there are relatively large variations in P_2O_5-REE and P_2O_5-incompatible trace element ratios between groups A and B (e.g., > 20%), which may be indicative of contrasting source characteristics.

Incompatible trace element plots

The variations in incompatible trace element abundances for the SAVF lavas are summarised in Fig. 5.12 where mantle-normalised diagrams are presented for samples of each group A and B rock type. There are distinct compositional differences between the group A and B rocks as well as among the various rock types within each group.

The basanites, nephelinites, and ne-hawaiites have ocean island basalt (OIB)-like mantle-normalised patterns characterised by Nb and Ta enrichment relative to the LILE (Cs, Rb, and Ba), distinct negative K and Pb anomalies, and an overall decrease in enrichment from Ta to Yb in LREE, HFSE, and HREE abundances. These patterns are similar to those of alkalic basalts from other continental intraplate settings, but contrast those of some intraplate basalts from the Northland Volcanic Province, which show clear negative Nb anomalies, considered by Smith *et al.* (1993) and Huang *et al.* (2000) to result from a subduction-related source component. Additionally, there is no apparent correlation between increases in incompatible element abundances with increasing degrees of silica-undersaturation such as those documented in similar rock types from the Okete Volcanics (Briggs and Goles, 1984) or volcanic provinces in eastern Australia (McDonough *et al.*,

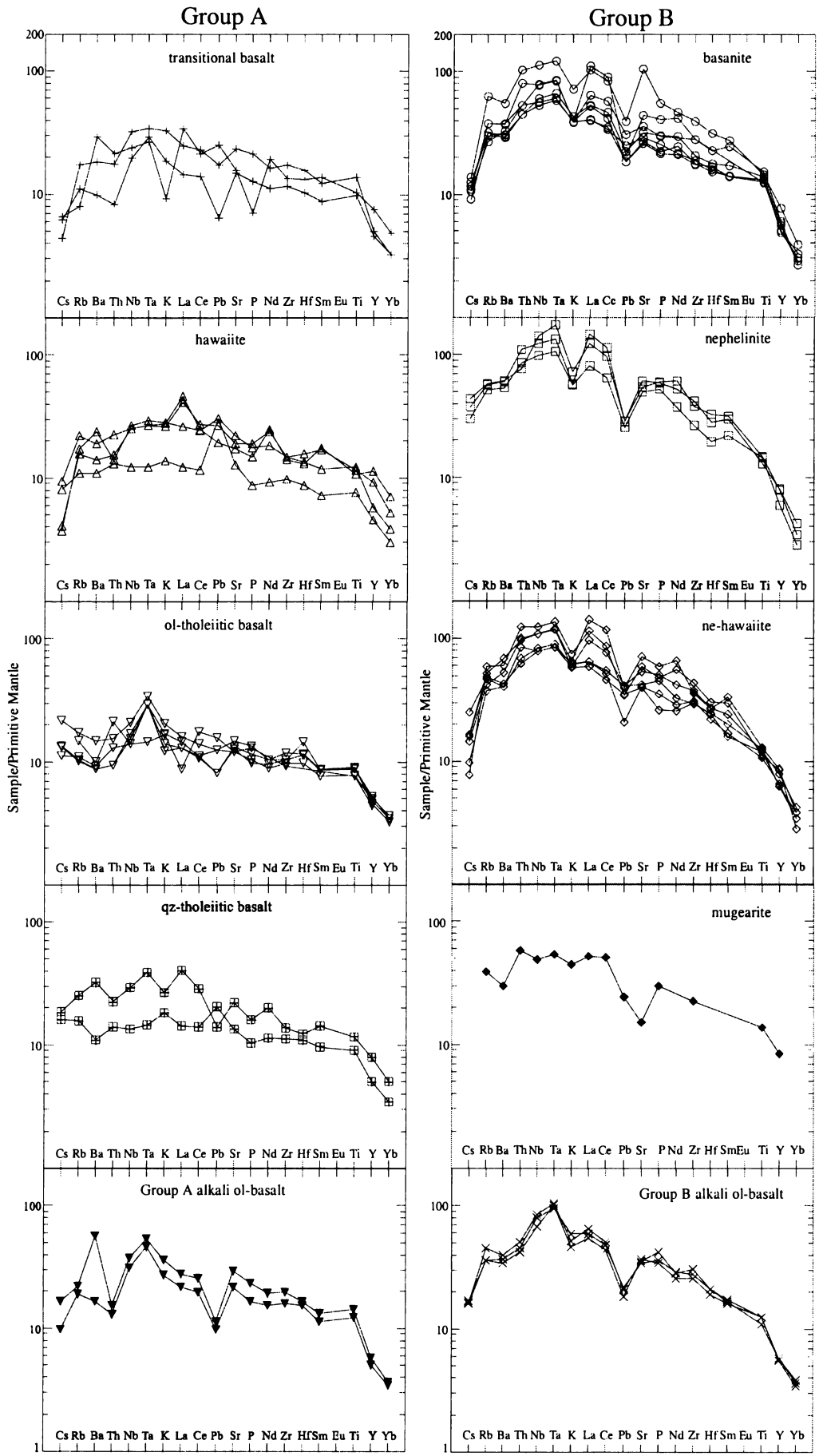

Fig. 5.12 Primitive mantle-normalised incompatible trace element diagrams for the 34 samples analysed for trace elements and REE by SSMS and ICP-MS, except for mugearite, for the South Auckland volcanic field. Normalisation factors are from Sun and McDonough (1989).

1985; Ewart, 1989). The patterns for the mugearite and group B alkali ol-basalts are similar to those of the other group B rock types except their K anomalies are less pronounced and the mugearite has overall lower trace element abundances and shows a strong negative Sr anomaly, indicative of plagioclase fractionation.

The patterns for the group A rocks are complex and exhibit a number of notable features:

1. Trace element abundances are lower than those of group B.
2. The patterns for each rock type, except the alkali ol-basalts, are generally flatter than those of group B. This is most pronounced from LREE to middle REE (MREE) abundances (La – Eu) and similar to the patterns of the low-Mg hawaiites and ol-tholeiitic basalts, and qz-tholeiitic basalts from eastern Australia (McDonough *et al.*, 1985; Ewart *et al.*, 1988; O'Reilly and Zhang, 1995). Abundances of Y and Yb are similar to those in OIB although there is some variation between samples.
3. Distinct variations in trace element abundances commonly occur not only between the different rock types but also among samples of the same rock type, especially the transitional basalts, hawaiites, and qz-tholeiitic basalts.
4. The enrichment of Nb and Ta in most samples is less prominent than in the group B rocks, except for the majority of ol-tholeiitic basalts and the alkali ol-basalts.
5. Most group A samples have a positive K anomaly. In addition, a number of samples from each rock type, except the alkali ol-basalts, have a positive Pb anomaly whereas, others of the same rock type have slightly negative anomalies. In contrast, the alkali ol-basalts have negative K and Pb anomalies similar to those of the OIB-like group B rocks.

Rare earth elements (REE)[51]

Rare earth element abundances for selected group A and B samples are presented in Tables 5.11 and 5.12 respectively. All SAVF lavas are enriched in LREE relative to HREE, a feature typical of alkaline intraplate basalts. In addition, the lavas from each group lack any significant negative or positive Eu-anomaly ($0.96 < Eu/Eu^{*} < 1.13$), which suggests negligible plagioclase fractionation.

The REE enrichment patterns for the group A and B rocks, shown in the chondrite-normalised REE plots (Fig. 5.13) are comparable with those of similar rock types from eastern Australia (e.g., Frey *et al.*, 1978; Ewart, 1989; Zhang and O'Reilly, 1997; Price *et al.*, 1997), the Okete Volcanics (Briggs and Goles, 1984), and the Ngatutura Basalts (Briggs *et al.*, 1990). Each group B rock type has a relatively broad range of LREE enrichment and similar HREE depletion resulting in steep REE patterns that are generally

[51] All REE data discussed in this and subsequent sections were derived by SSMS and ICP-MS analyses. See Appendix 7 Tables A7.3 and A7.4 for the complete REE data set for group A and B samples and for identification of those samples analysed by each technique.

subparallel to, but commonly cross over, each other. Strong HREE depletion relative to LREE, and crossing patterns, such as those observed in the group B rocks, are commonly attributed to residual garnet in the mantle source during initial basaltic melt generation (e.g., Langmuir *et al.*, 1977; Frey *et al.*, 1978; Hanson, 1980, Briggs and Goles, 1984; Clague and Dalrymple, 1988, Briggs *et al.*, 1990; Rollinson, 1993; Panter *et al.*, 2000). In addition, Langmuir *et al.* (1977) argued that crossing REE patterns together with near-constant La/Ce and large variations in La/Yb values, such as those exhibited by the group B rocks (Table 5.11; Fig. 5.14) are due, in part, to dynamic melting processes of a homogeneous source.

Table 5.11 REE analyses and chondrite-normalised ratios for selected group A samples from the SAVF.

	Group A										
	transitional basalt		hawaiite			ol-tholeiitic basalt		qz-tholeiitic basalt		alkali ol-basalt	
Sample	SA07[2]	SAB150[1]	SA11[2]	SA14[2]	SA69[2]	SA16[1]	SAB174[1]	SA76[2]	SAB198[1]	SA19[1]	SAB162[1]
La	24	10	29	8	32	9	9	10	28	15	19
Ce	38	25	48	21	44	19	20	25	51	35	46
Pr	5.8	3.5	7.0	2.5	7.5	3.0	2.8	3.2	6.9	4.9	6.2
Nd	26	15	32	12	34	13	12	16	27	21	26
Sm	6.1	3.9	7.5	3.2	7.8	3.8	3.4	4.3	6.4	5.1	5.9
Eu	2.0	1.4	2.6	1.2	2.5	1.3	1.2	1.5	2.1	1.7	2.0
Gd	6.0	4.4	7.6	3.7	8.3	4.6	4.1	4.7	7.2	5.4	6.1
Tb	0.99	0.69	1.1	0.55	1.4	0.72	0.67	0.74	1.1	0.82	0.90
Dy	6.0	3.7	6.8	3.3	7.9	3.9	3.7	4.4	5.9	4.3	4.7
Ho	1.2	0.72	1.4	0.69	1.7	0.80	0.75	0.88	1.2	0.80	0.87
Er	3.0	1.8	3.6	1.7	4.6	2.0	1.9	2.1	2.9	2.0	2.2
Tm	-	0.25	-	-	-	0.27	0.27	-	0.41	0.27	0.29
Yb	2.4	1.6	2.6	1.5	3.5	1.8	1.7	1.7	2.5	1.7	1.8
Lu	-	0.23	-	-	-	0.26	0.24	-	0.36	0.24	0.26
Eu/Eu*	1.01	1.01	1.06	1.03	0.96	0.97	1.01	1.02	0.97	1.01	1.03
$(Ce)_N$	44	29	56	24	50	23	23	29	59	41	53
$(La/Ce)_N$	1.6	1.1	1.6	1.1	1.9	1.3	1.1	1.1	1.5	1.1	1.1
$(La/Sm)_N$	3.9	2.6	3.8	2.6	4.1	2.5	2.5	2.3	4.5	2.9	3.2
$(La/Yb)_N$	6.5	4.3	7.3	3.8	6.1	3.5	3.4	3.8	7.6	5.9	7.2

[1] = trace element abundances determined by ICP-MS analyses
[2] = trace element abundances determined by SSMS analyses.

Table 5.12 REE analyses and chondrite-normalised ratios for selected group B samples from the SAVF.

	Group B										
	basanite			nephelinite			ne-hawaiite			alkali ol-basalt	
Sample	SA05[2]	SA56[2]	SAB179[1]	SA28[1]	SA51[2]	SAB135[1]	SA25[1]	SA66[2]	SAB218[1]	SAB188[1]	SAB227[1]
La	76	37	28	86	102	56	67	98	45	38	45
Ce	160	82	60	173	205	115	137	210	92	78	90
Pr	16	9.7	7.4	20	21	14	16	22	10	9.2	10.5
Nd	56	40	29	71	84	51	57	90	39	35	38
Sm	11	7.5	6.1	13	14	9.8	11	15	7.5	7.1	7.4
Eu	3.2	2.3	2.0	4.1	4.2	3.0	3.4	4.4	2.4	2.2	2.4
Gd	7.4	5.2	6.1	12	11	9.1	10	11	6.9	6.7	6.9
Tb	1.0	0.78	0.85	1.6	1.5	1.2	1.4	1.5	0.94	0.95	0.94
Dy	5.4	4.3	4.2	7.3	7.5	5.6	6.5	7.2	4.7	4.9	4.8
Ho	0.89	0.78	0.77	1.3	1.2	0.92	1.2	1.2	0.87	0.89	0.87
Er	2.1	1.7	1.8	2.9	2.7	2.1	2.6	2.4	2.1	2.2	2.1
Tm	-	-	0.24	0.36	-	0.25	0.35	-	0.29	0.30	0.29
Yb	1.3	1.3	1.5	2.1	1.7	1.4	2.1	1.4	1.7	1.9	1.8
Lu	-	-	0.21	0.28	-	0.20	0.28	-	0.26	0.26	0.26
Eu/Eu*	1.08	1.13	0.98	0.98	1.05	0.99	1.00	1.07	1.02	1.00	1.02
$(Ce)_N$	185	95	69	200	237	133	158	243	107	90	104
$(La/Ce)_N$	1.3	1.2	1.2	1.3	1.3	1.3	1.3	1.2	1.3	1.3	1.3
$(La/Sm)_N$	7.1	4.9	4.6	6.4	7.2	5.7	6.2	6.6	6.1	5.3	6.1
$(La/Yb)_N$	39	19	12	27	40	26	22	47	17	14	17

[1] = trace element abundances determined by ICP-MS analyses
[2] = trace element abundances determined by SSMS analyses.

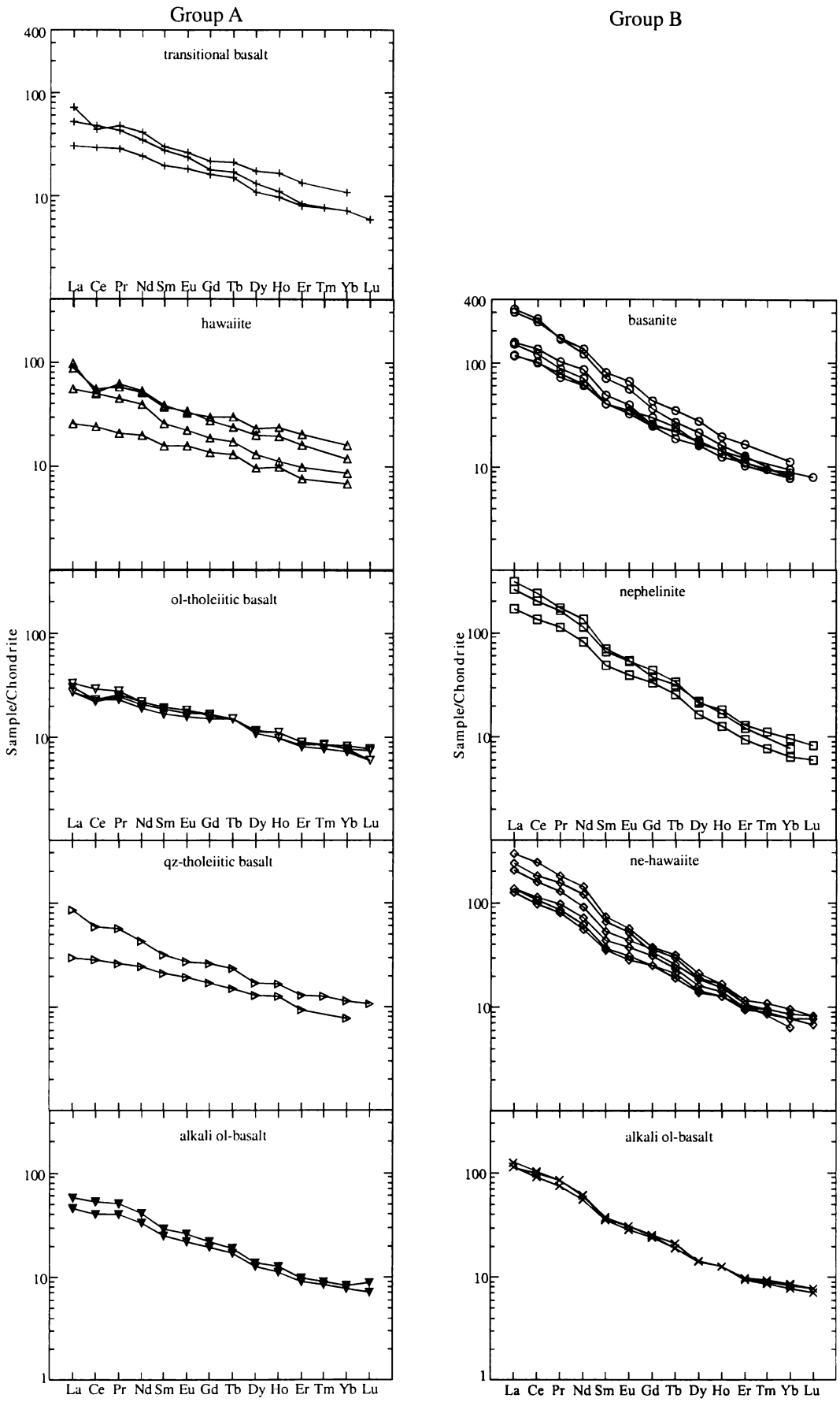

Fig. 5.13 Chondrite-normalised REE diagrams for South Auckland volcanic field lavas analysed by SSMS and ICP-MS. Normalisation factors are those of Nakamura (1974).

The group A rocks also display subparallel and crossing patterns, but have lower LREE abundances than those in group B. Additionally, in contrast to group B, MREE and HREE are enriched relative to LREE resulting in flatter slopes and crossing patterns, which cross over with those of group B. Briggs and Goles (1984) observed similar enrichment patterns in hawaiites and basanites from the Okete Volcanics and concluded that with extensive partial melting, garnet could be totally consumed resulting in HREE-enriched melts. The lower LREE of group A compared to those in group B are consistent with other distinct geochemical characteristics of group A (e.g., lower trace element abundances, Figs. 5.10, 5.11 and 5.12). A number of samples of each rock type, except the alkali ol-basalts, exhibit a positive La anomaly, possibly indicative of post-emplacement weathering (Price *et al.* 1991).

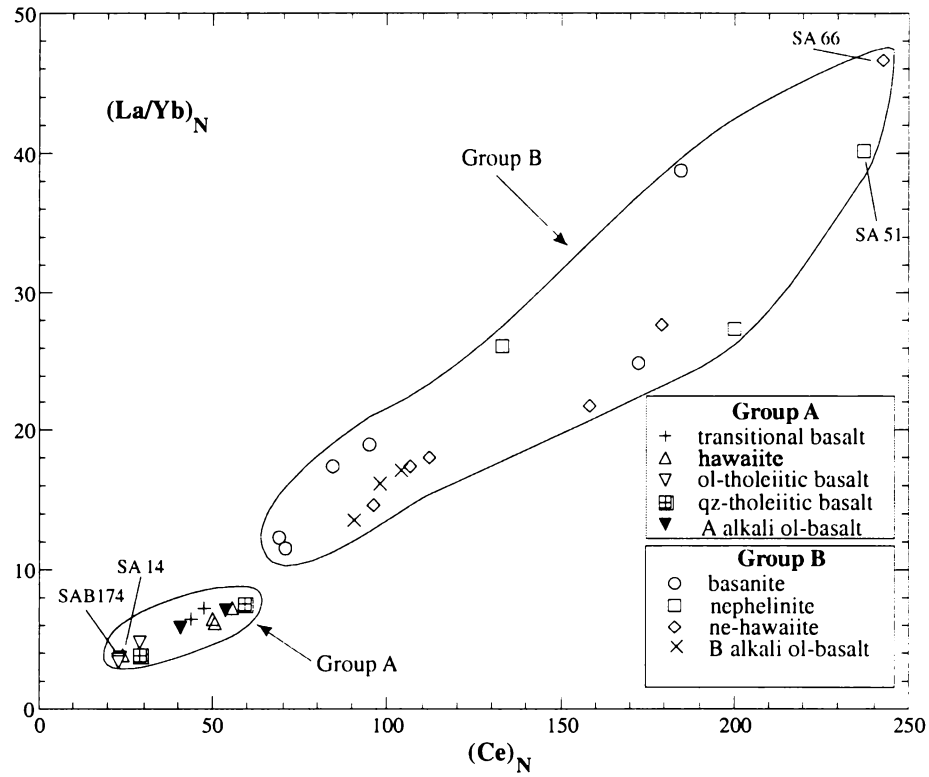

Fig. 5.14 $(La/Yb)_N$ vs. $(Ce)_N$ for the South Auckland volcanic field lavas analysed by SSMS and ICP-MS techniques. Refer to Tables 5.9 and 5.10 for values of labelled samples.

The chondrite-normalised REE data plotted in Fig. 5.14 illustrates the LREE depletion of the group A rocks relative to those in group B. The group A rocks exhibit a relatively small range of LREE enrichment [$(La/Yb)_N$ = 3.4 – 7.6], with ol-tholeiitic basalt SAB174 $(La/Yb)_N$ = 3.4 and hawaiite SA14 $(La/Yb)_N$ = 3.8 among the least LREE-enriched SAVF samples. In contrast, group B rocks exhibit a broad range of LREE enrichment [$(La/Yb)_N$ = 12 – 47], with nephelinite SA51 $(La/Yb)_N$ = 40 and ne-hawaiite SA66 $(La/Yb)_N$ = 47 among the most enriched SAVF samples. Although the data in Fig. 5.14 indicate that there is a strong correlation between the degree of REE fractionation and LREE content

(r^2 = 0.97), there is no apparent correlation between REE fractionation and the degree of silica-undersaturation of the samples in either group. This is evident by the similar REE patterns exhibited by the various rock types within their respective groups as shown in Fig. 5.13, and overlapping $(La/Yb)_N$ values for many of the samples within each group, illustrated in Fig. 5.14.

5.5 General radiogenic isotopic characteristics

5.5.1 Sr and Nd isotopic compositions

The SAVF lavas have Sr and Nd isotopic compositions characterised by a narrow range of relatively small $^{87}Sr/^{86}Sr$ (0.702729 – 0.703301) and relatively large ε_{Nd} (+ 5.97 to + 6.89) values, typical of magmas derived from depleted source regions (see Tables 5.13 and 5.14 for selected samples from groups A and B respectively). The Sr-Nd isotopic compositions for selected group A and B rocks are illustrated in Fig. 5.15 along with fields for similar rock types from other Cenozoic continental intraplate provinces and fields, subduction-related basalts from the Taupo Volcanic Zone (TVZ), Atlantic, Pacific, and Indian Ocean MORBs, HIMU-type alkalic basalts from Marie Byrd Land, Antarctica, Hawaiian Islands ocean island basalts (OIB), back-arc basin basalts (BABB) from the Lau and North Fiji Basins and the Mairana Trough of the western Pacific, and the Waipapa Terrane basement rocks, which underlie part of the SAVF. The SAVF rocks have $^{87}Sr/^{86}Sr$ compositions and ε_{Nd} values that range between HIMU (mantle with a high U-Pb ratio; Zindler and Hart, 1986), MORB (Ito *et al.*, 1987), and BABB (e.g., Stern *et al.*, 1990; Eissen *et al.*, 1991, 1994; Hergt and Hawkesworth, 1994), and strongly overlap those of basalts from Tasmania (McDonough *et al.*, 1985), the Northland Volcanic Province (Huang *et al.*, 2000), and some eastern Australia provinces and fields (Ewart *et al.*, 1988; O'Reilly and Zhang, 1995), which suggests that they may be products of a mixture between MORB- and HIMU OIB-like sources.

Overall, the SAVF lavas have smaller Sr and larger Nd isotopic compositions than the majority of eastern Australia basalts and notably smaller $^{87}Sr/^{86}Sr$ and larger ε_{Nd} values than those of the Newer basalts (McDonough *et al.*, 1985), TVZ basalts (Gamble *et al.*, 1993), and Waipapa metasediments (Graham *et al.*, 1992; McCulloch *et al.*, 1994). In addition, rocks from groups A and B have Sr isotopic compositions similar to some of the HIMU-type basalts from Marie Byrd Land, Antarctica (Panter *et al.*, 2000) but larger Nd

Table 5.13 Sr, Nd, Sm, and Pb isotope data, Δ7/4 and Δ8/4 values, and selected trace element data for selected group A SAVF lavas.

Sample #	Rock Type	$^{87}Sr/^{86}Sr$	Rb (ppm)	Sr (ppm)	$^{143}Nd/^{144}Nd$	$^{147}Sm/^{144}Nd$	$(Sm/Nd)_N$	ε_{Nd}	Sm (ppm)	Nd (ppm)	$^{206}Pb/^{204}Pb$	$^{207}Pb/^{204}Pb$	$^{208}Pb/^{204}Pb$	Pb (ppm)	Δ7/4	Δ8/4
SA19	alkali ol-basalt	0.703127±20	12	460	0.512980	-	-	6.67	5.1	21	19.204	15.587	38.814	1.8	1.4	-3.1
SAB162	alkali ol-basalt	0.702809±16	14	621	0.512971	-	-	6.50	5.9	26	19.226	15.586	38.828	2.1	1.1	-4.3
SA11	hawaiite	0.702949±17	10	400	0.512984	0.1367±16	0.72	6.75	7.5	32	-	-	-	4.9	-	-
SA14	hawaiite	0.703150±17	7.0	271	0.512966	0.1630±16	0.80	6.40	3.2	12	-	-	-	5.7	-	-
SA52	hawaiite	0.702955±17	11	463	0.512962	0.1448±12	0.65	6.32	5.2	25	-	-	-	5.6	-	-
SA69	hawaiite	0.703069±17	14	366	0.512944	0.1404±15	0.71	5.97	7.8	34	-	-	-	3.6	-	-
SA15	ol-tholeiitic basalt	0.702987±17	6.6	280	0.512965	-	-	6.38	3.9	14	19.075	15.597	38.731	1.5	3.8	4.2
SA16	ol-tholeiitic basalt	0.703053±14	6.5	270	0.512961	-	-	6.30	3.8	13	19.076	15.592	38.723	1.5	3.3	3.3
SA36	ol-tholeiitic basalt	0.703214±17	10	252	0.512985	0.1699±16	-	6.77	-	-	-	-	-	3.0	-	-
SA93	ol-tholeiitic basalt	0.703099±17	13	335	0.512949	0.1440±15	-	6.07	-	-	-	-	-	3.0	-	-
SAB174	ol-tholeiitic basalt	0.703176±19	7.0	255	0.512946	-	-	6.01	3.4	12	18.95	15.613	38.744	2.3	6.8	20.6
SAB187	ol-tholeiitic basalt	0.702833±18	11	315	0.512960	-	-	6.28	3.9	14	19.016	15.608	38.778	2.3	5.6	16.1
SA76	qz-tholeiitic basalt	0.703301±17	10	283	0.512991	0.1677±15	0.85	6.89	4.3	16	-	-	-	3.8	-	-
SAB198	qz-tholeiitic basalt	0.702939±18	16	469	0.512959	-	-	6.26	6.4	27	19.127	15.597	38.823	2.6	3.3	7.1
SA07	transitional basalt	0.703079±17	5.0	332	0.512956	0.1462±17	0.73	6.20	6.1	26	-	-	-	4.6	-	-
SA48	transitional basalt	0.702876±17	11	495	0.512979	0.1405±16	0.77	6.65	5.5	22	-	-	-	3.2	-	-
SAB150	transitional basalt	0.702876±13	6.6	314	0.512975	-	-	6.57	3.9	15	19.277	15.596	38.876	1.2	1.5	-5.7

$$\varepsilon_{Nd} = \left[\frac{\left(^{143}Nd/^{144}Nd\right)_{Sample}}{\left(^{143}Nd/^{144}Nd\right)_{CHUR}} - 1 \right] 10^4 \text{ , where } (^{143}Nd/^{144}Nd)_{CHUR} = 0.512638.$$

Table 5.14 Sr, Nd, Sm, and Pb isotope data, Δ7/4 and Δ8/4 values, and selected trace element data for selected group B SAVF lavas.

Sample #	Rock Type	$^{87}Sr/^{86}Sr$	Rb (ppm)	Sr (ppm)	$^{143}Nd/^{144}Nd$	$^{147}Sm/^{144}Nd$	$(Sm/Nd)_N$	ε_{Nd}	Sm (ppm)	Nd (ppm)	$^{206}Pb/^{204}Pb$	$^{207}Pb/^{204}Pb$	$^{208}Pb/^{204}Pb$	Pb (ppm)	Δ7/4	Δ8/4
SAB188	alkali ol-basalt	0.702843±17	23	774	0.512980	-	-	6.67	7.1	35	19.237	15.573	38.837	3.4	-0.3	-4.8
SAB224	alkali ol-basalt	0.702729±19	23	726	0.512972	-	-	6.52	7.5	39	19.294	15.576	38.887	4.1	-0.6	-6.6
SAB227	alkali ol-basalt	0.702835±17	29	754	0.512953	-	-	6.14	7.4	38	19.201	15.589	38.857	3.9	1.7	1.6
SA03	basanite	0.702847±17	24	746	0.512967	0.1191±16	-	6.42	-	-	-	-	-	5.7	-	-
SA05	basanite	0.702784±15	24	932	0.512959	0.1184±17	0.59	6.26	11	56	-	-	-	3.8	-	-
SA27	basanite	0.703228±17	40	2193	0.512963	0.1146±16	0.61	6.34	12	62	-	-	-	7.2	-	-
SA55	basanite	0.702914±17	20	547	0.512972	0.1296±17	0.67	6.52	6.1	29	-	-	-	3.4	-	-
SA56	basanite	0.702849±15	20	666	0.512965	0.1238±17	0.59	6.38	7.5	40	-	-	-	4.1	-	-
SA60	basanite	0.702829±17	19	568	0.512975	0.1289±16	0.57	6.57	6.2	33	-	-	-	3.4	-	-
SAB179	basanite	0.702845±18	20	581	0.512964	-	-	6.36	6.1	29	19.221	15.573	38.833	2.3	-0.2	-3.2
SA02	ne-hawaiite	0.702834±19	33	783	0.512978	-	-	6.63	7.1	35	19.274	15.578	38.873	4.4	-0.2	-5.6
SA24	ne-hawaiite	0.702818±14	26	822	0.512957	-	-	6.22	8.9	45	19.296	15.575	38.877	3.3	-0.8	-7.9
SA25	ne-hawaiite	0.702738±20	31	1053	0.512963	-	-	6.34	11	57	19.304	15.572	38.879	5.1	-1.2	-8.7
SA65	ne-hawaiite	0.702782±17	38	1253	0.512989	0.1076±11	0.55	6.85	13	75	-	-	-	6.4	-	-
SA66	ne-hawaiite	0.702816±17	33	1517	0.512963	0.1095±15	0.51	6.34	15	90	-	-	-	7.4	-	-
SAB218	ne-hawaiite	0.702751±20	32	759	0.512966	-	-	6.40	7.5	39	19.293	15.578	38.892	4.1	-0.4	-6.0
SA28	nephelinite	0.702788±22	37	469	0.512978	-	-	6.63	13	71	19.285	15.568	38.863	5.3	-1.3	-8.0
SA51	nephelinite	0.702800±17	36	1161	0.512986	0.1125±12	0.53	6.79	14	84	-	-	-	5.3	-	-
SAB135	nephelinite	0.702774±19	38	937	0.512971	-	-	6.50	9.8	51	19.323	15.576	38.906	4.0	-1.0	-8.3

$$\varepsilon_{Nd} = \left[\frac{\left(^{143}Nd/^{144}Nd\right)_{Sample}}{\left(^{143}Nd/^{144}Nd\right)_{CHUR}} - 1 \right] 10^4 \text{ , where } (^{143}Nd/^{144}Nd)_{CHUR} = 0.512638.$$

isotopic compositions, which overlap basalts from the Hawaiian Islands (Garcia *et al.*, 1996; Holcomb *et al.*, 1997; Reiners and Nelson, 1998; Pietruszka and Garcia, 1999). In contrast, all group B rocks have Sr isotopic compositions smaller than the Hawaiian basalts. Generally, the SAVF basalts have smaller ε_{Nd} values than BABBs, although Fig. 5.15 illustrates that some BABBs, primarily those from the North Fiji Basin (Eissen *et al.* 1994) and the Mariana Trough (Stern *et al.* 1990), have overlapping or smaller ε_{Nd} values.

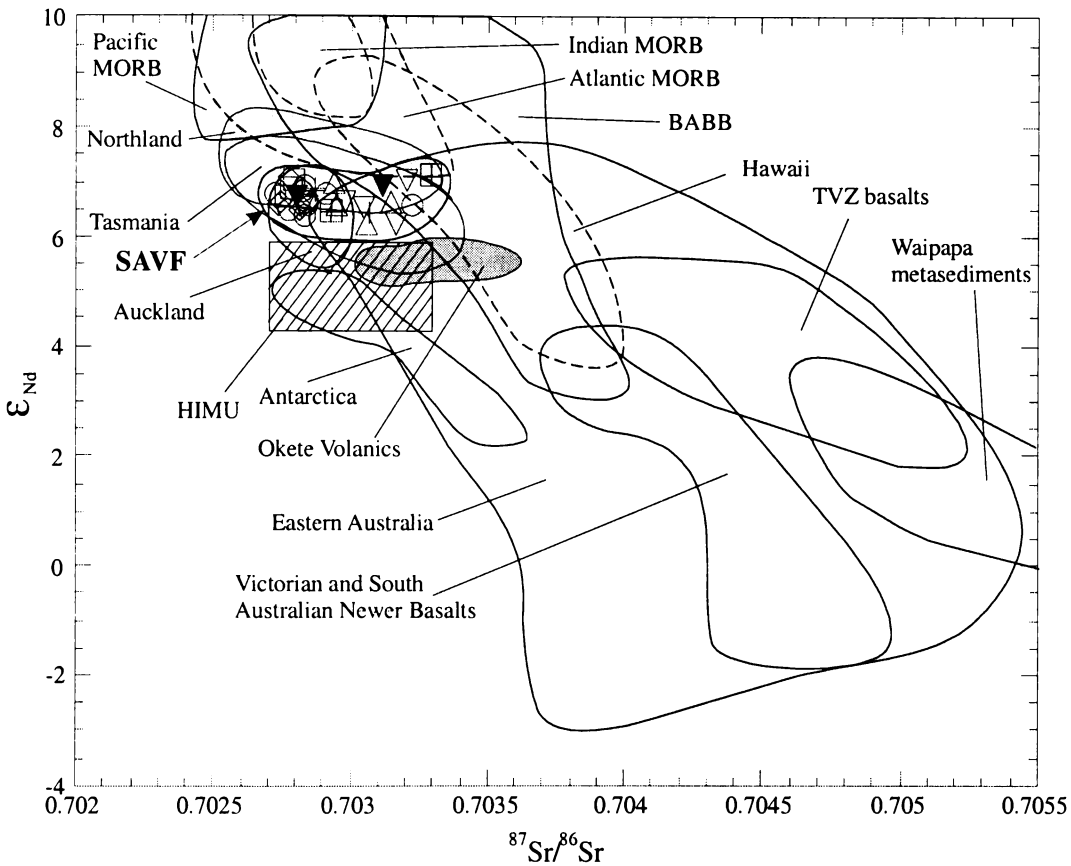

Fig. 5.15 $^{87}Sr/^{86}Sr$ vs. ε_{Nd} variation for selected group A and B lavas from the SAVF compared with basalts from the Okete Volcanics (Briggs and McDonough, 1990), Northland Volcanic Province (Huang *et al.*, 2000), Auckland volcanic field (Huang *et al.*, 1997), Eastern Australia (Ewart *et al.*, 1988; O'Reilly and Zhang, 1995), Tasmania and the Newer Volcanic Province of Victoria and South Australia (McDonough *et al.*, 1985), Marie Byrd Land, Antarctica (Panter *et al.*, 2000), Hawaiian Islands (Maaløe *et al.*, 1992; Kurz *et al.*, 1995; Rhodes and Hart, 1995; Cohen *et al.*, 1996; Garcia *et al.*, 1996, 2000; Holcomb *et al.*, 1997; Reiners and Nelson, 1998; Pietruszka and Garcia, 1999; Abouchami *et al.*, 2000), TVZ (Gamble *et al.*, 1993), Atlantic, Pacific, and Indian Ocean MORB (Ito *et al.*, 1987), back-arc basin basalts (BABB) from Lau Basin, North Fiji Basin, and Mairana Trough (Stern *et al.*, 1990; Eissen *et al.*, 1991,1994; Sinton *et al.*, 1993; Hergt and Hawkesworth, 1994), the Waipapa metasediments (Graham *et al.*, 1992; McCulloch *et al.*, 1994), and the HIMU (mantle with high U/Pb ratio) mantle reservoir end-member composition of Zindler and Hart (1986). Where ε_{Nd} is not reported in the literature ε_{Nd} values were calculated using reported $^{143}Nd/^{144}Nd$ analyses and $\varepsilon_{Nd} = \left[\frac{\left(^{143}Nd/^{144}Nd\right)_{Sample}}{\left(^{143}Nd/^{144}Nd\right)_{CHUR}} - 1\right] 10^4$, where $(^{143}Nd/^{144}Nd)_{CHUR} = 0.512638$. Symbols as in Fig. 5.16.

Relative to the Okete basalts (Briggs and McDonough, 1990), a large number of group A rocks have similar $^{87}Sr/^{86}Sr$ compositions but all SAVF rock types have larger ε_{Nd} values. In contrast, the majority of group B rocks have Sr-Nd isotopic compositions similar to those from the Auckland volcanic field (Huang *et al.*, 1997), indicating regional variation in $^{87}Sr/^{86}Sr$ and $^{143}Nd/^{144}Nd$ compositions, possibly reflecting source heterogeneity between the various fields within the Auckland Volcanic Province.

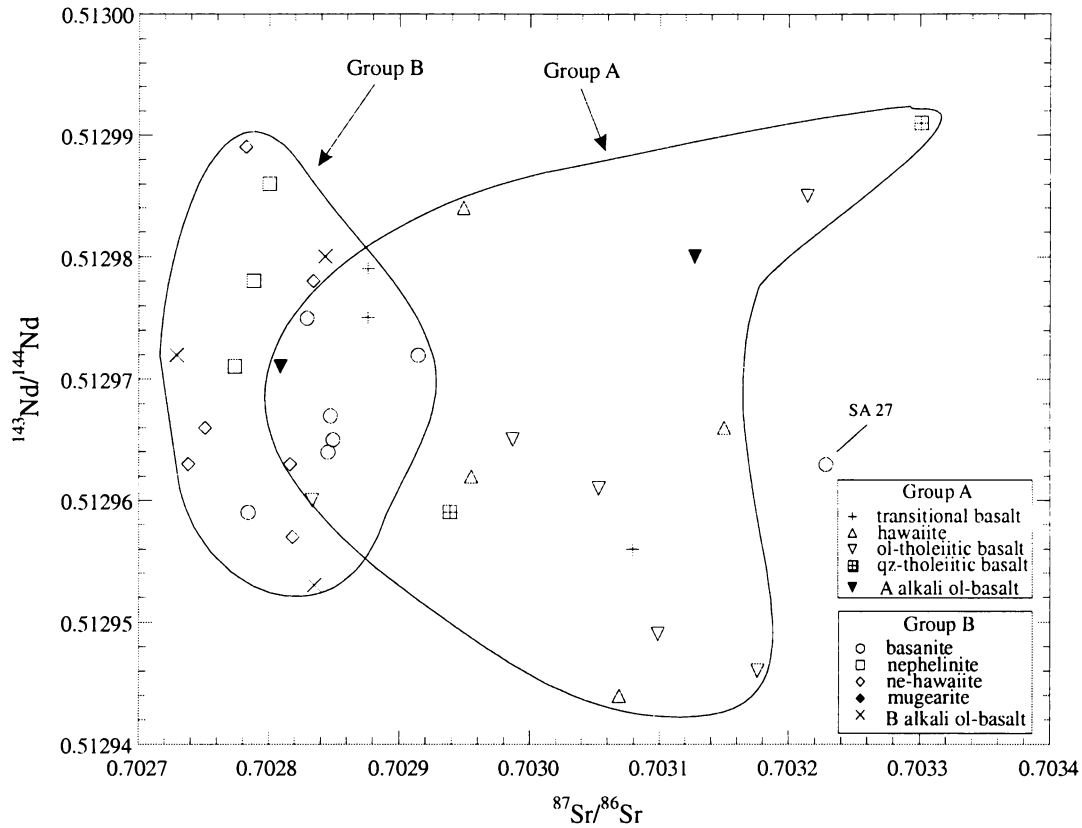

Fig. 5.16 $^{87}Sr/^{86}Sr$ vs. $^{143}Nd/^{144}Nd$ for selected group A and B lavas, South Auckland volcanic field.

Although there are relatively large variations in major and trace element and REE compositions between the group A and B rocks, they have similar Nd isotopic compositions (mean ε_{Nd} = + 6.47 ± 0.05; mean $^{143}Nd/^{144}Nd$ = 0.512972 ± 1.4 x 10^{-5}) and (mean ε_{Nd} = + 6.41 ± 0.19; mean $^{143}Nd/^{144}Nd$ = 0.512967 ± 9.7 x 10^{-6}) respectively (see Figs. 5.15 and 5.16). In contrast, the distinct major and trace element and REE compositions that characterise each group are also observed in their Sr isotopic compositions (Fig. 5.16). The most alkaline lavas (e.g., group B) generally have the least radiogenic Sr isotopic compositions (e.g., $^{87}Sr/^{86}Sr$ = 0.702729 – 0.702914), with SA27 the notable exception ($^{87}Sr/^{86}Sr$ = 0.703228), whereas the majority of the predominantly

subalkalic group A lavas have slight but notably more radiogenic $^{87}Sr/^{86}Sr$ compositions (e.g., $^{87}Sr/^{86}Sr = 0.702809 - 0.703214$).

5.5.2 Pb isotopic compositions

The Pb isotopic compositions for groups A and B are illustrated in Figs. 5.17 and 5.18. The $^{206}Pb/^{204}Pb$ compositions of SAVF lavas are more radiogenic than Indian and Pacific MORBs, Hawaiian Island OIBs, Newer basalts, TVZ basalts (Graham *et al.*, 1992), back-arc basin basalts (BABB) from the Lau and North Fiji Basins and the Mairana Trough (Stern *et al.*, 1990; Hergt and Hawkesworth, 1994), and the depleted mantle (DM), enriched mantle (EMI), and prevalent mantle (PREMA) reservoirs of Zindler and Hart (1986), and the majority of eastern Australia basalts. However, they are similar to basalts from Tasmania, Northland, Auckland, Okete, and Atlantic MORB, and less radiogenic than the HIMU-type alkalic basalts from Marie Byrd Land, Antarctica. Unlike the Sr-Nd isotope system shown in Fig. 5.15, the SAVF lavas plot away from HIMU, a characteristic shared by basalts from the other continental intraplate provinces and fields shown in Fig. 5.17A. However, as with their Sr and Nd isotopic compositions, the majority of group A rocks have Pb isotopic compositions similar to those of the Okete Volcanics, whereas the compositions of group B rocks are comparable to those from the Auckland volcanic field (Fig. 5.17A, B), indicative of possible contrasting source characteristics on a regional scale.

The group A and B lavas have contrasting $^{207}Pb/^{204}Pb$ and $^{206}Pb/^{204}Pb$ isotopic compositions (Fig. 5.18A). The rocks from groups A and B have $^{207}Pb/^{204}Pb$ compositions that overlap some Hawaiian basalts (e.g., Chen *et al.*, 1996) and BABBs, primarily from the Mariana Trough (Stern *et al.*, 1990), but are distinctly smaller than the Antarctica basalts. The group A rocks generally have smaller $^{206}Pb/^{204}Pb$ compositions (18.950 – 19.277) that only slightly overlap those of group B (19.201 – 19.323). In addition, they have $^{207}Pb/^{204}Pb$ compositions that negatively correlate with $^{206}Pb/^{204}Pb$ in the range 15.586 – 15.613 with $\Delta 7/4$ varying from 1.1 to 6.8. Most of the ol-tholeiitic basalts plot in the Okete Volcanics field and overlap the Northland Volcanic Province. The group A alkali ol-basalts, in contrast, are slightly less radiogenic with $^{207}Pb/^{204}Pb$ compositions similar to the group B alkali ol-basalts and basalts from Tasmania and the Auckland volcanic field. Compared to the group A rocks, those from group B have generally lower and relatively homogeneous $^{207}Pb/^{204}Pb$ compositions (15.568 – 15.578) that plot below the NHRL, with $\Delta 7/4$ in the range -0.2 to -1.3. Alkali ol-basalt, SAB227, ($^{207}Pb/^{204}Pb$ =

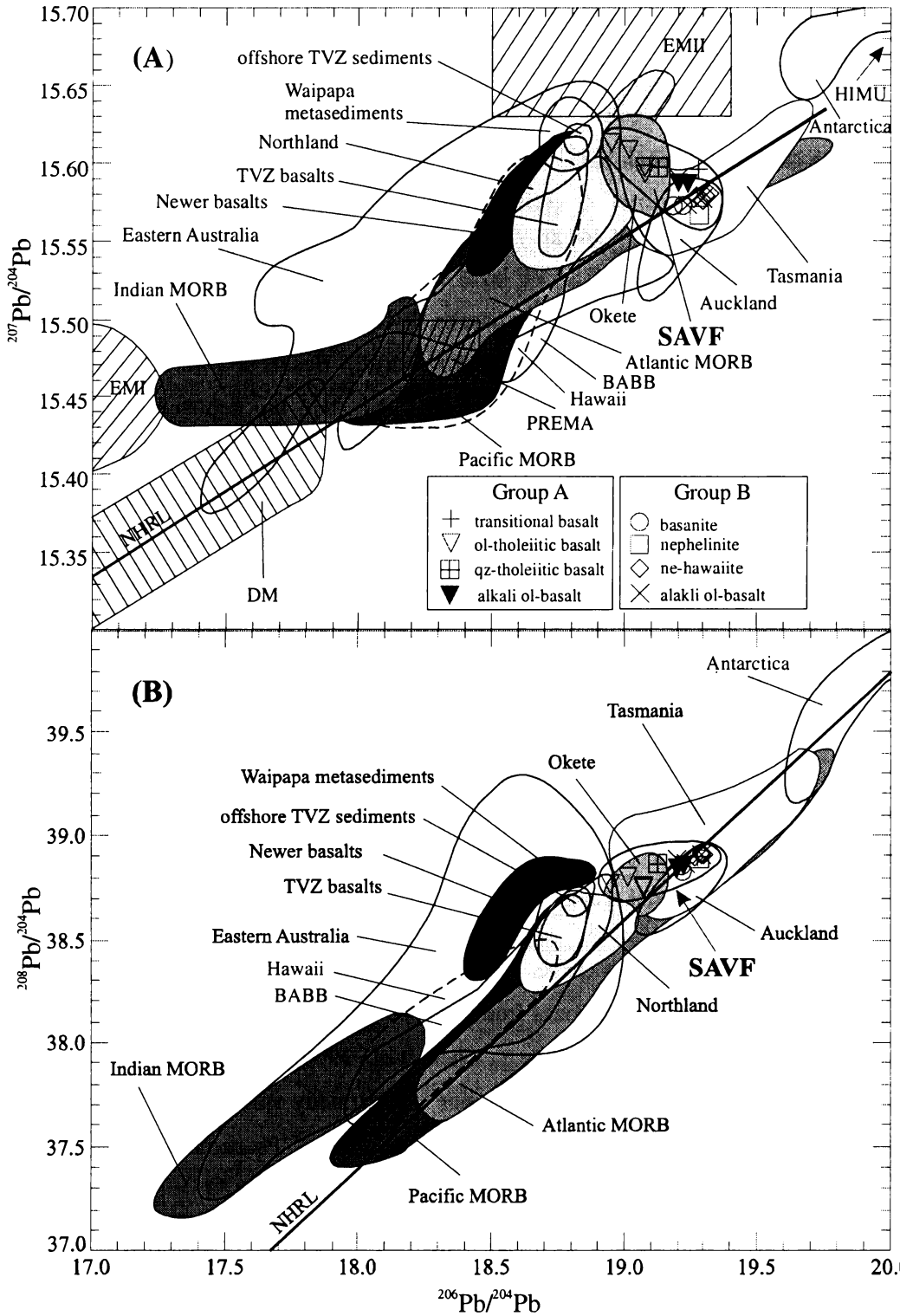

Fig. 5.17 (A) $^{207}Pb/^{204}Pb$ vs. $^{206}Pb/^{204}Pb$ and (B) $^{208}Pb/^{204}Pb$ vs. $^{206}Pb/^{204}Pb$ for selected group A and B lavas from the SAVF compared with fields for the Okete Volcanics (Briggs and McDonough, 1990), Northland Volcanic Province (Huang *et al.*, 2000), Auckland volcanic field (Huang *et al.*, 1997), basalts from Eastern Australia, Tasmania, and the Newer Volcanic Province of Victoria and South Australia (McDonough *et al.*, 1985; Ewart *et al.*, 1988), Marie Byrd Land, Antarctica (Panter *et al.*, 2000), Hawaiian Islands (Kurz and Kammer, 1991; Kurz *et al.*, 1995; Rhodes and Hart, 1995; Chen *et al*, 1996; Garcia *et al.*, 1996, 2000; Holcomb *et al.*, 1997; Hauri *et al.*, 1999; Pietruszka and Garcia, 1999; Abouchami *et al.*, 2000; Lassiter *et al.*, 2000), TVZ basalts (Graham *et al.*, 1992), Atlantic, Pacific, and Indian Ocean MORB (Ito *et al.*, 1987), back-arc basin basalts (BABB) from Lau Basin, North Fiji Basin, and Mairana Trough (Stern *et al.*, 1990; Hergt and Hawkesworth, 1994),Waipapa metasediments (Graham *et al.*, 1992; McCulloch *et al.*, 1994), offshore TVZ sediments (Gamble *et al.*, 1996), and the mantle reservoir end-member compositions; PREMA (prevalent mantle), DM (depleted mantle), and EMI and EMII (enriched mantle) of Zindler and Hart (1986). The Northern Hemisphere Reference Line (NHRL) is from Hart (1984).

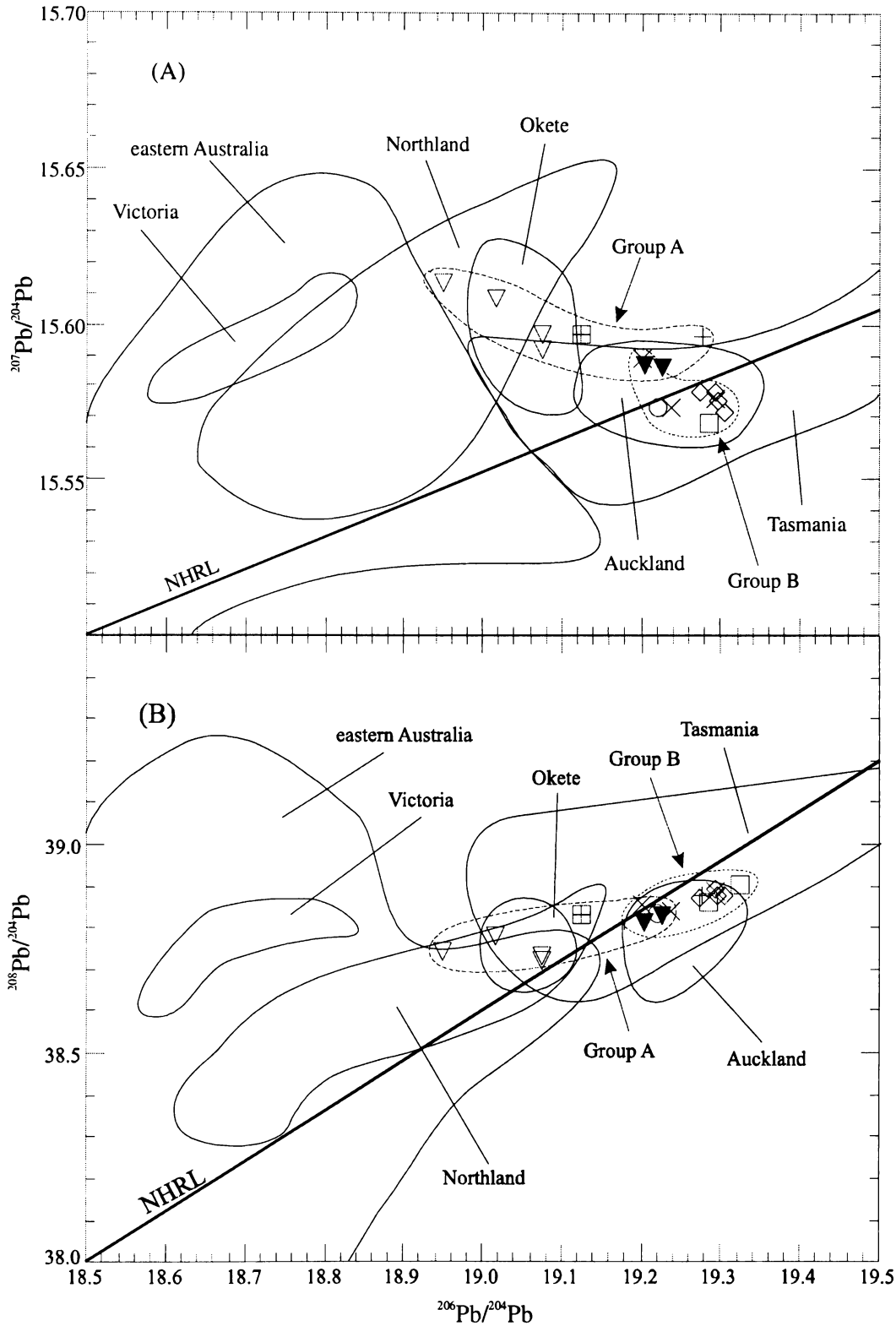

Fig. 5.18 (A) $^{207}Pb/^{204}Pb$ vs. $^{206}Pb/^{204}Pb$ and (B) $^{208}Pb/^{204}Pb$ vs. $^{206}Pb/^{204}Pb$ for selected SAVF Group A and B lavas compared with data for similar basalts from other continental intraplate settings; eastern Australia, Victoria, Tasmania, Northland Volcanic Province, the Okete Volcanics, and Auckland volcanic field (references and symbols as in Fig. 5.16).

15.589; Δ7/4 = 1.7) is the notable exception, plotting above the NHRL in the group A field. An unusual feature of the SAVF lavas is the negative correlation of $^{207}Pb/^{204}Pb$ with $^{206}Pb/^{204}Pb$ (Fig. 5.17A), with the group A rocks plotting furthest away from the Northern Hemisphere Reference Line (NHRL) of Hart (1984) towards the EMII mantle reservoir, the Waipapa metasediments, and sediments offshore from the TVZ (Gamble *et al.*, 1996). This trend contrasts those depicted by the other data fields shown in Fig. 5.17A, which represent either relatively homogeneous compositions (e.g., Auckland and Okete) or broad trends oriented subparallel to the NHRL (e.g., eastern Australia, Victoria, Tasmania, Antarctica, and the back-arc basalts).

The group A and B rocks have a similar narrow range of $^{208}Pb/^{204}Pb$ compositions (38.723 – 38.876, and 38.833 – 38.906, respectively) that slightly overlap and collectively exhibit a weak positive trend with $^{206}Pb/^{204}Pb$ (Fig. 5.18B). Rocks from each group have $^{208}Pb/^{204}Pb$ compositions smaller than the Antarctica basalts but larger than those from Hawaii and the BABBs. As with $^{207}Pb/^{204}Pb$ compositions, the group B rocks have $^{208}Pb/^{204}Pb$ compositions similar to those from Tasmania and Auckland, whereas the group A rocks share $^{208}Pb/^{204}Pb$ characteristics similar to those from the Northland Volcanic Province, Okete Volcanics, and Tasmania. The majority of group A rocks plot above the NHRL and have values of Δ8/4 that range from -3.1 to 20.6, whereas most group B rocks tend to cluster along the NHRL resulting in distinct Δ8/4 values in the range -8.7 to 1.6.

5.6 Summary

The South Auckland volcanic field lavas have geochemical compositions comparable to silica-undersaturated mafic magmas erupted in other continental intraplate tectonic settings. However, unlike suites of alkalic basalts elsewhere, which show systematic variations in composition (e.g., from nephelinite and basanite to hawaiite through to ol-tholeiitic and qz-tholeiitic basalt), the rocks that comprise the group A and B lavas in the SAVF have distinctive, contrasting geochemical characteristics marked by dissimilar trends of major elements and incompatible trace elements when plotted against MgO and contrasting degrees of LREE enrichment. These distinguishing geochemical features are also observed in their radiogenic isotopic compositions. Salient geochemical features include:

1. The majority of SAVF rocks have relatively primitive compositions (e.g., $100Mg/(Mg + Fe^{2+}) > 60$). Based on $100Mg/(Mg + Fe^{2+})$ and Ni and Cr contents,

the basanites have the most primitive compositions, whereas the ne-hawaiites from group B and a variety of group A rocks tend to be the most differentiated.

2. Group A and B rocks have distinctive major element and incompatible trace element characteristics. Each group is characterised by dissimilar trends of the major elements P_2O_5, Na_2O, and K_2O, and a large number of trace elements when plotted against MgO. Collectively, the group A rocks exhibit only small variations in incompatible trace element concentrations, and relative to those in group B, they are depleted in LILE and HFSE and have smaller LILE/HFSE values. In contrast, there are distinct variations in trace element abundances between the various group B rock types as well as among samples of the same rock type. The group B rocks have OIB-like trace element characteristics and show little variation between samples of the same rock type. In addition, the group B lavas are enriched in LREE and depleted in HREE and have lower LREE/HFSE ratios compared to those in group A.

3. All rock types from each group have Sr, Nd, and Pb isotopic compositions typical of a depleted mantle source. Generally, the SAVF lavas have Sr and Nd isotopic compositions similar to the continental intraplate basalts from Tasmania, the Okete Volcanics, Northland Volcanic Province, and Auckland volcanic field, but contrast those from intraplate fields elsewhere, e.g., eastern Australia. The rocks from groups A and B have Sr isotopic compositions that (i) are similar to MORB and HIMU, (ii) overlap BABB from the western Pacific, and (iii) are predominantly less radiogenic than Hawaiian OIBs, with most group A rocks slightly more radiogenic than those in group B. The Sr isotopic compositions of the SAVF lavas are distinctly less radiogenic than the Newer Basalts of eastern Australia, subduction-related TVZ basalts, and the Waipapa Terrane metasediments. All SAVF lavas have similar Nd isotopic characteristics intermediate between HIMU and MORB and overlap some Hawaiian and back-arc basin basalts. The group A and B rocks have Pb isotopic compositions that are smaller than HIMU, larger than PREMA and BABB, and generally overlap those of Atlantic MORB on the NHRL. The SAVF lavas have ^{206}Pb and ^{208}Pb compositions larger than OIB (i.e., Hawaiian basalts) and TVZ basalts, whereas they have ^{207}Pb compositions similar to those from Hawaii and the TVZ. The group A rocks have small but distinct differences in ^{206}Pb and ^{207}Pb compositions compared to those from group B, resulting in a trend of increasing $^{207}Pb/^{204}Pb$ with decreasing $^{206}Pb/^{204}Pb$ between the NHRL and the EMII mantle reservoir.

Chapter Six:
Petrogenesis of the SAVF Basalts

Chapter Six

Petrogenesis of the SAVF basalts

6.1 Introduction

The data presented in the preceding chapters show that at least two distinct groups of alkalic basalts were erupted in the SAVF during the one million year life of the field. The basalts that comprise groups A and B have dissimilar petrographic, mineral chemical, and major and incompatible trace element characteristics, as well as small but distinct differences in their Sr, Pb, and Sm isotopic compositions. Collectively, these dissimilarities suggest that the basalts from each group had distinct petrogenetic histories.

The focus of this chapter is on the petrogenesis and evolution of the range of magma types erupted throughout the SAVF. The main objectives are to (i) evaluate the genetic relationship between the group A and B basalts and the various rock types within each group, (ii) characterise the nature of the mantle source (or sources) for groups A and B, and (iii) determine if the contrasting compositions of groups A and B are source or process controlled, with the aim of developing a general model for intraplate volcanism in the South Auckland region.

6.2 Primary magma compositions

The identification of primary magmas (magmas unmodified by fractional crystallisation or other processes while en route to the surface) is important to the understanding of the generation and evolution of suites of cogenetic basalts, especially those with contrasting geochemical characteristics such as the group A and B basalts of the SAVF. Primary magma compositions can provide general constraints on the nature of the mantle source (or sources) for the group A and B basalts and can be used to estimate the temperatures and pressures at which melt segregation of discrete magma batches occurred. In addition, knowledge of primary magma compositions is important in the identification of those magmas parental to the various lineages of group A and B lava types.

Although none of the samples analysed in this investigation meet all criteria commonly invoked to be considered a primary magma in equilibrium with its mantle source (see section 5.4.1, p.144), nine of the 61 centres sampled erupted "near-primary" magmas that have undergone minor olivine fractionation. These samples, the majority of which are

basanites, have 100Mg/(Mg + Fe^{2+}) values ≥ 64, between 10 and 13 wt.% MgO, Ni abundances from 200 to 337 ppm, and contain rare ultramafic xenoliths. Representative primitive compositions from groups A and B are listed in Table 6.1.

Studies of upper mantle-derived peridotite xenoliths (e.g., harzburgites and lherzolites) in alkalic basalts from a variety of continental intraplate settings (e.g., northern Hessian Depression, Wedepohl, 1985; eastern Australia, O'Reilly *et al.*, 1989) indicate their source regions have compositions with 100Mg/(Mg + Fe^{2+}) values from 88 to 91 and contain olivine from Fo_{86} to Fo_{91}. The spinel-bearing harzburgite and lherzolite xenoliths observed in some SAVF basanites and ne-hawaiites by Sanders (1994) have similar compositions [i.e., 100Mg/(Mg + Fe^{2+}) values (88 – 91) and olivine Fo_{90} – Fo_{91}]. Although not cognate, they can be used as possible analogues to the source composition for the SAVF basalts for the purpose of estimating primary magma compositions. Studies by Green (1973a), Frey *et al.* (1978), and Hanson and Langmuir (1978) determined that primary basaltic melts equilibrated with peridotite source rocks such as these have 100Mg/(Mg + Fe^{2+}) values from 68 to 75 for up to 30% melting. In addition, experimental studies on MgO-Ni relationships of primary magmas show that they can have MgO concentrations between 11 and 13 wt.% and Ni abundances from 300 to 400 ppm for up to 20 % melting (Hart and Davis, 1978; Hirschmann and Ghiorso, 1994).

Experimental studies have shown that olivine is the low-pressure liquidus phase for basaltic compositions derived from peridotite source rocks under hydrous and anhydrous conditions (e.g., Green and Ringwood, 1967; Green, 1973a; Herzberg and Zhang, 1996). Therefore, near-primary magmas, such as those listed in Table 6.1, can be derived from primary partial melts of a peridotite source solely by olivine fractionation. Primary compositions were calculated by adding olivine Fo_{90} back to each composition in one percent increments, while maintaining a constant $K_{d_{Fe-Mg}}^{ol-melt}$ = 0.30 (Roeder and Emslie, 1970), until a composition having 11 – 13 wt.% MgO and 100Mg/(Mg + Fe^{2+}) ≥ 68 was reached. This is equivalent to producing a melt in equilibrium with a mantle olivine of Fo_{90}, which is a reasonable mantle composition in terms of the xenoliths described by Sanders (1994) from the SAVF basalts.

The amount of olivine required to reach 100Mg/(Mg + Fe^{2+}) = 68 by Rayleigh fractionation for the group A rocks ranges from 3 to 11% and for group B, < 1 to 9%. The calculated major element compositions and CIPW norms of representative SAVF primary magmas are presented in Table 6.1.

Table 6.1 Compositions and CIPW norms of representative group A and B 'primary' magmas (prime) derived by olivine addition to differentiated basalts (obs).

	Group A										Group B									
Rock Type	transitional		hawaiite		ol-tholeiitic		ol-tholeiitic		alkali ol-basalt		basanite		basanite		basanite		basanite		basanite	
Sample #	SA13		SA32		SAB181		SAB187		SA33		SA55		SA56		SA60		SAB179		SAB204	
	obs	prime	obs	prime	obs	prime	obs	prime	obs	prime	obs	prime	obs	prime	obs	prime	obs	prime	obs	prime
olivine added (%)		5		6		6		3		5		2		4		<1		<1		4
SiO_2	48.98	47.83	48.60	47.27	49.78	48.36	49.57	48.87	47.47	46.41	44.97	44.60	43.54	42.85	44.63	44.45	44.03	43.86	43.23	42.57
TiO_2	1.70	1.68	1.96	1.93	2.05	2.02	1.92	1.91	2.14	2.11	2.69	2.67	2.99	2.95	2.80	2.79	2.70	2.69	3.06	3.02
Al_2O_3	14.44	14.22	13.31	13.07	13.30	13.06	13.26	13.14	13.43	13.23	12.92	12.83	12.83	12.65	12.71	12.67	12.28	12.24	12.45	12.29
Fe_2O_3	1.97	1.94	2.16	2.12	2.01	1.98	1.99	1.97	2.12	2.08	2.09	2.08	2.22	2.19	2.06	2.05	2.15	2.15	2.32	2.29
FeO	9.84	9.71	10.78	10.56	10.07	9.9	9.93	9.83	10.58	10.39	10.47	10.38	11.08	10.88	10.28	10.23	10.77	10.71	11.60	11.37
MnO	0.17	0.17	0.16	0.16	0.17	0.17	0.18	0.17	0.18	0.18	0.19	0.19	0.19	0.19	0.17	0.17	0.20	0.20	0.20	0.20
MgO	9.92	11.7	10.55	12.62	9.93	12.05	10.65	11.71	10.59	12.32	11.73	12.41	11.71	13.04	12.20	12.54	12.99	13.32	12.39	13.69
CaO	9.47	9.32	8.76	8.6	9.00	8.84	8.95	8.87	9.39	9.24	10.28	10.21	10.40	10.26	10.49	10.46	10.31	10.27	10.18	10.05
Na_2O	2.89	2.85	2.86	2.81	2.69	2.64	2.65	2.62	3.03	2.99	3.02	3.00	3.09	3.05	3.00	2.99	2.86	2.85	2.64	2.60
K_2O	0.39	0.39	0.59	0.58	0.66	0.65	0.62	0.61	0.74	0.73	1.18	1.17	1.30	1.29	1.17	1.17	1.16	1.15	1.21	1.20
P_2O_5	0.21	0.21	0.28	0.27	0.34	0.33	0.29	0.29	0.33	0.33	0.46	0.46	0.65	0.64	0.49	0.48	0.55	0.55	0.74	0.73
$\frac{100Mg}{Mg + Fe^{2+}}$	64	68	64	68	64	68	66	68	64	68	67	68	65	68	68	69	68	69	66	68
Q	-	-	-	-	-	-	-	-	-	-	-	-	-	-	-	-	-	-	-	-
Or	2.3	2.3	3.5	3.4	3.9	3.8	3.6	3.6	4.4	4.3	7.0	6.9	7.7	7.6	6.9	6.9	7.0	6.8	7.2	7.1
Ab	24.4	24.1	24.1	23.8	22.7	22.3	22.4	22.2	23.6	19.5	11.2	9.8	7.0	4.4	9.5	8.9	8.3	7.6	8.4	5.8
An	25.2	24.8	21.6	21.3	22.2	21.8	22.4	22.3	20.8	20.5	18.2	18.1	17.2	17.0	17.7	17.7	16.7	17.2	18.4	18.3
Ne	-	-	-	-	-	-	-	-	1.1	3.1	7.7	8.4	10.4	11.6	8.6	8.9	9.0	8.9	7.6	8.7
Di	16.6	16.3	16.3	16.0	16.6	16.2	16.4	16.2	19.3	18.9	24.3	24.1	24.7	24.3	25.3	25.3	25.6	24.6	22.3	22.0
Hy	9.2	2.3	8.7	1.1	17.6	9.0	16.2	12.1	-	-	-	-	-	-	-	-	-	-	-	-
Ol	15.6	23.7	18.2	27.1	9.4	19.4	11.8	16.6	22.9	25.9	22.5	23.6	22.8	24.9	22.6	23.1	24.0	25.4	25.3	27.4
Mt	2.9	2.8	3.2	3.1	2.9	2.9	2.9	2.9	3.1	3.0	3.1	3.0	3.3	3.2	3.0	3.0	3.2	3.1	3.4	3.3
Il	3.2	3.2	3.7	3.7	3.9	3.8	3.7	3.6	4.1	4.0	5.1	5.1	5.7	5.6	5.3	5.3	5.1	5.1	5.8	5.7
Ap	0.5	0.5	0.6	0.6	0.7	0.7	0.6	0.6	0.7	0.7	1.0	1.0	1.4	1.4	1.1	1.1	1.1	1.2	1.6	1.6

Calculations based on volatile-free whole-rock XRF analyses with major element oxides normalised to total 100% and an adjusted Fe_2O_3/ FeO = 0.2.

6.3 Mantle source characteristics

The petrogenesis and evolution of the wide range of alkalic basaltic magmas erupted within continental intraplate environments is commonly attributed to the generation of partial melts at localised mantle peridotite source regions, subsequently modified by processes such as fractional crystallisation. Source regions often have OIB-like characteristics and are commonly a mixture between one or more of the mantle reservoir end-members; DM, HIMU, EMI, or EMII of Zindler and Hart (1986)[52]. In addition, the compositions of these basalts may be modified by interaction with the continental crust as they ascend toward the surface.

Regardless of the processes that may have affected compositions of the primary group A and B magmas, the petrographic, mineralogical, and geochemical evidence strongly suggests that the suites of group A and B lavas are not related to a single mantle source.

Evidence for the existence of distinct upper mantle sources for the subalkaline (group A) and alkaline (group B) lavas in the SAVF has been discussed previously by Rafferty and Heming (1979). It is expanded upon here based on the following observations of the group A and B lavas and their calculated primary compositions:

1. Small but distinct differences in their Sr, Pb, and Sm isotopic compositions.

2. Large differences in LILE and HFSE abundances between groups A and B and corresponding dissimilar ratios (e.g., K/Nb, Zr/Nb, Ti/Zr, Zr/Y, Ce/Pb, Th/Yb, and Ta/Yb; see Table 5.10, p.155).

3. The contrasting REE patterns that suggest a garnet-bearing source for the group B lavas (see Fig. 5.13, p.161) but perhaps not for group A, and pressure estimates based on primary magma compositions that indicate that melt segregation for groups A and B occurred at very different pressures: the spinel stability field for group A and the garnet stability field for group B primary magmas.

6.3.1 Isotopic characteristics

The group A and B lavas have Sr, Nd, and Pb isotopic compositions that are intermediate between HIMU and MORB (see Figs. 5.15 and 5.17, p.166 and 169, respectively). Each group has relatively unradiogenic $^{87}Sr/^{86}Sr$ and similar Nd isotopic compositions, but they exhibit small but distinct differences in their Sr and Pb isotopic compositions (Fig. 6.1). Relatively small differences such as these might reflect relatively small-scale heterogeneities within a common source region. These differences may also be indicative

[52] Mantle reservoirs; DM = depleted mantle (i.e., N-MORB), HIMU = high U/Pb; EM = enriched mantle. See Zindler and Hart (1986) for details.

of minor amounts of crustal contamination as described by O'Reilly and Zhang (1995) for similar rock types from eastern Australia, rather than contrasting mantle source characteristics. However, McDonough *et al.* (1985) considered similar contrasts observed between basalts from Tasmania and the Newer Volcanic Province, Australia, as evidence for distinct mantle sources.

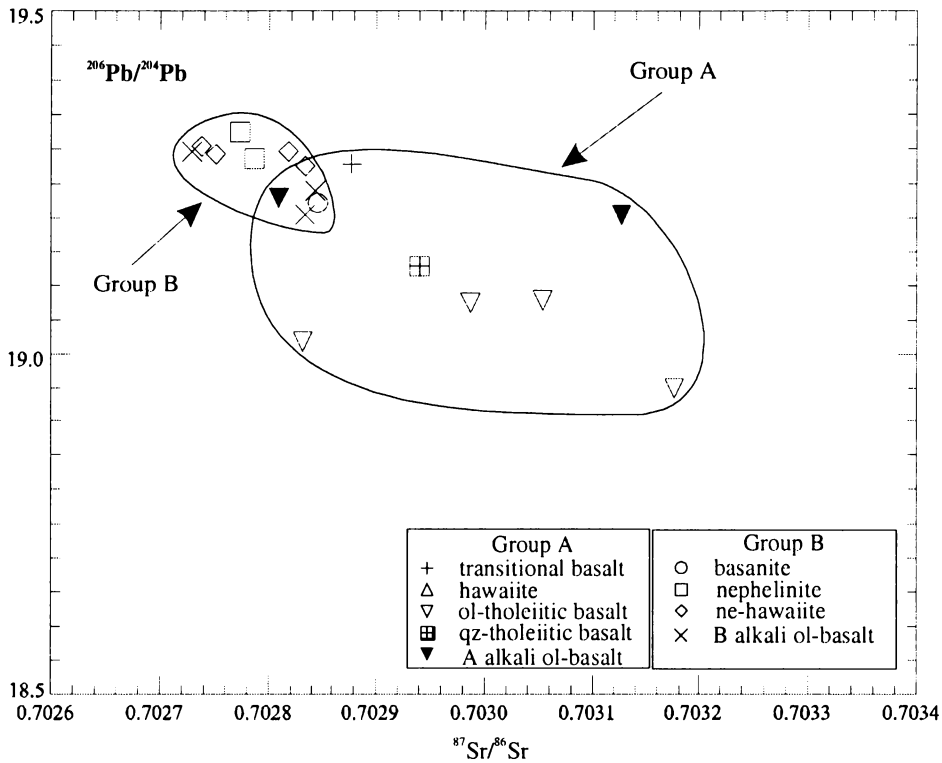

Fig. 6.1 $^{87}Sr/^{86}Sr$ vs. $^{206}Pb/^{204}Pb$ for the group A and B basalts of the South Auckland volcanic field.

It has long been recognised that the $^{87}Sr/^{86}Sr$, $^{143}Nd/^{144}Nd$, and $^{206}Pb/^{204}Pb$ ratios are not fractionated during igneous processes such as partial melting or fractional crystallisation (Hart and Allègre, 1980). Therefore, the distinctive $^{87}Sr/^{86}Sr$ and $^{206}Pb/^{204}Pb$ ratios of the group A and B lavas might reflect the ratios of dissimilar mantle sources, provided that magma modification by post-melt segregation processes, such as magma mixing, crustal assimilation, or assimilation/fractional crystallisation (AFC), has not occurred. Additional evidence for distinct sources for groups A and B are illustrated in the $^{143}Nd/^{144}Nd$ vs. $^{147}Sm/^{144}Nd$ diagram shown in Fig. 6.2. Despite having a similar $^{143}Nd/^{144}Nd$ composition, the group A rocks have more radiogenic Sm than those in group B. In addition, the larger $^{147}Sm/^{144}Nd$ values in the group A rocks are reflected in their larger Sm/Nd values (0.21 – 0.29) compared to those in group B (0.16 – 0.21) indicative of contrasting source characteristics.

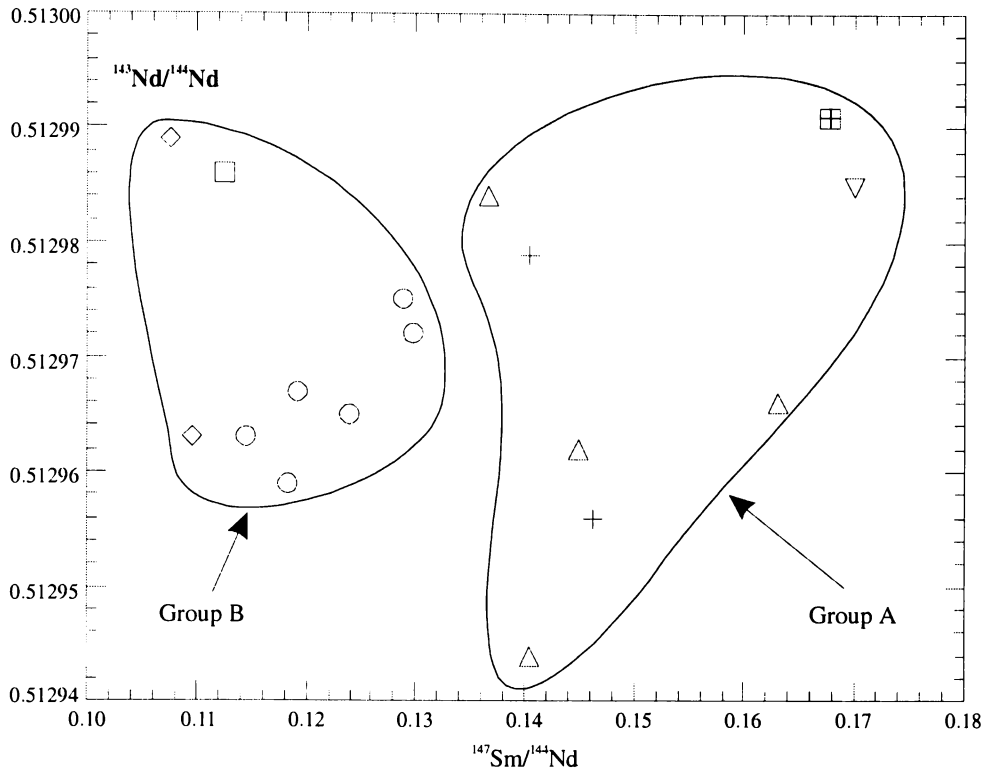

Fig. 6.2 $^{147}Sm/^{144}Nd$ vs. $^{143}Nd/^{144}Nd$ for selected South Auckland volcanic field lavas. Symbols as in Fig. 6.1

6.3.2 Trace element characteristics

The dissimilar incompatible trace element and LREE characteristics of the group A and B lavas further illustrate the contrasting geochemical characteristics of their sources. For example, the ratio-ratio plots shown in Fig. 6.3 illustrate that although the sources for groups A and B have similar Th/Ta and Ce/Nb values, each source has very different K/Nb and Th/Tb values. McKenzie and O'Nions (1991) argued that because REE (and by inference LILE and HFSE) have partition coefficients greater than 10^{-4} for the principal minerals in a mantle peridotite source: olivine, orthopyroxene, clinopyroxene, garnet, and spinel, they should not be considered to be totally incompatible for the purpose of melt generation. However, the highly incompatible nature for LILE, HFSE, and REE (i.e., K_d << 1; Table 6.2) indicate that, except for the compatible nature of HREE and Y in garnet, they are highly incompatible for these mineral phases. Because of this, it is unlikely that LILE/HFSE or LREE/HFSE will be strongly fractioned from each other during partial melting of a homogeneous source with these minerals as residues, or by fractional crystallisation of these phases, provided that (i) the degree of melting is sufficiently large (e.g., > 5%; Hart and Allègre, 1980) and (ii) fractional crystallisation is less than ~ 25% (see Wilson, 1989; Fig. 4.10, p.90). Therefore, the observed ratio of these elements most likely reflects the ratio of their concentration in the source.

Table 6.2 Mineral/melt partition coefficients used in the primary magma and mantle source calculations.

	$K^{ol/melt}$	Ref.	$K^{opx/melt}$	Ref.	$K^{cpx/melt}$	Ref.	$K^{gt/melt}$	Ref.	$K^{sp/melt}$	Ref.	$K^{plag/melt}$	
Sc	0.25	[7]	1.1	[7]	1.31	[10]	3.3	[14]	2.0	[15]	0.008	[17]
V	0.09	[7]	0.3	[7]	3.1	[10]	3.45	[14]	1.62	[16]	0.10	[18]
Cr	0.6	[2]	1.9	[2]	3.8	[10]	2.01	[13]	24	[15]	0.02	[18]
Ni	8.62	[1]	1.1	[8]	2.6	[8]	5.1	[12]	9.0	[15]	0.06	[18]
Cs	0.0001	[2]	0.001	[2]	0.002	[2]	-	-	-	-	0.14	[19]
Rb	0.00018	[3]	0.006	[3]	0.011	[3]	0.0007	[3]	0.001	[15]	0.10	[3]
Ba	0.0005	[2]	0.0006	[2]	0.00068	[10]	0.0007	[13]	0.001	[15]	0.68	[17]
Th	0.01	[2]	0.0001	[3]	0.00026	[3]	0.00137	[13]	-	-	0.05	[3]
Nb	0.01	[3]	0.004	[2]	0.001	[11]	0.015	[14]	0.08	[16]	0.01	[3]
Ta	0.02	[2]	0.007	[2]	0.004	[11]	0.051	[14]	0.06	[16]	0.01	[20]
K	10^{-9}	[9]	0.0001	[9]	0.0072	[10]	0.0002	[13]	-	-	0.156	[21]
Sr	0.00019	[3]	0.007	[3]	0.1283	[10]	0.006	[14]	0.001	[15]	2.0	[3]
P	0.019	[4]	0.014	[4]	0.0044	[12]	-	-	-	-	-	-
Zr	0.003	[2]	0.16	[2]	0.1234	[10]	0.41	[14]	0.06	[16]	0.03	[20]
Hf	0.01	[3]	0.01	[3]	0.256	[10]	0.23	[3]	0.05	[16]	0.01	[3]
Ti	0.006	[3]	0.024	[3]	0.10	[3]	0.1	[3]	0.048	[3]	0.04	[3]
Y	0.002	[2]	0.17	[2]	0.467	[10]	4.2	[14]	-	-	0.031	[22]
La	0.0005	[7]	0.0005	[7]	0.02	[7]	0.001	[7]	0.01	[3]	0.27	[3]
Ce	0.0008	[7]	0.0009	[7]	0.04	[7]	0.0033	[7]	0.01	[3]	0.20	[3]
Pr	0.0008	[3]	0.0048	[3]	0.15	[3]	0.054	[3]	0.01	[3]	0.17	[3]
Nd	0.0013	[7]	0.0019	[7]	0.09	[7]	0.0184	[7]	0.01	[3]	0.14	[3]
Sm	0.0019	[7]	0.0028	[7]	0.14	[7]	0.0823	[7]	0.01	[3]	0.11	[3]
Eu	0.0019	[7]	0.0036	[7]	0.16	[7]	0.1333	[7]	0.01	[3]	0.73	[3]
Gd	0.0015	[3]	0.016	[3]	0.30	[3]	0.498	[3]	0.01	[3]	0.066	[3]
Tb	0.0019	[7]	0.0059	[7]	0.19	[7]	0.2568	[7]	0.01	[3]	0.06	[3]
Dy	0.0017	[3]	0.022	[3]	0.33	[3]	1.06	[3]	0.01	[3]	0.055	[3]
Ho	0.002	[7]	0.0089	[7]	0.195	[7]	1.083	[7]	0.01	[3]	0.048	[3]
Er	0.0015	[3]	0.03	[3]	0.30	[3]	2.00	[3]	0.01	[3]	0.041	[3]
Tm	0.0015	[3]	0.04	[3]	0.29	[3]	3.00	[3]	0.01	[3]	0.036	[3]
Yb	0.004	[7]	0.0286	[7]	0.2	[7]	4.0	[7]	0.01	[3]	0.031	[3]
Lu	0.0048	[7]	0.038	[7]	0.19	[7]	7.0	[7]	0.01	[3]	-	-

References for $K^{mineral/melt}$ values: 1 = Takahashi (1978); 2 = Beattie (1994); 3 = McKenzie and O'Nions (1991); 4 = Anderson and Greenland (1969); 7 = Frey *et al.* (1978) data Set 1; 8 = Mysen (1978); 9 = Keleman *et al.* (1992); 10 = Hart and Dunn (1993); 11 = Skulski *et al.* (1994); 12 = Baker and Wyllie (1992) ; 13 = Hauri *et al.* (1994); 14 = Jenner *et al.* (1994); 15 = Wedepohl (1984); 16 = Horn *et al.* (1994); 17 = Paster *et al.* (1974); 18 = Bougault and Hekinian (1974); 19 = Villemant *et al.* (1981); 20 = Lemarchand *et al.* (1987); 21 = Philpotts and Schnetzler (1970); 22 = Bindeman *et al.* (1998). ol = olivine; opx = orthopyroxene; cpx = clinopyroxene; gt = garnet; sp = spinel; plag = plagioclase

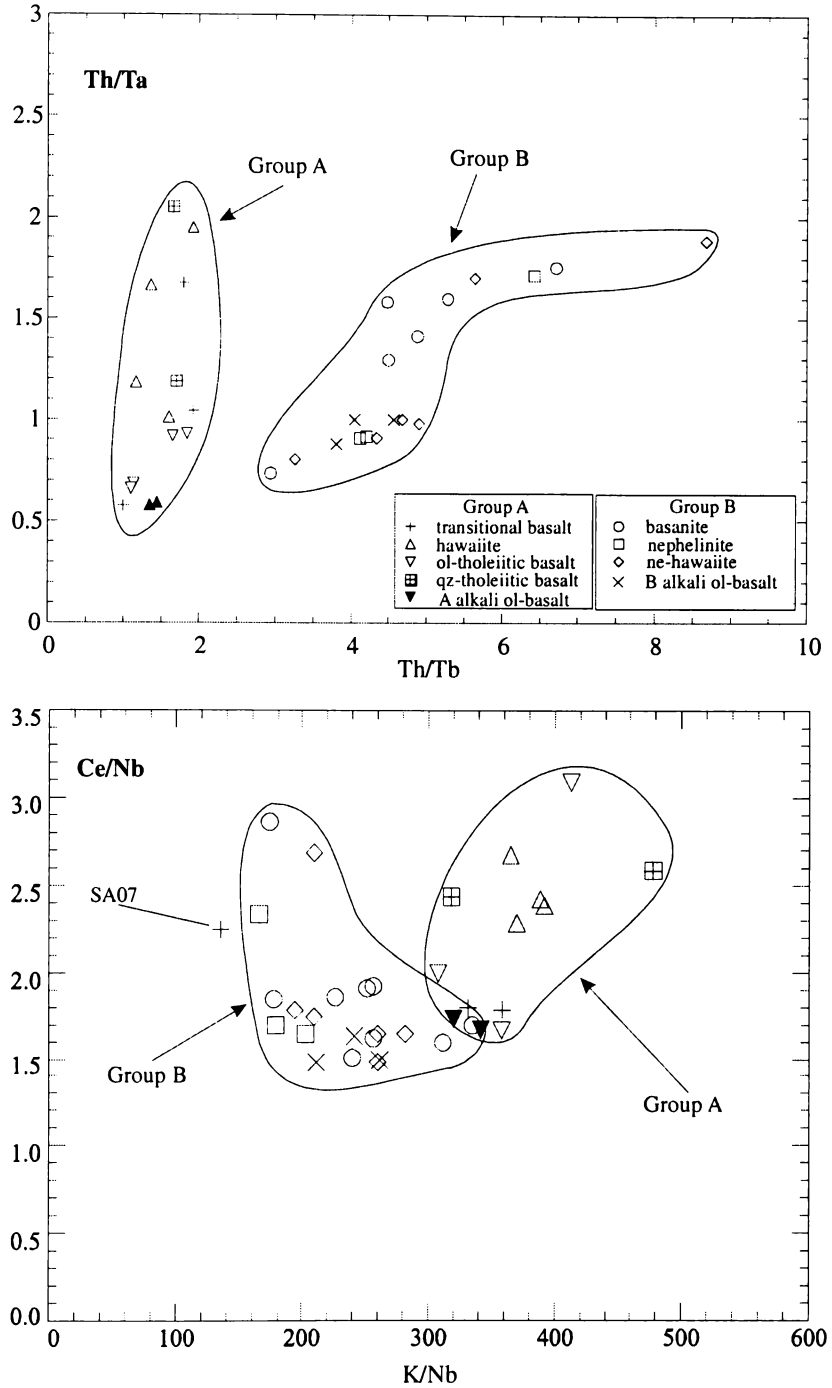

Fig. 6.3 Th/Tb vs. Th/Ta and K/Nb vs. Ce/Nb illustrating the contrasting characteristics of the mantle sources for groups A and B, South Auckland volcanic field. The small K/Nb values for group A transitional basalt SA07 reflect its small K_2O contents (0.27 wt.%)

The group B lavas have OIB-like incompatible trace element characteristics (Fig. 5.12, p.158) similar to strongly silica-undersaturated alkalic continental intraplate basalts elsewhere (see Table 1.1, p.2.). In addition, the group B lavas have Ce/Pb (25 ± 7)[53] and Nb/U (39 ± 6) values typical of an OIB-like source (Ce/Pb ~ 25 ± 5, Nb/U ~ 47 ± 10, Hoffman, 1986; Sims and DePaolo, 1997), which contrasts with the smaller Ce/Pb (12 ±

[53] means = ± 1 standard deviation

5) but similar Nb/U (42 ± 10) values of group A lavas. The group B lavas are enriched in LILE (i.e., Ba, Th, and K), HFSE (i.e., Zr and Nb), and LREE relative to the group A lavas but generally have smaller Ba/Nb, Rb/Nb, Sr/Nb, K/Nb, and Zr/Nb and larger Zr/Y values than those of group A (Fig. 6.4). Marked differences such as these are indicative of contrasting source characteristics (e.g., Hart and Allègre, 1980; Wilson, 1989; Frey and Rhodes, 1993).

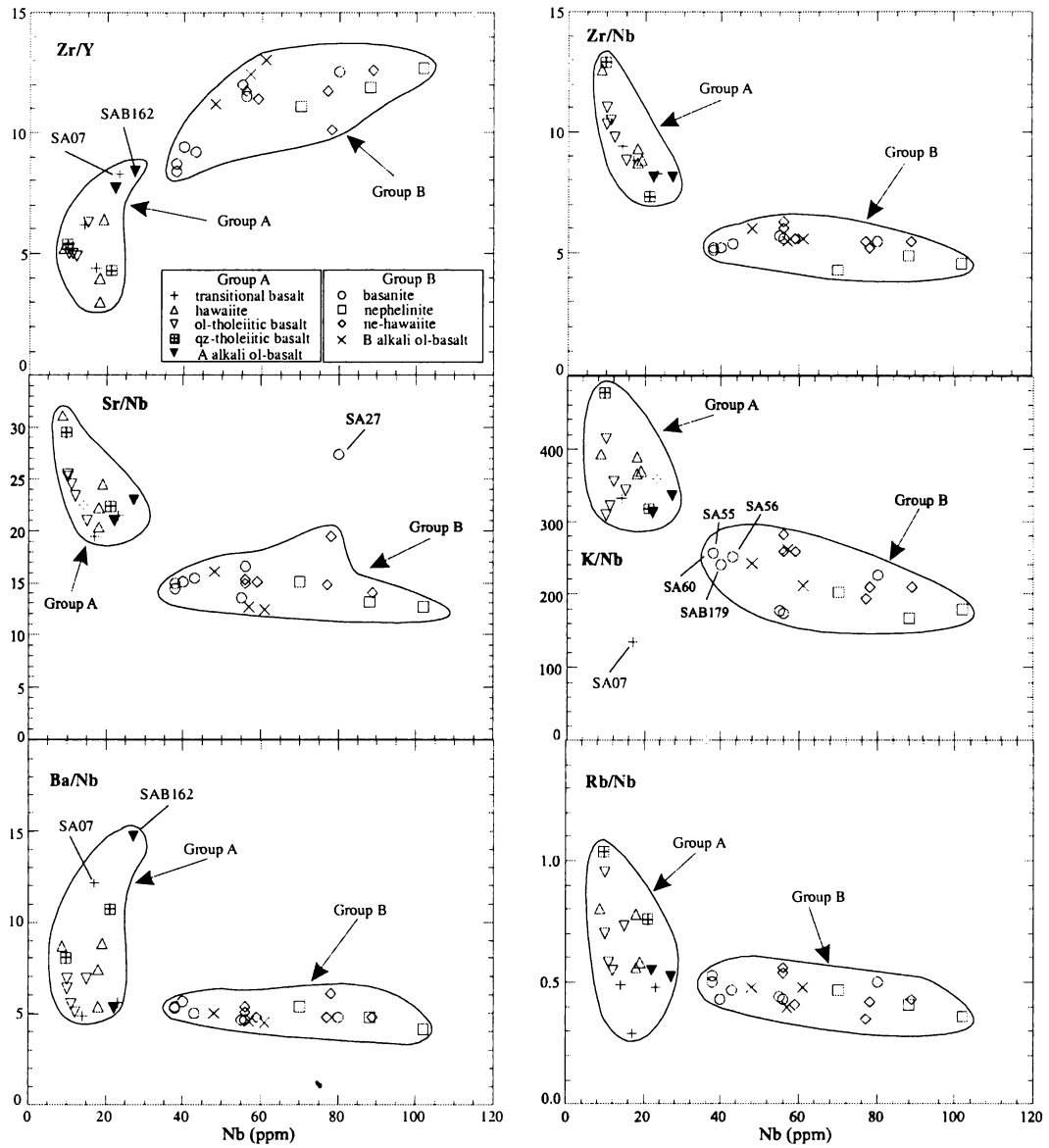

Fig. 6.4 Ba/Nb, Rb/Nb, Sr/Nb, K/Nb, Zr/Nb, and Zr/Y vs. Nb (ppm) plots illustrating the contrasting characteristics of the mantle sources for groups A and B, South Auckland volcanic field.

An important feature of the ratio-Nb plots shown in Fig. 6.4 is that the values of Ba/Nb, Rb/Nb, Sr/Nb, K/Nb, Zr/Nb, and Zr/Y for the group B lavas remain relatively constant over a wide range of Nb concentrations. This suggests that igneous processes such as partial melting or fractional crystallisation apparently had little effect on these ratios.

Furthermore, Frey and Rhodes (1993) noted that uniformity in such ratios is indicative of genetically related basalts.

The slight increase in Rb/Nb and K/Nb and decrease in Zr/Y could be indicative of phlogopite or clinopyroxene as residual phases in the group B source during the initial generation of the alkalic magmas, provided that melting was under very high pressure (e.g., Clague and Frey, 1982; Sun and McDonough, 1989). However, the samples for which these variations occur are among the most primitive group B lavas (basanites SA55, SA56, SA60, and SAB179) and their small Nb abundances suggest that they are comparatively large degree melts. Therefore, these weak trends are opposite to that expected had phlogopite and clinopyroxene remained in the source. In addition, Sun and McDonough (1989) concluded that small variations in incompatible element ratios (e.g., K/Nb) with decreasing Nb abundances, such as those characterised by the group B rocks, indicate that K-bearing phases (e.g., phlogopite) do not play a role in the generation of such magmas. Therefore, these ratios are not only the ratio of the primary magmas for group B but also of their mantle source.

In contrast to the group B lavas, Fig.6.4 shows that Ba, Rb, K, Sr, and Zr have been strongly fractionated from Nb during the petrogenesis of the group A lavas, resulting in large ratio variations over a narrow range of Nb abundances. Clague and Dalrymple (1988) argued that changes in incompatible trace element ratios such as Zr/Nb in samples from the Koloa Volcanics, Hawaii, represent changes in source composition during a 3 m.y. hiatus in volcanic activity. Frey and Rhodes (1993) however, maintained that such changes in some Hawaiian lavas do not necessarily reflect long-term differences in source composition, but may result from processes such as magma mixing or metasomatism. Alternatively, because there is no apparent correlation between magma differentiation and values of the ratios shown in Fig 6.4 for the group A lavas, the differences in ratio values between samples could reflect either of these scenarios:

1. **Source heterogeneity and variable degrees of melting.** Variable degrees of partial melting of a compositionally heterogeneous source can result in a wide range of incompatible trace element ratios such as those illustrated in Fig. 6.4 for the suite of group A lavas rather than the similar ratio values that would be expected for similar melting of a homogeneous source.

2. **Post-emplacement weathering processes.** The possible effect of incipient alteration accompanying weathering of some samples is illustrated by the large Ba/Nb values for alkali ol-basalt SAB162 and transitional basalt SA07 in Fig. 6.4, which are most likely due to Ba mobility during weathering processes (Price *et al.*, 1991). This is also evident by their large positive Ba anomalies on the mantle-normalised trace element plots (Fig. 5.12, p.158). In addition, re-examination of thin-sections of these samples suggest that they might have been

slightly weathered. It is unlikely however, that weathering processes can account for all of the large ratio variations involving the more mobile elements such as Ba or Y. For example, Price *et al.* (1991) demonstrated that the mobility of Y is highly variable on a localised scale. Therefore, the large Zr/Y value for SAB162 and SA07 is opposite to that expected for weathering-derived Y enrichment.

6.3.3 Spinel or garnet in the source regions of the SAVF basalts?

Because cognate spinel- or garnet-bearing xenoliths were not observed in the SAVF basalts, the presence or absence of garnet in the source regions for groups A and B can be inferred from the dissimilar REE abundances and LREE/HREE values between each group. Because the mineral/liquid partition coefficients for the HREE are much larger for garnet than for any of the other phases common in a peridotite source (Table 6.2), garnet is the only phase able to significantly fractionate HREE from LREE. Residual garnet during partial melting and melt segregation will result in large differences in LREE and HREE abundances, steep REE patterns, and small but very similar HREE abundances, such as Yb, in suites of alkalic basalts. These geochemical features have been cited in the studies of the alkalic basalts from the Okete, Ngatutura, and Auckland fields, and some of the fields in Northland as evidence for residual garnet in their respective source regions (Briggs and Goles, 1984; Briggs and McDonough, 1990; Briggs *et al.*, 1990; Huang *et al.*, 1997, 2000).

Comparable features of strong HREE depletion relative to LREE and steep chondrite-normalised REE patterns are apparent in the group B basalt patterns shown in Fig. 6.5 (see also Fig. 5.13, p.161) demonstrating that garnet is required as a residue in the group B source. In contrast, the group A lavas are HREE enriched resulting in relatively flat REE patterns that cross over those of group B (Fig. 6.5). These features suggest that the primary group A magmas could have been derived either from (i) a LREE-enriched garnet-bearing source, in which garnet was totally consumed during relatively large degrees of melting, thus enriching the melt in HREE, or (ii) a LREE-depleted source in which garnet is entirely absent, or present in very small amounts.

High-pressure melting experiments show that garnet is a solidus phase at pressures > 25 kbar for anhydrous conditions (Takahashi, 1986; Herzberg and Zhang, 1995) or > 20 kbar in the presence of small amounts of water (i.e., ~ 0.2 wt% H_2O) (Green and Ringwood, 1967; Green, 1973c). Pressure estimates for the primary magmas of groups A and B (Table 6.1) can be used therefore, to further constrain the nature of their source mineralogy. Calculations based on the empirical relationship proposed by Albarède (1992) to estimate the pressure at which melts segregate from their peridotite source

$$P(kbar) = \left[\exp^{5.04MgO/(SiO_2+MgO)-0.12SiO_2+7.47}\right] \pm 2.7kbar$$

indicate that the primary magmas of group B were generated at pressures ranging from 25 to 36 kbar (± 2.7 kbar) for basanites SA55 and SAB204 respectively, whereas those from group A range from 13 to 19 kbar (± 2.7 kbar) for ol-tholeiitic basalt SAB187 and alkali ol-basalt SA33 respectively. These pressures support the argument that the group B magmas were derived from a garnet-bearing source and indicate that the magmas primary to the group A lavas were generated outside the garnet stability field.

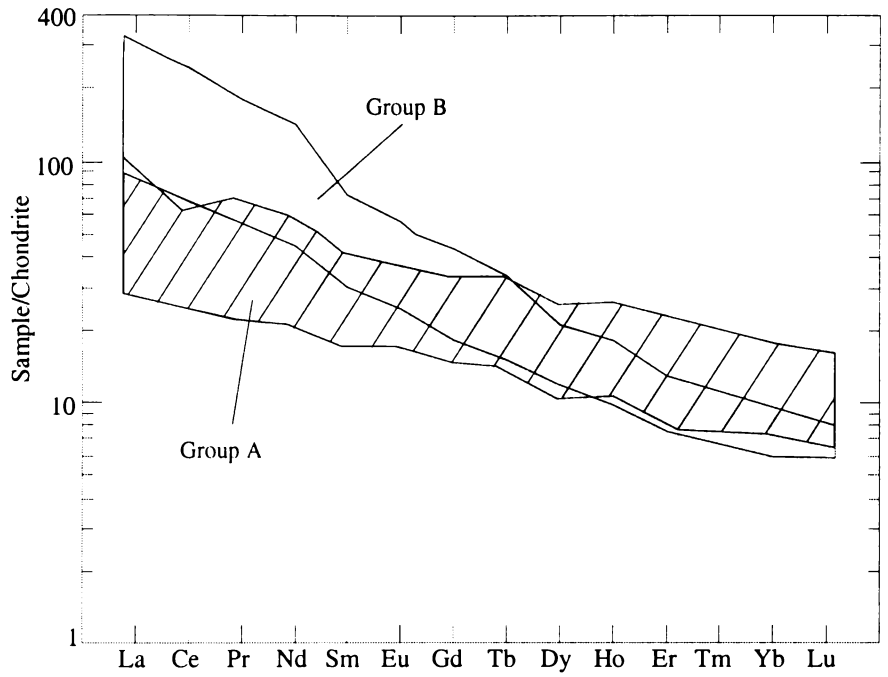

Fig 6.5 Chondrite-normalised REE diagrams for group A and B lavas analysed by SSMS and ICP-MS. Normalisation factors are those of Nakamura (1974).

All REE are highly incompatible in the principal mineral phases of a spinel peridotite source; olivine, orthopyroxene, clinopyroxene, and spinel (Table 6.2), and will be preferentially enriched in a melt. Therefore, partial melting of a source with these phases as residues or the fractional crystallisation of these phases is unlikely to fractionate LREE from HREE. Melting experiments of spinel peridotite compositions have shown that if melting occurs at pressures below the spinel-garnet transition then the resultant liquids will be less silica-undersaturated and hypersthene normative compared to the strongly silica-undersaturated and ne-normative basanitic and nephelinitic liquids generated at higher pressures (Jaques and Green, 1980; Takahashi and Kushiro, 1983; Hirose and Kushiro, 1993; Falloon *et al.*, 1999, 2001). The REE data for the SAVF basalts together with the experimental results suggests that the primary magmas for the group A lavas

were most likely derived from a spinel peridotite source at pressures that range from 10 to 20 kbar.

The results of these experiments are supported by Sanders' (1994) study of the spinel-bearing lherzolite and harzburgite xenoliths found in a number of SAVF basalts. Although these xenoliths were observed in the group B basanites and ne-hawaiites, Sanders argued that they represent accidental fragments derived from an upper mantle source between 15 and 17 kbar. In addition, a number of experimental studies on spinel peridotite compositions have shown that melts with major element compositions and normative mineralogy similar to that of the ol-tholeiitic basalt, alkali ol-basalt, and transitional basalt primary magmas (Table 6.1) can be generated by the partial melting of a spinel peridotite source over a broad range of pressures and temperatures (Takahashi and Kushiro, 1983; Hirose and Kushiro, 1993; Robinson *et al.*, 1998; Falloon *et al.*, 1999, 2001). Furthermore, the experiments of Green (1970, 1973a) demonstrated that because qz-tholeiitic basalts do not have olivine as a liquidus phase, they cannot be in equilibrium with the same residual phases as a garnet-bearing peridotite source. Therefore, qz-tholeiitic basalts "cannot be generated by equilibrium partial melting of a peridotitic source, even under water-saturated conditions at pressures greater than 20 kbar" (Green, 1970; see also Green, 1970, Fig. 6). The implications of Green's findings as they relate to the SAVF basalts is important because (i) they establishes that the qz-tholeiitic basalts and probably the other group A lava types were derived from magmas generated within the spinel stability field, and (ii) they imply that the depths of melt generation for the subalkaline (group A) magmas occurred at pressures less than those proposed by Rafferty and Heming (1979) who hypothesised that group A-type magmas probably formed at pressures > 30 kbar.

6.3.4 Evaluation of source modification by subduction processes

The Pb isotope data discussed in Chapter 5 indicate that the group A lavas are enriched in $^{207}Pb/^{204}Pb$ relative to the group B lavas. In addition, the group A lavas have positive $\Delta 7/4$ values (1.1 to 6.8) and all samples plot above the NHRL on the $^{207}Pb/^{204}Pb$ vs. $^{206}Pb/^{204}Pb$ diagram shown in Fig. 5.17A (p.169), and trend toward the field for the sediments offshore from the TVZ. In contrast, the group B lavas have negative $\Delta 7/4$ values (-0.2 to -1.3) and plot near or below the NHRL. It is possible therefore, that the $^{207}Pb/^{204}Pb$ and $\Delta 7/4$ characteristics of the group A lavas may result, in part, from the incorporation of sediments in relation to the subduction of the Pacific plate beneath this region.

Using the mixing models of Langmuir *et al.* (1978), this hypothesis was tested by mixing offshore TVZ sediment sample A302 (Gamble *et al.*, 1996) with a number of the OIB-like group B samples and samples from group A over their range of $^{207}Pb/^{204}Pb$ and $^{206}Pb/^{204}Pb$ compositions (see Tables 5.13 and 5.14, pp. 164 and 165). Modelling results indicate that the group A and B lavas plot outside any OIB-offshore-sediment mixing line or any mixing line involving group A Pb isotopic compositions and these sediments (see Fig. 5.17, p.169). This suggests that it is unlikely that the sources for the SAVF basalts represent a mixture with subducted oceanic or terrigenous sediments. In addition, although data for the group A basalts plotted on the Ta/Yb vs. Th/Yb tectonic discrimination diagram (Fig. 6.6) of Pearce (1982) exhibit similar Th/Yb values as the TVZ back arc basalts, the group A as well as the group B basalts plot in the mantle array that characterises basalts from non-subduction settings. Furthermore, the SAVF basalts lack the strong negative Nb, Ta, and Ti anomalies that would be expected for source regions modified by subducted sediments (*cf.* the intraplate alkalic basalts of the Chugoku district, southwest Japan, Iwamori, 1992, and the Whangarei field, Northland, New Zealand, Huang *et al.*, 2000).

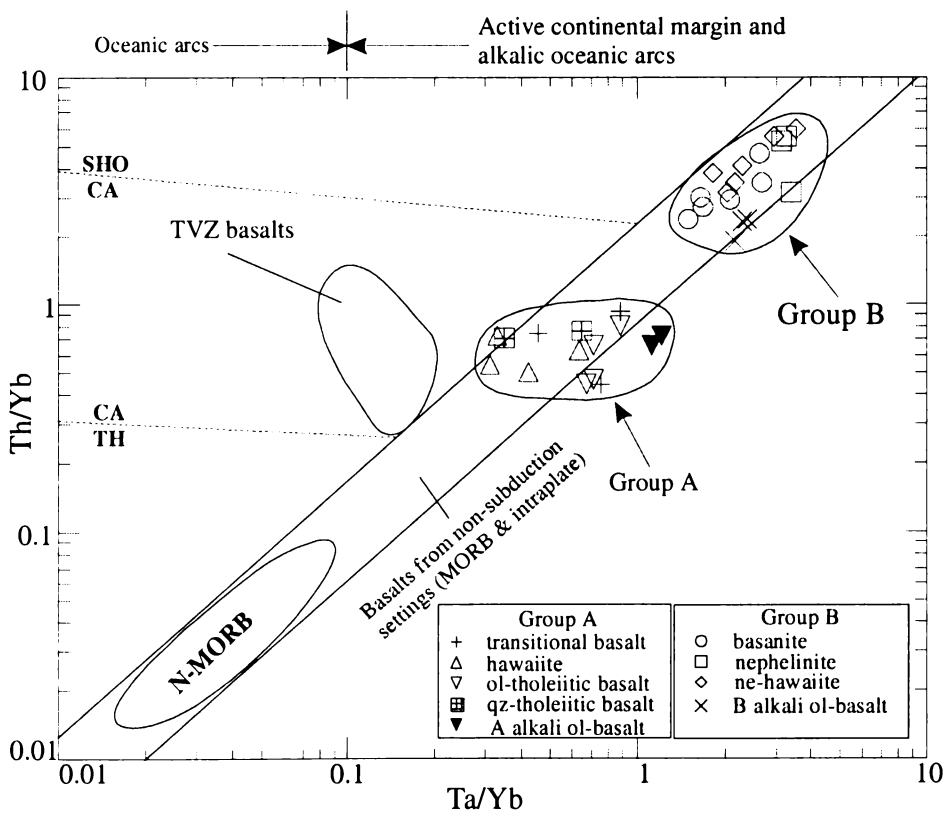

Fig. 6.6 Ta/Yb vs. Th/Yb showing the compositions of group A and B basalts from the South Auckland volcanic field relative to the TVZ basalts, the array for MORB and intraplate alkalic basalts, fields for shoshonitic (SHO), calc-alkaline (CA), and tholeiitic (TH) compositions, and the boundaries for oceanic arcs and active continental margin and alkalic oceanic arc basalts are from Pearce (1982). TVZ basalt data are from Gamble *et al.* (1993).

6.4 Partial Melting

The predominantly monogenetic nature of volcanism in the SAVF and lack of an apparent spatial or temporal correlation in compositions between or among the group A and B lavas suggests that (i) relatively small magma batches were generated from different parts of the mantle source regions for groups A and B at similar times, and (ii) melting of these sources occurred near-continuously during the life of the field.

The progressive increase in incompatible trace element and LREE abundances with decreasing MgO contents for the primitive group B lavas (i.e., basanite and nephelinites with MgO > 11 wt. %; Fig 5.10, p.154) is presumed, based on the work of Green (1970, 1973a), to result mainly from variable degrees of melting of a garnet peridotite source, although a single magmatic process cannot explain the increase in incompatible trace element concentrations from basanites to nephelinites to ne-hawaiites. The lavas with evolved compositions [i.e., $100Mg/(Mg + Fe^{2+}) < 60$] most likely are derivatives of primitive basanites and nephelinites by fractional crystallisation, as discussed in section 6.5. In contrast, group A rocks lack a distinct trend of progressively decreasing incompatible trace element and LREE abundances that would be indicative of either a range of degrees of melting or variable degrees of fractional crystallisation.

Experimental studies generally suggest that alkali basalts, comparable in composition to the primary group B magmas, form by degrees of partial melting that range from < 2 to 15%, whereas basalts with compositions similar to those from group A result from degrees of melting in the range 7 – 30%, for various peridotite source compositions (Green, 1970; Green 1973a,b,c; Jaques and Green, 1980; Hirose and Kushiro, 1993; Hirose and Kawamoto, 1995; Robinson *et al.*, 1998; Falloon *et al.*, 1999, 2001). According to the melting experiments of Green (1973a) on a lherzolite-bearing ol-basanite from Mt. Leura, Newer Volcanics Province, Australia, olivine-rich basanites with compositions similar to the primary magmas from group B (Table 6.1) can be generated from a garnet-bearing peridotite source (60% olivine, 18% orthopyroxene, 14% clinopyroxene, 8% garnet) by 6 – 8% partial melting at approximately 30 kbar under anhydrous conditions. The experiments of Green (1970) also demonstrated that with the addition of > 2% H_2O to the system, nephelinitic magmas (but not basanitic magmas) could be produced by smaller degrees of melting within the garnet stability field between 25 and 30 kbar. In the case of the group A basalts, a number of experimental studies have shown that melts with major element and normative compositions similar to the primary ol-tholeiitic basalts, transitional basalts, and alkali ol-basalts listed in Table 6.1 can be

generated from a variety of spinel peridotite compositions over a range of P – T conditions (Hirose and Kushiro, 1993; Falloon *et al.*, 1999, 2001).

The degree of melting required to generate the SAVF basalts has been addressed previously by Rafferty and Heming (1979) and Heming (1980b), but only qualitatively. They argued that the subalkalic (group A-type) magmas formed by larger degrees of melting than their alkalic (group B-type) counterparts. On the basis of REE data and equilibrium batch melting models, Briggs and Goles (1984) determined that the basanites of the Okete field formed by 5% melting whereas, 12% melting generated the Okete hawaiite lavas. Smaller degrees of melting have been determined for the alkalic basalts of the Auckland field (0.6 – 4.0%) by Huang *et al.* (1997) and the Northland fields (~ 4%) by Heming (1980a), whereas the subalkalic magmas in Northland, and by inference Auckland, were derived by 15 – 20% melting (Heming, 1980a: Heming and Barnet, 1986). In addition, the major element and REE melting models for basalts from eastern Australia by Frey *et al.* (1978) have shown that alkali ol-basalts, basanites, and ol-nephelinites can be generated by 11, 6, and < 6% melting, respectively, of a garnet peridotite source while, ol-tholeiitic basalts formed by ≥ 20% partial melting and that garnet was not a residual phase.

Based on the findings of the experimental and petrological studies discussed here, it is suggested that the primary group A magmas were derived from a spinel peridotite source (e.g., KLB-1; 58% olivine, 25% orthopyroxene, 15% clinopyroxene, and 2% spinel; Hirose and Kushiro, 1993) by larger degrees of partial melting than the group B magmas, which were derived by relatively small degrees of melting of a garnet peridotite source (e.g., 60% olivine, 18% orthopyroxene, 14% clinopyroxene, 8% garnet; Green, 1973a).

Although it is envisaged that the SAVF volcanoes represent the eruption of distinct magma batches, dynamic partial melting may appear to be a more plausible mechanism than simple non-modal equilibrium batch partial melting. The dynamic melting model implies that partial melting is continuous, and therefore melt extraction takes place from a source that always contains a mixture of melt plus residue. Langmuir *et al.* (1977) argued that this model could account for the variations in La/Yb and the crossing REE patterns for the suite of basalts from the FAMOUS region of the Mid-Atlantic Ridge. The SAVF basalts exhibit similar REE features. In addition, K-Ar age and spatial data, and pressure estimates for melt segregation suggest that melting of the group A and B sources was continuous and occurred in different parts of each source region and at different depths. Since it appears that the magma batches were randomly derived from different parts of the system at different times, dynamic melting could account, in part, for the lack of

distinct geochemical trends for the group A and B lavas that would be expected for variable degrees of equilibrium batch partial melting of a homogeneous source.

The degree of melting required to produce the primary compositions of basanites SAB179 and SA05, nephelinite SAB135, ol-tholeiitic basalt SAB187, and hawaiite SA69 (Table 6.1) was derived by the dynamic melting inversion (DMI) method of Zou and Zindler (1996) and modified by Zou (1998, 2000). This method was used because (i) it is based on the concentration ratios of incompatible trace elements and REE (e.g., Th, La, Nd) of cogenetic magmas, (ii) modal melting compositions do not have to be assumed, and (iii) the degrees of partial melting and the composition of the source from which the magmas are derived can be calculated independently without assuming one in order to calculate the other. Other melting models for similar rock types, such as the one proposed by Briggs and Goles (1984) for the Okete basalts, require the assumption of either the degree of melting or source composition for what is usually the most primitive sample in the suite. The degrees of melting and source compositions for other samples within the suite are made relative to this sample. This approach is practical provided that the suite of lavas is derived from the same source, as is inferred for the Okete basalts. However, such a model would be inappropriate for the SAVF basalts because it is believed that groups A and B were derived from different sources.

Because the DMI method involves solving a system of non-linear equations with two unknowns by Newton's method, a MATLAB programme was written for use in this investigation to solve these equations[54]. Details of the DMI method and the MATLAB programme are presented in Appendix 8. The data given in Zou and Zindler (1996; Table 3) and Zou (2000; Table 3) were used to verify the accuracy of the MATLAB program. In each model, values for the degree of melting were within 5% of those given in Zou and Zindler (1996) and Zou (2000). Based on this degree of accuracy, the MATLAB program is considered to be an acceptable substitute of the original FORTRAN version (Zou, pers. comm. 2001). The criteria for the DMI method are summarised in Zou (2000). The model assumes a constant bulk distribution coefficient. The partition coefficients used to calculate the bulk distribution coefficients for the models are given in Table 6.2. An example of the calculations used to determine the degrees of melting and the source concentration of selected trace elements, based on results of the MATLAB programme, are given in Appendix 8.

[54] The original programme developed by Zou and Zindler (1996) to solve these equations was written in FORTRAN and was not available for use in this investigation.

Samples SAB187 and SAB179 were chosen for modelling purposes because they have the most primitive compositions of the group A and B lavas, respectively. They have the largest $100Mg/(Mg + Fe^{2+})$ values and Ni abundances thus requiring the least amount of olivine addition (3% and < 1% respectively) to derive their primary compositions. In addition, they have the smallest incompatible trace element and REE abundances of their respective group. Therefore, the degrees of partial melting required to produce them most likely reflect the largest amount of melting for their group. The group A sample SA69 and group B samples SA05 and SAB135 and were chosen because of their relatively primitive nature [i.e., requiring the addition of 11%, 8%, and 9% olivine, respectively, to obtain $100Mg/(Mg + Fe^{2+})$ values = 68] and they have larger incompatible trace element and REE abundances than their more primitive counterparts (SAB187 and SAB179), which suggests that their incompatible trace element and REE compositions are controlled to a large extent by variable degrees of partial melting. The smaller degrees of melting required to produce these compositions could be indicative of the least amount of melting for each suite.

The calculated degrees of melting and abundances for a number of incompatible trace elements and REE for the sources of these samples are presented in Table 6.3. The modelling results show that degrees of melting for the group A and B primary magmas are likely to vary by more than a factor of two over the range of 5 to 12% and 3 to 8% respectively. The degree of melting for basanite SA05 and SAB179, nephelinite SAB135, and ol-tholeiitic basalt SAB187 are consistent with the amount of melting predicted for similar rock types in the melting experiments cited above. The 5% melting for hawaiite SA69 seems small when compared to the estimated degrees of melting for the hawaiites from the Okete field (9 – 12%) by Briggs and Goles (1984), and those melts with similar major element compositions as SA69 formed by 11% melting in the experiments of Jaques and Green (1980). However, the melting experiments of Hirose and Kawamoto (1995) on KLB-1 show that the addition of 0.3 wt.% H_2O in the lherzolite source can generate a 7% partial melt at 10 kbar.

The calculated source compositions for the group A and B magmas are LILE- and HFSE-enriched relative to chondrite values. Olivine tholeiitic basalt SAB187, basanite SAB179, and nephelinite SAB135 have similar Rb, Sr, Zr, Ba, and Th concentrations but very different Nb and Ta, whereas hawaiite SA69 and basanite SA05 exhibit different degrees of enrichment from the other samples in their respective groups. The differences in Nb and Ta most likely reflect differences between the mantle source regions for groups A and B. The large variations exhibited by SA69 and SA05 could be related to source

heterogeneity, although mantle heterogeneity is not reflected in the isotopic compositions of either source. Another plausible explanation for these variations is the melting history of the source and its effect on the abundances of the incompatible trace elements and REE. In systems undergoing dynamic partial melting, some melts may be extracted from their immediate source while others are at various stages of continuous melting but have not segregated from the residue. This could result in localised enrichment or, in the case of SA69 and SA05, depletion in these elements relative to other magmas generated within the region (Langmuir *et al.*, 1977; Pearce and Norry, 1979).

Table 6.3 Calculated degrees of partial melting and mantle source compositions for selected group A and B basalts, South Auckland volcanic field. F = degree of partial melting, C_L = primary magma concentration; C_o = source concentration; $(C_o)_N$ = chondrite-normalised source concentration. Values for F and C_o are calculated from the Dynamic Melting Inversion (DMI) method of Zou and Zindler (1996) and Zou *et al.* (2000) referred to in the text. Chondrite values used in normalising the incompatible trace elements are from Sun (1980), and from Nakamura (1974) for REE.

	Group A						Group B								
Sample	ol-tholeiitic basalt SAB187			hawaiite SA69			basanite SAB179			basanite SA05			nephelinite SAB135		
	C_L	C_o	$(C_o)_N$	C_L	C_o	$(C_o)_N$	C_L	C_o	$(C_o)_N$	C_L	C_o	$(C_o)_N$	C_L	C_o	$(C_o)_N$
F	0.12			0.05			0.08			0.03			0.04		
Rb	11	1.15	3.28	12	0.54	1.54	20	1.42	4.07	22	0.58	1.65	35	1.31	3.73
Sr	306	34	3.07	326	18	1.65	575	41	3.76	857	23	2.05	853	32	2.93
Zr	128	17	2.52	139	13	1.87	213	18	2.66	286	15	2.21	281	17	2.51
Nb	15	1.57	4.48	16	0.74	2.11	45	3.24	9.25	52	1.57	4.48	66	2.71	7.75
Ba	101	11	2.86	119	5.09	1.34	198	14	3.75	242	6.35	1.67	331	13	3.30
Ta	1.36	0.15	7.39	1.00	0.05	2.55	3.4	0.25	13	3.2	0.12	5.83	4.92	0.22	11
Th	1.26	0.14	2.72	1.67	0.07	1.48	2.5	0.18	3.59	4.2	0.12	2.49	4.46	0.18	3.60
La	11	1.17	3.57	28	1.23	3.75	28	1.99	6.04	70	1.80	5.46	51	1.91	5.81
Ce	24	2.60	3.01	39	1.75	2.02	59	4.26	4.93	147	3.79	4.38	105	3.93	4.55
Pr	3.31	0.37	3.30	6.63	0.39	3.45	7.32	0.53	4.70	14	0.38	3.37	13	0.48	4.25
Nd	14	1.52	2.42	30	1.52	2.42	28	2.04	3.24	52	1.35	2.15	47	1.76	2.80
Sm	3.77	0.42	2.06	6.91	0.40	1.95	6.04	0.43	2.14	9.9	0.26	1.30	8.92	0.34	1.67
Eu	1.33	0.15	1.94	2.25	0.13	1.75	1.94	0.14	1.81	2.9	0.078	1.01	2.76	0.11	1.37
Gd	4.28	0.54	1.96	7.41	0.60	2.19	6.03	0.44	1.58	6.8	0.20	0.73	8.24	0.33	1.19
Tb	0.68	0.08	1.67	1.22	0.08	1.67	0.84	0.06	1.29	0.93	0.025	0.54	1.08	0.042	0.89
Dy	3.63	0.47	1.38	7.06	0.62	1.80	4.17	0.31	0.89	5.0	0.16	0.47	5.07	0.21	0.63
Ho	0.70	0.08	1.16	1.50	0.10	1.41	0.77	0.055	0.79	0.82	0.024	0.34	0.84	0.033	0.48
Er	1.70	0.22	0.97	4.11	0.35	1.55	1.82	0.14	0.60	1.9	0.069	0.31	1.88	0.085	0.38
Tm	0.24	0.03	1.04	-	-	-	0.24	0.019	0.62	-	-	-	0.23	0.011	0.38
Yb	1.50	0.18	0.82	3.1	0.22	1.01	1.49	0.11	0.52	1.2	0.047	0.22	1.31	0.063	0.29
Lu	0.22	0.03	0.77	-	-	-	0.20	0.016	0.49	-	-	-	0.18	0.010	0.29

The range of Sr abundances in the group A samples illustrates the importance of source heterogeneity in group A petrogenesis. The absence of negative Sr anomalies in the mantle-normalised trace element plots (see Fig. 5.12, p.158) suggests that Sr behaves incompatibly for the entire suite of group A lavas. This is evident from the similar degree of Sr enrichment relative to that of the other incompatible elements shown in Fig. 6.4 for

the same samples. This also suggests that regardless of the cause of the ratio variations between the group A lavas, plagioclase is unlikely to have been involved, to a large extent, in the petrogenesis of the group A lavas either as a residual phase in their mantle source or as a fractionating phase.

The calculated REE abundances show that the group A and B sources are LREE-enriched and have contrasting but larger LREE/HREE values than that of chondrites. The LREE abundances for the group A source range from 2.4 to 3.8 times the abundances for chondrites, whereas LREE in group B range from 2.5 to over 5 times that of chondrites. The group A source is generally more enriched in the MREE and HREE than the group B source with all MREE and some HREE abundances exceeding that of chondrites. In contrast, the group B source is depleted in some MREE and all HREE relative to chondrites with variations between samples indicative of source heterogeneity.

6.5 Fractional crystallisation

6.5.1 Qualitative observations

Although variable degrees of partial melting can account for the depletion in the incompatible trace elements and REE to a large extent, it cannot explain the depletion in the concentrations of the compatible trace elements such as Ni and Cr. Fifty-two centres in the SAVF erupted magmas with evolved compositions [i.e., $100Mg/(Mg + Fe^{2+})$ values < 68, MgO contents < 10 wt.%, Ni abundances < 300 ppm]. The lavas from the majority of these centres (18 of 27 for group A and 15 of 25 for group B) have $100Mg/(Mg + Fe^{2+})$ values ≤ 60, MgO contents between 6 and 9 wt.%, and relatively small Ni and Cr abundances (group A means = 156 ± 63 ppm and 265 ± 68 ppm respectively; group B means = 151 ± 62 ppm and 198 ± 85 ppm respectively). The various rock types from each group collectively show relatively strong progressive depletion of Ni and Cr with decreasing MgO (Fig. 5.9, p.152), which suggests that they are products of differentiated magmas that have undergone various degrees of fractional crystallisation. The minerals most likely to exert strong control on these trends are olivine and clinopyroxene, respectively.

Petrographic observations show that olivine and clinopyroxene are the dominant phenocryst phases in the majority of group A samples, and the only phenocryst phases in those from group B. The importance of olivine and clinopyroxene fractionation in the evolution of each group is illustrated by the positive correlations between the compatible

elements Ni, Cr, V, and Sc and MgO (Fig. 5.9)[55]. Olivine control is inferred because of its prevalence as a phenocryst phase in the majority of samples, it is a liquidus phase at 1 atm in all SAVF basalts except qz-tholeiitic basalts (*cf.* Green, 1973a), the strong partitioning of Ni into olivine, and the relatively good positive Ni-MgO correlations in groups A and B (r^2 = 0.78 and 0.93 respectively). Clinopyroxene fractionation is also inferred in each group based on the strong partitioning of Ni and Cr into clinopyroxene and the positive Cr-MgO correlations (r^2 = 0.68 and 0.83 for groups A and B respectively). Ewart *et al.* (1988) and Ewart (1989) concluded that comparable trends in suites of similar rocks from southeastern Australia are controlled predominantly by the fractionation of olivine and clinopyroxene. In addition, Ewart *et al.* (1988) and Ewart (1989) determined that notably small Ni and Cr abundances (e.g., < 100 ppm) together with small MgO contents (e.g., < 6 wt.%), such as those observed in a number of group A and B rock types requires extensive fractionation of these phases.

The positive correlations of V-MgO and Sc-MgO (r^2 = 0.91 and 0.81 respectively), CaO-MgO (r^2 = 0.91), and CaO/Na_2O-MgO (r^2 = 0.83; Fig. 6.7), and the negative correlation of Al_2O_3/CaO-MgO (r^2 =0.80; Fig. 5.7, p.149)[56] also support clinopyroxene fractionation in the group B rocks. In contrast, such trends are not apparent in the group A suite, which might be due to the large variability of clinopyroxene abundance among the group A rocks and also suggests that clinopyroxene was not the only CaO- and Na_2O-bearing fractionating phase in these rocks.

Petrographic observations, supported by mineral chemical analyses, suggest that Ca- and Na-bearing plagioclase is an additional fractionating phase in some group A rocks, although its effect is not clearly identified by the geochemical data shown in Figs. 5.6 (p.145), 5.12 (p.158), and 5.13 (p.161) or Fig. 6.7 as a critical fractionating mineral in these rocks. In addition, the absence of a strong negative Eu anomaly in the group A rocks (Fig. 5.13) suggests that plagioclase fractionation was not extensive. Kyle *et al.* (1992) noted that Eu depletion by feldspar fractionation ($K_{Eu}^{plag/melt}$ = 0.73; McKenzie and O'Nions, 1991) could be negated by the enrichment of Eu due to clinopyroxene fractionation ($K_{Eu}^{cpx/melt}$ = 0.31; McKenzie and O'Nions, 1991). However, the mantle-normalised incompatible trace element patterns of the group A rocks (Fig 5.12) lack the

[55] Concentrations of transition metals (e.g., Ni, Cr, V, and Sc) in basaltic melts significantly change during fractional crystallisation of olivine and clinopyroxene because of their highly compatible nature in these minerals (e.g., $K_{Ni}^{ol/melt}$ = 8.6, Takahashi, 1978; $K_{Cr}^{ol/melt}$ = 1.2, Beattie, 1994; $K_{Ni}^{cpx/melt}$ = 2.6, Mysen, 1978; and $K_{Cr}^{cpx/melt}$ = 3.8, $K_{V}^{cpx/melt}$ = 3.1, and $K_{Sc}^{cpx/melt}$ = 1.3, Hart and Dunn, 1993).

[56] Clinopyroxene is the dominant host for CaO and Na_2O in primitive, plagioclase-free parental magmas such as those for the group B rocks. CaO/Na_2O and Al_2O_3/CaO ratios are independent of olivine fractionation but very sensitive to clinopyroxene fractionation.

strong negative Sr anomaly that would be expected if fractionation of plagioclase (in which Sr is compatible, $K_{Sr}^{plag/melt}$ = 2.0; McKenzie and O'Nions, 1991) occurred on a large scale. In addition, the trend of increasing Al_2O_3 with decreasing MgO (Fig. 5.6) is inconsistent with plagioclase-dominated fractionation, indicating that the mineral assemblage olivine ± clinopyroxene ± plagioclase was very variable among the group A parent magmas. This is supported by modal abundance data (Appendix 3, Table 3.1), which shows the considerable range of clinopyroxene and plagioclase abundances in each group A rock type.

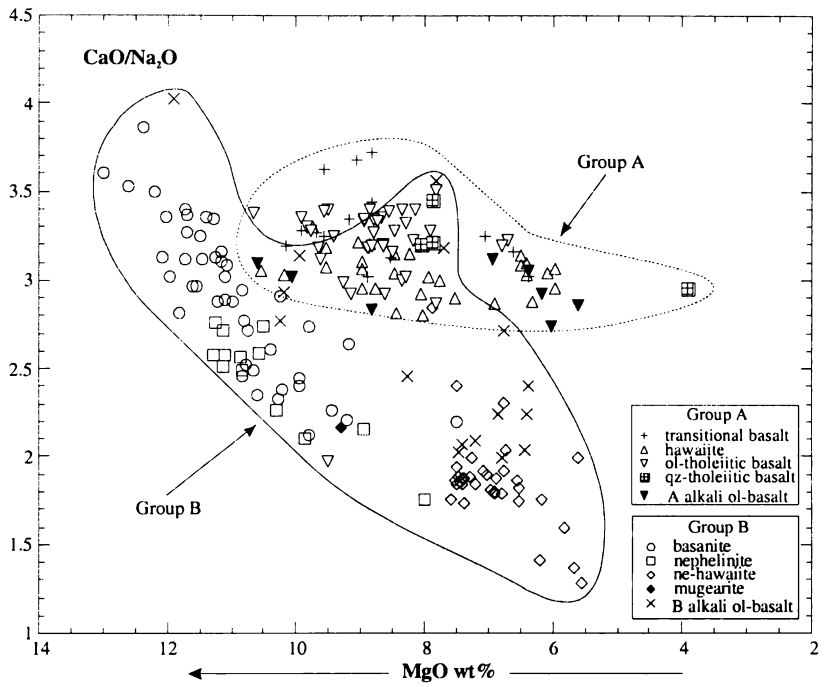

Fig. 6.7 CaO/Na_2O values vs. MgO for the group A and B lavas of the South Auckland volcanic field.

The Cr-titanomagnetite inclusions in olivine of most group A and all group B rock types, except mugearite, and titanomagnetite inclusions in the clinopyroxene of the group B rocks might have been fractionated together with their respective host phase, effectively depleting the residual liquids in Ni, Cr, Fe, and Ti[57]. The titanomagnetite microphenocrysts in many group A rocks could be an additional fractionating phase, although TiO_2 in these rocks show little correlation with MgO contents. However the modal abundance of the inclusions and microphenocrysts is typically very small[58] and fractional crystallisation models for similar rock types suggest that they would have only

[57] Ni, Cr, Fe, and Ti are strongly partitioned into magnetite and, by inference, Cr-titanomagnetite and titanomagnetite ($K_{Ni}^{magnetite/melt}$ = 31; Nielsen *et al.*, 1994, $K_{Cr}^{magnetite/melt}$ = 153; Schock, 1979, $K_{Fe}^{magnetite/melt}$ = 19.2 (for basaltic andesite); Okamoto, 1979, $K_{Ti}^{magnetite/melt}$ = 8; Nielsen *et al.*, 1994).

[58] Cr-titanomagnetite and titanomagnetite inclusions are typically << 1 modal %, and titanomagnetite is commonly < 1 modal % in the majority of group A rock types.

a nominal effect on magma compositions (e.g., Ewart, 1989; Briggs *et al.*, 1990; Kyle *et al.*, 1992).

The contrasting compositions of the primary magmas estimated for groups A and B (Table 6.1) indicate that each group evolved independently from distinct primary magmas. The geochemical trends of increasing SiO_2, Na_2O, and K_2O, and incompatible trace elements (e.g., Rb, Ba, Sr, Nb, Zr, La, and Ce) with decreasing MgO exhibited by the group B rocks (Fig. 5.6, p.145 and Fig. 5.10, p.154) suggests that their evolution includes fractional crystallisation of one or more parent magmas. The two distinct compositional trends in the suite of group B rocks, illustrated in Figs. 5.6 and 5.10, also suggest that they may have evolved as multiple lineages, analogous to those described by Coombs and Wilkinson (1969) for the silica-undersaturated lavas from the East Otago Volcanic Province, New Zealand.

The distinctive geochemical trends of group B are in marked contrast to the relatively weak trends of group A, which also suggests that each group evolved as a separate lineage. In addition, fractionation trends similar to those described by Ewart *et al.* (1988) and Ewart (1989) for alkali ol-basalts, transitional basalts, and ol-tholeiitic and qz-tholeiitic basalts from eastern Australia [e.g., values of $100Mg/(Mg + Fe^{2+})$ that positively correlate with decreasing degrees of silica-undersaturation; see Figure 5.2.3, p.192 of Ewart, 1989] are not apparent in the suite of similar rock types from group A. However, the wide range of $100Mg/(Mg + Fe^{2+})$ that characterises the group A lavas suggests that the majority of them were derived from more Mg-rich parental magmas. With the exception of the alkali ol-basalts, none of the group A rock types show a systematic trend that would suggest strong fractional crystallisation.

6.5.2 Quantitative modelling of fractional crystallisation

The qualitative data suggest the following hypotheses:

H1. The group A and B rocks evolved as separate lineages, and the various rock types within each group are genetically related by fractional crystallisation to distinct parent magmas.

H2. Fractional crystallisation is an important process in the evolution of the group A rocks based on the relatively strong positive correlations of the compatible trace elements, Ni and Cr, with MgO (despite the generally weak major and incompatible trace element trends exhibited by the suite of group A rocks).

H3. The group B rocks evolved as multiple lineages, each related to distinct parent magmas. Two major lineages consist of (i) silica-undersaturated basanites to less undersaturated basanites, and highly silica-undersaturated nephelinites to

less undersaturated basanites and nephelinites, and (ii) silica-undersaturated basanites to less undersaturated alkali ol-basalts and ne-hawaiites. These lineages are best illustrated in the incompatible trace element-MgO plots shown in Fig. 5.10 (p.154).

These hypotheses were tested quantitatively by a step-wise least-squares model, after Bryan *et al.* (1969) and modified by Stormer and Nicholls (1978) [59], for major elements, and mass balance calculations for selected compatible and incompatible trace elements using the equilibrium fractional crystallisation (Rayleigh fractionation) equation

$$C_l = C_i F^{(D-1)}$$

where C_l is the concentration of an element in the fractionated liquid, C_i is the concentration of an element in the parental magma, F is the melt fraction remaining during fractionation, and D is the bulk distribution coefficient for the element of interest. The mineral/melt partition coefficients used to calculate the bulk distribution coefficients are given in Table 6.2.

To explain the observed compositional trends satisfactorily by fractional crystallisation the following assumptions were made:

1. Each rock used as a parent magma represents an original liquid.
2. All phenocryst phases are in equilibrium with their host-rock composition.
3. The fractional crystallisation process is isobaric and occurred within a closed magmatic system.

Sample selection was restricted to the 26 samples chosen from each rock group for electron microprobe analyses[60]. The compositions of primary mantle-derived magmas and those primitive magmas not necessarily primary magmas form the basis of the fractional crystallisation models used here, which relate such compositions to those of possible "evolved" derivative magmas. Because none of the SAVF basalts represent primary compositions, the most primitive samples from each group were considered as possible parental magmas for their respective lineage. These include: alkali ol-basalt SA33, hawaiite SA32, ol-tholeiitic basalt SAB187, and transitional basalt SA13 from group A, and alkali ol-basalt SAB207 and basanites SA60, SAB179, SAB180, and SAB204 from group B. These samples generally have the largest $100Mg/(Mg + Fe^{2+})$ values (i.e., > 64) and compatible trace element abundances (i.e., Ni > 270 ppm and Cr > 300 ppm) in their respective groups (see Appendix 7, Tables A7.1 and A7.2). Each potential parent-

[59] The least squares computer programme, XLFRAC, of Stormer and Nicholls (1978) was modified for use in an EXCEL spreadsheet by J.P. Davidson and supplied by B.J. Hobden.
[60] These samples are listed in Appendix 6.

daughter pair was checked for similar incompatible trace element ratios (e.g., Ba/Rb, Ba/Nb, K/Rb, Zr/Nb), considered an indication of a possible genetic link by fractional crystallisation (Hart and Allégre, 1980; Briggs and McDonough, 1990).

Models were tested initially for major elements using the compositions of phenocryst cores and Cr-titanomagnetite inclusions in the proposed parental magma for each step. Models for which the calculated mineral proportions required to produce the derivative magma were geologically and mineralogically reasonable, and yielded $\sum r^2 < 0.2$ were accepted[61]. These models were mass balance tested to calculate trace element abundances predicted for the daughter magma. To test the validity of the model, the calculated abundances were compared with those observed in the daughter magma. An acceptable model was considered to be one that satisfies the major element and trace element variations exhibited by the suite of group A and B rocks.

The following were undertaken to test the hypotheses H1 – H3 respectively:

1. A variety of combinations of the available samples with the most primitive compositions from groups A and B was evaluated to identify a possible genetic link between the lavas in each group that resulted from fractional crystallisation processes after melt segregation. The aim was to determine if the less Si-undersaturated group A lavas represent residual melts from a more Si-undersaturated group B parental magma.

2. Numerous combinations were tested to model the range in geochemical compositions that define the group A lineage and identify distinct fractionation sequences within it using the step-wise least-squares modelling technique. Because of the large sample size, a large number of combinations of parental, intermediate, and evolved daughter magma compositions were available. One possible fractionation sequence for group A consists of: alkali ol-basalt SA33 → hawaiite SAB151 → qz -tholeiitic basalt SA77→ ol-tholeiitic basalt SAB169). The aim was to determine if selected parental magmas could generate the various rock types identified in group A (e.g., can parental alkali ol-basalts generate hawaiite or tholeiitic compositions).

3. The above procedure was repeated for the major lineages in group B to determine if they represent distinct fractionation sequences. Possible sequences for these lineages consist of: basanite SAB179 → nephelinite SAB135 → nephelinite SA28; and alkali ol-basalt SAB207 → basanite SAB102 → ne-hawaiite SA02 → ne-hawaiite SA65).

[61] Values of $\sum r^2$ (sum of squares of oxide residuals) used to identify acceptable least-squares models are not clearly defined. Reported $\sum r^2$ values for modelling basalts similar to those from the SAVF range from < 0.1 (e.g., Kyle *et al.*, 1992) to < 1.0 (e.g., Briggs and McDonough, 1990). In the case of the SAVF basalts, models that yield $\sum r^2 < 0.2$ provided the most geologically and mineralogically reasonable results. In many models, numerically acceptable solutions were obtained but required the addition of various mineral phases to the parent magma. These solutions were rejected because such additions are inconsistent with the modal mineralogy of the parent rock, and therefore suggest that fractional crystallisation is not the sole process relating the proposed parent-daughter pair.

Results of major element modelling

Models that tested the first hypothesis yielded large discrepancies between the major element oxides, and values of $\Sigma r^2 >> 1$. These results support the hypothesis that the group A and B lavas are not genetically related. They also support the isotopic and geochemical evidence previously discussed and the compositional data for the primary magmas of each group.

Table 6.4 Crystal fractionation models for the group A and B rocks of the South Auckland volcanic field.

	Group A						**Group B**			
	Step 1		Step 2		Step 3		Step 1		Step 2	
	alkali ol-basalt SA33 to alkali ol-basalt SA18		alkali ol-basalt SA18 to alkali ol-basalt SA19		alkali ol-basalt SA19 to alkali ol-basalt SAB159		basanite SAB179 to basanite SA37		basanite SA37 to basanite SA12	
	(observed)	(calculated)	(observed)	(calculated)	(observed)	(calculated)	(observed)	(calculated)	(observed)	(calculated)
SiO_2	47.20	47.36	47.64	47.70	47.40	47.27	43.53	43.61	43.73	43.89
TiO_2	2.28	2.44	2.61	2.77	2.99	3.23	2.76	2.89	2.83	2.91
Al_2O_3	13.98	14.71	15.23	16.27	15.98	16.56	12.60	13.18	13.69	14.80
FeO_T	13.71	11.96	13.28	11.26	13.32	12.87	13.86	13.71	14.04	14.48
MgO	8.74	8.85	6.88	7.30	5.91	5.42	11.58	10.31	9.34	7.09
CaO	9.37	9.58	9.99	9.76	9.62	9.76	10.53	10.82	9.73	8.96
Na_2O	3.30	3.37	3.20	3.22	3.26	3.60	3.37	3.55	4.29	4.95
K_2O	0.91	0.96	0.82	0.84	1.02	1.07	1.15	1.21	1.61	1.87
P_2O_5	0.50	0.77	0.36	0.88	0.49	0.21	0.61	0.73	0.74	1.04
Total	100.00	100.00	100.00	100.00	99.99	99.99	99.99	100.01	100.00	99.99
	$\Sigma r^2 = 0.05$		$\Sigma r^2 = 0.10$		$\Sigma r^2 = 0.08$		$\Sigma r^2 = 0.19$		$\Sigma r^2 = 0.15$	
Subtracted phases wt.%										
Olivine		5.2		6.1		2.1		4.1		6.0
Clinopyroxene		2.4		1.9		5.6		1.0		11.0
Plagioclase		1.4		0.3		3.8		-		-
Cr-titanomagnetite		-		-		-		0.02		0.4
% Crystallised		9.0		8.3		11.5		5.1		17.4
% melt fraction remaining		91.0		91.7		88.5		94.9		82.9
Trace-element calculations										
	SA18 (observed)	SA18 (calculated)	SA19 (observed)	SA19 (calculated)	SAB163 (observed)	SAB163 (calculated)	SA37 (observed)	SA37 (calculated)	SA12 (observed)	SA12 (calculated)
Sc	20	24	24	20	19	24	23	30	19	24
V	228	213	254	220	256	243	277	284	243	241
Cr	242	272	210	152	55	71	342	337	288	255
Ni	173	134	66	109	40	30	268	264	166	117
Rb	15	12	11	16	11	12	19	18	27	23
Ba	375	136	145	406	148	164	247	242	299	299
Th	4.7	3.0	3.0	5.0	2.9	3.4	6.6	4.7	8.5	8.0
Nb	29	22	16	31	22	18	57	42	59	69
La	30	20	15	32	20	17	49	36	55	59
Ce	70	53	47	76	49	53	105	68	121	126
Sr	585	447	450	632	534	507	717	634	901	856
Zr	177	172	167	191	188	188	275	220	332	328
Y	23	23	23	25	23	26	27	23	27	31

The models for hypotheses 2 and 3 produced only one fractionation sequence each for groups A and B, and neither sequence consists of a range of the lavas found within these groups. The group A sequence consists entirely of alkali ol-basalts: SA33 → SA18 → SA19 → SAB159.

Hypothesis 3 proposed two major lineages for group B. Models of the first lineage produced a single sequence consisting entirely of basanites; SAB179 → SA37 → SA12 (note that the parent-daughter pair SAB179 and SA37 is from the same deposit – Barriball Tuff Ring). Attempts to model the second lineage defined by the alkali ol-basalt – basanite – ne-hawaiite sequence proved unsuccessful. Modelling results for each sequence are presented in Table 6.4 and illustrated in Fig. 6.8.

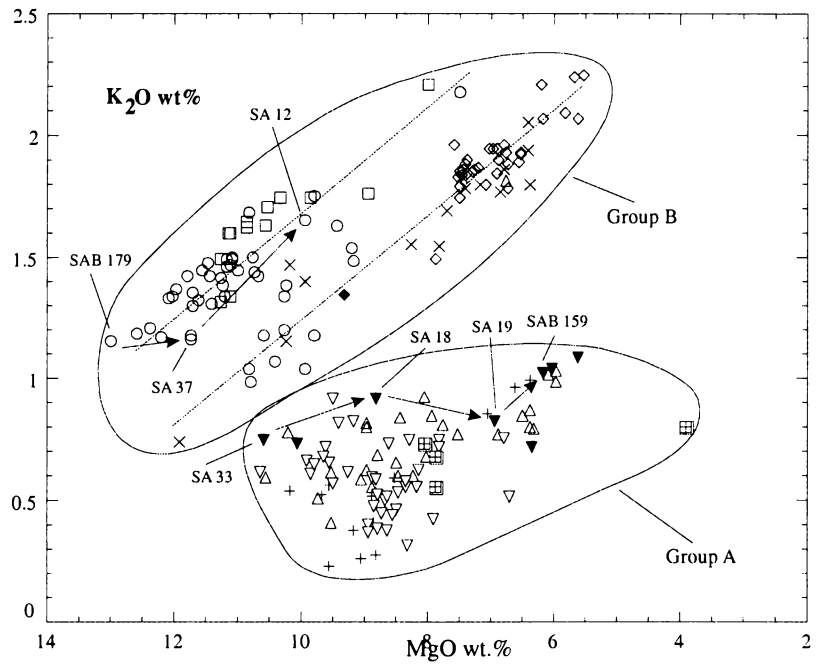

Fig. 6.8 Parent-daughter pairs (joined by the arrows) for the sequence of group A and B lavas based on least-squares approximation models. The dashed lines illustrate the two major lineages in the group B rocks referred to in the text. Symbols as in Fig. 6.7.

All other models of prospective sequences for hypotheses 2 and 3 yielded unacceptable results after the first step irrespective of (i) the large number of combinations of prospective parental, intermediate, or evolved daughter magmas tested, (ii) the selection of potential parent-daughter pairs with similar incompatible trace element ratios, and (iii) incorporation of the range of mineral compositions available for prospective parent magmas. The majority of these models generally resulted in large residuals of FeO, MgO, CaO, Na_2O, K_2O, and P_2O_5, $\Sigma r^2 > 0.2$, or yielded mineralogically unacceptable results

(i.e., the removal of a mineral phase from the parental magma in excess of that considered reasonable for its observed modal abundance).

The models for the group A sequence indicate that olivine and clinopyroxene are the main fractionating phases in Steps 1 and 2 with olivine the dominant phase and plagioclase a minor phase in each step, whereas clinopyroxene and plagioclase are the dominant phases in Step 3. In each step, the fractionating phases and the proportions in which they are removed from the parental magma are consistent with their observed modal abundances. Although titanomagnetite is a minor fractionating phase in the parental magmas for Steps 1 and 3, its inclusion in these steps yielded unsatisfactory results ($\sum r^2 > 1$), which indicates that titanomagnetite is not required as a fractionating phase to derive each of the daughter magmas.

For the basanites in the group B sequence, Cr-titanomagnetite was also fractionated (albeit in very minor amounts) in addition to the main phenocryst phases, olivine and clinopyroxene. As with the group A sequence, this is also consistent with the modal abundances of these phases in the parental magmas.

Results of trace-element modelling

The results of trace element modelling are given in Table 6.4 and the degrees of fit for selected compatible and incompatible trace elements in each step for the group A and B sequences are shown in Fig. 6.9. In the group A sequence, the trace element modelling failed to reproduce closely the observed daughter trace element abundances in Steps 1 and 2 with notably poor fits for the majority of elements, especially Ba, which range up to 75 % from the observed daughter values. For Step 3, the majority of trace elements exhibit marginal fits, with Sc, Cr, and Ni the notable exceptions, ranging up to 25 % outside the observed daughter values. In contrast, the predicted trace element abundances in each of the daughter magmas in the group B models are similar to their measured values with the exception of Th, Nb, La, and Ce in Step 1 and Ni in Step 2, which range up to 30 % lower than measured daughter abundances. Predicted Sc abundances exceed measured values by up to 20 % in each step.

Discussion

Qualitative observations suggest that fractionation of olivine and clinopyroxene could account for the geochemical variations of the basalts in the group A and B lineages. However, the overall poor results of step-wise least-squares modelling and mass balance calculations indicate that there is no adequate way to relate the lavas of group A to those

of group B or the various rock types within each group to one another solely by fractional crystallisation processes. Nevertheless, these results do not rule out fractional crystallisation as an important process in the evolution of the group A and B lavas because unacceptable models do not necessarily prove that fractional crystallisation was not an effective process, only that it is not mathematically realistic. For example, the importance of olivine fractionation in the evolution of the group A and B lavas is illustrated by the Ni-MgO data plotted on the olivine fractionation curves of Hart and Davis (1978) shown in Fig. 6.10.

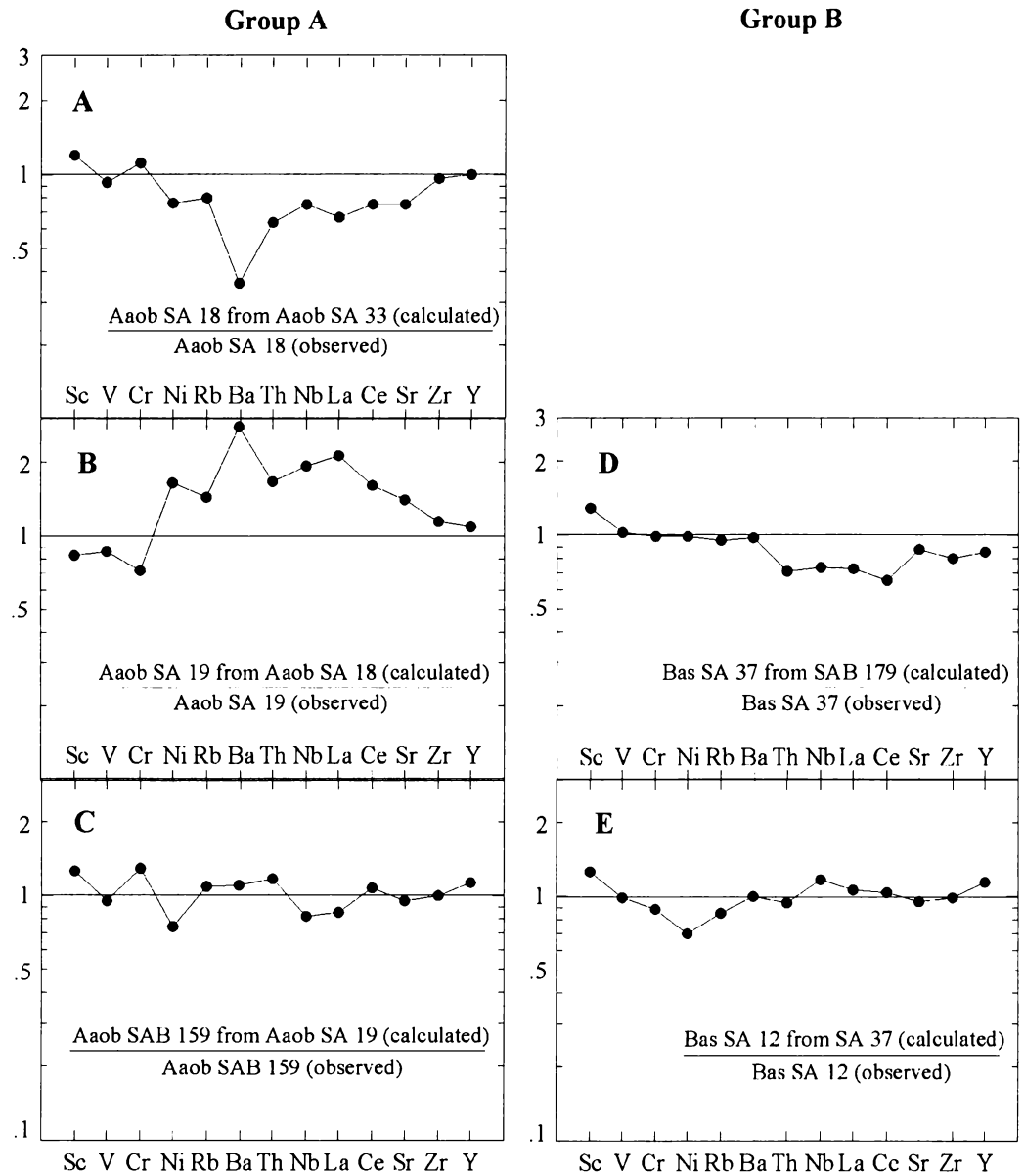

Fig. 6.9 The degree of fit for selected trace elements in each step of the fractional crystallisation sequence of the group A and B magmas discussed in the text. Incompatible trace elements are arranged in the order of increasing degree of incompatibility similar to that used in the mantle-normalised trace element plots shown in Fig. 5.12. Each point represents the ratio between the predicted trace element abundance in the daughter magma (calculated by the Rayleigh equation using its parent magma) and the observed (XRF-derived) abundance in the daughter magma. The solid lines represent the ideal trace element fit between parent-daughter pairs, defined as a ratio of one. Aaob = group A alkali ol-basalt; Bas = basanite.

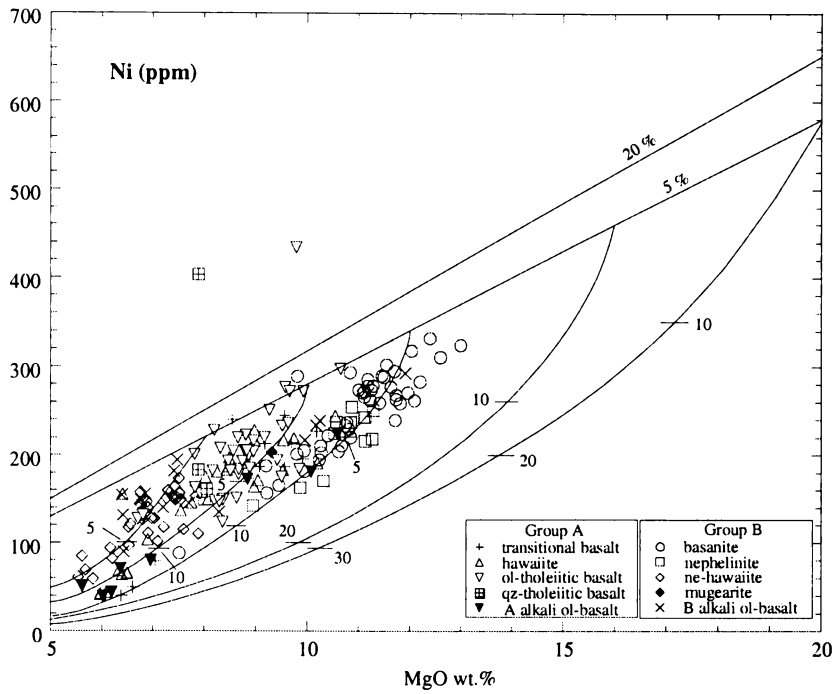

Fig. 6.10 The Ni-MgO relationships for each rock type from groups A and B, South Auckland volcanic field, superimposed on the batch partial-melting and olivine-fractionation trajectories of Hart and Davis (1978). The straight diagonal lines labelled 5% and 20% are for batch partial melts for an assumed peridotite source containing 2300 ppm Ni. Each fractionation curve starts at the 5% melting curve at initial liquids containing 8, 10, 12, 16, and 20 wt.% MgO. The numbers on these curves represent percentages of olivine crystallisation.

The trajectory that originates at the 12 wt. % MgO – 5 % partial melting intercept is dominated by the progressive decrease in Ni and MgO from basanites to nephelinites. This suggests that although not proven by the fractional crystallisation models, the first part of hypothesis 3 may be valid – less silica-undersaturated basanites are derived from a near-primary, highly silica-undersaturated basanite, and less silica-undersaturated basanites and nephelinites are derived from near-primary nephelinites.

The trajectory originating at the 8 wt. % MgO – 5 % partial melting intercept is dominated by alkali ol-basalts and ne-hawaiites. The notable feature of this trend is the absence of near-primary basanites from which these magmas could have been derived as suggested by the second part of hypothesis 3 (i.e., the alkali ol-basalts and ne-hawaiites represent residual liquids of a fractionated basanite parental magma). In addition, the restriction of the ne-hawaiites to the lower Ni-MgO region is suggestive of extensive olivine fractional crystallisation at relatively low pressures. The experimental studies of Irving and Green (1972) demonstrated that ne-hawaiites could be produced by the fractionation of olivine and kaersutite from a basanitic magma at pressures between 13 and 15 kbar, which is consistent with the estimated clinopyroxene crystallisation pressures of some ne-hawaiite samples (see Table 4.17, p.94). Although kaersutite was not observed in thin section in any of the SAVF samples, Rafferty and Heming (1979)

reported kaersutite megacrysts in some alkaline basalts and tuff deposits. However, the presence of harzburgite and lherzolite xenoliths in ne-hawaiites (Sanders, 1994) argues against significant fractional crystallisation at shallow levels in their evolution, although the presence of such xenoliths does not preclude olivine ± Cr-titanomagnetite + clinopyroxene fractionation prior to xenolith entrainment. Alternatively, it is possible that these samples represent residual liquids of low-MgO primary melts with relatively low Ni abundances, and therefore the Ni and MgO contents of the ne-hawaiites and some group B alkali ol-basalts is a feature of their source characteristic as opposed to a consequence of fractional crystallisation. Zhi *et al.* (1990) argued that lavas of the Hannuoba basalts, China, that are poorer in Ni and MgO, and similar to those from the SAVF, could be products of parental magmas derived from sources with comparatively small Ni and MgO contents, e.g., a veined pyroxenite-garnet lherzolite mantle.

The majority of group A lavas plot between the trajectories that originate at the 8 and 10 wt. % MgO – 5 % melting intercepts indicating that they were derived from magmas that have undergone between 5 and 10% olivine fractionation, although the scatter in these data suggests that clinopyroxene was probably an important fractionating phase.

There are a number of possible reasons for the poor modelling results, some of which are discussed below:

1. The models assumed crystal-melt equilibrium for all fractionating phases. However, olivine–host-rock disequilibrium is a common feature in most group A and many group B samples (Table 4.7, p.59 and Fig. 4.6, p.58).

2. The models assumed that fractional crystallisation processes operated in a closed system under isobaric conditions. The pressure and temperature data for the principal phases, olivine and clinopyroxene, discussed in Chapter 4, indicate that these phases commonly crystallised over a range of temperatures under polybaric conditions, not only for crystals from different samples but among crystals within the same sample.

3. The discrepancies in the mass balance calculations illustrated in Fig. 6.9 could be due to the sensitivity of the Rayleigh equation to the mineral/melt partition coefficients selected for each trace element. Briggs and Goles (1984), Briggs (1986), and Briggs *et al.* (1990) demonstrated that reduction in the discrepancies between observed and calculated abundances for the compatible trace elements (e.g., Ni, Cr, and V) could be achieved by selecting alternative partition coefficient values.

4. Although the fractionation of olivine and clinopyroxene probably accounts for the range of observed compatible trace elements, the fractionation of these phases most likely had little effect on the incompatible trace element abundances. This is regardless of the partition coefficient chosen when considering that at relatively large residual melt fractions such as those shown in Table 6.4 (i.e., $F > 83$ %), the distribution coefficients for such elements is very small (e.g., $<< 0.1$; see Cox *et*

al., 1979, Fig 14.1, p.341). Furthermore, even if the partition coefficients are set to zero, large discrepancies still occur between measured and observed values. Therefore, the discrepancies observed in the SAVF models are not merely a function of the choice of partition coefficients. Variable degrees of partial melting affect the behaviour of the highly incompatible elements shown in Fig. 6.9, resulting in decreasing abundances with increasing degrees of melting, but generally has little effect on trace elements such as Sc, V, Ni, and Cr because of their highly compatible nature. This suggests that the whole-rock compositions were controlled to some extent by varying degrees of partial melting.

5. The large variations of Ba and Rb in Steps 1 and 2 of the group A models, shown in Figs. 6.9 A and B, could be due to their mobility during post-eruption alteration, although the calculated and observed abundances of Y, which has been shown to be highly mobile during weathering processes (Price *et al.*, 1991), exhibit values of $Y_{calc}/Y_{obs} \sim 1$ in these models. Discrepancies in Th may also be suspect because of the large XRF analytical errors (relative standard deviation for Th = 27.4).

6. The limited geochemical variation exhibited by the suite of group A lavas argues against extensive fractional crystallisation. They also have larger Al_2O_3/CaO values than those of the group B lavas, but lack of Al_2O_3/CaO-MgO correlation and the absence of modal clinopyroxene and/or calcic plagioclase in a large number of group A samples suggests that differences in Al_2O_3/CaO are source-related rather than due to processes such as fractional crystallisation (Frey *et al.*, 1978; Clague and Dalrymple, 1988; Zhi et al., 1990; Gardner, 1994; Jung and Masberg, 1998).

7. There are no apparent REE fractionation trends between groups A and B or among the various rock types within each group with increasing differentiation (see Fig. 5.13, p.161). If individual members of a suite of SAVF lavas are related by fractional crystallisation then REE abundances should uniformly increase with progressive differentiation throughout the sequence resulting in consistent subparallel REE patterns. The contrasting slopes between the group A and B rocks and irregular REE patterns suggest that it is unlikely that the SAVF lavas were fractionated from a common parental magma.

8. Most, perhaps all, group A and B lavas are derived from distinct parental magmas, each with unique petrological characteristics. Therefore, it is unlikely that the geochemical trends exhibited by the suites of group A and B lavas represent the liquid line of descent that would be expected for lavas derived from a single parental magma.

6.6 Evaluation of crustal contamination

The alkali basaltic lavas erupted in the various intraplate fields of North Island, New Zealand, summarised in section 2.6 are generally considered essentially uncontaminated by the continental crust (Briggs and Goles, 1984; Heming and Barnet, 1986; Briggs and McDonough, 1990; Briggs *et al.*, 1990; Huang *et al.*, 2000). Their relatively small $^{87}Sr/^{86}Sr$ values (< 0.7035) and positive ε_{Nd} values (> +4) argue against a large-scale crustal influence in their genesis or during their ascent through the lithosphere to the

surface. However, studies of continental intraplate volcanics elsewhere (e.g., the Laacher See Province, Wörner *et al.*, 1985; eastern Australia, Ewart *et al.*, 1988; Vietnamese basalts, Nguyen *et al.*, 1996; the Newer Volcanic Province, McBride *et al.*, 2001) have shown that magma compositions can be affected by (i) bulk assimilation of crustal material – incorporation of wall rock material into magma as it ascends to the surface, and (ii) assimilation and fractional crystallisation (AFC; DePaolo, 1981) – assimilation of melted crustal material into a mafic magma during ongoing fractional crystallisation processes. Given the distinct geochemical characteristics of the SAVF basalts compared with those from the other intraplate fields of North Island, important questions regarding crustal contamination as it relates to the SAVF basalts are: (1) to what extent are the dissimilarities in compositions observed between and among the group A and B lavas the result of interaction with the crust or merely a reflection of the heterogeneity of their mantle sources, and (2) are the group A magmas derived from group B magmas through the assimilation of crustal material.

Table 6.5 Incompatible trace element, SiO_2, and Sr and Pb isotopic data used to evaluate the possible effects of assimilation of the Murihiku and Waipapa Terranes on the compositions of the group A and B magmas referred to in the text. Incompatible trace element and SiO_2 data for the Murihiku Terrane are from Middleton (1993) and the Waipapa Terrane from N. Mortimer (unpublished). Sr and Pb isotopic compositions for the Waipapa Terrane are from Graham *et al.* (1992). All data are mean values ± 1 standard deviation.

	Murihiku	Waipapa	Group A	Group B
SiO_2 wt.%	63.03 ± 8.85	63.99 ± 3.05	49.03 ± 1.20	45.33 ± 2.16
K (ppm)	20503 ± 7053	19184 ± 7387	5546 ± 1874	13377 ± 2610
Rb (ppm)	74 ± 36	68 ± 28	10 ± 4	27 ± 6
Pb (ppm)	19 ± 4	18 ± 5	3.1 ± 1.5	4.6 ± 1.3
Ce/Pb	2.7 ± 0.5	2.9 ± 1.5	12 ± 5	25 ± 7
$^{87}Sr/^{86}Sr$	-	0.70718[1]	0.703025 ± 0.00014	0.702832 ± 0.00011
$^{206}Pb/^{204}Pb$	-	18.788 ± 0.032	19.119 ± 0.111	19.273 ± 0.035

[1]Standard deviation was not given.

Petrographic observations show that a number of SAVF samples contain quartz and quartzofeldspathic xenoliths and evidence of their incorporation into the magma. This suggests that the compositions of some magmas may have been modified by the assimilation of crustal material. Strontium and Pb isotopic data and the abundances of a number of incompatible trace elements (e.g., K, Rb, and Pb) can be used to identify possible effects of crustal contamination on SAVF basalts because the upper crustal rocks in the South Auckland region – the Murihiku and Waipapa Terrane metasediments – are enriched in these elements and have larger $^{87}Sr/^{86}Sr$ and smaller $^{206}Pb/^{204}Pb$ and Ce/Pb values relative to the SAVF basalts (Table 6.5). In addition, because Ce/Pb in mafic magmas is generally unaffected by fractional crystallisation or partial melting, suites of continental intraplate magmas derived from such sources that have been variably

contaminated by the crust might be expected to show Ce/Pb values that trend towards crust-like compositions and strong negative $^{87}Sr/^{86}Sr$-Ce/Pb correlations.

6.6.1 Crustal contamination by bulk assimilation

The OIB-like geochemical characteristics of the group B lavas and the occurrence of ultramafic xenoliths in a number of samples, especially those with relatively primitive compositions, e.g., $100Mg/(Mg + Fe^{2+}) > 60$, indicates that these magmas ascended rapidly through the lithosphere. Their strong silica-undersaturated nature, large OIB-like Ce/Pb values (25 ± 7 ppm) (Fig. 6.11), negative Pb anomalies (Fig. 5.12, p.158), and lack of SiO_2-$^{87}Sr/^{86}Sr$ correlation (Fig. 6.12), together with the presence of the xenoliths indicate that they arrived at the surface largely uncontaminated by the assimilation of high SiO_2, and high $^{87}Sr/^{86}Sr$ and Pb components such as crustal-derived material. Sanders (1994), however, concluded that the ultramafic xenoliths found in the SAVF basalts represent accidental fragments derived from an upper mantle source between 15 and 17 kbar.

In contrast, the group A basalts have relatively small Ce/Pb values (12 ± 5 ppm) that trend towards those of the Murihiku and Waipapa metasediments (Fig. 6.11), a feature also exhibited by their $^{206}Pb/^{204}Pb$ compositions (Fig. 5.17A, p.169). In addition, although the group A lavas do not exhibit strong negative Ce/Pb-$^{87}Sr/^{86}Sr$ correlation (Fig. 6.12) that would be expected for large-scale crustal assimilation, they do show a broad trend of decreasing Ce/Pb with increasing $^{87}Sr/^{86}Sr$, and some samples of each group A rock type exhibit strong positive Pb anomalies (Fig. 5.12, p.158), indicating the possible influence of a crustal component.

The larger $^{87}Sr/^{86}Sr$ values of the group A rocks may reflect minor amounts of crustal contamination. In addition, the group A lavas have Pb isotopic compositions that trend towards the Waipapa Terrane basement rocks and the offshore TVZ sediments (see Fig. 5.17, p.169) and have large Δ7/4 values compared with those of group B (see Tables 5.13 and 5.14, pp.164 and 165), features that may be indicative of crustal contamination rather than contrasting mantle source characteristics.

To assess the effects of crustal contamination by bulk assimilation, a number of binary mixing models (after Faure, 1986; pp.141-151) were tested using the average $^{87}Sr/^{86}Sr$ and $^{206}Pb/^{204}Pb$ compositions and Pb and Sr abundance of the Waipapa metasediments

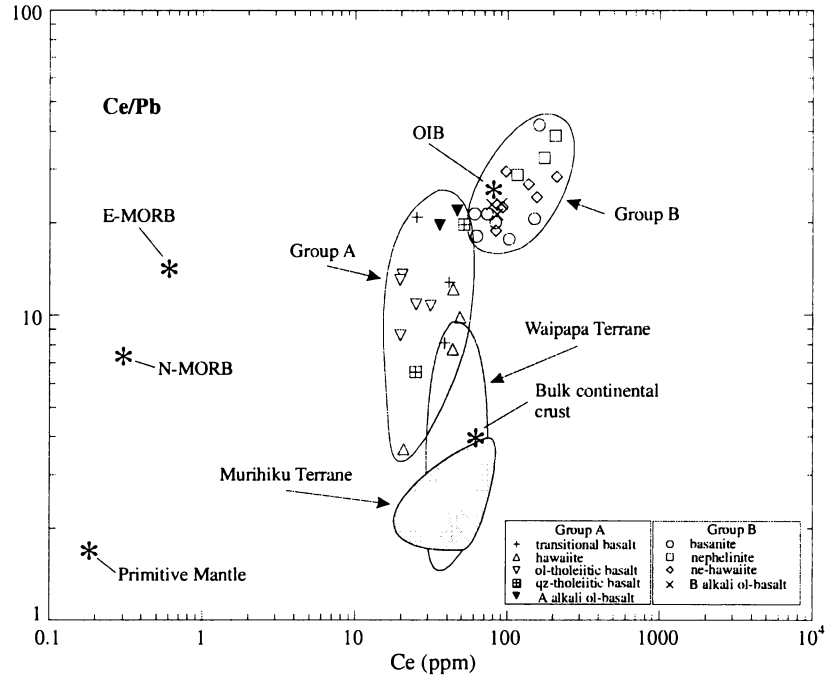

Fig. 6.11 Ce (ppm) vs. Ce/Pb for the group A and B lavas of the South Auckland volcanic field and the Waipapa Terrane (light shaded area), which underlies the SAVF east of the Drury Fault, and the Murihiku Terrane (dark shaded area), which underlies the SAVF west of the Drury Fault (see Fig. 2.4, p.16). Shown for comparison are plots of average Ce (ppm) contents vs. Ce/Pb values (stars) for the Primitive Mantle, E-type MORB, N-type MORB, and OIB (Sun and McDonough, 1989), and bulk continental crust (Wedepohl, 1995).

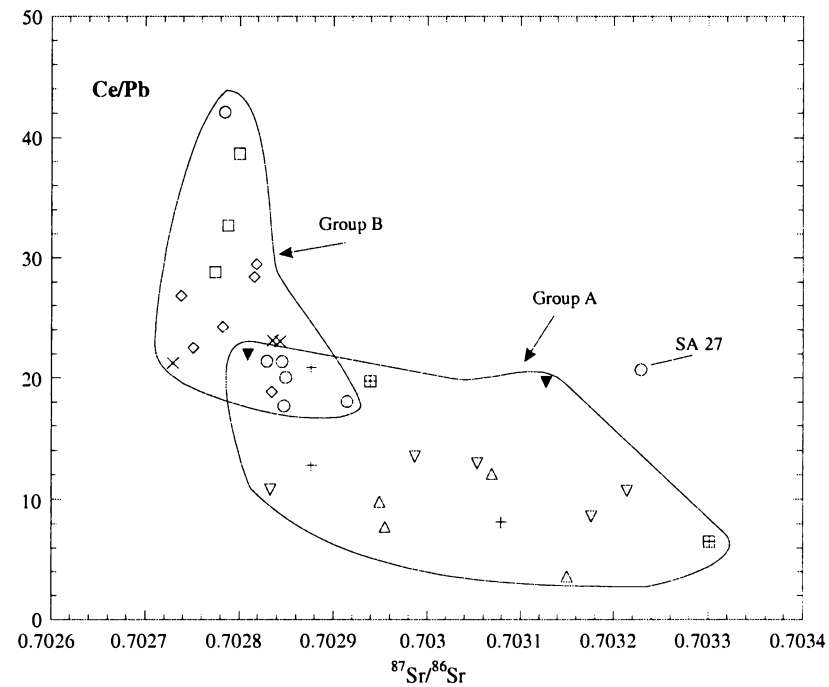

Fig. 6.12 $^{87}Sr/^{86}Sr$ vs. Ce/Pb for selected group A and B lavas, South Auckland volcanic field. Symbols as in Fig. 6.11

(Table 6.5)[62] together with a variety of group A and B samples as end-members to derive a SAVF basalt with relatively large $^{87}Sr/^{86}Sr$ and small $^{206}Pb/^{204}Pb$ values. For example, to produce ol-tholeiitic basalt SAB174 ($^{87}Sr/^{86}Sr$ = 0.703176 and $^{206}Pb/^{204}Pb$ = 18.950) required the mixing of 91% basanite SA179 ($^{87}Sr/^{86}Sr$ = 0.702845, $^{206}Pb/^{204}Pb$ = 19.221, Sr = 581ppm, and Pb = 2.8 ppm) with 9% melt derived from the Waipapa. This result was further tested by major element mass balance calculations. These calculations revealed large discrepancies in a number of the major elements between the end-member SAB179 and the mixing product SAB174, most notably in Al_2O_3 (18%), MgO (26%), K_2O (71%), and P_2O_5 (58%). Similar results were produced when other low-SiO_2, low-$^{87}Sr/^{86}Sr$ group B samples were mixed with the Waipapa, which suggests that the geochemical characteristics of the less Si-undersaturated group B and all group A magmas were not acquired via the mixing of relatively primitive group B-like magmas with the regional basement rocks.

An alternative model was tested which considered mixing the primitive, less Si-undersaturated group A ol-tholeiitic basalt SAB187 ($^{87}Sr/^{86}Sr$ = 0.702833, Sr = 315 ppm) with the Waipapa to produce SAB174. The results of the model and major element mass balance calculations show that a mix with ~ 5% Waipapa melt was required to produce SAB174. However, this also resulted in large differences in MgO (13%), K_2O (48%), and P_2O_5 (14%). Assuming that SAB174 represents a discrete magma batch, these results suggest that the incorporation of large amounts of basement rock did not occur in the group A magmas while en route through the crust.

6.6.2 Evaluation of contamination by AFC

Because the basement rocks of the South Auckland region have large SiO_2 contents and Sr isotopic compositions relative to the group A and B lavas, variable contamination by this material during magma fractionation might be expected to show relatively strong positive SiO_2-$^{87}Sr/^{86}Sr$ correlations. In addition, Price *et al.* (1997) hypothesised that trends such as these could be an indicator of the effectiveness of crustal contamination on controlling the geochemical variations from alkalic to tholeiitic compositions. In Fig. 6.13 SiO_2 is plotted against $^{87}Sr/^{86}Sr$ for the group A and B lavas. The diagram shows a relatively broad positive correlation between SiO_2 and $^{87}Sr/^{86}Sr$ values, especially from the nephelinites and basanites to a number of hawaiites and ol-tholeiitic basalts, indicating

[62] Because of the absence of Sr, Nd, and Pb isotopic data for the Murihiku Terrane, only Waipapa Terrane data has been used in these mixing models. The arguments presented here however, should be relevant for both Terranes given the geochemical characteristics of the upper continental crust as reported in Wedepohl (1995).

that while some magmas fractionated without associated crustal contamination, AFC processes may have affected others.

The importance of fractional crystallisation in the evolution of the various rock types within groups A and B has been discussed in section 6.3. If assimilation of upper or lower crustal material was accompanied by fractional crystallisation then those lavas with evolved compositions, e.g., basanite SA27, ne-hawaiite SA25, and alkali ol-basalt SAB162 with comparatively small 100Mg/(Mg + Fe^{2+}) values of 53, 52, and 53 respectively, are probably most likely to show the effects of AFC processes (DePaolo, 1981; Kinzler *et al.*, 2000), e.g., positive $^{87}Sr/^{86}Sr$-K and $^{87}Sr/^{86}Sr$-Rb correlation. With the exception of SA27, which exhibits qualitative evidence for AFC modification, the $^{87}Sr/^{86}Sr$-K and $^{87}Sr/^{86}Sr$-Rb plots shown in Fig. 6.14 suggest that this is not the case for the SAVF basalts. The broad range of K and Rb abundances in the group B lavas decrease markedly over a very narrow range of $^{87}Sr/^{86}Sr$ values. In contrast, the group A lavas have the lowest abundances of these elements that decrease slightly over a broader range of increasing $^{87}Sr/^{86}Sr$ values. These trends are opposite to that expected had high K- and Rb-bearing material such as the Murihiku (K = 20530 ± 7053 ppm, Rb = 74 ± 36 ppm; Middleton, 1993) or Waipapa terranes (K = 19184 ± 7387 ppm, Rb = 68 ± 28 ppm; Mortimer, pers. comm., 2002) been assimilated into the group A and B magmas.

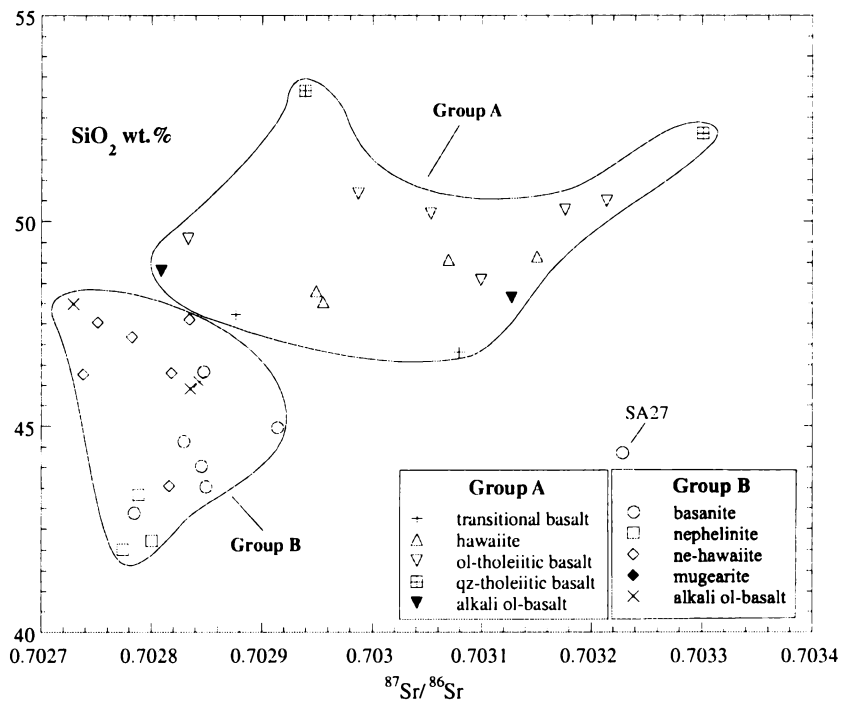

Fig. 6.13 $^{87}Sr/^{86}Sr$ vs. SiO_2 for selected group A and B rocks, South Auckland volcanic field.

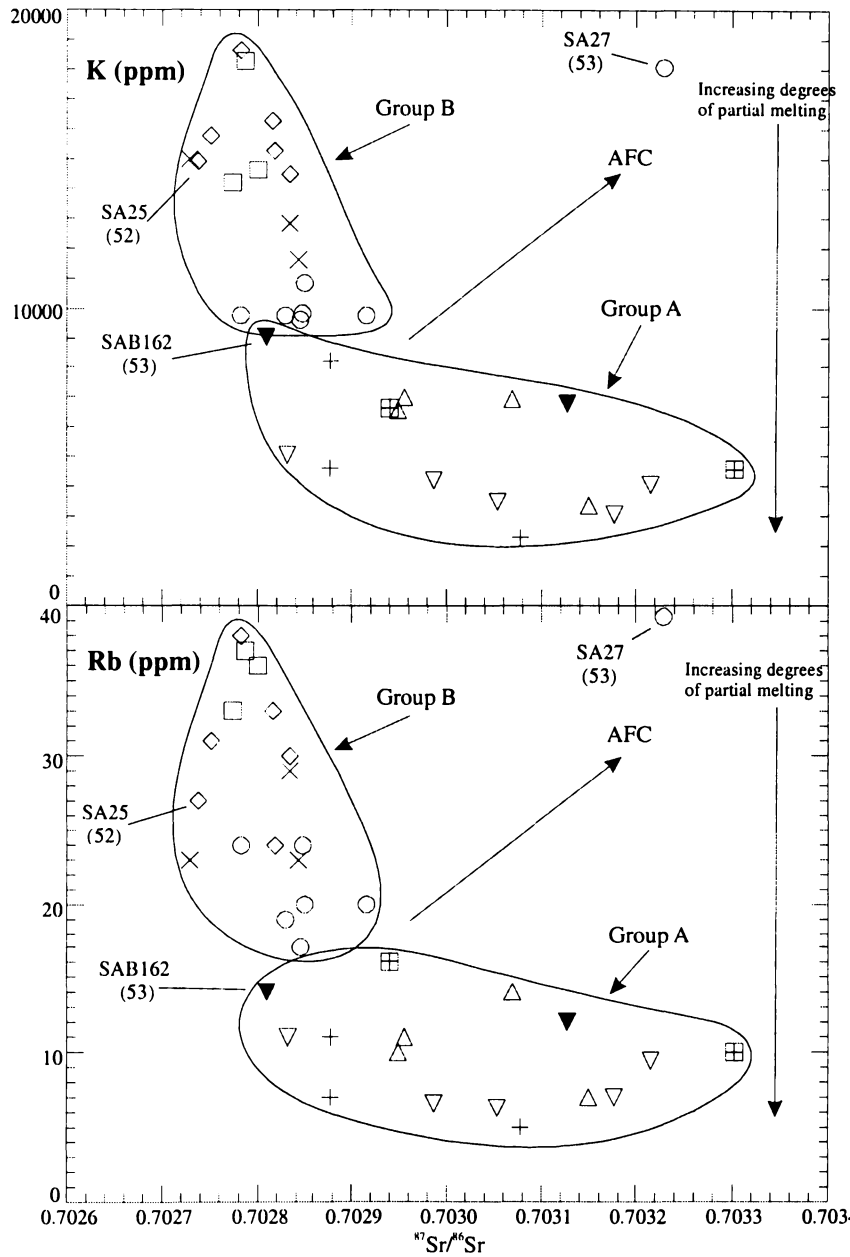

Fig. 6.14 Variation of K and Rb abundances (ppm) with $^{87}Sr/^{86}Sr$ for selected group A and B lavas, South Auckland volcanic field. The general effect that processes such as assimilation/fractional crystallisation (AFC) and increasing degrees of partial melting could have on the suites of SAVF basalts is indicated on each plot. The labelled samples in each plot are referred to in the text. The number in parenthesis below the sample number is its $100Mg/(Mg + Fe^{2+})$ value. Symbols as in Fig. 6.13.

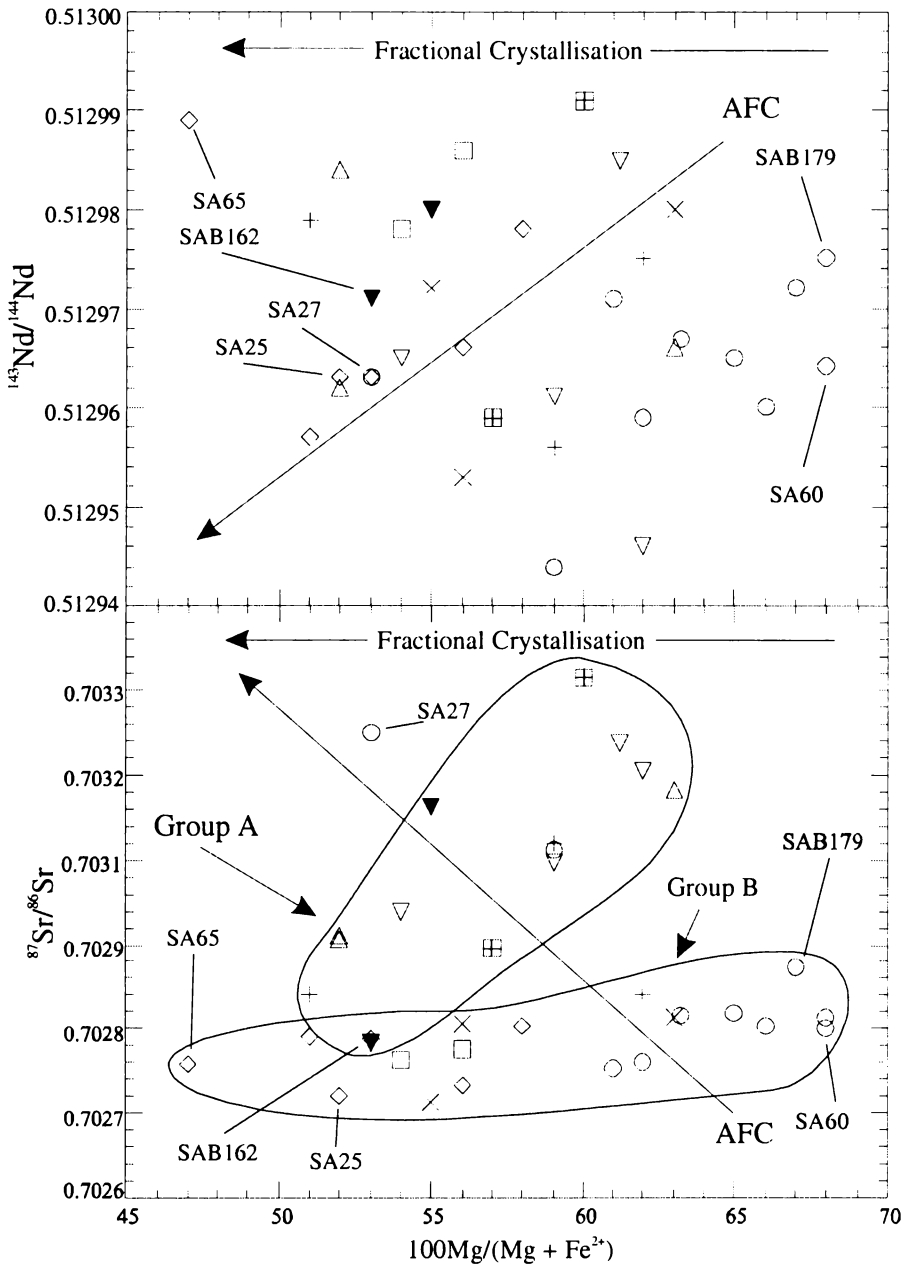

Fig. 6.15 100Mg/(Mg + Fe^{2+}) values vs. $^{143}Nd/^{144}Nd$ and $^{87}Sr/^{86}Sr$ for selected South Auckland volcanic field lavas. Symbols as in Fig. 5.20. The labelled samples in each figure are referred to in the text. The fields for the group A and B lavas in the 100Mg/(Mg + Fe^{2+}) vs. $^{143}Nd/^{144}Nd$ plot have been omitted because they strongly overlap.

Suites of basalts strongly affected by AFC show strong positive $^{143}Nd/^{144}Nd$-100Mg/(Mg + Fe^{2+}) and negative $^{87}Sr/^{86}Sr$-100Mg/(Mg + Fe^{2+}) correlations (*cf.* the flood basalts of Sana'a, Yemen; Baker *et al.*, 1997). The group A and B rocks however, exhibit no apparent $^{143}Nd/^{144}Nd$ correlation with magma differentiation (Fig. 6.15). For example, ne-hawaiite SA65 [100Mg/(Mg + Fe^{2+}) = 47] has one of the largest $^{143}Nd/^{144}Nd$ values (0.512989) of all analysed SAVF samples, whereas the relatively primitive samples SA60 and SAB179 [100Mg/(Mg + Fe^{2+}) = 68] have $^{143}Nd/^{144}Nd$ compositions (0.512964 and 0.512975 respectively) similar to samples with much smaller 100Mg/(Mg + Fe^{2+}) values.

In addition, lavas within each group have $^{87}Sr/^{86}Sr$ compositions that broadly correlate positively (albeit weakly in the group B lavas) with decreasing $100Mg/(Mg + Fe^{2+})$ (Fig. 6.15) with SA25, SA65, and SAB162 having among the smallest $^{87}Sr/^{86}Sr$ values (0.702738, 0.702782, and 0.702809 respectively) indicating that their isotopic compositions are not distinct from those basalts considered to have near primary compositions (e.g., basanite SAB179). These features are similar to those of some intraplate basalts from eastern Australia (e.g., O'Reilly and Zhang, 1995) where no significant crustal assimilation has been characterised, and are opposite to what would be expected for magma modification by AFC.

Discussion

Petrographic, geochemical, and isotopic evidence suggests that the group B rocks have not been contaminated by continental crust, or at least not by any detectable amount. In the case of the group A rocks, the modelling results show that although crustal contamination may provide a plausible explanation for some of the variations observed in them, their distinctive geochemical and radiogenic isotopic characteristics are not consistent with an interpretation of large-scale modification by an upper crustal component such as the Murihiku or Waipapa Terranes. Therefore, the comparatively low Ce/Pb values of the group A lavas most likely reflects their derivation from a Ce-depleted source rather than crustal contamination. In addition, modelling results supported by geochemical evidence do not support an interpretation that the group A rocks were derived from group B magmas through crustal assimilation and fractional crystallisation processes.

6.7 Model for volcanism in the SAVF

The data presented in the previous sections show that the contrasting geochemical features observed between the group A and B lavas of the South Auckland volcanic field cannot be explained by variable degrees of partial melting of a common mantle source, or by fractional crystallisation of a common parental magma. Evidence from incompatible trace element and REE data supports the hypothesis that the major geochemical differences between groups A and B are due principally to the contrasting geochemical characteristics of their respective mantle source regions. Although the group A and B lavas have contrasting REE abundances, each group has REE abundances and LREE/HREE ratios that are larger than those of chondrites, consistent with sources that are geochemically enriched. In addition, each group has similar, positive ε_{Nd} values,

suggesting that each source has been "recently" enriched (*cf.*, Briggs and McDonough, 1990). Therefore, there remains the question of the origin and nature of the enrichment that accounts for the different source characteristics of groups A and B. There is evidence that supports four possible enrichment scenarios:

1. The group B lavas are derived from a HIMU-OIB like source.
2. OIB-like characteristics resulted from subduction-related enrichment via incorporation of fluids from oceanic crust into the upper mantle.
3. The group A lavas are derived from a source that is a mixture of two or more of the OIB mantle reservoir end-members of Zindler and Hart (1986).
4. Enrichment due to metasomatism of the lithospheric mantle produced alkalic basalts with OIB-like characteristics.

The group B lavas have Ce/Pb and Nb/U values, incompatible trace element characteristics, and $^{87}Sr/^{86}Sr$ values, which support the hypothesis that a HIMU OIB-like geochemical signature dominates their source. Evidence for a HIMU signature is illustrated in the ratio-ratio plots in Fig. 6.16, which show that values of Zr/Nb, La/Nb, Th/Nb, Ba/Nb, and K/Nb predominantly overlap those of HIMU-OIB. A number of studies have concluded that HIMU-OIB geochemical characteristics can be obtained by the recycling of ancient basaltic oceanic crust into an OIB source region (e.g., Palacz and Saunders, 1986; Weaver *et al.*, 1986; Dupuy *et al.*, 1988; Ringwood, 1990; Weaver, 1991a,b), although Sun and McDonough (1989) noted that because Nb is less incompatible than La (and Zr), low La/Nb, and by inference, low Zr/Nb values could also be due to mantle metasomatism and/or small degrees of partial melting. Weaver (1991a,b) argued however, that the characteristic positive Nb and Ta anomaly imparted on OIB-like magmas is the result of dehydration processes associated with the subducting slab, whereby the HFSE-enriched slab is recycled into the mantle. For HIMU-OIBs, this process occurs deep in the mantle and may take between 1 to 2 billion years (Weaver, 1991b). This scenario has important implications regarding the group B source because, as with the alkalic basalts from the Auckland field, the group B basalts have distinctly smaller Pb isotopic compositions than typical HIMU-OIB basalts (e.g., St. Helena; Sun and McDonough, 1989).

Chauvel *et al.* (1992) have demonstrated that long-term storage and isotopic evolution of recycled oceanic crust (MORB) can reproduce the Sr, Nd, and Pb isotopic characteristics of a HIMU source. Huang *et al.* (1997) interpreted the small Pb isotopic compositions of the Auckland field (e.g., $^{206}Pb/^{204}Pb$ = 19.321; sample 43364) relative to HIMU as evidence that the HIMU features are relatively young and that the source region for the

Auckland field will develop St. Helena-like Pb isotopic values (e.g., $^{206}Pb/^{204}Pb = 20.896$; Sun and McDonough, 1989) in approximately 500 m.y.

Source enrichment of this nature for group B could not have been related to the subduction of the Pacific plate in association with the development of the Coromandel or Taupo Volcanic Zones (see Fig. 2.2, p.9). The New Zealand tectonic setting is too young for OIB-like source enrichment via subduction-related processes. Evidence for this is the negative Nb and Ta anomalies for some of the alkalic basalts from the Whangarei field (Huang *et al.*, 2000). Therefore, the group B source enrichment was probably affected by some other subduction-related event. One possibility is the subduction of the Phoenix plate beneath New Zealand when it was located at the eastern margin of Gondwanaland during mid Triassic to late Jurassic. Metasomatic fluids generated by the partial melting of the Pheonix plate could have caused this metasomatism, thus enriching this region in LILE, HFSE, and LREE, which are now reflected in the group B lava compositions.

The origin of the mantle components contributing to the group A basalts are more difficult to define. The K/Nb and Zr/Nb values shown in Fig. 6.16 indicate the involvement of EM-type continental lithospheric mantle components in their generation, whereas values of La/Nb, Th/Nb, and Ba/Nb indicate a HIMU component (i.e., overlap on the vertical scale in Fig. 6.16). In addition, the group A lavas have $^{207}Pb/^{204}Pb$ and $^{206}Pb/^{204}Pb$ values that trend toward the EMII component (see Fig. 5.17A, p.169) and have OIB-like (albeit weak; Fig. 5.12, p.158) incompatible trace element characteristics indicating the possible mixing between the EMII end-member and a HIMU-OIB-like source.

Weaver *et al.* (1986) and Weaver (1991a,b) argued that the EM-type source characteristic is due largely to mixing between HIMU-OIB and terrigenous sediment, which has been subducted with oceanic crust. Alternatively, Hawkesworth *et al.* (1986) proposed that EM-type geochemical features could result from the delamination of metasomatised-enriched continental lithosphere. Since New Zealand was located at the eastern margin of Gondwanaland prior to Cenozoic continental rifting associated with the opening of the Southern Ocean and Tasman Sea (see Weaver *et al.*, 1994; Fig. 1), the EM-type component of the group A lavas may have been inherited from the supercontinent. Processes associated with plume-related magmatism that may have begun in mid-Cretaceous time (Weaver *et al.*, 1994) and subsequent melting could have imparted an EM-type signature into the Gondwanaland subcontinental lithosphere. Evidence for plume-related magmatism during this time, discussed in Lanyon *et al.* (1993) and Weaver *et al.* (1994), includes plume-related HIMU-OIB basalts found in: Marie Byrd Land,

Antarctica; Tasmania, Australia; the Balleny Islands; and Chatham Island, New Zealand. Sanders (1994) argued that the upper mantle and lower crust of northern North Island have been metasomatised and cited the presence of volatile-bearing minerals (i.e., amphibole, mica, apatite, carbonate, and sulphide globules) in a variety of xenolith types from the alkalic basalts in the Okete, Ngatutura, South Auckland volcanic fields as evidence for this. Therefore, the group A basalts could have resulted from the partial melting of the remnants of a metasomatised and HIMU plume-modified Gondwanaland lithosphere, following continental fragmentation.

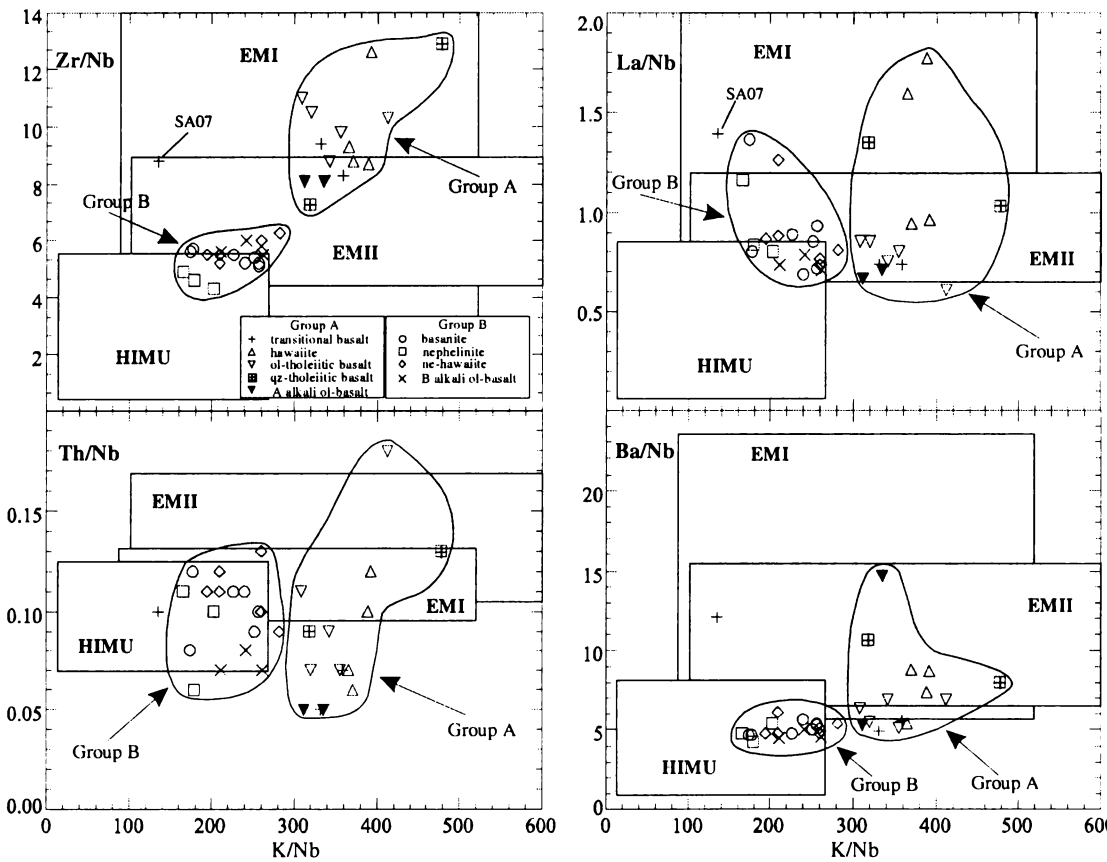

Fig. 6.16 Incompatible trace element ratios Zr/Nb, La/Nb, Th/Nb, and Ba/Nb plotted against K/Nb for HIMU, EMI, and EMII mantle reservoirs and selected group A and B lavas from the South Auckland volcanic field. Mantle reservoir fields are based on data compiled from Saunders *et al.* (1988), Weaver (1991a,b), and Lanyon *et al.* (1993). SAVF data are from ICP-MS analyses.

In intraplate continental tectonic settings, the eruption of alkaline magmas of basanitic and nephelinitic compositions are commonly associated with the eruption of magmas with subalkaline, e.g., tholeiitic, compositions. A number of models have been proposed to account for the spectrum of geochemical and isotopic compositions commonly associated with these basalt types (e.g., Rafferty and Heming, 1979; McDonough *et al.*, 1985; Sun and McDonough, 1989; O'Reilly and Zhang, 1995; Zhang *et al.*, 2001). These works are interpreted pictorially in Fig.6.17a as they may apply to the generation of the SAVF basalts. However, this model is inconsistent with the evidence presented above,

which was not available when Rafferty and Heming (1979) proposed that the group A-type magmas were generated at depths greater than the group B-type magmas.

Model (a) Plume model for the petrogenesis of the SAVF basalts

As discussed in section 6.3.3, the inference of garnet in the group B source requires melt generation at pressures greater than 20 kbar. Magma generation for the group B magmas takes place in a zone of partial melting beneath the South Auckland region within the low velocity zone (LVZ). Because group A-type magmas are generally considered the result of relatively large degrees of partial melting by Rafferty and Heming (1979), this model requires that group A magma generation takes place at depths greater than those of group B. Melting at such depths most likely would require a heat source near the base of the lithosphere such as the hot ascending mantle plume model invoked by McDonough *et al.* (1985), Sun *et al.* (1989), and Zhang *et al.* (2001) for southeastern Australia intraplate magmatism (see McDonough *et al.*, 1985; Fig. 7). The interaction of a plume with this region would raise the temperature above the mantle solidus and initiate melting in the LVZ (McDonough *et al.*, 1985). Generally, these models invoke that the spectrum of magmas observed in eastern Australia, similar to those from the SAVF, result from the mixing of asthenosphere-derived melts with melts generated in the lithosphere. In this model (Fig. 6.17a), a separate source for groups A and B is maintained.

This model requires some extension or transtension to allow the group A and B magmas to ascend through the continental lithosphere. Partial melts generated from the plume component could have group A characteristics provided that sufficient melting occurred to consume most of the garnet in the residue. Partial melting at these depths could also take place over the time that Rafferty and Heming (1979) considered necessary to generate the relatively large degree subalkalic group A-type melts. Unlike the McDonough *et al.* (1985) model however, the group A magmas pass through the LVZ without mixing with the smaller degree alkalic (group B-type) melts generated there.

Another possible explanation for the geochemical features of the group A lavas is the mixing of asthenosphere-derived melts with a metasomatised subcontinental lithospheric mantle (SCLM). O'Reilly and Zhang (1995) and Zhang *et al.* (2001) proposed that the HIMU signature of some eastern Australian basalts could have been acquired by the mixing of relatively small degree asthenosphere-melts with partial melts from the SCLM. The strong OIB characteristics of the group B magmas suggest that they passed unimpaired through the SCLM. In contrast, the interaction of the plume-derived group A

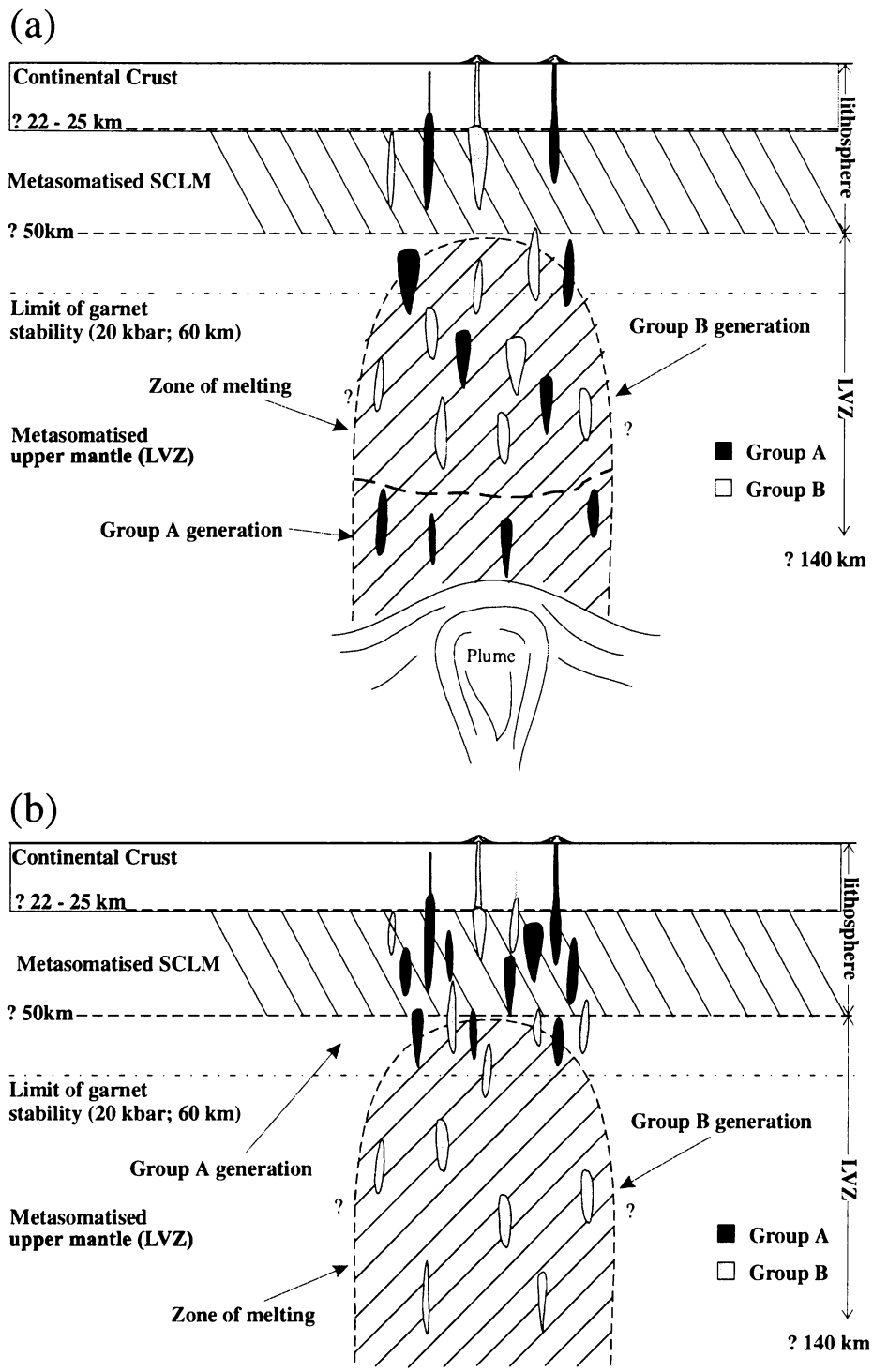

Fig. 6.17 Models for petrogenesis of the SAVF basalts. (a) Model (a) based on the interpretations of Rafferty and Heming, 1979; McDonough *et al.*, 1985; Sun and McDonough, 1989; O'Reilly and Zhang, 1995; Zhang *et al.*, 2001) for the generation of magmas similar to the group A and B magmas described in this study. The generation of the group A magmas occurs near the low velocity zone (LVZ)-asthenosphere interface at depths greater than that for the group B magmas. Melting of the LVZ is initiated due to the hot ascending plume that intrudes the base of the lithosphere. The group B magmas form in a zone of melting within the LVZ due to the heat from the plume. The group B magmas ascend rapidly to the surface without mixing with group A magmas, melts from the SCLM or incorporation of the continental crust. The group A magmas rise through the LVZ without mixing with the group B magmas but mix with melts generated within the SCLM. (b) Model (b). The group B magmas are generated and ascend to the surface as in the model (a), but the group A magmas are generated at pressures < 20 kbar, within the spinel stability field. In this model, tensional forces allow for mantle upwelling and decompressional melting.

melts with partial melts from the enriched lithospheric mantle could partially mask their OIB-like features and overprint the enriched source signature (McDonough *et al.*, 1985; Sun *et al.*, 1989).

A plume model (hot spot) for the SAVF such as those proposed by McDonough *et al.* (1985), Sun *et al.* (1989), and O'Reilly and Zhang (1995) for similar basalts from eastern Australia is not likely as it would require the spontaneous and fortuitous initiation of plume activity in the South Auckland region. Furthermore, there is no evidence for hot spot activity because this is contrary to the direction of the relative plate motion and the age trend of the four volcanic fields in the Auckland Province. An alternative model to a stationary magma source is the northward migration of the source for the fields. An experimental study by Kerr and Lister (1988) on linear sources of buoyant fluids concluded that regularly spaced volcanism, such as the age-progressive volcanic lines described by Lister and Etheridge (1989) and O'Reilly and Zhang (1995) for volcanic fields in eastern Australia, might be due to gravitational instability of buoyant regions of partial melt in the upper mantle. This mechanism has been suggested for the volcano spacing in the East African rift valley (Mohr and Wood, 1976). The experiments of Kerr and Lister (1988), however, did not produce the spatial or temporal periodicity of diapiric plumes required to account for the time-space relationships of the volcanic fields in the Auckland Province.

Model (b) Extension model for the petrogenesis of the SAVF basalts

Based on the new evidence presented above, a new model for the generation of the group A and B magmas is presented in Fig. 6.17b where partial melting may have been triggered by tensional forces associated with earlier orogenic events and the later subduction of the Pacific plate beneath North Island. This would allow for crustal extension, mantle upwelling, and subsequent decompressional melting due to elevated mantle temperatures caused by lithospheric attenuation (e.g., McKenzie and Bickle, 1988). In this model the group B magmas are generated in the low velocity zone as in the previous model. However, the evidence presented for the generation of the group A magmas from a spinel-peridotite source requires that they formed at depths shallower than those for group B, within the spinel stability field, e.g., < 20 kbar.

This model also requires mantle metasomatism as the cause for the distinct incompatible trace element and REE characteristics observed in the group A lavas. One of the problems with this model is how can large volumes of subalkalic (group A-type) melts such as those proposed by Rafferty and Heming (1979) be generated in the SCLM. In contrast to

models that require the melting temperatures to generate tholeiitic (group A-type) magmas to be higher than that for alkalic (group B-type) magmas, this model proposes that the group A magmas could have been generated under hydrous conditions. Evidence for this is the presence of amphibole in some of the spinel-peridotite xenoliths described by Sanders (1994). This would lower the solidus temperature, and therefore the group A magmas could be generated at lower temperatures and by relatively lower degrees of partial melting implied by the DMI melting models than that suggested by e.g., Rafferty and Heming (1979), Frey *et al.* (1978), and McDonough *et al.* (1985) for similar rock types. The large scatter in the incompatible trace elements and LREE between the various rock types, and lack of any coherent geochemical trend in the group A lavas (see Fig. 5.10, p.154), is most likely due to the heterogeneous nature of the SCLM, together with variable degrees of partial melting and fractional crystallisation.

Chapter Seven: Summary and Conclusions

Chapter Seven

Summary and Conclusions

The South Auckland volcanic field (SAVF) is one of a number of geographically isolated Pliocene to Recent continental basaltic intraplate volcanic fields in North Island, New Zealand. The SAVF formed between 0.51 and 1.59 Ma and is situated in an extensional tectonic environment behind the active volcanic front of the Taupo Volcanic Zone. The field consists of eroded basaltic lava flows, scoria cones, and tuff deposits, produced from approximately 100, predominantly monogenetic volcanic centres over an area of ~ 300 km^2. The SAVF basalts have mineralogical and major element characteristics of magmas that range from basanites to quartz tholeiites.

In many cases elsewhere in the world in continental intraplate settings, volcanic fields consist of a single suite of alkalic rocks that show a spectrum of compositions that range from strongly silica-undersaturated to less undersaturated compositions (e.g., southeastern Australia, Frey *et al.*, 1978, McDonough *et al.*, 1985; northern Hessian Depression, Wedepohl, 1985; Garrotxa NE Volcanic Province, Spain, Cebriá *et al.*, 2000). In some suites, the basalts evolved as multiple lineages (e.g., East Otago Volcanic Province, New Zealand, Coombs and Wilkinson, 1969), whereas others exhibit a temporal relationship between rock types (e.g. Whangarei-Puhipuhi, New Zealand; Heming, 1980a).

However, the basalts from the South Auckland volcanic field are different from continental intraplate alkalic basalts elsewhere because they can be divided into two broad groups (A and B) based on their distinctive mineralogy and geochemical compositions. The distinguishing feature of the SAVF basalts is that each group evolved as a distinct lineage from a separate mantle source and there is no apparent temporal or spatial association between or among the various lava types that comprise each group. Salient features of group A and B lavas are presented in Table 7.1.

Group A basalts are predominantly hypersthene normative and consist of transitional basalts, hawaiites, olivine- and quartz-tholeiites, and alkali olivine basalts, whereas group B are predominantly nepheline normative and consist of basanites, nephelinites, nepheline hawaiites, mugearites, and alkali olivine basalts. Olivine and clinopyroxene are the main phenocryst phases in each group and plagioclase occurs in some group A lavas. In most group A lavas olivine tends to be less forsteritic, and clinopyroxene less calcic,

Table 7.1 Summary of salient features of the group A and B lavas of the South Auckland volcanic field. Means = ± 1 standard deviation.

	Group A	Group B
Rock types	hypersthene normative transitional basalts, hawaiites, ol-tholeiitic basalts, qz-tholeiitic basalts, alkali ol-basalts	nepheline normative basanites, nephelinites, ne-hawaiites, mugearites, alkali ol-basalts
Mineral chemistry		
Olivine	Fo_{59} - Fo_{82}; Fo_{mean} = 75 ± 5	Fo_{60} to Fo_{92}; Fo_{mean} = 78 ± 6
Clinopyroxene	augite Wo_{35} - Wo_{47}; Wo_{mean} = 43 ± 3 En_{36} - En_{50}; En_{mean} = 43 ± 3 Fs_{11} - Fs_{23}; Fs_{mean} = 14± 3	diopside Wo_{42} - Wo_{52}; Wo_{mean} = 48 ± 2 En_{32} - En_{46}; En_{mean} = 38 ± 3 Fs_{10} - Fs_{20}; Fs_{mean} = 13± 2
Geochemistry		
$Na_2O + K_2O$	3.0 - 4.8 wt.%; mean = 3.6 ± 0.4 wt.%	3.3 - 7.9 wt.%; mean = 5.5 ± 0.9 wt.%
Nb	9 - 29 ppm; mean = 16 ± 6 ppm	35 - 102 ppm; mean = 58 ± 6 ppm
Zr	97 - 210 ppm; mean = 142 ± 34 ppm	194 - 491 ppm; mean = 320 ± 62 ppm
$(La/Yb)_n$	3.4 - 7.6; mean = 5.4 ± 1.6	12 - 47; mean = 23 ± 10
isotopes:		
$^{87}Sr/^{86}Sr$	0.702809 - 0.703301 mean = 0.703025 ± 0.00014	0.702738 - 0.703228; mean = 0.702832 ± 0.00011
$^{206}Pb/^{204}Pb$	18.95 - 19.277 mean = 19.119 ± 0.111	19.201 - 19.323 mean = 19.273 ± 0.035
$^{207}Pb/^{204}Pb$	15.586 - 15.613 mean = 15.597 ± 0.009	15.568 - 15.589 mean = 15.576 ± 0.0001
$^{208}Pb/^{204}Pb$	38.731 - 38.876 mean = 38.790 ± 0.54	38.833 - 38.906 mean = 38.870 ± 0.025
Mantle source	spinel-peridotite (< 20 kbar)	garnet-peridotite (> 25 kbar)

than those from the majority of group B basalts. Although Fe, Mg, Ca, and Na partitioning calculations indicate that a large number of olivine and clinopyroxene phenocrysts are not in equilibrium with their host magma, estimated crystallisation pressures and temperatures show that these phases crystallised over a similar range of P – T conditions and suggest polybaric crystallisation of distinct magma batches.

The group A basalts have notably smaller LILE, HFSE, and LREE abundances than those from group B and have relatively flat REE patterns that cross over the steep REE patterns of the group B basalts. In addition, the group A basalts exhibit relatively weak and variable OIB-like incompatible trace element characteristics, whereas the group B lavas have a strong OIB-like signature.

Petrogenetic modelling suggests that the group A and B basalts evolved as discrete volcanic lineages that do not appear to be related by processes such as variable degrees of melting of a common mantle source or by fractional crystallisation of a common parental magma. Results of partial melting models, using the dynamic melting inversion (DMI) method of Zou and Zindler (1996), together with estimated melt segregation pressures, indicate that the primary magma compositions for the group A basalts were derived by 5 – 12 % partial melting of a spinel-peridotite source at depths of < 66 km. In contrast, the primary magmas for group B were derived by comparatively smaller degrees of melting (i.e., 3 – 8 %) of a garnet-peridotite at depths of > 75 km. This is supported by the relatively small LREE abundances and $(La/Yb)_N$ values (3.4 – 7.6) exhibited by the group A basalts, indicative of magma generation in the spinel stability field, compared with the group B basalts which have large LREE abundances and $(La/Yb)_N$ values (12 – 47), indicative of magma generation of a source with residual garnet. Based on the modelling results and estimated incompatible trace element and REE abundances for the group A and B sources, group A magmas were derived from an enriched upper mantle source with relatively depleted LILE, HFSE, and LREE and small LREE/HREE values, whereas those from group B exhibit strong incompatible trace element affinities with a LREE-enriched garnet-bearing OIB-like source.

The strong positive correlation between decreasing Ni and Cr with MgO indicate that fractionation of olivine and clinopyroxene was an important process in the evolution of the suites of group A and B lavas. However, results of fractional crystallisation models and mass balance calculations suggest that the group A and B basalts are not genetically related to a common parental magma. Furthermore, the modelling results strongly suggest that although fractional crystallisation played a role in the evolution of the lineages that define groups A and B, it cannot account for the broad range of compositions exhibited by each group. Therefore, the group A and B basalts most likely are derived from discrete magma batches formed by variable degrees of partial melting and evolved independently by variable degrees of fractional crystallisation.

The group A and B basalts have Sr isotopic compositions similar to HIMU-OIB, Nd isotopic composition intermediate between HIMU-OIB and MORB, and Pb isotopic compositions that are unradiogenic relative to HIMU-OIB. Although the group A lavas have ε_{Nd} values (+ 5.97 to + 6.89) similar to those of group B (+ 6.14 to + 6.85), they exhibit small but distinct differences in their $^{87}Sr/^{86}Sr$, $^{207}Pb/^{204}Pb$, and $^{206}Pb/^{204}Pb$ compositions. Because there is no isotopic or geochemical evidence to suggest that any of the lavas from either group have been extensively contaminated by continental crust or

have been modified by subduction-related processes, these differences in isotopic compositions are considered to be source related. Variations in incompatible element ratios, such as K/Nb, Zr/Nb, Sr/Nb and Zr/Y, and the trend of $^{207}Pb/^{204}Pb$ and $^{206}Pb/^{204}Pb$ compositions towards EMII for the group A basalts, further support this and indicate that the SAVF lavas were derived from at least two distinct sources: a HIMU-OIB-like source for group B, and a mixture of OIB and EMII sources for the group A magmas.

Partial melting of a metasomatised subcontinental lithospheric source that was modified by a HIMU-OIB plume prior to the breakup of the Gondwanaland supercontinent could account for the generation of the group A lavas. In contrast, the group B lavas have Pb isotopic characteristics indicative of a relatively young HIMU-OIB signature that may have resulted from processes related to the subduction of the Phoenix plate beneath New Zealand when it was at the eastern margin of Gondwanaland. Both basalt groups are associated with partial melting of lithospheric remnants following continental fragmentation. Extensional tectonics related to orogenic events affecting the South Auckland region could have created conditions that promoted adiabatic decompression melting of these widely dispersed lithospheric fragments.

References

References Cited

Abouchami, W., Galer, S.J.G., Hofmann, A.W., 2000, High precision lead isotope systematics of lavas from the Hawaiian scientific drilling project. Chemical Geology. v. 169, pp. 187-209.

Adam, J. and Green, T.H., 1994, The effects of pressure and temperature on the partitioning of Ti, Sr and REE between amphibole, clinopyroxene and basaltic melts. Chemical Geology. v. 117, pp. 219-233.

Adams, C.J., Graham, I.J., Seward, D., and Skinner, D.N.B., 1994, Geochronological and geochemical evolution of late Cenozoic volcanism in the Coromandel Volcanic Zone. New Zealand Journal of Geology and Geophysics. v. 37, pp. 359-379.

Adams, R.D. and Ware, D.E., 1977, Subcrustal earthquakes beneath New Zealand; Locations determined with a laterally inhomogeneous velocity model. New Zealand Journal of Geology and Geophysics. v. 20, no. 1, pp. 59-83.

Albarède, F., 1992, How deep do common basaltic magmas from and differentiate? Journal of Geophysical Research. v. 97, no. B7, pp. 10997-11009.

Allan, J.F., Sack, R.O., and Batiza, R., 1988, Cr-rich spinels as petrogenetic indicators: MORB-type lavas from the Lamont seamount chain, eastern Pacific. American Mineralogist. v. 73, pp. 741-753.

Anderson, A.T. and Greenland, L.P., 1969, Phosphorous fractionation diagrams as a quantitative indicator of crystallisation differentiation of basaltic liquids. Geochimica et Cosmochimica Acta. v. 33, pp. 493-505.

Ashcroft, 1986, The Kerikeri volcanics: A basalt-Pantellerite association in Northland. In: Late Cenozoic volcanism in New Zealand. Smith, I.E.M., (ed). The Royal Society of New Zealand. Bulletin 23, pp. 49-63.

Aspen, P., Upton, B.G.J., and Dichin, A.P., 1990, Anorthoclase, sanidine and associated megacrysts in Scottish alkali basalts: High-pressure syenitic debris from upper mantle sources? European Journal of Mineralogy. v. 2, pp 503-517.

Bacon, C.R. and Hirschmann, M.M., 1988, Mg/Mn partitioning as a test for equilibrium between coexisting Fe-Ti oxides. American Mineralogist. v. 73, pp. 57-61.

Baker, J.A., Menzies, M.A., Thirlwall, M.F., MacPherson, C.G., 1997, Petrogenesis of Quaternary intraplate volcanism, Sana'a, Yemen: Implications for plume-lithosphere interaction and polybaric melt hybridisation. Journal of Petrology. v. 38, no., 10, pp. 1359-1390.

Baker, M.B. and Wyllie, P.J., 1992. High-pressure apatite solubility in carbonate-rich liquids: Implications for mantle metasomatism. Geochimica et Cosmochimica Acta. v. 56, pp. 3409-3422.

Ballance, P.F., 1976, Evolution of the Upper Cenozoic magmatic arc and plate boundary in northern New Zealand. Earth and Planetary Science Letters. v. 28, pp. 356-370.

Ballance, P.F., Pettinga, J.R., and Webb, C., 1982, A model of Cenozoic evolution of northern New Zealand and adjacent areas of the southwest Pacific. Tectonophysics. v. 87, pp. 37-48.

Ballance, P.F. and Campbell, J.D., 1993, The Murihiku arc-related basin of New Zealand (Triassic-Jurassic). In: *Sedimentary Basins of the World South Pacific Sedimentary Basins.* Hsü, K.J. and Ballance, P.F. (eds.), pp. 21-33.

Basu, A.R., Junwen, W., Wankang, H., Guanghong, X., and Tatsumoto, M., 1991, Major element, REE, and Pb, Nd, and Sr isotopic geochemistry of Cenozoic volcanic rocks of eastern China: implications for their origin from suboceanic-type mantle reservoirs. Earth and Planetary Science Letters. v. 105, pp. 149-169.

Beattie, P., 1994. Systematics and energetics of trace-element partitioning between olivine and silicate melts: Implications for the nature of mineral/melt partitioning. Chemical Geology. v. 117, pp. 57-71.

Bednarz U. and Schmincke, H-U. 1990, Evolution of the Quaternary melilite-nephelinite Herchenberg volcano (East Eifel). Bulletin of Volcanology. v. 52, pp. 426-444.

Bell, A.R., Cochrane, P.R., Depledge, D., and Maggs, G.R., 1991, Pukekawa-Onewhero area water resources. Waikato Regional Council Technical Report 1991/29. Environment Waikato, Hamilton, New Zealand. 90 pp.

Bindeman, I.N., Davis, A.M., and Drake, M.J., 1998, Ion microprobe study of plagioclase-basalt partition experiments at natural concentration levels of trace elements. Geochimica et Cosmochimica Acta. v. 62, no. 7, pp. 1175-1193.

Black, P.M., Briggs, R.M., Itaya, T., Dewes, E.R., Dunbar, H.M., Kawasaki, K., Kuschel. E., and Smith, I.E.M., 1992, K-Ar age data and geochemistry of the Kiwitahi Volcanics, western Hauraki Rift, North Island, New Zealand. New Zealand Journal of Geology and Geophysics. v. 35, pp. 403-413.

Blundy, J.D., Falloon, T.J., Wood, B.J., and Dalton, J.A., 1995, Sodium partitioning between clinopyroxene and silicate melts. Journal of Geophysical Research. v. 100, No. B8, pp. 15501-15515.

Bougault, H. and Hekinian, R., 1974. Rift valley in the Atlantic ocean near 36° 50' N: Petrology and geochemistry of basaltic rocks. Earth and Planetary Science Letters. v. 24, pp. 249-261.

Bradshaw, J.D., 1989, Cretaceous geotectonic patterns in the New Zealand region. Tectonics. v. 8, no. 4, pp. 803-820.

Briggs, R.M., 1986, Petrology and geochemistry of Maungatautari, a medium-K andesite-dacite volcano. New Zealand Journal of Geology and Geophysics. v. 29, pp 273-289.

Briggs, R.M. and Goles, G.G., 1984, Petrological and trace element geochemical features of the Okete Volcanics, western North Island, New Zealand. Contributions to Mineralogy and Petrology. v. 86, pp. 77-88.

Briggs, R.M., Itaya, T., Lowe, D.J., and Keane, A.J., 1989, Ages of the Pliocene-Pleistocene Alexandra and Ngatutura volcanics, western North Island, New Zealand, and some geological implications. New Zealand Journal of Geology and Geophysics. v. 32, pp. 417-427.

Briggs, R.M. and McDonough W.F., 1990, Contemporaneous convergent margin and intraplate magmatism, North Island, New Zealand. Journal of Petrology. v. 31. no. 4, pp. 813-851.

Briggs, R.M., Utting, A.J., and Gibson, I.L., 1990, The origin of alkaline magmas in an intraplate setting near a subduction zone: The Ngatutura Basalts, North Island, New Zealand. Journal of Volcanology and Geothermal Research. v. 40, pp. 55-70.

Briggs, R.M., Okada, T., Itaya, T., Shibuya, H., and Smith, I.E.M., 1994, K-Ar ages, palaeomagnetism, and geochemistry of the South Auckland volcanic field, North Island, New Zealand. New Zealand Journal of Geology and Geophysics. v. 37, pp. 143-153.

Briggs, R.M., Rosenberg, M.D., De Lange, P.J., Itaya, T., King, P.R., and Price, R.C., 1997, Geology and geochemistry of Gannet (Karewa) Island, Tasman Sea: A rift-related nephelinitic tuff ring. New Zealand Journal of Geology and Geophysics. v. 40, no. 3, pp. 263-273.

Brothers, R.N., 1975, Kaikoura Orogeny in Northland, New Zealand. New Zealand Journal of Geology and Geophysics. v. 17, no. 1, pp. 1-18.

Bryan, W.B., Finger, L.W., and Chayes, 1969, Estimating proportions in petrographic mixing equations by least-squares approximation. Science, v. 163, pp. 926-927.

Cameron, M. and Papike, J.J., 1981, Structural and chemical variations in pyroxenes. American Mineralogist. v. 66, pp. 1-50.

Carmichael, I.S.E., 1967, The iron-titanium oxides of salic volcanic rocks and their associated ferromagnesian silicates. Contributions to Mineralogy and Petrology. v. 14, pp. 36-64.

Carmichael, I.S.E., 1991, The redox states of basic and silicic magmas: A reflection of their source regions. Contributions to Mineralogy and Petrology. v. 106, no. 2, pp. 129 – 141.

Cas, R.A.F., 1989, Framework for volcanism: Regional influences on magma emplacement. In: *Intraplate Volcanism in Eastern Australia and New Zealand.* Johnson, R.W., Knutson, J., and Taylor, S.R., (eds.), Cambridge University Press, Cambridge. pp. 408.

Cashman, K.V., 1993, Relationship between plagioclase crystallisation and cooling rate in basaltic melts. Contributions to Mineralogy and Petrology. v. 113, pp. 126-142.

Cashman, K.V. and Marsh, B.D., 1988, Crystal size distribution (CSD) in rocks and the kinetics and dynamics of crystallisation II. Makaopuhi lava lake. Contributions to Mineralogy and Petrology. v. 99, pp. 292-305.

Cebriá, J. M. and López-Ruiz, J., 1995, Alkali basalts and leucites in an extensional intracontinental plate setting: The late Cenozoic Calatrava Volcanic Province (central Spain). Lithos. v. 35, pp. 27-46.

Cebriá, J. M., López-Ruiz, J., Doblas, M., Oyarzun, R., Hertogen, J., and Benito, R., 2000, Geochemistry of the Quaternary alkali basalts of Garrotxa (NE Volcanic Province, Spain): A case of double enrichment of the mantle lithosphere. Journal of Volcanology and Geothermal Research. v. 102, pp. 217-235.

Chauvel, C., Hofmann, A.W., Vidal, P., 1992, HIMU-EM: The French Polynesian connection. Earth and Planetary Science Letters. v. 110, pp. 99-119.

Chen, C, -Y, Frey, F.A., Rhodes, J.M., Easton, R.M., 1996, Temporal geochemical evolution of Kilauea volcano: Comparison of Hilina and Puna basalt. In*: Earth processes, reading the isotopic code. Basu*, A. and Hart, S.R. (eds). American Geophysical Union. Washington D.C. pp. 161-181.

Chung, S-L., Sun, S-s, Tu, K., Chen, C-H., Lee, C-y., 1994, Late Cenozoic basaltic volcanism around the Taiwan Strait, SE China: Product of lithosphere-asthenosphere interaction during continental extension. Chemical Geology. v. 112, pp. 1-20.

Chung, S-L., Jahn, B-M., Chen, S-J., Lee, T., Chen, C-H., 1995, Miocene basalts in northwestern Taiwan: Evidence for EM-type mantle sources in the continental lithosphere. Geochimica et Cosmochimica Acta. v. 59, no. 3, pp. 549-555.

Clague, D.A. and Frey, F.A., 1982, Petrology and trace element geochemistry of the Honolulu Volcanics, Oahu: Implications for the oceanic mantle below Hawaii. Journal of Petrology. v. 23, no. 3, pp. 447-504.

Clague, D.A. and Dalrymple, G.B., 1988, Age and petrology of alkalic postshield and rejuvenated-stage lava from Kauai, Hawaii. Contributions to Mineralogy and Petrology. v. 99, pp. 202-218.

Clark, A.H., Pearce, T.H., Roeder, P.L., and Wolfson, I., 1986, Oscillatory zoning and other microstructures in magmatic olivine and augite: Nomarski interference contrast observations on etched polished surfaces. American Mineralogist. v. 71, pp. 734-741.

Clynne, M.A. and Borg, L.E., 1997, Olivine and chromian spinel in primitive calc-alkaline and tholeiitic lavas from the southernmost Cascade Range, California: A reflection of relative fertility of the source. The Canadian Mineralogist. v. 35, pp. 453-472.

Coblentz, D.D., Sandiford, M., Richardson, R.M., Zhou, S., and Hillis, R., 1995, The origins of the intraplate stress field in continental Australia. Earth and Planetary Science Letters. v. 135, pp. 299-309.

Cohen, A.S., O'Nions, R.K., Kurz, M.D., 1996, Chemical and isotopic variations in Mauna Loa tholeiites. Earth and Planetary Science Letters. v. 143, pp. 111-124.

Cole, J.W. and Lewis, K.B., 1981, Evolution of the Taupo-Hikurangi subduction system. Tectonophysics, v. 72, no. 1, pp. 1-21.

Cole, J.W., 1986, Distribution and tectonic setting of late Cenozoic volcanism in New Zealand. In: *Late Cenozoic Volcanism in New Zealand.* Smith, I.E.M. (ed). The Royal Society of New Zealand. Bulletin 23, pp. 7-20.

Cole, J.W., 1990, Structural control and origin of volcanism in the Taupo Volcanic Zone, New Zealand. Bulletin of Volcanology, v. 52, no. 6, pp.445-459.

Colson, R.O., McKay, G.A., and Taylor, L.A., 1988, Temperature and composition dependencies of trace element partitioning: Olivine/melt and low-Ca pyroxene/melt. Geochimica et Cosmochimica Acta. v. 52, pp. 539-553.

Coombs, D.S. and Wilkinson, J.F.G., 1969, Lineages and fractionation trends in undersaturated volcanic rocks from the East Otago Volcanic Province (New Zealand) and related rocks. Journal of Petrology. v. 10, part 3, pp. 440-501.

Coombs, D.S., Cas, R.A.F., Kawachi, Y., Landis, C.A., McDonough, W.F., and Reay, A., 1986, Cenozoic volcanism in north, east, and central Otago. In: *Late Cenozoic Volcanism in New Zealand.* The Royal Society of New Zealand. Smith, I.E.M. (ed.), Bulletin 23, pp. 313-336.

Corrigan, G.M., 1982, Supercooling and the crystallisation of plagioclase, olivine, and clinopyroxene from basaltic magmas. Mineralogical Magazine. v. 46, pp. 31-42.

Cotton, J., Le Dez, J. A., Bau, M., Caroff, M., Maury, R.C., Dulski, P., Fourcade, S., Bohn, M., and Brousse, R., 1995, Origin of anomalous rare-earth element and yttrium enrichment in subaerially exposed basalts: Evidence from French Polynesia. Chemical Geology. v. 119, nos. 1-4, pp. 115-138.

Cox, K.G., Bell, J.D., Pankhurst, R.J., 1979, *The interpretation of Igneous Rocks.* Unwin Hyman Ltd., London. pp. 450.

Deer, W.A., Howie, R.A., and Zussman, J., 1992, *An introduction to the rock forming minerals.* Harlow, Essex, England: Longman Scientific & Technical; New York, NY: Wiley. pp. 696

DePaolo, D.J., 1981, Trace element and isotopoic effects of combined wallrock assimilation and fractional crystallisation. Earth and Planetary Science Letters. v. 53, pp. 189-202.

Dobosi, G., 1989, Clinopyroxene zoning patterns in the young alkali basalts of Hungary and their petrogenetic significance. Contributions to Mineralogy and Petrology. v. 101, pp. 112-121.

Donaldson, C.H., 1976, An experimental investigation of olivine morphology. Contributions to Mineralogy and Petrology. v. 57, pp. 187-213.

Duda, A and Schmincke, H.U., 1978, Quaternary basanites, melilite nephelinites and tephrites from the Laacher See Area (Germany). N Jb Miner Abh, v. 132, pp. 1-33.

Duda, A and Schmincke, H.U., 1985, Polybaric differentiation of alkali basaltic magmas: Evidence from green-core clinopyroxenes (Eifle, FRG). Contributions to Mineralogy and Petrology. v. 91, pp. 340-353.

Duncan, R.A. and Clague, D.A., 1985, Pacific plate motion recorded by linear volcanic chains. In: *The Ocean Basins and Margins, Volume 7A, the Pacific Ocean.* Nairn, A.E.M. (ed.), Plenum, New York.

Duncan, R.A. and McDougall, I., 1989, Framework for volcanism: Volcanic time-space relationships. In: *Intraplate Volcanism in Eastern Australia and New Zealand.* Johnson, R.W., Knutson, J., and Taylor, S.R., (eds.), Cambridge University Press, Cambridge. pp. 43-53.

Dungan, M., 1987, Open system magmatic evolution of the Taos Plateau Volcanic Field, northern New Mexico: II. The genesis of cryptic hybrids. Journal of Petrology. v. 28, Part 5, pp. 955-977.

Dupuy, C., Barsczus, H.G., Liotard, J.M., Dostal, J., 1988, Trace element evidence for the origin of ocean island basalts: an example from the Austral Islands (French Polynesia). Contributions to Mineralogy and Petrology. v. 98, pp. 293-302.

Eissen, J.P., Lefevre, C., Maillet, P., Morvan, G., Nohara, M., 1991, Petrology and geochemistry of the central North Fiji Basin spreading center (southwest Pacific) between 16° and 22° S. Marine Geology. v. 98, nos. 2-4, pp. 201-239.

Eissen, J.P., Nohara, M., Cotton, M., Hirose, K., 1994, North Fiji Basin basalts and their magma sources: Part I. Incompatible element constraints. Marine Geology. v. 116, nos. 1-2, pp. 153-178.

Ewart, A., Chappell, B.W., and Menzies, M.A., 1988, An overview of the geochemical and isotopic characteristics of the eastern Australian Cainozoic volcanic provinces. Journal of Petrology. Special Lithosphere Issue. pp. 225-273.

Ewart, A, 1989, East Australian petrology and geochemistry: Mineralogy and mineral chemistry. In: *Intraplate Volcanism in Eastern Australia and New Zealand.* Johnson, R.W., Knutson, J., and Taylor, S.R., (eds.), Cambridge University Press, Cambridge. pp. 189 – 217.

Falloon, T.J., Green, D.H., Danyushevshy, L.V., Faul, U.H., 1999, Peridotite melting at 1.0 and 1.5 GPa: An experimental evaluation of techniques using diamond aggregates and mineral mixes for determination of near-solidus melts. Journal of Petrology. v. 40, no. 9, pp. 1343-1375.

Falloon, T.J., Danyushevshy, L.V., Green, D.H., 2001, Peridotite melting at 1 GPa: Reversal experiments on partial melt compositions produced by peridotite-basalt sandwich experiments. Journal of Petrology. v. 42, no. 12, pp. 2363-2390.

Faure, G., 1986, *Principles of Isotope Geology* (*2nd edition*), John Wiley and Sons, Inc. New York, 598 pp.

Ferguson, A.K., 1978, Ca-enrichment in olivines from volcanic rocks. Lithos. v. 45, pp. 189-194.

Fitton, J.G., James, D., and Leeman, W.P., 1991, Basic magmatism associated with late Cenozoic extension in the western United States: Compositional variations in space and time. Journal of Geophysical Research. v. 96, pp. 13693-13711.

Forsythe, L.M., Nielsen, R.L., and Fish, M.R., 1994, High-field-strength element partitioning between pyroxene and basaltic to dacitic magmas. Chemical Geology, v. 117, nos. 1-4, pp. 107-125.

Frey, F.A., Green, D.H., and Roy, S.D., 1978, Integrated models of basalt petrogenesis: A study of quartz tholeiites to olivine melilitites from southeastern Australia utilizing geochemical and experimental petrologic data. Journal of Petrology. v. 19, part 3, pp. 463-513.

Frey, F.A., Wise, W.S., Garcia, M.O., West, H., Kwon, S. –T., and Kennedy, A., 1990, Evolution of Mauna Kea volcano, Hawaii: Petrologic and geochemical constraints on post-shield volcanism. Journal of Geophysical Research. v. 95, no.B2, pp. 1271-1300.

Frey, F.A. and Rhodes, J.M., 1993, Intershield geochemical differences among Hawaiian volcanoes: Implications for source compositions, melting process and magma ascent paths. Philosophical Transactions of the Royal Society of London. v. A342, pp. 121-136.

Gamble, J.A., Smith, I.E.M., Graham, I.J., Kokelaar, B.P., Cole, J.W., Houghton, B.F. and Wilson, C.J.N., 1990, The petrology, phase relations and tectonic setting of basalts from the Taupo Volcanic Zone, New Zealand and the Kermadec Island Arc - Havre Trough, SW Pacific. Journal of Volcanology and Geophysical Research. v. 43, pp. 235-270.

Gamble, J.A., Smith, I.E.M., McCulloch, M.T., Graham, I.J., and Kokelaar, B.P., 1993, The geochemistry and petrogenesis of basalts from the Taupo volcanic Zone and Kermadec Island Arc, S.W. Pacific. Journal of Volcanology and Geophysical Research. v. 54, pp. 265-290.

Gamble, J., Woodhead, J., Wright, I., Smith, I., 1996, Basalt and sediment geochemistry and magma petrogenesis in a transect from oceanic island arc to rifted continental margin arc: The Kermadec-Hikurangi Margin, SW Pacific. Journal of Petrology. v. 37, no. 6, pp. 1523-1546.

Garcia, M.O., Rhodes, J.M., Trusdall, F.A., and Pietruszka, A.J., 1996, Petrology of lavas from the Puu O'o eruption of Kilauea Volcano: III. The Kupaianaha episode (1986-1992). Bulletin of Volcanology. v. 58, pp. 359-379.

Garcia, M.O., Pietruszka, A.J., Rhodes, J.M., Swanson, K., 2000, Magmatic processes during the prolonged Puu O'o eruption of Kilauea volcano, Hawaii. Journal of Petrology. v. 41, pp. 967-990.

Gardner, C.A., 1994, Temporal, spatial, and petrologic variations of lava flows from the Mount Bachelor volcanic chain, central Oregon High Cascades. U.S. Geological Survey. Open-file report 94-261. 100 pp.

Gee, L. and Sack, R.O., 1988, Experimental petrology of melilite nephelinites. Journal of Petrology. v. 29, pp. 1233-1255.

Gertsenberger, H. and Hasse, 1997, A highly effective emitter substance for mass stretrometric Pb isotope ratio determinations. Chemical Geology. v. 136, pp. 309-312.

Graham, I.J., Gulson, B.L., Hedenquist, J.W., and Nizon, K., 1992, Petrogenesis of Late Cenozoic volcanic rocks from the Taupo Volcanic Zone, New Zealand, in the light of new lead data. Geochimica et Cosmochimica Acta. v. 56, pp. 2797-2819.

Green, D.H. and Ringwood, A.E., 1967, The genesis of basaltic magmas. Contributions to Mineralogy and Petrology. v. 15, pp. 103-190.

Green, D.H., 1970, The origin of basaltic and nephelinitic magmas in the Earth's mantle. Leicester Literary and Philosophical Society. pp. 28-54.

Green, D.H., 1973a, Conditions of melting of basanite magma from garnet peridotite. Earth and Planetary Science Letters. v. 17, pp. 456-465.

Green, D.H., 1973b, Contrasted melting relations in a pyrolite upper mantle under mid-oceanic ridge, stable crust and island arc environments. Tectonophysics. v. 17, pp. 285-297.

Green, D.H., 1973c, Experimental melting studies on a model upper mantle composition at high pressure under water-saturated and water-undersaturated conditions. Earth and Planetary Science Letters. v. 19, pp. 37-53.

Green, T.H., 1992, Petrology and geochemistry of basaltic rocks from the Balleny Is, Antarctica. Australian Journal of Earth Sciences. v. 39, pp. 603-617.

Green, T.H., 1995, Significance of Nb/Ta as an indicator of geochemical processes in the crust-mantle system. Chemical Geology. v. 120, nos. 3 and 4, pp. 347-359.

Hamilton, D.L., 1961, Nephelines as crystallisation temperature indicators. Journal of Geology. v. 69, pp. 321-369.

Hanson, G.N., 1980, Rare earth elements in petrogenetic studies of igneous systems. Annual Review of Earth and Planetary Sciences. v. 8, pp. 371-406.

Hanson, G.N. and Langnuir, C.H., 1978, Modelling of major and trace elements in mantle-melt systems using trace element approaches. Geochimica et Cosmochimica Acta. v. 42, pp. 725-741.

Hart, S.R., 1984, A large-scale isotope anomaly in the Southern Hemisphere mantle. Nature. v. 309, pp. 753-757.

Hart, S.R. and Davis, K.E., 1978. Nickel partitioning between olivine and silicate melt. Earth and Planetary Science Letters. v. 40, pp. 203-219.

Hart, S.R. and Allègre, C.J., 1980, Trace-element constraints on magma genesis. In: *Physics of Magmatic Processes.* Princeton University Press. pp. 121-159.

Hart, S.R., and Dunn, T., 1993, Experimental clinopyroxene/melt partitioning of 24 trace elements. Contributions to Mineralogy and Petrology. v. 113, no. 1, pp 1-8.

Hatherton, T, and Sibson, R.H., 1969, Junction Magnetic Anomaly north of the Waikato River. New Zealand Journal of Geology and Geophysics. v. 13, no. 3, pp. 655-662.

Hatherton, T., Davey, F.J., and Hunt, T.M., 1979, Geophysical anomalies and igneous bodies off the west coast, New Zealand. Journal of the Royal Society of New Zealand. v. 9, no. 1, pp. 13-28.

Hauri, E.H., Wagner, T.P. and Grove, T.L., 1994. Experimental and natural partitioning of Th, U, Pb and other trace elements between garnet, clinopyroxene and basaltic melts. Chemical Geology. v. 117, pp. 149-166.

Hawkesworth, C.J., Mantovani, M.S.M., Taylor, P.N., Palacz, A., 1986, Evidence from the Parana of south Brazil for a continental contribution to Dupal basalts. Nature. v. 322, pp. 356-359.

Hayward, B.W., Black, P.M., Smith, I.E.M., Ballance, P.F., Itaya, T., Doi, M., Takagi, M., Bergman, S., Adams, C.J., Herzer, R.H., Robertson, D.J., 2001, K-Ar ages of early Miocene arc-type volcanoes in northern New Zealand. New Zealand Journal of Geology and Geophysics. v. 44, no. 2, pp. 285-311.

Helz, R.T., 1987, Diverse olivine types in lava of the 1959 eruption of Kilauea Volcano and their bearing on eruption dynamics. In: *Volcanism in Hawaii, Volume 1.* (eds. Decker, R.W., Wright, T.L., and Stauffer, P.H.), U.S. Geological Survey Professional Paper 1350, pp. 691-722.

Helz, R.T. and Wright, T., 1992, Differentiation and magma mixing on Kilauea's east rift zone: A further look at the eruptions of 1955 and 1960. Part I. The late 1955 lavas. Bulletin of Volcanology. v. 54, pp. 361-384.

Heming, R.F., 1980a, Petrology and geochemistry of Quaternary basalts from Northland, New Zealand. Journal of Volcanology and Geothermal Research. v. 8, pp. 23-44.

Heming, R.F., 1980b, Patterns of Quaternary basaltic volcanism in the northern North Island, New Zealand. New Zealand Journal of Geology and Geophysics. v. 23, pp. 335-344.

Heming, R.F. and Barnet, P.R., 1986, The petrology and petrochemistry of the Auckland volcanic field. In: *Late Cenozoic Volcanism in New Zealand.* Smith, I.E.M. (ed). The Royal Society of New Zealand. Bulletin 23, pp. 64-75.

Henderson, C.M.B. and Gibb F.G.F., 1983, Felsic mineral crystallization trends in differentiating alkaline basic magmas. Contributions to Mineralogy and Petrology. v. 84, pp. 355-364.

Henderson, J. and Grange, L.I., 1926, The geology of the Huntly – Kawhia subdivision, Pirongia Division. New Zealand Geological Survey Bulletin, Number 28.

Hergt, J.M. and Hawkesworth, C.J., 1994, Pb-, Sr-, and Nd-isotopic evolution of the Lau Basin: Implications for mantle dynamics during bark-arc opening. In: Hawkins, J., Parson, L., Allan, J., *et al.* (eds.), *Proc. OPD Sci. Results.* v. 135, College Station, TX, (Ocean Drilling Program), pp. 505-517.

Herzberg, C., and Zhang, J., 1996, Melting experiments on anhydrous peridotite KLB-1: Compositions of magmas in the upper mantle and transition zone. Journal of Geophysical Research. v. 101, no. B4, pp. 8271-8295.

Herzer, R.H., 1995, Seismic stratigraphy of a buried volcanic arc, Northland, New Zealand and implications for Neogene subduction. Marine and Petroleum Geology. v. 12, pp. 511-531.

Hirose, K. and Kushiro, 1993, Partial melting of dry peridotites at high pressures: Determination of compositions of melts segregated from peridotite using aggregates of diamond. Earth and Planetary Science Letters. v. 114, pp. 477-489.

Hirose, K. and Kawamoto, T., 1995, Hydrous partial melting of lherzolite at 1 GPa: The effect of H_2O on the genesis of basaltic magmas. Earth and Planetary Science Letters. v. 133, pp. 463-473.

Hirschmann, M.M. and Ghiorso, M.S., 1994, Activities of nickel, cobalt, and manganese silicates in magmatic liquids and applications to olivine/liquid and to silicate/metal partitioning. Geochimica et Cosmochimica Acta. v. 58, no. 19, pp. 4109-4126.

Hoang, N., Flower, M., Carlson, 1996, Major, trace element, and isotopic compositions of Vietnamese basalts: Interaction of hydrous EM1-rich asthenosphere with thinned Eurasian lithosphere. Geochimica et Cosmochimica Acta. v. 60, no. 22, pp. 4329-4351.

Hoang, N. and Flower, M., 1998, Petrogenesis of Cenozoic basalts from Vietnam: Implication for origins of a 'diffuse igneous province'. Journal of Petrology. V. 39, no. 3, pp. 369-395.

Hochstein, M.P. and Nixon, I.M., 1979, Geophysical study of the Hauraki Depression, North Island, New Zealand. New Zealand Journal of Geology and Geophysics. v. 22, pp. 1-22.

Hochstein, M.P. and Ballance, P.F., 1993, Hauraki Rift: A young, active, intra-continental rift in a back-arc setting. In: *South Pacific Sedimentary basins.* Sedimentary Basins of the World, 2. Ballance, P.F. (ed). Elsevier, New York, New York. pp. 295-305.

Hodder, A.P.W., 1984, Late Cenozoic rift development and intra-plate volcanism in northern New Zealand inferred from geochemical discrimination diagrams. Tectonophysics. v. 101, pp. 293-318.

Hodder, A.P.W., 1988, A mantle heterogeneity in the southwest Pacific. Tectonophysics. v. 156, pp. 145-165.

Hofmann, A.W., 1986, Nb in Hawaiian magmas: Constraints on source compositions and evolution. Chemical Geology. v. 57, pp. 17-30.

Holcomb, R.T., Reiners, P.W., Nelson, B.K., Sawyer, N. –L.E., 1997, Evidence for two shield volcanoes exposed on the island of Kauai, Hawaii. Geology. v. 25, pp. 811-814.

Horn, I., Foley, S.F., Jackson, S.E. and Jenner, G.A., 1994. Experimentally determined partitioning of high field strength- and selected transition elements between spinel and basaltic melt. Chemical Geology. v. 117, pp. 193-218.

Huang, Y., Hawkesworth, C., van Calsteren, P., Smith, I., and Black, P., 1997, Melting generation models for the Auckland volcanic field, New Zealand: constraints from U-Th isotopes. Earth and Planetary Science Letters. v. 149, pp. 477-489.

Huang, Y., Hawkesworth, C., Smith, I.E.M., van Calsteren, P., and Black, P.M., 2000, Geochemistry of late Cenozoic basalt volcanism in Northland and Coromandel, New Zealand: implications for mantle enrichment processes. Chemical Geology. v. 164, pp. 219-238.

Huebner, J.S. and Sato, M., 1970, The oxygen fugacity-temperature relationships of manganese oxide and nickel oxide buffers. American Mineralogist. v. 55, pp. 934-952.

Hunt, T.M., 1978, Stoke's magnetic anomaly system. New Zealand Journal of Geology and Geophysics. v. 21, pp. 595-606.

Irvine, T.L.I. and Baragar, W. R. I., 1971, A guide to chemical classification to common volcanic rocks. Canadian Journal of Earth Science. v. 8, pp. 523-548.

Irving, A.J., 1978, A review of experimental studies of crystal/liquid trace element partitioning. Geochimica et Cosmochimica Acta. v. 42, pp. 743-770.

Irving, A.J. and Green, D.H., 1972, Experimental study of phase relationships in a high-pressure mugearitic basalt as a function of water content. Abstract; Abstracts with Programs, Geological Society of America Meetings. v. 4, pp. 550-551.

Irving, A.J. and Frey, F.A., 1984, Trace element abundances in megacrysts and their host basalts: Constraints on partition coefficients and magacryst genesis. Geochimica et Cosmochimica Acta. v. 48, pp. 1201-1221.

Ito, E., White, W.M., and Göpel, C., 1987, The O, Sr, Nd and Pb isotope geochemistry of MORB. Chemical Geology. V. 62, pp. 157-176.

Iwanori, H., 1992, Degree of melting and source composition of Cenozoic basalts in Southwest Japan: Evidence for mantle upwelling by flux melting. Journal of Geophysical Research. v. 97, no. B7, pp. 10983-10995.

Jaques, A.L. and Green, D.H., 1980, Anhydrous melting of peridotite at 0 – 15 kb pressure and the genesis of tholeiitic basalts. Contributions to Mineralogy and Petrology. v. 73, pp. 287-310.

Jenner, G.A., Foley, S.F., Jackson, S.E., Green, T.H., Fryer, B.J. and Longerich, H.P., 1994. Determination of partition coefficients for trace elements in high pressure-temperature experimental run products by laser ablation microprobe-inductively coupled plasma-mass spectrometry (LAM-ICP-MS). Geochimica et Cosmochimica Acta. v. 58, pp. 5099-5103.

Johnson, R.W. and Duggan, M.B., 1989, Rock classification and analytical data bases. In: *Intraplate Volcanism in Eastern Australia and New Zealand.* Johnson, R.W., Knutson, J., and Taylor, S.R., (eds.), Cambridge University Press, Cambridge. pp. 12-13.

Jukic, M.F., 1995, A geological and geophysical subsurface investigation of the South Auckland volcanic field. Unpublished MSc thesis lodged in the library at University of Auckland, Auckland, New Zealand.

Jung, S. and Masberg, P., 1998, Major- and trace-element systematics and isotope geochemistry of Cenozoic mafic volcanic rocks from the Vogelsberg (central Germany): Constraints on the origin of continental alkaline and tholeiitic basalts and their mantle sources. Journal of Volcanology and Geothermal Research. V. 86. Pp. 151-177.

Jurewicz, A.J.G. and Watson, E. B., 1988a, Cations in olivine, Part 1: Calcium partitioning and calcium – magnesium distribution between olivines and coexisting melts, with petrologic applications. Contributions to Mineralogy and Petrology. v. 99, pp. 176-185.

Jurewicz, A.J.G. and Watson, E. B., 1988b, Cations in olivine, Part 2: Diffusion in olivine xenocrysts, with applications to petrology and mineral physics. Contributions to Mineralogy and Petrology. v. 99, pp. 186-201.

Kamp, P.J.J. and Liddell, I.J., 2000, Thermochronology of northern Murihiku Terrane, New Zealand, derived from apatite FT analysis. Journal of the Geological Society, London. v. 157, pp. 345-354.

Kear, D., 1964, Volcanic alignments north and west of New Zealand's Central Volcanic Region. New Zealand Journal of Geology and Geophysics. v. 7, pp. 24-44.

Keleman, P.B. and Dunn, J.T., 1992. Depletion of Nb relative to other highly incompatible elements by melt/rock reaction in the upper mantle (abst.). EOS v. 73, pp. 656-657.

Kelsey, H.M., Cashman, S.M., Beanland, S., and Berryman, K.R., 1995, Structural evolution along the inner forearc of the obliquely convergent Hikurangi Margin, New Zealand. Tectonics. v. 14, no. 1, pp. 1-18.

Kempton, P.D., Dungan, M.A., and Blanchard, D.P., 1987, Petrology and geochemistry of xenolith-bearing alkalic basalts from the Geranimo volcanic field, southeast Arizona; Evidence for polybaric fractionation and implications for mantle heterogeneity. In: *Mantle Metasomatism and Alkaline Magmatism.* Geological Society of America Special Paper 215. Morris, E.M. and Pasteris, J.D. (eds.). pp. 347-370.

Kerr, R.C. and Lister, J.R., 1988, Island arc and mid-ocean ridge volcanism, modelled by diapirism from linear source regions. Earth and Planetary Science Letters. v. 88, pp. 143-152.

Kinzler, R.J. and Grove, T.L., 1992, Primary magmas of Mid-Ocean Ridge basalts 1. Experiments and methods. Journal of Geophysical Research. v. 97, no. B5, pp. 6885-6906.

Kinzler, R.J., Donnelly-Nolan, J.M., Grove, T.L., 2000, Late Holocene hydrous mafic magmatism at the Paint Pot Crater and Callahan flows, Medicine Lake Volcano, N. California, and the influence of H_2O in the genesis of silicic magmas. Contributions to Mineralogy and Petrology. v. 138, pp. 1-16.

Kohn, S.C. and Schofield, P.F., 1994, The importance of melt composition in controlling trace-element behaviour: An experimental study of Mn and Zn partitioning between forsterite and silicate melts. Chemical Geology. v. 117, pp. 73-87.

Kurz, M.D. and Kammer, D.P., 1991, Isotopic evolution of Mauna Loa volcano. Earth and Planetary Science Letters. v. 103, pp. 257-269.

Kurz, M.D., Kenna, T.C., Kammer, D.P., Rhodes, J.M., Garcia, M.O., 1995, Isotopic evolution of Mauna Loa volcano: A view from the submarine southwest rift zone. In: *Mauna Loa revealed.* Rhodes, J.M. and Lockwood, J.P. (eds). American Geophysical Union. Washington D.C. pp. 289-306.

Kyle, P.R., Moore, J.A., and Thirlwall, M.F., 1992, Petrologic evolution of anorthoclase phonolite lavas and Mount Erebus, Ross Island, Antarctica. Journal of Petrology. v. 33, no. 4, pp. 849-875.

Langmuir, C.H., Bender, J.F., Bence, A.E., Hanson, G.N., and Taylor, S.R., 1977, Petrogenesis of basalts from the FAMOUS area: Mid-Atlantic ridge. Earth and Planetary Science Letters. v. 36, pp. 133-156.

Langmuir, C.H., Vocke, R.D., Hanson, G.N., and Hart, S.R., 1978, A general mixing equation with applications to Icelandic basalts. Earth and Planetary Science Letters. v. 37, pp. 380-392.

Lanyon, R., Varne, R., Crawford, A.J., 1993, Tasmanian Tertiary basalts, the Balleny plume, and opening of the Tasman Sea (southwest Pacific Ocean. Geology, v. 21, pp. 555-558.

Lassiter, J.C., Hauri, E.H., Reiners, P.W., Garcia, M.O., 2000, Generation of Hawaiian post-erosional lavas by melting of a mixed lherzolites/pyroxenite source. Earth and Planetary Science Letters. v. 178, pp. 269-284.

Le Bas, M.J., Le Maitre, R.W., and Streckeisen, A., 1986, A chemical classification of volcanic rocks based on the total alkali – silica diagram. Journal of Petrology. v. 27, pp. 745-750.

Le Maitre, R.W., Bateman, P., Dudek, A., Keller J., Lameyre Le Bas, M.J., Sabine, P.A., Schmid, R., Sorenson, H., Streckeisen, A., Wooley, A.R., and Zanettin, B., 1989, *A classification of igneous rocks and glossary of terms*. Blackwell, Oxford.

Lemarchande, F., Benoit, V., and Calais, G., 1987, Trace element distribution coefficients in alkaline series. Geochimica et Cosmochimica Acta. v. 51, pp. 1071-1081.

Libourel, G., 1999, Systematics of calcium partitioning between olivine and silicate melt: Implications for melt structure and calcium content of magmatic olivines. Contributions to Mineralogy and Petrology. v. 136, pp. 63-80.

Lindsley, D.H., 1983, Pyroxene thermometry. American Mineralogist. v. 68, pp. 477-493.

Lindstrom, C.C., Shaw, H.F., Ryerson, F.J., Williams, Q., and Gill, J., 1998, Crystal chemical control of clinopyroxene-melt partitioning in the Di-Ab-An system: Implications for elemental fractionations in the depleted mantle. Geochimica et Cosmochimica Acta. v. 62, no. 16, pp. 2849-2862.

Liotard, J.M., Briot, D., and Boivin, P., 1988, Petrological and geochemical relationships between pyroxene megacrysts and associated alkali-basalts from Massif Central (France). Contributions to Mineralogy and Petrology. v. 98, pp. 81-90.

Lister, G.S. and Etheridge, M.A., 1989, Detachment models for uplift and volcanism in the Eastern Highlands, and their application to the origin of passive margin mountains. In: *Intraplate Volcanism in Eastern Australia and New Zealand*. Johnson, R.W., Knutson, J., and Taylor, S.R., (eds.), Cambridge University Press, Cambridge. pp. 297-312.

Liu, C-Q., Masuda, A., and Xie, G-H., 1994, Major and trace element compositions of Cenozoic basalts in eastern China: Petrogenesis and mantle source. Chemical Geology. v. 114, pp. 19-42.

MacDonald, G.A. and Katsura, T., 1964, Chemical compositions of Hawaiian lavas. Journal of Petrology. v. 5, p. 82-133.

Maaløe, S., 1982, Geochemical aspects of permeability controlled partial melting and fractional crystallization. Geochimica et Cosmochimica Acta. v. 46, pp. 43-57.

Maaløe, S. and Hansen, B., 1982, Olivine phenocrysts of Hawaiian olivine tholeiite and oceanite. Contributions to Mineralogy and Petrology. v. 81, pp. 203-211.

Maaløe, S., James, D.E., Smedley, P., Petersen, S., Garmann. L.B., 1992, The Koloa volcanic suite of Kauai, Hawaii. Journal of Petrology. v. 33, pp. 761-784.

MacKenzie, W.S., Donaldson, C.H., Guilford, C., 1982, *Atlas of igneous rocks and their textures*. Longman Group Limited. Essex, England. 148 p.

Malpas, J., Spörli, R.B., Black, P.M., and Smith, I.E.M., 1992, Northland Ophiolite, New Zealand, and implications for plate-tectonic evolution of the southwest Pacific. Geology. v. 20, pp. 149-152.

Marsh, B.B., 1988, Crystal size distribution (CSD) in rocks and the kinetics and dynamics of crystallisation I. Theory. Contributions to Mineralogy and Petrology. v. 99, pp. 277-291.

McBride, J.S, 1998, *Re-Os isotopic evidence for the age and evolution of the southeastern Australian sub-continental lithosphere mantle*. Unpublished PhD thesis, lodged in the library, Monash University, Melbourne, Australia.

McBride, J.S, Lambert, D.D., Nicholls, Price, R.C., 2001, Osmium isotopic evidence for crust-mantle interaction in the genesis of continental intraplate basalts form the Newer Volcanics Province, southeastern Australia. Journal of Petrology. v. 42, no. 6, pp. 1197-1218.

McCulloch, M.T., Kyser, T.K., Woodhead, J.D., and Kinsley, L., 1994, Pb-Sr-Nd-O isotopic constraints on the origin of rhyolites from the Taupo Volcanic Zone of New Zealand: Evidence for assimilation followed by fractionation from basalt. Contributions to Mineralogy and Petrology. v. 115, no. 3, pp. 303-312.

McDonough, W.F., McCulloch, M.T., and Sun, S.S., 1985, Isotopic and geochemical systematics in Tertiary-Recent basalts from southeastern Australia and implications for the evolution of the sub-continental lithosphere. Geochimica et Cosmochimica Acta. v. 49?, pp. 2051-2067.

McKenzie, D. and Bickle, M.J., 1988, The volume and composition of melt generation by extension of the lithosphere. Journal of Petrology. v. 29, no. 3, pp. 625-679.

McKenzie, D. and O'Nions, R.K., 1991, Partial melt distribution from inversion of rare earth element concentrations. Journal of Petrology. v. 32, no. 5, pp. 1021-1091.

Meschede, M., 1986, A method of discriminating between different types of mid-ocean ridge basalts and continental thoeiites with the Nb-Zr-Y diagram. Chemical Geology. v. 56, pp. 207-218.

Middlemost, E.A.K., 1989, Iron oxidation ratios, norms and the classification of volcanic rocks. Chemical Geology. v. 77, pp. 19-26.

Middleton, M.P., 1993, *A provenance study of the Triassic-Jurassic Murihiku Terrane, North Island.* Unpublished MSc thesis lodged in the library. University of Waikato, Hamilton, New Zealand.

Mitropoulos, P. and Tarney, J., 1992, Significance of mineral composition variations in the Aegean Island Arc. Journal of Volcanology and Geophysical Research. v. 51, pp. 283-303.

Miyashiro A., 1978, Nature of alkalic volcanic rock series. Contributions to Mineralogy and Petrology. v. 66, pp. 91-104.

Mohr, P.A. and Wood, C.A., 1976, Volcano spacing and lithospheric attenuation in the eastern rift of Africa. Earth and Planetary Science Letters. v. 33, pp. 126-144.

Mooney, H.M., 1970, Upper mantle inhomogeneity beneath New Zealand: Seismic evidence. Journal of Geophysical Research. v. 75, pp. 285-309.

Morimoto, N., Fabries, J., Ferguson, A.K., Ginzburg, I.V., Ross, M., Seifert, F.A., Zussman, J., Aoki, K., and Gottardi, G., 1988, Nomenclature of pyroxenes. American Mineralogist. v. 73, pp. 1123-1133.

Mortimer, N. and Smith-Lyttle, B., 2001, New Zealand's geological foundations. Wall poster. Institute of Geological and Nuclear Sciences. Lower Hutt, New Zealand.

Mysen, B.O., 1978, Limits of solution of trace elements in minerals according to Henry's Law: Review of experimental data. Geochimica et Cosmochimica Acta. v. 42, pp. 871-885.

Nakada, M., Yanagi, T., and Maida, S., 1997, Lower crustal erosion induced by mantle diapiric upwelling: Constraints from sedimentary basin formation followed by voluminous basalt volcanism in northwest Kyushu, Japan. Earth and Planetary Science Letters. v. 146, pp. 415-429.

Nakamura, N, 1974, Determination of REE, Ba, Fe, Mg, Na, and K in carbonaceous and ordinary chondrites. Geochimica et Cosmochimica Acta. v. 38, pp.757-775.

Nguyen, H., Flower, M.F., Carlson, R.W., 1996, Major, trace element, and isotopic compositions of Vietnamese basalts: Implication of hydrous EM1-rich asthenosphere with thinned Eurasian lithosphere. Geochimica et Cosmochimica Acta. v. 60, no. 22, pp. 4329-4351.

Nielson, J.E. and Noller, J.S., 1987, Processes of mantle metasomatism; Constraints from observations of composite peridotite xenoliths. In: *Mantle Metasomatism and Alkaline Magmatism.* Geological Society of America Special Paper 215. Morris, E.M. and Pasteris, J.D. (eds.). pp. 61-76.

Nielsen, R.L., Forsythe, L.M., Gallahan, W.E., and Fisk, M.R., 1994, Major- and trace-element magnetite-melt equilibria. Chemical Geology. v. 117, pp. 167-191.

Nimis, P., 1995, A clinopyroxene geobarometer for basaltic systems based on crystal-structure modelling. Contributions to Mineralogy and Petrology. v. 121, pp. 115-125.

Nimis, P. and Ulmer, P., 1998, Clinopyroxene geobarometry of magmatic rocks Part 1: An expanded structural geobarometer for anhydrous and hydrous basic and ultrabasic systems. Contributions to Mineralogy and Petrology. v. 133, pp. 122-135.

Nixon, G.T. and Pearce, T.H., 1987, Laser-interferometry study of oscillatory zoning in plagioclase: The record of magma mixing and phenocryst recycling in calc-alkaline magma chambers, Iztaccíhautl volcano, Mexico. American Mineralogist. v. 72, nos. 11-12, pp. 1144-1162.

Nohara, M., Hirose, K., Eissen, J.P., Urabe, T., Joshima, M., 1994, The North Fiji Basin basalts and their magma sources: Part II. Sr-Nd isotopic and trace element constraints. Marine Geology. v. 116, nos. 1-2, pp. 179-195.

Norman, M.D., 1998, Melting and metasomatism in the continental lithosphere: Laser ablation ICPMS analysis of minerals in spinel lherzolites from eastern Australia. Contributions to Mineralogy and Petrology. v. 130, pp. 240-255.

O'Brien, H.E., Irving, A.J., and McCallum. I.S., 1988, Complex zoning and resorption of phenocrysts in mixed potassic mafic magmas of the Highwood Mountains, Montana. American Mineralogist. v. 73, pp. 1007-1024.

O'Reilly, S.Y. and Griffin, W.L., 1988, Mantle metasomatism beneath western Victoria, Australia: I. Metasomatic processes in Cr-diopside lherzolites. Geochimica et Cosmochimica Acta. v. 52, pp. 433-447.

O'Reilly, S.Y., Nicholls, I.A., Griffin, W.L., 1989, Xenoliths and megacrysts of mantle origin. In: In: *Intraplate Volcanism in Eastern Australia and New Zealand.* Johnson, R.W., Knutson, J., and Taylor, S.R., (eds.), Cambridge University Press, Cambridge. pp. 254-274.

O'Reilly, S.Y. and Zhang, M, 1995, Geochemical characteristics of lava-field basalts from eastern Australia and inferred sources: Connections with the subcontinental lithospheric mantle? Contributions to Mineralogy and Petrology. v. 121, pp. 148-170.

Okamoto, K., 1979. Geochemical study on magmatic differentiation of Asama volcano, Central Japan. Journal of the Geological Society of Japan. v. 85, pp. 525-535.

Palacz, Z.A. and Sanders, A.D., 1986, Coupled trace element and isotope enrichment in the Cook-Austral-Samoa islands, southwest Pacific. Earth and Planetary Science Letters. v. 79, pp. 270-280.

Panter, K.S., Hart, S.R., Kyle, P., Blusztanjn, J., and Wilch, T., 2000, Geochemistry of Late Cenozoic basalts from the Crary Mountains: Characterisation of mantle sources in Marie Byrd Land, Antarctica. Chemical Geology. v. 165, pp. 215-241.

Parker, R.J., Smith, I.E.M., and Wilmshurst, J.K., 1993, *Sample preparation for XRF and ICP analysis. Department of Geology – Report No. 2*, University of Auckland, New Zealand. 14 pp.

Paslick, C., Halliday, A., James, D., and Dawson, J.B., 1995, Enrichment of the continental lithosphere by OIB melts: Isotopic evidence from the volcanic province of northern Tanzania. Earth and Planetary Science Letters. v. 130, pp. 109-126.

Paster, T.P, Schauwecher, D.S. and Haskin, L.A., 1974. The behaviour of some trace elements during solidification of the Skaergarrd layered series. Geochimica et Cosmochimica Acta. v. 38, pp. 1549-1577.

Pearce, J.A., 1982, Trace element characteristics of lavas from destructive plate boundaries. In: *Andesites.* Thorpe, R.S. (ed). Chinchester: Wiley, pp. 525-548.

Pearce, J.A. and Norry, M.J., 1979, Petrogenetic implications of Ti, Zr, Y, and Nb variations in volcanic rocks. Contributions to Mineralogy and Petrology. v. 69, pp. 33-47.

Pearce, T.H., Russell, J.K., and Wolfson, I., 1987, Laser-interference and Nomarski interference imaging of zoning profile in plagioclase phenocrysts from the May 18. 1980 eruption of Mount St. Helens, Washington. American Mineralogist. v. 72, nos. 11-12, pp. 1131-1143.

Peck, D.L., 1978, Cooling and vesiculation of Alae lava lake, Hawaii. U.S. Geological Survey Professional Paper, 935-B, 59 pp.

Petch, R.A., Bell, A.R., Depledge, D., Hadfield, J.C., Maggs, G.R., and Ringham, K.L., 1991, An assessment of ground and surface water resources in the Pukekohe/Tuakau area. Waikato Regional Council Technical Report 1991/12. Environment Waikato, Hamilton, New Zealand. 141 pp.

Philpotts, J.A. and Schnetzler, C.C., 1970. Phenocryst-matrix partition coefficients for K, Rb, Sr, and Ba, with applications to anorthosite and basalt genesis. Geochimica et Cosmochimica Acta. v. 34, pp. 307-322.

Pietruszka, A.J. and Garcia, M.O., 1999, A rapid fluctuation in the mantle source and melting history of Kilauea volcano inferred from the geochemistry of its historical summit lavas (1790-1982). Journal of Petrology. v. 40, pp. 1321-1342.

Pilaar, W.F.H. and Wakefield, L.L., 1978, Structural and stratigraphic evolution of the Taranaki Basin, offshore North Island, New Zealand. APEA Journal. v. 18, pp. 93-101.

Price, R.C., Gray, C.M., Wilson, R.E., Frey, F.A., and Taylor, S.R., 1991, The effects of weathering on rare-earth element, Y and Ba abundances in Tertiary basalts from southeastern Australia. Chemical Geology. v. 93, pp. 245-265.

Price, R.C., Gray, C.M., and Frey, F.A., 1997, Strontium isotopic and trace element heterogeneity in the plains basalts of the Newer Volcanic Province, Victoria, Australia. Geochimica et Cosmochimica Acta. v. 61, no. 1, pp. 171-192.

Price, R.C., Stewart, R.B., Woodhead, J.D., and Smith, I.E.M., 1999, Petrogenesis of high-K arc magmas: Evidence from Egmont Volcano, North Island, New Zealand. Journal of Petrology. v. 40, no. 1, pp. 167-197.

Putirka, K., 1999, Clinopyroxene + liquid equilibria to 100 kbar and 2450 K. Contributions to Mineralogy and Petrology. v. 135, pp. 151-163.

Putirka, K., Johnson, M., Kinzler, R., Longhi, J., and Walker, D., 1996, Thermobarometry of mafic igneous rocks based on clinopyroxene-liquid equilibria, 0-30 kbar. Contributions to Mineralogy and Petrology. v. 123, pp. 92-108.

Rafferty, W.J., 1977, *The volcanic geology and petrology of South Auckland.* Unpublished MSc thesis, lodged in the library. University of Auckland, Auckland, New Zealand.

Rafferty, W.J. and Heming, R.F., 1979, Quaternary alkalic and sub-alkalic volcanism in South Auckland, New Zealand. Contributions to Mineralogy and Petrology. v. 71, no. 2, pp. 139-150.

Reiners, P.W. and Nelson, B.K., 1998, Temporal-compositional-isotopic trends in rejuvenated-stage magmas of Kauai, Hawaii, and implications for mantle melting processes. Chemical Geology. v. 62, pp. 2347-2368.

Rhodes, J.M. and Hart, S.R., 1995, Episodic trace element and isotopic variations in historical Mauna Loa lavas: Implications for magma and plume dynamics. In: *Mauna Loa Revealed.* Rhodes, J.M. and Lockwood, J.P. (eds), American Geophysical Union. Washington D.C. pp. 263-288.

Richards, J.R., 1986, Lead isotopic signatures: Further examination of comparisons between South Africa and Western Australia. Transactions of the Geological Society of South Africa. v. 89, pp. 285-290.

Richter, D.H., Eaton, J.P., Murata, K.J., Ault, W.U., and Kirvoy, H.L., 1970, The 1959-1960 eruption of Kilauea Volcano, Hawaii. U.S. Geological Survey Professional Paper, 537-E, pp. 73.

Ringwood, A.E., 1990, Slab-mantle interactions: 3. Petrogenesis of intraplate magmas and structure of the upper mantle. Chemical Geology. v. 82, pp. 187-207.

Robinson, J.A.C., Wood, B.J., Blundy, J.D., 1998, The beginning of melting of fertile and depleted peridotite at 1.5 GPa. Earth and Planetary Science Letters. v. 155, pp. 97-111.

Roeder, P.L and Emslie, R.F., 1970, Olivine-liquid equilibrium. Contributions to Mineralogy and Petrology. v. 29, pp. 275-289.

Rollinson, H., 1993, *Using Geochemical Data: Evaluation, Presentation, Interpretation.* Longman Group Limited. Essex, England. 352 pp.

Rosenberg, M.D., 1991, *The nature and mechanism of phreatomagmatic volcanism in the South Auckland Volcanic Field.* Unpublished MSc thesis lodged in the library. University of Waikato, Hamilton, New Zealand.

Sack R.O. and Carmichael, I.S.E., 1984, $Fe^{2+} \leftrightarrow Mg_2$ and $TiAl_2 \leftrightarrow MgSi_2$ exchange reactions between clinopyroxenes and silicate melts. Contributions to Mineralogy and Petrology. v. 85, pp. 103-115.

Sack, R.O. and Ghiorso, M.S., 1994, Thermodynamics of multicomponent pyroxenes: III. Calibration of $Fe^{2+}(Mg)_{-1}$, $TiAl_2(MgSi_2)_{-1}$, $TiFe_2^{3+}(MgSi_2)_{-1}$, $AlFe^{3+}(MgSi)_{-1}$, $NaAl(CaMg)_{-1}$, $Al_2(MgSi)_{-1}$, and $Ca(Mg)_{-1}$, exchange reactions between pyroxenes and silicate melts. Contributions to Mineralogy and Petrology. v. 118, pp. 271-296.

Sanders, R.J., 1994, Ultramafic and mafic xenoliths from the Okete, Ngatutura, and South Auckland volcanics. Unpublished MSc thesis lodged in the library. University of Waikato, Hamilton, New Zealand.

Sato, M and Valenza, M., 1980, Oxygen fugacities of the layered series of the Skaergaard Intrusion, East Greenland. American Journal of Science. v. 280-A, Part 1, pp. 134-158.

Saunders, A.D., Norry, M.J., and Tarney, J., 1988, Origin of MORB and chemically-depleted mantle reservoirs: Trace element constraints. Journal of Petrology, *Special Lithosphere Issue.* pp. 415-445.

Schock, H.H., 1979, Distribution of rare earth and other trace elements in magnetites. Chemical Geology. v. 26, pp. 119-133.

Schofield, J.C., 1976, Sheet N48, Mangatawhiri, 1st (ed). Geological Map of New Zealand, 1:63360. Map and notes, pp. 28. New Zealand Geological Survey. Department of Scientific and Industrial Research, Wellington, New Zealand.

Schofield, J.C., 1988, Sheet QM 281, Manukau. Interim Geological Map of New Zealand, 1:250000. Map and notes. New Zealand Geological Survey. Department of Scientific and Industrial Research, Wellington, New Zealand.

Schwindinger, K.R., Roppo, P.S., and Anderson, A.T., Jr., 1983, Synneusis of olivine phenocrysts into glomerophophyritic clusters (abs.): Geological Society of America Abstracts with Programs. v. 15, p. 682.

Schwindinger, K.R. and Anderson Jr, A.T., 1989, Synneusis of Kilauea Iki olivines. Contributions to Mineralogy and Petrology. v. 103, no. 2, pp. 187-198.

Shaw, H.R., 1980, The fracture mechanisms of magma transport from the mantle to the surface. In: *Physics of Magmatic Processes.* Hargraves, R.B. (ed.), Princeton University Press, New Jersey, pp. 201-254.

Shelley, D., 1993, *Igneous and Metamorphic Rocks Under the Microscope; classification, textures, microstructures, and mineral preferred orientations.* Chapman and Hall. London, England. 445 pp.

Shimizu, N. and Le Roex, A.P., 1986, The chemical zoning of augite phenocrysts in alkaline basalts from Gough Island, south Atlantic. Journal of Volcanology and Geophysical Research. v. 29, pp. 159-188.

Simkin, T. and Smith, J.V., 1970, Minor element distribution in olivine. Journal of Geology. v. 78, pp. 304-325.

Sims, K.W.W. and DePaolo, D.J., 1997, Inferences about mantle magma sources from incompatible element concentrations ratios in oceanic basalts. Geochimica et Cosmochimica Acta. v. 61, no. 4, pp. 765-784.

Sinton, J.M., Price, R.C., Johnson, K.T., Staudigel, H., Zindler, A., 1993, Petrology and geochemistry of submarine lavas from the Lau and North Fiji back-arc basins. Circum Pacific Council for Energy and Mineral Resources.

Skulski, T., Minarik, W., And Watson, E.B., 1994, High-pressure experimental trace-element partitioning between clinopyroxene and basaltic melts. Chemical Geology. v. 117, nos. 1-4, pp. 127-147.

Smith, I.E.M., 1989, New Zealand intraplate volcanism: North Island. In: *Intraplate Volcanism in Eastern Australia and New Zealand.* Johnson, R.W., Knutson, J., and Taylor, S.R., (eds.), Cambridge University Press, Cambridge. pp. 157-162.

Smith, I.E.M., Okada, T., Itaya, T., and Black, P.M., 1993, Age relationships and tectonic implications of late Cenozoic basaltic volcanism in Northland, New Zealand. New Zealand Journal of Geology and Geophysics. v. 36, pp. 385-393.

Song, Y., Frey, F.A., and Zhi, X., 1990, Isotopic characteristics of Hannuoba basalts, eastern China: Implications for their petrogenesis and the composition of subcontinental mantle. Chemical Geology. v. 85, pp. 35-52.

Spence, D.A. and Turcotte, D.L., 1985, Magma-driven propagation of cracks. Journal of Geophysical Research. v. 90, no. B1, pp. 575-580.

Spencer, K.J. and Lindsley, D.H., 1981, A solution model for coexisting iron-titanium oxides. American Mineralogist. v. 66, pp. 1189-1201.

Spörli, K.B., 1978, Mesozoic tectonics, North Island, New Zealand. Geological Society of America Bulletin 89. pp. 415-425.

Spörli, K.B., 1980, New Zealand and oblique-slip margins: Tectonic development up to and during the Cainozoic. Special Publication of the International Association of Sedimentologist. v. 4, pp. 147-170.

Spörli, K.B. and Ballance, P.F., 1989, Mesozoic ocean floor/continent interaction and terrane configuration, southwest Pacific area around New Zealand. In: *The Evolution of the Pacific Ocean Margins.* Oxford Monographs of Geology and Geophysics 8. Abraham Z.B. (ed.). Oxford University Press, Oxford. pp. 176-190.

Spörli, K.B. and Eastwood, V.R., 1997, Elliptical boundary of an intraplate volcanic field, Auckland, New Zealand. Journal of Volcanology and Geothermal Research. v. 79, pp. 169-179.

Stern, R.J., Ping, N., Morris, J.D., Jackson, M.C., Fryer, P., Bloomer, S.H., Ito, E., 1990, Enriched back-arc basin basalts from the northern Mariana trough: Implications for the magmatic evolution of back-arc basins. Earth and Planetary Science Letters. v. 100, nos. 1-3, pp. 210-225.

Stern, T.A., 1985, A back-arc basin formed within continental lithosphere: The Central Volcanic Region of New Zealand. Tectonophysics. v. 112, pp. 385-409.

Stern, T.A., 1987, Asymmetric back-arc spreading, heat flux and structure associated with the Central Volcanic Region of New Zealand. Earth and Planetary Science Letters. v. 85, pp. 265-276.

Stipp, J.J., 1968, *The geochronology and petrogenesis of the Cenozoic volcanics of North Island, New Zealand.* Unpublished PhD thesis, lodged in the library, Australian National University, Canberra.

Stipp, J.J. and Thompson, B.N., 1971, K/Ar ages from the volcanics of Northland, New Zealand. New Zealand Journal of Geology and Geophysics. v. 14, pp. 403-413.

Stormer, J.C., 1973, Calcium zoning in olivine and its relationship to silica activity and pressure. Geochimica et Cosmochimica Acta. v. 37, pp. 1815-1821.

Stormer, J.C., and Nicholls, J., 1978, XLFRAC: A program for the interactive testing of magmatic differentiation models. Computers and Geosciences. v. 4., pp. 143-159.

Sun, S. -s., 1980, Lead isotope study of young volcanic rocks from mid-ocean ridges, ocean islands and island arcs. Philosophical Transactions of the Royal Society of London. v. A97, pp. 409-445.

Sun, S. -s, and McDonough, W.F., 1989, Four component dynamic model for East Australian basalts. In: *Intraplate Volcanism in Eastern Australia and New Zealand.* Johnson, R.W., Knutson, J., and Taylor, S.R., (eds.), Cambridge University Press, Cambridge. pp. 333-347.

Sun, S. -s. and McDonough, W.F., 1989, Chemical and isotopic systematics of oceanic basalts: Implications for mantle composition and processes. In: *Magmatism in the Ocean Basins*, Saunders, A.D. and Norry, M. J. (eds), Geological Society Special Publication No. 42, pp. 313-345.

Swanson, D.A., Duffield, W.A., Jackson, D.B., and Peterson, D.W., 1972, The complex cooling filling of Alae crater, Kilauea Volcano, Hawaii. Bulletin of Volcanology, v. 36, pp. 105-126.

Swanson, D.A., Duffield, W.A., Jackson, D.B., and Peterson, D.W., 1979, Chronological narrative of the 1969-1971 Mauna Ulu eruption of Kilauea Volcano, Hawaii. U.S. Geological Survey Professional Paper, 1065, 55 pp.

Takahashi, E., 1978. Partitioning of Ni^{2+}, Co^{2+}, Fe^{2+}, Mn^{2+}, and Mg^{2+} between olivine and silicate melts: compositional dependence of partition coefficients. Geochimica et Cosmochimica Acta. v. 42, 1829-1854.

Takahashi, E., 1986, Melting of dry peridotite KLB-1 up to 14 GPa: Implications on the origin of peridotitic upper mantel. Journal of Geophysical Research. v. 91, no. B9, pp. 9367-9382.

Takahashi, E. And Kushiro, I. 1983, Melting of a dry peridotite at high pressure and basalt magma genesis. American Mineralogist. v. 68, pp. 859-879.

Takahashi, E., Shimazaki, T., Tsuzaki, Y., and Yoshida, H., 1993, Melting study of a peridotite KLB-1 to 6.5 GPa, and the origin of basalt magmas. Philosophical Transactions of the Royal Society of London. v. A342, pp. 105-120.

Thompson, R.H., 1974, Some high-pressure pyroxenes. Mineralogical Magazine. v. 39, pp. 768-787.

Thompson, R.N., Morrison, M.A., Dickin, A.P., Gibson, I.L., and Harmon, R.S., 1986, Two contrasting styles of interaction between basic magmas and continental crust in the British Tertiary Volcanic Province. Journal of Geophysical Research. v. 91, no. B6, pp. 5985-5997.

Trønnes, R.G., Canil, D., Wei, K., 1992, Element partitioning between silicate minerals and coexisting melts at pressures of 1 – 27 GPa, and implications for mantle evolution. Earth and Planetary Science Letters. v. 111, pp. 241-255.

Tsuchiyama, A., 1986, Melting and dissolution kinetics: Application to partial melting and dissolution of xenoliths. Journal of Geophysical Research. v. 91, no. B9, pp. 9395-9406.

Turcotte, D.L. and Oxburgh, E.R., 1976, Stress accumulation in the lithosphere. Tectonophysics. v. 35, pp. 183-199.

Turcotte, D.L. and Oxburgh, E.R., 1978, Intra-plate volcanism. Philosophical Transactions of the Royal Society of London. v. A288, no. 1355, pp. 561-579.

Velde, B. and Kushiro, I., 1978, Structure of sodium alumino-silica melts quenched at high pressure: Infrared and aluminium K-radiation data. Earth and Planetary Science Letters. v. 4, pp. 137-140.

Villemant, B., Jaffrezic, H., Joron, J-L., and Treuil, M., 1981, Distribution coefficients of major and trace elements: Fractional crystallisation in the alkali basalt series of Chaîne des Puys (Massif Central, France). Geochimica et Cosmochimica Acta. v. 45, pp. 1997-2016.

Wass, S.Y., 1979, Multiple origins of clinopyroxenes in alkali basaltic rocks. Lithos. v. 12, pp. 115-132.

Waterhouse, B.C., 1978, Sheet Nature.51, Onewhero, 1st (ed). Geological Map of New Zealand, 1:63360. Map and notes, pp. 32. New Zealand Geological Survey. Department of Scientific and Industrial Research, Wellington.

Watson, B.E., 1977, Partitioning of manganese between forsterite and silicate liquid. Geochimica et Cosmochimica Acta. v. 41, pp. 1363-1374.

Watson, B.E., 1979, Calcium content of forsterite coexisting with silicate liquid in the system Na_2O-CaO-MgO-Al_2O_3-SiO_2. American Mineralogist. v. 64, pp. 824-829.

Watson, E.B. and Green, T.H., 1981, Apatite liquid partition coefficients for the rare earth elements and strontium. Earth and Planetary Science Letters. v. 56, pp. 405-421.

Weaver, B.L., 1991a, The origin of ocean island basalts end-member compositions: trace element and isotopic constraints. Earth and Planetary Science Letters. v. 104, pp. 381-397.

Weaver, B.L., 1991b, Trace element evidence for the origin of ocean-island basalts. Geology. v. 19, pp. 123-126.

Weaver, B.L., Wood, D.A., Tarney, J., Joron, J.-L., 1986, Role of subducted sediment in the genesis of ocean island basalts: Geochemical evidence from South Atlantic ocean islands. Geology. v. 14, pp. 275-278.

Weaver, S.D., Smith, I.E.M., Sewell, R.J., Gamble, J.A., Morris, P.A., and Gibson, I.L., 1989, New Zealand Intraplate Volcanism: Trace element geochemistry. In: *Intraplate Volcanism in Eastern Australia and New Zealand.* Johnson, R.W., Knutson, J., and Taylor, S.R., (eds.), Cambridge University Press, Cambridge. pp. 180-183.

Weaver, S.D., Storey, B.C., Pankhurst, R.J., Mukasa, S.B., DiVenere, V.J., and Bradshaw, J.D., 1994, Antarctica-New Zealand rifting and Marie Byrd Land lithospheric magmatism linked to ridge subduction and mantle plume activity. Geology. v. 22, pp. 811-814.

Wedepohl, H.K., 1985, Origin of the Tertiary basaltic volcanism in the northern Hessian Depression. Contributions to Mineralogy and Petrology. v. 89, pp. 122-143.

Wedepohl, K.H., 1987, Kontinentaler Intraplatten-Vulkanismus am Beispiel der tertiären Basalte der Hessischen Senke. Fortschritte der Mineralogie. v. 65, no. 1, pp. 19-47

Wedepohl, K.H., 1995, The composition of the continental crust. Geochimica et Cosmochimica Acta. v. 59, no. 7, pp. 1217-1232.

Weertman, J., 1971, Theory of water-filled crevasses in glaciers applied to vertical magma transport beneath ocean ridges. Journal of Geophysical Research. v. 76, no. 5, pp. 1171-1183.

Weissel, J.K., Hayes, D.E., and Herron, E.M., 1977, Plate tectonics synthesis: The displacements between Australian New Zealand and Antarctica since the late Cretaceous. Marine geology. v. 25, pp. 231-277.

White, J.P. and Waterhouse, 1993, Lithostratigraphy of the Te Kuiti Group: A revision. New Zealand Journal of Geology and Geophysics. v. 36, p.255-266.

Wilkinson, J.F.G., 1991, Mauna Loan, and Kilauean tholeiites with low 'ferromagnesian-fractionated' 100 Mg/(Mg + Fe^{2+}) ratios: primary liquids from the upper mantle? Journal of Petrology. v. 32, no.5, pp. 863-907.

Wilson, C.J.N., Houghton, B.F., McWilliams, M.O., Lanphere, M.A., Weaver, S.D., and Briggs, R.M., 1995, Volcanic and structural evolution of Taupo Volcanic Zone, New Zealand: A review. Journal of Volcanology and Geothermal Research. v. 68, pp. 1-28.

Wilson, M., 1989, *Igneous Petrogenesis: A Global Tectonic Approach.* Unwin Hyman Ltd. London, 466 pp.

Wood, D.A., 1980, The application of a Th-Hf-Ta diagram to problems of tectonomagmatic classification and to establishing the nature of crustal contamination of basaltic lavas of the British Tertiary volcanic province. Earth and Planetary Science Letters. v. 50, pp. 11-30.

Wood, I.A., 1991, Thermoluminescence dating gives new ages for some Auckland basalts. Abstract. Geological Society of New Zealand miscellaneous publication 59A, p. 147.

Wörner, G. and Schmincke, H. -U., 1984a, Mineralogical and chemical zonation of the Laacher See Tephra sequence (West Eifel, W. Germany). Journal of Petrology. v. 25, no. 4, pp. 805-835.

Wörner, G. and Schmincke, H. –U., 1984b, Petrogenesis of the Zoned Laacher See Tephra, Journal of Petrology. v. 25, no. 4, pp. 836-851.

Wörner, G., Staudigel, H., and Zindler, A., 1985, Isotopic constraints on open system evolution of the Laacher See magma chamber (Eifel), West Germany. Earth and Planetary Science Letters. v. 75, pp. 37-49.

Wright, T.L. and Okamura, R.T., 1977, Cooling and crystallisation of tholeiitic basalt, 1965 Makaopuhi lava lake, Hawaii. U.S. Geological Survey Professional Paper, 1004, 78 pp.

Zhang, M. and O'Reilly, 1997, Multiple sources for basaltic rocks from Dubbo, eastern Australia: Geochemical evidence for plume-lithospheric mantle interactions. Chemical Geology. v. 136, pp. 33-54.

Zhang, M., Stephenson, P.J., O'Reilly, S.Y., McCulloch, M.T., Norman, M., 2001, Petrogenesis and geodynamic implications of late Cenozoic basalts in North Queensland, Australia: Trace-element and Sr-Nd-Pb isotope evidence. Journal of Petrology. v. 42, no. 4, pp. 685-719.

Zhi, X., Song, Y., Frey, F.A., Feng, J., and Zhai, M., 1990, Geochemistry of Hannuoba basalts, eastern China: Constraints on the origin of continental alkalic and tholeiitic basalts. Chemical Geology. v. 88, pp. 1-33.

Zhou, P., and Mukasa, S.B., 1997, Nd-Sr-Pb isotopic, and major and trace element geochemistry of Cenozoic lavas from the Khorat Plateau, Thailand: Sources and petrogenesis. Chemical Geology. v. 137, pp. 175-193.

Zindler, A. and Hart, S., 1986, Chemical geodynamics. Annual Review of Earth and Planetary Sciences. v. 14, pp. 493-571.

Zou, H., 1998, Trace element fractionation during modal and non-modal dynamic melting and open-system melting: A mathematical treatment. Geochimica et Cosmochimica Acta. v. 62, no. 11, pp. 1937-1945.

Zou, H., 2000, Modelling of trace element fractionation during non-modal dynamic melting with linear variations in mineral/melt distribution coefficients. Geochimica et Cosmochimica Acta. v. 64, no. 6, pp. 1095-1102.

Zou, H. and Zindler, A., 1996, Constraints on the degree of dynamic partial melting and source composition using concentration ratios in magmas. Geochimica et Cosmochimica Acta. v. 60. no. 4, pp. 711-717.

Zou, H., Zindler, A., Xu, X., Qi, Q., 2000, Major, trace element, and Nd, Sr and Pb isotope studies of Cenozoic basalts in SE China: Mantle sources, regional variations, and tectonic significance. Chemical Geology. v. 171, pp. 33-47.

Personal Communication:

Goles, G., University of Oregon, USA; goles@oregon.uoregon.edu

Mortimer, N., Institute of Geological and Nuclear Research, New Zealand; n.mortimer@gns.cri.nz

Nelson, C., University of Waikato, New Zealand; c.nelson@waikato.ac.nz

Putirka, K., University of Indiana, Pennsylvania, USA; kputirka@grove.iup.edu

Zou, H., University of California at Los Angles (UCLA), USA; hzou@ess.ucla.edu

Appendices

Appendix One: General Reference Information

Appendix 1

General reference information

General reference information e.g., sample numbers, geographic locations and corresponding grid references, university archive numbers, rock type and group, analyses performed, and the K-Ar age[1] for all samples used in this investigation are presented in Table A1.1.

Sample numbers and archive numbers are divided into two groups. Samples with the prefix "SA", were collected by R.M. Briggs, University of Waikato, Hamilton, New Zealand and are assigned University of Auckland archive numbers (e.g., sample number SA01 corresponds to University of Auckland archive number AU41602). Samples numbers with the prefix "SAB", were collected by the author, and are assigned University of Waikato archive numbers (e.g., sample number SAB101 corresponds to University of Waikato archive number W970050). SAB samples also have corresponding field numbers.

Locations for samples are given by geographic location and grid references for the NZMS 260 (1:50000) series.

Rock classification abbreviations

bas	basanite
neph	nephelinite
ne-haw	nepheline hawaiite
aob	alkali olivine basalt
mug	mugearite
trans	transitional basalt
haw	hawaiite
ol-th	olivine tholeiitic basalt
qz-th	quartz tholeiitic basalt

Analytical technique abbreviations

XRF	X-ray fluorescence
SSMS	Spark source mass spectrometry
ICP-MS	Inductively coupled plasma emission mass spectrometry
TIMS	Thermal ionisation mass spectrometry

The rock classification assigned to each sample is according to the scheme of Johnson and Duggan (1989). Details are discussed in Chapter 3. Because this scheme requires whole-rock geochemical data, those samples not analysed by XRF have been classified based on petrographic characteristics similar to those of classified rocks provided that these samples have a close spatial association (i.e., from the same lava flow or ponded lava. The classifications of these samples are given in italics.

[1] All K-Ar ages were determined by and are reported in Briggs *et al.* (1994).

Table A1.1 Sample location, grid reference, and analytical treatment, and general information for each SAVF sample.

Sample number	Field number	Archive number	Rock group	Rock type	Grid reference	Volcanic centre/ location	Geology description	Field occurrence	thin section	modal analysis	Microprobe analysis	XRF	SSMS	ICP-MS	TIMS	K-Ar age (Ma)	Comments
SA01		AU41602	B	ne-haw	R12/872463	Stevenson's Quarry	platy lava flow	lower flow	X	X		X				1.19 ± 0.04	abundant 30mm ultramafic xenoliths
SA02		AU41603	B	ne-haw	R12/872463	Stevenson's Quarry	lava flow	upper flow unit	X	X	X	X	X		X	1.32 ± 0.05	stratigraphically younger than SA01
SA03		AU41604	B	bas	R12/869383	Wilkins & Davies Quarry	ponded lava	middle of deposit	X	X		X				1.31 ± 0.12	abundant, up to 40mm, ultramafic xenoliths
SA05		AU41606	B	bas	R12/862329	Smeed's Quarry	ponded lava	centre of deposit	X	X		X	X		X	0.77 ± 0.05	platy jointed lava
SA06		AU41607	B	neph	R12/862329	Smeed's Quarry	ponded lava	western margin of deposit	X	X		X				0.82 ± 0.05	columnar jointed
SA07		AU41608	A	trans	R12/772333	Onepoto Volcano	ballistic bomb	strombolian scoria deposit	X	X	X	X	X		X	0.65 ± 0.10	volcano summit, youngest stratigraphically
SA08		AU41609	A	trans	R12/772333	Onepoto Volcano	ballistic bomb	strombolian scoria deposit	X	X		X					
SA09		AU41610	A	trans	R12/772333	Onepoto Volcano	ballistic bomb	strombolian scoria deposit	X	X		X					
SA10		AU41611	A	trans	R12/772333	Onepoto Volcano	ballistic bomb	strombolian scoria deposit	X	X	X	X					volcano summit, oldest stratigraphically
SA11		AU41612	A	haw	R12/796411	Pukekohe, Kitchener Road	boulder	boulder field float	X	X		X	X		X	0.56 ± 0.05	
SA12		AU41613	B	bas	R12/872361	Pokeno-Tuakau Road	lava flow	outcrop	X	X	X	X				0.64 ± 0.04	columnar jointed

Table A1.1 continued.

Sample number	Field number	Archive number	Rock group	Rock type	Grid reference	Volcanic centre/ location	Geology description	Field occurrence	thin section	modal analysis	Microprobe analysis	XRF	SSMS	ICP-MS	TIMS	K-Ar age (Ma)	Comments
SA13		AU41614	A	trans	R13/693282	Volcanic Centre, Port Waikato Road	lava flow	outcrop	X	X	X	X				0.70 ± 0.24	SAVF westernmost volcanic centre
SA14		AU41615	A	haw	R13/682274	Volcanic Centre, Port Waikato Road	lava flow	outcrop	X	X		X	X		X	0.75 ± 0.28	SAVF westernmost volcanic centre (waterfall)
SA15		AU41616	A	ol-th	R12/736313	Te Kohanga tuff ring	ballistic bomb	in tuff beds	X	X		X	X		X	1.59 ± 0.51	juvenile clast
SA16		AU41617	A	ol-th	R12/736313	Te Kohanga tuff ring	boulder	edge of tuff ring	X	X		X	X		X	1.00 ± 0.09	possibly accidental clast
SA17		AU41618	A	aob	R13/792290	Onewhero tuff ring, Kaipo Flats Road	boulder	in tuff deposit	X	X	X	X				0.88 ± 0.06	possibly older lava not related to Onewhero eruption
SA18		AU41619	A	aob	R13/787245	Kauri Road Cone	lava flow	outcrop	X	X	X	X				0.84 ± 0.07	north side of road
SA19		AU41620	A	aob	R12/843309	Smeed's Volcano	west lava flow	boulder field	X	X	X	X	X		X	0.91 ± 0.06	fresh basalt
SA20		AU41621	A	haw	R12/878308	Mile Bush Volcano	north lava flow	boulder in creek	X	X	X	X				0.66 ± 0.03	probably stransported to this location
SA21		AU41622	B	neph	R12/878308	Pukekawa Volcano	north lava flow	boulder field/ weathered flow	X	X	X	X				0.85 ± 0.05	8 mm ultramafic nodules
SA22		AU41623	B	ne-haw	S12/926342	Kellyville tuff ring	ponded lava	quarry	X	X		X				1.48 ± 0.10	
SA23		AU41624	B	bas	S12/919405	Pinnacle Hill Cone, Pokeno-Thames Hwy	lava flow	boulder field/ weathered flow	X	X		X				0.73 ± 0.04	uncertain about source of lava

Table A1.1 continued.

Sample number	Field number	Archive number	Rock group	Rock type	Grid reference	Volcanic centre/ location	Geology description	Field occurrence	thin section	modal analysis	Microprobe analysis	XRF	SSMS	ICP-MS	TIMS	K-Ar age (Ma)	Comments
SA24		AU41625	B	ne-haw	S12/986432	Mangatawhiri Cone	lava flow	boulder field/ weathered flow	X	X		X	X		X	1.38 ± 0.04	platy jointed lava
SA25		AU41626	B	ne-haw	S12/963457	Paparata Cone	ponded lava	quarry	X	X	X	X	X		X	1.59 ± 0.13	
SA26		AU41627	B	bas	R12/863569	Red Hill Cone, Papakura	large clast	volcanic breccia	X	X		X				1.10 ± 0.04	abundant ultramafic and crustal xenoliths
SA27		AU41628	B	bas	S12/571962	Hunua Falls	lava flow	outcrop	X	X	X	X	X		X	1.30 ± 0.05	complex closely-spaced jointing pattern (waterfall)
SA28		AU41629	B	neph	S12/971519	Otua Cone	boulder	boulder in creek	X	X	X	X	X		X	1.38 ± 0.04	probably stransported to location
SA29		AU41630	B	ne-haw	S12/919500	Ararime Cone	lava flow	quarry	X	X	X	X				1.34 ± 0.04	platy jointed lava
SA30		AU41631	A	haw	R12/894442	Puketutu Cone	lava flow	boulder field/ weathered flow	X	X		X				0.59 ± 0.03	
SA31		AU41632	A	qz-th	R12/864528	Drury Fault, unnamed centre	lava flow	boulder field/ weathered flow	X	X		X				2.09 ± 0.37	
SA32		AU41633	A	haw	R12/712435	Patumahoe Quarry, near Mauku	lava flow	outcrop	X	X	X	X				0.68 ± 0.07	
SA33		AU41634	A	aob	R12/712436	Patumahoe Quarry, near Mauku	ponded lava	outcrop	X	X	X	X				0.64 ± 0.04	waterfall located in quarry
SA34		AU41635	A	ol-th	R12/646403	Waitangi Falls	lava flow	outcrop	X	X		X				1.07 ± 0.22	base of waterfall

Table A1.1 continued.

Sample number	Field number	Archive number	Rock group	Rock type	Grid reference	Volcanic centre/ location	Geology description	Field occurrence	thin section	modal analysis	Microprobe analysis	XRF	SSMS	ICP-MS	TIMS	K-Ar age (Ma)	Comments
SA35		AU41636	A	ol-th	R12/684377	Waiuku Cone	boulder	boulder in creek	X	X		X				1.16 ± 0.27	possibly in situ
SA36		AU41637	A	ol-th	R12/702397	Bald Hill Cone	ballistic bomb	in lapilli tuff	X	X	X	X			X	0.94 ± 0.07	possibly accidental clast, at road cut
SA37		AU41638	B	bas	R12/702389	Barriball Road tuff ring	ballistic bomb	in tuff bed	X	X	X	X				1.00 ± 0.06	10m thich base surge deposit
SA38		AU41639	B	bas	R12/736375	Riverview Road Cone	boulder	boulder field/ weathered flow	X	X		X				0.64 ± 0.05	
SA39		AU41640	A	trans	R12/768378	Puni Domain Cone	ponded lava	quarry	X	X		X				0.66 ± .011	
SA40		AU41641	B	bas	R12/825432	Pukekohe East tuff ring	boulder	boulder field/ weathered flow	X	X		X				0.68 ± 0.03	
SA41		AU41642	B	bas	R12/828424	Jericho Road Cone	boulder	edge of lava flow	X	X		X				0.68 ± 0.03	
SA42		AU41643	B	bas	R12/836444	Rutherford Road Cone	lava flow	boulder field/ weathered flow	X	X		X				0.65 ± 0.03	
SA43		AU41644	A	ol-th	R12/848470	Raventhorpe tuff ring	ponded lava	quarry	X	X		X				0.73 ± 0.13	5 mm olivine nodules
SA44		AU41645	A	haw	R12/797325	Onewhero	lava flow	outcrop	X	X		X					
SA45		AU41646	B	bas	R13/703285	Tauranganui Cone	lava flow	boulder field/ weathered flow	X	X		X					
SA46		AU41647	B	neph	R13/739292	Pukeotahinga Cone	lava flow	boulder field/ weathered flow	X	X		X					small olivine nodules or large phenocrysts

Table A1.1 continued.

Sample number	Field number	Archive number	Rock group	Rock type	Grid reference	Volcanic centre/ location	Geology description	Field occurrence	thin section	modal analysis	Microprobe analysis	XRF	SSMS	ICP-MS	TIMS	K-Ar age (Ma)	Comments
SA47		AU41648	A	haw	R13/814262	Onewhero Cone, Kauri Road	lava flow	boulder field/ weathered flow	X	X		X					contain small ultramafic nodules
SA48		AU41649	A	trans	R13/839253	Pukekawa Volcano	lava flow	escarpment, S.W. flow terminus	X	X		X	X		X		contains white amygdales
SA49		AU41650	A	trans	R13/888258	Pukekawa Volcano	lava flow	boulder field/ weathered flow, S.E. flow	X	X		X					
SA50		AU41651	B	neph	R13/841279	Pukekawa Volcano	lava flow	boulder field/ weathered flow, W. flow	X	X		X					possible small ultramafic nodules
SA51		AU41652	B	neph	R13/873277	Pukekawa Volcano	lava flow	boulder field/ weathered flow, E. flow	X	X	X	X	X		X		
SA52		AU41653	A	haw	R13/848292	Mile Bush Volcano	lava flow	boulder field at edge of escarpment, W. flow	X	X		X	X		X		
SA53		AU41654	A	ol-th	R12/852345	Cone N.E. of Roberts Road, Tuakau	lava flow	boulder field/ weathered flow	X	X		X					
SA54		AU41655	B	aob	R12/895359	Bluff Road Cone, Pokeno	boulder	boulder field/ weathered flow	X	X	X	X					
SA55		AU41656	B	bas	R12/882402	Belle Fleur Cone, S.H.1	boulder	boulder field/ weathered flow	X	X		X	X		X		

Table A1.1 continued.

Sample number	Field number	Archive number	Rock group	Rock type	Grid reference	Volcanic centre/ location	Geology description	Field occurrence	thin section	modal analysis	Microprobe analysis	XRF	SSMS	ICP-MS	TIMS	K-Ar age (Ma)	Comments
SA56		AU41657	B	bas	R12/876398	Ridge Road tuff ring	boulder	summit edge of tuff ring	X	X		X	X		X		4 mm olivine phenocryst clusters or nodules
SA57		AU41658	B	bas	R12/897405	Pokeno Cone	lava flow	outcrop	X	X		X					in situ; well developed columnar jointing
SA58		AU41659	B	bas	S12/920424	Pinnacle Hill Road, Cone 1	lava flow	outcrop	X	X		X					
SA59		AU41660	A	ol-th	R12/873435	Razorback Road, Cone 1	boulder	stream bed	X	X		X					possibly transported to this location
SA60		AU41661	B	bas	R12/875423	Belle Fleur Cone	boulder	float N. flow	X	X		X	X		X		
SA61		AU41662	B	bas	R12/860436	Bombay Cones	boulder	stream bed	X	X		X					possibly transported to this location
SA62		AU41663	B	ne-haw	R12/868498	Peach Hill Road Cone	lava flow	outcrop	X	X		X					in situ
SA63		AU41664	B	ne-haw	R12/890510	Bellamys Basalt	boulder	stream bed	X	X		X					downstream from waterfall
SA64		AU41665	B	ne-haw	R12/875491	Pratts Road Cone	ballistic bomb	in tuff bed	X	X		X					in situ
SA65		AU41666	B	ne-haw	R12/875491	Pratts Road Cone	boulder	base tuff bed	X	X	X	X	X		X		possibly accidental clast
SA66		AU41667	B	ne-haw	R12/872512	Ballards Road Cone	lava flow	boulder field/ weathered flow	X	X		X	X		X		

Table A1.1 continued.

Sample number	Field number	Archive number	Rock group	Rock type	Grid reference	Volcanic centre/ location	Geology description	Field occurrence	thin section	modal analysis	Microprobe analysis	XRF	SSMS	ICP-MS	TIMS	K-Ar age (Ma)	Comments
SA67		AU41668	A	ol-th	R12/865543	Ponga Road Cone	lava flow	boulder field/ weathered flow	X	X		X					small ultramafic nodules
SA68		AU41669	A	ol-th	R12/854456	Raventhorpe tuff ring	lava flow	boulder field/ weathered flow	X	X		X					south side of tuff ring
SA69		AU41670	A	haw	R12/836454	Rutherfords Road Cone	boulder	N. lava flow, in stream bed	X	X		X	X		X		near edge of tuff ring
SA70		AU41671	A	haw	R12/685435	Somerville Road Cone	boulder	N.W. lava flow, in stream bed	X	X		X					weathered; zeolites in vesicles
SA71		AU41672	A	ol-th	R12/680402	Somerville Road Cone	boulder	S.W. lava flow, in stream bed	X	X		X					
SA72		AU41673	A	trans	R12/665374	Waiuku Cone	boulder	W. lava flow, in stream bed	X	X		X					
SA73		AU41674	A	ol-th	R12/746388	Puni Domain Cone	boulder	boulder field/ weathered flow	X	X		X					small ultramafic nodules
SA74		AU41675	A	haw	R12/835412	Red Crater tuff ring, Pukekohe East	boulder	rim of tuff ring	X	X		X					
SA75		AU41676	B	bas	R12/835412	Red Crater tuff ring, Pukekohe East	boulder	same tuff deposit as SA74	X	X		X					possible accessory lithic
SA76		AU41677	A	qz-th	R12/865560	Mt Calm Cone, Drury	boulder	boulder field/ weathered flow	X	X	X	X	X		X		
SA77		AU41678	A	qz-th	R12/863532	Waihoihoi Cone, Drury			X	X	X	X					7 mm olivine phenocryst clots; vesicles with zeolites

Table A1.1 continued.

Sample number	Field number	Archive number	Rock group	Rock type	Grid reference	Volcanic centre/ location	Geology description	Field occurrence	thin section	modal analysis	Microprobe analysis	XRF	SSMS	ICP-MS	TIMS	K-Ar age (Ma)	Comments
SA78		AU41679	A	haw	R12/874472	Maxted Road Cone			X	X		X					weathered; zeolites in vesicles
SA79		AU41680	A	ol-th	R12/871478	Maxted Road Tuff Cone			X	X		X					stratigraphically younger than SA80
SA80		AU41681	A	ol-th	R12/871478	Maxted Road Tuff Cone	lava flow	top of tuff cone	X	X	X	X					stratigraphically older than SA79
SA81		AU41682	A	ol-th	R12/866454	Bombay Cones	ponded lava	from quarry	X	X		X					
SA82		AU41683	B	bas	R12/895435	Puketutu Cone	boulder	from high up on cone	X	X		X					
SA83		AU41684	A	trans	R12/826377	Bucklands Cone	boulder	boulder field/ weathered flow; S.W. flow	X	X		X					
SA84		AU41685	A	trans	R12/816383	Bucklands Cone	boulder	boulder field/ weathered flow; W.S.W. flow	X	X		X					
SA85		AU41686	A	haw	R12/737443	Patumahoe Cone	boulder	boulder field/ weathered flow; E. flow	X	X		X					
SA86		AU41687	B	bas	R12/717453	Patumahoe Cone	boulder	boulder field/ weathered flow; N.W. flow	X	X		X					
SA87		AU41688	A	haw	R12/687448	Sommerville Road Cone	boulder	boulder field/ weathered flow; N. flow	X	X		X					
SA88		AU41689	B	mug	R12/687448	Sommerville Road Cone	segregation vein	boulder field/ weathered flow; N. flow	X	X	X	X					same flow as SA87

Table A1.1 continued.

Sample number	Field number	Archive number	Rock group	Rock type	Grid reference	Volcanic centre/ location	Geology description	Field occurrence	thin section	modal analysis	Microprobe analysis	XRF	SSMS	ICP-MS	TIMS	K-Ar age (Ma)	Comments
SA89		AU41690	A	ol-th	R12/657399	Waiuku Cone	in situ	outcrop; N.W. flow	X	X		X					in situ
SA90		AU41691	A	haw	R12/662354	Waiuku Cone		boulder field/ weathered flow; S.W. flow	X	X		X					secondary minerals in vesicles
SA91		AU41692	A	ol-th	R12/671367	Waiuku Cone	boulder	boulder field/ weathered flow; S. flow	X	X		X					
SA92		AU41693	A	haw	R12/645422	Sommerville Road Cone	boulder	boulder field/ weathered flow; W. flow	X	X		X					
SA93		AU41694	A	ol-th	R12/645422	Sommerville Road Cone		boulder field/ weathered flow; W. flow	X	X		X	X				may be stratigraphically younger than SA92
SA94		AU41695	A	aob	R12/774401	Pukekohe Cone	boulder	boulder field/ weathered flow; W. flow	X	X		X					
SA95		AU41696	B	aob		Pukekohe Volcano		drill core	X	X		X					
SAB101	SQV-1	W970050	B	*bas*	R12/863329	Smeed's Quarry	ponded lava	centre of deposit	X	X							vertical profile, lowest stratigraphically
SAB102	SQV-2	W970051	B	bas	R12/863329	Smeed's Quarry	ponded lava	quarry	X	X	X	X					vertical profile columnar jointed
SAB103	SQV-3	W970052	B	*bas*	R12/863329	Smeed's Quarry	ponded lava	quarry	X	X							vertical profile
SAB104	SQV-41	W970053	B	neph	R12/863329	Smeed's Quarry	ponded lava	quarry	X	X		X					vertical profile

Table A1.1 continued.

Sample number	Field number	Archive number	Rock group	Rock type	Grid reference	Volcanic centre/ location	Geology description	Field occurrence	thin section	modal analysis	Microprobe analysis	XRF	SSMS	ICP-MS	TIMS	K-Ar age (Ma)	Comments
SAB105	SQV-413	W970054	B	neph	R12/863329	Smeed's Quarry	ponded lava	quarry	X	X		X					baked zone between SAB104 and SAB107
SAB106	SQV-42	W970055	B	*neph*	R12/863329	Smeed's Quarry	ponded lava	quarry	X	X							vertical profile platy cleavage
SAB107	SQV-43	W970056	B	bas	R12/863329	Smeed's Quarry	ponded lava	quarry	X	X		X					vertical profile platy cleavage
SAB108	SQV-5	W970057	B	*bas*	R12/863329	Smeed's Quarry	ponded lava	quarry	X	X							vertical profile platy cleavage
SAB109	SQV-6	W970058	B	*bas*	R12/863329	Smeed's Quarry	ponded lava	quarry	X	X							vertical profile columnar jointed
SAB110	SQV-7	W970059	B	*bas*	R12/863329	Smeed's Quarry	ponded lava	quarry	X	X							vertical profile
SAB111	SQV-8	W970060	B	bas	R12/863329	Smeed's Quarry	ponded lava	quarry	X	X	X	X					vertical profile highest stratigraphically
SAB112	SQH-1	W970061	B	*neph*	R12/862329	Smeed's Quarry	ponded lava	quarry	X	X							horizontal profile columnar jointed
SAB113	SQH-2	W970062	B	neph	R12/862329	Smeed's Quarry	ponded lava	quarry	X	X	X	X					horizontal profile rare apatite
SAB114	SQH-3	W970063	B	*bas*	R12/862329	Smeed's Quarry	ponded lava	quarry	X	X							horizontal profile
SAB115	SQH-4	W970064	B	*bas*	R12/862329	Smeed's Quarry	ponded lava	quarry	X	X							horizontal profile
SAB116	SQH-5	W970065	B	bas	R12/862329	Smeed's Quarry	ponded lava	quarry	X	X		X					horizontal profile

Table A1.1 continued.

Sample number	Field number	Archive number	Rock group	Rock type	Grid reference	Volcanic centre/ location	Geology description	Field occurrence	thin section	modal analysis	Microprobe analysis	XRF	SSMS	ICP-MS	TIMS	K-Ar age (Ma)	Comments
SAB117	SQH-6	W970066	B	*bas*	R12/863329	Smeed's Quarry	ponded lava	quarry	X	X							horizontal profile
SAB118	SQH-7	W970067	B	*bas*	R12/863329	Smeed's Quarry	ponded lava	quarry	X	X							horizontal profile
SAB119	SQH-8	W970068	B	neph	R12/863329	Smeed's Quarry	ponded lava	quarry	X	X		X					horizontal profile large columnar joints
SAB120	SQH-9	W970069	B	*neph*	R12/863329	Smeed's Quarry	ponded lava	quarry	X	X							horizontal profile
SAB121	SQH-10	W970070	B	*neph*	R12/863329	Smeed's Quarry	ponded lava	quarry	X	X							horizontal profile
SAB122	SQH-11	W970071	B	*bas*	R12/863329	Smeed's Quarry	ponded lava	quarry	X	X							horizontal profile
SAB123	SQH-12	W970072	B	*bas*	R12/863329	Smeed's Quarry	ponded lava	quarry	X	X							horizontal profile calcite-filled amygdales
SAB124	SQH-13	W970073	B	*bas*	R12/864329	Smeed's Quarry	ponded lava	quarry	X	X							horizontal profile
SAB125	SQH-14	W970074	B	*bas*	R12/864329	Smeed's Quarry	ponded lava	quarry	X	X							horizontal profile
SAB126	SQH-15	W970075	B	*neph*	R12/864329	Smeed's Quarry	ponded lava	quarry	X	X							horizontal profile
SAB127	SQH-16	W970076	B	neph	R12/864329	Smeed's Quarry	ponded lava	quarry	X	X		X					horizontal profile
SAB128	SQH-17	W970077	B	bas	R12/865329	Smeed's Quarry	ponded lava	quarry	X	X	X	X					horizontal profile
SAB129	CDR-1	W970078	B	bas	S13/902282	Pukekawa Volcano	lava flow	boulder field/ weathered flow, E. flow	X	X							Clarke-Denize Road

Table A1.1 continued.

Sample number	Field number	Archive number	Rock group	Rock type	Grid reference	Volcanic centre/ location	Geology description	Field occurrence	thin section	modal analysis	Microprobe analysis	XRF	SSMS	ICP-MS	TIMS	K-Ar age (Ma)	Comments
SAB130	CDR-2	W970079	B	*bas*	S13/902281	Pukekawa Volcano	lava flow	boulder field/ weathered flow, E. flow	X	X							
SAB131	CDR-3	W970080	B	*bas*	S13/904280	Pukekawa Volcano	lava flow	boulder field/ weathered flow, E. flow	X	X							
SAB132	CDR-4	W970081	B	bas	R13/898277	Pukekawa Volcano	lava flow	boulder field/ weathered flow, E. flow	X	X		X					near waterfall
SAB133	CDR-5	W970082	A	haw	S13/902289	Mile Bush Volcano	lava flow	boulder field/ weathered flow, E. flow	X	X		X					
SAB134	CDR-6	W970083	A	haw	S13/906289	Mile Bush Volcano	lava flow	boulder field/ weathered flow, E. flow	X	X		X					flow terminus
SAB135	CDR-7	W970084	B	neph	S13/907288	Mile Bush Volcano	lava flow	boulder field/ weathered flow, E. flow	X	X	X	X		X	X		
SAB136	CDR-8	W970085	A	*neph*	S13/908288	Mile Bush Volcano	lava flow	outcrop E. flow	X	X							
SAB137	GR-1	W970086	B	*haw*	S13/908277	Pukekawa Volcano	lava flow	boulder field/ weathered flow, E. flow	X	X							Geraghty Road
SAB138	GR-2	W970087	A	haw	R13/899274	Pukekawa Volcano	lava flow	boulder field/ weathered flow, E. flow	X	X		X					near pond
SAB139	GR-31	W970088	A	*haw*	R13/899273	Pukekawa Volcano	lava flow	boulder field/ weathered flow, E. flow	X	X							

Table A1.1 continued.

Sample number	Field number	Archive number	Rock group	Rock type	Grid reference	Volcanic centre/ location	Geology description	Field occurrence	thin section	modal analysis	Microprobe analysis	XRF	SSMS	ICP-MS	TIMS	K-Ar age (Ma)	Comments
SAB140	GR-32	W970089	A	haw	R13/899273	Pukekawa Volcano	lava flow	boulder field/ weathered flow, E. flow	X	X		X					
SAB141	GR-4	W970090	A	*haw*	R13/890268	Pukekawa Volcano	lava flow	boulder field/ weathered flow, E. flow	X	X							
SAB142	GR-5	W970091	A	haw	R13/893/268	Pukekawa Volcano	lava flow	boulder field/ weathered flow, E. flow	X	X		X					
SAB143	CHR-1	W970092	A	*haw*	R13/877243	Pukekawa Volcano	lava flow	outcrop, S.E. flow	X	X							Churchill Road columnar jointed
SAB144	CHR-2	W970093	A	ol-th	R13/877243	Pukekawa Volcano	lava flow	outcrop, S.E. flow	X	X		X					
SAB145	CHR-3	W970094	A	trans	R13/877242	Pukekawa Volcano	lava flow	boulder field/ weathered flow, S.E. flow	X	X		X					
SAB146	CHR-4	W970095	A	*haw*	R13/896247	Pukekawa Volcano	lava flow	boulder field/ weathered flow, S.E. flow	X	X							flow terminus
SAB147	CHR-5	W970096	A	haw	R13/888246	Pukekawa Volcano	lava flow	boulder field/ weathered flow, S.E. flow	X	X		X					
SAB148	CHR-6	W970097	A	*haw*	R13/887247	Pukekawa Volcano	lava flow	boulder field/ weathered flow, S.E. flow	X	X							
SAB149	CHR-7	W970098	A	ol-th	R13/879234	Pukekawa Volcano	lava flow	boulder field/ weathered flow, S.E. flow	X	X		X					

Table A1.1 continued.

Sample number	Field number	Archive number	Rock group	Rock type	Grid reference	Volcanic centre/ location	Geology description	Field occurrence	thin section	modal analysis	Microprobe analysis	XRF	SSMS	ICP-MS	TIMS	K-Ar age (Ma)	Comments
SAB150	CHR-8	W970099	A	trans	R13/879234	Pukekawa Volcano	lava flow	boulder field/ weathered flow, S.E. flow	X	X		X		X	X		same site as SAB149
SAB151	CHR-9	W970100	A	haw	R13/882238	Pukekawa Volcano	lava flow	boulder field/ weathered flow, S.E. flow	X	X	X	X					
SAB152	CHR-10	W970101	A	ol-th	R13/882238	Pukekawa Volcano	lava flow	boulder field/ weathered flow, S.E. flow	X	X	X	X					same site as SAB151
SAB153	CHR-11	W970102	A	*haw*	R13/887237	Pukekawa Volcano	lava flow	boulder field/ weathered flow, S.E. flow	X	X							
SAB154	CHR-12	W970103	A	*trans*	R13/887237	Pukekawa Volcano	lava flow	boulder field/ weathered flow, S.E. flow	X	X							same site as SAB153
SAB155	BRR-1	W970104	A	*aob*	R13/848240	Logan Road, unnamed centre	lava flow	boulder field/ weathered flow, S. flow	X	X							
SAB156	BRR-2	W970105	A	*aob*	R13/847239	Logan Road, unnamed centre	lava flow	boulder field/ weathered flow, S. flow	X	X							
SAB157	BRR-3	W970106	A	*aob*	R13/847237	Logan Road, unnamed centre	lava flow	boulder field/ weathered flow, S. flow	X	X							
SAB158	BRR-5	W970107	A	*aob*	R13/846241	Logan Road, unnamed centre	lava flow	boulder field/ weathered flow, S. flow	X	X							
SAB159	BRR-6	W970108	A	aob	R13/846243	Logan Road, unnamed centre	lava flow	boulder field/ weathered flow, S. flow	X	X		X					

Table A1.1 continued.

Sample number	Field number	Archive number	Rock group	Rock type	Grid reference	Volcanic centre/ location	Geology description	Field occurrence	thin section	modal analysis	Microprobe analysis	XRF	SSMS	ICP-MS	TIMS	K-Ar age (Ma)	Comments
SAB160	BR-1	W970109	A	*trans*	R13/834221	Logan Road, unnamed centre	lava flow	boulder field/ weathered flow, S. flow	X	X							
SAB161	BR-2	W970110	A	trans	R13/836220	Logan Road, unnamed centre	lava flow	boulder field/ weathered flow, S. flow	X	X		X					
SAB162	BR-3	W970111	A	aob	R13/834215	Logan Road, unnamed centre	lava flow	boulder field/ weathered flow, S. flow	X	X	X	X		X	X		
SAB163	BR-4	W970112	A	haw	R13/833223	Logan Road, unnamed centre	lava flow	boulder field/ weathered flow, S. flow	X	X	X	X					above outcrop of light-grey mudstone
SAB164	BR-5	W970113	A	*haw*	R13/834225	Logan Road, unnamed centre	lava flow	boulder field/ weathered flow, S. flow	X	X							
SAB165	BR-6	W970114	A	*haw*	R13/836227	Logan Road, unnamed centre	lava flow	boulder field/ weathered flow, S. flow	X	X							
SAB166	BR-7	W970115	A	haw	R13/846237	Logan Road, unnamed centre	lava flow	boulder field/ weathered flow, S. flow	X	X		X					
SAB167	LR-1	W970116	A	haw	R13/836251	Logan Road, unnamed centre	lava flow	boulder field/ weathered flow, S.W. flow	X	X		X					
SAB168	LR-1a	W970117	A	aob	R13/836251	Logan Road, unnamed centre	lava flow	boulder field/ weathered flow, S.W. flow	X	X		X					
SAB169	HWY22a	W970118	A	ol-th	R13/841298	Mile Bush Volcano	lava flow	outcrop, W. flow	X	X	X	X					Hwy22 roadcut

Table A1.1 continued.

Sample number	Field number	Archive number	Rock group	Rock type	Grid reference	Volcanic centre/ location	Geology description	Field occurrence	thin section	modal analysis	Microprobe analysis	XRF	SSMS	ICP-MS	TIMS	K-Ar age (Ma)	Comments
SAB170	BBT010	W970119	A	ol-th	R12/701398	Barriball Volcano	juvenile pyroclast	tuff deposit	X	X	X	X					bomb base of section
SAB171	BBT010A	W970120	A	ol-th	R12/701398	Barriball Volcano	juvenile pyroclast	tuff deposit	X	X	X	X					6m from SAB170, same stratagraphic horizon
SAB172	BBT055	W970121	A	ol-th	R12/701398	Barriball Volcano	juvenile pyroclast	tuff deposit	X	X	X	X					bomb
SAB173	BBT104	W970122	A	ol-th	R12/701398	Barriball Volcano	juvenile pyroclast	tuff deposit	X	X	X	X					bomb impact sag structure
SAB173-1	BBT110	W990400	B	bas	R12/701398	Barriball Volcano	juvenile pyroclast	tuff deposit	X			X					bomb
SAB174	BBT116	W970123	A	ol-th	R12/701398	Barriball Volcano	juvenile pyroclast	tuff deposit	X	X	X	X		X	X		bomb impact sag structure
SAB175	BBT136	W970124	B	bas	R12/701398	Barriball Volcano	block	tuff deposit	X	X	X	X					rounded block, possibly recycled clast, impact sag structure
SAB176	BBT143	W970125	B	bas	R12/701398	Barriball Volcano	juvenile pyroclast	tuff deposit	X	X	X	X					bomb
SAB176-1	BBT145	W990401	B	bas	R12/701398	Barriball Volcano	juvenile pyroclast	tuff deposit	X			X					bomb, in same bed as SAB176 impact sag structure
SAB177	BBT153	W970126	B	bas	R12/701398	Barriball Volcano	juvenile pyroclast	tuff deposit	X	X	X	X					bomb, impact sag structure
SAB177-1	BBT154	W990402	B	bas	R12/701398	Barriball Volcano	juvenile pyroclast	tuff deposit	X			X					bomb

Table A1.1 continued.

Sample number	Field number	Archive number	Rock group	Rock type	Grid reference	Volcanic centre/ location	Geology description	Field occurrence	thin section	modal analysis	Microprobe analysis	XRF	SSMS	ICP-MS	TIMS	K-Ar age (Ma)	Comments
SAB177-2	BBT157	W990403	A	ol-th	R12/701398	Barriball Volcano	block	tuff deposit	X			X					rounded block, recycled clast
SAB177-3	BBT161	W990404	A	ol-th	R12/701398	Barriball Volcano	block	tuff deposit	X			X					rounded block, recycled clast
SAB178	BBT162	W970127	B	neph	R12/701398	Barriball Volcano	juvenile pyroclast	tuff deposit	X	X	X	X					bomb, impact sag structure
SAB178-1	BBT194	W990405	B	bas	R12/701398	Barriball Volcano	block	tuff deposit	X			X					rounded block, recycled clast impact sag structure
SAB178-2	BBT199A	W990406	A	ol-th	R12/701398	Barriball Volcano	block	tuff deposit	X			X					recycled clast
SAB178-3	BBT199B	W990407	B	bas	R12/701398	Barriball Volcano	block	tuff deposit	X			X					recycled block in contact with SAB178-2
SAB179	BBT204	W970128	B	bas	R12/701398	Barriball Volcano	juvenile pyroclast	tuff deposit	X	X	X	X		X	X		bomb
SAB180	BBT225	W970129	B	bas	R12/701398	Barriball Volcano	juvenile pyroclast	tuff deposit	X	X	X	X					bomb
SAB181	RTR-1	W970130	A	ol-th	R12/850462	Raventhorpe tuff ring	juvenile pyroclast	tuff deposit	X	X	X	X					bomb impact sag structure
SAB182	RTR-2	W970131	A	*ol-th*	R12/850462	Raventhorpe tuff ring	juvenile pyroclast	tuff deposit	X	X							bomb
SAB183	RTR-3	W970132	A	*ol-th*	R12/850462	Raventhorpe tuff ring	juvenile pyroclast	tuff deposit	X	X							bomb

Table A1.1 continued.

Sample number	Field number	Archive number	Rock group	Rock type	Grid reference	Volcanic centre/ location	Geology description	Field occurrence	thin section	modal analysis	Microprobe analysis	XRF	SSMS	ICP-MS	TIMS	K-Ar age (Ma)	Comments
SAB184	RTR-4	W970133	A	ol-th	R12/850462	Raventhorpe tuff ring	juvenile pyroclast	tuff deposit	X	X		X					bomb impact sag structure
SAB185	RTR-4a	W970134	B	aob	R12/850462	Raventhorpe tuff ring	block	tuff deposit	X	X		X					accidental clast
SAB186	RTR-5	W970135	A	*aob*	R12/850462	Raventhorpe tuff ring	block	tuff deposit	X	X							rounded block, accidental clast
SAB187	RTR-6	W970136	A	ol-th	R12/850462	Raventhorpe tuff ring	juvenile pyroclast	tuff deposit	X	X	X	X		X	X		bomb
SAB188	RTR-6a	W970137	B	aob	R12/850462	Raventhorpe tuff ring	pyroclast	tuff deposit	X	X	X	X		X	X		accidental clast
SAB189	PP-1	W970138	A	haw	R13/884252	Pukekawa Volcano	lava flow	boulder field/ weathered flow S.E. flow	X	X		X					
SAB190	PP-2a	W970139	A	ol-th	R13/890261	Pukekawa Volcano	lava flow	boulder field/ weathered flow S.E. flow	X	X		X					
SAB191	PP-2b	W970140	A	ol-th	R13/893261	Pukekawa Volcano	lava flow	boulder field/ weathered flow S.E. flow	X	X		X					
SAB192	MOR-1	W970141	B	*neph*	S13/916301	Mile Bush Volcano	lava flow	boulder field/ weathered flow E. flow	X	X							flow terminus
SAB193	MOR-2	W970142	B	neph	S13/898297	Mile Bush Volcano	lava flow	boulder field/ weathered flow E. flow	X	X		X					

Table A1.1 continued.

Sample number	Field number	Archive number	Rock group	Rock type	Grid reference	Volcanic centre/ location	Geology description	Field occurrence	thin section	modal analysis	Microprobe analysis	XRF	SSMS	ICP-MS	TIMS	K-Ar age (Ma)	Comments
SAB194	MOR-3	W970143	B	bas	R12/902305	Mile Bush Volcano	lava flow	boulder field/ weathered flow E. flow	X	X		X					
SAB195	MOR-4	W970144	B	*bas*	R12/899311	Mile Bush Volcano	lava flow	boulder field/ weathered flow E. flow	X	X							
SAB196	HR-1	W970145	B	bas	R12/885319	Mile Bush Volcano	boulder	boulder field float	X	X		X					
SAB197	HR-1a	W970146	B	bas	R12/885319	Mile Bush Volcano	boulder	boulder field float	X	X							
SAB198	HR-2	W970147	A	qz-th	R12/882322	Smeed's Volcano	boulder	boulder field float	X	X	X	X		X	X		
SAB199	HR-3	W970148	A	*ol-th*	R12/880322	Smeed's Volcano	boulder	boulder field/ weathered flow N. flow	X	X							
SAB200	SR-1	W970149	A	*ol-th*	R12/873315	Smeed's Volcano	lava flow	boulder field/ weathered flow N. flow	X	X							
SAB201	SR-2a	W970150	A	ol-th	R12/871327	Smeed's Volcano	lava flow	boulder field/ weathered flow N. flow	X	X		X					
SAB202	SR-2b	W970151	A	ol-th	R12/871327	Smeed's Volcano	lava flow	boulder field/ weathered flow N. flow	X	X		X					
SAB203	SR-3a	W970152	A	haw	R12/874327	Smeed's Volcano	block	tuff deposit	X	X		X					

Table A1.1 continued.

Sample number	Field number	Archive number	Rock group	Rock type	Grid reference	Volcanic centre/ location	Geology description	Field occurrence	thin section	modal analysis	Microprobe analysis	XRF	SSMS	ICP-MS	TIMS	K-Ar age (Ma)	Comments
SAB204	SR-3b	W970153	B	bas	R12/874327	Smeed's Volcano	block	tuff deposit	X	X	X	X					in contact with SAB203
SAB205	SR-4a	W970154	A	ol-th	R12/875326	Smeed's Volcano	lava flow	boulder field/ weathered flow N. flow	X	X		X					
SAB206	SR-4b	W970155	A	*ol-th*	R12/875326	Smeed's Volcano	lava flow	boulder field/ weathered flow N. flow	X	X							
SAB207	SQT	W970156	A	aob	R12/836329	Smeed's Volcano	top of ponded lava	outcrop	X	X	X	X					
SAB208	MR-1	W970157	A	haw	R12/854311	Smeed's Volcano	lava flow	outcrop W. flow	X	X		X					
SAB209	HWY22b	W970158	A	*trans*	R13/840295	Mile Bush Volcano	lava flow	boulder field/ weathered flow W. flow	X	X							
SAB210	HWY22c	W970159	A	trans	R13/839289	Mile Bush Volcano	lava flow	boulder field/ weathered flow W. flow	X	X		X					
SAB211	HWY22d	W970160	A	*trans*	R13/841297	Mile Bush Volcano	lava flow	boulder field/ weathered flow W. flow	X	X							
SAB212	REF 1	W970161	A	*aob*	R13/848240	Logan Road, unnamed centre	lava flow	outcrop S. flow	X	X							
SAB213	REF 2	W970162	A	*aob*	R13/848240	Logan Road, unnamed centre	lava flow	outcrop S. flow	X	X							

Table A1.1 continued.

Sample number	Field number	Archive number	Rock group	Rock type	Grid reference	Volcanic centre/ location	Geology description	Field occurrence	thin section	modal analysis	Microprobe analysis	XRF	SSMS	ICP-MS	TIMS	K-Ar age (Ma)	Comments
SAB214	MQS	W970163	B	bas	R12/869409	Bombay quarry	weathered boulder	float	X	X		X					top of ash-covered tuff deposit
SAB215	MQW	W970164	B	ne-haw	R12/869409	Bombay quarry	ponded lava	quarry	X			X					W. wall
SAB216	MQUW	W970165	B	*ne-haw*	R12/869409	Bombay quarry	ponded lava	quarry	X								upper W. wall
SAB217	MQE	W970166	B	ne-haw	R12/869409	Bombay quarry	ponded lava	quary	X			X					E. wall
SAB218	MQ1685 A	W970167	B	ne-haw	R12/869409	Bombay quarry	ponded lava	quarry	X			X		X	X		quarry floor level peg RL168.5m
SAB219	MQ1685 B	W970168	B	*ne-haw*	R12/869409	Bombay quarry	ponded lava	quarry	X								quarry floor level peg RL168.5m
SAB220	MQD1	W970169	B	ne-haw	R12/869409	Bombay quarry	dike	quarry	X			X					cuts through ponded lava
SAB221	MQD2	W970170	B	ne-haw	R12/869409	Bombay quarry	dike	quarry	X			X					cuts through ponded lava
SAB222	MQS0B	W990408	B	aob	R12/869409	Bombay quarry	spatter	scoria deposit	X			X					stratigraphically younger than ponded lava; base of section
SAB223	MQS036	W990409	B	ne-haw	R12/869409	Bombay quarry	spatter	scoria deposit	X			X					interlayered with scoria
SAB224	MQS063	W990410	B	aob	R12/869409	Bombay quarry	spatter	scoria deposit	X			X		X	X		interlayered with scoria
SAB225	MQS114	W990411	B	aob	R12/869409	Bombay quarry	spatter	scoria deposit	X			X					interlayered with scoria

Table A1.1 continued.

Sample number	Field number	Archive number	Rock group	Rock type	Grid reference	Volcanic centre/ location	Geology description	Field occurrence	thin section	modal analysis	Microprobe analysis	XRF	SSMS	ICP-MS	TIMS	K-Ar age (Ma)	Comments
SAB226	MQS130	W990412	B	haw	R12/869409	Bombay quarry	spatter	scoria deposit	X			X					top of section, interlayered with scoria
SAB227	MQT020	W990413	B	aob	R12/869409	Bombay quarry	juvenile pyroclast	tuff deposit	X			X					above rhyolitic ash stratigraphically younger than scoria and lava; large lapilli base of section,
SAB228	MQT034	W990414	B	ne-haw	R12/869409	Bombay quarry	juvenile pyroclast	tuff deposit	X			X		X	X		large lapilli very vesicular
SAB229	MGT035	W990415	B	aob	R12/869409	Bombay quarry	juvenile pyroclast	tuff deposit	X			X					large lapilli very vesicular
SAB230	MQT039	W990416	B	*aob*	R12/869409	Bombay quarry	juvenile pyroclast	tuff deposit	X								large lapilli very vesicular
SAB231	MQT0455	W990417	B	ne-haw	R12/869409	Bombay quarry	juvenile pyroclast	tuff deposit	X			X					large lapilli few vesicles
SAB232	MQT078	W990418	B	aob	R12/869409	Bombay quarry	juvenile pyroclast	tuff deposit	X			X					bomb
SAB233	MQT125	W990419	B	ne-haw	R12/869409	Bombay quarry	juvenile pyroclast	tuff deposit	X			X					bomb
SAB234	MQT134	W990420	B	ne-haw	R12/869409	Bombay quarry	juvenile pyroclast	tuff deposit	X			X					bomb
SAB235	MQT150	W990421	B	ne-haw	R12/869409	Bombay quarry	juvenile pyroclast	tuff deposit	X			X					bomb
SAB236	MQT174	W990422	B	ne-haw	R12/869409	Bombay quarry	juvenile pyroclast	tuff deposit	X			X					bomb

Table A1.1 continued.

Sample number	Field number	Archive number	Rock group	Rock type	Grid reference	Volcanic centre/ location	Geology description	Field occurrence	thin section	modal analysis	Microprobe analysis	XRF	SSMS	ICP-MS	TIMS	K-Ar age (Ma)	Comments
SAB237	MQT180	W990423	B	ne-haw	R12/869409	Bombay quarry	juvenile pyroclast	tuff deposit	X			X					bomb
SAB238	MQT260A	W990424	B	*ne-haw*	R12/869409	Bombay quarry	juvenile pyroclast	tuff deposit	X								large lapilli
SAB239	MQT260B	W990425	B	ne-haw	R12/869409	Bombay quarry	juvenile pyroclast	tuff deposit	X			X					adjacent to SAB260A and C
SAB240	MQT260C	W990426	B	*ne-haw*	R12/869409	Bombay quarry	juvenile pyroclast	tuff deposit	X								adjacent to SAB260A and B
SAB241	MQT272A	W990427	B	ne-haw	R12/869409	Bombay quarry	juvenile pyroclast	tuff deposit	X			X					large lapilli
SAB242	MQT272B	W990428	B	*ne-haw*	R12/869409	Bombay quarry	juvenile pyroclast	tuff deposit	X								adjacent to SAB272A
SAB243	MQT278	W990429	B	*ne-haw*	R12/869409	Bombay quarry	juvenile pyroclast	tuff deposit	X								bomb
SAB244	MQT286A	W990430	B	*ne-haw*	R12/869409	Bombay quarry	juvenile pyroclast	tuff deposit	X								large lapilli
SAB245	MQT286B	W990431	B	ne-haw	R12/869409	Bombay quarry	juvenile pyroclast	tuff deposit	X			X					adjacent to SAB286A
SAB246	MQT296A	W990432	B	*ne-haw*	R12/869409	Bombay quarry	juvenile pyroclast	tuff deposit	X								large lapilli
SAB247	MQT296B	W990433	B	ne-haw	R12/869409	Bombay quarry	juvenile pyroclast	tuff deposit	X			X					adjacent to SAB296A and C
SAB248	MQT296C	W990434	B	*ne-haw*	R12/869409	Bombay quarry	juvenile pyroclast	tuff deposit	X								adjacent to SAB272A and B

Table A1.1 continued.

Sample number	Field number	Archive number	Rock group	Rock type	Grid reference	Volcanic centre/ location	Geology description	Field occurrence	thin section	modal analysis	Microprobe analysis	XRF	SSMS	ICP-MS	TIMS	K-Ar age (Ma)	Comments
SAB249	MQT303A	W990435	B	ne-haw	R12/869409	Bombay quarry	juvenile pyroclast	tuff deposit	X			X					large lapilli
SAB250	MQT303B	W990436	B	*ne-haw*	R12/869409	Bombay quarry	juvenile pyroclast	tuff deposit	X								adjacent to SAB303A,C, D, E
SAB251	MQT303C	W990437	B	*ne-haw*	R12/869409	Bombay quarry	juvenile pyroclast	tuff deposit	X								adjacent to SAB303A, B, D, E
SAB252	MQT303D	W990438	B	*aob*	R12/869409	Bombay quarry	juvenile pyroclast	tuff deposit	X								adjacent to SAB303A, B, C, E
SAB253	MQT303E	W990439	B	aob	R12/869409	Bombay quarry	juvenile pyroclast	tuff deposit	X			X					adjacent to SAB303A, B, C, D
SAB254	MQT306A	W990440	B	*ne-haw*	R12/869409	Bombay quarry	juvenile pyroclast	tuff deposit	X								large lapilli
SAB255	MQT306B	W990441	B	*ne-haw*	R12/869409	Bombay quarry	juvenile pyroclast	tuff deposit	X								adjacent to SAB306A and C
SAB256	MQT306C	W990442	B	*ne-haw*	R12/869409	Bombay quarry	juvenile pyroclast	tuff deposit	X								adjacent to SAB306A and B
SAB257	MQT313A	W990443	B	*ne-haw*	R12/869409	Bombay quarry	juvenile pyroclast	tuff deposit	X								large lapilli
SAB258	MQT313B	W990444	B	*ne-haw*	R12/869409	Bombay quarry	juvenile pyroclast	tuff deposit	X								adjacent to SAB313A
SAB259	MQT321A	W990445	B	ne-haw	R12/869409	Bombay quarry	juvenile pyroclast	tuff deposit	X			X					large lapilli
SAB260	MQT321B	W990446	B	ne-haw	R12/869409	Bombay quarry	juvenile pyroclast	tuff deposit	X			X					adjacent to SAB321A and C

Table A1.1 continued.

Sample number	Field number	Archive number	Rock group	Rock type	Grid reference	Volcanic centre/ location	Geology description	Field occurrence	thin section	modal analysis	Microprobe analysis	XRF	SSMS	ICP-MS	TIMS	K-Ar age (Ma)	Comments
SAB261	MQT321C	W990447	B	*ne-haw*	R12/869409	Bombay quarry	juvenile pyroclast	tuff deposit	X								adjacent to SAB321A and B
SAB262	MQT330A	W990448	B	ne-haw	R12/869409	Bombay quarry	juvenile pyroclast	tuff deposit	X			X					large lapilli
SAB263	MQT330B	W990449	B	*ne-haw*	R12/869409	Bombay quarry	juvenile pyroclast	tuff deposit	X								adjacent to SAB330A
SAB264	MQT340A	W990450	B	ne-haw	R12/869409	Bombay quarry	juvenile pyroclast	tuff deposit	X								large lapilli
SAB265	MQT340B	W990451	B	*ne-haw*	R12/869409	Bombay quarry	juvenile pyroclast	tuff deposit	X								adjacent to SAB340A
SAB266	MQT346A	W990452	B	*ne-haw*	R12/869409	Bombay quarry	juvenile pyroclast	tuff deposit	X			X					large lapilli
SAB267	MQT346B	W990453	B	*ne-haw*	R12/869409	Bombay quarry	juvenile pyroclast	tuff deposit	X								adjacent to SAB346A
SAB268	MQT356A	W990454	B	*ne-haw*	R12/869409	Bombay quarry	juvenile pyroclast	tuff deposit	X								large lapilli
SAB269	MQT356B	W990455	B	*ne-haw*	R12/869409	Bombay quarry	juvenile pyroclast	tuff deposit	X								adjacent to SAB356A
SAB270	MQT361A	W990456	B	aob	R12/869409	Bombay quarry	juvenile pyroclast	tuff deposit	X			X					large lapilli
SAB271	MQT361B	W990457	B	ne-haw	R12/869409	Bombay quarry	juvenile pyroclast	tuff deposit	X			X					adjacent to SAB361A and C
SAB272	MQT361C	W990458	B	*ne-haw*	R12/869409	Bombay quarry	juvenile pyroclast	tuff deposit	X								adjacent to SAB361A and B

Table A1.1 continued.

Sample number	Field number	Archive number	Rock group	Rock type	Grid reference	Volcanic centre/ location	Geology description	Field occurrence	thin section	modal analysis	Microprobe analysis	XRF	SSMS	ICP-MS	TIMS	K-Ar age (Ma)	Comments
SAB273	MQT374A	W990459	B	*aob*	R12/869409	Bombay quarry	juvenile pyroclast	tuff deposit	X								large lapilli
SAB274	MQT374B	W990460	B	*aob*	R12/869409	Bombay quarry	juvenile pyroclast	tuff deposit	X								adjacent to SAB374A
SAB275	MQT375	W990461	B	aob	R12/869409	Bombay quarry	juvenile pyroclast	tuff deposit	X			X					bomb
SAB276	MQT392A	W990462	B	*aob*	R12/869409	Bombay quarry	juvenile pyroclast	tuff deposit	X								large lapilli
SAB277	MQT392B	W990463	B	aob	R12/869409	Bombay quarry	juvenile pyroclast	tuff deposit	X			X					adjacent to SAB392A and C
SAB278	MQT392C	W990464	B	*aob*	R12/869409	Bombay quarry	juvenile pyroclast	tuff deposit	X								adjacent to SAB392A and B

Appendix Two:
Petrographic Descriptions for the SAVF Basalts

Appendix 2

Petrographic descriptions for the SAVF basalts

Detailed petrographic descriptions for each rock type from groups A and B are given in the following sections together with modal mineralogy data for phenocryst and groundmass phases for representative samples of each rock type.

A2.1 Group A – alkali ol-basalts, transitional basalts, hawaiites, ol-tholeiitic basalts, qz-tholeiitic basalts

A2.1.1 Group A alkali ol-basalts

Group A alkali ol-basalts exhibit porphyritic and glomeroporphyritic textures, range from relatively coarse-grained (Fig. A2.1) to fine-grained (Fig. A2.2), and are slightly vesicular to very vesicular. They are typically holocrystalline and consist of olivine megacrysts, and phenocrysts and microphenocrysts of olivine, clinopyroxene and plagioclase set in an intergranular plagioclase-rich groundmass (described in Table A2.4). Titanomagnetite is generally restricted to the groundmass in most samples. However, it occurs in SAB159, SAB162, and SAB168 as irregular-shaped crystals that frequently partially enclose plagioclase laths and clinopyroxene groundmass crystals and rare blocky microphenocrysts up to 500 μm.

Samples SA19, SA33, SAB159, SAB162, and SAB168 are glomeroporphyritic and commonly contain monomineralic clusters of either olivine, clinopyroxene, or plagioclase and polymineralic clusters characterised by a variety of mineral assemblages described in Table A2.3.

Total phenocryst phases range from 7.4 to 24.4 modal %. The modal abundance of phenocrysts and groundmass phases of selected samples are presented in Table A2.1. Descriptions of the main mineral phases olivine, clinopyroxene, and plagioclase are given in Table A2.2.

Groundmass

The groundmass (54.2 to 86.0 modal %) is commonly coarse-grained and predominantly intergranular (see Fig. A2.1). Only SA18 has a relatively fine-grained intergranular groundmass (see Fig. A2.2). Plagioclase and clinopyroxene are abundant with plagioclase

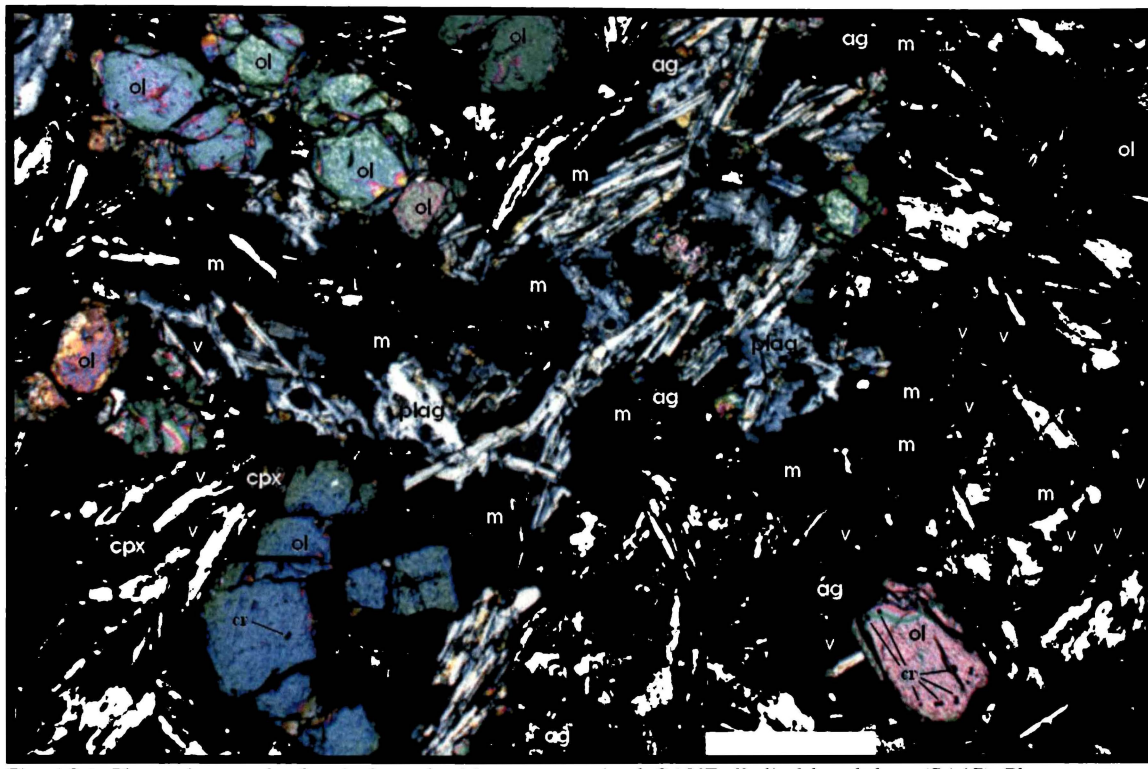

Fig. A2.1. Photomicrograph of typical porphyritic, coarse-grained, SAVF alkali ol-basalt lava (SA17). Phenocrysts and microphenocrysts of olivine (ol) with Cr-titanomagnetite inclusions (cr), anhedral clinopyroxene microphenocrysts (cpx), and microphenocrysts and small clusters of titanomagnetite grains (m) are set in an intergranular groundmass composed primarily of slender laths and interstitial crystals of plagioclase (plag), and aggregates of small blocky titanomagnetite and clinopyroxene grains (ag). The euhedral olivine in the lower left of the image is shattered and partially mantled by grains of clinopyroxene. Polarised light; scale bar is 500μm.

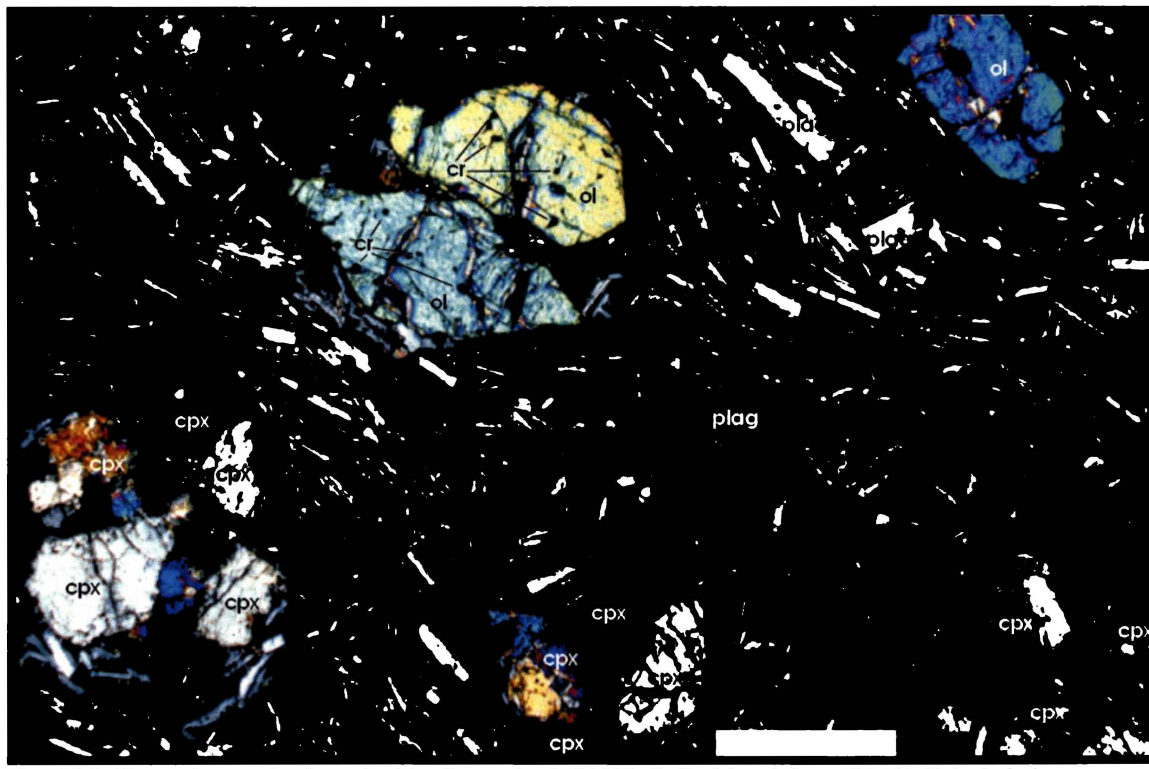

Fig. A2.2. Photomicrograph of porphyritic, fine-grained, SAVF alkali ol-basalt lava (SA18). Euhedral phenocrysts of olivine (ol) with Cr-titanomagnetite inclusions (cr), small monomineralic clusters of interlocking clinopyroxene microphenocrysts (cpx), and rare plagioclase microphenocrysts (plag) are set in a black devitrified glassy groundmass with abundant plagioclase laths that exhibit trachytic texture. Polarised light; scale bar is 500μm.

Table A2.1 Modal abundances of phenocrysts and the main groundmass phases of selected group A alkali ol-basalts. Abundances were determined by counting 1000 points.

Lava type:	Group A - alkali ol-basalts								
Sample:	SA17	SA19	SA33	SAB159	SAB162	SAB168	All Samples (n=8)		
Phenocrysts							Max	Min	Mean
olivine	13.0	6.2	14.8	4.2	0.8	7.0	14.8	0.8	7.2
clinopyroxene	2.8	3.8	7.8	2.6	0.4	1.2	7.8	0.4	3.1
plagioclase	2.8	5.6	0.8	7.2	12.4	11.6	12.4	0.8	5.4
magnetite	2.6	1.2	1.0	3.2	4.0	0.8	4.0	tr	1.7
ilmenite	-	-	-	-	-	-	tr	tr	tr
Total	21.2	16.8	24.4	17.2	17.6	20.6	20.6	7.4	17.9
Vesicles	7.4	8.6	21.0	1.8	4.0	3.4	21.0	2.8	7.0
Groundmass	71.4	74.6	54.2	81.0	78.0	76.0	86.0	54.2	75.3
Groundmass							n = 7		
olivine	2.7	4.6	3.8	4.6	4.4	2.2	4.6	2.2	3.6
clinopyroxene	32.0	21.3	33.3	22.6	21.6	26.0	38.8	21.3	28.0
plagioclase	59.6	69.2	54.0	62.0	63.7	62.8	69.2	48.9	60.0
magnetite	3.3	2.0	3.5	7.7	5.7	4.7	7.7	2.0	4.4
ilmenite	1.6	1.7	3.8	2.0	3.5	1.3	4.7	1.3	2.7
apatite	tr	tr	tr	tr	tr	1.7	1.7	tr	0.2
glass	-	-	-	-	-	-	-	-	-

n = number of samples; tr = trace; - = none counted.

Table A2.2 General description of the main mineral phases in the group A alkali ol-basalts.

	Group A – alkali ol-basalt		
Mineral	**Olivine**	**Clinopyroxene**	**Plagioclase**
Megacrysts	Rare < 3.25 mm euhedral, subhedral, and elongate - embayed and occasionally skeletal.		
Phenocrysts / microphenocrysts	Phenocrysts and microphenocrysts: subhedral and anhedral, often embayed. Some compositionally zoned phenocrysts.	Light brown to pale purple brown. Phenocrysts and microphenocrysts: subhedral and occasionally twinned. Rare subhedral 8-sided phenocrysts. Some with strong purple margins in SA17 and SA33.	Phenocrysts: < 750 μm prismatic. Microphenocrysts: prismatic and tabular, less frequently as interstitial patches. Some tabular crystals with oscillatory zones.
Textures	Phenocryst populations in SA17, SA19, SA33 samples with disequilibrium textures: 1. Optically continuous sheaths of light brown clinopyroxene. 2. Aggregates of groundmass-size crystals randomly orientated and apparently annealed to its margins. 3. Thin, dark grey rims of opaque crystals (e.g., SAB159, SAB162, SAB 168) giving margins a mottled appearance.	Frequent sieved-textured cores.	
Alteration			
Inclusions	Blocky titanomagnetite up to 75 μm (e.g., SAB159, SAB162, SAB168). Rare < 10 μm Cr-titanomagnetite.	Phenocrysts and microphenocrysts: < 25 μm titanomagnetite and Cr-bearing titanomagnetite.	< 10 μm apatite
Comments	Often the dominant phenocryst phase. Monomineralic clusters in SA17 and SA18. Phenocrysts with large angular cavities.	Monomineralic clusters in SA17 and SA18.	Dominant phenocryst phase in SAB159, SAB162, and SAB168.

the dominant phase in all samples. Titanomagnetite, ilmenite, olivine, and apatite are additional groundmass phases (see Table A2.1). Titanomagnetite occurs either as blocky grains or as irregular-shaped crystals that often partially enclose plagioclase laths and clinopyroxene crystals. Ilmenite is either prismatic or irregular-shaped, often partially enclosing plagioclase laths. Olivine commonly occurs as anhedral grains, frequently in the clinopyroxene-dominated aggregates. Apatite occurs in trace amounts in many samples as small, e.g., < 100 μm, needle-like crystals. A general description of the major groundmass phases, plagioclase and clinopyroxene, and other features of the groundmass in the group A alkali ol-basalt samples are given in Table A2.4.

Table A2.3 General description of glomeroporphyritic clusters in group A alkali ol-basalts.

Group A alkali ol-basalts
Glomeroporphyritic Clusters
Glomeroporphyritic samples may contain: 1. Monomineralic clinopyroxene clusters up to 3.25 mm diameter composed of interlocking clinopyroxene phenocrysts and microphenocrysts (see Fig, A2.2). Many crystals contain opaque and other inclusions resulting in a sieve-like texture. Many clusters are embayed, have irregular margins, and have cavities filled with groundmass plagioclase. 2. Monomineralic olivine clusters up to 4 mm across typically consist of (i) less than six annealed subhedral 6-sided phenocrysts and microphenocrysts and (ii) open clusters of rounded phenocrysts and microphenocrysts. The textures of the open clusters suggest that they may be disaggregated or partially melted olivine xenoliths. 3. Monomineralic plagioclase clusters up to 750 μm diameter composed of (i) microphenocrysts and groundmass crystals (SA19) and (ii) radiating prismatic and tabular microphenocrysts with groundmass crystals (SAB159, SAB162, and SAB168). 4. Polymineralic clusters up to 5.25 mm across composed of primarily of light brown or pale purple-brown clinopyroxene with subordinate phases that may include olivine, plagioclase, or rare titanomagnetite. These clusters may be embayed and have irregular margins.

Table A2.4 Summarised groundmass characteristics of the group A alkali ol-basalts.

	Group A alkali ol-basalt	
Mineral	**Clinopyroxene**	**Plagioclase**
Crystal habit	< 100 μm light-brown anhedral	< 500 μm prismatic laths, tabular and irregular-shaped crystals, and in interstitial pools.
Textures		Trachytic (SA18; see Fig. A2.2).
Alteration		
Inclusions		< 10 μm apatite
Comments	Commonly in small monomineralic clusters between plagioclase. Also in aggregates with titanomagnetite and ilmenite.	Dominant phase in all samples. Occurs in small clusters in SAB159. SAB162, and SAB168.
Secondary mineralisation	Minor patchy areas of a brownish-yellow alteration product (possibly smectite) typically associated with partially altered titanomagnetite and ilmenite microphenocrysts (e.g., SAB159, SAB162, and SAB168).	
Crystal clusters	Sample SA33 contains a 1.25mm x 1.0 cm vein composed of light brown, euhedral and subhedral, 6-sided, groundmass-size clinopyroxene, minor amounts of titanomagnetite grains, and slender ilmenite crystals. The clinopyroxene crystals contain small opaque inclusions (possibly titanomagnetite) and other unidentified inclusions.	

A2.1.2 Transitional basalts

Transitional basalts exhibit porphyritic or glomeroporphyritic textures or rare vitrophyric texture and range from vesicle-poor to highly vesicular. The transitional basalts are either hypocrystalline or holocrystalline. This distinction in crystallinity is marked by the absence of plagioclase phenocrysts in the hypocrystalline lavas. Total phenocryst phases range from 8.2 to 19.8 modal %. Olivine always exceeds clinopyroxene which is either rare or absent in all samples. Titanomagnetite is a minor mineral phase in most transitional basalts. However, sample SAB161 contains comparatively abundant (5.0 modal %) blocky to irregular-shaped crystals that are uniformly distributed throughout the sample and occasionally occur along the margins of olivine phenocrysts.

The holocrystalline samples SA48, SA49, SAB161, and SAB210 are glomeroporphyritic and contain clinopyroxene and plagioclase monomineralic clusters and polymineralic clusters composed of a variety of mineral assemblages that include olivine, clinopyroxene, and plagioclase, described in Table A2.8.

The groundmass (described in Table A2.9) ranges from fine- to coarse-grained and is dominated by plagioclase laths and microlites. The modal abundances of phenocrysts and groundmass minerals for selected samples are presented in Table A2.5. Descriptions of the main mineral phases olivine, clinopyroxene, and plagioclase for the hypocrystalline and holocrystalline samples are given in Tables A2.6 and A2.7 respectively.

Table A2.5 Modal abundances of phenocrysts and the main groundmass phases of selected transitional basalts. Abundances were determined by counting 1000 points.

Lava type:	transitional basalts								
Sample:	SA09	SA13	SA48	SA83	SAB145	SAB161	All Samples (n=14)		
Phenocrysts							Max	Min	Mean
olivine	12.2	12.0	4.2	14.8	4.8	2.0	14.8	2.0	8.4
clinopyroxene	0.6	0.6	1.4	0.2	2.2	1.2	2.2	tr	0.8
plagioclase	-	2.8	7.8	1.4	6.4	10.8	10.8	tr	2.8
magnetite	-	-	0.2	0.6	1.4	5.0	5.0	tr	0.6
ilmenite	-	-	-	-	0.2	-	0.2	tr	tr
Total	12.8	15.4	13.6	17.0	15.0	19.0	19.8	8.2	12.6
Vesicles	16.8	17.4	0.8	5.4	1.8	3.8	21.0	0.8	8.7
Groundmass	70.4	67.2	85.6	77.6	83.2	77.6	89.2	67.2	78.7
Groundmass							n = 6		
olivine	5.7	1.6	0.2	9.4	6.5	0.5	9.4	0.2	4.0
clinopyroxene	13.3	24.3	20.5	19.9	24.1	25.1	25.1	13.3	21.2
plagioclase	53.4	68.8	69.5	63.8	62.7	66.6	69.5	53.4	64.1
magnetite	3.8	2.9	9.8	4.3	2.6	5.7	9.8	2.6	4.8
ilmenite	-	2.4	tr	2.3	4.1	2.2	4.1	tr	-
glass	19.2	-	-	0.3	-	-	19.2	-	-

n = number of samples; tr = trace; - = none counted.

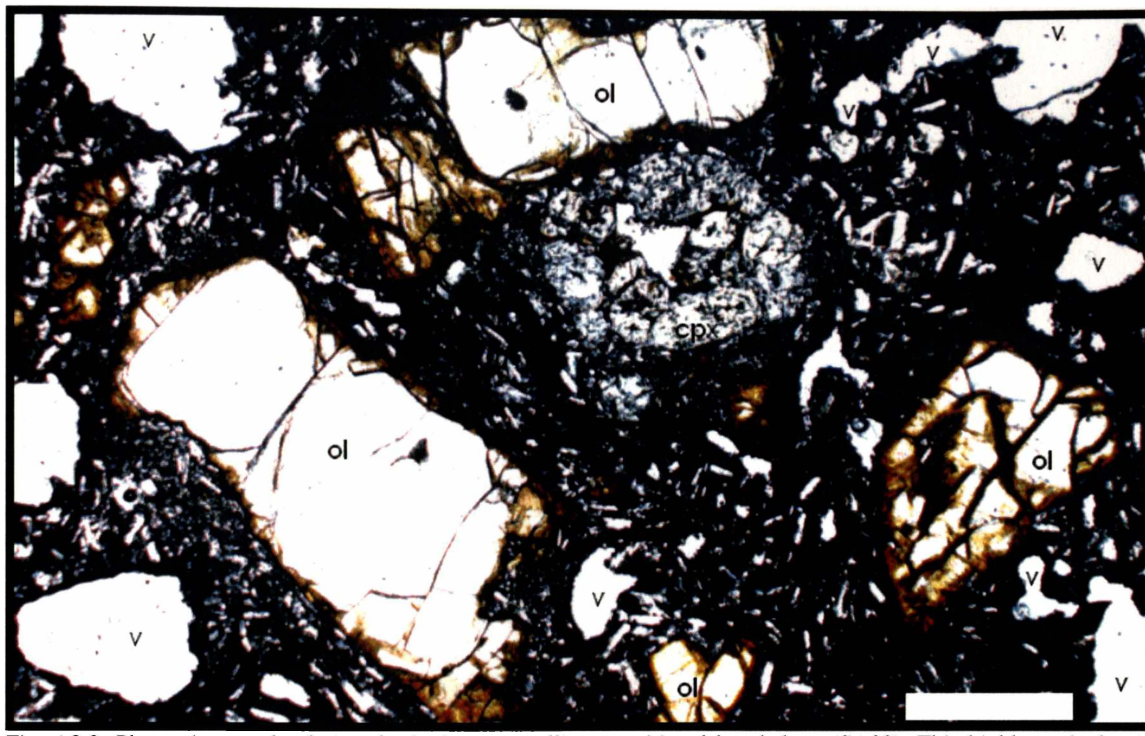

Fig. A2.3. Photomicrograph of vitrophyric, hypocrystalline transitional basalt lava (SA09). This highly vesicular (v) sample consists of rounded phenocrysts and microcrysts of olivine (ol) and clinopyroxene (cpx) set in a black, devitrified, glassy groundmass with abundant small plagioclase laths (white crystals). Olivine crystals have rims altered to reddish-orange iddingsite with alteration spreading from rims towards the interiors of some crystals (note the skeletal crystal at the right of the image). Opaque reaction products occur adjacent to the rims. The clinopyroxene shown at the centre of the image is a cluster of 11 interlocked clinopyroxene microphenocrysts each exhibiting sieve texture. The rounded cluster is mantled with opaque reaction products. Plane polarised light. Scale bar is 500μm.

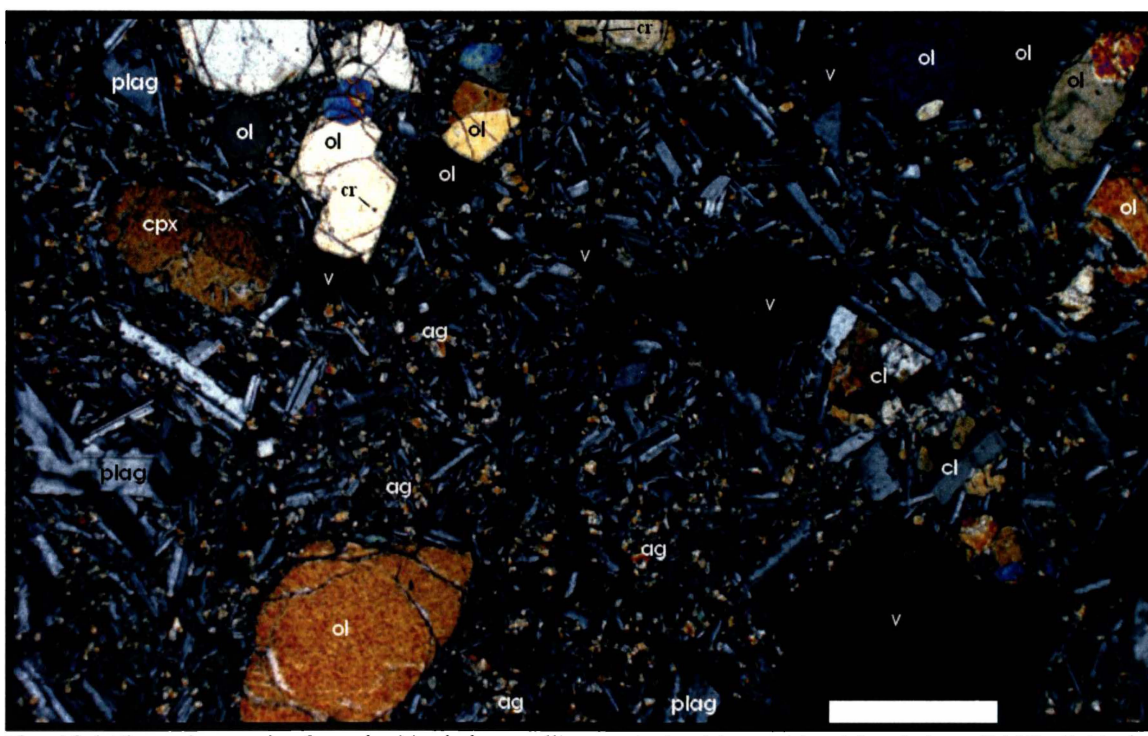

Fig. A2.4 Photomicrograph of porphyritic, holocrystalline, vesicular (v) transitional basalt lava (SA13). Subhedral olivine phenocrysts and microphenocrysts (ol) with Cr-titanomagnetite inclusions (cr), and clinopyroxene (cpx) and plagioclase (plag) microphenocrysts are set in a relatively coarse-grained intergranular groundmass composed of abundant plagioclase laths and microlites and aggregates of clinopyroxene and titanomagnetite grains (ag) between the laths. The small cluster to the right of the image (cl) is composed of clinopyroxene and plagioclase microphenocrysts. The margin of the twinned, euhedral clinopyroxene shown is corroded, a feature that may be indicative of mineral-liquid disequilibrium. Polarised light; scale bar is 500 μm.

Hypocrystalline transitional basalts

The hypocrystalline lavas (SA07, SA08, and SA09; Fig. A2.3; Table A2.6) are relatively fine-grained, porphyritic or vitrophyric, and vesicular to highly vesicular. They contain olivine megacrysts, and phenocrysts and microphenocrysts of olivine and clinopyroxene. Plagioclase is restricted to the groundmass.

Table A2.6 General description of the main mineral phases in the hypocrystalline transitional basalts.

	Hypocrystalline transitional basalt	
Mineral	**Olivine**	**Clinopyroxene**
Megacrysts	< 1.75 mm subhedral, often skeletal or embayed	
Phenocrysts / microphenocrysts	Phenocrysts: commonly subhedral, often skeletal or embayed. Microphenocrysts: subhedral and anhedral.	Rare. Pale green or pale brown. Phenocrysts: subhedral Microphenocrysts: subhedral and anhedral.
Textures	Occasional graphic textures of opaque worm-like intergrowths (e.g., SA08). Some megacrysts and phenocrysts with disquilibrium textures: margins and embayments lined with dense aggregates of opaque crystals (see Fig. A2.3).	
Alteration	Megacrysts and phenocrysts: Rims often altered to golden-yellow or reddish-orange iddingsite. Phenocrysts: patchy overgrowths of iddingsite. Microphenocrysts: often completely altered to iddingsite.	
Inclusions	Rare < 5 μm Cr-titanomagnetite inclusions in many crystals.	< 250 μm titanomagnetitie and other smaller opaque inclusions.
Comments	Dominant mineral phase.	Phenocrysts and microphenocrysts in clusters up to 1.0 mm across but insufficient to consider samples glomeroporphyritic.

Holocrystalline transitional basalts

The holocrystalline lavas (Fig. A2.4) are porphyritic (e.g., SA13) or glomeroporphyritic (e.g., SA48), vesicle-poor to vesicular, and relatively coarse-grained. They contain olivine megacrysts, olivine and clinopyroxene phenocrysts and microphenocrysts, phenocrysts and microphenocrysts of prismatic or tabular plagioclase, and rare titanomagnetite microphenocrysts. Plagioclase is the dominant phase in a minor number of holocrystalline samples.

Table A2.7 General description of the main mineral phases in the holocrystalline transitional basalts.

	Holocrystalline transitional basalts		
Mineral	**Olivine**	**Clinopyroxene**	**Plagioclase**
Megacrysts	< 3.25 mm subhedral to anhedral occasionally skeletal and embayed.		
Phenocrysts / microphenocrysts	Phenocrysts and microphenocrysts: subhedral to anhedral, occasionally skeletal and embayed (e.g., SA13).	Rare. Pale brown Phenocrysts and microphenocrysts: anhedral, usually in monomineralic glomeroporphyritic clusters (<2.75 mm) or polymineralic clusters with olivine. Rare purplish-brown titaniferous clinopyroxene in SA48.	Phenocrysts: up to 1.25 mm prismatic and tabular. Microphenocrysts: prismatic and tabular, less frequently as interstitial patches.
Textures			
Alteration	Phenocrysts and microphenocrysts: Reddish-orange iddingsite or greenish-brown bowlingite along rims, margins of embayments, and fractures. Dark greenish-brown bowlingite alteration is extensive, along fractures and spreading to crystal interiors as patchy overgrowths radiating from the fractures (e.g. SA48 and SAB161).		Sercite along fractures and as patchy overgrowths in some samples (e.g., SA49 and SAB145).
Inclusions	Rare < 5 μm Cr-titanomagnetite in some crystals in most samples. Greatest abundance in SAB150.	< 80 μm titanomagnetite inclusions (e.g., SA72 and SAB161).	< 5 μm apatite
Comments	Dominant phase in many samples (e.g., SA13 and SA83). Phenocrysts and microphenocrysts occur in monomineralic or polymineralic clusters with clinopyroxene.	Phenocrysts and microphenocrysts usually in monomineralic clusters or polymineralic clusters with olivine < 2.75 mm across.	Dominant phase in a number of samples (e.g., SA48, SAB145 and SAB161). Phenocrysts and microphenocrysts, in monomineralic clusters.

Table A2.8 General description of glomeroporphyritic clusters in transitional basalts.

Transitional basalts
Glomeroporphyritic Clusters
Glomeroporphyritic samples may contain: 1. Monomineralic clusters of interlocking anhedral clinopyroxene phenocrysts and microphenocrysts. Corroded margins lined with opaque reaction products indicative of cluster-magma disequilibrium and therefore, possibly an exotic origin (e.g., SA48). 2. Monomineralic plagioclase clusters up to 2.25 mm across: Abundant, prismatic phenocrysts and microphenocrysts, small laths, and anhedral groundmass crystals. Many are dominated by large, radiating prismatic phenocrysts and microphenocrysts that occur together with groundmass plagioclase (e.g., SA48 and SAB210). A number of phenocrysts in these clusters contain numerous oscillatory zones. 3. Polymineralic clusters up to 4.25 mm across: Phenocrysts and microphenocrysts of olivine ± clinopyroxene ± plagioclase. A number of plagioclase phenocrysts contain numerous oscillatory zones. In the largest clusters, clinopyroxene commonly occurs as an assemblage of interlocked anhedral crystals surrounded almost entirely by olivine and plagioclase (e.g., SA48). These clusters commonly have corroded margins, indicative of cluster-magma disequilibrium, suggesting a possible exotic origin.

Groundmass

The groundmass of the hypocrystalline samples (70.4 to 80.6 modal %) is commonly hyalopilitic (e.g., SA07 and SA08) and consists primarily of relatively short, e.g., < 350 μm, plagioclase laths and microlites, and rare interstitial plagioclase crystals, colourless clinopyroxene, titanomagnetite, and minor olivine (typically completely altered to iddingsite), and rare skeletal opaque crystals. Interstitial patches of dark brown devitrified glass are common. The vitrophyric sample (SA09) has a black, devitrified glassy matrix.

The groundmass of the holocrystalline samples (67.2 to 85.6 modal %) is commonly intergranular and coarse-grained. In all samples, the groundmass is composed primarily of abundant plagioclase and clinopyroxene, together with variable amounts of olivine, titanomagnetite, and ilmenite. Titanomagnetite occurs as blocky crystals, smaller grain-size crystals, and irregular-shaped crystals that commonly partially enclose plagioclase laths or groundmass clinopyroxene crystals. Ilmenite commonly occurs as irregular-shaped prismatic crystals that frequently partially enclose plagioclase laths. Sample SAB161 contains rare skeletal opaques that typically occur in areas containing devitrified glass. Olivine is commonly completely altered to iddingsite. It occurs as abundant anhedral crystals in sample SA83 but more often as small grain-size crystals in the other samples. Apatite microlites occur as small, e.g., < 100 μm, needle-like crystals in all samples. A general description of the major groundmass phases, plagioclase and clinopyroxene, and other features of the groundmass in the holocrystalline transitional basalts are given in Table A2.9.

Table A2.9 Summarised groundmass characteristics of the holocrystalline transitional basalts.

	Holocrystalline transitional basalts	
Mineral	**Clinopyroxene**	**Plagioclase**
Crystal habit	Colourless to pale greenish-brown anhedral crystals < 100 μm	< 500 μm prismatic laths, tabular and slender microlites - less common as irregular-shaped interstitial crystals.
Textures		Trachytic (SA72).
Alteration		
Inclusions		< 10 μm apatite
Comments	Commonly aggregates with titanomagnetite between plagioclase crystals.	Dominant phase in all samples.
Secondary mineralisation	Interstitial patches of a dark greenish-brown bowlingite in SA48, SA49, SAB150, SAB161, and SA210.	
Crystal clusters	Plagioclase crystals commonly in relatively small clusters throughout samples.	
Vesicles	Vesicles in SA48, SA49, SAB150, SAB161, and SA210 are often either lined or partially filled with greenish-brown bowlingite.	

A2.1.3 Hawaiites

Hawaiites exhibit either porphyritic (Fig. A2.5) or glomeroporphyritic (Fig. A2.6) textures and are usually vesicular. They are typically holocrystalline and consist of mineral assemblage olivine + clinopyroxene + plagioclase ± titanomagnetite ± ilmenite. Titanomagnetite and ilmenite occur as rare microphenocrysts in a small number of samples. Titanomagnetite commonly occurs as euhedral and occasionally as irregular-shaped crystals that partially enclose groundmass plagioclase laths or clinopyroxene grains. SAB163 is the only sample with a comparatively high titanomagnetite content (6.6 modal %). Ilmenite occurs as prismatic crystals up to 300 μm. Total phenocryst phases range from 6.6 to 47 modal %. Xenocrysts, xenoliths, and glomeroporphyritic clusters occur in a number of samples and are described in Table A2.12. The groundmass, described in Table A2.13, ranges from fine- to coarse-grained and is dominated by plagioclase and clinopyroxene.

The modal abundance of phenocrysts and groundmass phases of selected samples are presented in Table A2.10. Descriptions of the main mineral phases, olivine, clinopyroxene, and plagioclase are given in Table A2.11.

Table A2.10 Modal abundances of phenocrysts and the main groundmass phases of selected hawaiites. Abundances were determined by counting 1000 points.

Lava type:	hawaiites								
Sample:	SA11	SA32	SA74	SA140	SAB163	SAB203	All Samples (n=29)		
Phenocrysts							Max	Min	Mean
olivine	6.8	16.0	11.8	14.8	2.4	7.8	17.2	1.6	8.8
clinopyroxene	0.6	10.0	0.6	0.2	2.0	3.8	10.0	0.2	3.7
plagioclase	2.4	21.0	7.4	1.4	8.0	0.2	21.0	0.2	4.3
magnetite	-	-	-	0.6	6.6	-	6.6	tr	1.0
ilmenite	-	-	-	-	-	-	1.0	tr	-
Total	9.8	47.0	19.8	17.0	19.0	11.8	47.0	6.6	17.9
Vesicles	8.4	0.8	2.0	5.4	1.8	7.2	24.8	tr	6.8
Groundmass	81.8	52.2	78.2	77.6	91.4	81.0	92.6	52.2	75.3
Groundmass							n = 6		
olivine	0.5	2.0	2.4	1.6	tr	2.9	2.9	tr	16
clinopyroxene	35.2	29.9	40.3	32.7	27.0	37.8	40.3	27.0	33.8
plagioclase	52.7	63.3	51.5	51.0	62.5	51.3	63.3	51.0	55.4
magnetite	11.7	1.4	2.9	14.4	8.4	5.5	14.4	2.9	7.4
ilmenite	-	3.4	2.9	0.2	2.0	2.6	2.6	-	-
apatite	-	-	tr	tr	tr	tr	tr	-	-
glass	-	-	-	-	-	-	-	-	-

n = number of samples; tr = trace; - = none counted

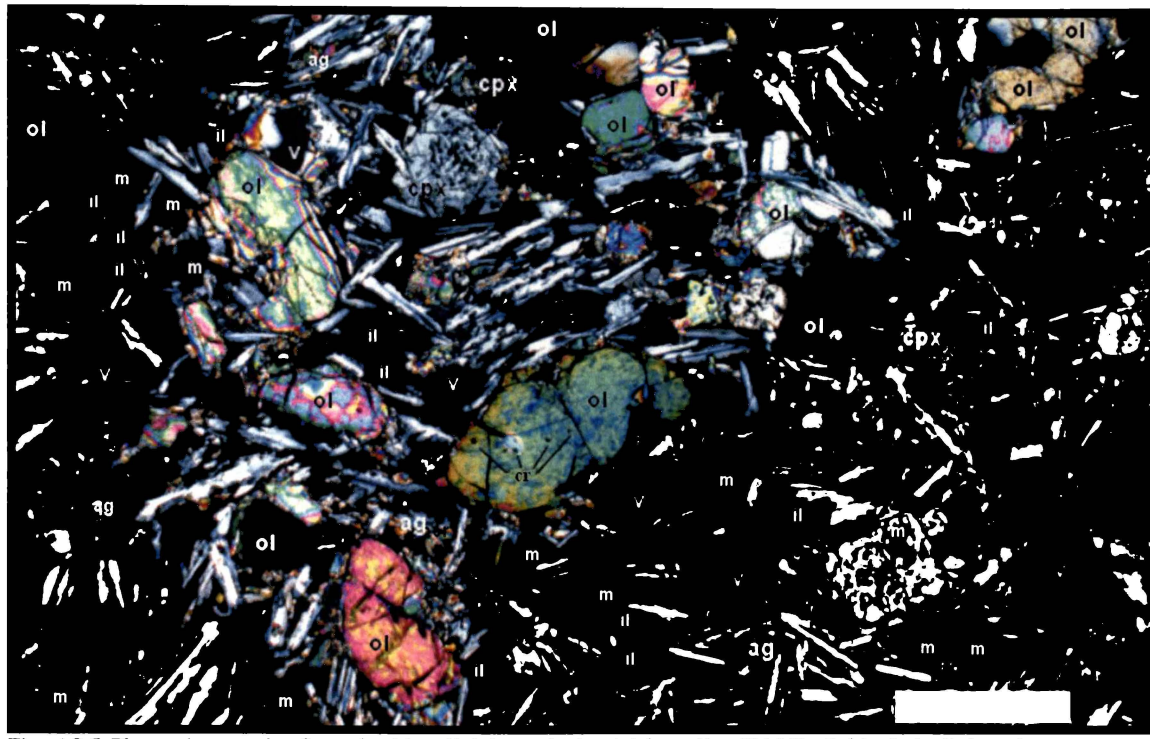

Fig. A2.5 Photomicrograph of porphyritic, slightly vesicular (v) hawaiite (SA32). Subhedral olivine phenocrysts and microphenocrysts (ol), occasionally with Cr-titanomagnetite inclusions (Cr), and clinopyroxene microphenocrysts (cpx) are set in a relatively coarse-grained groundmass composed of abundant plagioclase laths (white crystals), and grains of olivine, clinopyroxene, titanomagnetite (m), and ilmenite (il) that occasionally occur together in small aggregates (ag). Some clinopyroxene microphenocrysts contain titanomagnetite, clear, and unidentified opaque inclusions resulting in sieve-like textures (typical of many clinopyroxene crystals in the hawaiites). Polarised light; scale bar is 500 μm.

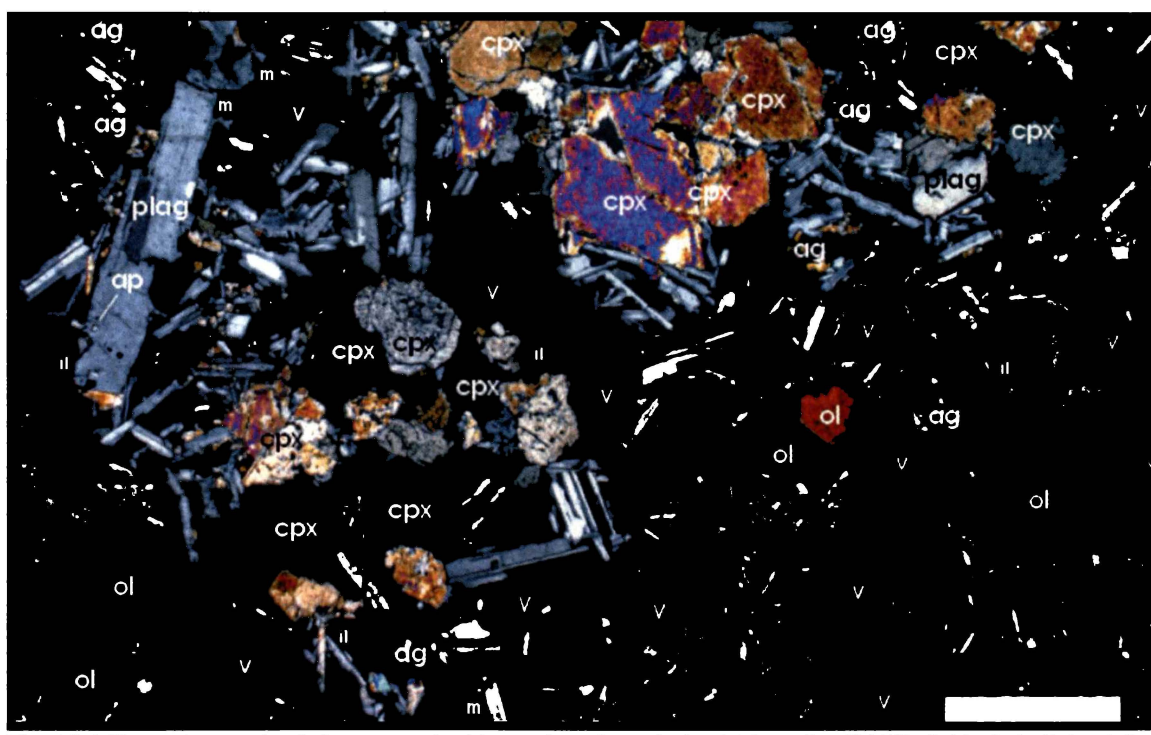

Fig. A2.6 Photomicrograph of glomeroporphyritic, moderately vesicular (v) hawaiite (SA78). Subhedral olivine (ol) and clinopyroxene (cpx) and tabular plagioclase (plag) microphenocrysts are set in a relatively coarse-grained groundmass composed of abundant plagioclase laths, aggregates of clinopyroxene, olivine, and titanomagnetite grains (ag) between the laths, and small titanomagnetite (m) and ilmenite (il) grains. The clusters are composed predominantly of interlocking anhedral clinopyroxene microphenocrysts. The margins of the clusters do not exhibit disequilibrium textures. The plagioclase phenocryst at the left of the image contains an apatite inclusion, typical of most plagioclase crystals in the group A rocks. Polarised light; scale bar is 500 μm.

Table A2.11 General description of the main mineral phases in the hawaiites.

	Hawaiite		
Mineral	**Olivine**	**Clinopyroxene**	**Plagioclase**
Megacrysts	< 3 mm subhedral to anhedral, typically embayed and often skeletal. Common in many samples.		
Phenocrysts / microphenocrysts	Phenocrysts and microphenocrysts: subhedral. Rare subhedral 6-sided phenocrysts. Phenocrysts typically embayed and often skeletal.	Pale brown, pale greenish-brown, or pale purplish-brown. Phenocrysts: subhedral, occasionally twinned, rare distinct marginal zones or oscillatory zoning. Microphenocrysts: subhedral	Phenocrysts: up to 1.5 mm prismatic and untwinned irregular-shaped, crystals. Microphenocrysts: prismatic and untwinned irregular-shaped, less frequently as tabular crystals up to 750 um. Some phenocrysts and microphenocrysts have distinct marginal zones or oscillatory zoning.
Textures		Phenocrysts: occasional partially resorbed interiors, irregular margins, some with rare aegerine augite rims. Phenocrysts and microphenocrysts occur in rare subophitic texture (e.g., SA90) partially enclosing large plagioclase groundmass laths.	Large phenocrysts in SA11 often have black, anisotropic, worm-like and patchy overgrowths in symplectite texture. Some phenocrysts in SA69 have partially resorbed cores mantled with "fresh" plagioclase.
Alteration	Phenocrysts: dark reddish-orange iddingsite, extensive along rims, margins of embayments, fractures, and crystal interiors. Phenocrysts: occasionally with extensively altered interiors mantled with fresh olivine. Microphenocrysts: often extensively altered to iddingsite.	Sieve texture in many samples.	
Inclusions	Rare < 50 μm opaque inclusions (possibly Cr-titanomagnetite).	Abundant < 20 μm opaque inclusions.	< 20 μm apatite
Comments	Dominant mineral phase in 22 of 29 samples.	Exceeds olivine in abundance in SA20, SAB140, and SAB142.	Dominant phase in 5 of 29 samples. Exceeds clinopyroxene in 9 samples.

Xenoliths, xenocrysts, and glomeroporphyritic clusters

Many olivine megacrysts and phenocrysts are interpreted as having a xenocrystic origin or are products of xenolith disaggregation based on several lines of evidence, outlined in Table A2.12. In addition, a number of samples contain relatively small xenoliths and/or glomeroporphyritic clusters up to 5.25 mm across, each of which may be characterised by a variety of mineral assemblages described in Table A2.12.

Table A2.12 General description of xenocrysts, xenoliths, and glomeroporphyritic clusters in hawaiites.

	Hawaiites
Xenocrysts	Typically subhedral crystals. Skeletal olivine up to 2.5 mm with rounded margins rims mantled with opaque alteration products, and kink-band metamorphic texture (e.g., SAB163).
Xenoliths	Xenoliths occur as: 1. Clusters up to 5.25 mm across of rounded subhedral and anhedral olivine phenocrysts and microphenocrysts. Deeply incised, rounded embayments and irregular, severely corroded margins indicates partial melting or dissolution - suggests possible derivation from xenolith disaggregation (e.g., SA11, SA14, SA30, SA44, SA69 and SAB189). 2. Clusters up to 3.7 mm diameter of clinopyroxene with minor olivine. Some clinopyroxene have kink-band metamorphic textures (e.g., SAB167). 3. Monomineralic olivine clusters of subhedral or elongate olivine megacrysts, phenocrysts, and microphenocrysts. Disequilibrium textures; (i) irregular margins with reaction rims of pale purple-brown clinopyroxene or aggregates or colourless clinopyroxene grains, (ii) partially resorbed interiors, and (iii) margins that are mantled with opaque crystals.
Glomeroporphyritic Clusters	Glomeroporphyritic samples may contain: 1. Monomineralic clinopyroxene clusters up to 3 mm across of subhedral to anhedral phenocrysts and microphenocrysts. 2. Monomineralic plagioclase clusters up to 2 mm diameter of radiating phenocrysts, microphenocrysts, and groundmass-size crystals. 3. Polymineralic clusters up to 5 mm across of olivine, clinopyroxene and plagioclase phenocrysts and microphenocrysts. Many clusters have disequilibrium textures e.g., severely corroded margins and clinopyroxene with partially resorbed interiors. Cavities and embayments in many clusters are often filled with groundmass plagioclase and granular titanomagnetite.

Groundmass

The groundmass (52.2 to 92.6 modal %) is generally coarse-grained and predominantly intergranular. Intersertal textures are rare. In all samples, the groundmass is composed primarily of abundant plagioclase and clinopyroxene. Titanomagnetite is relatively abundant in many samples and occurs as blocky grains or as irregular-shaped crystals with both crystal habits often occurring in the same sample. Ilmenite is less common but often occurs as prismatic crystals in the coarse-grained samples. Olivine typically occurs as anhedral grains and is often completely altered to iddingsite. Apatite microlites occur in many samples, but only in trace amounts. A general description of the major groundmass phases, plagioclase and clinopyroxene, and other features of the groundmass in hawaiites are given in Table A2.13.

Table A2.13 Summarised groundmass characteristics of the hawaiites.

	Hawaiite	
Mineral	**Clinopyroxene**	**Plagioclase**
Crystal habit	< 500 μm colourless to pale brown anhedral crystals.	< 500 μm prismatic laths, irregular-shaped crystals, and interstitial pools.
Textures		Trachytic (SA30).
Alteration		
Inclusions		< 10 μm apatite
Comments	Commonly as grains in aggregates between plagioclase crystals. Rare aggregates that partially encloses titanomagnetite microphenocrysts.	Dominant phase in all samples.
Secondary mineralisation	Opaques altered to a dark reddish-brown mineral (possibly leucoxene). Interstitial patches of a greenish-brown alteration product, possibly derived from devitrified glass.	
Crystal clusters	Clinopyroxene grains - interpreted as locations of resorbed quartzose xenoliths or xenocrysts, occur in a number of samples.	
Vesicles	Vesicles partially or completely filled with dark reddish-yellow-brown to brownish-yellow unidentified minerals.	

A2.1.4 Ol-tholeiitic basalts

Olivine tholeiitic basalts have predominantly porphyritic textures, range from medium- to relatively coarse-grained (Figs. A2.7 and Fig. A2.8 respectively), and are slightly vesicular to very vesicular. The ol-tholeiitic basalts are principally holocrystalline and there is no apparent glass in the samples. Mineral assemblages are typically dominated by olivine phenocrysts together with lesser amounts of clinopyroxene ± plagioclase. Clinopyroxene and plagioclase phenocrysts are rare or absent in a number of samples, especially those from the suite of Barriball tuff ring samples (SAB170 – SAB174). Titanomagnetite and ilmenite are minor phenocryst phases in a number of samples, each typically < 1.6 modal %. Titanomagnetite occurs as irregular-shaped and blocky crystals. Ilmenite typically occurs as prismatic crystals < 300 μm. The groundmass (described in Table A2.16) is generally medium- to coarse-grained.

Monomineralic and polymineralic clusters occur in a number of samples but generally in insufficient quantities for these samples to be considered to have glomeroporphyritic textures. SAB169 is the only sample characterised as glomeroporphyritic. It contains comparatively large numbers of polymineralic clusters of clinopyroxene ± olivine ± plagioclase as well as large monomineralic clusters of radiating plagioclase phenocrysts and microphenocrysts.

Total phenocryst phases range from 5.8 to 31.4 modal %. The modal abundance of phenocrysts and groundmass phases of selected samples are presented in Table A2.14. Descriptions of the main mineral phases, olivine, clinopyroxene, and plagioclase are given in Table A2.15.

Table A2.14 Modal abundances of phenocrysts and the main groundmass phases of selected ol-tholeiitic basalts. Abundances were determined by counting 1000 points.

Lava type	ol-tholeiitic basalt										
Sample	SA35	SA53	SA81	SA89	SAB149	SAB169	SAB171	SAB184	All Samples (n=34)		
Phenocysts									Max	Min	Mean
olivine	7.8	9.4	10.0	10.8	9.0	6.2	8.8	10.2	16.6	0.2	8.9
clinopyroxene	3.0	4.8	6.0	4.0	2.2	3.6	-	2.0	8.0	tr	3.2
plagioclase	4.2	-	1.2	1.0	2.0	9.2	0.6	1.8	20.8	tr	3.0
magnetite	0.6	-	-	-	1.6	-	-	-	2.6	tr	0.5
ilmenite	-	-	-	-	0.6	-	-	0.2	2.2	tr	0.2
Total	15.6	14.2	17.2	15.8	15.4	19.0	9.4	14.2	31.4	5.8	15.8
Vesicles	6.0	10.4	4.8	7.6	5.2	7.2	16.6	9.8	20.2	tr	8.8
Groundmass	78.4	75.4	78.0	80.2	79.4	73.8	74.0	76.0	87.2	52.8	75.6
Groundmass									n = 8		
olivine	8.7	8.8	8.9	9.5	6.8	1.8	9.2	4.6	9.5	1.8	7.3
clinopyroxene	22.9	18.1	19.6	21.8	24.7	9.7	21.0	22.6	24.7	9.7	20.1
plagioclase	61.0	37.2	62.4	54.1	58.4	34.1	48.8	56.7	62.4	34.1	51.6
magnetite	4.3	30.6	2.0	3.6	5.5	1.6	2.4	2.0	30.6	1.6	6.5
ilmenite	3.1	tr	7.0	3.6	2.0	tr	0.5	3.7	7.0	tr	2.5
apatite	tr	5.3	tr	tr	2.5	1.3	tr	tr	5.3	tr	1.1
carbonate	-	-	-	7.3	-	-	-	-	7.3	-	-
glass	-	-	-	-	-	51.4	18.1	10.3	51.4	-	-

n = number of samples; tr = trace; - = none counted.

Groundmass

The groundmass (52.8 to 87.2 modal %) is generally medium- to coarse-grained with textures that range from intersertal to intergranular. In all samples, the groundmass is composed primarily of abundant plagioclase and clinopyroxene together with variable amounts of olivine, titanomagnetite, and ilmenite. Olivine typically occurs as anhedral grains. Titanomagnetite occurs predominantly as distinct blocky crystals, < 50 μm, or aggregates of crystals, although the majority of crystals in sample SA53 (Fig. A2.7) are < 5 μm. Ilmenite commonly occurs as thin, needle-like crystals oriented adjacent and parallel to the margins of phenocrysts, and as irregular-shaped prismatic crystals that occasionally partially enclose plagioclase laths. A number of samples (e.g., SA68, SA81, SAB181, and SAB184) contain skeletal opaques, which are commonly associated with interstitial patches of dark brown devitrified glass. A general description of the major groundmass phases, plagioclase and clinopyroxene, and other features of the groundmass in the ol-tholeiitic basalts are given in Table A2.16.

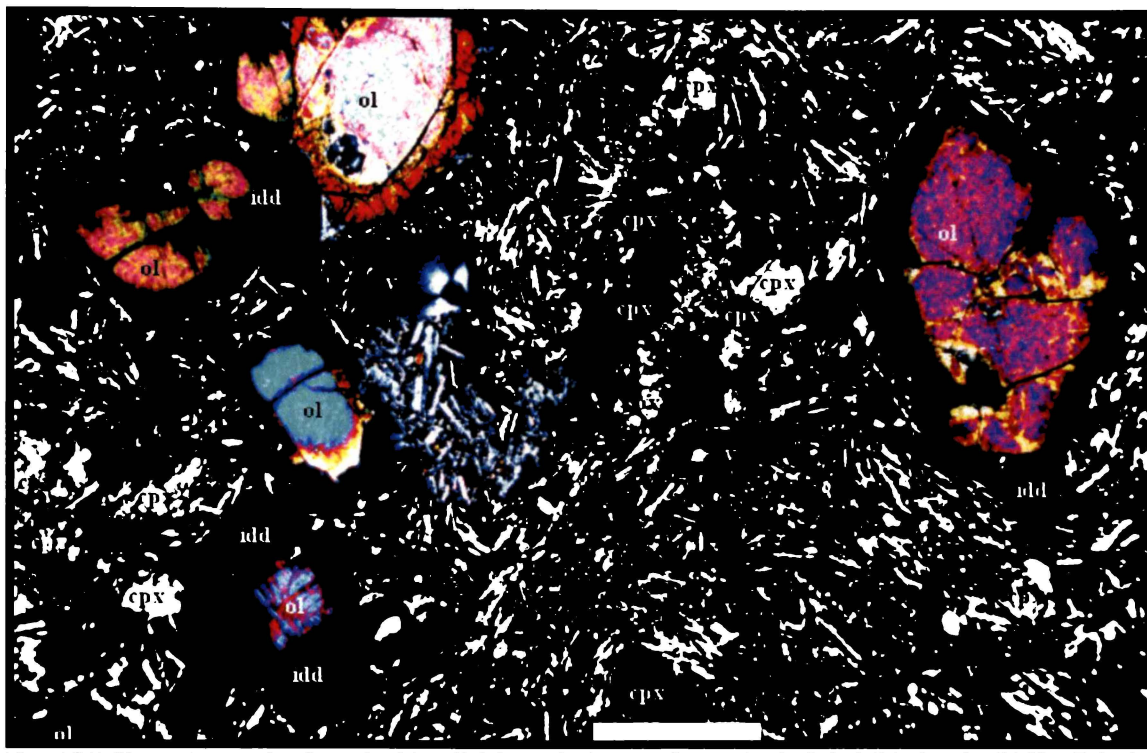

Fig. A2.7 Photomicrograph of porphyritic, slightly vesicular (v), fine-grained ol-tholeiitic basalt (SA53). Euhedral olivine phenocrysts (ol) with rims heavily altered to iddingsite (idd) are set in a plagioclase-rich groundmass. Clinopyroxene (cpx) occurs as anhedral microphenocrysts, predominantly in small clusters (centre and lower left of the image). In addition to plagioclase, the groundmass contains, < 5μm, clinopyroxene (high birefringence) and titanomagnetite (black) grains that are uniformly distributed throughout the sample. Polarised light; scale bar is 500μm.

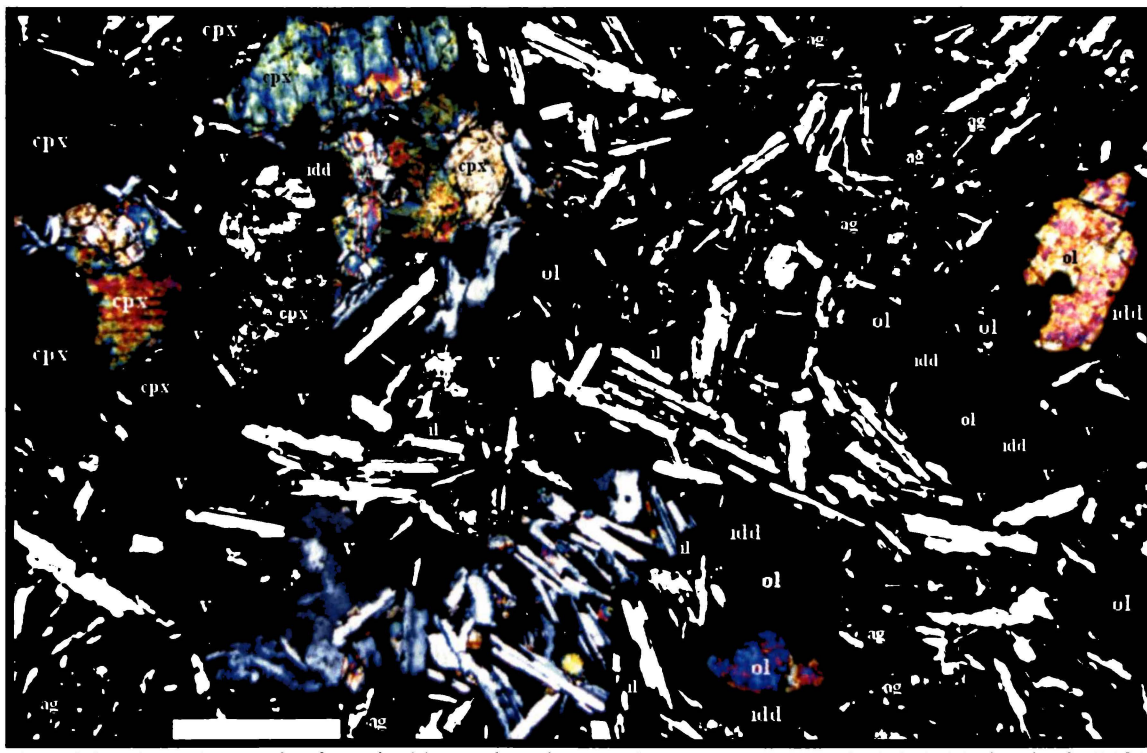

Fig. A2.8 Photomicrograph of porphyritic, moderately vesicular (v) coarse-grained ol-tholeiitic basalt (SAB184). Subhedral olivine (ol) and anhedral clinopyroxene (cpx) phenocrysts are set in a plagioclase-rich (low birefringence) groundmass. Olivine crystals are often annealed to one another and may form small clusters. Their rims are typically heavily altered to iddingsite (idd). The large cluster at the upper left of the image is composed of interlocking anhedral cpx microphenocrysts, which surround an olivine microphenocryst. Clinopyroxene grains occur in small aggregates (ag) between plagioclase laths. Ilmenite (il) is a minor groundmass phase. Polarised light; scale bar is 500μm.

Table A2.15 General description of the main mineral phases in the ol-tholeiitic basalts.

	Ol-tholeiitic basalts		
Mineral	**Olivine**	**Clinopyroxene**	**Plagioclase**
Megacrysts	Rare < 3 mm subhedral to anhedral, often skeletal, occur in only a few samples (e.g., SA34, SA35, SA80, SA81).		
Phenocrysts / microphenocrysts	Phenocrysts and microphenocrysts: subhedral to anhedral. Occasionally in small, loosely consolidated clusters of < 6 crystals.	Colourless, pale green, or pale brown. Phenocrysts and microphenocrysts: subhedral to anhedral, with irregular margins. Often occurs in: 1. Monomineralic clusters < 1.25 mm of few crystals. 2. Monomineralic clusters up to 3 mm of numerous interlocked subhedral and anhedral crystals. 3. Polymineralic clusters up to 7.5 mm with olivine and plagioclase (e.g., SA16), with intersticies filled with groundmass material.	Phenocrysts: up to 1.5 mm prismatic and untwinned irregular-shaped crystals (e.g., SA93 and SAB169). Microphenocrysts: up to 750 μm prismatic, untwinned irregular-shaped, and tabular crystals. Some phenocrysts and microphenocrysts have distinct marginal zones or oscillatory zoning. Occasionally in small monomineralic clusters up to 1.25 mm of radiating crystals (e.g. SAB169).
Textures	Megacrysts and larger phenocrysts with disequilibrium textures: 1. Crystal margins partially sheathed with clinopyroxene grains and microphenocrysts. 2. Deeply incised embayments with corroded margins.		
Alteration	Megacrysts: frequently extensively altered to reddish-orange iddingsite or dark greenish-brown bowlingite. Phenocrysts: rims and fractures often heavily altered to iddingsite (e.g., SA53). Bowlingite is less commonly which also occurs along crystal fractures and frequently spreads towards the crystal's interior (e.g., SA73). Large-scale bowlingite overgrowths in the extensively altered samples SA93, SAB152, SAB201 and SAB205.	Phenocryst rims green aegerine-augite.	

Continued on next page.

Table 3.18 continued.

	Ol-tholeiitic basalts		
Mineral	**Olivine**	**Clinopyroxene**	**Plagioclase**
Inclusions	Phenocrysts and microphenocrysts: < 5 μm Cr-titanomagnetite - abundant in a number of samples (e.g., SA43 and SA59).		< 5 μm apatite
Comments	Dominant phenocryst phase in 28 of 34 samples. Some phenocrysts with large angular cavities.		Dominant phenocryst phase in 3 samples and exceeds clinopyroxene in modal abundance in 11 other samples. Rare zoned crystals.

Table 3.19 Summarised groundmass characteristics of the ol-tholeiitic basalts.

	Ol-tholeiitic basalts	
Mineral	**Clinopyroxene**	**Plagioclase**
Crystal habit	< 500 μm colourless, pale green, pale brown anhedral crystals.	< 500 μm prismatic laths and tabular crystals.
Textures		
Alteration		
Inclusions		< 5 μm apatite
Comments	Intergranular samples: Small aggregates of clinopyroxene grains, and minor amounts of olivine, titanomagnetite, and ilmenite, occur between plagioclase.	Dominant phase in all samples.
Secondary mineralisation	1. Interstitial patches of a light to dark brown mineraloid, possibly devitrified glass or smectite (e.g., SA34, SA93, and SAB181). 2. Interstitial patches of greenish-brown mineraloid, possibly smectite (e.g., SA73). 3. Interstitial patches of chlorite (e.g., SA73). 4. Carbonate in interstitial pools (e.g., SA67) and amygdales (e.g., SA71). 5. Extensive bowlingite and smectite overgrowths on phenocryst phases.	
Crystal clusters	< 2 mm in diameter, composed of clinopyroxene grains (e.g., SA16). Interpreted as locations of resorbed quartzose xenoliths or xenocrysts.	
Vesicles	1. Filled with greenish-brown (possibly smectite, e.g., SA73). 2. Partially filled with yellow carbonate (possibly siderite, e.g., SA89).	

A2.1.5 Qz-tholeiitic basalt

Four samples are classified as qz-tholeiitic basalts. Each is porphyritic, holocrystalline, and vesicular. The groundmass, described in Table A2.19, is relatively fine- to coarse-grained. With the exception of sample SAB198, they consist of the mineral assemblage olivine + clinopyroxene + plagioclase ± titanomagnetite and ± ilmenite (Fig A2.7). Sample SAB198 is the only SAVF rock examined that does not contain olivine phenocrysts. Total phenocryst phases range from 3.6 to 17.6 modal %. The modal abundance of phenocrysts and groundmass phases of selected samples are presented in Table A2.17. Descriptions of the main mineral phases, olivine and clinopyroxene, are given in Table A2.18.

Table A2.17 Modal abundances of phenocrysts and the main groundmass phases of the qz-tholeiitic basalts. Abundances were determined by counting 1000 points.

Lava type:	qz-tholeiitic basalts						
Sample:	SA31	SA76	SA77	SAB198	All Samples (n=4)		
Phenocrysts					Max	Min	Mean
olivine	5.2	14.8	6.8	-	14.8	0.8	6.9
clinopyroxene	3.4	0.8	3.0	2.8	3.4	0.8	2.5
plagioclase	1.0	2.0	1.2	0.4	2.0	0.4	1.2
magnetite	-	-	-	0.4	0.4	tr	0.1
ilmenite	0.4	-	-	-	0.4	tr	0.1
Total	10.0	17.6	11.0	3.6	17.6	3.6	10.6
Vesicles	5.0	1.2	4.8	15.0	15.0	1.2	6.5
Groundmass	85.4	79.2	83.4	81.4	85.4	79.2	82.4
Groundmass					n = 4		
olivine	1.4	1.1	1.2	2.4	2.4	1.1	1.5
clinopyroxene	42.1	44.2	44.7	36.7	44.7	36.7	41.9
plagioclase	48.5	47.8	47.6	52.6	52.6	47.6	49.1
magnetite	1.1	1.8	0.2	3.3	3.3	0.2	1.6
ilmenite	5.1	3.9	5.7	4.0	5.7	3.9	4.7
apatite	1.8	1.1	0.5	0.9	1.8	0.5	1.1
carbonate	-	2.0	1.0	-	2.0	-	-
glass	-	-	-	-	-	-	-

n = number of samples; tr = trace; - = none counted.

Groundmass

The groundmass (79.2 to 89.4 modal %) is intergranular, relatively fine- to coarse-grained, and composed of abundant plagioclase and clinopyroxene with minor amounts of titanomagnetite, ilmenite, and apatite. Titanomagnetite is often irregular-shaped and frequently partially encloses plagioclase laths and clinopyroxene grains. Ilmenite typically occurs as < 300 μm slender prismatic or irregular-shaped crystals. Apatite microlites occurs throughout the groundmass. A general description of the major groundmass phases, plagioclase and clinopyroxene, and other features of the groundmass in the qz-tholeiitic basalts are given in Table A2.19.

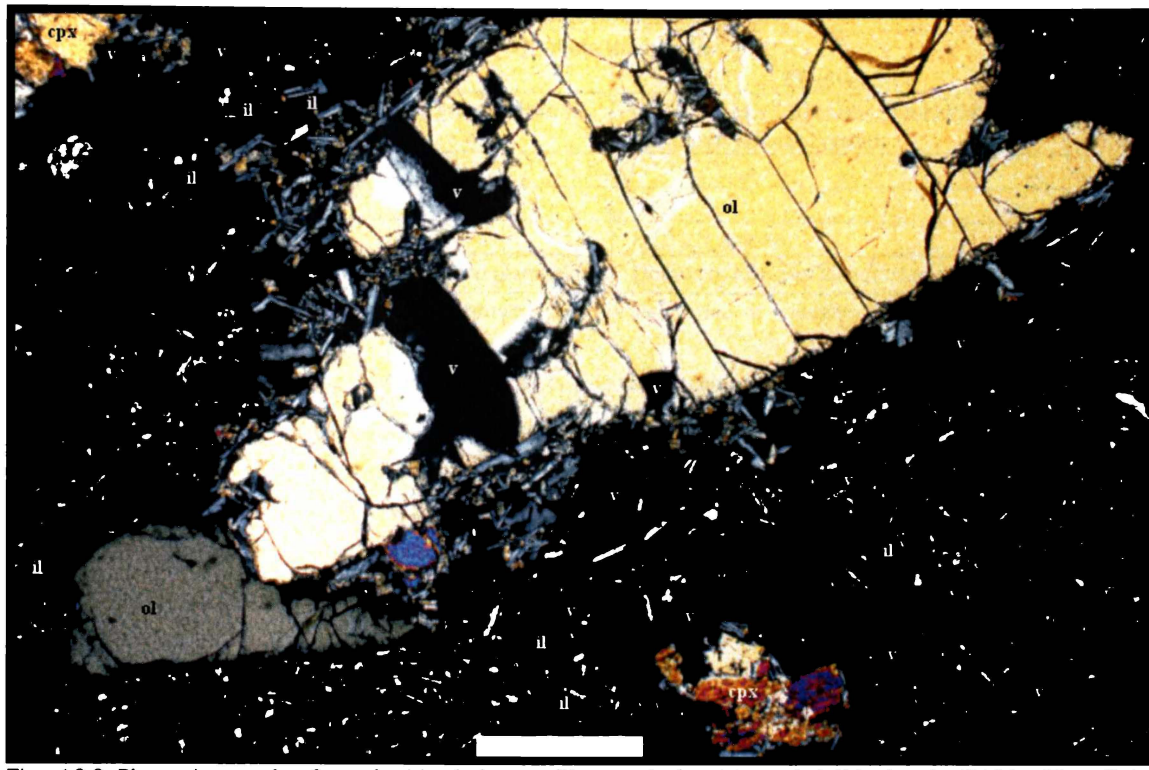

Fig. A2.9 Photomicrograph of porphyritic, holocrystalline, vesicular (v) qz-tholeiitic basalt (SA31). The olivine xenocryst (ol) is typical of the olivine crystals that occur in each qz-tholeiitic sample, except SAB198. Clinopyroxene grains typically rim xenocryst margins, indicative of crystal-melt disequilibrium,. Clinopyroxene microphenocrysts (cpx) often occur in small clusters. Plagioclase laths (low birefringence) dominates the medium-grained, intergranular groundmass. Clinopyroxene grains (high birefringence) occur in aggregates between the plagioclase. Prismatic ilmenite (il) is a minor groundmass phase. Polarised light; scale bar is 500μm.

Table A2.18 General description of the main mineral phases in the qz-tholeiitic basalts.

	Qz-tholeiitic basalts		
Mineral	**Olivine**	**Clinopyroxene**	**Plagioclase**
Megacrysts	up to 4 mm unaltered, skeletal, and embayed.		
Phenocrysts / microphenocrysts	Phenocrysts: subhedral Microphenocrysts: subhedral and anhedral.	Colourless or pale greenish-brown. Phenocrysts and. microphenocrysts: subhedral and anhedral.	Rare.Phenocrysts: prismatic or poorly formed prism-like crystals. Microphenocrysts: tabular (less common).
Textures	Megacrysts and larger phenocrysts with disequilibrium textures: rounded, irregular margins lined with clinopyroxene grains.	Some crystals with sieve-like texture.	
Alteration	Phenocrysts with rims, fractures, and embayments, slightely altered to greenish-brown bowlingite.		
Inclusions		< 30 μm opaque inclusions.	< 10 μm apatite
Comments	Dominant phenocryst phase (except in SAB198).	Often in clusters up to 1.75 mm across but in insufficient quantities for samples to be considered glomeroporphyritic.	

Table A2.19 Summarised groundmass characteristics of the qz-tholeiitic basalts.

Mineral	Qz-tholeiitic basalts	
	Clinopyroxene	**Plagioclase**
Crystal habit	< 200 μm colourless to pale green anhedral crystals.	< 400 μm prismatic laths, interstitial patches and minor tabular crystals.
Textures		
Alteration		
Inclusions		< 10 μm apatite
Comments	Commonly in aggregates between plagioclase.	Dominant phase in all samples.
Secondary mineralisation	1. Occasional dark reddish-brown (possibly leucoxene or smectite) that often occurs proximal to Fe-Ti-oxides. 2. Interstitial patches and amygdales of pale yellow carbonate. 3. Small, widespread patches of light brown devitrified glass (e.g., SA31).	
Crystal clusters	None observed.	

A2.2 Group B – basanites, nephelinites, ne-hawaiites, alkali ol-basalts, mugearites

A2.2.1 Basanites

Basanites have either porphyritic or glomeroporphyritic textures and tend to be slightly vesicular. They are typically hypocrystalline (Fig. A2.10), crystal-rich hypocrystalline, or holocrystalline (Fig. A2.11) and consist of olivine megacrysts, and phenocrysts and microphenocrysts of olivine and clinopyroxene. Total phenocryst phases range from 10.2 to 34.2 modal %. Plagioclase is generally restricted to the groundmass (described in Table A2.23), which is relatively fine-grained. The modal abundance of phenocrysts and groundmass phases of selected samples are presented in Table A2.20. Descriptions of the main mineral phases, olivine and clinopyroxene, are given in Table A2.21. Xenocrysts, xenoliths, and glomeroporphyritic clusters occur in a number of samples and are described in Table A2.22.

Table A2.20 Modal abundances of phenocrysts and the main groundmass phases of selected basanites. Abundances were determined by counting 1000 points.

Lava type:	basanite								
Sample:	SA27	SA42	SA75	SAB111	SAB176	SAB204	All Samples (n=33)		
							Max	Min	Mean
Phenocrysts									
olivine	5.2	13.6	7.0	15.0	21.2	15.6	21.2	5.2	12.9
clinopyroxene	6.0	20.2	2.8	2.0	7.0	6.4	20.2	2.0	8.3
plagioclase	-	0.4	-	-	-	-	0.6	tr	0.1
magnetite	0.2	-	0.6	0.2	-	-	2.0	tr	0.4
Total	11.4	34.2	10.4	17.2	28.2	22.0	34.2	10.2	21.7
Vesicles	6.4	8.2	0.4	7.8	4.2	16.6	16.6	tr	4.2
Groundmass	82.2	57.0	89.2	75.0	67.6	61.4	89.2	57.0	74.3
Groundmass							n = 8		
olivine	8.4	3.0	1.8	2.3	6.7	2.4	8.4	tr	-
clinopyroxene	54.6	31.8	31.7	30.2	35.0	28.3	54.6	28.3	35.3
plagioclase	9.1	51.5	45.0	36.4	43.8	20.5	51.5	9.1	34.4
magnetite	25.2	13.7	21.4	10.4	12.9	13.2	25.2	10.4	16.1
apatite	tr	tr	tr	tr	tr	-	tr	tr	-
glass	2.9	-	-	20.7	1.7	35.6	35.6	-	-

n = number of samples; tr = trace; - = none counted

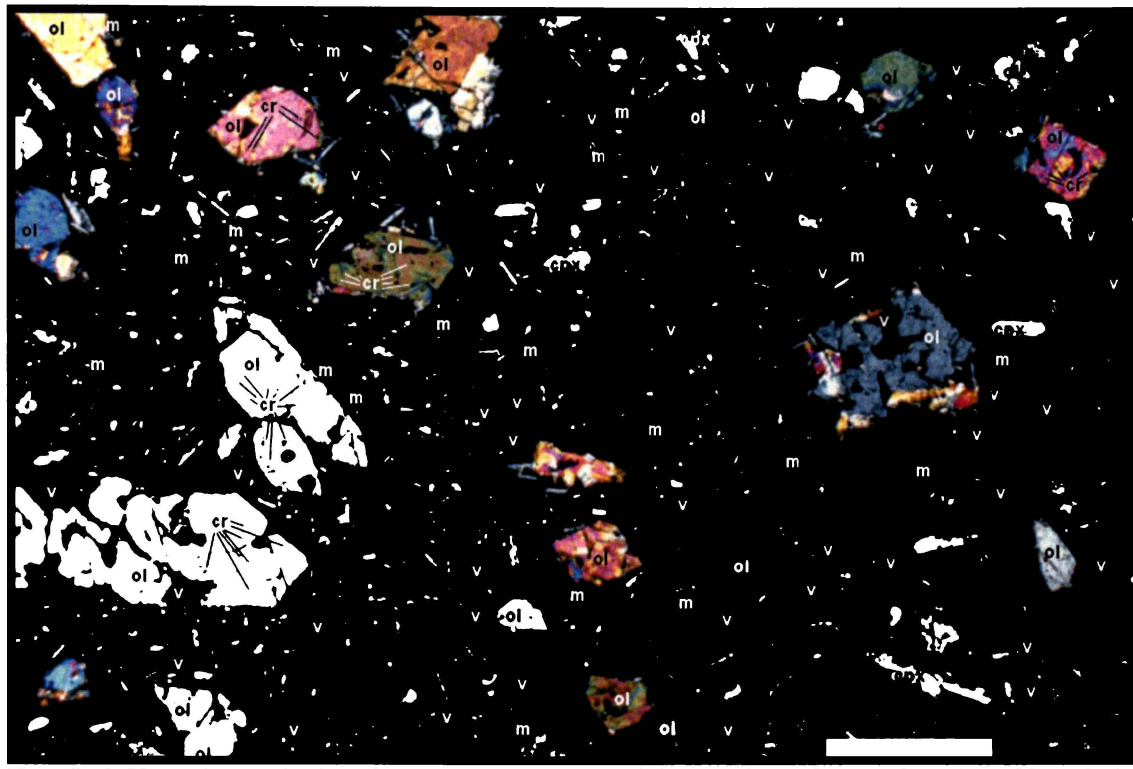

Fig. A2.10 Photomicrograph of porphyritic, hypocrystalline slightly vesicular (v) basanite lava (SAB128). Euhedral and subhedral olivine (ol), some with Cr-titanomagnetite inclusions (cr), and clinopyroxene (cpx) are set in a fine-grained intersertal groundmass of dark devirtrified glass with plagioclase laths and microlites (low birefringence), euhedral grains and laths of clinopyroxene (high birefringence), and titanomagnetite grains (m). Note the large, deeply incised olivine at the right and left of the image. Polarised light: scale bar is 500 μm.

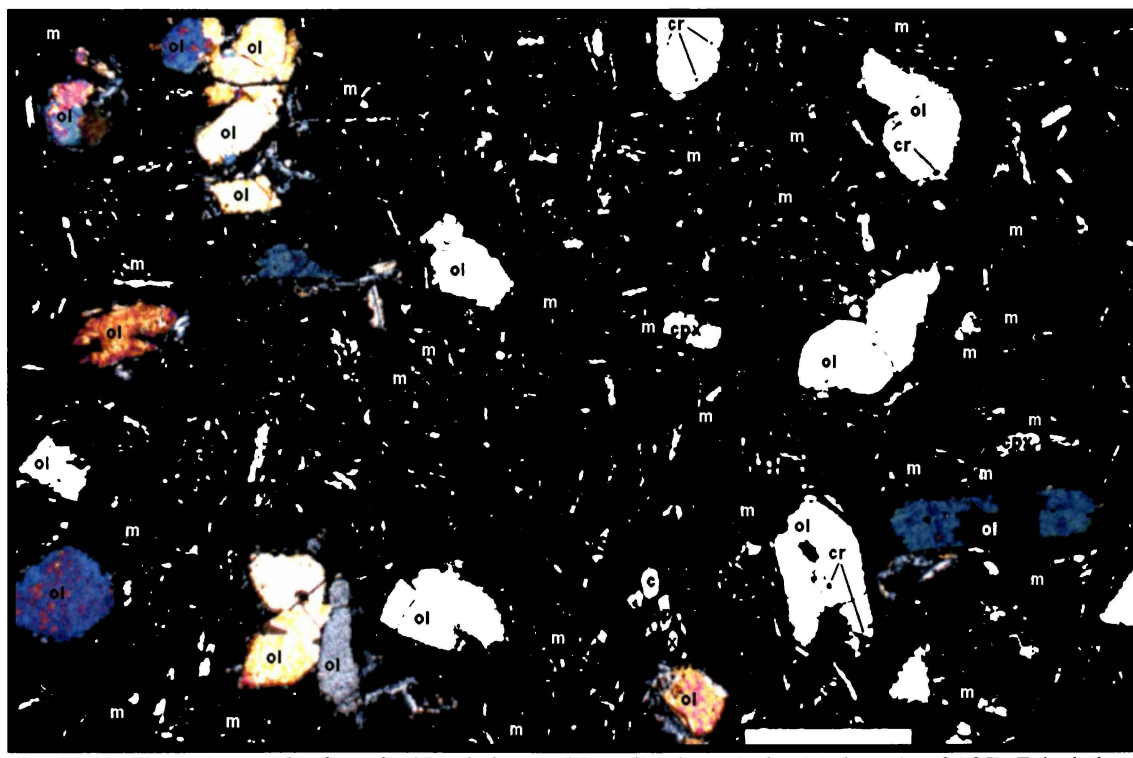

Fig. A2.11 Photomicrograph of porphyritic, holocrystalline, slightly vesicular (v), basanite (SA05). Euhedral and subhedral olivine (ol), some with Cr-titanomagnetite inclusions, and clinopyroxene (cpx) set in an intergranular groundmass composed of abundant plagioclase laths, microlites, and interstitial patches (low birefringence), euhedral grains and laths of clinopyroxene (high birefringence), and titanomagnetite grains (m). Many olivine crystals have slightly rounded margins with thin reaction rims.. Polarised light: scale bar is 500 μm.

Table A2.21 General description of the main mineral phases in basanites.

	Basanites	
	Olivine	**Clinopyroxene**
Megacrysts	Infrequent < 2.5 mm subhedral or elongate, occasionally skeletal.	
Phenocrysts / microphenocrysts	Phenocrysts: commonly euhedral and subhedral 6-sided or elongate, occasionally skeletal. Microphenocrysts: subhedral and anhedral, rare euhedral and subhedral 6-sided.	Purplish-brown and titaniferous Phenocrysts: rare 6- or 8-sided euhedral and subhedral; rare sector zoned prismatic (< 750 μm) Microphenocrysts: euhedral and subhedral 6- and 8-sided, often twinned, many with distinct marginal zones and oscillatory zoning; less common sector zoned prismatic.
Textures	Phenocryst populations in SA27, SA38, SA55, SA56, SA75, SA86, SAB107, SAB129, SAB132) with disequilibrium textures that may include one or more of the following features: 1. Crystals mantled with opaque crystals. 2. Reaction rims of pyroxene. 3. Irregular margins partially enclosed by Ti-clinopyroxene ± titanomagnetite ± devitrified glass. 4. Partially dissolved crystals overgrown by fresh olivine (e.g., SA75).	Partially resorbed cores with groundmass-filled cavities (e.g., SA03 and SA26)
Alteration	Common in most samples Phenocrysts: varying degrees of reddish-yellow to reddish-orange iddingsite; extensive alteration along rims and fractures. Microphenocrysts: often extensively altered to reddish-yellow iddingsite.	
Inclusions	<75 μm Cr-titanomagnetite; less common clear inclusions in phenocrysts.	< 40 μm titanomagnetite often abundant, some Cr-bearing.
Comments	Dominant phase in 25 of 34 samples.	Dominant phase in 9 of 34 samples. Occasional bimodal populations; crystals with resorbed cores together with those without resorbed cores indicative of disequilibrium phenocryst assemblages.

Xenocrysts, xenoliths, and glomeroporphyritic clusters

Many olivine megacrysts are interpreted as having a xenocrystic origin. In addition, a number of samples contain relatively small (e.g., < 5 mm) xenoliths and/or glomeroporphyritic clusters up to 2 mm across, each of which may be characterised by a variety of mineral assemblages described in Table A2.22.

Table A2.22 General description of xenocrysts, xenoliths, and glomeroporphyritic clusters in basanites.

	Basanites
Xenocrysts	Up to 3.25 mm subhedral olivine with: 1. Deeply incised or embayed with severely corroded margins. 2. Margins lined with Ti-clinopyroxene microphenocrysts and grains. 3. Kink-band metamorphic texture. Some xenocrysts in SA82 contain carbonate inclusions.
Xenoliths	Xenoliths occur as: 1. Clusters up to 4.75 mm across of olivine phenocrysts and microphenocrysts. The clusters have irregular margins that are partially enclosed by Ti-clinopyroxene microphenocrysts or grains. 2. Clusters up to 3.25 mm diameter of pale purple-brown titaniferous clinopyroxene phenocrysts and microphenocrysts. They often have embayed, irregular margins and partially resorbed interiors. 3. Clusters up to 4.75 mm across of feldspar, quartz, and quartz + feldspar. They are commonly partially resorbed and enclosed by the mineral assemblage; Ti-clinopyroxene ± olivine ± plagioclase. Sample SA82 contains a 7 mm greywacke xenolith.
Glomeropophyritic Clusters	Glomeroporphyritic samples may contain: 1. Monomineralic olivine clusters up to 2 mm across of subhedral 6-sided phenocrysts and subhedral microphenocrysts. 2. Monomineralic Ti-clinopyroxene clusters up to 1.5 mm across of subhedral 6- and 8-sided and prismatic phenocrysts and microphenocrysts. 3. Polymineralic clusters up to 1.25 mm across of olivine and Ti-clinopyroxene phenocrysts and microphenocrysts. Many clusters have disequilibrium textures, e.g., corroded margins. Many crystals in these clusters, especially clinopyroxene, have partially resorbed interiors.

Groundmass

Groundmass (57 to 89.2 modal %) textures are generally fine-grained, and range from hyalopilitic, to intersertal, to intergranular. Plagioclase and Ti-clinopyroxene are abundant with plagioclase the dominant phase in the majority of samples. Titanomagnetite, olivine, and nepheline[1] are additional groundmass phases (see Table A2.20). A general description of these phases and other features of the groundmass in the basanites are given in Table A2.23.

[1] Few nepheline crystals in the groundmass of the group B rocks were identified using optical mineralogy techniques, because of its relatively small size (e.g., < 75μm). The nepheline referred to in the text was identified in samples selected for electron microprobe analyses (see Appendix 1 for identification of these samples). Therefore, the occurrence of nepheline in basanite and the other group B rocks is inferred and its relative abundance in each sample is uncertain.

Table A2.23 Summarised groundmass characteristics of the basanites.

	Basanites			
Mineral	**Olivine**	**Clinopyroxene**	**Titanomagnetite**	**Plagioclase/ Nepheline**
Crystal habit	< 100 μm anhedral grains	< 150 μm laths and 6-sided euhedral and subhedral crystals	< 100 μm blocky grains, abundant in interstitial and intergranular samples. Hyalopilitic samples contain abundant < 5 μm grains.	< 350 μm laths, microlites, and interstitial pools. Nepheiline: < 75 μm, laths and interstitial pools.
Textures		Partially resorbed interiors in some samples.		
Alteration	Often completely altered to iddingsite			
Inclusions		Titanomagnetite grains		< 10 μm apatite
Comments	Rare in many samples	Abundant in most samples. Interstitial and intergranular samples - often occurs in aggregates (i) frequently between plagioclase and nepheline, (ii) infrequently partially enclose plagioclase laths.	Relatively abundant in most samples. Skeletal opaques restricted to samples with hyalopilitic textures. Concentrated in areas with abundant devitrified glass.	Abundant in most samples.
Secondary mineralisation	1. Veins and patches of reddish-yellow-orange alteration product (possibly smectite), bright green patches (possibly chlorite), and rare interstitial patches of calcite. 2. Hyalopilitic samples often contain abundant (up to 35.6 modal %) dark brown and greyish-black devitrified glass. 3. Intersertal, and less frequently intergranular, samples contain light brown devitrified glass and minor patches of greenish black devitrified glass.			
Crystal clusters	Occur in many samples. Up to 2.0 mm across, composed of fibrous pyroxene or Ti-clinopyroxene laths and grains. Interpreted as locations of completely resorbed quartzose or feldspar xenoliths or xenocrysts.			
Vesicles	1. Partially or completely filled with analcime or pale yellow to pale brown carbonate (possibly magnesite or siderite). 2. Partially filled with fan-like prismatic pyroxene radiating from the cavity's wall. 3. Enclosed by relatively thin, e.g., < 20 μm, fine-grained assemblages of plagioclase ± Ti-clinopyroxene ± titanomagnetite.			

A2.2.2 Nephelinites

Nephelinite lavas are porphyritic and tend to be slightly vesicular. They are typically hyalocrystalline (Fig. A2.12) or crystal-rich hypocrystalline (Fig. A2.13) and consist of olivine megacrysts, phenocrysts and microphenocrysts of olivine and clinopyroxene, and rare titanomagnetite microphenocrysts. Plagioclase and nepheline are restricted to the groundmass, described in Table A2.26, which ranges from very fine-grained to relatively

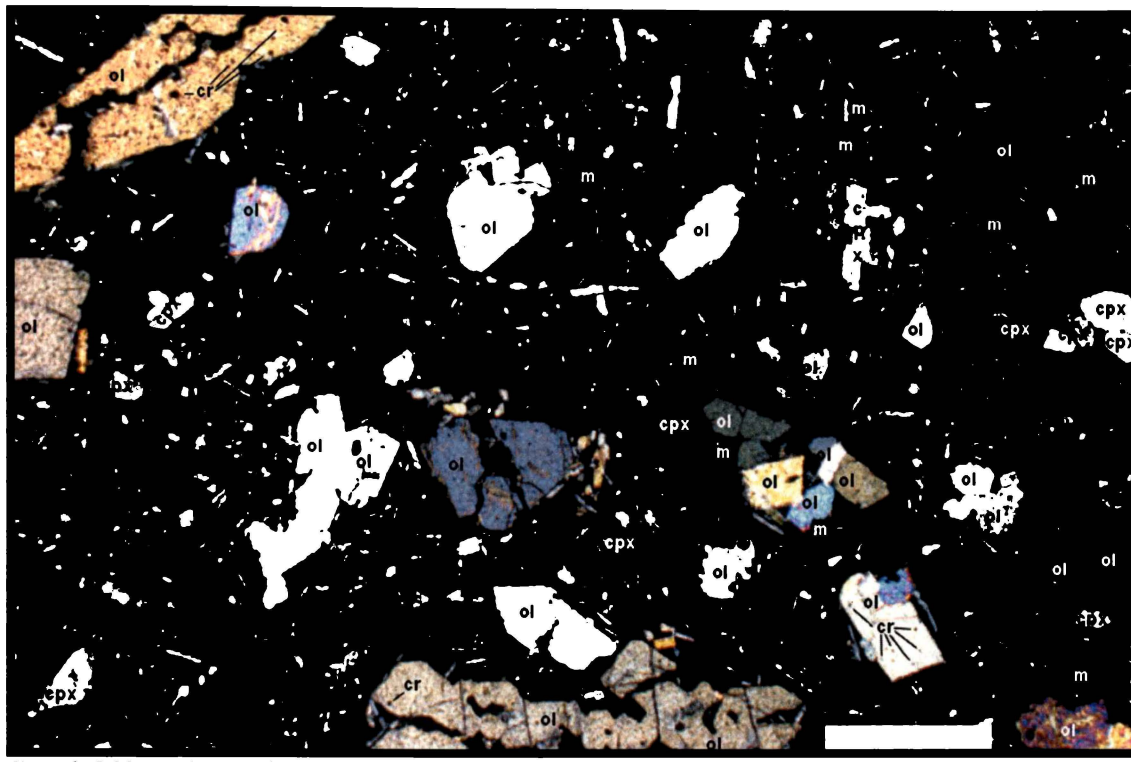

Fig. A212 Photomicrograph of porphyritic, hyalocrystalline nephelinite (SA06). Euhedral and subhedral olivine (ol) phenocrysts and microphenocrysts, some with Cr-titanomagnetite inclusions (cr), and clinopyroxene microphenocrysts (cpx) set in a fine-grained groundmass of devitrified glass with abundant plagioclase laths (low birefringence), clinopyroxene laths to euhedral grains (high birefringence), and titanomagnetite (m). Olivine phenocrysts are often deeply incised and corroded. Many olivine and clinopyroxene microphenocrysts occur in small monomineralic clusters. Polarised light: scale bar is 500 μm.

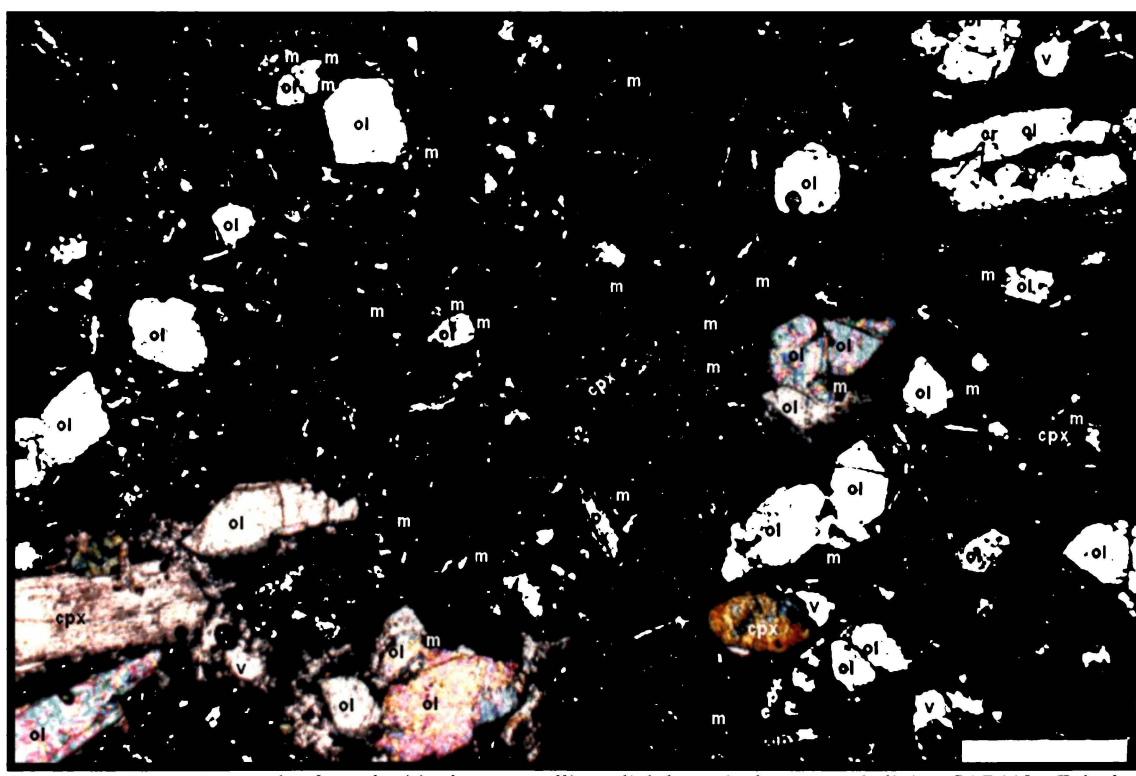

Fig. A2.13 Photomicrograph of porphyritic, hypocrystalline, slightly vesicular (v) nephelinite (SAB119). Euhedral and subhedral olivine (ol), some with Cr-titanomagnetite inclusions (cr), and clinopyroxene (cpx) phenocrysts and microphenocrysts set in a fine-grained intersertal groundmass of devitrified glass with abundant clinopyroxene laths and euhedral to subhedral grains (high birefringence), titanomagnetite grains (m), and a minor amount of plagioclase laths (low birefringence). Polarised light: scale bar is 500 μm.

coarse-grained. Total phenocryst phases range from 8.2 to 21.0 modal %. The modal abundance of phenocrysts and groundmass phases of selected samples are presented in Table A2.24. Descriptions of the main mineral phases, olivine and clinopyroxene, are given in Table A2.25.

Table A2.24 Modal abundances of phenocrysts and the main groundmass phases of selected nephelinites. Abundances determined by counting 1000 points.

Lava type:	nephelinite								
Sample:	SA06	SA50	SA51	SAB104	SAB178	SAB193	All Samples (n=13)		
Phenocrysts							Max	Min	Mean
olivine	16.2	6.6	7.8	6.8	6.0	12.0	16.2	6.0	9.4
clinopyroxene	3.6	1.8	0.8	1.4	4.0	4.8	4.8	0.8	2.9
plagioclase	-	-	-	-	-	-	-	-	-
magnetite	1.2	0.2	0.4	-	-	-	1.2	tr	0.4
Total	21.0	8.6	9.0	8.2	10.0	16.8	21.0	8.2	12.6
Vesicles	0.8	1.8	7.6	8.8	3.0	2.4	8.8	0.4	4.0
Groundmass	78.2	89.6	83.4	83.0	87.0	80.8	89.6	76.8	83.3
Groundmass							n = 9		
olivine	tr	4.3	1.1	2.1	1.6	tr	4.3	tr	-
clinopyroxene	40.9	55.7	60.5	55.5	45.8	40.6	60.5	38.9	49.8
plagioclase	17.0	20.4	20.7	19.9	10.7	30.1	30.1	10.0	19.8
magnetite	12.7	19.2	17.7	14.4	10.6	14.1	19.2	10.4	14.8
apatite	-	-	tr	tr	-	-	tr	-	-
glass	29.0	tr	tr	8.1	27.8	14.5	32.7	tr	-

n = number of samples; tr = trace; - = none counted

Table A2.25 General description of the main mineral phases in nephelinites.

	Nephelinites	
	Olivine	**Clinopyroxene**
Megacrysts	Rare > 1.5 mm subhedral or elongate, frequently skeletal in SA06, SA21, SA28, SA46, SA50, SAB105, and SAB193.	
Phenocrysts / microphenocrysts	Phenocrysts and microphenocrysts: Typically euhedral and subhedral 6-sided, often embayed, infrequently skeletal, occasionally in monomineralic clusters. Less commonly as elongate phenocrysts (some as parallel growth crystals (e.g., SAB119).	Purplish-brown and titaniferous. Phenocrysts: Rare - euhedral and subhedral. Microphenocrysts: Typically 6- and 8-sided euhedral and subhedral, often twinned and zoned, often with distinct marginal zones. Prismatic microphenocrysts common, often twinned with distinct sector zones, occasionally in monomineralic clusters (< 600 μm) and in polymineralic clusters 1.25 mm across with olivine phenocrysts.
Textures	Megacrysts and a large number of phenocrysts in most samples have disequilibrium textures; 1. Partially resorbed interiors. 2. Corroded margins, with rims and embayments mantled by relatively thin (<10 μm) assemblages that may include black devitrified glass, granular opaque crystals, and small clinopyroxene grains.	Some of the largest crystals have crystal-melt disequilibrium textures; partially resorbed interiors (e.g., in SA06 and SA50)
Alteration	Rims occasionally slightly altered golden-yellow iddingsite.	
Inclusions	< 50 μm Cr-titanomagnetite or clear inclusions.	< 50 μm titanomagnetite
Comments	Dominant phase in all samples.	

Xenoliths and xenocrysts

Xenoliths were not observed in the nephelinite samples. However, as with the basanites, some olivine megacrysts up to 2.25 mm across exhibit morphologies that suggest an exotic origin. These crystals commonly have partially resorbed interiors or deeply incised rounded embayments, whereas others have kink-band metamorphic textures and severely corroded margins.

Groundmass

The groundmass (76.8 to 89.6 modal %) ranges from very fine-grained to relatively coarse-grained, and may be hyalopilitic, intersertal, or intergranular with poikilitic texture. In contrast to other group B rock types in which plagioclase is typically the dominant groundmass phase, clinopyroxene is the dominant phase in most nephelinites, ranging from 42.1 to 60.5 modal %. Titanomagnetite, olivine, nepheline, and apatite are additional groundmass phases (see Table A2.24). A general description of the major groundmass phases, clinopyroxene, plagioclase, and titanomagnetite, and other features of the groundmass in the nephelinites are given in Table A2.26.

Table A2.26 Summarised groundmass characteristics of the nephelinite samples.

	Nephelinites			
Mineral	**Olivine**	**Clinopyroxene**	**Titanomagnetite**	**Plagioclase/ Nepheline**
Crystal habit	< 100 μm anhedral grains	< 150 μm 6-sided euhedral and subhedral crystals (often with distinct marginal zones), anhedral grains, and laths.	< 100 μm blocky grains	< 200 μm laths, microlites, and interstitial pools. Nepheline: < 75 μm, laths and interstitial pools.
Textures		Partially resorbed interiors in some samples.		
Alteration				
Inclusions		Titanomagnetite grains		< 10 μm apatite
Comments	Absent or rare in most samples.	Dominant phase in most samples. Aggregates of euhedral crystals, laths, and anhedral grains are common.	Abundant in all samples. Skeletal opaques common and often abundant in most samples. Concentrated in interstitial patches of devitrified glass.	Abundant in most samples. Apatite microlites are common but typically occur in trace amounts.
Secondary mineralisation	Patches of reddish-yellow-orange alteration product (possibly smectite) often in hyalopilitic and intersertal samples, e.g., SA28 and SAB178 respectively.			
Crystal clusters	Less common than in basanites. Occur as < 1 mm diameter aggregates of euhedral and subhedral Ti-clinopyroxene grains and laths. Interpreted as locations of completely resorbed quartzose or feldspar xenoliths or xenocrysts.			
Vesicles	Rare in all samples.			

3.5.9 Ne-hawaiites

The ne-hawaiites are typically porphyritic and generally slightly vesicular although samples SA63 and SA65 are moderately vesicular. The ne-hawaiites are predominantly holocrystalline and consist of olivine phenocrysts and microphenocrysts, and microphenocrysts of clinopyroxene (Fig. A2.14). Total phenocryst phases range from 2.4 to 19.0 modal %. Plagioclase is generally restricted to the groundmass (described in Table A2.32). The modal abundance of phenocrysts and groundmass phases of selected samples are presented in Table A2.30. Descriptions of the main mineral phases, olivine and clinopyroxene, are given in Table A2.31.

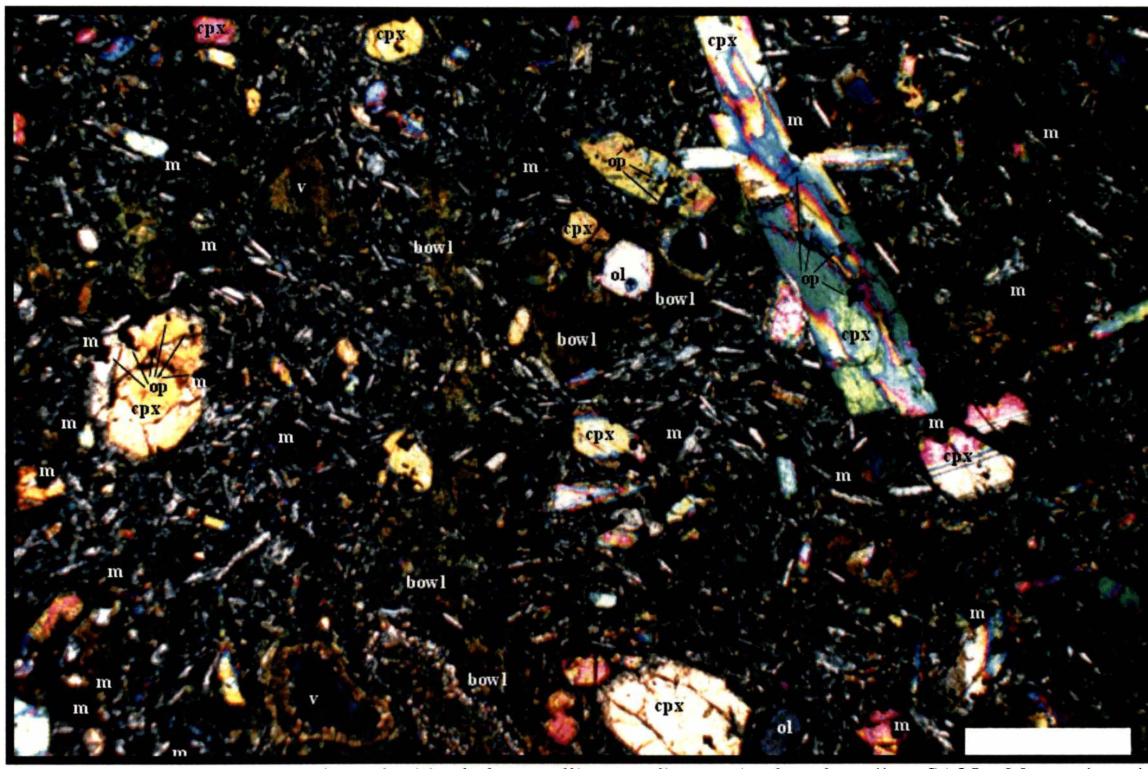

Fig. A2.14 Photomicrograph of porphyritic, holocrystalline, medium-grained ne-hawaiite (SA25). Most prismatic, euhedral, and subhedral titaniferous clinopyroxene (cpx) contain abundant opaque inclusions (probably titanomagnetite and Cr-bearing titanomagnetite; cr). Phenocrysts are set in plagioclase-rich (low birefringent laths and interstitial crystals) groundmass that also includes abundant clinopyroxene laths and euhedral grains (high birefringence). The olivine phenocrysts (ol) are extensively altered to brownish-green bowlingite (bowl). Bowlingite and possibly smectite and chlorite also occur as interstitial patches. The vesicles commonly have walls lined with fibrous, radiating clinopyroxene crystals and are infilled with zeolite. Polarised light; scale bar is 500μm.

Table 3.30 Modal abundances of phenocrysts and the main groundmass phases of selected ne-hawaiites. Abundances determined by counting 1000 points.

Lava type:	ne-hawaiite								
Sample:	SA01	SA22	SA24	SA25	SA63	SA65	All Samples (n=9)		
Phenocrysts							Max	Min	Mean
olivine	7.4	2.4	12.0	4.0	3.2	6.8	12.0	2.4	5.6
clinopyroxene	8.2	-	7.0	10.4	0.6	1.8	10.4	tr	4.2
plagioclase	0.8	-	-	-	-	-	0.8	tr	-
magnetite	0.2	-	-	-	-	-	0.2	tr	-
Total	16.6	2.4	19.0	14.4	3.8	8.6	19.0	2.4	9.9
Vesicles	4.8	tr	1.2	1.2	10.8	11.6	11.6	tr	4.2
Groundmass	78.6	95.2	79.8	84.0	85.4	79.8	95.2	78.6	85.5
Groundmass							n = 8		
olivine	2.1	-	tr	-	2.3	1.3	2.3	-	-
clinopyroxene	30.7	38.0	32.0	27.9	13.6	22.6	38.0	13.6	27.0
plagioclase	54.2	34.7	54.7	50.2	54.9	61.4	61.4	34.7	50.8
magnetite	9.2	22.1	13.3	14.4	23.5	14.5	23.5	6.9	14.9
apatite	tr	tr	tr	tr	tr	tr	tr	tr	tr
glass	3.8	5.2	-	2.5	5.6	tr	22.1	-	-

n = number of samples; tr = trace; - = none counted

Table 3.31 General description of the main mineral phases in ne-hawaiites.

	Ne-hawaiites	
	Olivine	**Clinopyroxene**
Megacrysts	Rare	
Phenocrysts / microphenocrysts	Phenocrysts and microphenocrysts: euhedral and subhedral 6-sided, often skeletal or embayed.	Purplish-brown to brown and titaniferous. Phenocrysts: rare 6- or 8-sided euhedral and subhedral, sector-zoned in SA25. Microphenocrysts: < 750 μm, euhedral and subhedral 6- and 8-sided, often with distinct marginal zones, less common sector zoned prismatic. Occasionally in < 1 mm diameter monomineralic clusters, many crystals with partially resorbed interiors.
Textures	Phenocryst populations in most samples with disequilibrium textures: 1. Partially resorbed interiors and/or corroded margins lined with Ti-clinopyroxene grains. 2. Deeply incised, rounded embayments.	A large number of microphenocrysts in most samples have partially resorbed interiors with numerous opaque and clear inclusions resulting in sieve-textured cores.
Alteration	Unaltered in SA01, SA24, SA29, SA65, SA66. Phenocrysts and microphenocrysts: extensive alteration in SA22 and SA25along rims and fractures to brownish-green bowlingite.	
Inclusions	< 75 μm Cr-titanomagnetite	< 50 μm blocky, opaque inclusions (probably titanomagnetite) are common.
Comments	Dominant phase in most samples.	Dominant phase in SA01, SA25. Occurs only as rare microphenocrysts in SA22, SA62, SA63, SA64, SA65 and SA66.

Xenoliths and xenocrysts

A number of samples contain ultramafic and quartzofeldspathic xenoliths. Sample SA01 contains xenoliths up to 5 mm diameter composed entirely of olivine phenocrysts and microphenocrysts. These xenoliths have corroded margins partially rimmed with

clinopyroxene grains, indicative of disequilibrium conditions. Sample SA02 contains xenoliths up to 7.5 mm across composed of olivine, clinopyroxene, and orthopyroxene. The rounded margins of orthopyroxene phenocrysts, at the exterior of the largest xenolith, are mantled by fresh clinopyroxene overgrowths, indicating reaction with the melt possibly during partial solution at lower pressures (e.g., Tsuchiyama, 1986). Olivine crystals in most xenoliths in the ne-hawaiites often exhibit kink-band metamorphic textures. Sample SA22 contains quartzofeldspathic xenoliths with reaction rims of clinopyroxene.

Groundmass

The groundmass (78.6 to 95.2 modal %) is fine- to medium-grained and either intergranular or intersertal. Plagioclase, Ti-clinopyroxene, and titanomagnetite are abundant with plagioclase the dominant phase in the majority of samples. Olivine, nepheline, and apatite are additional groundmass phases. A general description of the major groundmass phases, clinopyroxene, plagioclase, and titanomagnetite, and other features of the groundmass in the ne-hawaiites are given in Table 3.32.

Table 3.32 Summarised groundmass characteristics of the ne-hawaiites.

	Ne-hawaiites			
Mineral	**Olivine**	**Clinopyroxene**	**Titanomagnetite**	**Plagioclase/ Nepheline**
Crystal habit	< 100 μm anhedral grains.	< 100 μm 6-sided euhedral and subhedral crystals (often with distinct marginal zones), anhedral grains, and laths.	< 5 μm blocky grains in fine-grained samples. < 100 μm blocky grains in course-grained samples.	< 400 μm laths, microlites, and interstitial pools. Nepheline: < 75 μm, laths and interstitial pools.
Textures		Partially resorbed interiors.		
Alteration				
Inclusions		Titanomagnetite grains		< 10 μm apatite
Comments	Absent or rare	Dominant phase Aggregates of euhedral crystals, laths, and anhedral grains often between plagioclase laths and pools.	Abundant Skeletal opaques in SA02 in areas with interstitial patches of devitrified glass.	Abundant Apatite microlites and anhedral grains are common but typically occur in trace amounts.
Secondary mineralisation	1. Veins and amygdales infilled with zeolite. 2. Interstitial patches of chlorite and a dark greenish-brown mineraloid (possibly smectite)			
Crystal clusters	Up to 2.5 mm diameter aggregates of euhedral and subhedral Ti-clinopyroxene grains and laths in SA01, SA25, SA29, SA62, SA65. Interpreted as locations of completely resorbed quartzose or feldspar xenoliths or xenocrysts.			
Vesicles	1. Filled with calcite and carbonates in SA29, SA63, SA64, SA65. 2. Lined with radiating growths of fine-grained chlorite in SA22.			

A2.2.4 Group B alkali ol-basalt

The group B alkali ol-basalts (Fig. A2.15) are porphyritic, predominantly hypocrystalline, and generally slightly vesicular. They are composed of olivine megacrysts and phenocrysts, and olivine, clinopyroxene, and rare titanomagnetite and plagioclase microphenocrysts set in a plagioclase-rich relatively course-grained groundmass. Some samples contain olivine and clinopyroxene megacrysts up to 3 mm, interpreted as having a xenocrystic origin. Plagioclase occurs as rare prismatic microphenocrysts < 900 μm that commonly contain apatite inclusions. The largest plagioclase crystals occur in SA54. Total phenocryst phases range from 7.8 to 18.6 modal %. The modal abundance of phenocrysts and groundmass phases of selected samples are presented in Table A2.33. Descriptions of the main mineral phases, olivine and clinopyroxene, are given in Table A2.34. The groundmass is described in Table A2.35.

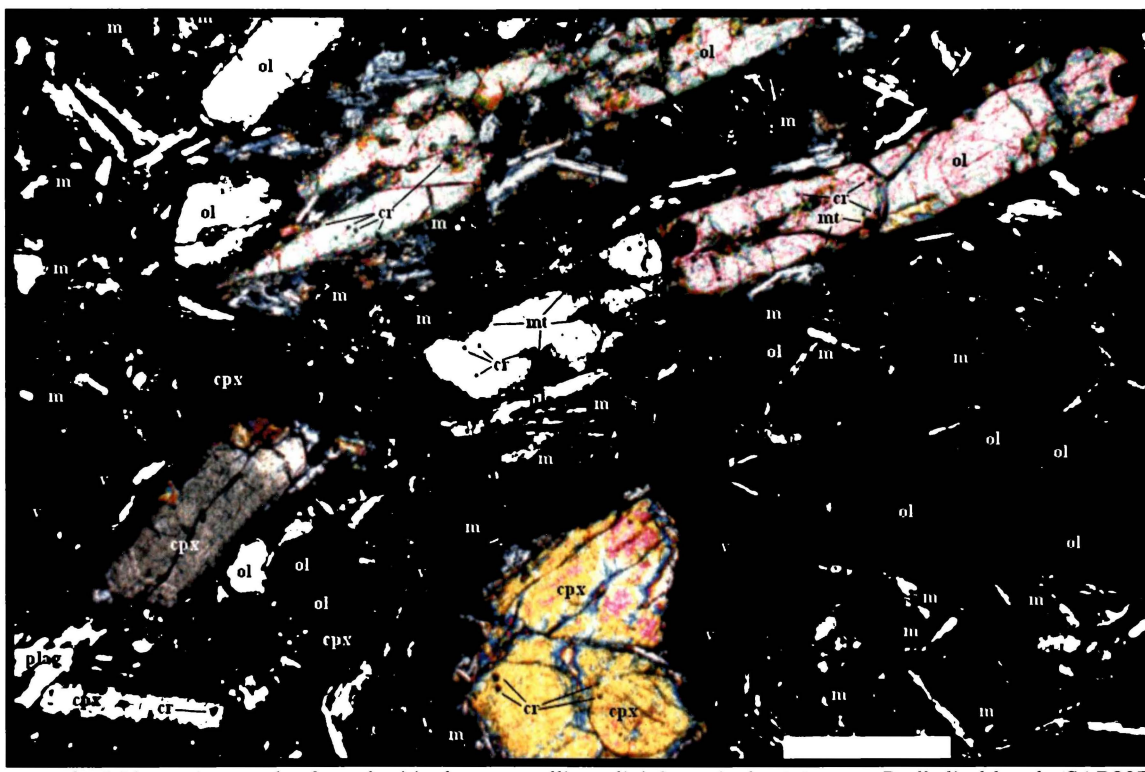

Fig. A2.15 Photomicrograph of porphyritic, hypocrystalline, slightly vesicular (v) group B alkali ol-basalt (SAB207). Euhedral and subhedral olivine (ol), rare, elongate, skeletal olivine parallel growth phenocrysts, and clinopyroxene (cpx) phenocrysts are set in a glassy, intersertal groundmass composed predominantly of plagioclase (low birefringence), titanomagnetite grains (m), and small clinopyroxene crystals (high birefringence). Olivine and clinopyroxene phenocrysts commonly contain Cr-titanomagnetite inclusions (cr). The euhedral clinopyroxene phenocryst at the lower left of the image is compositionally zoned (white bands). Polarised light; scale bar is 500μm.

Table 3.33 Modal abundances of phenocrysts and the main groundmass phases of selected group B alkali ol-basalts. Abundances determined by counting 1000 points.

Lava type:	Group B: alkali ol-basalt						
Sample:	SA54	SAB185	SAB188	SAB207	All Samples (n=4)		
Phenocrysts					Max	Min	Mean
olivine	4.8	6.4	3.4	13.0	13.0	3.4	5.4
clinopyroxene	11.2	1.2	4.0	4.2	11.2	4.0	3.2
plagioclase	2.0	2.0	0.4	0.6	2.0	0.4	4.8
magnetite	0.6	0.4	-	-	0.6	tr	1.2
Total	18.6	10.0	7.8	17.8	18.6	7.8	14.6
Vesicles	4.4	0.2	0.4	6.4	6.4	0.2	3.4
Groundmass	77.0	89.8	91.8	75.8	91.8	75.8	81.9
Groundmass					n = 4		
olivine	7.2	8.4	9.8	6.4	9.8	6.4	7.9
clinopyroxene	23.7	27.8	20.5	34.5	34.5	23.7	26.6
plagioclase	59.3	56.3	55.9	42.1	59.3	42.1	53.4
magnetite	9.9	7.5	14.2	16.5	16.5	7.5	12.0
apatite	tr	tr	tr	tr	tr	-	-
glass	tr	tr	tr	tr	tr	-	-

n = number of samples; tr = trace; - = none counted

Table 3.34 General description of the main mineral phases in group B alkali ol-basalts.

	Alkali ol-basalts	
	Olivine	**Clinopyroxene**
Megacrysts	Up to 3 mm subhedral or elongate.	
Phenocrysts / microphenocrysts	Phenocrysts and microphenocrysts: euhedral and subhedral 6-sided or elongate. Infrequently in clusters (< 5 crystals). Rare parallel growth crystals (e.g., SAB207; Fig. 3.15).	Purplish-brown and titaniferous. Microphenocrysts: euhedral and subhedral 6- and 8-sided, many with distinct marginal zones. Rare oscillatory zoning. Less common sector zoned prismatic crystals, generally restricted to SA54. Occasional < 1.5 mm monomineralic clusters. Less frequent with olivine in < 1.5 mm polimineralic clusters. Most clusters in SA54.
Textures	Megacrysts and phenocryst populations with disequilibrium textures: 1. Reaction rims of pyroxene. 2. Incised margins that are rounded or corroded.	Many crystals in SA54 have partially resorbed interiors with abundant opaque and clear inclusions and groundmass-filled cavities resulting in sieve-textured cores surrounded by clinopyroxene.
Alteration	Common along rims and fractures in most samples. Reddish-orange iddingsite (e.g., SAB207) Dark greenish-brown bowlingite (e.g., SAB185, SAB188).	
Inclusions	< 5 μm Cr-titanomagnetite	< 10 μm titanomagnetite often abundant, some Cr-bearing.
Comments	Dominant phase in most samples.	SA54 has a bimodal population of sieve-textured and unaltered clinopyroxene crystals, indicative of disequilibrium phenocryst assemblages.

Xenoliths and xenocrysts

A number of subhedral to elongate olivine xenocrysts, ranging from 500μm to > 3 mm occur in SAB185 and SAB188[2]. Each crystal has corroded margins rimmed with dark greenish-brown bowlingite, and exhibit kink-band metamorphic textures.

Samples SAB185 and SAB188 also contain pyroxene xenocrysts. SAB185 contains a well-rounded, 1.25mm xenocryst with concentric reaction rims. The interior rim (up to 100 μm) consists of a continuous sheath of aggregated prismatic clinopyroxene microphenocrysts oriented parallel to one another and perpendicular to the xenocryst's margin. The outer rim (up to 200 μm) is composed of small olivine crystals and titanomagnetite grains. Many olivines contain < 0.75 μm opaque inclusions (possibly Cr-titanomagnetite or Cr-spinel).

Sample SAB188 contains a subhedral, pale brown, 3 mm pyroxene xenocryst that has irregular margins mantled with < 100 μm plagioclase laths, a partially resorbed interior that exhibits a felty texture, and contains rare, small olivine crystals and opaque grains.

Groundmass

The groundmass (75.8 to 91.8 modal %) is generally coarse-grained and intersertal. Plagioclase and Ti-clinopyroxene are abundant with plagioclase the dominant phase in all samples. Olivine, nepheline, and apatite are additional groundmass phases (see Table 3.33). A general description of the major groundmass phases, clinopyroxene, plagioclase, and titanomagnetite, and other features of the groundmass in the group B alkali ol-basalt samples are given in Table 3.35.

[2] SAB185 and SAB188 are accidental clasts collected from the Raventhorpe tuff ring.

Table 3.35 Summarised groundmass characteristics of the group B alkali ol-basalts.

	Group B alkali ol-basalt			
Mineral	**Olivine**	**Clinopyroxene**	**Titanomagnetite**	**Plagioclase/ Nepheline**
Crystal habit	< 100 μm anhedral grains.	< 100 μm frequent 6-sided euhedral and subhedral crystals (often with distinct marginal zones), anhedral grains, and laths.	< 100 μm blocky grains. Irregular shaped crystals that partially enclose plagioclase laths and clinopyroxene grains (e.g., SA54 and SAB185).	Plagioclase: < 500 μm laths, microlites, and interstitial pools. Nepheline: < 75 μm, laths and interstitial pools (e.g., SA54 and SAB185).
Textures		Partially resorbed interiors common in SA54.		Trachytic (SAB185).
Alteration				
Inclusions		Blocky titanomagnetite grains.		< 10 μm apatite
Comments		Occurs in aggregates with titanomagnetite and olivine grains between plagioclase laths.		Dominant phase in most samples. Needle-like apatite crystals are common but typically occur in trace amounts.
Secondary mineralisation	1. Interstitial light brown devitrified glass. 2. Interstitial patches and veins of dark greenish-brown bowlingite (possibly smectite) in SA54 and SAB188. 3. Interstitial bright green patches (possibly chlorite) in SA54.			
Crystal clusters	Up to 1 mm diameter aggregates of euhedral and subhedral Ti-clinopyroxene grains and laths in SA54 and SAB185. Interpreted as locations of completely resorbed quartzose xenoliths.			
Vesicles	Some partially filled with dark greenish-brown bowlingite (possibly smectite) in SA54 and SAB188.			

A2.2.5 Mugearite

The only mugearite sample, SA88 (Fig. 3.16), was collected from a segregation vein in a hawaiite lava flow. It is porphyritic, holocrystalline, coarse-grained, and vesicular with gabbroic texture. Descriptions of the main mineral phases, olivine (18.0 modal %), clinopyroxene (4.0 modal %), and plagioclase (3.0 modal %) are given in Table 3.36. The coarse-grained groundmass is dominated by prismatic plagioclase (73.6 modal %) and anhedral, pale brown clinopyroxene (13.8 modal %). Aegerine-augite (2.2 modal %), granular titanomagnetite (2.6 modal %), prismatic ilmenite (4.6 modal %), and long needle-like apatite crystals (trace amounts) are additional groundmass phases.

Fig.A2.16. Photomicrograph of porphyritic, hypocrystalline, vesicular (v) mugearite (SA88). Phenocrysts of olivine (ol), clinopyroxene (cpx), and plagioclase (plag) are set in a coarse-grained groundmass composed of abundant plagioclase crystals (low birefringence), clinopyroxene, and titanomagnetite (m). The rims and interiors of the olivine are heavily altered to dark reddish-orange iddingsite (idd). Polarised light; scale bar is 500μm.

Table A2.36 General description of the main mineral phases in mugearite SA88.

	Mugearite		
Mineral	**Olivine**	**Clinopyroxene**	**Plagioclase**
Megacrysts	Up to 2.25 mm		Rare prismatic up to 2 mm.
Phenocrysts / microphenocrysts	Phenocrysts and microphenocrysts; subhedral and anhedral	Phenocrysts and microphenocrysts; pale brown, subhedral and anhedral. Rare bright green aegerine-augite.	Phenocrysts and microphenocrysts; prismatic and irregular-shaped crystals.
Textures	Skeletal megacrysts		
Alteration	Phenocryst rims; dark red-orange iddingsite. Microphenocrysts interiors; dark red-orange iddingsite.	Some crystals with green aegerine-augite rims.	< 5 μm apatite <1.25 reddish-brown (undetermined)
Inclusions	< 10 μm opaque (possibly Cr-titanomagnetite) in many crystals.		
Comments	Dominant phenocryst phase.	Occasionally in monomineralic clusters of polymineralic clusters with olivine and plagioclase.	

Appendix Three: Modal Mineralogy

Appendix 3

Modal percentage of phenocryst phases and groundmass proportions for point-counted representative samples.

The modal percentage of phenocryst phases and groundmass proportions were determined by counting one thousand points per thin section. Modal analyses results for selected SAVF samples from groups A and B are given in Tables A3.1 and A3.2 respectively. Each table is organised according to rock type. Note that the term "phenocryst" includes megacrysts, phenocrysts, and microphenocrysts. Each term is defined in Chapter 3, section 3.4.

Abbreviations used in tables:

ol	olivine
cpx	clinopyroxene
plag	plagioclase feldspar
mag	magnetite
ilm	ilmenite
gnd	groundmass

Table A3.1 Modal percent phenocryst phases and groundmass proportions for selected SAVF group A rocks.

	alkali ol-basalt								hawaiite															
Sample	SA17	SA18	SA19	SA33	SA94	SAB159	SAB162	SAB168	SA11	SA14	SA20	SA30	SA32	SA44	SA47	SA52	SA69	SA70	SA74	SA78	SA85	SA87	SA90	SA92	SAB133
Mineral																									
ol	13.0	7.4	6.2	14.8	3.8	4.2	0.8	7.0	6.8	9.4	7.8	11.6	16.0	12.4	7.6	6.4	17.2	14.4	11.8	6.8	12.0	12.8	5.0	10.2	11.6
cpx	2.8	5.4	3.8	7.8	0.8	2.6	0.4	1.2	0.6	0.2	8.2	4.6	10.0	0.4	2.4	2.6	2.4	6.6	2.6	6.0	6.0	8.6	4.2	4.2	1.2
plag	2.8	3.6	5.6	0.8	2.4	7.2	12.4	11.6	2.4	3.4	11.6	1.0	21.0	1.2	2.8	5.6	2.2	6.2	7.4	7.8	8.8	7.6	3.8	4.2	1.0
mag	2.6	-	1.2	1.0	0.4	3.2	4.0	0.8	-	1.6	0.6	2.2	-	1.6	3.0	2.2	-	0.6	-	1.0	1.2	0.8	-	1.2	-
ilm	-	-	-	-	-	-	-	-	-	-	-	1.0	-	-	0.2	0.4	-	1.0	-	0.2	0.4	1.0	-	-	-
total	21.2	16.4	16.8	24.4	7.4	17.2	17.6	20.6	9.8	14.6	28.2	20.4	47.0	15.6	16.0	17.2	21.8	28.8	21.8	21.8	28.4	30.8	13.0	19.8	13.8
gnd	71.4	80.8	74.6	54.2	86.0	81.0	78.0	76.0	81.8	79.6	63.8	77.8	52.2	74.0	80.0	76.0	76.8	65.2	76.2	68.6	62.2	57.8	62.2	66.8	78.2
vesicles	7.4	2.8	8.6	21.0	6.6	1.8	4.0	3.4	8.4	5.8	8.0	1.8	0.8	10.4	4.0	6.8	1.4	6.2	2.0	9.8	9.4	11.4	24.8	13.4	8.0

Table A3.1 continued.

	hawaiite												ol-tholeiitic basalt											
Sample	SAB134	SAB138	SAB140	SAB142	SAB147	SAB151	SAB163	SAB166	SAB167	SAB189	SAB203	SAB208	SA15	SA16	SA34	SA35	SA36	SA43	SA53	SA59	SA67	SA68	SA73	SA79	SA80
Mineral																									
ol	9.8	9.4	1.6	3.4	13.2	7.6	2.4	4.2	3.8	7.4	7.8	4.0	4.8	8.2	7.8	7.8	11.6	7.8	9.4	5.8	7.8	7.8	3.4	15.4	10.6
cpx	2.4	3.0	2.4	8.2	1.2	4.6	2.0	3.6	0.4	1.8	3.8	1.8	0.6	2.6	-	3.0	0.8	8.0	4.8	7.2	3.0	5.8	6.8	6.4	2.8
plag	0.8	0.6	2.6	2.4	0.6	1.0	8.0	6.6	2.4	1.4	0.2	1.2	6.4	4.8	2.2	4.2	0.4	2.0	-	0.6	0.2	3.6	2.0	6.4	5.4
mag	-	-	0.2	0.6	0.4	0.8	6.6	3.2	-	0.8	-	0.4	-	-	-	0.6	-	0.4	-	-	-	-	0.6	-	-
ilm	-	-	-	-	-	-	-	-	-	-	-	-	-	-	-	-	-	-	-	-	-	-	-	-	-
total	13.0	13.0	6.8	14.6	15.4	14.0	19.0	17.6	6.6	11.4	11.8	7.4	11.8	15.6	10.0	15.6	12.8	18.2	14.2	13.6	11.0	17.2	12.8	28.2	18.8
gnd	84.6	84.6	91.4	81.0	73.8	78.2	75.4	73.6	89.6	78.0	81.0	92.6	69.8	71.8	82.6	78.4	69.4	74.0	75.4	85.2	84.2	78.0	87.2	71.8	74.0
vesicles	2.4	2.4	1.8	4.4	10.8	7.8	4.2	8.8	3.8	10.6	7.2	nil	18.4	12.6	7.4	6.0	17.8	7.8	10.4	1.2	4.8	4.8	nil	nil	7.2

Table A3.1 continued.

	ol-tholeiitic basalt																			
Sample	SA81	SA89	SA91	SA93	SAB144	SAB149	SAB152	SAB169	SAB170	SAB171	SAB172	SAB173	SAB174	SAB181	SAB184	SAB187	SAB190	SAB191	SAB201	SAB202	SAB205
Mineral																					
ol	10.0	10.8	9.4	0.2	10.4	9.0	6.8	6.2	9.0	8.8	5.8	7.4	7.2	16.6	10.2	15.6	8.4	13.4	10.6	10.8	8.2
cpx	6.0	4.0	3.0	7.6	3.6	2.2	5.2	3.6	-	-	-	0.2	0.0	2.2	2.0	2.2	1.2	1.2	4.4	3.0	6.0
plag	1.2	1.0	6.4	20.8	2.6	2.0	3.2	9.2	0.2	0.6	-	1.0	0.2	3.0	1.8	4.2	2.6	2.0	0.2	0.2	-
mag	-	-	-	1.6	2.6	1.6	1.4	-	-	-	-	0.2	-	1.6	-	0.8	-	1.6	1.6	0.4	1.0
ilm	-	-	-	1.2	2.2	0.6	1.0	-	-	-	-	-	-	0.6	0.2	0.8	-	1.0	-	-	0.2
total	17.2	15.8	18.8	31.4	21.4	15.4	17.6	19.0	9.2	9.4	5.8	8.8	7.4	24.0	14.2	23.6	12.2	19.2	16.8	14.4	15.4
gnd	78.0	80.2	81.0	52.8	72.2	79.4	72.4	73.8	78.0	74.0	74.0	74.8	81.8	70.2	76.0	59.2	82.0	75.0	82.4	65.8	84.4
vesicles	4.8	7.6	0.2	15.8	6.4	5.2	10.0	7.2	12.8	16.6	20.2	16.4	10.8	5.8	9.8	17.2	5.8	5.8	0.8	19.8	0.2

Table A3.1 continued.

	qz-tholeiitic basalt				transitional basalt													
Sample	SA31	SA76	SA77	SAB198	SA07	SA08	SA09	SA10	SA13	SA48	SA49	SA72	SA83	SA84	SAB145	SAB150	SAB161	SAB210
Mineral																		
ol	5.2	14.8	6.8	-	12.2	9.8	7.0	7.8	12.0	4.2	6.2	8.6	14.8	9.8	4.8	5.0	2.0	13.4
cpx	3.4	0.8	3.0	2.8	0.6	0.8	1.2	-	0.6	1.4	2.0	0.8	0.2	-	2.2	-	1.2	0.8
plag	1.0	2.0	1.2	0.4	-	-	-	0.4	2.8	7.8	3.2	-	1.4	2.4	6.4	3.0	10.8	1.4
mag	-	-	-	0.4	-	-	-	-	-	0.2	0.2	-	0.6	-	1.4	-	5.0	0.4
ilm	0.4	-	-	-	-	-	-	-	-	-	-	-	-	-	0.2	-	-	-
total	10.0	17.6	11.0	3.6	12.8	10.6	8.2	8.2	15.4	13.6	11.6	9.4	17.0	12.2	15.0	8.0	19.0	16.0
gnd	85.4	79.2	83.4	81.4	70.4	82.6	70.8	74.0	67.2	85.6	83.6	79.6	77.6	77.4	83.2	89.2	77.6	83.0
vesicles	4.6	3.2	4.6	15.0	16.8	6.8	21.0	17.8	17.4	0.8	4.8	11.0	5.4	10.4	1.8	2.8	3.8	1.0

Table A3.2 Modal percent phenocryst phases and groundmass proportions for selected SAVF group B rocks.

	alkali ol-basalt				basanite																		
Sample	SA54	SAB185	SAB188	SAB207	SA03	SA05	SA12	SA23	SA26	SA27	SA37	SA38	SA40	SA41	SA42	SA45	SA55	SA56	SA57	SA58	SA60	SA61	SA75	SA82	SA86
Mineral																									
ol	4.8	6.4	3.4	13.0	8.0	15.2	10.6	14.4	8.2	5.2	9.6	12.4	16.8	14.0	13.6	15.2	15.4	11.0	12.6	12.6	15.8	10.2	7.0	8.2	11.6
cpx	11.2	1.2	4.0	4.2	11.0	2.8	12.6	6.2	11.4	6.0	9.8	5.6	12.0	17.0	20.2	7.8	10.4	10.0	8.4	5.4	5.2	12.4	2.8	2.0	13.2
plag	2.0	2.0	0.4	0.6	-	-	-	-	0.2	-	0.4	-	-	-	0.4	-	0.4	-	-	-	-	-	-	-	-
mag	0.6	0.4	-	-	0.4	0.6	-	-	-	-	-	-	-	0.6	-	1.8	-	0.2	0.4	-	-	-	0.6	-	-
ilm	-	-	-	-	-	-	-	-	-	-	-	-	-	-	-	-	-	-	-	-	-	-	-	-	-
total	18.6	10.0	7.8	17.8	19.4	18.6	23.2	20.6	19.8	11.2	19.8	18.0	28.8	31.6	34.2	24.8	26.2	21.2	21.4	18.0	21.0	22.6	10.4	10.2	24.8
gnd	77.0	89.8	91.8	75.8	77.6	78.8	69.6	76.8	78.4	82.4	66.2	78.6	68.2	66.4	57.0	73.6	68.2	78.8	76.8	88.4	66.6	72.0	89.2	87.2	73.2
vesicles	4.4	0.2	0.4	6.4	3.0	2.6	7.2	2.6	1.8	6.4	14.0	3.4	3.0	2.0	8.2	1.6	5.6	nil	1.8	1.6	12.4	5.4	0.4	2.6	2.0

Table A3.2 continued.

	basanite												
Sample	SAB102	SAB107	SAB111	SAB116	SAB128	SAB129	SAB132	SAB176	SAB179	SAB180	SAB194	SAB196	SAB204
Mineral													
ol	12.0	12.8	15.0	18.8	15.6	13.8	10.4	21.2	18.4	14.0	10.4	14.6	15.6
cpx	3.0	2.6	2.0	9.6	4.0	9.8	8.0	7.0	14.8	11.4	2.8	7.6	6.4
plag	-	-	-	0.6	-	-	-	-	-	-	-	-	-
mag	2.0	1.4	0.2	1.0	1.0	1.4	0.4	-	0.2	0.2	-	0.2	-
ilm	-	-	-	-	-	-	-	-	-	-	-	-	-
total	17.0	16.8	17.2	30.0	20.6	25.0	18.8	28.2	33.4	25.6	13.2	22.4	22.0
gnd	78.0	81.4	75.0	68.8	79.2	73.4	79.8	67.6	61.8	69.6	83.8	74.2	61.4
vesicles	5.0	1.8	7.8	1.2	0.2	1.6	1.2	4.2	4.8	4.8	3.0	3.4	16.6

Table A3.2 continued.

	nephelinite													ne-hawaiite								
Sample	SA06	SA21	SA28	SA46	SA50	SA51	SAB104	SAB105	SAB113	SAB119	SAB127	SAB178	SAB193	SA01	SA02	SA22	SA24	SA25	SA62	SA63	SA65	SA66
Mineral																						
ol	16.2	13.0	9.6	7.8	6.6	7.8	6.8	8.4	10.2	9.4	8.4	6.0	12.0	7.4	5.0	2.4	12.0	4.0	3.6	3.2	6.8	6.0
cpx	3.6	4.2	4.6	2.2	1.8	0.8	1.4	1.2	4.2	1.6	2.8	4.0	4.8	8.2	6.6	0.0	7.0	10.4	1.8	0.6	1.8	1.6
plag	-	-	-	-	-	-	-	-	-	-	-	-	-	0.8	-	-	-	-	-	-	-	-
mag	1.2	0.8	0.6	0.4	0.2	0.4	-	-	0.6	-	0.6	-	-	0.2	-	-	-	-	-	-	-	-
ilm	-	-	-	-	-	-	-	-	-	-	-	-	-	-	-	-	-	-	-	-	-	-
total	21.0	18.0	14.8	10.4	8.6	9.0	8.2	9.6	15.0	11.0	11.8	10.0	16.8	16.6	11.6	2.4	19.0	14.4	5.4	3.8	8.6	7.6
gnd	78.2	80.4	76.8	88.0	89.6	83.4	83.0	85.2	78.6	87.8	83.8	87.0	80.8	78.6	85.0	95.2	79.8	84.0	92.6	85.4	79.8	89.4
vesicles	0.8	1.6	8.4	1.6	1.8	7.6	8.8	5.2	6.4	0.4	4.4	3.0	2.4	4.8	3.4	0.0	1.2	1.2	2.0	10.8	11.6	3.0

Appendix Four:
CIPW Normative Compositions

Appendix 4

CIPW normative compositions

The CIPW normative mineral compositions for selected SAVF samples from groups A and B are given in Tables A4.1 and A4.2 respectively. Each table is organised according to rock type. Norm calculations for the minerals; quartz (Q), orthoclase (Or), albite (Ab), anorthite (An), nepheline (Ne), luecite (Lc), diposide (Di), hypersthene (Hy), olivine (Ol), magnetite (Mt), ilmenite (Il), and apatite (Ap), and the differentiation index (D.I.) were determined by Minpet PowerNorm software (version 2.02) using volatile-free whole-rock analyses normalised to total 100%, and an adjusted $Fe_2O_3/FeO = 0.20$ (Middlemost, 1989).

Table A4.1 CIPW normative compositions for selected group A samples from the South Auckland volcanic field.

Rock type	alkali ol-basalt								hawaiite													
Sample #	SA17	SA18	SA19	SA33	SA94	SAB159	SAB162	SAB168	SA11	SA14	SA20	SA30	SA32	SA44	SA47	SA52	SA69	SA70	SA74	SA78	SA85	SA87
Q	-	-	-	-	-	-	-	-	-	-	-	-	-	-	-	-	-	-	-	-	-	-
Or	4.33	5.42	4.87	4.39	4.23	6.10	6.44	6.03	4.37	2.43	4.55	5.43	3.50	3.64	4.60	5.01	4.97	4.68	4.01	4.83	3.28	4.71
Ab	20.62	24.81	26.85	23.58	28.04	26.91	29.23	26.98	28.45	24.98	27.61	25.33	24.13	25.68	24.22	27.26	26.53	24.72	26.57	26.58	25.22	25.65
An	21.22	20.82	24.96	20.81	25.21	24.88	26.50	25.59	25.98	24.66	24.46	23.88	21.61	23.19	22.34	25.48	22.27	24.10	24.98	21.26	23.64	23.28
Ne	3.23	1.82	0.27	1.10	0.17	1.39	0.18	0.63	-	-	-	-	-	-	-	-	-	-	-	-	-	-
Lc	-	-	-	-	-	-	-	-	-	-	-	-	-	-	-	-	-	-	-	-	-	-
$100\frac{An}{An+Ab}$	50.72	45.63	48.18	46.88	47.34	48.04	47.55	48.68	47.73	49.68	46.98	48.53	47.25	47.45	47.98	48.31	45.64	49.37	48.46	44.44	48.38	47.58
Di	19.38	18.91	18.83	19.31	19.07	16.21	16.51	16.38	16.22	16.98	16.67	14.15	16.34	17.56	15.43	17.80	16.04	15.00	14.05	18.83	18.12	17.06
Hy	-	-	-	-	-	-	-	-	1.57	9.36	7.96	6.26	8.71	1.67	5.51	0.10	7.46	8.46	9.12	5.28	7.06	2.50
Ol	22.86	19.67	15.47	22.94	14.79	14.75	11.55	14.70	14.70	15.09	10.95	16.55	18.20	20.73	20.00	15.39	14.50	14.07	13.47	15.55	15.40	18.58
Mt	3.31	3.07	2.96	3.08	3.01	3.06	2.56	2.98	3.05	2.95	2.99	3.33	3.19	3.10	3.18	3.07	3.07	3.86	3.08	2.89	3.07	3.04
Il	4.28	4.38	5.00	4.06	4.61	5.63	5.92	5.64	4.76	3.14	4.17	4.24	3.72	3.84	4.04	5.06	4.45	4.39	4.15	4.14	3.64	4.46
Ap	0.77	1.10	0.79	0.72	0.88	1.06	1.12	1.08	0.90	0.42	0.64	0.85	0.60	0.60	0.69	0.84	0.71	0.73	0.57	0.64	0.57	0.73
D.I.	28.18	32.05	31.99	29.07	32.44	34.41	35.84	33.64	32.82	27.41	32.16	30.75	27.63	29.33	28.82	32.27	31.51	29.40	30.58	31.41	28.50	30.36

Table A4.1 continued.

Rock type	hawaiite															ol-tholeiitic basalt					
Sample #	SA90	SA92	SAB133	SAB134	SAB138	SAB140	SAB142	SAB147	SAB151	SAB163	SAB166	SAB167	SAB189	SAB203	SAB208	SA15	SA16	SA34	SA35	SA36	SA43
Q	-	-	-	-	-	-	-	-	-	-	-	-	-	-	-	-	-	-	-	-	-
Or	4.53	4.98	3.69	4.04	2.98	5.02	5.12	3.57	3.46	6.07	5.98	5.80	3.51	3.87	4.77	3.04	2.51	3.12	2.22	2.93	4.33
Ab	27.18	26.16	24.10	26.00	24.01	27.05	27.22	25.68	25.16	27.82	27.16	26.91	25.23	26.36	26.74	25.94	25.14	23.58	24.23	23.45	26.00
An	23.78	23.33	23.10	22.74	23.99	25.71	25.24	24.63	24.39	26.16	26.42	26.22	25.07	23.02	23.91	24.68	24.74	25.00	26.90	25.25	23.87
Ne	-	-	-	-	-	-	-	-	-	-	-	-	-	-	-	-	-	-	-	-	-
Lc	-	-	-	-	-	-	-	-	-	-	-	-	-	-	-	-	-	-	-	-	-
$100\frac{An}{An+Ab}$	46.66	47.14	48.94	46.66	49.98	48.73	48.11	48.96	49.22	48.46	49.31	49.35	49.84	46.62	47.21	48.76	49.60	51.46	52.61	51.85	47.86
Di	16.93	17.17	15.67	16.79	17.01	17.82	17.99	17.29	17.50	15.70	15.76	15.87	16.27	17.79	17.38	18.88	18.37	15.75	14.14	15.67	15.62
Hy	8.63	5.08	9.55	6.93	8.57	0.73	1.12	5.39	4.19	0.06	0.80	1.31	6.75	4.07	7.21	17.18	15.45	21.60	15.17	20.49	14.80
Ol	11.09	14.94	16.04	15.72	15.98	14.71	14.22	15.52	17.55	14.37	14.14	14.08	15.35	17.09	12.22	2.93	6.77	4.45	10.17	5.59	8.60
Mt	2.89	3.08	3.42	3.10	3.04	3.03	3.05	3.09	3.03	2.98	3.00	3.12	3.09	3.12	2.86	2.92	2.92	2.90	3.00	2.88	2.69
Il	4.29	4.51	3.77	3.95	3.85	5.08	5.14	4.19	4.12	5.74	5.68	5.63	4.12	3.82	4.17	3.90	3.64	3.18	3.64	3.12	3.50
Ap	0.68	0.75	0.66	0.72	0.57	0.86	0.90	0.64	0.62	1.10	1.06	1.06	0.61	0.86	0.75	0.55	0.46	0.42	0.53	0.62	0.59
D.I.	31.71	31.15	27.79	30.04	26.99	32.06	32.34	29.25	28.62	33.90	33.13	32.71	28.73	30.23	31.50	28.97	27.65	26.70	26.45	26.38	30.33

Table A4.1 continued.

Rock type	ol-tholeiitic basalt																					
Sample #	SA53	SA59	SA67	SA68	SA71	SA73	SA79	SA80	SA81	SA89	SA91	SA93	SAB144	SAB149	SAB152	SAB169	SAB170	SAB171	SAB172	SAB173	SAB174	SAB177-2
Q	-	-	-	-	-	-	-	-	-	-	-	-	-	-	-	-	-	-	-	-	-	-
Or	5.37	3.25	4.39	4.23	3.69	3.41	3.65	4.88	4.40	3.28	2.71	4.78	3.52	3.34	3.63	4.46	3.10	2.79	2.55	2.38	2.20	1.89
Ab	28.31	25.10	24.16	24.18	23.11	23.84	25.46	26.09	24.38	24.14	24.81	22.70	24.10	22.83	23.02	26.74	23.34	23.02	23.14	23.20	23.32	24.00
An	20.58	25.28	22.28	21.55	29.84	26.17	22.39	21.98	31.49	24.78	24.93	23.81	25.79	25.40	25.36	26.43	25.24	25.67	26.22	25.80	26.18	26.33
Ne	-	-	-	-	-	-	-	-	-	-	-	-	-	-	-	-	-	-	-	-	-	-
Lc	-	-	-	-	-	-	-	-	-	-	-	-	-	-	-	-	-	-	-	-	-	-
$100\frac{An}{An+Ab}$	42.09	50.18	47.98	47.12	56.36	52.33	46.79	45.72	56.36	50.65	50.12	51.19	51.69	52.66	52.42	49.71	51.96	52.72	53.12	52.65	52.89	52.31
Di	8.24	14.08	21.09	17.28	12.18	15.87	16.84	17.14	8.24	16.20	15.94	14.23	14.30	15.04	14.32	17.61	15.32	15.12	15.03	14.94	14.86	15.67
Hy	15.19	18.23	18.72	14.94	18.45	10.04	13.59	10.86	12.57	14.37	18.14	12.13	11.50	11.33	10.65	10.79	21.17	20.96	21.59	20.62	20.93	19.43
Ol	14.04	6.96	2.02	10.53	6.18	12.69	10.81	11.77	12.29	10.39	6.39	13.95	12.93	14.29	15.30	6.35	5.16	5.76	4.74	6.49	5.97	6.02
Mt	3.18	2.88	2.67	2.92	2.64	3.08	2.87	2.71	2.67	3.22	2.85	3.17	3.02	3.08	3.02	2.52	2.81	2.87	2.89	2.93	2.86	2.96
Il	4.30	3.58	4.10	3.83	3.44	4.19	3.82	3.95	3.38	3.18	3.66	4.47	4.23	4.08	4.11	4.31	3.20	3.15	3.35	3.19	3.19	3.21
Ap	0.80	0.64	0.58	0.55	0.48	0.72	0.57	0.61	0.59	0.45	0.56	0.75	0.62	0.62	0.61	0.79	0.66	0.66	0.48	0.46	0.48	0.50
D.I.	33.68	28.35	28.55	28.41	26.79	27.25	29.11	30.97	28.78	27.42	27.53	27.49	27.61	26.17	26.64	31.20	26.44	25.82	25.69	25.58	25.52	25.89

Table A4.1 continued.

Rock type	ol-tholeiitic basalt										qz-tholeiitic basalt			
Sample #	SAB177-3	SAB178-2	SAB181	SAB184	SAB187	SAB190	SAB191	SAB201	SAB202	SAB205	SA31	SA76	SA77	SAB198
Q	-	-	-	-	-	-	-	-	-	-	0.66	1.27	0.16	1.85
Or	2.66	2.31	3.92	3.88	3.63	3.04	3.45	4.00	4.25	3.83	4.30	3.26	4.02	4.76
Ab	23.66	23.92	22.67	23.01	22.39	24.45	23.89	23.37	24.39	22.82	23.99	23.35	24.61	32.34
An	25.47	25.51	22.24	22.87	22.40	25.18	25.79	23.81	25.28	24.18	22.84	22.55	22.32	28.95
Ne	-	-	-	-	-	-	-	-	-	-	-	-	-	-
Lc	-	-	-	-	-	-	-	-	-	-	-	-	-	-
$100\frac{An}{An+Ab}$	51.84	51.61	49.52	49.85	50.01	50.74	51.91	50.47	50.90	51.45	48.77	49.13	47.56	47.23
Di	15.56	15.34	16.63	16.80	16.38	15.64	14.10	14.64	11.22	14.43	16.79	19.21	18.37	20.29
Hy	19.07	18.82	17.57	15.86	16.18	11.03	12.12	10.97	18.66	12.90	24.16	23.38	23.24	4.79
Ol	6.92	7.42	9.43	10.10	11.82	13.04	12.83	15.54	8.08	14.27	0.00	0.00	0.00	0.00
Mt	2.91	2.94	2.93	2.94	2.91	3.13	3.09	3.18	3.26	3.12	2.67	2.78	2.71	1.52
Il	3.12	3.14	3.89	3.74	3.66	3.91	4.11	3.78	4.02	3.71	4.01	3.72	3.97	4.73
Ap	0.63	0.61	0.72	0.81	0.64	0.59	0.61	0.73	0.84	0.73	0.60	0.49	0.60	0.77
D.I.	26.32	26.22	26.59	26.88	26.02	27.49	27.34	27.37	28.64	26.65	28.95	27.88	28.79	38.95

Table A4.1 continued.

Rock type	transitional basalts														
Sample #	SA07	SA08	SA09	SA10	SA13	SA39	SA48	SA49	SA72	SA83	SA84	SAB145	SAB150	SAB161	SAB210
Q	-	-	-	-	-	-	-	-	-	-	-	-	-	-	-
Or	1.63	3.12	1.56	1.38	2.32	3.02	5.86	3.09	3.17	2.40	2.21	3.46	3.28	5.68	5.02
Ab	22.98	24.36	23.60	23.06	24.41	25.28	26.14	23.32	23.93	25.00	24.17	25.01	23.75	24.68	25.10
An	28.99	25.24	27.35	27.19	25.22	25.51	26.22	24.66	24.39	26.05	25.13	25.21	24.91	27.52	26.21
Ne	-	-	-	-	-	-	-	-	-	-	-	-	-	-	-
Lc	-	-	-	-	-	-	-	-	-	-	-	-	-	-	-
$100\frac{An}{An+Ab}$	55.78	50.89	53.68	54.11	50.82	50.23	50.08	51.40	50.48	51.03	50.97	50.20	51.19	52.72	51.08
Di	16.60	18.30	18.18	16.87	16.64	14.38	14.32	15.24	15.64	16.02	17.45	15.55	15.15	12.75	15.85
Hy	2.45	4.04	4.52	6.49	9.20	7.35	3.46	9.31	7.26	5.85	6.97	7.51	9.80	7.27	7.78
Ol	19.53	17.34	17.45	17.59	15.64	16.82	14.18	16.68	18.61	17.75	17.09	15.31	15.34	12.27	11.10
Mt	3.25	3.09	3.07	3.13	2.87	3.17	3.21	3.21	3.08	3.20	3.22	3.13	3.07	3.16	3.00
Il	4.24	3.93	3.75	3.84	3.23	3.84	5.61	3.96	3.44	3.31	3.36	4.18	4.10	5.61	5.09
Ap	0.33	0.58	0.53	0.44	0.46	0.65	1.00	0.54	0.49	0.42	0.40	0.62	0.62	1.06	0.86
D.I.	24.61	27.49	25.16	24.44	26.73	28.30	32.00	26.41	27.11	27.40	26.38	28.47	27.03	30.36	30.11

Table A4.2 CIPW normative compositions for selected group B samples from the South Auckland volcanic field.

Rock type	alkali ol-basalt														basanite						
Sample #	SA54	SA95	SAB185	SAB188	SAB207	SAB222	SAB224	SAB225	SAB227	SAB229	SAB232	SAB270	SAB275	SAB277	SA03	SA05	SA12	SA23	SA26	SA27	SA37
Q	-	-	-	-	-	-	-	-	-	-	-	-	-	-	-	-	-	-	-	-	-
Or	9.18	6.82	8.66	8.28	4.37	10.47	10.65	10.65	9.17	10.00	12.18	10.53	11.00	11.48	6.96	6.94	9.62	8.89	7.10	12.78	6.86
Ab	21.72	21.70	18.63	19.46	13.08	26.49	25.04	27.64	18.37	18.28	26.00	24.94	25.68	29.19	19.27	7.08	7.76	9.16	11.84	10.75	7.51
An	18.69	18.46	20.81	21.56	21.24	18.75	17.40	20.18	21.66	20.96	18.39	16.89	17.04	21.76	19.99	11.84	13.47	13.63	16.71	12.29	15.98
Ne	4.31	3.39	3.82	2.78	4.51	2.55	4.34	1.01	3.19	3.93	4.00	4.53	4.68	0.17	5.11	15.56	15.63	12.58	9.30	13.02	11.54
Lc	-	-	-	-	-	-	-	-	-	-	-	-	-	-	-	-	-	-	-	-	-
$100\frac{An}{An+Ab}$	46.25	45.97	52.76	52.56	61.89	41.45	41.00	42.20	54.11	53.41	41.43	40.38	39.89	42.71	50.92	62.58	63.45	59.81	58.53	53.34	68.03
Di	16.70	19.68	15.43	15.69	20.26	14.65	15.19	13.75	19.34	17.84	13.90	15.58	15.24	9.83	18.24	26.26	25.11	24.37	23.93	21.13	26.76
Hy	-	-	-	-	-	-	-	-	-	-	-	-	-	-	-	-	-	-	-	-	-
Ol	19.68	21.96	22.82	22.40	25.30	17.55	17.88	17.08	17.38	17.93	16.48	18.05	16.95	18.15	21.01	20.69	18.22	21.20	20.69	17.93	21.60
Mt	3.22	3.01	3.06	3.08	3.47	3.09	3.07	3.10	3.19	3.26	2.91	3.05	3.02	2.99	3.01	3.44	3.13	3.20	3.34	3.63	3.10
Il	5.13	3.96	5.14	5.13	6.16	4.81	4.73	4.83	5.72	5.93	4.39	4.71	4.65	4.54	5.03	6.24	5.43	5.38	5.79	5.88	5.30
Ap	1.35	1.02	1.63	1.63	1.61	1.66	1.70	1.77	1.99	1.88	1.75	1.72	1.75	1.90	1.38	1.94	1.63	1.58	1.30	2.59	1.35
D.I.	35.22	31.92	31.11	30.52	21.96	39.50	40.03	39.29	30.73	32.21	42.19	40.00	41.36	40.84	31.34	29.58	33.01	30.63	28.25	36.55	25.91

Table A4.2 continued.

Rock type	basanite																					
Sample #	SA38	SA40	SA41	SA42	SA45	SA55	SA56	SA57	SA58	SA60	SA61	SA75	SA82	SA86	SAB102	SAB107	SAB111	SAB116	SAB128	SAB129	SAB132	SAB173-1
Q	-	-	-	-	-	-	-	-	-	-	-	-	-	-	-	-	-	-	-	-	-	-
Or	6.31	7.86	8.41	8.08	6.12	6.96	7.69	8.41	8.50	6.92	8.17	7.90	8.79	9.10	5.78	6.14	7.69	7.81	7.91	10.36	9.81	8.52
Ab	15.51	6.93	5.79	7.02	8.84	11.23	6.98	7.56	10.75	9.53	10.81	9.84	13.67	6.18	10.39	8.50	7.11	7.82	5.9	5.50	6.67	6.47
An	16.48	15.03	13.51	14.87	13.76	18.16	17.19	14.27	15.25	17.70	14.70	12.86	20.12	11.69	15.55	13.15	16.72	15.71	14.71	10.53	13.04	14.18
Ne	8.37	11.29	13.45	11.58	14.44	7.74	10.36	14.15	10.53	8.57	12.94	13.91	9.03	17.27	10.94	13.92	10.23	11.00	12.92	17.63	14.54	13.07
Lc	-	-	-	-	-	-	-	-	-	-	-	-	-	-	-	-	-	-	-	-	-	-
$100\frac{An}{An+Ab}$	51.52	68.44	70.00	67.93	60.88	61.79	71.12	65.37	58.65	65.00	57.62	56.65	59.54	65.42	59.95	60.74	70.16	66.77	71.37	65.69	66.16	68.67
Di	22.10	26.09	26.99	25.74	25.29	24.29	24.66	24.90	23.22	25.33	24.24	25.15	19.13	25.51	23.10	24.75	23.84	23.49	24.72	25.04	23.62	27.18
Hy	-	-	-	-	-	-	-	-	-	-	-	-	-	-	-	-	-	-	-	-	-	-
Ol	21.71	22.91	21.89	22.87	19.82	22.46	22.78	20.73	21.53	22.57	19.69	20.23	19.53	18.96	22.40	21.79	22.93	23.26	22.34	19.64	20.88	20.56
Mt	3.22	3.19	3.16	3.20	3.46	3.05	3.27	3.17	3.21	3.01	3.01	3.21	3.05	3.45	3.49	3.47	3.42	3.35	3.43	3.34	3.46	3.18
Il	4.89	5.36	5.41	5.31	6.28	5.10	5.67	5.27	5.40	5.31	4.96	5.15	5.43	5.48	6.18	6.17	6.17	5.99	6.19	5.68	5.72	5.32
Ap	1.41	1.35	1.39	1.35	1.99	1.01	1.42	1.54	1.61	1.06	1.47	1.76	1.26	2.36	2.16	2.11	1.89	1.58	1.89	2.29	2.27	1.53
D.I.	30.19	26.08	27.66	26.68	29.40	25.93	25.02	30.12	29.78	25.02	31.92	31.64	31.48	32.55	27.12	28.56	25.04	26.62	26.73	33.49	31.01	28.06

Table A4.2 continued.

Rock type	basanite																mugearite
Sample #	SAB175	SAB176	SAB176-1	SAB177	SAB177-1	SAB178-1	SAB178-2A	SAB179	SAB179D	SAB180	SAB180D	SAB194	SAB196	SAB204	SAB214		SA88
Q	-	-	-	-	-	-	-	-	-	-	-	-	-	-	-		-
Or	8.75	8.52	8.81	8.87	8.40	8.40	8.70	6.85	6.98	7.93	8.04	8.59	8.80	7.17	8.16		7.94
Ab	5.73	6.85	7.20	5.93	7.15	6.02	6.16	8.18	8.28	8.60	8.30	9.80	7.41	8.36	6.48		28.32
An	15.33	14.86	14.80	14.36	15.08	15.82	13.97	17.23	16.69	16.83	16.25	17.21	16.07	18.44	15.00		11.29
Ne	11.87	12.16	11.54	12.73	11.38	11.53	13.20	8.63	8.98	9.27	9.93	8.82	10.91	7.55	11.74		-
Lc	-	-	-	-	-	-	-	-	-	-	-	-	-	-	-		-
$100\frac{An}{An+Ab}$	72.79	68.45	67.27	70.77	67.84	72.44	69.40	67.81	66.84	66.18	66.19	63.72	68.44	68.81	69.83		28.50
Di	27.12	25.86	26.78	27.00	26.46	27.43	27.19	24.66	25.63	24.43	25.46	21.70	23.26	22.34	26.34		17.12
Hy	-	-	-	-	-	-	-	-	-	-	-	-	-	-	-		1.04
Ol	21.34	21.79	20.96	20.89	21.65	20.96	20.71	24.96	24.02	23.20	22.31	23.20	22.37	25.33	21.64		23.28
Mt	3.15	3.13	3.15	3.20	3.18	3.18	3.16	3.14	3.16	3.14	3.15	3.33	3.34	3.40	3.32		3.92
Il	5.28	5.27	5.24	5.40	5.28	5.26	5.32	5.13	5.13	5.28	5.32	5.71	5.94	5.80	5.74		5.68
Ap	1.42	1.56	1.53	1.62	1.42	1.40	1.59	1.21	1.14	1.32	1.24	1.65	1.92	1.61	1.57		1.41
D.I.	26.36	27.54	27.55	27.53	26.93	25.95	28.05	23.66	24.24	25.80	26.27	27.21	27.11	23.09	26.39		36.26

Table A4.2 continued.

Rock type	ne-hawaiite																					
Sample #	SA01	SA02	SA22	SA24	SA25	SA29	SA62	SA63	SA64	SA65	SA66	SAB215	SAB217	SAB218	SAB220	SAB221	SAB223	SAB228	SAB231	SAB233	SAB234	SAB235
Q	-	-	-	-	-	-	-	-	-	-	-	-	-	-	-	-	-	-	-	-	-	-
Or	11.07	10.30	8.77	10.88	10.59	13.05	13.19	12.36	12.19	13.25	11.56	11.36	11.00	11.24	11.12	11.00	10.53	12.24	11.53	11.42	10.94	11.24
Ab	18.36	19.70	18.56	20.68	20.05	14.40	18.53	22.24	17.02	20.09	6.71	23.42	23.78	21.03	23.68	22.26	26.13	26.43	23.72	24.62	22.48	24.62
An	15.84	18.60	16.00	13.72	13.52	7.16	8.76	14.06	14.03	8.74	6.45	14.53	15.79	13.12	16.38	14.51	19.46	16.48	15.76	16.30	14.36	15.86
Ne	11.15	7.01	5.66	9.21	8.93	18.11	15.47	9.89	11.47	15.16	20.68	8.66	5.98	10.00	6.04	8.00	2.37	5.74	6.61	5.94	8.02	6.26
Lc	-	-	-	-	-	-	-	-	-	-	-	-	-	-	-	-	-	-	-	-	-	-
$100\frac{An}{An+Ab}$	46.32	48.56	46.30	39.88	40.27	33.21	32.10	38.73	45.19	30.32	49.01	38.29	39.90	38.42	40.89	39.46	42.68	38.41	39.92	39.83	38.98	39.18
Di	18.66	19.69	20.68	16.51	17.41	20.73	18.79	15.49	20.51	17.76	26.45	17.48	16.57	18.38	16.90	17.27	14.31	13.95	16.19	15.70	17.35	15.78
Hy	-	-	-	-	-	-	-	-	-	-	-	-	-	-	-	-	-	-	-	-	-	-
Ol	15.84	15.71	18.81	17.96	18.52	15.48	14.71	15.68	13.71	14.86	16.40	15.33	17.41	16.90	16.40	17.49	17.58	16.04	16.95	16.76	17.46	16.89
Mt	2.90	2.84	3.55	3.43	3.49	3.42	3.29	3.19	3.35	3.25	3.58	2.93	3.05	3.02	3.06	3.04	3.12	2.91	2.97	3.00	3.02	2.99
Il	4.89	4.90	5.28	5.45	5.08	4.94	4.93	5.21	5.53	4.62	5.33	4.60	4.69	4.64	4.73	4.71	4.83	4.39	4.54	4.56	4.66	4.56
Ap	1.27	1.25	2.69	2.16	2.40	2.72	2.33	1.89	2.19	2.28	2.83	1.70	1.72	1.68	1.70	1.72	1.68	1.81	1.72	1.70	1.72	1.81
D.I.	40.59	37.01	32.99	40.77	39.57	45.55	47.19	44.48	40.68	48.50	38.96	43.43	40.77	42.26	40.83	41.25	39.03	44.41	41.86	41.98	41.44	42.12

Table A4.2 continued.

Rock type	ne-hawaiite											
Sample #	SAB236	SAB237	SAB239	SAB241	SAB245	SAB247	SAB249	SAB259	SAB260	SAB262	SAB264	SAB271
Q	-	-	-	-	-	-	-	-	-	-	-	-
Or	10.88	10.88	11.48	10.82	11.53	11.60	11.00	10.88	11.18	10.59	11.12	11.41
Ab	23.03	22.85	23.78	22.61	24.16	23.71	22.78	22.43	24.39	22.90	23.40	24.33
An	15.31	15.13	15.07	14.93	14.94	14.94	15.10	14.69	16.08	15.45	15.05	15.64
Ne	7.17	7.32	7.31	7.53	7.15	7.63	7.40	7.95	6.80	6.97	6.83	7.24
Lc	-	-	-	-	-	-	-	-	-	-	-	-
$100\frac{An}{An+Ab}$	39.93	39.84	38.79	39.77	38.21	38.65	39.86	39.57	39.73	40.29	39.14	39.13
Di	16.51	16.65	16.36	16.68	16.21	16.44	16.41	17.01	16.16	16.91	16.08	16.43
Hy	-	-	-	-	-	-	-	-	-	-	-	-
Ol	17.66	17.75	16.76	17.92	16.73	16.45	17.58	17.54	16.06	17.71	17.92	15.66
Mt	3.05	3.03	2.97	3.06	2.99	2.97	3.06	3.05	2.97	3.05	3.06	2.93
Il	4.69	4.67	4.54	4.71	4.54	4.52	4.73	4.73	4.62	4.71	4.73	4.62
Ap	1.70	1.72	1.72	1.75	1.75	1.75	1.94	1.72	1.75	1.72	1.81	1.75
D.I.	41.08	41.05	42.57	40.96	42.84	42.93	41.18	41.27	42.37	40.45	41.35	42.98

Table A4.2 continued.

Rock type	nephelinite													
Sample #	SA06	SA21	SA28	SA46	SA50	SA51	SAB104	SAB105	SAB113	SAB119	SAB127	SAB135	SAB178	SAB193
Q	-	-	-	-	-	-	-	-	-	-	-	-	-	-
Or	7.75	7.90	13.00	6.05	8.89	10.39	9.70	9.65	8.85	9.48	9.45	10.07	9.94	9.62
Ab	4.59	4.22	4.79	-	-	3.15	3.67	4.75	4.71	3.46	3.81	1.79	3.93	1.34
An	13.69	13.42	5.43	6.43	8.99	8.46	11.92	12.68	12.69	11.89	12.23	12.10	13.75	11.31
Ne	14.49	14.96	21.18	22.97	20.22	19.59	16.30	15.37	15.10	16.13	15.58	16.47	14.06	17.73
Lc	-	-	-	3.34	1.08	-	-	-	-	-	-	-	-	-
$100\frac{An}{An + Ab}$	74.89	76.08	53.13	100.00	100.00	72.87	76.46	72.75	72.93	77.46	76.25	87.11	77.77	89.41
Di	26.39	26.39	26.46	31.70	28.42	27.45	25.81	25.84	25.59	25.88	25.69	26.84	26.69	27.47
Hy	-	-	-	-	-	-	-	-	-	-	-	-	-	-
Ol	21.76	21.70	17.28	17.59	20.15	18.37	20.94	20.03	21.68	21.59	21.72	20.65	20.94	20.71
Mt	3.43	3.46	3.63	3.44	3.66	3.67	3.35	3.28	3.33	3.39	3.40	3.49	3.31	3.41
Il	6.19	6.14	5.41	5.95	6.48	6.06	6.17	6.27	6.15	6.19	6.13	6.10	5.49	6.08
Ap	1.71	1.80	2.82	2.54	2.13	2.88	2.13	2.13	1.90	1.98	1.99	2.51	1.89	2.34
D.I.	26.83	27.08	38.98	32.35	30.19	33.13	29.67	29.76	28.66	29.08	28.84	28.32	27.92	28.68

Appendix Five:
Analytical Procedures and Instrument Precision

Appendix 5

Analytical procedures and instrument precision

A5.1 Electron microprobe analysis

Mineral chemical analyses for 52 South Auckland volcanic field samples were obtained using a JEOL-JXA(5A) electron probe micro-analyser, housed at the Department of Geology, University of Auckland, Auckland, New Zealand, under the direction of R. Simms. Samples chosen for microprobe analysis from each rock type and their corresponding sample number are given in Appendix 6. R. Simms provided the information regarding electron microprobe operation and analytical precision, sections A5.12 and A5.13 respectively.

A5.1.1 Sample preparation

A 30μm-thick polished thin-section was prepared from each sample. After polishing, each thin-section was cleaned with acetone. Prior to microprobe analyses each thin-section was cleaned with ethanol and acetone then placed in an Edwards vacuum evaporator and coated with an ~ 25 ηm-thick carbon film. For microprobe analyses, each thin-section was mounted on a brass sample holder. The points of contact between the holder and thin-section were painted with Aquadag colloidal graphite in order to ground any charge build-up during the analysis session.

A5.1.2 Electron microprobe operation

Mineral crystals were analysed by a modified JEOL-JXA(5A) electron microprobe (Simms, pers comm. 1998). The operating parameters of the JEOL-JXA(5A) for major element analysis of silicate and oxide minerals were; an electron gun accelerating voltage of 15 kV, approximately 600 pA sample absorption current, and an electron spot diameter ~ 3 μm.

X-ray measurements are made by energy dispersive spectrometry, using a LINK SYSTEMS (now Oxford Instruments) LZ-5 Si(Li) Be-window detector and a LINK SYTEMS QX2000 pulse-processor/computer, running ZAF-4/FLS software, version QX20-ZF4-1291. Each spectrum was collected for 100 seconds of live time.

Analytical spot positioning is done using back-scattered electron imaging, with the signal being processed by LINK SYSTEMS software on the QX2000.

A5.1.3 Analytical precision

The operating standard, for hour-to-hour standardisation, is Co metal. During each session, a pure Co standard was analysed every three hours and, if necessary, the probe was re-calibrated to correct for instrument drift.

Microprobe calibration for the suite of major elements Si, Ti, Al, Fe, Mn, Mg, Ca, Na, K, and V is determined on a weekly basis using nine Department of Geology mineral standards. The precision of microprobe analyses is determined by 10 replicate analyses of the nine mineral standards (Table A5.1). Precision estimates based on one standard deviation (1σ) yield percent relative standard deviation values (%RSD) that range from << 1% RSD for element oxides that comprise > 25 wt% of a given mineral phase to >> 10% RSD for element oxide contents that range from < 2 wt%. The relationship between %RSD and element oxide wt% for the nine mineral standards is illustrated in Fig. A5.1. Since analytical precision is concentration dependent, the precision for those oxides not accounted for in the mineral standards (e.g., Cr_2O_5) may be estimated from Fig. A5.1.

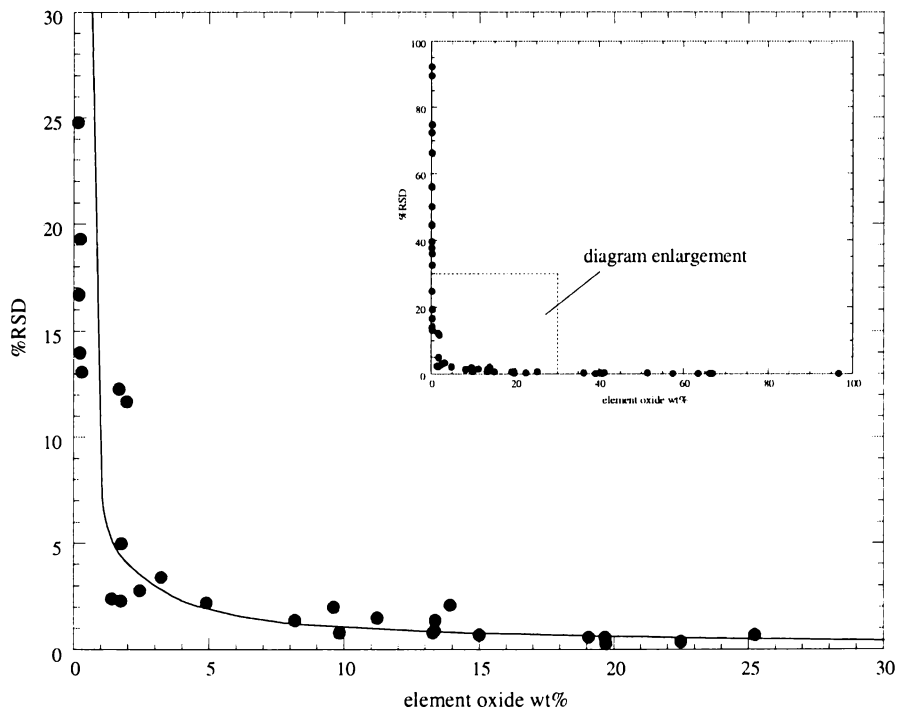

Fig. A5.1 Percent relative standard deviation (%RSD) versus element oxide wt% for electron microprobe mineral standards. The best-fit power curve shown in the enlarged diagram is for the data set of the nine mineral standards given in Table A5.1 (see inset for plot of all data).

Table A5.1 Electron microprobe mineral standard analyses (in wt.%), average compositions (Avg), one standard deviation (1σ), and percent relative standard deviation (%RSD) values for each element oxide (after Simms, pers. comm., 2001). %RSD = 100(1σ/Avg).

Standard	Albite F												
analysis	1	2	3	4	5	6	7	8	9	10	Avg	1σ	%RSD
SiO_2	66.97	66.53	66.53	66.72	66.70	66.77	66.97	66.61	66.87	66.69	66.74	0.16	0.2
Al_2O_3	19.49	19.72	19.78	19.80	19.61	19.58	19.70	19.54	19.56	19.80	19.66	0.12	0.6
CaO	-	0.19	0.26	0.24	0.07	0.13	0.18	0.14	-	0.26	0.15	0.10	66.3
Na_2O	13.44	13.42	13.32	13.10	13.51	13.37	13.16	13.63	13.48	13.06	13.35	0.19	1.4
K_2O	0.01	0.14	0.12	0.15	0.11	0.15	-	0.09	0.09	0.19	0.11	0.05	44.7
Standard	albite K												
SiO_2	66.66	66.74	66.54	66.70	66.99	66.65	66.43	66.58	66.80	66.89	66.70	0.17	0.2
Al_2O_3	19.76	19.71	19.73	19.66	19.61	19.68	19.80	19.76	19.60	19.71	19.70	0.07	0.3
CaO	0.11	0.15	0.08	0.08	0.09	0.14	0.17	0.04	0.13	0.06	0.11	0.04	39.6
Na_2O	13.30	13.25	13.48	13.43	13.10	13.34	13.43	13.51	13.31	13.24	13.34	0.13	0.9
K_2O	0.16	0.16	0.16	0.14	0.21	0.20	0.16	0.11	0.17	0.08	0.15	0.04	24.8
Standard	Andularia												
SiO_2	65.17	65.34	65.20	65.06	65.16	64.93	65.16	65.28	65.16	65.07	66.15	0.11	0.2
TiO_2	0.25	0.10	0.26	0.16	0.01	0.21	0.20	0.14	0.09	0.19	0.17	0.06	36.0
Al_2O_3	18.95	19.06	18.93	19.13	19.14	19.11	19.96	19.97	19.08	19.28	19.06	0.11	0.6
CaO	0.08	-	-	0.14	0.19	-	0.06	0.07	0.07	0.10	0.07	0.06	89.7
Na_2O	1.50	1.79	1.46	1.74	1.82	1.49	1.55	1.92	1.33	1.85	1.65	0.20	12.3
K_2O	14.05	13.71	14.14	13.77	13.59	14.26	14.08	13.62	14.27	13.51	13.90	0.29	2.1
Standard	Olivine												
SiO_2	40.30	40.27	40.28	40.01	40.16	40.19	40.24	40.07	40.24	40.03	40.18	0.11	0.3
Al_2O_3	0.22	0.20	0.18	0.16	0.18	0.17	0.27	0.18	0.21	0.17	0.19	0.03	16.7
FeO	8.05	8.19	8.14	8.34	8.02	8.16	8.11	8.11	8.02	8.35	8.15	0.12	1.4
MnO	0.10	0.12	0.13	0.06	0.12	0.13	0.10	-	0.08	0.16	0.10	0.04	44.5
MgO	51.33	51.22	51.28	51.43	51.52	51.36	51.28	51.64	51.45	51.28	51.38	0.13	0.3
Standard	Enstatite												
SiO_2	57.50	57.49	57.58	57.30	57.19	57.36	57.41	57.35	57.55	57.42	57.41	0.12	0.2
Al_2O_3	1.78	1.74	1.69	1.69	1.69	1.75	1.69	1.78	1.71	1.68	1.72	0.04	2.3
FeO	0.19	0.18	0.18	0.24	0.26	0.18	0.19	0.25	0.19	0.20	0.21	0.03	14.0
MgO	40.49	40.52	40.46	40.66	40.75	40.61	40.60	40.59	40.48	40.64	40.58	0.09	0.2
CaO	0.04	0.07	0.09	0.11	0.11	0.10	0.11	0.04	0.06	0.05	0.08	0.03	37.7
Standard	Kaersuitite												
SiO_2	41.17	41.15	40.90	41.12	41.36	41.02	41.20	41.06	40.86	41.17	41.10	0.15	0.4
TiO_2	4.76	4.92	4.88	4.90	4.92	4.90	4.82	4.72	4.92	5.10	4.88	0.11	2.2
Al_2O_3	15.07	14.87	14.94	14.94	14.93	15.11	15.21	14.92	14.97	14.97	14.99	0.10	0.7
FeO	11.32	11.29	11.32	11.41	11.05	11.41	10.95	11.01	11.22	11.09	11.21	0.17	1.5
MnO	0.00	0.10	0.09	0.11	0.11	0.11	0.14	0.13	0.13	-	0.09	0.05	56.0
MgO	13.18	13.23	13.29	13.25	13.12	13.11	13.29	13.44	13.43	13.29	13.26	0.11	0.8
CaO	9.78	9.82	9.74	9.78	9.84	9.92	9.65	9.83	9.75	9.90	9.80	0.08	0.8
Na_2O	3.27	3.27	3.28	3.13	3.31	3.04	3.22	3.33	3.18	3.03	3.21	0.11	3.4
K_2O	1.35	1.35	1.45	1.37	1.37	1.37	1.42	1.40	1.38	1.34	1.38	0.03	2.4
V_2O_5	0.11	-	0.11	-	-	-	0.10	0.15	0.17	0.10	0.07	0.07	92.3
Standard	Almandine												
SiO_2	38.95	39.10	38.99	39.15	39.02	39.02	38.95	39.18	38.94	38.97	39.03	0.09	0.2
Al_2O_3	22.46	22.43	22.47	22.49	22.63	22.62	22.52	22.54	22.43	22.33	22.49	0.09	0.4
FeO	25.18	24.89	25.23	25.19	25.11	25.43	25.35	25.03	25.32	25.46	25.22	0.18	0.7
MnO	1.92	2.40	1.81	1.77	1.85	2.16	2.14	1.76	1.72	1.78	1.93	0.23	11.7
MgO	9.71	9.51	9.65	9.63	9.52	9.17	9.39	9.67	9.86	9.68	9.58	0.19	2.0
CaO	1.78	1.66	1.85	1.78	1.86	1.61	1.65	1.82	1.74	1.77	1.75	0.09	5.0
Standard	Sillimanite												
SiO_2	36.37	36.11	36.37	36.24	36.28	36.37	36.20	36.32	36.14	36.26	36.27	0.10	0.3
Al_2O_3	63.39	63.66	63.41	63.55	63.41	63.42	63.50	63.50	63.64	63.44	63.49	0.10	0.2
FeO	0.23	0.24	0.23	0.21	0.31	0.21	0.30	0.17	0.23	0.30	0.24	0.05	19.3
Standard	Hematite												
SiO_2	0.28	0.31	0.28	0.24	0.34	0.29	0.32	0.35	0.31	0.23	0.29	0.04	13.1
TiO_2	2.43	2.42	2.51	2.50	2.38	2.42	2.26	2.41	2.39	2.46	2.42	0.07	2.8
Al_2O_3	0.14	0.09	0.20	0.14	-	0.14	0.07	0.07	0.15	0.11	0.11	0.06	50.1
Fe_2O_3	96.69	96.59	96.72	96.64	96.70	96.88	96.46	96.65	96.69	97.03	96.70	0.15	0.2
MgO	0.13	0.10	-	0.09	0.11	-	0.09	-	0.08	0.08	0.07	0.05	72.4
Na_2O	0.16	0.27	0.14	0.16	0.30	-	0.49	0.36	0.16	-	0.20	0.15	74.8
V_2O_5	0.16	0.22	0.14	0.23	0.18	0.28	0.31	0.15	0.21	0.09	0.20	0.06	32.5

A5.2 X-ray fluorescence analysis

Samples SA01 – SA95 were analysed for major and trace elements by a Phillips 1404 fully automated X-ray fluorescence (XRF) spectrometer housed at the Analytical Facility, Victoria University, Wellington, New Zealand[2]. One hundred and ten "SAB" samples were analysed by XRF for major and trace elements using the Siemens SRS3000 with Spectra 3000 software V2.0 housed at the Department of Geology, University of Auckland, Auckland, New Zealand. Operation of the XRF was under the direction of J. Wilmshurst who provided the information regarding operating conditions and analytical precision, sections A5.22 and A5.23 respectively.

A5.2.1 Sample preparation

The SAB samples that showed obvious signs of weathering or alteration in hand specimen or in thin sections were rejected for geochemical analyses[3].

Samples were prepared for analysis from slices sawn by a water-cooled, diamond-tipped blade. Sawn surfaces were inspected for metal streaks from the blade and if present, a water-cooled table grinder equipped with a diamond-studded brass wheel was used to remove all streaks. The rock slices were broken into small fragments e.g., < 1 cm^3 in size using a hammer and anvil, the surfaces of which were covered with heavy paper to prevent contamination. Fragments that showed any indication of contamination from the paper, hammer, or anvil were rejected. Additionally, fragments containing xenolithic material or filled vesicles were rejected.

The rock fragments were ground in a tungsten carbide ring mill, which was thoroughly cleaned between uses for each rock sample. Grinding times were minimised (typically less than three minutes) in order to reduce potential contamination from the mill, especially Co due to the binding agent used in commercial tungsten carbide mills (Goles, pers. comm., 2000) and Ta (see Price *et al.*, 1999).

The rock powder was prepared for major and trace element analyses by XRF according to the sample preparation techniques of Parker *et al.* (1993) with the following modifications: (1) major element glass fusion disks (d = 40mm) were prepared with

[2] Fourteen of these analyses are reported in Briggs *et al.* (1994).
[3] Replacement of olivine by iddingsite is the most apparent form of alteration observed in the SAVF lavas. Since iddingsite alteration may occur at the vapour-rich top of a magma column prior to eruption (Shelley, 1993), samples that contain iddingsitised olivine were considered for geochemical analysis.

1.2600 ± 0.0005g of ignited sample powder[4] mixed with 6.7500 ± 0.0005g of dried Norrish flux (Lanthanum oxide heavy, absorber flux), (2) trace element briquettes (d = 40mm) were prepared with 10g of dried rock powder combined with 10 – 20 drops of liquid PVP/Methyl Cellulose binder.

A5.2.2 Operating conditions

The trace calibration uses the Compton peak as the matrix correction with intensity based jump corrections for trace element lines below Fe. Major and trace elements are calibrated using 37 international standards.

A5.2.3 Analytical precision

Analytical precision for the Siemens SRS3000 for basalts analyses is based on the Mount Eden Basalt (MEB) reference standard determined by 48 replicate analyses for the major elements and 38 replicate analyses for trace elements. Precision data for major and trace elements and the limits of detection for trace elements are given in Table A5.2.

Table A5.2 Precision for XRF major (wt.%) and trace element (ppm) data and limits of detection for trace elements (ppm) for MEB. Avg = average in wt.% for major elements or ppm for trace elements; SD = standard deviation; RSD = analysis precision (100SD/Avg); LLD = Lower limit of detection – the smallest signal that can be qualitatively measured using 3σ confidence (3sp); LoD = Limit of determination – the smallest signal that can be quantitatively measured using 3σ confidence (6sp); LoQ = Limit of quantitation – the smallest signal that can be quantitatively measured with sufficient confidence to be quoted for commercial or statutory use (10sp); sp = standard deviation in a net line intensity.

	Precision for XRF data							Limits of detection (ppm)		
	Avg	SD (n = 48)	RSD		Avg	SD (n = 38)	RSD	LLD	LoD	LoQ
SiO_2	46.04	0.28	0.6	Sc	21.7	1.9	8.9	2.6	5.2	8.7
TiO_2	2.24	0.01	0.7	V	244.3	1.4	0.6	2.3	4.6	7.7
Al_2O_3	13.69	0.11	0.8	Cr	322.8	1.5	0.5	1.6	3.2	5.3
Fe_2O_3	13.52	0.09	0.6	Ni	220.8	1.3	0.6	1.3	2.6	4.3
MnO	0.19	0.02	11.6	Cu	102.6	1.0	0.9	1.6	3.2	5.3
MgO	10.35	0.13	1.3	Zn	117.6	1.0	0.8	1.6	3.2	5.3
CaO	9.68	0.06	0.6	Ga	21.9	0.4	1.9	0.7	1.4	2.4
Na_2O	3.40	0.07	2.2	Rb	17.0	0.3	1.7	0.7	1.4	2.3
K_2O	0.98	0.01	1.1	Sr	509.1	1.4	0.3	0.7	1.3	2.2
P_2O_5	0.44	0.01	2.2	Y	24.6	0.4	1.5	0.4	0.7	1.2
$H2O^-$	0.06	0.00	7.3	Zr	173.5	0.5	0.3	0.5	1.0	1.6
LOI	-0.57	0.03	5.2	Nb	35.0	0.2	0.7	0.4	0.8	1.4
Total	100.02			Ba	205.0	5.8	2.9	4.8	9.6	16.0
				La	24.2	1.5	6.4	2.2	4.4	7.3
				Pb	3.6	0.8	23.3	1.5	3.0	5.0
				Ce	46.5	2.4	5.1	6.4	12.8	21.3
				Th	2.7	0.7	27.4	1.0	2.0	3.3
				U	1.0	1.0	104.3	1.2	2.4	4.0

[4] Four grams of rock powder was ignited at 950°C for two hours.

A5.3 High-precision trace element and REE analyses

Fifteen "SA" samples were analysed for REE by spark source mass spectrometry (SSMS) at the Research School of Earth Sciences, Australian National University, Canberra, Australia by Dr. R.M. Briggs.

Eleven "SAB" samples and an additional subset of 7 "SA" samples were analysed for 23 trace elements and REE by ICP-MS at the Victoria Institute of Earth and Planetary Sciences (VIEPS) Trace Analysis Laboratory, Monash University, Melbourne, Australia under the direction of Dr. L. Frick. XRF results were used to select these samples for ICP-MS analyses. Sample selection was based on the following criteria:

1. Samples that appeared to have "unusually high" Ba and Y abundances and Ba/Nb ratio were considered unsuitable for REE analysis based in part on the experimental work by Price *et al.* (1991) and Cotton *et al.* (1995)[5] on the origins of anomalous REE and Y enrichments in subaerially exposed basalts.
2. Thin section examination indicates that some analysed samples contain vesicles filled with low-temperature secondary phases, e.g. carbonate or zeolite species. Although such vesicles tend to comprise << 1% total rock volume (see Appendix 3 for details), samples containing filled vesicles were rejected.
3. Petrographic examination showed that some SAVF samples contain olivine extensively altered to iddingsite, especially microphenocrysts and groundmass crystals. Although Price *et al.* (1991) concluded that there is no correlation between anomalous Ba, Y, and REE abundances and the degree of iddingsite alteration in olivine, samples with extremely altered crystals were not considered for REE analysis.

A5.3.1 Sample preparation

SAVF samples and the BHVO-1 standard was prepared from100 mg or rock powder that was leached in SAVILLEX beakers with 2D NHO_3 and 2D HF prior to dissolution in hot 2D NHO_3. Samples were centrifuged for three minutes to remove any solid residue. The solution was loaded onto the resin-filled columns used for Sr purification. REE were purified by conventional anion exchange techniques using two column passes of 2M HCl to collect Sr. One pass of 2.5M NHO_3 was used to remove Ba interference from the resin followed by on pass of 6.2M HCl to collect REE.

[5] Price *et al.* (1991) and Cotton *et al.* (1995) showed that abundances of highly mobile elements such as Ba, Y, and REE in basaltic rocks may be affected by low levels of surface weathering or hydrothermal alteration (e.g. post magmatic supergene processes). They cited "unusually high" concentrations of these elements as possible evidence for post-depositional alteration. While such anomalies in REE may become obvious only after chemical analysis has been completed, Price *et al.* (1991) and Cotton *et al.* (1995) established criteria using ratios between easily mobilised elements, e.g. Ba and relatively immobile elements, e.g. Nb, to help ascertain if incipient alteration may have occurred. In volcanic fields dominated by monogenetic centres, such as the SAVF, mobile element enrichment within suites of samples that predominantly have comparatively low abundances in these elements may be an original magmatic feature. Nevertheless, samples that appeared to have "abnormal" Ba, Y, or Ba/Nb were rejected.

A5.3.2 ICP-MS operating conditions

Diluted rock and acid-leached samples were analysed using a high-resolution Finnigan MAT ELEMENT magnetic sector ICP-MS. One or two isotopes listed in Table A5.3 were chosen for each element of interest based on no or minimal isobaric interferences. Twenty-five runs of one mass spectrometer sweep through the mass spectrum were performed. The run specifications resulted in approximately 10 sample points per peak.

Table A5.3 Isotopes used for ICP-MS analyses.

Element	Isotope	Element	Isotope
Sc	45	La	139
Ti	47	Ce	140
V	51	Pr	141
Cr	52	Nd	146
Mn	55	Sm	147
Co	59	Eu	151
Ni	60	Gd	158
Cu	63	Tb	159
Zn	66	Dy	161
Rb	85	Ho	165
Sr	88	Er	166
Y	89	Tm	169
Zr	90	Yb	172
Nb	93	Lu	175
Mo	97	Hf	180
In	115	Ta	181
Sn	118	Pb	208
Cs	133	Th	232
Ba	137	U	238

Integrated count data from the instrument was reduced using a custom, off-line, spreadsheet-based program. During each analysis a series of dummy samples were run to provide a check on instrument drift. The count data was then corrected by a polynomial in time for each element analysed to provide constant counting efficiency in the dummy samples. Next, calibration curves were constructed for each element using a simple, least-squares linear regression of BHVO-1 standard data points at dilution factors of 4, 6, 8, and 10 thousand. Using these calibration curves, the data were resolved into ppb in solution. The count data was then corrected by polynomial in time for each element to provide constant counting efficiency in the dummy samples. Next, calibration curves were constructed for each element using a simple, least squares linear regression of the BHVO-1 standard data points.

A5.3.3 Analytical precision and data quality

Precision (in-run statistics quoted as RSD = 100SD/mean) is better than 5% for each analysis. As described above, determination of analytical accuracy is based on analysis of the solution standards, and is typically better than 5% for most elements at the 95% confidence level.

A5.4 Thermal ionisation mass spectrometry

Ratios for the radiogenic isotopes, Sr, Nd, and Sm for 18 "SA" samples were determined at the Institut für Mineralogie, Petrologie und Geochemie, Universität Tübingen, Tübingen, Germany, by Dr. E. Hegner. Ratios for the radiogenic isotopes, Sr, Nd, and Pb were determined for 14 "SAB" samples and an additional four "SA" samples at the VIEPS Radiogenic Isotope Laboratory, Department of Earth Sciences, La Trobe University, Melbourne, Australia under the direction of Dr. R. Maas.

Samples were selected from those analysed by SSMS or ICP-MS.

A5.4.1 Sample preparation for Sr – Nd – Pb

150 mg of small (i.e., < 2 mm) rock chips were leached with hot 6M HCl for 60 minutes prior to dissolution in HF-HNO3-HCl. Samples were centrifuged for three minutes to remove any solid residue. The solution was loaded onto the columns used for Sr and Nd purification. Sr and Nd were purified by conventional anion exchange techniques using two column passes and 2M HCl to collect Sr and 0.2M HCl to collect Nd.

Pb was purified by conventional HBr-HCl anion exchange techniques using two column passes (columns made from heat-shrink TFE teflon, internal diameter 4 mm; resin is AG1-X8, 200-400 mesh, 1.pass 0.1 mlresin, 2.pass 0.05 ml resin).

A5.4.2 Operating conditions

Sr, Nd, and Pb isotopic ratios ($^{87}Sr/^{86}Sr$, $^{143}Nd/^{144}Nd$, $^{206}Pb/^{204}Pb$, $^{207}Pb/^{204}Pb$, $^{208}Pb/^{204}Pb$) were measured on a Finnigan MAT 262 multiple collector mass spectrometer in static mode. Sr isotopic ratios were measured in static mode for masses 84,85,86,87, and 88. Mass 84 was used to monitor the possible presence of Rb in the sample during analysis. None was detected. $^{87}Sr/^{86}Sr$ ratios were normalised to $^{88}Sr/^{86}Sr$ = 8.3752. Pb loaded with Si-gel onto a single Re filaments was pre-degassed at 3.5A for 20 minutes. The Si-gel used was made from silicic acid following Gerstenberger and Haas (1997).

A5.4.3 Analytical precision and data quality

$^{87}Sr/^{86}Sr$ ratios were adjusted to the NBS-987 = 0.71024 standard ± 0.2 (95% confidence level). Only results with a 2σ uncertainty of ± 0.000015 were accepted. Duplicate analyses run on samples were within this uncertainty. Nd isotopic ratios were based on the La Jolla $^{143}Nd/^{144}Nd$ = 0.511860 standard. Because the La Trobe TIMS was measuring below this value (e.g., $^{143}Nd/^{144}Nd$ = 0.511850 to 0.511830), 0.000025 was added to all measured $^{143}Nd/^{144}Nd$ values for the SAVF samples to make them compatible with the La Jolla standard.

Measured Pb isotopic ratios were corrected for thermal fractionation by 0.11% per mass unit based on hundreds of runs of Pb standards NBS-981 and NBS-982. Total uncertainties are 0.1% or less based on multiple runs of standards and samples. A separate aliquot of the Pb fractions (taken from the same beaker as the unspiked fraction) was spiked on the TIMS filament with a $^{207}Pb/^{204}Pb$ double-spike to correct for instrumental mass fractionation (see Woodhead *et al*, 1995). Unspiked and spiked runs were done at ^{208}Pb ion currents of at least 10^{-11} amps. Four sets of SRM981 loads were also run with the double-spike and yielded the following double-spike-corrected ratios (±2σ of population):

$^{206}Pb/^{204}Pb$ = 16.934±0.004 (16.937 recommended); $^{207}Pb/^{204}Pb$ = 15.489±0.005 (15.491 recommended); $^{208}Pb/^{204}Pb$ = 36.698±0.012 (36.700* recommended; *as amended by Richards, 1986).

Two repeat dissolutions (for SAB198 and SAB135) give double-spike-corrected ratios that produced results within the range observed for the SRM981 standard. Analytical blanks were on the order of 200 pg and are negligible to the amounts of sample Pb (500-2500 ng).

No age correction was applied to the data due to the young age of the rocks.

Appendix Six: Mineral Chemistry

Appendix 6

Mineral chemical analyses for selected samples

A subset of 52 South Auckland volcanic field samples representing the range of rock types within rock groups A and B was selected for electron microprobe mineral chemical analysis.

Samples from group A according to rock type are:

alkali ol-basalts – SA17, SA18, SA19, SA33, SAB162

transitional basalts – SA07, SA10, SA13

hawaiites – SA20, SA32, SAB151, SAB163

ol-tholeiitic basalts – SA36, SA80, SAB152, SAB169, SAB170, SAB171, SAB172, SAB173, SAB174, SAB181, SAB187

qz-tholeiitic basalts – SA76, SA77, SAB198

Samples from group B according to rock type are:

alkali ol-basalts – SA54, SAB188, SAB207

basanites – SA12, SA27, SA37, SAB102, SAB111, SAB128, SAB175, SAB176, SAB177, SAB178, SAB179, SAB180, SAB204

nephelinites – SA21, SA28, SA51, SAB113, SAB135

ne-hawaiites – SA02, SA25, SA29, SA65

mugearite – SA88

Sample preparation, electron microprobe operation procedures, and data quality and precision of the analyses are described in Appendix 5, Sections A5.1.1 through 5.1.3. Mineral chemical data for the predominant phenocryst and groundmass phases described in Chapters 3 and 4 are presented in Tables A6.1 to A6.19 for group A samples and Tables A6.20 to A6.39 for group B samples in the following order:

- Group A lavas - alkali ol-basalts, transitional basalts, hawaiites, ol-tholeiitic basalts, and qz-tholeiitic basalts: olivine (A6.1 - A6.5), clinopyroxene (A6.6 - A6.10), plagioclase (A6.11 - A6.15), alkali feldspar (A6.16), chromian titanomagnetite (A6.17), titanomagnetite (A6.18), and ilmenite (A6.19).

- Group B lavas - alkali ol-basalts, basanites, nephelinites, ne-hawaiites, mugearite: olivine (A6.20 - 6.24), clinopyroxene (A6.24 - A6.29), plagioclase (A6.30 - A6.34), alkali feldspar (A6.35), nepheline (A6.36), chromian titanomagnetite (A6.37), titamomagnetite (A6.38), and ilmenite (A6.39).

All oxide data are reported as originally analysed and computed by the microprobe software. The microprobe software calculated all cation concentrations on the basis of 10 oxygens. Therefore, cation concentrations were recalculated using the appropriate oxygens per formula unit for each mineral phase. Since this recalculation does not change cation ratios originally derived using 10 oxygens, the recalculated cation concentrations are reported in the tables as original data.

Total iron is reported as FeO for all mineral phases. Estimated Fe^{3+} content and Fe_2O_3 wt% were determined for the ferromagnesian oxides (chromian titanomagnetite, titanomagnetite, and ilmenite) and the iron-bearing silicate (olivine) according to the method described in Droop (1987). The estimated Fe^{3+} content in clinopyroxene was determined according to the method described in Lindsley (1983). Recalculated Fe^{2+} contents and FeO wt%s for Fe^{3+}-corrected analyses for all mineral phases were determined by the method given in Droop (1987). Recalculated Fe^{2+}, Fe^{3+}, FeO, and Fe_2O_3 values are reported in the tables for each mineral.

Total aluminium is reported as Al in each table for all mineral phases. Aluminium in clinopyroxene has been recalculated into Al^{IV} and Al^{VI} according to the procedure given in Lindsley (1983) which assumes that Al^{IV} = 2.000 – Si and Al^{VI} = Al - Al^{IV}. Calculated values for Al^{IV} and Al^{VI} are reported in the clinopyroxene tables.

End-member compositions (expressed as mol.%) for olivine, clinopyroxene, plagioclase and alklai feldspar are based on formula given in (Deer et al, 1993, pp. 683 - 685). End-member compositions for the Cr-Fe-Ti-oxides (e.g. Usp and Ilmenite) were determined using the procedure given in Stormer (1982). All end-member compositions are based on the ideal number of cations per formula unit for the respective mineral and therefore were derived using normalised cation concentrations. Because the calculations for olivine and clinopyroxene end-members require Fe^{3+}, their compositions were derived from Fe^{3+}-corrected analyses.

Nepheline end-member compositions are based on the ternary system (Q) SiO_2 – (Ne) $NaAlSiO_4$ – (Ks) $KAlSiO_4$. Each component of this system can be derived empirically by using the molecular weight of SiO_2, Na_2O, K_2O and Al_2O_3 determined from electron microprobe analyses.

Each chromian titanomagnetite inclusion analysis is accompanied with its host mineral type and the host's corresponding analysis number. The atomic percentages reported for

chromium, magnesium and iron ($Cr^{\#}$, $Mg^{\#}$, and $Fe^{\#}$ respectively) are derived from normalised cation data assuming total cations = 24 per ideal formula unit where,

$Cr^{\#} = 100Cr/(Cr + Al)$,

$Mg^{\#} = 100\ Mg/(Mg + Fe^{2+})$, and

$Fe^{\#} = 100Fe^{3+}/(Fe^{3+} + Cr + Al)$.

Note that cation totals for chromian titanomagnetite and Cr-bearing titanomagnetite (Tables A6.17 and A6.37), and titanomagnetite (Tables A6.18 and A6.38) commonly exceed the idealised 24 cations per formula unit from 1.2 to 14.5%. This cation "excess" may reflect impurities within the crystals or different mineral species whose formula cannot be accurately derived by the microprobe software calculation routine.

Analysis abbreviations are as follows:

Sample	= South Auckland volcanic field sample number
Analysis	= microprobe analysis number
C	= core of phenocryst
R	= rim of phenocryst Note: alphanumeric code (e.g., C1 and R1) used to identify core/rim pairs
G	= groundmass phase
I	= inclusion in another crystal
Fo	= forsterite end-member mol%, olivine
Wo, En, Fs	= wollastonite, enstatite, ferrosilite end-members mole%, clinopyroxene
Or, Ab, An	= orthoclase, albite, anorthite end-members mol%, plagioclase and alkali feldspar
$Cr^{\#}$, $Mg^{\#}$, $Fe^{\#}$	= atomic percentages for chrome, magnesium and iron respectively
Usp	= ulvöspinel, $2Fe_2TiO_4$
Ilm	= ilmenite, $2FeTiO_3$
-	= either no analysis or below detection limit

A6.1 Microprobe analyses of olivine in group A lavas: alkali ol-basalt

Table A6.1 Electron microprobe analyses of olivine for group A alkali ol-basalt

Sample	SA17							SA18									
Analysis	137-C1	138-R1	140-C2	141-R2	424-C3	425-R3	139-G	1772-C1	1773-R1	1776-C2[1]	1777-R2	1794-C3	1795-R3	1774G	1780-G	1785-G	1797-G
SiO_2	38.30	35.79	38.75	35.74	38.84	36.96	35.61	38.33	37.13	37.38	37.16	38.25	37.54	36.78	35.08	34.27	33.83
TiO_2	-	-	-	-	-	-	-	-	-	-	-	-	-	-	-	-	0.20
Al_2O_3	-	-	0.28	-	0.30	-	-	-	-	-	1.00	-	-	-	0.33	-	-
FeO_T	24.76	34.85	23.46	37.22	22.50	33.38	38.62	19.46	26.97	23.65	27.23	20.04	26.44	28.35	37.75	40.23	42.27
MnO	0.31	0.54	-	0.42	-	0.44	0.63	0.22	0.31	0.24	0.30	0.26	0.31	0.27	0.61	0.68	0.72
MgO	36.02	28.61	37.98	26.18	37.97	29.55	25.22	40.68	34.57	36.86	32.81	39.85	34.27	33.34	24.56	22.97	21.19
CaO	0.29	0.47	0.28	0.45	0.28	0.37	0.51	0.25	0.33	0.28	0.33	0.27	0.33	0.33	0.54	0.47	0.55
Total	99.68	100.26	100.75	100.01	99.89	100.70	100.59	98.94	99.31	98.41	98.83	98.67	98.89	99.07	98.87	99.52	98.76
Number of ions on the basis of 4 oxygen																	
Si	1.005	0.972	0.997	0.997	1.009	1.008	0.996	0.991	0.991	0.992	0.996	0.993	1.016	0.992	0.997	0.988	0.989
Ti	-	-	-	-	-	-	-	-	-	-	-	-	-	-	-	-	0.004
Al	-	-	0.008	-	0.009	-	-	-	-	-	0.032	-	-	-	0.011	-	-
Fe^{2+}	0.543	0.792	0.505	0.869	0.489	0.761	0.903	0.420	0.602	0.524	0.610	0.435	0.598	0.640	0.898	0.970	1.034
Mn	0.007	0.012	-	0.010	-	0.010	0.015	0.005	0.007	0.005	0.007	0.006	0.007	0.006	0.015	0.016	0.018
Mg	1.408	1.159	1.457	1.089	1.471	1.202	1.051	1.568	1.376	1.457	1.311	1.542	1.383	1.340	1.040	0.987	0.924
Ca	0.008	0.014	0.008	0.014	0.008	0.011	0.015	0.007	0.010	0.008	0.010	0.008	0.010	0.010	0.016	0.014	0.017
Cations	2.971	2.949	2.974	2.979	2.986	2.992	2.980	2.990	2.986	2.986	2.965	2.984	3.014	2.988	2.978	2.976	2.987
Recalculated Fe ions and oxides																	
Fe^{2+}	0.543	0.792	0.505	0.869	0.489	0.761	0.903	0.420	0.602	0.524	0.610	0.435	0.511	0.640	0.898	0.970	1.034
Fe^{3+}	-	-	-	-	-	-	-	-	-	-	-	-	0.087	-	-	-	-
FeO	24.76	34.85	23.46	37.22	22.50	33.38	38.62	19.46	26.97	23.65	27.23	20.04	22.58	28.35	37.75	40.23	42.27
Fe_2O_3	-	-	-	-	-	-	-	-	-	-	-	-	4.29	-	-	-	-
End-member composition																	
Fo	71.9	59.0	74.3	55.3	75.0	60.9	53.4	78.7	69.3	73.3	68.0	77.8	69.5	67.5	53.3	50.0	46.8

Table A6.1 Electron microprobe analyses of olivine for group A alkali ol-basalt (continued).

Sample	SA19			SA33								SAB162								
Analysis	1992-C	1999-C	2001-C[1]	1704-C1	1706-R1	1709-C2	1710-R2	1711-C3	1712-R3	1725-G	1726-G	1742-C1	1743-R1	1747-C2	1748-R2	1761-C3	1762-R3	1763-C	1767-G	1768-G
SiO_2	37.67	37.34	37.94	38.78	37.32	39.34	37.04	36.70	36.28	34.09	33.97	37.43	36.80	37.46	37.02	37.52	36.19	37.26	35.86	34.81
TiO_2	-	-	-	-	-	-	-	-	-	-	-	-	-	-	-	-	-	-	-	-
Al_2O_3	-	-	-	-	0.26	-	-	-	-	-	-	-	-	-	-	-	-	-	2.12	-
FeO_T	23.94	24.04	23.32	18.71	24.49	18.90	29.50	32.42	31.92	43.11	40.97	25.04	28.70	25.39	27.63	25.55	29.91	25.29	32.28	36.86
MnO	0.24	0.27	0.29	0.24	0.30	0.26	0.35	0.50	0.31	0.60	0.56	0.31	0.38	0.36	0.37	0.30	0.31	0.33	0.44	0.57
MgO	36.92	37.03	36.95	41.22	35.33	41.76	33.13	30.77	30.76	21.80	24.01	36.13	32.80	35.94	33.45	36.36	31.80	36.02	27.21	26.12
CaO	0.28	0.25	0.31	0.24	0.28	0.26	0.31	0.38	0.45	0.42	0.42	0.20	0.33	0.27	0.35	0.24	0.30	0.32	0.56	0.48
Total	99.05	98.93	98.81	99.19	97.98	100.52	100.33	100.77	99.72	100.02	99.93	99.11	99.01	99.42	98.82	99.97	98.51	99.22	98.47	98.84
Number of ions on the basis of 4 oxygen																				
Si	0.992	0.987	1.007	0.994	1.005	0.995	0.990	0.992	0.990	0.986	0.959	0.992	0.996	0.991	1.003	0.988	0.991	0.988	0.999	0.988
Ti	-	-	-	-	-	-	-	-	-	-	-	-	-	-	-	-	-	-	-	-
Al	-	-	-	-	0.008	-	-	-	-	-	-	-	-	-	-	-	-	-	0.070	-
Fe^{2+}	0.528	0.531	0.518	0.401	0.551	0.400	0.660	0.733	0.728	1.042	0.967	0.555	0.650	0.562	0.626	0.563	0.685	0.560	0.752	0.874
Mn	0.005	0.006	0.007	0.005	0.007	0.006	0.008	0.012	0.007	0.015	0.014	0.007	0.009	0.008	0.008	0.007	0.007	0.007	0.010	0.014
Mg	1.450	1.458	1.462	1.576	1.417	1.575	1.320	1.240	1.252	0.940	1.010	1.427	1.323	1.418	1.351	1.428	1.298	1.424	1.130	1.104
Ca	0.008	0.007	0.009	0.007	0.008	0.007	0.009	0.011	0.013	0.013	0.013	0.006	0.010	0.008	0.010	0.007	0.009	0.009	0.017	0.015
Cations	2.983	2.990	3.002	2.983	2.996	2.983	2.987	2.989	2.991	2.996	2.962	2.986	2.987	2.987	2.999	2.992	2.990	2.988	2.978	2.995
Recalculated Fe ions and oxides																				
Fe^{2+}	0.528	0.531	0.489	0.401	0.551	0.400	0.660	0.733	0.728	1.042	0.967	0.555	0.650	0.562	0.626	0.563	0.685	0.560	0.752	0.874
Fe^{3+}	-	-	0.028	-	-	-	-	-	-	-	-	-	-	-	-	-	-	-	-	-
FeO	23.94	24.04	22.05	18.71	24.49	18.90	29.50	32.42	31.92	43.11	40.97	25.04	28.70	25.39	27.63	25.55	29.91	25.29	32.28	36.86
Fe_2O_3	-	-	1.41	-	-	-	-	-	-	-	-	-	-	-	-	-	-	-	-	-
End-member composition																				
Fo	73.1	73.1	73.6	79.5	71.7	79.5	66.4	62.5	63.0	47.1	50.8	71.8	66.8	71.3	68.0	71.5	65.2	71.5	59.7	55.4

A6.2 Microprobe analyses of olivine in group A lavas: transitional basalts

Table A6.2 Electron microprobe analyses of olivine for group A transitional basalt

Sample	SA07						SA10									
Analysis	1889-C1	1890-R1	1895-C2	1896-R2	1904-C3	1906-R3	1808-C1[1]	1809-R1	1811-C2	1812-R2	1823-C3	1824-R3	1815-C[1]	1817-C[1]	1810-G	1832-G
SiO_2	38.40	37.53	38.70	39.49	38.74	35.17	38.30	38.05	38.46	38.06	39.33	38.75	38.31	37.98	37.34	37.62
TiO_2	-	-	-	-	-	-	-	-	-	-	-	-	-	-	-	-
Al_2O_3	-	0.29	-	-	-	3.85	-	-	-	0.30	-	-	-	-	0.32	-
FeO_T	19.74	21.89	19.50	21.16	18.60	40.42	20.99	22.17	18.39	23.03	18.72	20.72	20.89	20.84	31.66	21.59
MnO	0.32	0.31	0.26	0.36	0.26	0.22	0.22	0.29	0.24	0.31	-	0.37	0.27	0.27	0.39	0.30
MgO	40.38	38.07	40.68	37.58	41.25	18.75	38.94	37.83	41.14	36.42	40.28	39.05	39.17	39.16	27.94	38.35
CaO	0.31	0.25	0.23	0.32	0.23	0.58	0.30	0.37	0.25	0.47	0.27	0.73	0.39	0.29	0.63	0.36
Total	99.15	98.34	99.37	98.91	99.08	98.99	98.75	98.71	98.48	98.59	98.60	99.62	99.03	98.54	98.28	98.22
Number of ions on the basis of 4 oxygen																
Si	0.991	0.987	0.994	1.053	0.994	1.072	1.004	1.005	0.993	1.016	1.024	0.999	0.996	0.992	1.059	0.991
Ti	-	-	-	-	-	-	-	-	-	-	-	-	-	-	-	-
Al	-	-	-	-	-	-	-	-	-	0.010	-	-	-	-	0.011	-
Fe^{2+}	0.426	0.482	0.419	0.472	0.399	1.030	0.460	0.490	0.397	0.514	0.408	0.447	0.454	0.455	0.751	0.476
Mn	0.007	0.007	0.006	0.008	0.006	0.006	0.005	0.006	0.005	0.007	-	0.008	0.006	0.006	0.010	0.006
Mg	1.553	1.489	1.558	1.494	1.577	0.852	1.521	1.489	1.584	1.450	1.564	1.501	1.517	1.525	1.182	1.506
Ca	0.009	0.007	0.006	0.009	0.006	0.019	0.008	0.010	0.007	0.014	0.008	0.020	0.011	0.008	0.019	0.010
Cations	2.986	2.972	2.984	3.036	2.982	2.979	2.998	3.000	2.987	3.010	3.004	2.975	2.984	2.987	3.032	2.988
Recalculated Fe ions and oxides																
Fe^{2+}	0.426	0.482	0.419	0.468	0.399	1.030	0.460	0.452	0.397	0.431	0.380	0.447	0.454	0.455	0.751	0.476
Fe^{3+}	-	-	-	0.004	-	-	-	0.038	-	0.084	0.027	-	-	-	-	-
FeO	19.74	21.89	19.50	20.98	18.60	40.42	20.99	20.45	18.39	19.28	17.46	20.72	20.89	20.84	31.66	21.59
Fe_2O_3	-	-	-	0.20	-	-	-	1.91	-	4.17	1.40	-	-	-	-	-
End-member composition																
Fo	78.2	75.3	78.6	75.7	79.6	45.1	76.6	75.0	79.7	73.6	79.3	76.7	76.7	76.8	60.8	75.7

Table A6.2 Electron microprobe analyses of olivine for group A transitional basalts (continued).

Sample	SA13										
Analysis	562-C1	563-R1	571-C2	572-R2	583-C3	584-R3	44-C	45-C	33-G	37-G	47-G
SiO_2	39.88	36.70	39.27	36.18	39.58	36.30	38.99	38.22	34.15	36.09	36.65
TiO_2	-	-	-	-	-	-	-	-	-	-	-
Al_2O_3	-	-	-	-	-	-	-	0.28	-	-	-
FeO_T	18.90	30.72	21.04	30.43	18.67	32.01	21.58	23.40	45.24	37.33	32.09
MnO	-	0.46	-	0.47	0.25	0.41	0.27	0.34	0.78	0.62	0.34
MgO	41.29	32.40	38.47	33.13	41.76	31.09	38.50	37.46	19.32	26.04	30.62
CaO	0.21	0.27	0.24	0.38	0.22	0.31	0.24	0.31	0.42	0.37	0.29
Total	100.28	100.55	99.02	100.59	100.48	100.12	99.58	100.01	99.91	100.45	99.99
Number of ions on the basis of 4 oxygen											
Si	1.014	0.978	1.035	0.952	1.006	0.978	1.007	0.993	0.998	1.002	0.995
Ti	-	-	-	-	-	-	-	-	-	-	-
Al	-	-	-	-	-	-	-	0.008	-	-	-
Fe^{2+}	0.402	0.685	0.464	0.670	0.396	0.722	0.466	0.509	1.106	0.867	0.729
Mn	-	0.010	-	0.010	0.005	0.009	0.006	0.008	0.019	0.014	0.008
Mg	1.565	1.287	1.512	1.300	1.581	1.249	1.482	1.452	0.842	1.078	1.240
Ca	0.006	0.008	0.007	0.010	0.006	0.009	0.007	0.008	0.013	0.011	0.008
Cations	2.986	2.969	3.017	2.943	2.994	2.967	2.968	2.978	2.978	2.973	2.980
Recalculated Fe ions and oxides											
Fe^{2+}	0.402	0.685	0.462	0.670	0.396	0.722	0.466	0.509	1.106	0.867	0.729
Fe^{3+}	-	-	0.002	-	-	-	-	-	-	-	-
FeO	18.90	30.72	20.95	30.43	18.67	32.01	21.58	23.40	45.24	37.33	32.09
Fe_2O_3	-	-	0.10	-	-	-	-	-	-	-	-
End-member composition											
Fo	79.6	64.9	76.5	65.7	79.7	63.1	75.8	73.8	42.8	55.0	62.7

A6.3 Microprobe analyses of olivine in group A lavas: hawaiites

Table A6.3 Electron microprobe analyses of olivine for group A hawaiites

Sample	SA20								SA32											
Analysis	1858-C1	1859-R1	1879-C	1880-C	1849-G	1862-G	1863-G	1871-G	1919-C1	1920-R1	1921-C2	1922-R2	1923-C3	1924-R3	1925-C4	1926-R4	1930-G	1933-G	1940-G	1941-G
SiO_2	36.68	35.59	39.70	38.86	30.90	34.14	33.37	32.48	37.00	37.30	36.84	37.03	39.27	36.30	37.90	36.55	31.09	34.61	33.50	33.31
TiO_2	-	-	-	0.27	-	-	-	-	-	-	-	-	-	-	-	-	-	-	-	-
Al_2O_3	-	-	0.53	0.45	-	-	-	-	-	-	-	-	-	-	-	-	-	-	-	-
FeO_T	31.92	36.69	30.93	26.05	57.84	43.86	46.10	52.17	28.60	26.87	28.96	28.52	17.11	29.48	23.52	28.61	56.39	40.23	43.27	46.02
MnO	0.37	0.45	0.27	-	1.00	0.53	0.65	0.82	0.33	0.46	0.31	0.38	-	0.37	0.30	0.36	1.06	0.59	0.67	0.72
MgO	31.18	26.56	26.96	32.63	8.88	21.28	19.88	13.77	33.29	34.87	32.79	33.91	42.16	32.47	37.53	33.55	9.45	23.58	20.35	18.26
CaO	0.36	0.40	0.24	0.29	0.56	0.47	0.43	0.55	0.39	0.38	0.35	0.40	0.26	0.42	0.36	0.35	0.78	0.59	0.53	0.62
Total	100.51	99.69	98.63	98.55	99.18	100.28	100.43	99.79	99.61	99.88	99.25	100.24	98.80	99.04	99.61	99.42	98.77	99.60	98.32	98.93
Number of ions on the basis of 4 oxygen																				
Si	0.991	0.995	1.130	1.062	0.982	0.988	0.964	0.992	0.993	0.990	0.995	0.987	1.009	0.987	0.992	0.984	0.981	0.990	0.992	1.000
Ti	-	-	-	0.006	-	-	-	-	-	-	-	-	-	-	-	-	-	-	-	-
Al	-	-	-	-	-	-	-	-	-	-	-	-	-	-	-	-	-	-	-	-
Fe^{2+}	0.722	0.858	0.736	0.596	1.536	1.062	1.114	1.333	0.642	0.596	0.654	0.636	0.368	0.670	0.515	0.644	1.489	0.963	1.071	1.155
Mn	0.008	0.011	0.006	-	0.027	0.013	0.016	0.021	0.008	0.010	0.008	0.008	-	0.008	0.007	0.008	0.028	0.014	0.017	0.018
Mg	1.256	1.107	1.144	1.330	0.420	0.918	0.856	0.627	1.332	1.380	1.320	1.348	1.614	1.316	1.464	1.347	0.444	1.006	0.898	0.817
Ca	0.010	0.012	0.007	0.008	0.019	0.014	0.013	0.018	0.011	0.011	0.010	0.012	0.007	0.012	0.010	0.010	0.026	0.018	0.017	0.020
Cations	2.988	2.983	3.023	3.001	2.984	2.996	2.964	2.992	2.986	2.988	2.986	2.991	2.998	2.994	2.987	2.994	2.969	2.991	2.994	3.011
Recalculated Fe ions and oxides																				
Fe^{2+}	0.722	0.858	0.726	0.535	1.536	1.062	1.114	1.333	0.642	0.596	0.654	0.636	0.368	0.670	0.515	0.644	1.489	0.963	1.071	1.061
Fe^{3+}	-	-	0.010	0.060	-	-	-	-	-	-	-	-	-	-	-	-	-	-	-	0.094
FeO	31.92	36.69	30.52	23.41	57.84	43.86	46.10	52.17	28.60	26.87	28.96	28.52	17.11	29.48	23.52	28.61	56.39	40.23	43.27	42.27
Fe_2O_3	-	-	0.45	2.93	-	-	-	-	-	-	-	-	-	-	-	-	-	-	-	4.17
End-member composition																				
Fo	63.2	56.0	60.6	69.1	21.2	46.1	43.1	31.7	67.2	69.5	66.6	67.7	81.4	66.0	73.7	67.4	22.7	50.7	45.2	41.0

Table A6.3 Electron microprobe analyses of olivine for group A hawaiites (continued).

Sample	SAB151						SAB163									
Analysis	197-C1	198-R1	211-C2	212-R2	669-C3	670-R3	1956-C1	1957-R1	1976-C2	1977-R2	1982-C3	1983-R3	1964-G	1968-G	1972-G	1979-G
SiO_2	39.31	34.89	36.96	35.37	38.68	37.14	37.11	36.12	37.52	37.10	37.17	35.78	34.70	32.70	34.30	34.44
TiO_2	-	-	-	-	-	-	-	-	-	-	-	-	-	-	-	-
Al_2O_3	-	0.43	-	0.32	-	-	-	-	-	-	-	-	-	-	-	-
FeO_T	20.07	36.56	30.84	35.45	20.47	30.74	25.73	33.95	25.02	30.17	28.13	37.04	40.72	49.90	40.45	41.74
MnO	0.32	0.52	0.39	0.49	0.24	0.28	0.35	0.44	0.28	0.45	0.26	0.48	0.68	0.73	0.67	0.68
MgO	40.48	25.27	31.20	28.35	39.85	31.64	36.81	30.03	36.83	32.77	34.07	26.33	23.55	15.57	23.59	22.61
CaO	0.24	0.38	0.30	0.35	0.27	0.33	0.26	0.39	0.32	0.40	0.27	0.46	0.50	0.63	0.51	0.57
Total	100.42	98.05	99.69	100.33	99.51	100.13	100.26	100.93	99.97	100.89	99.90	100.09	100.15	99.53	99.52	100.04
Number of ions on the basis of 4 oxygen																
Si	1.000	0.994	1.000	0.963	1.002	0.992	0.964	0.984	0.985	0.991	0.991	0.998	0.989	0.989	0.984	0.988
Ti	-	-	-	-	-	-	-	-	-	-	-	-	-	-	-	-
Al	-	0.014	-	0.010	-	-	-	-	-	-	-	-	-	-	-	-
Fe^{2+}	0.427	0.871	0.698	0.808	0.444	0.687	0.559	0.773	0.549	0.674	0.628	0.864	0.970	1.262	0.971	1.001
Mn	0.007	0.012	0.009	0.011	0.005	0.006	0.008	0.010	0.006	0.010	0.006	0.011	0.016	0.019	0.016	0.016
Mg	1.535	1.072	1.259	1.151	1.539	1.260	1.425	1.219	1.441	1.304	1.354	1.094	1.000	0.702	1.013	0.967
Ca	0.007	0.012	0.009	0.010	0.008	0.010	0.007	0.011	0.009	0.011	0.008	0.014	0.015	0.020	0.016	0.017
Cations	2.976	2.975	2.976	2.954	2.998	2.954	2.962	2.997	2.990	2.990	2.987	2.981	2.991	2.993	3.000	2.990
Recalculated Fe ions and oxides																
Fe^{2+}	0.427	0.871	0.698	0.808	0.444	0.687	0.559	0.773	0.549	0.674	0.628	0.864	0.970	1.262	0.971	1.001
Fe^{3+}	-	-	-	-	-	-	-	-	-	-	-	-	-	-	-	-
FeO	20.07	36.56	30.84	35.45	20.47	30.74	25.73	33.95	25.02	30.17	28.13	37.04	40.72	49.90	40.45	41.74
Fe_2O_3	-	-	-	-	-	-	-	-	-	-	-	-	-	-	-	-
End-member composition																
Fo	78.0	54.8	64.0	58.4	77.4	64.5	71.6	60.9	72.2	65.6	68.1	55.6	50.3	35.4	50.6	48.7

A6.4 Microprobe analyses of olivine in group A lavas: ol-tholeiitic basalts

Table A6.4 Electron microprobe analyses of olivine for group A ol-tholeiitic basalts

Sample	SA80							SAB152					
Analysis	115-C1	116-R1	119-C2	120-R2	541-C3	543-R3	118-G	247-C1	248-R1	250-C2	251-R2	701-C3	702-R3
SiO_2	38.43	37.27	39.13	37.64	39.71	38.15	37.95	38.92	37.76	39.23	36.19	39.77	35.36
TiO_2	-	-	-	-	-	-	-	-	-	-	-	-	-
Al_2O_3	-	-	-	-	0.33	-	0.28	-	-	0.29	-	-	-
FeO_T	23.53	30.36	20.69	26.61	17.90	26.53	25.64	21.55	28.64	18.73	34.54	19.14	38.61
MnO	0.36	0.33	-	0.29	-	0.47	0.31	0.23	0.37	0.23	0.43	0.30	0.48
MgO	37.24	32.06	39.78	34.12	41.78	34.76	35.67	39.19	33.38	40.63	27.27	41.15	24.82
CaO	0.22	0.33	0.27	0.25	0.18	0.34	0.28	0.22	0.30	0.22	0.38	0.21	0.37
Total	99.78	100.35	99.87	98.91	99.90	100.25	100.13	100.11	100.45	99.33	98.81	100.57	99.64
Number of ions on the basis of 4 oxygen													
Si	1.001	0.999	1.003	1.005	1.009	1.010	0.995	1.000	1.002	1.002	1.016	1.011	1.004
Ti	-	-	-	-	-	-	-	-	-	-	-	-	-
Al	-	-	-	-	0.010	-	0.009	-	-	0.009	-	-	-
Fe^{2+}	0.513	0.680	0.444	0.594	0.380	0.588	0.562	0.463	0.636	0.400	0.811	0.407	0.917
Mn	0.008	0.008	-	0.006	-	0.010	0.007	0.005	0.008	0.005	0.010	0.006	0.012
Mg	1.446	1.281	1.520	1.358	1.582	1.372	1.395	1.502	1.320	1.547	1.141	1.559	1.051
Ca	0.006	0.010	0.008	0.007	0.005	0.010	0.008	0.006	0.008	0.006	0.012	0.006	0.011
Cations	2.974	2.977	2.974	2.971	2.986	2.990	2.976	2.976	2.974	2.970	2.989	2.989	2.996
Recalculated Fe ions and oxides													
Fe^{2+}	0.513	0.680	0.444	0.594	0.380	0.588	0.562	0.463	0.636	0.400	0.811	0.407	0.917
Fe^{3+}	-	-	-	-	-	-	-	-	-	-	-	-	-
FeO	23.53	30.36	20.69	26.61	17.90	26.53	25.64	21.55	28.64	18.73	34.54	19.14	38.61
Fe_2O_3	-	-	-	-	-	-	-	-	-	-	-	-	-
End-member composition													
Fo	73.5	65.1	77.4	69.3	80.6	69.6	71.0	76.2	67.2	79.2	58.2	79.1	53.1

Table A6.4 Electron microprobe analyses of olivine for group A ol-tholeiitic basalts (continued).

Sample	SAB169								SA36									
Analysis	17-C1	18-R1	20-C2	21-R2	420-C3	421-R3	19-C	27-C	800-C1	801-R1	804-C2	805-R2	808-C3	809-R3	802-C	803-C	806-C	807-C
SiO_2	38.14	37.06	37.95	35.88	38.58	37.22	38.00	36.56	39.27	36.34	39.04	38.48	39.11	37.17	37.48	38.14	38.88	38.43
TiO_2	-	-	-	-	-	-	-	-	-	-	-	-	-	-	-	-	-	-
Al_2O_3	-	-	-	0.35	-	-	-	-	-	0.30	0.32	0.34	0.36	-	0.32	-	-	-
FeO_T	25.85	28.31	26.78	32.25	24.75	31.17	26.68	31.31	18.35	38.12	18.40	21.33	18.34	26.80	27.04	24.03	19.67	21.72
MnO	0.32	0.26	0.37	0.43	0.25	0.49	0.36	0.49	0.26	0.31	-	0.27	-	0.27	0.35	0.31	-	0.28
MgO	35.59	34.35	35.11	30.72	37.15	31.38	35.22	30.38	42.11	23.52	42.42	39.61	42.37	34.92	35.13	37.70	40.90	39.60
CaO	0.21	0.32	0.23	0.47	0.22	0.43	0.22	0.42	0.16	0.35	0.26	0.19	0.23	0.26	0.27	0.24	0.26	0.25
Total	100.11	100.30	100.44	100.10	100.95	100.69	100.48	99.16	100.15	98.94	100.44	100.22	100.41	99.42	100.59	100.42	99.71	100.28
Number of ions on the basis of 4 oxygen																		
Si	1.001	0.972	0.998	0.964	1.004	1.005	0.998	0.999	1.000	1.040	0.989	0.994	0.991	0.996	0.992	0.996	1.000	0.994
Ti	-	-	-	-	-	-	-	-	-	-	-	-	-	-	-	-	-	-
Al	-	-	-	0.011	-	-	-	-	-	0.010	0.010	0.010	0.011	-	0.010	-	-	-
Fe^{2+}	0.568	0.621	0.589	0.724	0.539	0.704	0.586	0.716	0.391	0.912	0.390	0.461	0.388	0.600	0.599	0.525	0.423	0.470
Mn	0.007	0.006	0.008	0.010	0.006	0.011	0.008	0.011	0.006	0.008	-	0.006	-	0.006	0.008	0.007	-	0.006
Mg	1.393	1.343	1.376	1.230	1.442	1.263	1.380	1.238	1.599	1.004	1.602	1.525	1.600	1.395	1.386	1.468	1.569	1.528
Ca	0.006	0.009	0.006	0.014	0.006	0.012	0.006	0.012	0.004	0.011	0.007	0.005	0.006	0.007	0.008	0.007	0.007	0.007
Cations	2.975	2.952	2.978	2.953	2.996	2.995	2.978	2.976	3.000	2.984	2.997	3.001	2.996	3.004	3.003	3.004	3.000	3.006
Recalculated Fe ions and oxides																		
Fe^{2+}	0.568	0.621	0.589	0.724	0.539	0.704	0.586	0.716	0.391	0.912	0.390	0.451	0.388	0.585	0.553	0.518	0.423	0.468
Fe^{3+}	-	-	-	-	-	-	-	-	-	-	-	0.010	-	0.015	0.045	0.007	-	0.002
FeO	25.85	28.31	26.78	32.25	24.75	31.17	26.68	31.31	18.35	38.12	18.40	20.89	18.34	26.13	24.99	23.69	19.67	21.62
Fe_2O_3	-	-	-	-	-	-	-	-	-	-	-	0.49	-	0.74	2.28	0.38	-	0.11
End-member composition																		
Fo	70.8	68.2	69.7	62.6	72.6	63.9	69.9	63.0	80.1	52.2	80.4	76.6	80.5	69.7	69.6	73.4	78.8	76.2

Table A6.4 Electron microprobe analyses of olivine for group A ol-tholeiitic basalts (continued).

Sample	SAB170												SAB171					
Analysis	864-C1	866-R1	867-C2	868-R2	882-C3	883-R3	860-C	862-C	872-C	881-G	884-G	888-G	939-C1	940-R1	943-C2	944-R2	976-C3	978-R3
SiO_2	38.97	38.44	38.52	38.36	38.79	37.73	39.15	38.85	38.34	37.43	37.62	37.73	37.88	36.67	38.85	36.88	37.93	36.30
TiO_2	-	-	-	-	-	-	-	-	-	-	-	-	-	-	-	-	-	-
Al_2O_3	0.38	0.39	-	0.27	0.33	-	-	-	0.52	-	-	-	-	-	-	-	0.32	-
FeO_T	18.40	20.96	19.51	21.11	19.35	23.48	18.69	18.33	20.57	25.76	25.87	25.71	25.07	29.25	19.90	28.75	22.33	34.70
MnO	-	0.31	0.29	-	0.22	0.27	0.25	0.30	0.29	0.35	0.38	0.30	0.38	0.35	-	0.33	0.26	0.47
MgO	41.95	40.19	40.96	39.68	41.12	37.45	41.92	41.23	40.06	35.79	35.83	35.86	36.58	32.27	40.67	32.95	38.31	28.88
CaO	0.20	0.26	0.20	0.24	0.20	0.28	0.25	0.27	0.28	0.37	0.38	0.33	0.24	0.29	0.27	0.27	0.26	0.29
Total	99.90	100.55	99.48	99.66	100.01	99.21	100.26	98.98	100.06	99.70	100.08	99.93	100.15	98.83	99.69	99.18	99.41	100.64
Number of ions on the basis of 4 oxygen																		
Si	0.992	0.988	0.993	0.995	0.994	0.996	0.998	1.002	0.989	0.995	0.996	0.999	0.998	1.008	1.001	1.000	0.994	0.999
Ti	-	-	-	-	-	-	-	-	-	-	-	-	-	-	-	-	-	-
Al	0.012	0.012	-	0.008	0.010	-	-	-	0.016	-	-	-	-	-	-	-	0.010	-
Fe^{2+}	0.392	0.451	0.421	0.458	0.415	0.518	0.398	0.396	0.444	0.573	0.573	0.570	0.552	0.672	0.429	0.652	0.489	0.798
Mn	-	0.007	0.006	-	0.005	0.006	0.006	0.006	0.006	0.008	0.009	0.007	0.008	0.008	-	0.008	0.006	0.011
Mg	1.592	1.540	1.574	1.534	1.571	1.475	1.593	1.586	1.540	1.418	1.415	1.416	1.436	1.322	1.562	1.332	1.496	1.184
Ca	0.006	0.007	0.006	0.006	0.006	0.008	0.007	0.007	0.008	0.010	0.011	0.010	0.007	0.008	0.008	0.008	0.007	0.009
Cations	2.994	3.006	3.000	3.002	3.001	3.004	3.002	2.998	3.003	3.005	3.004	3.001	3.002	3.019	3.000	3.000	3.001	3.002
Recalculated Fe ions and oxides																		
Fe^{2+}	0.392	0.445	0.406	0.457	0.402	0.516	0.387	0.396	0.439	0.565	0.563	0.560	0.513	0.667	0.429	0.652	0.476	0.795
Fe^{3+}	-	0.005	0.015	0.001	0.013	0.002	0.012	-	0.004	0.007	0.010	0.010	0.039	0.005	-	-	0.013	0.003
FeO	18.40	20.71	18.82	21.06	18.75	23.38	18.14	18.33	20.37	25.42	25.44	25.28	23.29	29.02	19.90	28.75	21.75	34.56
Fe_2O_3	-	0.28	0.77	0.05	0.66	0.11	0.61	-	0.22	0.37	0.48	0.48	1.98	0.26	-	-	0.65	0.15
End-member composition																		
Fo	80.2	77.1	78.7	77.0	78.9	73.8	79.8	79.8	77.4	70.9	70.9	71.1	71.9	66.0	78.5	66.9	75.1	59.4

Table A6.4 Electron microprobe analyses of olivine for group A ol-tholeiitic basalts (continued).

Sample	SAB171 (continued)					SAB172											
Analysis	981-C4	982-R4	941-C	971-C	972-C	93-C1	94-R1	99-C2	100-R2	603-C3	604-R3	101-G	927-G	928-G	929-G	930-G	934-G
SiO_2	37.04	36.56	37.96	37.91	36.77	38.86	36.12	39.74	38.81	39.73	39.69	33.42	34.08	36.17	34.97	35.17	37.32
TiO_2	-	-	-	-	-	-	-	-	-	-	0.21	0.24	-	-	-	-	-
Al_2O_3	-	-	0.33	-	-	-	-	0.29	-	-	-	0.64	0.27	-	-	0.27	-
FeO_T	25.81	30.51	23.84	22.76	28.65	22.76	32.86	18.08	21.88	17.76	31.24	51.16	42.22	30.61	39.59	35.90	26.85
MnO	0.28	0.35	0.24	0.24	0.32	0.28	0.45	-	0.28	0.25	0.41	0.68	0.52	0.45	0.38	0.43	0.27
MgO	35.50	31.34	36.95	38.74	33.35	37.88	30.45	41.91	38.87	42.18	27.46	13.68	21.04	31.23	23.23	26.96	34.02
CaO	0.27	0.30	0.26	0.29	0.25	0.30	0.33	0.19	0.25	0.30	1.33	0.39	0.36	0.35	0.35	0.33	0.36
Total	98.90	99.06	99.58	99.94	99.34	100.08	100.21	100.21	100.09	100.22	100.34	100.21	98.49	98.81	98.52	99.06	98.82
Number of ions on the basis of 4 oxygen																	
Si	0.994	1.002	0.999	0.990	0.995	1.005	0.971	1.001	1.000	1.008	1.069	1.003	1.009	1.003	1.026	0.992	1.013
Ti	-	-	-	-	-	-	-	-	-	-	0.004	0.005	-	-	-	-	-
Al	-	-	0.010	-	-	-	-	0.008	-	-	-	0.023	0.010	-	-	0.009	-
Fe^{2+}	0.579	0.699	0.525	0.497	0.649	0.492	0.739	0.381	0.471	0.377	0.704	1.284	1.045	0.710	0.971	0.847	0.609
Mn	0.006	0.008	0.005	0.005	0.008	0.006	0.010	-	0.006	0.005	0.009	0.017	0.013	0.011	0.010	0.010	0.006
Mg	1.420	1.280	1.450	1.509	1.346	1.460	1.221	1.574	1.493	1.595	1.102	0.612	0.928	1.291	1.016	1.134	1.376
Ca	0.008	0.009	0.007	0.008	0.007	0.008	0.010	0.005	0.007	0.008	0.038	0.013	0.012	0.010	0.011	0.010	0.010
Cations	3.006	2.998	2.996	3.010	3.005	2.972	2.951	2.970	2.976	2.992	2.927	2.956	3.017	3.025	3.033	3.003	3.015
Recalculated Fe ions and oxides																	
Fe^{2+}	0.575	0.699	0.525	0.447	0.623	0.492	0.739	0.381	0.471	0.377	0.704	1.284	1.023	0.665	0.905	0.759	0.601
Fe^{3+}	0.004	-	-	0.050	0.026	-	-	-	-	-	-	-	0.022	0.045	0.066	0.088	0.009
FeO	25.62	30.51	23.84	20.46	27.52	22.76	32.86	18.08	21.88	17.76	31.24	51.16	41.32	28.69	36.89	32.17	26.47
Fe_2O_3	0.21	-	-	2.55	1.25	-	-	-	-	-	-	-	1.00	2.13	3.00	4.14	0.42
End-member composition																	
Fo	70.8	64.4	73.2	75.0	67.2	74.6	62.0	80.5	75.8	80.7	60.7	32.0	46.7	64.2	50.9	56.9	69.1

Table A6.4 Electron microprobe analyses of olivine for group A ol-tholeiitic basalts (continued).

Sample	SAB173														SAB174				
Analysis	983-C1	985-R1	986-C2	987-R2	1014-C3	1016-R3	1011-C	1013-C	998-G	1000-G	1001-G	1004-G	1007-G	1019-G	1066-C1	1067-R1	1079-C2	1080-R2	1086-C3
SiO_2	38.48	35.69	38.33	36.29	37.02	34.13	36.96	37.17	34.21	35.19	34.56	34.03	34.45	36.03	39.16	37.66	37.98	37.72	38.25
TiO_2	-	0.22	-	-	-	-	-	-	-	-	-	-	-	-	-	-	-	-	-
Al_2O_3	-	-	0.27	0.28	-	-	-	-	-	-	-	-	2.67	0.42	0.31	-	-	0.28	0.29
FeO_T	18.67	35.58	20.60	31.32	27.25	42.05	31.16	26.02	42.70	37.04	42.22	44.30	45.10	29.87	17.98	24.52	23.64	25.87	21.79
MnO	0.22	0.43	-	0.35	0.36	0.45	0.29	0.32	0.62	0.36	0.49	0.47	0.62	0.48	-	0.36	0.22	0.30	0.27
MgO	41.28	27.19	39.52	31.20	34.41	22.28	30.36	36.11	21.83	26.66	23.04	20.03	15.68	31.38	41.86	36.51	37.83	36.26	39.71
CaO	0.24	0.28	0.24	0.24	0.19	0.27	0.21	0.30	0.32	0.34	0.30	0.38	0.43	0.33	0.23	0.29	0.21	0.32	0.19
Total	98.89	99.39	98.96	99.68	99.23	99.18	98.98	99.92	99.68	99.59	100.61	99.21	98.95	98.51	99.54	99.34	99.88	100.75	100.50
Number of ions on the basis of 4 oxygen																			
Si	0.996	1.000	0.997	0.992	0.994	0.994	1.029	0.988	0.995	0.993	0.991	1.002	1.054	0.992	1.000	0.998	0.996	0.991	0.982
Ti	-	0.005	-	-	-	-	-	-	-	-	-	-	-	-	-	-	-	-	-
Al	-	-	0.008	0.009	-	-	-	-	-	-	-	-	0.096	0.014	0.009	-	-	0.009	0.009
Fe^{2+}	0.404	0.834	0.448	0.716	0.612	1.024	0.725	0.578	1.039	0.874	1.012	1.092	1.154	0.688	0.384	0.544	0.518	0.568	0.468
Mn	0.005	0.010	-	0.008	0.008	0.011	0.007	0.007	0.015	0.009	0.012	0.012	0.016	0.011	-	0.008	0.005	0.007	0.006
Mg	1.592	1.136	1.532	1.271	1.378	0.968	1.260	1.430	0.946	1.121	0.984	0.880	0.716	1.288	1.594	1.443	1.479	1.420	1.519
Ca	0.007	0.008	0.007	0.007	0.006	0.008	0.006	0.008	0.010	0.010	0.009	0.012	0.014	0.010	0.006	0.008	0.006	0.009	0.005
Cations	3.004	2.995	2.992	3.004	2.998	3.006	3.027	3.012	3.005	3.007	3.009	2.997	3.050	3.001	2.994	3.002	3.004	3.005	2.988
Recalculated Fe ions and oxides																			
Fe^{2+}	0.387	0.834	0.448	0.705	0.612	0.991	0.593	0.508	1.029	0.860	0.993	1.092	1.130	0.672	0.384	0.527	0.514	0.558	0.468
Fe^{3+}	0.017	-	-	0.011	-	0.033	0.132	0.070	0.010	0.014	0.019	-	0.024	0.016	-	0.017	0.004	0.011	-
FeO	17.88	35.58	20.60	30.85	27.25	40.70	25.47	22.85	42.31	36.45	41.42	44.30	44.14	29.18	17.98	23.75	23.45	25.39	21.79
Fe_2O_3	0.87	-	-	0.52	-	1.50	6.32	3.52	0.44	0.65	0.89	-	1.06	0.77	-	0.85	0.22	0.54	-
End-member composition																			
Fo	79.6	57.4	77.4	63.7	68.9	48.3	63.2	71.0	47.3	55.9	49.0	44.4	37.9	64.8	80.6	72.3	73.9	71.2	76.2

Table A6.4 Electron microprobe analyses of olivine for group A ol-tholeiitic basalts (continued).

Sample	SAB174 (continued)											
Analysis	1087-R3	1088-C	1091-C	1092-C	1093-C	1090-G	1094-G	1095-G	1098-G	1099-G	1102-G	1103-G
SiO_2	37.77	37.86	38.13	38.67	38.72	38.09	38.33	37.21	35.68	38.64	32.64	34.20
TiO_2	-	-	-	-	-	-	-	-	-	-	-	-
Al_2O_3	0.41	0.46	0.41	0.29	0.31	-	0.34	0.29	0.39	1.05	-	0.27
FeO_T	24.79	22.80	21.14	21.00	20.64	25.33	23.19	26.20	36.01	30.11	52.77	42.65
MnO	0.31	0.29	0.28	-	0.27	0.30	0.32	0.37	0.36	0.38	0.61	0.49
MgO	36.33	37.89	39.04	40.53	40.17	35.33	38.12	34.79	27.44	28.17	13.50	21.82
CaO	0.39	0.31	0.26	0.22	0.26	1.11	0.32	0.32	0.49	0.52	0.50	0.43
Total	10-	99.61	99.26	100.71	100.37	100.16	100.62	99.18	100.37	98.87	100.02	99.86
Number of ions on the basis of 4 oxygen												
Si	0.995	0.992	0.994	0.991	0.995	1.006	0.995	0.996	0.992	1.087	1.000	0.992
Ti	-	-	-	-	-	-	-	-	-	-	-	-
Al	0.013	0.014	0.013	0.009	0.010	-	0.010	0.009	0.013	0.035	-	0.009
Fe^{2+}	0.546	0.500	0.461	0.450	0.444	0.559	0.503	0.587	0.837	0.708	1.352	1.034
Mn	0.007	0.006	0.006	-	0.006	0.007	0.007	0.008	0.008	0.009	0.016	0.012
Mg	1.427	1.480	1.518	1.549	1.539	1.391	1.475	1.389	1.137	1.181	0.616	0.944
Ca	0.011	0.008	0.007	0.006	0.007	0.032	0.009	0.009	0.015	0.016	0.016	0.013
Cations	2.998	3.001	3.000	3.005	3.001	2.994	3.000	2.999	3.002	3.036	3.000	3.004
Recalculated Fe ions and oxides												
Fe^{2+}	0.546	0.487	0.461	0.448	0.431	0.559	0.503	0.587	0.835	0.702	1.257	1.033
Fe^{3+}	-	0.013	-	0.002	0.013	-	-	-	0.002	0.006	0.095	0.001
FeO	24.79	22.22	21.14	20.90	20.05	25.33	23.19	26.20	35.92	29.84	49.07	42.61
Fe_2O_3	-	0.65	-	0.11	0.66	-	-	-	0.10	0.30	4.11	0.05
End-member composition												
Fo	72.1	74.5	76.4	77.5	77.4	71.1	74.3	70.0	57.4	62.2	31.1	47.4

Table A6.4 Electron microprobe analyses of olivine for group A ol-tholeiitic basalts (continued).

Sample	SAB181								SAB187					
Analysis	181-C1	182-R1	190-C2	191-R2	520-C3	521-R3	183-C	518-C	264-C1	265-R1	274-C2	275-R2	526-C3	527-R3
SiO_2	39.20	36.92	39.27	37.64	38.87	37.94	36.12	38.87	37.14	37.14	36.08	36.61	39.73	36.57
TiO_2	-	-	-	-	-	-	-	-	-	-	-	-	-	-
Al_2O_3	-	0.33	-	-	0.29	0.31	-	-	-	-	-	-	-	-
FeO_T	21.62	31.69	20.52	28.17	21.56	24.51	33.36	21.63	29.29	32.01	35.14	34.50	17.82	33.47
MnO	0.23	0.26	0.24	0.36	0.25	0.29	0.42	0.28	0.31	0.40	0.41	0.43	0.27	0.35
MgO	38.99	30.21	39.94	33.80	38.62	35.54	28.90	38.47	32.79	30.41	28.00	28.54	41.84	29.39
CaO	0.17	0.36	0.23	0.26	0.22	0.23	0.28	0.20	0.34	0.33	0.29	0.33	0.27	0.25
Total	100.21	99.77	100.20	100.23	99.81	98.82	99.08	99.45	99.87	100.29	99.92	100.41	99.93	100.03
Number of ions on the basis of 4 oxygen														
Si	1.006	1.002	1.003	0.999	1.008	1.009	0.998	1.012	0.996	1.004	0.996	1.002	1.010	1.006
Ti	-	-	-	-	-	-	-	-	-	-	-	-	-	-
Al	-	0.010	-	-	0.009	0.010	-	-	-	-	-	-	-	-
Fe^{2+}	0.464	0.719	0.438	0.625	0.468	0.545	0.771	0.471	0.657	0.724	0.812	0.789	0.379	0.770
Mn	0.005	0.006	0.005	0.008	0.006	0.006	0.010	0.006	0.007	0.009	0.010	0.010	0.006	0.008
Mg	1.491	1.222	1.520	1.338	1.493	1.409	1.191	1.493	1.311	1.226	1.153	1.164	1.587	1.204
Ca	0.005	0.010	0.006	0.007	0.006	0.007	0.008	0.006	0.010	0.010	0.009	0.010	0.007	0.007
Cations	2.970	2.969	2.973	2.977	2.988	2.986	2.978	2.988	2.980	2.972	2.980	2.974	2.990	2.995
Recalculated Fe ions and oxides														
Fe^{2+}	0.464	0.719	0.438	0.625	0.468	0.545	0.771	0.471	0.657	0.724	0.812	0.789	0.379	0.770
Fe^{3+}	-	-	-	-	-	-	-	-	-	-	-	-	-	-
FeO	21.62	31.69	20.52	28.17	21.56	24.51	33.36	21.63	29.29	32.01	35.14	34.50	17.82	33.47
Fe_2O_3	-	-	-	-	-	-	-	-	-	-	-	-	-	-
End-member composition														
Fo	76.1	62.7	77.4	67.9	75.9	71.9	60.4	75.8	66.4	62.6	58.4	59.3	80.5	60.8

A6.5 Microprobe analyses of olivine in group A: qz-tholeiitic basalts

Table A6.5 Electron microprobe analyses of olivine for group A qz-tholeiitic basalts.

Sample	SA76							SA77					
Analysis	124-C1	125-R1	132-C2	133-R2	465-C3	466-R3	134-G	169-C1	170-R1	177-C2	178-R2	625-C3	626-R3
SiO_2	39.53	38.34	38.50	37.18	39.88	39.32	36.99	39.47	38.30	39.55	39.63	39.94	39.18
TiO_2	-	-	-	-	-	-	-	-	-	-	-	-	-
Al_2O_3	-	0.29	-	-	-	-	-	-	-	0.34	-	-	-
FeO_T	17.27	22.18	23.50	23.97	17.35	20.55	30.57	19.70	24.22	16.95	19.89	16.53	20.87
MnO	0.26	0.27	0.32	0.30	-	0.34	0.38	0.23	0.28	-	0.32	0.23	0.25
MgO	42.34	39.09	38.11	37.74	42.39	40.14	31.42	40.69	37.61	43.04	40.84	43.20	39.80
CaO	0.21	0.20	0.27	0.30	0.20	0.26	0.34	0.26	0.28	0.27	0.27	0.19	0.26
Total	99.61	100.37	100.70	99.49	99.82	100.61	99.70	100.35	100.69	100.15	100.95	100.09	100.36
Number of ions on the basis of 4 oxygen													
Si	1.001	0.974	0.994	0.957	1.012	1.007	1.000	1.002	0.980	0.981	1.002	1.008	1.007
Ti	-	-	-	-	-	-	-	-	-	-	-	-	-
Al	-	0.009	-	-	-	-	-	-	-	0.010	-	-	-
Fe^{2+}	0.366	0.471	0.507	0.516	0.368	0.440	0.691	0.418	0.518	0.352	0.420	0.349	0.449
Mn	0.006	0.006	0.007	0.006	-	0.008	0.009	0.005	0.006	-	0.007	0.005	0.005
Mg	1.598	1.481	1.466	1.448	1.603	1.532	1.266	1.540	1.434	1.591	1.538	1.625	1.525
Ca	0.006	0.006	0.008	0.008	0.005	0.007	0.010	0.007	0.008	0.007	0.007	0.005	0.007
Cations	2.975	2.947	2.982	2.936	2.988	2.994	2.976	2.973	2.945	2.940	2.974	2.992	2.993
Recalculated Fe ions and oxides													
Fe^{2+}	0.366	0.471	0.507	0.516	0.368	0.440	0.691	0.418	0.518	0.352	0.420	0.349	0.449
Fe^{3+}	-	-	-	-	-	-	-	-	-	-	-	-	-
FeO	17.27	22.18	23.50	23.97	17.35	20.55	30.57	19.70	24.22	16.95	19.89	16.53	20.87
Fe_2O_3	-	-	-	-	-	-	-	-	-	-	-	-	-
End-member composition													
Fo	81.1	75.6	74.0	73.5	81.3	77.4	64.4	78.4	73.2	81.9	78.3	82.1	77.1

A6.6 Microprobe analyses of clinopyroxene in Group A lavas: alkali ol-basalts

Table A6.6 Electron microprobe analyses of clinopyroxene in group A alkali ol-basalts.

Sample	SA17					SA18										SA19		
Analysis	429-C	430-C	147-G	148-G	150-G	1778-C1	1779-R1	1783-C2	1784-R2	1790-C3	1791-R3	1781-G	1786-G	1792-G	1798-G	1994-C	1997-C	2002-C
SiO_2	50.47	49.56	50.83	50.30	50.40	50.34	46.56	45.99	49.11	49.38	48.82	48.12	49.38	49.32	48.54	48.69	50.16	48.13
TiO_2	1.93	1.80	1.72	1.70	2.06	0.78	2.42	2.30	1.67	1.37	1.70	2.25	1.75	1.62	2.07	1.37	1.20	1.27
Al_2O_3	2.49	4.37	2.27	2.51	3.64	3.90	5.23	7.91	3.16	5.16	3.35	3.18	4.63	2.75	3.81	4.50	2.09	6.30
Cr_2O_3	-	-	-	-	-	0.70	-	0.40	-	0.43	-	-	-	-	-	0.78	0.38	0.91
FeO_T	10.51	7.70	9.58	9.51	9.75	6.81	9.51	8.77	10.02	9.05	9.63	11.91	10.07	9.74	11.17	8.27	8.90	7.59
MnO	0.22	0.28	0.24	0.26	-	-	-	-	-	-	-	-	-	-	-	-	-	0.21
MgO	12.38	13.39	13.32	13.35	11.75	15.47	12.52	12.61	12.29	11.96	12.76	12.13	10.94	13.01	12.12	14.02	14.35	14.92
CaO	21.81	21.89	21.57	21.79	21.03	19.85	21.55	20.60	21.51	20.20	21.94	20.47	19.82	21.38	20.36	21.03	21.05	19.38
Na_2O	0.55	-	0.43	0.41	-	0.85	0.84	0.90	1.01	1.09	1.00	0.97	1.91	0.93	0.80	0.81	0.66	0.89
Total	100.36	98.99	99.96	99.83	98.63	98.70	98.63	99.48	98.77	98.64	99.20	99.03	98.50	98.75	98.87	99.47	98.79	99.60
Number of ions on the basis of 6 oxygen																		
Si	1.897	1.874	1.894	1.879	1.942	1.894	1.785	1.736	1.876	1.880	1.858	1.849	1.894	1.894	1.849	1.832	1.895	1.796
Ti	0.055	0.051	0.048	0.048	0.060	0.022	0.070	0.065	0.048	0.039	0.049	0.065	0.050	0.047	0.059	0.039	0.034	0.036
Al	0.110	0.195	0.100	0.110	0.166	0.173	0.236	0.352	0.142	0.232	0.150	0.144	0.209	0.124	0.171	0.200	0.093	0.277
Cr	-	-	-	-	-	0.021	-	0.012	-	0.013	-	-	-	-	-	0.023	0.011	0.027
Fe^{2+}	0.331	0.244	0.298	0.297	0.314	0.214	0.305	0.277	0.320	0.288	0.307	0.383	0.323	0.313	0.356	0.260	0.281	0.237
Mn	0.007	0.009	0.007	0.008	-	-	-	-	-	-	-	-	-	-	-	-	-	0.001
Mg	0.694	0.755	0.740	0.743	0.675	0.868	0.715	0.709	0.700	0.679	0.724	0.695	0.625	0.745	0.688	0.787	0.808	0.830
Ca	0.879	0.887	0.861	0.872	0.868	0.800	0.885	0.833	0.880	0.824	0.895	0.843	0.814	0.880	0.830	0.848	0.852	0.775
Na	0.040	-	0.031	0.030	-	0.062	0.063	0.066	0.074	0.080	0.073	0.073	0.142	0.069	0.059	0.059	0.048	0.064
Cations	4.013	4.014	3.979	3.988	4.026	4.055	4.059	4.051	4.042	4.035	4.055	4.051	4.058	4.070	4.013	4.048	4.023	4.043
Recalculated Al and Fe ions and Fe oxides																		
Al^{IV}	0.103	0.126	0.100	0.110	0.058	0.106	0.215	0.264	0.124	0.120	0.142	0.144	0.106	0.106	0.151	0.168	0.093	0.204
Al^{VI}	0.008	0.069	-	-	0.108	0.067	0.021	0.088	0.018	0.111	0.008	-	0.103	0.018	0.020	0.032	-	0.074
Fe^{2+}	0.304	0.244	0.263	0.253	0.314	0.179	0.187	0.177	0.237	0.288	0.196	0.297	0.278	0.249	0.283	0.166	0.220	0.142
Fe^{3+}	0.026	-	0.036	0.044	-	0.035	0.117	0.099	0.084	-	0.111	0.086	0.045	0.064	0.072	0.095	0.061	0.095
FeO	9.68	7.70	8.44	8.11	9.75	5.69	5.85	5.62	7.40	9.05	6.15	9.24	8.67	7.75	8.90	5.27	6.96	4.54
Fe_2O_3	0.93	-	1.27	1.55	-	1.25	4.07	3.50	2.91	-	3.87	2.97	1.56	2.22	2.53	3.34	2.15	3.39
End-member compositions*																		
Wo	46.0	46.8	45.2	45.4	46.7	42.5	46.5	45.8	46.3	46.0	46.5	43.9	46.2	45.4	44.3	44.7	43.9	42.1
En	36.3	39.8	38.8	38.7	36.3	46.1	37.5	39.0	36.8	37.9	37.6	36.2	35.5	38.4	36.7	41.5	41.6	45.0
Fs	17.7	13.3	16.0	15.9	16.9	11.4	16.0	15.2	16.9	16.1	15.9	19.9	18.3	16.1	19.0	13.7	14.5	12.9

Table A6.6 Electron microprobe analyses of clinopyroxene in group A alkali ol-basalts (contiued).

Sample	SA33								SAB162							
Analysis	1728-C1	1729-R1	1734-C2	1735-R2	1719-C	1722-G	1723-G	1727-G	1758-C1	1760-R1	1759-C	1769-C	1739-G	1746-G	1754-G	1757-G
SiO_2	49.87	46.96	49.43	49.53	50.46	50.27	49.73	50.45	47.83	47.28	49.10	48.04	49.67	49.43	48.08	50.50
TiO_2	1.31	1.62	1.95	1.91	1.28	1.17	0.92	1.38	1.45	1.65	1.69	1.49	1.78	1.59	2.07	1.76
Al_2O_3	3.43	2.70	3.34	3.16	1.63	1.36	0.84	1.54	5.58	5.52	3.50	5.19	2.32	1.63	3.77	1.83
Cr_2O_3	0.79	-	-	-	-	-	-	-	0.47	0.77	0.38	0.59	-	-	-	-
FeO_T	7.68	18.64	9.80	10.81	13.69	16.41	20.43	13.29	7.59	7.57	8.57	7.50	10.11	12.82	9.87	11.66
MnO	-	0.26	-	0.24	0.23	0.33	0.41	0.28	-	-	-	-	0.22	0.32	-	0.22
MgO	14.48	10.29	13.28	12.98	12.32	10.75	8.13	12.67	13.95	13.27	13.45	13.85	13.41	11.96	13.01	12.85
CaO	21.35	18.72	21.31	20.82	19.91	19.77	19.76	20.09	21.35	21.63	21.62	21.30	21.13	20.51	21.34	21.08
Na_2O	0.52	0.90	0.86	0.70	0.70	0.54	0.68	0.71	0.87	0.97	0.76	0.78	0.70	0.68	0.91	0.65
Total	99.43	100.092	99.97	100.15	100.22	100.60	100.90	100.41	99.09	98.66	99.07	98.74	99.34	98.94	99.05	100.55
Number of ions on the basis of 6 oxygen																
Si	1.869	1.818	1.861	1.868	1.919	1.928	1.941	1.914	1.804	1.796	1.859	1.816	1.886	1.906	1.834	1.904
Ti	0.037	0.047	0.055	0.054	0.037	0.034	0.027	0.039	0.041	0.047	0.048	0.043	0.051	0.046	0.059	0.050
Al	0.151	0.124	0.148	0.140	0.073	0.062	0.038	0.069	0.248	0.247	0.156	0.232	0.104	0.074	0.169	0.081
Cr	0.023	-	-	-	-	-	-	-	0.014	0.023	0.011	0.018	-	-	-	-
Fe^{2+}	0.241	0.604	0.308	0.341	0.436	0.526	0.667	0.422	0.239	0.241	0.271	0.237	0.321	0.413	0.315	0.368
Mn	-	0.008	-	0.008	0.007	0.011	0.014	0.009	-	-	-	-	0.007	0.010	-	0.007
Mg	0.809	0.594	0.745	0.730	0.698	0.615	0.473	0.716	0.784	0.751	0.759	0.781	0.758	0.688	0.740	0.722
Ca	0.857	0.777	0.860	0.841	0.811	0.812	0.826	0.817	0.862	0.880	0.877	0.863	0.859	0.847	0.872	0.851
Na	0.038	0.067	0.063	0.051	0.052	0.040	0.052	0.052	0.064	0.071	0.056	0.057	0.051	0.051	0.067	0.047
Cations	4.026	4.033	4.041	4.033	4.033	4.028	4.039	4.038	4.057	4.057	4.037	4.046	4.037	4.036	4.056	4.030
Recalculated Al and Fe ions and Fe oxides																
Al^{IV}	0.131	0.124	0.139	0.132	0.073	0.062	0.038	0.069	0.196	0.204	0.141	0.184	0.104	0.074	0.166	0.081
Al^{VI}	0.020	-	0.009	0.008	-	-	-	-	0.052	0.043	0.015	0.048	-	-	0.003	-
Fe^{2+}	0.189	0.507	0.226	0.274	0.384	0.491	0.632	0.379	0.129	0.126	0.196	0.147	0.268	0.381	0.203	0.339
Fe^{3+}	0.051	0.097	0.082	0.067	0.051	0.035	0.035	0.043	0.111	0.115	0.075	0.090	0.053	0.032	0.112	0.029
FeO	6.04	15.65	7.19	8.68	12.08	15.31	19.35	11.93	4.08	3.95	6.21	4.66	8.43	11.82	6.36	10.75
Fe_2O_3	1.82	3.32	2.90	2.36	1.79	1.22	1.20	1.51	3.90	4.02	2.63	3.16	1.86	1.11	3.90	1.01
End-member compositions																
Wo	45.0	39.2	44.9	43.8	41.5	41.4	41.7	41.6	45.7	47.0	46.0	45.9	44.2	43.3	45.3	43.7
En	42.4	30.0	38.9	38.0	35.8	31.3	23.9	36.5	41.6	40.1	39.8	41.5	39.0	35.1	38.4	37.0
Fs	12.6	30.9	16.1	18.2	22.7	27.3	34.4	21.9	12.7	12.9	14.2	12.6	16.9	21.6	16.4	19.2

A6.7 Microprobe analyses of clinopyroxene in group A: transitional basalts

Table A6.7 Electron microprobe analyses of clinopyroxene in group A transitional basalts.

Sample	SA07											SA10				SA13				
Analysis	1884-C1	1885-R1	1907-C2	1908-R2	1912-C3	1913-R3	1888-G	1894-G	1901-G	1902-G	1910-G	1813-G	1837-G	1838-G	1840-G	565-C1	566-R1	49-C	43-G	46-G
SiO_2	50.32	48.69	49.44	47.40	50.02	50.44	48.16	50.02	48.12	48.36	45.24	47.32	48.55	49.52	48.00	51.52	51.13	50.63	50.95	51.10
TiO_2	0.71	1.44	0.77	1.99	0.73	1.06	1.86	1.16	1.92	1.90	2.32	2.15	1.55	1.27	1.94	0.72	1.03	1.28	1.27	1.15
Al_2O_3	4.51	3.90	5.30	4.81	4.86	2.44	4.28	2.65	4.62	4.29	2.90	4.43	3.21	3.11	4.47	2.73	3.68	3.16	2.43	2.56
Cr_2O_3	0.63	0.36	1.05	0.26	1.10	0.27	0.27	0.32	-	0.34	-	-	-	-	0.26	-	-	-	-	-
FeO_T*	6.79	9.31	6.61	10.16	6.84	9.50	9.92	9.56	10.04	10.12	12.29	11.53	11.15	11.01	10.30	8.35	7.63	9.91	11.45	10.81
MnO	0.24	-	-	-	-	-	0.29	-	0.21	-	0.38	0.25	0.23	0.28	-	0.23	0.26	0.25	0.30	0.30
MgO	16.43	13.72	15.67	13.29	16.35	15.68	13.50	14.97	13.03	13.49	18.58	13.03	14.62	14.06	13.38	15.83	14.76	14.25	14.30	15.19
CaO	18.95	20.60	18.91	20.10	18.06	19.43	20.16	19.56	20.16	19.67	15.40	19.57	18.59	18.72	19.86	20.02	21.35	19.37	19.45	18.75
Na_2O	0.92	0.74	0.90	0.89	0.98	0.68	0.72	0.65	0.84	0.91	1.03	0.89	0.83	0.78	0.79	-	-	-	-	-
Total	99.50	98.76	98.65	98.90	98.94	99.50	99.16	98.89	98.94	99.08	98.14	99.17	98.73	98.75	99.00	99.40	99.84	98.85	100.15	99.86
Number of ions on the basis of 6 oxygen																				
Si	1.864	1.850	1.846	1.808	1.871	1.892	1.829	1.891	1.854	1.835	1.737	1.810	1.853	1.897	1.826	1.918	1.896	1.905	1.895	1.896
Ti	0.020	0.041	0.022	0.057	0.020	0.030	0.053	0.033	0.056	0.054	0.067	0.062	0.044	0.037	0.056	0.020	0.029	0.036	0.035	0.032
Al	0.197	0.175	0.233	0.217	0.214	0.108	0.191	0.118	0.210	0.192	0.131	0.200	0.145	0.140	0.200	0.120	0.161	0.140	0.107	0.112
Cr	0.019	0.011	0.031	0.008	0.032	0.008	0.008	0.010	-	0.010	-	-	-	-	0.008	-	-	-	-	-
Fe^{2+}	0.210	0.296	0.206	0.324	0.214	0.298	0.315	0.302	0.323	0.321	0.394	0.369	0.356	0.353	0.328	0.260	0.237	0.312	0.356	0.335
Mn	0.008	-	-	-	-	-	0.009	-	0.007	-	0.013	0.008	0.007	0.009	-	0.007	0.008	0.008	0.010	0.010
Mg	0.907	0.777	0.872	0.756	0.911	0.877	0.764	0.844	0.749	0.763	1.063	0.743	0.832	0.803	0.758	0.878	0.816	0.799	0.793	0.840
Ca	0.752	0.839	0.757	0.821	0.724	0.781	0.821	0.792	0.832	0.800	0.634	0.802	0.760	0.768	0.809	0.799	0.848	0.781	0.775	0.745
Na	0.066	0.055	0.065	0.066	0.071	0.049	0.053	0.048	0.063	0.067	0.077	0.067	0.062	0.058	0.058	-	-	-	-	-
Cations	4.042	4.043	4.033	4.057	4.058	4.044	4.044	4.037	4.094	4.042	4.116	4.060	4.060	4.064	4.043	4.002	3.995	3.980	3.971	3.971
Recalculated Al and Fe ions and Fe oxides																				
Al^{IV}	0.136	0.150	0.154	0.192	0.129	0.108	0.171	0.109	0.146	0.165	0.131	0.190	0.145	0.103	0.174	0.082	0.104	0.095	0.105	0.104
Al^{VI}	0.060	0.025	0.080	0.024	0.085	-	0.021	0.009	0.064	0.027	-	0.010	-	0.037	0.026	0.038	0.057	0.044	0.002	0.008
Fe^{2+}	0.126	0.210	0.141	0.212	0.173	0.210	0.226	0.229	0.290	0.235	0.321	0.246	0.237	0.302	0.241	0.256	0.237	0.312	0.323	0.304
Fe^{3+}	0.084	0.086	0.065	0.112	0.042	0.089	0.089	0.073	0.033	0.086	0.073	0.123	0.118	0.051	0.087	0.004	-	-	0.033	0.031
FeO	4.08	6.62	4.52	6.65	5.51	6.68	7.13	7.25	9.01	7.42	10.01	7.69	7.44	9.42	7.57	8.22	7.63	9.91	10.39	9.81
Fe_2O_3	3.01	2.99	2.32	3.90	1.48	3.14	3.10	2.56	1.14	3.00	2.53	4.26	4.12	1.77	3.03	0.14	-	-	1.17	1.11
End-member compositions																				
Wo	40.1	43.9	41.2	43.2	39.1	39.9	43.0	40.9	43.5	42.5	30.1	41.7	38.9	39.7	42.7	41.1	44.4	41.1	40.1	38.6
En	48.3	40.6	47.5	39.8	49.3	44.8	40.0	43.5	39.2	40.5	50.5	38.7	42.6	41.5	40.0	45.2	42.7	42.1	41.0	43.5
Fs	11.6	15.5	11.2	17.0	11.6	15.2	17.0	15.6	17.3	17.0	19.3	19.6	18.6	18.7	17.3	13.7	12.8	16.8	18.9	17.9

A6.8 Microprobe analyses of clinopyroxene in group A lavas: hawaiites

Table A 6.8 Electron microprobe analyses of clinopyroxene in group A hawaiites.

Sample	SA20											SAB163								
Analysis	1854-C1	1855-R1	1856-C2	1857-R2	1876-C3	1877-R3	1881-C	1851-G	1852-G	1864-G	1872-G	1960-C1	1961-R1	1986-C2	1987-R2	1990-C	1963-G	1969-G	1980-G	1988-G
SiO_2	48.19	50.10	50.26	49.31	48.04	49.49	48.22	49.53	49.71	50.80	49.13	47.87	47.94	48.44	48.29	48.75	50.22	50.66	50.29	50.72
TiO_2	1.80	1.27	0.79	1.73	1.69	1.77	1.44	1.89	1.52	1.43	1.79	1.61	1.90	2.12	2.26	1.62	1.68	1.55	1.57	1.47
Al_2O_3	6.02	1.67	4.64	2.96	5.28	2.92	4.53	3.04	2.24	1.64	2.47	6.12	5.73	3.73	3.13	5.03	2.08	1.79	1.52	1.77
Cr_2O_3	0.43	-	0.71	-	0.34	0.36	0.57	-	-	-	-	0.38	-	-	-	0.40	-	-	-	-
FeO_T	8.40	12.69	7.31	12.08	8.04	10.91	8.77	12.86	14.98	12.32	14.47	8.12	8.10	10.22	10.85	8.21	9.90	10.97	14.02	11.02
MnO	-	0.22	-	0.22	-	-	-	-	0.34	0.34	-	-	-	0.22	-	-	-	0.24	0.33	0.24
MgO	13.53	12.97	15.88	12.96	13.35	13.54	14.32	12.24	11.02	13.61	11.44	13.78	13.29	13.21	12.31	13.92	13.48	12.92	11.18	12.87
CaO	21.53	19.72	19.88	20.54	21.94	20.85	21.69	19.84	19.78	19.95	20.59	21.25	22.04	21.16	21.22	21.14	21.34	21.29	21.27	21.60
Na_2O	1.03	0.75	1.07	0.87	0.78	0.87	0.85	0.79	0.80	0.65	0.88	0.97	0.85	0.73	0.80	0.81	0.68	0.78	0.75	0.81
Total	100.93	99.39	100.54	100.67	99.46	100.71	100.39	100.19	100.39	100.74	100.77	100.10	99.85	99.83	98.86	99.88	99.38	100.20	100.93	100.50
Number of ions on the basis of 6 oxygen																				
Si	1.790	1.914	1.840	1.850	1.810	1.847	1.775	1.877	1.901	1.910	1.861	1.790	1.799	1.834	1.852	1.824	1.900	1.904	1.912	1.910
Ti	0.050	0.037	0.022	0.049	0.048	0.050	0.040	0.054	0.044	0.040	0.051	0.045	0.053	0.060	0.065	0.046	0.048	0.044	0.045	0.042
Al	0.263	0.075	0.200	0.131	0.235	0.128	0.196	0.136	0.101	0.073	0.110	0.270	0.253	0.167	0.142	0.222	0.093	0.080	0.068	0.079
Cr	0.013	-	0.020	-	0.003	0.003	0.004	-	-	-	-	0.011	-	-	-	0.012	-	-	-	-
Fe^{2+}	0.261	0.406	0.224	0.379	0.253	0.341	0.270	0.407	0.479	0.388	0.458	0.254	0.254	0.323	0.348	0.257	0.313	0.345	0.446	0.347
Mn	-	0.007	-	0.007	-	-	-	-	0.011	0.011	-	-	-	0.007	-	-	-	0.008	0.011	0.008
Mg	0.749	0.739	0.866	0.725	0.750	0.754	0.785	0.692	0.628	0.763	0.646	0.768	0.743	0.746	0.704	0.776	0.761	0.724	0.634	0.722
Ca	0.857	0.808	0.780	0.826	0.886	0.834	0.856	0.806	0.811	0.804	0.836	0.851	0.886	0.859	0.872	0.848	0.865	0.857	0.866	0.872
Na	0.074	0.056	0.076	0.064	0.057	0.064	0.061	0.058	0.059	0.047	0.065	0.070	0.062	0.054	0.060	0.059	0.050	0.056	0.055	0.059
Cations	4.058	4.040	4.028	4.030	4.042	4.020	3.987	4.030	4.035	4.036	4.027	4.060	4.051	4.050	4.042	4.043	4.030	4.018	4.037	4.039
Recalculated Al and Fe ions and Fe oxides																				
Al^{IV}	0.210	0.075	0.160	0.131	0.190	0.128	0.196	0.123	0.099	0.073	0.110	0.210	0.201	0.166	0.142	0.176	0.093	0.080	0.068	0.079
Al^{VI}	0.054	-	0.040	-	0.045	-	-	0.013	0.003	-	-	0.060	0.052	0.001	-	0.046	-	-	-	-
Fe^{2+}	0.144	0.348	0.092	0.282	0.150	0.252	0.098	0.348	0.412	0.348	0.386	0.135	0.150	0.225	0.275	0.171	0.266	0.296	0.413	0.292
Fe^{3+}	0.117	0.058	0.132	0.098	0.103	0.089	0.172	0.060	0.068	0.040	0.072	0.119	0.104	0.099	0.073	0.086	0.047	0.049	0.033	0.055
FeO	4.64	10.89	3.00	8.97	4.76	8.07	3.20	10.97	12.87	11.05	12.18	4.31	4.78	7.10	8.58	5.47	8.42	9.41	12.99	9.28
Fe_2O_3	4.18	2.00	4.78	3.46	3.65	3.16	6.19	2.10	2.35	1.41	2.54	4.24	3.69	3.47	2.52	3.04	1.64	1.73	1.15	1.94
End-member compositions																				
Wo	45.9	41.2	41.7	42.6	46.9	43.2	44.8	42.3	42.0	40.9	43.1	45.5	47.0	44.4	45.3	45.1	44.6	44.3	44.3	44.7
En	40.1	37.7	46.3	37.4	39.7	39.1	41.1	36.3	32.6	38.8	33.3	41.0	39.5	38.5	36.6	41.3	39.2	37.4	32.4	37.1
Fs	14.0	21.1	12.0	20.0	13.4	17.7	14.1	21.4	25.4	20.3	23.6	13.5	13.5	17.1	18.1	13.7	16.2	18.2	23.3	18.2

Table A 6.8 Electron microprobe analyses of clinopyroxene in group A hawaiites (continued).

Sample	SA32											SAB151							
Analysis	1935-C1	1936-R1	1943-C2	1944-R2	1945-C	1934-C	1932-G	1937-G	1938-G	1939-G	1942-G	202-C1	203-R1	208-C2	209-R2	691-C3	692-R3	210-G	213-G
SiO_2	48.93	48.38	49.33	48.71	48.89	49.73	49.01	50.25	48.53	50.76	50.44	50.51	50.55	51.86	50.71	50.53	50.82	50.84	49.96
TiO_2	1.20	2.27	1.26	1.41	1.48	1.11	1.69	1.64	2.09	1.18	1.21	1.36	1.15	1.11	1.38	0.94	1.23	1.35	1.53
Al_2O_3	3.66	3.77	3.63	3.90	3.82	2.95	4.04	2.12	2.85	2.38	2.94	3.38	2.92	1.99	2.98	4.02	1.84	1.89	2.24
Cr_2O_3	0.79	-	1.04	0.88	0.73	0.74	0.97	-	-	0.22	0.54	-	-	-	-	-	-	-	-
FeO_T	7.26	9.53	7.33	7.50	7.99	7.36	8.02	9.97	11.87	7.92	7.29	8.26	8.72	9.25	8.69	7.18	12.40	10.49	12.90
MnO	-	-	-	-	-	-	-	0.25	0.21	-	-	-	-	0.24	-	-	0.29	-	-
MgO	14.32	12.65	14.29	13.84	13.96	14.43	14.02	13.12	11.53	14.54	14.67	14.34	14.23	14.36	14.06	14.99	12.39	13.56	12.12
CaO	21.74	21.44	21.41	21.89	21.63	21.78	21.55	20.96	21.26	21.72	21.83	20.95	21.17	21.06	21.01	21.21	20.17	20.57	20.04
Na_2O	0.81	0.89	0.71	0.78	0.99	0.78	0.80	0.80	1.00	0.64	0.78	-	-	-	-	-	-	-	-
Total	98.71	98.93	99.00	98.91	99.49	98.88	100.10	99.11	99.34	99.36	99.70	98.80	98.74	99.87	98.83	98.87	99.14	98.70	98.79
Number of ions on the basis of 6 oxygen																			
Si	1.852	1.855	1.858	1.843	1.842	1.877	1.834	1.932	1.863	1.904	1.884	1.883	1.891	1.920	1.905	1.888	1.937	1.915	1.913
Ti	0.034	0.065	0.035	0.040	0.042	0.031	0.047	0.047	0.060	0.033	0.034	0.038	0.032	0.031	0.039	0.026	0.035	0.038	0.044
Al	0.163	0.170	0.161	0.174	0.170	0.131	0.178	0.096	0.129	0.105	0.130	0.148	0.129	0.087	0.132	0.177	0.083	0.084	0.101
Cr	0.023	-	0.031	0.026	0.022	0.022	0.029	-	-	0.007	0.016	-	-	-	-	-	-	-	-
Fe^{2+}	0.230	0.305	0.231	0.237	0.252	0.232	0.251	0.320	0.381	0.248	0.228	0.257	0.273	0.286	0.273	0.224	0.395	0.331	0.413
Mn	-	-	-	-	-	-	-	0.008	0.007	-	-	-	-	0.008	-	-	0.010	-	-
Mg	0.808	0.723	0.803	0.781	0.784	0.812	0.782	0.752	0.660	0.813	0.817	0.797	0.794	0.793	0.787	0.834	0.704	0.761	0.692
Ca	0.881	0.881	0.864	0.887	0.874	0.881	0.864	0.863	0.875	0.873	0.874	0.836	0.848	0.836	0.846	0.849	0.824	0.830	0.822
Na	0.059	0.066	0.052	0.058	0.073	0.058	0.058	0.059	0.074	0.046	0.056	-	-	-	-	-	-	-	-
Cations	4.051	4.066	4.036	4.046	4.058	4.044	4.043	4.079	4.049	4.029	4.038	3.960	3.967	3.960	3.982	3.998	3.988	3.960	3.985
Recalculated Al and Fe ions and Fe oxides																			
Al^{IV}	0.148	0.145	0.142	0.157	0.158	0.123	0.166	0.068	0.129	0.096	0.116	0.117	0.109	0.080	0.095	0.112	0.063	0.084	0.087
Al^{VI}	0.015	0.025	0.020	0.017	0.012	0.008	0.012	0.028	-	0.009	0.014	0.031	0.020	0.007	0.037	0.065	0.020	-	0.014
Fe^{2+}	0.129	0.250	0.159	0.145	0.139	0.144	0.163	0.316	0.298	0.187	0.153	0.248	0.248	0.274	0.273	0.224	0.395	0.323	0.413
Fe^{3+}	0.101	0.056	0.072	0.092	0.113	0.088	0.087	0.005	0.083	0.061	0.075	0.009	0.025	0.012	-	-	-	0.007	-
FeO	4.06	7.79	5.03	4.60	4.40	4.57	5.23	9.83	9.27	5.98	4.90	7.96	7.92	8.87	8.69	7.18	12.40	10.26	12.90
Fe_2O_3	3.55	1.93	2.55	3.22	3.99	3.10	3.11	0.16	2.89	2.16	2.66	0.34	0.89	0.42	-	-	-	0.25	-
End-member compositions																			
Wo	45.9	46.1	45.5	46.6	45.7	45.8	45.6	44.4	45.5	45.1	45.5	44.2	44.3	43.5	44.4	44.5	42.6	43.2	42.7
En	42.1	37.9	42.3	41.0	41.1	42.2	41.2	38.7	34.3	42.0	42.6	42.1	41.4	41.2	41.3	43.7	36.4	39.6	35.9
Fs	12.0	16.0	12.2	12.4	13.2	12.1	13.2	16.9	20.2	12.8	11.9	13.6	14.3	15.3	14.3	11.8	21.0	17.2	21.4

A6.9 Microprobe analyses of clinopyroxene in group A lavas: ol-tholeiitic basalts

Table A6.9 Electron microprobe analyses of clinopyroxene in group A ol-tholeiitic basalts.

Sample	SA80							SAB152						SAB169					
Analysis	104-C1	105-R1	109-C2	110-R2	547-C3	548-R3	117-G	717-C	718-C	719-C	260-G	261-G	263-G	422-C1	423-R1	22-C	26-C	28-C	30-C
SiO_2	51.59	49.70	51.91	51.42	51.69	51.68	51.53	50.79	51.34	49.70	49.99	50.43	50.60	50.04	49.85	50.95	49.65	49.51	49.02
TiO_2	0.79	1.18	0.84	1.26	1.04	1.03	1.02	1.05	1.27	1.98	1.35	1.60	1.40	1.17	1.25	0.82	1.33	1.32	2.42
Al_2O_3	3.88	4.57	2.00	2.42	1.44	1.27	1.18	3.10	2.86	2.89	1.87	2.84	1.77	4.10	4.18	5.28	4.15	4.04	3.96
Cr_2O_3	-	-	-	-	-	-	-	-	-	-	-	-	-	-	-	-	-	-	-
FeO_T	6.77	7.30	7.99	8.94	13.50	13.60	13.66	10.05	8.56	10.75	14.72	9.64	15.43	7.99	8.12	7.09	8.39	8.61	11.70
MnO	-	0.25	0.28	0.22	0.35	-	0.37	0.26	-	-	0.30	0.26	0.38	-	0.25	0.26	-	-	0.31
MgO	15.10	14.77	15.39	14.55	14.16	13.49	13.63	13.56	14.68	13.16	11.21	13.82	10.86	14.32	14.29	15.54	13.94	14.01	12.27
CaO	20.34	20.74	20.35	20.16	17.77	18.40	17.83	20.59	20.71	20.82	20.27	21.13	19.87	20.91	21.00	19.73	21.04	21.32	19.12
Na_2O	0.35	0.38	-	-	-	-	-	-	-	-	-	-	-	-	-	0.49	-	-	-
Total	98.82	98.89	98.76	98.97	99.95	99.47	99.22	99.40	99.42	99.30	99.71	99.72	100.31	98.53	98.94	100.16	98.50	98.81	98.80
Number of ions on the basis of 6 oxygen																			
Si	1.939	1.848	1.928	1.926	1.948	1.958	1.943	1.910	1.915	1.882	1.904	1.879	1.917	1.882	1.872	1.857	1.860	1.853	1.877
Ti	0.022	0.033	0.023	0.035	0.029	0.029	0.029	0.029	0.035	0.056	0.039	0.045	0.040	0.033	0.035	0.022	0.037	0.037	0.070
Al	0.172	0.200	0.088	0.107	0.064	0.057	0.053	0.137	0.126	0.129	0.084	0.125	0.079	0.182	0.185	0.227	0.183	0.178	0.179
Cr	-	-	-	-	-	-	-	-	-	-	-	-	-	-	-	-	-	-	-
Fe^{2+}	0.213	0.227	0.248	0.280	0.425	0.431	0.431	0.316	0.267	0.341	0.469	0.301	0.489	0.251	0.255	0.216	0.263	0.269	0.374
Mn	-	0.008	0.009	0.007	0.011	-	0.012	0.008	-	-	0.010	0.008	0.013	-	0.008	0.008	-	-	0.010
Mg	0.845	0.819	0.852	0.812	0.796	0.762	0.766	0.760	0.816	0.743	0.637	0.768	0.613	0.803	0.800	0.844	0.779	0.782	0.701
Ca	0.818	0.826	0.810	0.809	0.718	0.747	0.721	0.830	0.827	0.845	0.827	0.844	0.807	0.842	0.845	0.770	0.845	0.856	0.785
Na	0.025	0.028	-	-	-	-	-	-	-	-	-	-	-	-	-	0.035	-	-	-
Cations	4.034	3.989	3.959	3.976	3.991	3.984	3.955	3.991	3.986	3.996	3.970	3.970	3.958	3.994	4.000	3.979	3.967	3.976	3.996
Recalculated Al and Fe ions and Fe oxides																			
Al^{IV}	0.061	0.152	0.072	0.074	0.052	0.042	0.053	0.090	0.085	0.118	0.084	0.121	0.079	0.118	0.128	0.143	0.140	0.147	0.123
Al^{VI}	0.110	0.048	0.016	0.033	0.011	0.015	-	0.047	0.041	0.011	-	0.004	-	0.064	0.057	0.084	0.043	0.032	0.056
Fe^{2+}	0.213	0.162	0.240	0.280	0.425	0.431	0.431	0.316	0.267	0.341	0.463	0.274	0.489	0.251	0.255	0.166	0.240	0.229	0.374
Fe^{3+}	-	0.065	0.009	-	-	-	-	-	-	-	0.006	0.027	-	-	-	0.050	0.023	0.041	-
FeO	6.77	5.20	7.71	8.94	13.50	13.60	13.66	10.05	8.56	10.75	14.53	8.78	15.43	7.99	8.11	5.46	7.67	7.31	11.70
Fe_2O_3	-	2.33	0.31	-	-	-	-	-	-	-	0.21	0.96	-	-	0.01	1.81	0.80	1.44	-
End-member compositions																			
Wo	43.6	44.0	42.2	42.4	36.8	38.5	37.3	43.3	43.3	43.8	42.6	43.9	42.0	44.4	44.3	41.9	44.8	44.9	42.0
En	45.0	43.6	44.4	42.6	40.8	39.3	39.7	39.7	42.7	38.5	32.8	40.0	31.9	42.3	41.9	45.9	41.3	41.0	37.5
Fs	11.3	12.5	13.4	15.0	22.4	22.2	22.9	17.0	14.0	17.7	24.6	16.1	26.1	13.3	13.8	12.2	13.9	14.1	20.6

Table A6.9 Electron microprobe analyses of clinopyroxene in group A ol-tholeiitic basalts (continued).

Sample	SAB181			SAB187							SA36					
Analysis	187-G	189-G	192-G	266-C1	267-R1	272-C2	273-R2	539-C3	540-R3	268-G	825-G	826-G	830-G	831-G	832-G	834-G
SiO_2	51.49	51.03	51.02	50.73	52.28	50.95	51.88	52.09	51.64	51.77	49.48	50.50	49.24	50.64	51.24	50.91
TiO_2	0.95	0.99	1.38	1.09	0.95	0.83	1.05	0.98	0.87	1.24	1.13	0.89	0.94	1.21	0.96	0.93
Al_2O_3	2.32	1.12	1.80	3.19	2.68	4.10	3.00	2.55	2.98	1.50	2.72	1.89	3.03	2.13	2.25	2.41
Cr_2O_3	-	-	-	-	-	-	-	-	-	-	-	-	-	-	0.23	-
FeO_T	7.93	17.17	13.24	8.65	8.61	7.04	8.36	7.92	7.90	10.57	17.88	16.67	16.81	13.96	10.72	11.87
MnO	0.24	0.29	0.25	0.30	0.24	-	0.33	0.32	0.29	0.23	0.31	0.37	0.50	0.32	0.28	0.25
MgO	15.65	14.95	14.25	14.77	14.70	15.47	15.30	14.97	15.34	15.03	12.94	13.91	12.18	14.26	15.90	15.00
CaO	20.24	13.84	17.41	19.95	19.06	20.24	19.78	19.91	19.97	19.08	14.21	15.44	16.39	17.69	18.82	17.65
Na_2O	-	-	-	-	-	0.39	-	-	-	-	-	-	-	-	-	-
Total	98.82	99.39	99.35	98.68	98.52	99.02	99.70	98.74	98.99	99.42	98.67	99.67	99.09	100.21	100.40	99.02
Number of ions on the basis of 6 oxygen																
Si	1.912	1.933	1.917	1.892	1.964	1.880	1.908	1.982	1.937	1.927	1.925	1.927	1.900	1.911	1.907	1.922
Ti	0.026	0.028	0.039	0.031	0.027	0.023	0.029	0.028	0.025	0.035	0.033	0.025	0.027	0.034	0.027	0.026
Al	0.101	0.050	0.080	0.140	0.119	0.178	0.130	0.115	0.132	0.066	0.125	0.085	0.138	0.095	0.098	0.107
Cr	-	-	-	-	-	-	-	-	-	-	-	-	-	-	0.007	-
Fe^{2+}	0.246	0.544	0.416	0.270	0.271	0.217	0.257	0.252	0.248	0.329	0.582	0.532	0.543	0.440	0.334	0.375
Mn	0.007	0.009	0.008	0.010	0.008	-	0.010	0.010	0.009	0.007	0.010	0.012	0.016	0.010	0.008	0.008
Mg	0.866	0.844	0.798	0.821	0.823	0.851	0.838	0.849	0.857	0.834	0.751	0.791	0.701	0.802	0.882	0.844
Ca	0.805	0.562	0.701	0.797	0.767	0.800	0.779	0.812	0.803	0.761	0.592	0.631	0.678	0.715	0.751	0.714
Na	-	-	-	-	-	0.028	-	-	-	-	-	-	-	-	-	-
Cations	3.964	3.968	3.959	3.962	3.979	3.977	3.952	4.048	4.011	3.960	4.018	4.004	4.003	4.008	4.013	3.998
Recalculated Al and Fe ions and Fe oxides																
Al^{IV}	0.088	0.050	0.080	0.108	0.036	0.120	0.092	0.018	0.063	0.066	0.075	0.073	0.100	0.089	0.093	0.078
Al^{VI}	0.013	-	-	0.033	0.083	0.059	0.038	0.096	0.069	-	0.050	0.012	0.038	0.006	0.005	0.030
Fe^{2+}	0.223	0.544	0.414	0.256	0.271	0.174	0.257	0.252	0.248	0.329	0.582	0.522	0.535	0.426	0.306	0.375
Fe^{3+}	0.023	-	0.002	0.014	-	0.043	-	-	-	-	-	0.010	0.008	0.015	0.027	-
FeO	7.20	17.17	13.17	8.21	8.61	5.65	8.36	7.92	7.90	10.57	17.88	16.36	16.57	13.49	9.84	11.87
Fe_2O_3	0.81	-	0.08	0.48	-	1.55	-	-	-	-	-	0.35	0.26	0.52	0.98	-
End-member compositions																
Wo	41.8	28.7	36.4	42.0	41.1	42.8	41.3	42.2	41.9	39.4	30.6	32.1	35.0	36.3	38.0	36.8
En	45.0	43.1	41.5	43.3	44.0	45.5	44.5	44.1	44.7	43.2	38.8	40.2	36.2	40.8	44.7	43.5
Fs	13.2	28.2	22.1	14.7	14.9	11.6	14.2	13.6	13.4	17.4	30.6	27.7	28.9	22.9	17.3	19.7

Table A6.9 Electron microprobe analyses of clinopyroxene in group A ol-tholeiitic basalts (continued).

Sample	SAB170					SAB171										SAB172			
Analysis	880-G	886-G	887-G	889-G	890-G	945-G	946-G	947-G	948-G	950-G	951-G	952-G	953-G	954-G	955-G	97-C1	98-R1	608-C2	609-R2
SiO_2	49.33	50.07	48.92	49.68	49.72	51.41	51.82	51.56	50.94	51.87	49.54	51.17	51.76	51.24	50.91	50.67	49.44	50.90	50.19
TiO_2	1.67	1.26	1.91	1.55	1.47	0.79	0.71	0.87	0.93	0.82	0.85	0.93	0.45	0.92	0.63	1.40	1.85	1.27	1.27
Al_2O_3	3.45	4.02	3.86	3.45	3.23	1.96	1.10	2.49	1.55	1.59	0.93	1.44	0.64	1.95	5.88	2.95	2.16	3.02	2.13
Cr_2O_3	0.23	0.82	-	-	-	0.39	-	0.74	-	-	-	-	-	-	-	-	-	-	-
FeO_T	10.98	8.64	14.10	12.37	15.09	9.25	21.53	8.13	13.24	10.49	27.30	12.89	22.12	10.77	19.37	11.93	18.23	9.89	14.33
MnO	0.28	0.21	0.33	0.31	0.32	0.21	0.53	-	0.24	0.35	0.50	0.28	0.41	0.25	0.38	0.39	0.26	0.23	0.30
MgO	14.02	14.22	13.23	14.41	15.28	15.60	18.93	15.64	14.68	15.69	11.77	15.10	19.78	15.98	14.39	14.92	11.29	14.77	14.14
CaO	19.36	19.71	16.47	17.04	14.08	19.41	5.64	19.66	17.07	18.20	8.66	17.16	4.10	17.74	7.50	17.56	17.30	19.40	16.42
Na_2O	-	-	-	-	-	-	-	-	-	-	-	-	-	-	0.66	-	-	-	-
Total	99.32	98.95	98.82	98.81	99.19	99.02	100.26	99.09	98.65	99.01	99.55	98.97	99.26	98.85	99.72	99.82	100.53	99.48	98.78
Number of ions on the basis of 6 oxygen																			
Si	1.866	1.903	1.882	1.897	1.887	1.929	1.951	1.947	1.941	1.973	1.955	1.941	1.965	1.930	1.910	1.885	1.883	1.905	1.918
Ti	0.047	0.036	0.055	0.044	0.042	0.022	0.020	0.025	0.027	0.023	0.025	0.026	0.013	0.026	0.018	0.039	0.053	0.035	0.037
Al	0.154	0.180	0.175	0.155	0.145	0.087	0.049	0.110	0.070	0.071	0.043	0.064	0.029	0.086	0.260	0.130	0.097	0.133	0.096
Cr	0.007	0.025	-	-	-	0.011	-	0.022	-	-	-	-	-	-	-	-	-	-	-
Fe^{2+}	0.347	0.275	0.454	0.395	0.479	0.290	0.678	0.257	0.422	0.334	0.901	0.409	0.702	0.339	0.608	0.371	0.581	0.310	0.458
Mn	0.009	0.007	0.011	0.010	0.010	0.007	0.017	-	0.008	0.011	0.017	0.009	0.013	0.008	0.012	0.013	0.008	0.007	0.010
Mg	0.790	0.805	0.758	0.820	0.864	0.872	1.063	0.880	0.833	0.889	0.692	0.854	1.120	0.897	0.805	0.828	0.641	0.824	0.805
Ca	0.785	0.803	0.679	0.697	0.572	0.780	0.227	0.796	0.697	0.742	0.366	0.698	0.167	0.716	0.302	0.700	0.706	0.778	0.673
Na	-	-	-	-	-	-	-	-	-	-	-	-	-	-	0.048	-	-	-	-
Cations	4.005	4.033	4.014	4.020	3.999	3.999	4.004	4.037	3.997	4.044	3.998	4.001	4.008	4.001	3.964	3.966	3.970	3.992	3.997
Recalculated Al and Fe ions and Fe oxides																			
Al^{IV}	0.134	0.097	0.118	0.103	0.113	0.071	0.049	0.053	0.059	0.027	0.043	0.059	0.029	0.070	0.090	0.115	0.097	0.095	0.082
Al^{VI}	0.020	0.083	0.057	0.052	0.032	0.016	-	0.057	0.011	0.044	-	0.005	-	0.016	0.171	0.015	-	0.038	0.014
Fe^{2+}	0.334	0.275	0.454	0.395	0.479	0.290	0.668	0.257	0.422	0.334	0.901	0.408	0.698	0.336	0.608	0.349	0.581	0.310	0.458
Fe^{3+}	0.013	-	-	-	-	-	0.010	-	-	-	-	0.001	0.004	0.003	-	0.022	-	-	-
FeO	10.57	8.64	14.10	12.37	15.09	9.25	21.22	8.13	13.24	10.49	27.30	12.86	21.99	10.68	19.37	11.22	18.23	9.89	14.33
Fe_2O_3	0.46	-	-	-	-	-	0.35	-	-	-	-	0.04	0.14	0.10	-	0.79	-	-	-
End-member compositions																			
Wo	40.6	42.5	35.7	36.3	29.7	40.0	11.5	41.2	35.5	37.6	18.5	35.4	8.3	36.5	17.5	36.6	36.5	40.6	34.6
En	40.9	42.6	39.9	42.7	44.9	44.8	53.5	45.5	42.5	45.0	35.0	43.3	55.9	45.8	46.6	43.3	33.1	42.9	41.4
Fs	18.5	14.9	24.4	21.1	25.4	15.2	35.0	13.3	21.9	17.5	46.4	21.2	35.7	17.7	35.9	20.1	30.4	16.5	24.1

Table A6.9 Electron microprobe analyses of clinopyroxene in group A ol-tholeiitic basalts (continued).

Sample	SAB172 (continued)									SAB173								
Analysis	615-C3	616-R3	103-C	102-G	917-G	918-G	919-G	921-G	922-G	992-G	993-G	996-G	999-G	1002-G	1003-G	1012-G	1023-G	1025-G
SiO_2	50.45	50.29	50.93	51.81	50.39	51.53	48.65	48.76	48.77	49.66	50.80	50.90	50.23	49.72	49.85	51.71	5-	49.46
TiO_2	1.39	1.42	1.22	0.84	0.89	0.74	2.02	0.96	1.57	0.59	1.17	1.00	1.14	1.13	0.95	0.58	0.48	0.96
Al_2O_3	3.45	2.31	3.35	2.16	0.85	1.14	2.40	1.43	2.09	0.82	1.54	1.90	1.51	1.45	1.39	0.55	0.80	1.29
Cr_2O_3	-	-	-	-	-	-	-	-	-	-	-	-	-	-	-	-	-	-
FeO_T	9.97	14.46	9.53	10.27	21.32	15.57	18.28	21.39	17.63	27.08	15.60	11.04	18.71	22.06	18.76	22.44	27.32	20.51
MnO	0.34	0.28	0.28	0.35	0.48	0.39	0.32	0.37	0.32	0.56	0.32	0.29	0.41	0.45	0.29	0.51	0.57	0.43
MgO	14.99	14.24	14.32	15.74	13.86	15.94	10.40	9.07	11.56	14.70	15.50	15.09	15.43	12.28	13.73	19.04	14.51	12.75
CaO	18.27	15.69	20.05	18.20	11.10	13.74	18.49	17.21	16.79	5.40	14.25	18.38	11.76	12.77	13.68	4.28	5.43	13.26
Na_2O	-	-	-	-	-	-	-	-	-	-	-	-	-	-	-	-	-	-
Total	98.86	98.69	99.68	99.37	98.89	99.05	100.56	99.19	98.73	98.81	99.18	98.60	99.19	99.86	98.65	99.11	99.11	98.66
Number of ions on the basis of 6 oxygen																		
Si	1.908	1.932	1.888	1.922	1.971	1.969	1.877	1.929	1.902	1.954	1.932	1.929	1.927	1.931	1.934	1.971	1.961	1.937
Ti	0.040	0.041	0.034	0.023	0.026	0.021	0.059	0.029	0.046	0.017	0.034	0.028	0.033	0.033	0.028	0.017	0.014	0.028
Al	0.154	0.105	0.146	0.094	0.039	0.052	0.109	0.067	0.096	0.038	0.069	0.085	0.068	0.067	0.064	0.025	0.037	0.059
Cr	-	-	-	-	-	-	-	-	-	-	-	-	-	-	-	-	-	-
Fe^{2+}	0.316	0.464	0.295	0.319	0.697	0.497	0.590	0.707	0.575	0.892	0.496	0.350	0.600	0.716	0.609	0.715	0.896	0.671
Mn	0.011	0.009	0.008	0.011	0.016	0.013	0.010	0.013	0.010	0.019	0.010	0.009	0.013	0.014	0.010	0.016	0.019	0.014
Mg	0.845	0.815	0.791	0.870	0.808	0.908	0.599	0.535	0.672	0.862	0.878	0.853	0.882	0.711	0.794	1.082	0.848	0.744
Ca	0.740	0.646	0.796	0.723	0.465	0.562	0.764	0.730	0.702	0.227	0.581	0.746	0.483	0.531	0.569	0.175	0.229	0.556
Na	-	-	-	-	-	-	-	-	-	-	-	-	-	-	-	-	-	-
Cations	4.014	4.013	3.959	3.962	4.022	4.022	4.009	4.009	4.004	4.009	4.000	4.000	4.006	4.003	4.007	4.001	4.005	4.010
Recalculated Al and Fe ions and Fe oxides																		
Al^{IV}	0.092	0.068	0.112	0.078	0.029	0.031	0.109	0.067	0.096	0.038	0.068	0.071	0.068	0.066	0.063	0.025	0.037	0.059
Al^{VI}	0.062	0.037	0.034	0.016	0.010	0.021	-	-	-	-	0.001	0.014	-	0.001	0.001	-	-	-
Fe^{2+}	0.316	0.464	0.285	0.303	0.697	0.497	0.590	0.698	0.572	0.888	0.496	0.349	0.598	0.716	0.602	0.715	0.888	0.669
Fe^{3+}	-	-	0.010	0.015	-	-	-	0.010	0.004	0.003	-	0.001	0.002	-	0.007	-	0.008	0.002
FeO	9.97	14.46	9.21	9.77	21.32	15.57	18.28	21.09	17.52	26.98	15.60	11.01	18.66	22.06	18.54	22.44	27.08	20.44
Fe_2O_3	-	-	0.36	0.55	-	-	-	0.33	0.12	0.11	-	0.04	0.06	-	0.25	-	0.27	0.07
End-member compositions																		
Wo	38.7	33.4	42.1	37.6	23.4	28.4	38.9	36.8	35.8	11.4	29.5	38.1	24.4	26.9	28.7	8.8	11.5	28.0
En	44.2	42.2	41.8	45.3	40.7	45.9	30.5	26.9	34.3	43.1	44.7	43.5	44.6	36.0	40.1	54.4	42.6	37.5
Fs	17.1	24.5	16.1	17.1	35.9	25.7	30.6	36.3	29.9	45.5	25.8	18.3	31.0	37.0	31.2	36.8	45.9	34.5

Table A6.9 Electron microprobe analyses of clinopyroxene in group A ol-tholeiitic basalts (continued).

Sample	SAB174													
Analysis	1068-G	1069-G	1070-G	1074-G	1076-G	1078-G	1082-G	1085-G	1089-G	1101-G	1104-G	1105-G	1110-G	1112-G
SiO_2	50.35	49.35	50.51	47.41	50.29	50.46	48.81	48.21	48.18	49.02	50.86	47.99	47.33	51.43
TiO_2	1.14	1.56	1.24	1.55	1.25	1.08	1.64	1.46	1.81	0.83	0.68	1.31	0.82	0.66
Al_2O_3	3.08	2.40	2.84	3.58	2.52	2.60	2.15	1.69	2.06	3.57	0.99	1.98	1.59	0.68
Cr_2O_3	0.52	-	-	-	-	-	-	-	-	-	-	-	-	-
FeO_T	10.36	16.22	12.51	21.38	12.81	13.49	20.91	22.33	21.18	25.46	23.00	27.86	28.16	23.51
MnO	0.34	0.29	0.30	0.40	0.21	0.40	0.32	0.36	0.44	0.44	0.42	0.45	0.47	0.52
MgO	15.43	13.06	14.61	8.87	14.64	15.85	9.90	9.06	8.73	6.72	15.66	7.70	5.52	17.42
CaO	18.08	16.21	17.00	15.68	17.14	14.78	16.47	15.83	17.48	13.36	7.04	13.16	15.63	5.69
Na_2O	-	-	-	-	-	-	-	-	-	1.07	-	-	-	-
Total	99.30	99.09	99.01	98.87	98.86	98.66	100.20	98.94	99.88	100.47	98.65	100.45	99.52	99.91
Number of ions on the basis of 6 oxygen														
Si	1.891	1.911	1.935	1.887	1.922	1.914	1.901	1.915	1.895	1.927	1.982	1.898	1.924	1.963
Ti	0.032	0.046	0.036	0.047	0.036	0.031	0.048	0.044	0.053	0.025	0.020	0.039	0.025	0.019
Al	0.136	0.109	0.128	0.168	0.113	0.116	0.099	0.079	0.095	0.166	0.046	0.092	0.076	0.031
Cr	0.016	-	-	-	-	-	-	-	-	-	-	-	-	-
Fe^{2+}	0.325	0.525	0.401	0.712	0.410	0.428	0.681	0.742	0.697	0.837	0.749	0.922	0.957	0.751
Mn	0.011	0.010	0.010	0.014	0.007	0.013	0.011	0.012	0.015	0.015	0.014	0.015	0.016	0.017
Mg	0.864	0.754	0.834	0.526	0.834	0.896	0.575	0.536	0.512	0.394	0.910	0.454	0.335	0.991
Ca	0.727	0.673	0.698	0.669	0.702	0.601	0.687	0.674	0.737	0.563	0.294	0.557	0.681	0.233
Na	-	-	-	-	-	-	-	-	-	0.081	-	-	-	-
Cations	4.002	4.027	4.042	4.023	4.024	3.997	4.002	4.002	4.004	4.007	4.014	3.977	4.014	4.003
Recalculated Al and Fe ions and Fe oxides														
Al^{IV}	0.109	0.089	0.065	0.113	0.078	0.086	0.099	0.079	0.095	0.073	0.018	0.092	0.076	0.030
Al^{VI}	0.027	0.020	0.063	0.055	0.035	0.030	-	-	-	0.093	0.028	-	-	0.001
Fe^{2+}	0.323	0.525	0.401	0.712	0.410	0.428	0.679	0.742	0.697	0.825	0.749	0.908	0.931	0.751
Fe^{3+}	0.002	-	-	-	-	-	0.002	-	-	0.012	-	0.014	0.026	-
FeO	10.29	16.22	12.51	21.38	12.81	13.49	20.84	22.33	21.18	25.10	23.00	27.45	27.39	23.51
Fe_2O_3	0.08	-	-	-	-	-	0.08	-	-	0.40	-	0.46	0.86	-
End-member compositions														
Wo	37.7	34.3	35.9	34.8	36.0	31.0	35.2	34.3	37.6	31.1	14.9	28.6	34.2	11.7
En	44.8	38.4	42.9	27.4	42.7	46.3	29.4	27.3	26.1	21.8	46.2	23.3	16.8	49.8
Fs	17.4	27.3	21.1	37.8	21.3	22.7	35.4	38.4	36.3	47.1	38.8	48.1	48.9	38.5

A6.10 Microprobe analyses of clinopyroxene in group A lavas: qz-tholeiitic basalts

Table A6.10 Electron microprobe analyses of clinopyroxene in group A qz-tholeiitic basalts.

Sample	SA76								SA77									
Analysis	121-C1	122-R1	462-C2	463-R2	473-C3	474-R3	129-G	135-G	638-C1	639-R1	175-C	176-C	180-C	633-G	634-C	635-C	636-G	637-G
SiO_2	50.06	52.22	50.52	53.07	51.53	51.52	51.08	52.51	52.16	51.77	51.45	54.07	50.56	51.86	51.17	52.68	51.99	52.01
TiO_2	1.67	1.03	1.25	0.52	1.06	0.94	1.14	0.75	0.71	0.92	1.01	0.90	1.62	0.64	0.87	0.59	0.61	0.70
Al_2O_3	4.32	1.94	3.70	1.58	2.00	3.97	1.69	1.72	3.14	2.00	2.18	5.85	3.60	0.93	3.14	2.06	0.71	1.02
Cr_2O_3	-	-	-	-	-	-	-	-	-	-	-	-	-	-	-	-	-	-
FeO_T*	8.25	11.67	8.21	8.25	10.15	7.24	17.50	9.68	7.33	10.80	12.45	7.01	11.07	22.10	7.19	8.46	22.47	21.22
MnO	-	0.33	-	0.33	0.37	-	0.25	0.24	0.29	0.40	0.30	-	0.28	0.42	0.29	0.23	0.41	0.44
MgO	15.09	15.53	15.42	17.73	15.72	15.25	14.80	16.85	16.87	16.59	14.65	13.24	15.68	17.63	15.77	17.55	18.97	18.91
CaO	20.28	17.41	20.03	17.79	18.38	20.35	13.10	17.55	18.18	17.08	18.06	16.85	16.84	5.89	20.62	17.47	3.93	4.96
Na_2O	-	-	-	-	-	-	-	-	-	-	-	0.99	-	-	-	-	-	-
Total	99.67	100.13	99.13	99.27	99.21	99.27	99.56	99.30	98.68	99.56	100.10	98.91	99.65	99.47	99.05	99.04	99.09	99.26
Number of ions on the basis of 6 oxygen																		
Si	1.847	1.928	1.885	1.961	1.931	1.938	1.927	1.936	1.945	1.931	1.913	1.955	1.873	1.973	1.906	1.951	1.977	1.969
Ti	0.046	0.029	0.035	0.014	0.030	0.026	0.032	0.020	0.020	0.026	0.028	0.025	0.045	0.019	0.025	0.016	0.017	0.020
Al	0.188	0.085	0.163	0.069	0.088	0.176	0.075	0.075	0.138	0.088	0.095	0.250	0.157	0.041	0.138	0.090	0.032	0.046
Cr	-	-	-	-	-	-	-	-	-	-	-	-	-	-	-	-	-	-
Fe^{2+}	0.254	0.360	0.256	0.255	0.318	0.228	0.552	0.299	0.229	0.337	0.387	0.212	0.343	0.703	0.224	0.262	0.715	0.672
Mn	-	0.010	-	0.010	0.012	-	0.008	0.008	0.009	0.013	0.010	-	0.009	0.013	0.009	0.007	0.013	0.014
Mg	0.830	0.854	0.858	0.977	0.878	0.855	0.833	0.926	0.938	0.923	0.812	0.713	0.865	1.000	0.876	0.969	1.076	1.067
Ca	0.802	0.689	0.801	0.704	0.738	0.820	0.529	0.694	0.727	0.683	0.719	0.653	0.668	0.240	0.823	0.693	0.160	0.201
Na	-	-	-	-	-	-	-	-	-	-	-	0.069	-	-	-	-	-	-
Cations	3.968	3.955	3.998	3.991	3.995	4.043	3.957	3.958	4.004	4.000	3.964	3.876	3.960	3.989	4.000	3.988	3.990	3.989
Recalculated Al and Fe ions and Fe oxides																		
Al^{IV}	0.153	0.072	0.115	0.039	0.069	0.062	0.073	0.064	0.055	0.069	0.087	0.045	0.127	0.027	0.094	0.049	0.023	0.031
Al^{VI}	0.035	0.012	0.048	0.030	0.019	0.114	0.002	0.011	0.083	0.019	0.008	0.204	0.030	0.014	0.044	0.041	0.009	0.015
Fe^{2+}	0.229	0.358	0.256	0.255	0.318	0.228	0.546	0.287	0.229	0.337	0.364	0.212	0.335	0.703	0.223	0.262	0.715	0.672
Fe^{3+}	0.025	0.002	-	-	-	-	0.006	0.012	-	-	0.023	-	0.008	-	-	-	-	-
FeO	7.44	11.60	8.21	8.25	10.15	7.24	17.32	9.30	7.33	10.80	11.72	7.01	10.82	22.10	7.18	8.46	22.47	21.22
Fe_2O_3	0.90	0.08	-	-	-	-	0.20	0.42	-	-	0.81	-	0.27	-	0.01	-	-	-
End-member compositions																		
Wo	42.5	36.0	41.8	36.2	37.9	43.1	27.5	36.0	38.2	34.9	37.3	41.4	35.5	12.3	42.6	35.9	8.2	10.3
En	44.0	44.7	44.8	50.2	45.1	44.9	43.3	48.1	49.3	47.2	42.1	45.2	45.9	51.1	45.4	50.2	54.8	54.6
Fs	13.5	19.3	13.4	13.6	17.0	12.0	29.2	15.9	12.5	17.9	20.6	13.4	18.7	36.6	12.1	13.9	37.1	35.1

Table A6.10 Electron microprobe analyses of clinopyroxene in group A qz-tholeiitic basalts (continued).

Sample	SAB198										
Analysis	1571-C1	1572-R1	1574-C2	1575-R2	1582-C3	1583-R3	1569-C	1573-G	1576-G	1577-G	1578-G
SiO_2	49.46	50.36	49.66	50.63	50.61	50.96	51.12	48.72	49.86	49.46	5-
TiO_2	1.10	0.97	0.89	1.01	0.91	1.07	0.91	1.91	1.04	1.52	1.13
Al_2O_3	4.81	3.98	4.34	2.54	2.53	2.11	2.37	2.40	1.09	2.73	1.33
Cr_2O_3	0.86	0.57	0.71	0.47	0.65	-	0.29	-	-	-	-
FeO_T	8.13	7.94	7.16	8.61	8.41	9.81	8.75	13.65	16.48	10.77	16.32
MnO	-	-	-	-	-	0.22	-	0.30	0.41	-	0.35
MgO	14.44	14.27	15.09	14.74	15.85	14.53	15.94	12.05	10.86	13.15	11.36
CaO	19.97	20.46	20.94	20.46	19.45	20.23	19.71	18.91	19.08	20.39	19.06
Na_2O	0.91	0.78	0.73	0.72	0.58	0.72	0.75	0.88	0.68	0.71	0.68
Total	99.68	99.33	99.52	99.18	98.99	99.65	99.84	98.82	99.50	98.73	100.23
Number of ions on the basis of 6 oxygen											
Si	1.847	1.883	1.853	1.903	1.899	1.915	1.904	1.882	1.928	1.888	1.923
Ti	0.031	0.027	0.025	0.029	0.026	0.030	0.025	0.056	0.030	0.044	0.032
Al	0.212	0.175	0.191	0.112	0.112	0.094	0.104	0.109	0.050	0.123	0.061
Cr	0.025	0.017	0.021	0.014	0.019	-	0.008	-	-	-	-
Fe^{2+}	0.254	0.248	0.223	0.271	0.264	0.308	0.272	0.441	0.533	0.344	0.525
Mn	-	-	-	-	-	0.007	-	0.010	0.013	-	0.011
Mg	0.804	0.795	0.839	0.826	0.886	0.814	0.885	0.694	0.626	0.748	0.651
Ca	0.799	0.820	0.838	0.824	0.782	0.815	0.787	0.783	0.791	0.834	0.785
Na	0.066	0.056	0.053	0.053	0.042	0.053	0.054	0.066	0.050	0.053	0.051
Cations	4.037	4.021	4.042	4.033	4.030	4.036	4.040	4.041	4.022	4.033	4.040
Recalculated Al and Fe ions and Fe oxides											
Al^{IV}	0.153	0.117	0.147	0.097	0.101	0.085	0.096	0.109	0.050	0.112	0.061
Al^{VI}	0.059	0.058	0.044	0.015	0.011	0.009	0.008	-	-	0.011	-
Fe^{2+}	0.180	0.204	0.137	0.208	0.203	0.240	0.190	0.378	0.492	0.277	0.477
Fe^{3+}	0.074	0.045	0.086	0.062	0.061	0.069	0.083	0.063	0.041	0.067	0.048
FeO	5.75	6.51	4.39	6.63	6.47	7.62	6.10	11.69	15.22	8.67	14.84
Fe_2O_3	2.64	1.59	3.07	2.20	2.16	2.43	2.95	2.17	1.40	2.33	1.64
End-member compositions											
Wo	43.0	44.0	44.1	42.9	40.5	41.9	40.5	40.6	40.3	43.3	39.8
En	43.3	42.7	44.2	43.0	45.9	41.9	45.5	36.0	31.9	38.8	33.0
Fs	13.7	13.3	11.7	14.1	13.7	16.2	14.0	23.4	27.8	17.9	27.2

A6.11 Microprobe analyses of plagioclase feldspar in group A lavas: alkali ol-basalts

Table A6.11 Electron microprobe analyses of plagioclase feldspar in group A alkali ol-basalts.

Sample	SA17							SA18								
Analysis	143-C	146-C	433-C	142-G	426-G	427-G	432-G	1788-C1	1789-R1	1803-C2	1804-R2	1801-C	1796-G	1800-G	1805-G	1806-G
SiO_2	53.55	52.50	52.60	51.47	58.35	62.96	51.86	51.27	52.53	50.77	50.98	50.74	50.80	50.85	55.04	55.83
TiO_2	-	-	-	-	0.18	-	-	-	-	-	0.18	0.18	-	-	-	-
Al_2O_3	28.34	29.83	30.13	30.36	25.97	23.02	30.14	29.90	28.88	30.34	29.52	30.34	29.67	29.86	27.21	26.25
FeO_T	0.74	0.71	0.53	0.56	0.57	0.58	0.91	0.61	0.67	0.52	0.92	0.69	0.98	0.63	1.02	0.77
MgO	-	-	-	-	-	-	-	-	0.25	0.31	0.26	0.37	0.24	0.30	-	0.33
CaO	11.04	12.66	12.65	13.42	7.85	3.89	11.93	12.59	11.59	13.14	12.46	13.10	12.60	12.43	9.82	8.63
Na_2O	4.77	4.13	4.18	3.56	6.63	7.83	4.06	4.16	4.77	4.03	4.28	4.00	4.30	4.28	5.53	6.33
K_2O	0.36	0.23	0.21	0.23	0.73	2.49	0.27	0.19	0.27	0.15	0.22	0.24	0.23	0.22	0.35	0.57
Total	98.80	100.06	100.30	99.60	100.28	100.77	99.17	98.72	98.96	99.26	98.82	99.66	98.82	98.57	98.97	98.71
Number of ions on the basis of 32 oxygen																
Si	9.804	9.475	9.530	9.341	10.451	11.165	9.501	9.453	9.702	9.328	9.418	9.299	9.392	9.402	10.172	10.211
Ti	-	-	-	-	0.026	-	-	-	-	-	0.026	0.026	-	-	-	-
Al	6.118	6.346	6.432	6.496	5.482	4.810	6.509	6.499	6.285	6.570	6.426	6.554	6.467	6.506	5.926	5.661
Fe^{2+}	0.112	0.109	0.080	0.083	0.086	0.086	0.141	0.096	0.102	0.080	0.141	0.106	0.150	0.099	0.157	0.118
Mg	-	-	-	-	-	-	-	-	0.070	0.083	0.074	0.102	0.067	0.083	-	0.090
Ca	2.166	2.448	2.454	2.611	1.507	0.739	2.342	2.490	2.294	2.586	2.467	2.573	2.496	2.464	1.942	1.690
Na	1.693	1.443	1.469	1.251	2.301	2.691	1.443	1.488	1.706	1.437	1.533	1.421	1.542	1.533	1.984	2.246
K	0.083	0.054	0.048	0.054	0.166	0.563	0.064	0.045	0.064	0.035	0.051	0.054	0.054	0.051	0.083	0.131
Cations	19.976	19.875	20.013	19.837	20.019	20.054	20.000	20.070	20.224	20.118	20.134	20.134	20.170	20.138	20.265	20.147
End-member compositions																
An	55.0	62.0	61.8	66.7	37.9	18.5	60.8	61.9	56.5	63.7	60.9	63.6	61.0	60.9	48.4	41.5
Ab	42.9	36.6	37.0	31.9	57.9	67.4	37.5	37.0	42.0	35.4	37.8	35.1	37.7	37.9	49.5	55.2
Or	2.1	1.4	1.2	1.4	4.2	14.1	1.7	1.1	1.6	0.9	1.3	1.3	1.3	1.3	2.1	3.2

Group A lavas: alkali ol-basalts (continued)

Table A6.11 Electron microprobe analyses of plagioclase feldspar in group A alkali ol-basalts (continued).

Sample	SA19			SA33									
Analysis	1993-C	1996-C	1998-C	1707-C1	1708-R1	1713-C2	1714-R2	1715-C3	1716-R3	1731-G	1732-G	1733-G	1736-G
SiO_2	49.88	53.04	51.11	51.70	60.34	51.93	61.91	54.99	54.70	54.21	58.27	58.96	51.53
TiO_2	-	-	-	-	-	-	0.18	-	0.18	-	-	-	-
Al_2O_3	31.09	28.43	29.95	30.18	23.30	30.06	23.64	27.50	28.55	28.63	25.58	25.59	30.70
FeO_T	0.60	0.89	0.45	0.48	1.20	0.51	0.51	0.73	0.47	0.46	0.86	0.57	0.60
MgO	0.46	0.23	0.29	0.38	0.45	0.34	-	0.27	0.41	0.28	0.32	-	0.42
CaO	14.01	11.86	13.32	12.84	5.43	12.95	4.83	9.73	10.53	10.90	6.91	7.27	12.85
Na_2O	3.55	3.97	3.54	4.43	7.77	4.25	8.31	5.39	5.45	5.24	7.16	7.17	4.39
K_2O	0.12	0.25	-	0.19	1.07	0.15	1.28	1.11	0.35	0.27	0.64	0.65	0.12
Total	99.71	98.67	98.66	100.20	99.56	100.19	100.66	99.72	100.64	99.99	99.74	100.21	100.61
Number of ions on the basis of 32 oxygen													
Si	9.149	10.094	9.584	9.405	10.874	9.440	10.986	10.000	9.783	9.814	10.493	10.554	9.235
Ti	0.012	-	-	-	-	-	0.022	-	0.026	-	-	-	-
Al	6.723	6.378	6.618	6.474	4.947	6.442	4.944	5.894	6.019	6.109	5.430	5.398	6.486
Fe^{2+}	0.093	0.141	0.070	0.074	0.179	0.077	0.077	0.112	0.070	0.070	0.131	0.086	0.090
Mg	0.125	0.067	0.080	0.102	0.122	0.093	-	0.074	0.109	0.074	0.086	-	0.112
Ca	2.755	2.419	2.675	2.502	1.050	2.525	0.918	1.894	2.016	2.115	1.334	1.395	2.467
Na	1.264	1.466	1.286	1.565	2.717	1.498	2.858	1.901	1.891	1.840	2.499	2.490	1.526
K	0.029	0.061	-	0.045	0.246	0.035	0.291	0.259	0.080	0.061	0.147	0.147	0.029
Cations	20.150	20.625	20.313	20.166	20.134	20.109	20.096	20.134	19.994	20.083	20.122	20.070	19.946
End-member compositions													
An	68.1	61.3	67.5	60.9	26.2	62.2	22.6	46.7	50.6	52.7	33.5	34.6	61.3
Ab	31.2	37.1	32.5	38.1	67.7	36.9	70.3	46.9	47.4	45.8	62.8	61.7	37.9
Or	0.7	1.5	0.0	1.1	6.1	0.9	7.2	6.4	2.0	1.5	3.7	3.7	0.7

Group A lavas: alkali ol-basalts (continued)

Table A6.11 Electron microprobe analyses of plagioclase feldspar in group A alkali ol-basalts (continued).

Sample	SAB162									
Analysis	1737-C1	1738-R1	1752-C2	1753-R2	1764-C3	1765-R3	1745-G	1750-G	1770-G	1771-G
SiO_2	49.76	49.28	49.19	58.82	49.19	51.34	53.21	49.93	59.37	52.67
TiO_2	-	-	-	0.18	-	-	-	-	-	0.18
Al_2O_3	31.15	31.08	31.18	24.51	31.41	29.34	28.88	31.39	24.67	28.62
FeO_T	0.54	0.68	0.50	0.46	0.63	1.00	0.69	0.66	0.45	0.71
MgO	0.35	0.30	0.29	-	0.24	0.28	0.27	0.29	-	0.25
CaO	14.27	14.04	14.46	6.16	14.28	12.32	11.16	14.29	6.08	11.44
Na_2O	3.51	3.52	3.21	7.15	3.44	4.14	4.98	3.50	7.48	5.02
K_2O	-	0.14	0.15	1.26	0.10	0.26	0.43	0.13	1.04	0.33
Total	99.58	99.04	98.98	98.54	99.29	98.68	99.62	100.19	99.09	99.22
Number of ions on the basis of 32 oxygen										
Si	9.136	9.114	9.094	10.698	9.072	9.485	9.702	9.123	10.723	9.658
Ti	-	-	-	0.026	-	-	-	-	-	0.026
Al	6.742	6.774	6.794	5.254	6.829	6.390	6.208	6.758	5.251	6.186
Fe^{2+}	0.083	0.106	0.077	0.070	0.096	0.154	0.106	0.099	0.067	0.109
Mg	0.096	0.083	0.080	-	0.067	0.077	0.074	0.080	-	0.067
Ca	2.806	2.781	2.864	1.200	2.822	2.438	2.179	2.797	1.174	2.246
Na	1.251	1.261	1.152	2.518	1.232	1.485	1.763	1.242	2.621	1.782
K	-	0.032	0.035	0.291	0.022	0.061	0.099	0.032	0.240	0.077
Cations	20.115	20.150	20.096	20.058	20.141	20.090	20.131	20.131	20.077	20.150
End-member compositions										
An	69.2	68.3	70.7	29.9	69.2	61.2	53.9	68.7	29.1	54.7
Ab	30.8	31.0	28.4	62.8	30.2	37.3	43.6	30.5	64.9	43.4
Or	0.0	0.8	0.9	7.3	0.5	1.5	2.5	0.8	5.9	1.9

A6.12 Microprobe analyses of plagioclase feldspar in group A lavas: transitional basalt

Table A6.12 Electron microprobe analyses of plagioclase feldspar in group A transitional basalt.

Sample	SA07							SA10					
Analysis	1886-C	1891-C	1887-G	1897-G	1903-G	1909-G	1914-G	1828-C	1830-C	1818-G	1820-G	1825-G	1834-G
SiO_2	52.50	50.77	50.69	51.18	52.46	53.37	52.97	50.38	49.53	50.52	53.81	49.48	49.70
TiO_2	0.22	-	-	-	0.42	0.21	0.30	-	-	0.20	0.24	-	-
Al_2O_3	28.74	30.50	29.95	29.83	23.66	28.59	26.73	30.12	31.17	30.62	28.15	31.14	31.02
FeO_T	0.77	0.69	0.84	0.82	2.61	0.92	1.75	0.48	0.58	0.76	0.99	0.66	0.76
MgO	0.38	0.42	0.31	0.34	2.92	0.37	0.74	0.30	0.40	0.32	0.27	0.35	0.39
CaO	11.90	13.43	13.24	13.40	12.70	11.63	11.40	13.56	14.38	13.73	11.12	14.31	13.92
Na_2O	4.13	3.80	3.66	3.39	4.39	4.98	4.45	3.61	3.24	3.69	4.98	3.08	3.71
K_2O	0.24	0.10	0.14	-	0.22	0.20	0.27	-	-	0.10	0.24	-	0.10
Total	98.88	99.71	98.83	98.96	99.38	100.27	98.61	98.45	99.30	99.94	99.80	99.02	99.60
Number of ions on the basis of 32 oxygen													
Si	9.810	9.293	9.473	9.580	9.763	9.683	9.975	9.325	9.120	9.238	9.789	9.133	9.136
Ti	0.032	-	-	-	0.058	0.029	0.008	-	-	0.026	0.032	-	-
Al	6.330	6.582	6.557	6.582	5.190	6.115	5.933	6.573	6.765	6.602	6.038	6.774	6.723
Fe^{2+}	0.118	0.106	0.131	0.128	0.406	0.141	0.275	0.074	0.090	0.115	0.150	0.102	0.118
Mg	0.106	0.112	0.086	0.096	0.810	0.102	0.208	0.083	0.109	0.086	0.074	0.096	0.106
Ca	2.381	2.634	2.634	2.688	2.531	2.259	2.301	2.688	2.838	2.691	2.170	2.829	2.742
Na	1.498	1.350	1.315	1.229	1.584	1.754	1.626	1.293	1.155	1.309	1.757	1.101	1.325
K	0.058	0.026	0.032	-	0.051	0.045	0.064	-	-	0.026	0.054	-	0.026
Cations	20.331	20.102	20.228	20.303	20.394	20.128	20.390	20.035	20.077	20.093	20.064	20.035	20.176
End-member compositions													
An	60.5	65.7	66.2	68.6	60.8	55.7	57.7	67.5	71.1	66.9	54.5	72.0	67.0
Ab	38.0	33.7	33.0	31.4	38.0	43.2	40.7	32.5	28.9	32.5	44.1	28.0	32.4
Or	1.5	0.6	0.8	0.0	1.2	1.1	1.6	0.0	0.0	0.6	1.4	0.0	0.6

Group A lavas: transitional basalt (continued)

Table A6.12 Electron microprobe analyses of plagioclase feldspar in group A transitional basalt (continued).

Sample	SA13													
Analysis	34-C1	35-R1	40-C2	41-R2	581-C3	582-R3	48-C	42-G	560-G	561-G	564-G	567-G	568-G	570-G
SiO_2	51.93	53.78	51.14	54.28	50.96	53.56	57.41	54.29	54.25	54.71	56.64	54.98	53.80	53.01
TiO_2	-	-	-	-	-	-	-	-	-	-	0.20	0.20	-	-
Al_2O_3	30.09	28.41	30.88	28.44	31.35	28.47	25.67	28.94	27.88	28.24	27.07	27.80	29.24	29.30
FeO_T	0.46	0.97	0.72	0.90	0.56	1.19	0.83	0.85	1.17	0.94	1.16	1.10	0.90	0.89
MgO	-	-	-	-	-	-	-	-	-	-	-	-	-	-
CaO	13.40	11.41	14.32	11.46	14.32	11.61	8.22	11.60	10.68	11.01	9.27	10.68	12.09	12.35
Na_2O	4.02	4.51	3.48	4.81	3.62	4.74	6.38	4.96	5.05	4.96	6.12	5.18	4.77	4.54
K_2O	-	0.21	-	0.20	-	0.22	0.46	0.17	0.27	0.17	0.37	0.40	0.12	0.12
Total	99.90	99.29	100.5	100.09	100.81	99.79	98.97	100.81	99.30	100.03	100.83	100.34	100.92	100.21
Number of ions on the basis of 32 oxygen														
Si	9.392	9.744	9.226	9.760	9.180	9.760	10.407	9.702	9.904	9.898	10.096	9.936	9.690	9.622
Ti	-	-	-	-	-	-	-	-	-	-	0.026	0.026	-	-
Al	6.416	6.067	6.566	6.029	6.656	6.115	5.485	6.093	6.000	6.022	5.686	5.923	6.208	6.269
Fe^{2+}	0.070	0.147	0.109	0.134	0.083	0.182	0.125	0.125	0.179	0.144	0.173	0.166	0.134	0.134
Mg	-	-	-	-	-	-	-	-	-	-	-	-	-	-
Ca	2.598	2.214	2.768	2.208	2.765	2.266	1.597	2.221	2.090	2.134	1.770	2.067	2.333	2.403
Na	1.411	1.584	1.216	1.677	1.264	1.674	2.243	1.718	1.786	1.738	2.115	1.814	1.664	1.597
K	-	0.048	-	0.045	-	0.051	0.109	0.038	0.064	0.042	0.083	0.093	0.029	0.026
Cations	19.888	19.805	19.88	19.853	19.948	20.048	19.966	19.898	20.022	19.978	19.949	20.026	20.058	20.051
End-member compositions														
An	64.8	57.6	69.5	56.2	68.6	56.8	40.4	55.8	53.0	54.5	44.6	52.0	57.9	59.7
Ab	35.2	41.2	30.5	42.7	31.4	41.9	56.8	43.2	45.3	44.4	53.3	45.7	41.3	39.7
Or	0.0	1.2	0.0	1.1	0.0	1.3	2.8	1.0	1.6	1.1	2.1	2.3	0.7	0.6

A6.13 Microprobe analyses of plagioclase feldspar in group A lavas: hawaiites

Table A6.13 Electron microprobe analyses of plagioclase feldspar in group A hawaiites.

Sample	SA20												SA32				
Analysis	1843-C1	1844-R1	1860-C2	1861-R2	1867-C3	1868-R3	1873-G	1874-G	1875-G	1878-G	1882-C4	1883-R4	1950-G	1951-G	1953-G	1954-G	1955-G
SiO_2	51.17	51.27	54.07	53.60	50.86	54.52	54.96	53.45	53.73	54.04	51.47	53.77	51.57	58.76	58.96	51.82	51.61
TiO_2	-	-	0.18	-	-	0.37	-	-	-	0.18	-	-	0.32	-	-	-	-
Al_2O_3	30.73	30.86	28.46	28.40	30.36	28.45	27.93	29.08	28.48	28.38	30.28	28.45	29.00	24.60	24.64	29.49	29.63
FeO_T	0.62	0.50	0.68	1.47	0.56	1.84	0.93	0.58	1.09	0.84	0.47	0.78	1.16	0.54	0.47	1.08	0.72
MgO	0.34	0.35	-	0.24	0.29	0.30	-	0.26	0.31	0.39	0.28	0.33	0.22	0.23	-	-	0.27
CaO	13.49	13.44	10.91	9.97	13.46	9.87	10.22	11.47	10.92	10.49	13.11	10.98	11.45	6.25	6.58	12.06	12.38
Na_2O	4.07	4.04	5.09	4.90	4.01	4.96	5.38	5.16	5.02	5.30	4.19	5.29	4.37	7.06	6.99	4.38	4.41
K_2O	0.16	0.18	0.32	0.33	0.15	0.37	0.32	0.26	0.29	0.35	0.12	0.30	0.99	1.11	0.96	0.27	0.29
Total	100.58	100.64	99.71	98.91	99.69	100.68	99.74	100.26	99.84	99.97	99.92	99.90	99.08	98.55	98.60	99.10	99.31
Number of ions on the basis of 32 oxygen																	
Si	9.293	9.244	9.824	9.878	9.315	9.827	9.968	9.683	9.773	9.802	9.386	9.773	9.520	10.682	10.824	9.530	9.472
Ti	-	-	0.026	-	-	0.051	-	-	-	0.026	-	-	0.045	-	-	-	-
Al	6.579	6.557	6.093	6.166	6.554	6.045	5.971	6.211	6.106	6.067	6.509	6.096	6.310	5.270	5.331	6.390	6.410
Fe^{2+}	0.093	0.074	0.102	0.227	0.086	0.278	0.141	0.090	0.166	0.128	0.070	0.118	0.179	0.083	0.074	0.166	0.109
Mg	0.090	0.093	-	0.064	0.077	0.080	-	0.070	0.083	0.106	0.077	0.090	0.061	0.061	-	-	0.077
Ca	2.624	2.598	2.125	1.968	2.643	1.907	1.987	2.227	2.128	2.038	2.560	2.138	2.266	1.216	1.293	2.378	2.435
Na	1.434	1.414	1.795	1.750	1.424	1.734	1.891	1.811	1.773	1.862	1.482	1.866	1.565	2.486	2.486	1.565	1.568
K	0.035	0.042	0.074	0.080	0.035	0.086	0.074	0.061	0.067	0.080	0.029	0.070	0.234	0.259	0.224	0.064	0.067
Cations	20.147	20.022	20.038	20.134	20.134	20.010	20.032	20.154	20.096	20.109	20.112	20.150	20.179	20.058	20.232	20.093	20.138
End-member compositions																	
An	64.1	64.1	53.2	51.8	64.4	51.2	50.3	54.3	53.6	51.2	62.9	52.5	55.7	30.7	32.3	59.3	59.8
Ab	35.0	34.9	45.0	46.1	34.7	46.5	47.9	44.2	44.7	46.8	36.4	45.8	38.5	62.8	62.1	39.1	38.5
Or	0.9	1.0	1.8	2.1	0.9	2.3	1.9	1.5	1.7	2.0	0.7	1.7	5.7	6.5	5.6	1.6	1.7

Group A lavas: hawaiites (continued)

Table A6.13 Electron microprobe analyses of plagioclase feldspar in group A hawaiites (continued).

Sample	SAB151																
Analysis	665-C1	666-R1	667-C2	668-R2	671-C3	672-R3	199-C	207-C	206-G	689-C4	690-R4	673-C	675-G	676-G	677-G	679-G	680-G
SiO_2	55.55	53.65	52.75	53.76	51.32	60.44	53.72	50.64	59.46	53.27	55.76	53.12	55.67	58.73	63.36	53.27	63.42
TiO_2	0.18	-	0.18	0.19	-	-	0.21	-	0.25	-	0.23	0.20	-	-	-	-	0.25
Al_2O_3	27.25	29.53	28.69	29.31	31.02	23.87	28.63	30.54	24.22	28.95	27.50	29.90	28.29	25.78	21.47	29.29	22.74
FeO_T	0.96	0.65	0.84	0.80	0.55	0.67	0.77	0.58	0.58	0.54	1.06	0.70	0.65	0.56	0.82	0.59	0.80
MgO	-	-	-	-	-	-	-	-	-	-	-	-	-	-	-	-	-
CaO	10.18	12.19	11.85	11.72	13.96	5.62	11.34	13.81	6.15	12.13	10.08	12.23	10.52	7.64	3.48	11.98	3.77
Na_2O	5.42	4.54	4.27	4.85	3.27	7.30	4.75	3.07	7.21	4.45	5.64	4.50	5.44	6.74	7.94	4.47	8.24
K_2O	0.31	0.23	0.23	0.31	-	0.99	0.28	0.14	0.78	0.19	0.41	0.25	0.32	0.67	2.15	0.31	1.67
Total	99.85	100.79	98.81	100.94	100.12	98.89	99.70	98.78	98.65	99.53	100.68	100.90	100.89	100.12	99.22	99.91	100.89
Number of ions on the basis of 32 oxygen																	
Si	10.061	9.664	9.747	9.677	9.328	10.906	9.699	9.324	10.682	9.706	10.029	9.517	9.971	10.518	11.379	9.677	11.200
Ti	0.026	-	0.026	0.026	-	-	0.029	-	0.035	-	0.032	0.026	-	-	-	-	0.032
Al	5.818	6.269	6.246	6.221	6.646	5.075	6.093	6.627	5.130	6.218	5.830	6.314	5.974	5.443	4.544	6.272	4.733
Fe^{2+}	0.147	0.099	0.128	0.122	0.083	0.102	0.115	0.090	0.086	0.083	0.160	0.106	0.099	0.083	0.125	0.090	0.118
Mg	-	-	-	-	-	-	-	-	-	-	-	-	-	-	-	-	-
Ca	1.974	2.352	2.346	2.259	2.717	1.088	2.195	2.726	1.184	2.368	1.942	2.346	2.019	1.466	0.669	2.333	0.714
Na	1.901	1.587	1.530	1.696	1.152	2.554	1.664	1.098	2.512	1.574	1.968	1.562	1.891	2.339	2.765	1.574	2.822
K	0.070	0.054	0.054	0.070	-	0.227	0.064	0.032	0.179	0.045	0.096	0.058	0.074	0.154	0.493	0.070	0.378
Cations	19.997	20.026	20.076	20.070	19.926	19.952	19.859	19.897	19.808	19.994	20.058	19.926	20.029	20.003	19.974	20.016	19.997
End-member compositions																	
An	50.0	58.9	59.7	56.1	70.2	28.1	56.0	70.7	30.6	59.4	48.5	59.2	50.7	37.0	17.0	58.6	18.2
Ab	48.2	39.7	38.9	42.1	29.8	66.0	42.4	28.5	64.8	39.5	49.1	39.4	47.5	59.1	70.4	39.6	72.1
Or	1.8	1.4	1.4	1.7	0.0	5.9	1.6	0.8	4.6	1.1	2.4	1.5	1.8	3.9	12.6	1.8	9.6

Table A6.13 Electron microprobe analyses of plagioclase feldspar in group A hawaiites (continued).

Sample	SAB163								
Analysis	1958-C1	1959-R1	1966-C2	1967-R2	1984-C	1965-G	1970-G	1989-G	1991-G
SiO_2	50.10	49.44	49.10	56.04	51.29	54.97	56.20	54.18	54.84
TiO_2	-	-	-	-	-	0.20	0.19	0.21	0.37
Al_2O_3	30.94	31.26	31.13	27.97	3-	27.75	27.50	28.60	26.85
FeO_T	0.57	1.02	0.64	0.75	0.71	0.61	0.88	0.72	1.51
MgO	0.35	0.57	0.25	0.29	0.35	-	0.23	0.29	-
CaO	13.82	13.55	14.51	7.01	12.74	9.86	9.05	11.00	9.64
Na_2O	3.56	2.82	3.25	5.81	4.26	5.60	6.19	5.30	4.66
K_2O	0.13	0.21	0.13	0.67	0.24	0.50	0.59	0.36	0.95
Total	99.47	98.87	99.01	98.54	99.59	99.49	100.83	100.66	98.82
Number of ions on the basis of 32 oxygen									
Si	9.200	9.404	9.088	10.296	9.395	9.987	10.077	9.770	10.299
Ti	-	-	-	-	-	0.026	0.026	0.029	0.051
Al	6.698	7.008	6.790	6.058	6.477	5.942	5.814	6.080	5.942
Fe^{2+}	0.086	0.163	0.099	0.115	0.109	0.093	0.131	0.109	0.237
Mg	0.096	0.160	0.070	0.080	0.096	-	0.061	0.077	-
Ca	2.720	2.762	2.877	1.382	2.499	1.920	1.741	2.125	1.939
Na	1.267	1.040	1.165	2.070	1.514	1.974	2.150	1.856	1.699
K	0.029	0.051	0.032	0.157	0.054	0.115	0.134	0.083	0.227
Cations	20.096	20.588	20.122	20.158	20.144	20.058	20.134	20.128	20.395
End-member compositions									
An	67.7	71.7	70.6	38.3	61.4	47.9	43.2	52.3	50.2
Ab	31.6	27.0	28.6	57.4	37.2	49.2	53.4	45.7	44.0
Or	0.7	1.3	0.8	4.3	1.3	2.9	3.3	2.0	5.9

A6.14 Microprobe analyses of plagioclase feldspar in group A lavas: ol-tholeiitic basalts

Table A6.14 Electron microprobe analyses of plagioclase feldspar in group A ol-tholeiitic baslats.

Sample	SA80																
Analysis	106-C1	107-R1	112-C2	113-R2	550-C3	551-R3	557-C4	558-R4	111-G	544-G	545-G	546-G	549-G	552-G	554-G	556-G	559-G
SiO_2	52.41	52.57	52.66	53.81	50.82	58.21	52.27	53.22	52.61	51.81	54.48	53.99	56.17	56.43	54.33	53.07	54.21
TiO_2	-	-	-	-	-	-	-	-	-	-	-	-	-	0.20	-	-	-
Al_2O_3	29.58	29.45	29.67	28.15	31.97	25.34	30.31	29.09	29.99	29.79	28.75	28.93	27.80	26.20	28.96	29.76	28.66
FeO_T	0.59	0.60	0.41	0.60	0.41	0.64	0.40	0.65	0.71	0.52	0.64	0.52	0.56	0.56	0.65	0.50	0.59
MgO	-	-	-	-	-	-	-	-	-	-	-	-	-	-	-	-	-
CaO	12.75	12.66	12.79	11.16	12.38	7.75	13.38	11.88	12.39	12.71	11.63	11.94	10.25	9.15	11.94	12.64	11.41
Na_2O	4.21	4.07	3.98	4.86	4.02	6.74	4.06	4.77	4.76	3.85	4.83	4.67	5.57	5.83	4.73	4.43	4.78
K_2O	0.15	0.20	0.20	0.28	0.11	0.58	0.16	0.29	0.23	0.17	0.19	0.19	0.36	0.38	0.23	0.11	0.22
Total	99.69	99.55	99.71	98.86	99.71	99.26	100.58	99.90	100.69	98.85	100.52	100.24	100.71	98.75	100.84	100.51	99.87
Number of ions on the basis of 32 oxygen																	
Si	9.491	9.523	9.514	9.782	9.254	10.525	9.459	9.677	9.239	9.517	9.818	9.760	10.064	10.399	9.770	9.590	9.824
Ti	-	-	-	-	-	-	-	-	-	-	-	-	-	0.029	-	-	-
Al	6.314	6.288	6.320	6.032	6.861	5.402	6.464	6.237	6.208	6.451	6.106	6.166	5.872	5.690	6.141	6.339	6.122
Fe^{2+}	0.090	0.093	0.061	0.093	0.061	0.096	0.061	0.099	0.102	0.080	0.096	0.080	0.083	0.086	0.099	0.074	0.090
Mg	-	-	-	-	-	-	-	-	-	-	-	-	-	-	-	-	-
Ca	2.474	2.458	2.477	2.173	2.416	1.501	2.595	2.317	2.333	2.502	2.246	2.314	1.968	1.805	2.301	2.448	2.214
Na	1.478	1.427	1.395	1.712	1.421	2.362	1.424	1.683	1.622	1.370	1.686	1.635	1.936	2.083	1.651	1.552	1.680
K	0.035	0.048	0.048	0.064	0.026	0.134	0.035	0.067	0.051	0.038	0.042	0.042	0.083	0.090	0.051	0.026	0.051
Cations	19.882	19.837	19.814	19.856	20.038	20.019	20.038	20.080	19.556	19.958	19.994	19.997	20.006	20.181	20.013	20.029	19.981
End-member compositions																	
An	62.0	62.5	63.2	55.0	62.6	37.6	64.0	57.0	58.2	64.0	56.5	58.0	49.4	45.4	57.5	60.8	56.1
Ab	37.1	36.3	35.6	43.4	36.8	59.1	35.1	41.4	40.5	35.0	42.4	41.0	48.6	52.4	41.2	38.6	42.6
Or	0.9	1.2	1.2	1.6	0.7	3.4	0.9	1.7	1.3	1.0	1.0	1.0	2.1	2.3	1.3	0.6	1.3

Table A6.14 Electron microprobe analyses of plagioclase feldspar in group A ol-tholeiitic baslats (continued).

Sample	SAB152																	
Analysis	711-C1	712-R1	713-C2	714-R2	715-C3	716-R3	696-C4	697-R4	253-C	255-C	256-C	258-C	259-C	693-G	694-G	695-G	699-G	700-G
SiO_2	52.71	54.74	50.99	52.55	53.38	63.18	53.31	58.66	52.84	56.89	56.98	52.92	56.02	59.05	53.36	54.39	61.16	59.83
TiO_2	-	-	-	-	-	-	-	-	-	-	0.18	-	-	0.20	-	-	-	-
Al_2O_3	28.98	27.89	31.28	29.53	29.19	22.62	29.08	24.38	28.92	26.48	24.71	29.16	26.53	25.22	29.53	27.84	24.46	23.67
FeO_T	1.26	1.09	0.58	1.27	0.90	0.38	0.71	1.65	0.64	0.80	2.74	0.78	0.90	0.93	0.96	1.48	0.79	1.80
MgO	0.43	-	-	0.30	-	-	-	0.69	-	-	0.98	-	-	-	-	0.40	-	0.73
CaO	11.88	10.60	13.96	12.56	11.96	3.94	12.01	6.22	11.99	8.74	6.80	12.25	9.22	7.23	12.27	10.27	5.65	5.59
Na_2O	4.17	5.19	3.73	4.21	4.54	8.34	4.63	7.13	4.53	6.32	6.53	4.46	5.65	6.92	4.45	4.96	7.40	6.90
K_2O	0.19	0.30	-	0.18	0.22	1.46	0.21	0.61	0.20	0.54	0.55	0.17	0.63	0.70	0.22	0.33	1.24	0.97
Total	99.62	99.81	100.54	100.60	100.19	99.92	99.95	99.34	99.12	99.77	99.47	99.74	98.95	100.25	100.79	99.67	100.70	99.49
Number of ions on the basis of 32 oxygen																		
Si	9.626	9.936	9.149	9.530	9.680	11.238	9.686	10.618	9.606	10.202	10.304	9.574	10.141	10.576	9.629	9.898	10.858	10.794
Ti	-	-	-	-	-	-	-	-	-	-	0.026	-	-	0.029	-	-	-	-
Al	6.237	5.968	6.614	6.310	6.240	4.742	6.227	5.200	6.198	5.597	5.267	6.218	5.658	5.325	6.282	5.971	5.120	5.034
Fe^{2+}	0.192	0.166	0.086	0.192	0.138	0.058	0.109	0.250	0.099	0.118	0.416	0.118	0.134	0.138	0.144	0.224	0.118	0.272
Mg	0.115	-	-	0.080	-	-	-	0.186	-	0.019	0.262	-	-	-	-	0.109	-	0.195
Ca	2.323	2.061	2.685	2.442	2.323	0.752	2.339	1.206	2.336	1.680	1.315	2.374	1.789	1.389	2.374	2.000	1.075	1.082
Na	1.478	1.827	1.296	1.478	1.594	2.877	1.632	2.502	1.600	2.198	2.291	1.565	1.984	2.403	1.555	1.750	2.547	2.413
K	0.045	0.070	-	0.042	0.051	0.330	0.048	0.141	0.048	0.125	0.125	0.038	0.147	0.160	0.051	0.077	0.282	0.221
Cations	20.016	20.029	19.830	20.074	20.026	19.997	20.042	20.102	19.888	19.939	20.006	19.888	19.853	20.019	20.035	20.029	20.000	20.010
End-member compositions																		
An	60.4	52.1	67.4	61.6	58.5	19.0	58.2	31.3	58.6	42.0	35.2	59.7	45.6	35.1	59.6	52.3	27.5	29.1
Ab	38.4	46.2	32.6	37.3	40.2	72.7	40.6	65.0	40.2	54.9	61.4	39.3	50.6	60.8	39.1	45.7	65.2	64.9
Or	1.2	1.8	0.0	1.1	1.3	8.3	1.2	3.7	1.2	3.1	3.3	1.0	3.8	4.0	1.3	2.0	7.2	5.9

Table A6.14 Electron microprobe analyses of plagioclase feldspar in group A ol-tholeiitic basalts (continued).

Sample	SAB169														SAB181		
Analysis	16-R1	23-C2Z1*	24-C2Z2*	25-R2	411-C3Z1*	413-C3Z2*	414-C3Z3*	412-R3	416-C4	417-R4	29-G	415-G	418-G	419-G	512-C1	513-R1	514-C2
SiO_2	54.33	52.15	51.23	51.47	52.99	52.00	52.08	57.02	52.27	51.28	54.69	55.40	54.55	53.79	52.89	52.74	52.86
TiO_2	-	-	-	-	-	-	-	0.33	-	-	-	-	0.22	-	-	-	-
Al_2O_3	28.57	30.19	30.43	29.89	29.59	30.48	30.00	26.20	30.41	30.66	28.41	28.06	27.73	27.97	29.59	29.37	29.59
FeO_T	0.71	0.57	0.66	0.83	0.47	0.58	0.46	0.99	0.63	0.88	0.63	0.83	1.03	0.93	0.55	0.84	0.50
MgO	-	-	-	-	-	-	-	-	-	-	-	-	-	-	-	-	-
CaO	11.64	13.28	13.48	13.22	12.30	13.51	13.08	8.83	12.81	13.60	11.17	10.70	10.48	11.03	12.46	12.47	12.71
Na_2O	4.66	3.94	3.69	3.81	4.42	3.67	3.73	6.05	4.19	4.01	4.97	5.48	5.28	4.79	4.09	4.27	4.31
K_2O	0.22	0.15	0.13	0.18	0.12	0.13	0.11	0.51	0.16	0.12	0.26	0.32	0.41	0.22	0.17	0.20	0.15
Total	100.13	100.28	99.62	99.40	99.89	100.37	99.46	99.93	100.47	100.55	100.13	100.79	99.70	98.73	99.75	99.89	100.12
Number of ions on the basis of 32 oxygen																	
Si	9.757	9.398	9.306	9.376	9.622	9.427	9.507	10.288	9.380	9.270	9.808	9.955	9.923	9.926	9.616	9.603	9.590
Ti	-	-	-	-	-	-	-	0.045	-	-	-	-	0.032	-	-	-	-
Al	6.048	6.413	6.515	6.419	6.333	6.515	6.454	5.571	6.432	6.531	6.006	5.942	5.946	6.083	6.342	6.304	6.330
Fe^{2+}	0.106	0.086	0.099	0.128	0.070	0.090	0.070	0.150	0.096	0.131	0.096	0.125	0.157	0.144	0.083	0.128	0.077
Mg	-	-	-	-	-	-	-	-	-	-	-	-	-	-	-	-	-
Ca	2.240	2.563	2.624	2.579	2.394	2.624	2.560	1.709	2.464	2.634	2.147	2.061	2.042	2.182	2.429	2.432	2.470
Na	1.622	1.376	1.302	1.344	1.555	1.290	1.322	2.118	1.456	1.405	1.728	1.910	1.859	1.715	1.443	1.507	1.517
K	0.051	0.035	0.032	0.042	0.026	0.029	0.026	0.118	0.035	0.029	0.061	0.074	0.096	0.051	0.038	0.048	0.035
Cations	19.824	19.872	19.878	19.888	20.000	19.974	19.939	20.000	19.863	19.999	19.846	20.067	20.054	20.102	19.952	20.022	20.019
End-member compositions																	
An	57.2	64.5	66.3	65.1	60.2	66.6	65.5	43.3	62.3	64.8	54.6	50.9	51.1	55.3	62.1	61.0	61.4
Ab	41.5	34.6	32.9	33.9	39.1	32.7	33.8	53.7	36.8	34.5	43.9	47.2	46.5	43.4	36.9	37.8	37.7
Or	1.3	0.9	0.8	1.0	0.6	0.7	0.7	3.0	0.9	0.7	1.5	1.8	2.4	1.3	1.0	1.2	0.9

Table A6.14 Electron microprobe analyses of plagioclase feldspar in group A ol-tholeiitic basalts (continued).

Sample	SAB181 (continued)															SAB187		
Analysis	516-R2	184-C	194-C	511-C	185-G	193-G	503-G	504-G	505-G	506-G	507-G	508-G	509-G	510-G	515-G	530-C1	531-R1	533-C2
SiO_2	51.54	52.13	54.02	53.20	55.37	54.82	54.12	56.02	61.86	62.28	53.39	60.65	52.98	56.34	60.16	52.85	58.82	53.94
TiO_2	-	-	0.19	-	-	-	-	-	-	0.36	-	-	-	-	-	-	0.19	-
Al_2O_3	31.02	29.45	29.00	29.65	27.72	28.03	29.13	27.62	23.11	22.52	29.76	24.84	29.44	27.85	23.96	29.39	25.95	28.79
FeO_T	0.42	0.36	0.59	0.41	0.43	0.47	0.52	0.63	0.88	1.18	0.56	0.66	0.62	0.55	0.73	0.52	0.75	0.58
MgO	-	-	-	-	-	-	-	-	-	-	-	-	-	-	-	-	-	-
CaO	11.64	12.74	11.84	12.55	10.72	10.85	11.84	10.30	5.58	5.34	12.60	6.54	12.67	10.24	6.20	12.31	7.80	11.57
Na_2O	4.11	4.18	4.69	4.40	5.41	4.97	4.67	5.55	7.85	6.69	4.39	7.49	4.18	5.41	7.08	4.31	6.73	4.79
K_2O	0.14	0.12	0.24	0.16	0.25	0.26	0.18	0.31	0.98	1.74	0.18	0.70	0.16	0.31	0.74	0.17	0.54	0.24
Total	98.87	98.98	100.57	100.37	99.90	99.40	100.46	100.43	100.26	100.11	100.88	100.88	100.05	100.70	98.87	99.55	100.78	99.91
Number of ions on the basis of 32 oxygen																		
Si	9.490	9.498	9.670	9.619	9.936	9.882	9.757	10.070	10.966	11.120	9.613	10.752	9.619	10.083	10.923	9.632	10.477	9.782
Ti	-	-	0.026	-	-	-	-	-	-	0.048	-	-	-	-	-	-	0.026	-
Al	6.730	6.323	6.118	6.320	5.862	5.958	6.192	5.853	4.829	4.739	6.317	5.190	6.298	5.875	5.126	6.314	5.450	6.154
Fe^{2+}	0.064	0.054	0.090	0.064	0.064	0.070	0.077	0.096	0.131	0.176	0.083	0.096	0.096	0.083	0.112	0.080	0.112	0.086
Mg	-	-	-	-	-	-	-	-	-	-	-	-	-	-	-	-	-	-
Ca	2.294	2.486	2.272	2.432	2.061	2.096	2.288	1.984	1.059	1.021	2.432	1.242	2.464	1.965	1.206	2.403	1.488	2.246
Na	1.466	1.478	1.629	1.542	1.882	1.738	1.632	1.936	2.701	2.317	1.533	2.576	1.472	1.878	2.493	1.523	2.326	1.686
K	0.032	0.029	0.054	0.035	0.058	0.058	0.042	0.070	0.221	0.397	0.042	0.157	0.035	0.070	0.170	0.038	0.122	0.054
Cations	20.076	19.869	19.859	20.013	19.862	19.802	19.987	20.010	19.907	19.818	20.019	20.013	19.984	19.955	20.030	19.990	20.000	20.010
End-member compositions																		
An	60.5	62.3	57.4	60.7	51.5	53.9	57.8	49.7	26.6	27.3	60.7	31.2	62.0	50.2	31.2	60.6	37.8	56.3
Ab	38.6	37.0	41.2	38.5	47.0	44.7	41.2	48.5	67.8	62.0	38.3	64.8	37.1	48.0	64.4	38.4	59.1	42.3
Or	0.8	0.7	1.4	0.9	1.4	1.5	1.1	1.8	5.5	10.6	1.0	3.9	0.9	1.8	4.4	1.0	3.1	1.4

Table A6.14 Electron microprobe analyses of plagioclase feldspar in group A ol-tholeiitic basalts (continued).

Sample	SAB187 (continued)													SA36				
Analysis	535-R2	536-C3	537-R3	269-C	270-C	271-C	279-C	522-G	523-G	525-G	529-G	532-G	538-G	810-G	811-G	813-G	815-G	816-G
SiO_2	53.35	52.59	53.25	53.38	53.93	53.13	53.29	53.36	53.49	53.36	54.29	52.86	52.88	59.72	53.28	52.88	54.37	53.13
TiO_2	-	-	-	-	-	-	-	-	-	0.23	-	-	-	0.27	0.22	-	-	0.32
Al_2O_3	29.25	29.14	29.15	29.03	29.18	29.06	29.18	29.50	28.92	28.16	28.49	29.55	29.14	23.73	28.49	28.78	27.76	28.07
FeO_T	0.75	0.56	0.66	0.52	0.61	0.64	0.61	0.59	0.55	0.91	0.72	0.56	0.67	1.01	0.92	1.18	1.00	0.93
MgO	-	-	-	-	-	-	-	-	-	-	-	-	-	-	-	-	-	-
CaO	11.83	12.15	12.00	12.19	12.17	12.05	12.17	12.21	11.82	11.04	11.43	12.36	12.11	7.78	11.37	11.55	10.63	11.90
Na_2O	4.62	4.49	4.56	4.48	4.40	4.53	4.40	4.40	4.82	4.87	4.80	4.40	4.43	5.00	4.68	4.87	5.08	4.25
K_2O	0.20	0.18	0.18	0.17	0.23	0.19	0.22	0.23	0.25	0.25	0.23	0.24	0.17	1.52	0.24	0.24	0.32	0.32
Total	100.00	99.11	99.80	99.77	100.52	99.60	99.87	100.29	99.85	98.82	99.96	99.97	99.40	99.03	99.20	99.50	99.16	98.92
Number of ions on the basis of 32 oxygen																		
Si	9.683	9.635	9.683	9.619	9.725	9.613	9.613	9.654	9.722	9.795	9.837	9.606	9.658	10.932	9.747	9.677	9.933	9.757
Ti	-	-	-	-	-	-	-	-	-	0.032	-	-	-	0.038	0.032	-	-	0.045
Al	6.256	6.294	6.246	6.166	6.202	6.198	6.202	6.291	6.195	6.093	6.086	6.330	6.272	5.120	6.144	6.208	5.978	6.077
Fe^{2+}	0.112	0.086	0.099	0.080	0.093	0.096	0.093	0.090	0.083	0.141	0.109	0.083	0.102	0.157	0.141	0.182	0.154	0.144
Mg	-	-	-	-	-	-	-	-	-	-	-	-	-	-	-	-	-	-
Ca	2.301	2.384	2.339	2.355	2.352	2.336	2.352	2.368	2.301	2.173	2.218	2.406	2.368	1.526	2.227	2.266	2.080	2.342
Na	1.626	1.597	1.606	1.565	1.539	1.590	1.539	1.542	1.699	1.734	1.686	1.552	1.571	1.773	1.661	1.728	1.798	1.514
K	0.045	0.042	0.042	0.038	0.051	0.045	0.051	0.051	0.058	0.058	0.054	0.054	0.042	0.355	0.058	0.054	0.074	0.077
Cations	20.022	20.038	20.016	19.824	19.962	19.878	19.850	19.997	20.058	20.026	19.990	20.032	20.013	19.901	20.010	20.115	20.016	19.955
End-member compositions																		
An	57.9	59.3	58.7	59.5	59.7	58.8	59.7	59.8	56.7	54.8	56.0	60.0	59.5	41.8	56.4	56.0	52.6	59.6
Ab	40.9	39.7	40.3	39.5	39.0	40.0	39.0	38.9	41.9	43.7	42.6	38.7	39.5	48.5	42.1	42.7	45.5	38.5
Or	1.1	1.0	1.0	1.0	1.3	1.1	1.3	1.3	1.4	1.5	1.4	1.4	1.0	9.7	1.5	1.3	1.9	2.0

Table A6.14 Electron microprobe analyses of plagioclase feldspar in group A ol-tholeiitic basalts (continued).

Sample	SA36 (continued)				SAB170											SAB171		
Analysis	818-G	819-G	820-G	833-G	869-G	870-G	871-G	873-G	874-G	875-G	876-G	877-G	878-G	879-G	885-G	956-G	957-G	958-G
SiO_2	52.50	52.76	53.58	52.30	50.90	52.00	52.12	52.10	54.67	52.23	52.40	54.50	51.42	51.85	49.60	51.76	52.22	52.78
TiO_2	-	-	-	-	-	0.17	-	-	1.33	0.31	-	0.39	-	-	-	-	-	-
Al_2O_3	28.07	29.52	28.51	28.43	30.60	29.02	29.69	29.79	23.01	25.33	29.73	23.76	29.71	29.35	30.78	29.98	29.67	29.62
FeO_T	1.54	0.86	0.81	1.23	0.60	0.80	0.60	0.65	5.12	2.41	0.72	4.68	0.66	0.68	0.93	0.75	0.68	0.80
MgO	1.10	-	-	0.80	-	-	-	-	0.81	2.44	-	1.78	-	-	-	-	-	-
CaO	12.68	11.89	11.26	12.62	13.58	12.56	12.39	12.78	10.25	13.14	12.39	9.42	12.68	12.38	13.85	12.93	12.44	12.17
Na_2O	4.22	4.65	5.02	4.16	3.64	4.23	4.22	4.24	4.44	3.66	4.35	5.02	4.27	4.25	3.36	4.23	4.43	4.32
K_2O	-	0.15	0.24	0.17	-	0.15	0.14	0.11	0.58	0.12	0.16	0.22	0.14	0.14	-	0.13	0.10	0.14
Total	100.11	99.83	99.42	99.71	99.32	98.93	99.16	99.67	100.21	99.64	99.75	99.77	98.88	98.65	98.52	99.78	99.54	99.83
Number of ions on the basis of 32 oxygen																		
Si	9.587	9.606	9.779	9.578	9.334	9.625	9.546	9.510	10.102	9.658	9.552	10.067	9.526	9.555	9.200	9.456	9.539	9.600
Ti	-	-	-	-	-	0.022	-	-	0.186	0.042	-	0.054	-	-	-	-	-	-
Al	6.042	6.336	6.131	6.138	6.614	6.330	6.410	6.410	5.011	5.520	6.387	5.171	6.486	6.374	6.730	6.454	6.387	6.352
Fe^{2+}	0.237	0.131	0.125	0.189	0.093	0.125	0.093	0.099	0.790	0.374	0.109	0.723	0.102	0.106	0.144	0.115	0.106	0.122
Mg	0.301	-	-	0.218	-	-	-	-	0.224	0.672	-	0.490	-	-	-	-	-	-
Ca	2.483	2.320	2.202	2.477	2.669	2.490	2.432	2.499	2.029	2.605	2.419	1.866	2.518	2.445	2.755	2.531	2.435	2.371
Na	1.494	1.642	1.779	1.478	1.293	1.517	1.498	1.501	1.594	1.312	1.536	1.798	1.533	1.520	1.210	1.501	1.568	1.526
K	-	0.035	0.054	0.038	-	0.035	0.032	0.026	0.134	0.029	0.038	0.051	0.035	0.032	-	0.029	0.026	0.032
Cations	20.144	20.070	20.070	20.115	20.003	20.144	20.010	20.045	20.070	20.211	20.042	20.221	20.201	20.032	20.038	20.086	20.061	20.003
End-member compositions																		
An	62.4	58.0	54.6	62.0	67.4	61.6	61.4	62.1	54.0	66.0	60.6	50.2	61.6	61.2	69.5	62.3	60.4	60.3
Ab	37.6	41.1	44.1	37.0	32.6	37.5	37.8	37.3	42.4	33.3	38.5	48.4	37.5	38.0	30.5	37.0	38.9	38.8
Or	0.0	0.9	1.3	1.0	0.0	0.9	0.8	0.6	3.6	0.7	1.0	1.4	0.9	0.8	0.0	0.7	0.6	0.8

Table A6.14 Electron microprobe analyses of plagioclase feldspar in group A ol-tholeiitic basalt (continued).

Sample	SAB171 (continued)								SAB172									
Analysis	962-G	963-G	964-G	965-G	968-G	974-G	979-G	980-G	610-C1	611-R1	613-C2	614-R2	92-C	95-C	96-G	599-G	600-G	601-G
SiO_2	52.63	59.44	52.25	56.41	56.30	55.32	52.23	50.53	52.96	55.39	53.02	53.82	52.01	53.17	55.20	53.93	53.47	52.92
TiO_2	-	-	-	-	0.17	0.32	-	-	-	-	-	-	-	-	-	-	-	-
Al_2O_3	29.95	24.70	29.78	26.65	26.27	26.89	29.31	30.39	29.70	28.00	29.62	28.87	30.44	29.42	28.35	29.23	29.24	29.78
FeO_T	0.72	1.00	0.94	0.94	1.02	0.93	0.52	0.52	0.53	0.72	0.58	0.69	0.62	0.61	0.81	0.51	0.57	0.58
MgO	-	-	-	-	-	-	-	-	-	-	-	-	-	-	-	-	-	-
CaO	12.49	6.39	12.32	8.87	8.78	9.62	12.32	13.45	12.71	10.85	12.66	11.97	13.63	12.61	11.24	12.22	12.46	12.76
Na_2O	4.44	7.43	4.32	6.37	6.19	5.82	4.39	3.69	4.11	5.25	4.27	4.53	3.98	4.28	4.75	4.56	4.37	4.48
K_2O	0.19	0.62	0.13	0.33	0.38	0.31	0.17	0.13	0.13	0.16	-	0.15	-	0.14	0.19	0.11	0.10	0.17
Total	100.42	99.58	99.74	99.57	99.11	99.21	98.94	98.71	100.14	100.37	100.15	100.03	100.68	100.23	100.54	100.56	100.21	100.69
Number of ions on the basis of 32 oxygen																		
Si	9.536	10.694	9.533	10.221	10.246	10.083	9.644	9.331	9.597	9.974	9.606	9.754	9.293	9.565	9.853	9.718	9.680	9.507
Ti	-	-	-	-	0.022	0.045	-	-	-	-	-	-	-	-	-	-	-	-
Al	6.397	5.238	6.403	5.693	5.635	5.776	6.381	6.614	6.346	5.942	6.326	6.166	6.413	6.237	5.965	6.208	6.240	6.307
Fe^{2+}	0.109	0.150	0.144	0.144	0.157	0.141	0.080	0.080	0.080	0.109	0.086	0.106	0.093	0.093	0.122	0.077	0.086	0.086
Mg	-	-	-	-	-	-	-	-	-	-	-	-	-	-	-	-	-	-
Ca	2.426	1.232	2.406	1.722	1.712	1.878	2.438	2.659	2.467	2.093	2.458	2.326	2.608	2.432	2.150	2.362	2.416	2.458
Na	1.562	2.595	1.530	2.237	2.186	2.058	1.571	1.322	1.446	1.834	1.501	1.590	1.379	1.494	1.642	1.594	1.533	1.562
K	0.045	0.144	0.032	0.077	0.090	0.070	0.042	0.029	0.032	0.038	-	0.035	-	0.032	0.045	0.026	0.022	0.038
Cations	20.074	20.054	20.048	20.093	20.048	20.051	20.156	20.035	19.968	19.990	19.978	19.978	19.786	19.853	19.776	19.984	19.978	19.958
End-member compositions																		
An	60.2	31.0	60.6	42.7	42.9	46.9	60.2	66.3	62.5	52.8	62.1	58.9	65.4	61.4	56.0	59.3	60.8	60.6
Ab	38.7	65.4	38.5	55.4	54.8	51.4	38.8	33.0	36.7	46.2	37.9	40.2	34.6	37.8	42.8	40.0	38.6	38.5
Or	1.1	3.6	0.8	1.9	2.2	1.8	1.0	0.7	0.8	1.0	0.0	0.9	0.0	0.8	1.2	0.6	0.6	0.9

Table A6.14 Electron microprobe analyses of plagioclase feldspar in group A ol-tholeiitic basalts (continued).

Sample	SAB172 (continued)					SAB173										
Analysis	602-G	605-G	606-G	607-G	612-G	988-G	989-G	990-G	991-G	994-G	995-G	997-G	1005-G	1006-G	1008-G	1024-G
SiO_2	57.98	54.04	57.65	53.27	54.53	52.72	59.37	59.04	51.94	55.60	57.10	51.76	52.15	50.91	52.38	52.01
TiO_2	-	-	0.21	-	-	0.18	0.21	-	-	-	-	-	-	-	-	-
Al_2O_3	26.59	28.54	26.51	29.21	28.16	29.60	24.60	24.71	29.47	26.88	26.05	29.39	29.63	29.97	29.31	29.31
FeO_T	0.71	0.58	0.88	0.77	0.86	0.70	0.73	0.85	0.90	0.59	0.82	0.69	0.61	0.82	0.62	0.50
MgO	-	-	-	-	-	-	-	-	-	-	-	-	-	-	-	-
CaO	9.03	11.69	9.03	12.32	11.11	12.16	6.65	6.59	12.21	9.26	8.29	12.17	12.18	12.85	12.09	12.39
Na_2O	6.25	4.93	6.38	4.34	5.10	4.35	7.04	7.11	4.41	6.24	6.46	4.39	4.59	4.11	4.35	4.19
K_2O	0.33	0.15	0.30	0.11	0.22	0.14	0.59	0.54	0.18	0.36	0.39	0.13	0.11	0.13	0.13	0.16
Total	100.89	99.93	100.96	100.02	99.98	99.85	99.19	98.84	99.11	98.93	99.11	98.53	99.27	98.79	98.88	98.56
Number of ions on the basis of 32 oxygen																
Si	10.336	9.802	10.291	9.670	9.885	9.587	10.826	10.688	9.542	10.144	10.362	9.549	9.549	9.398	9.613	9.581
Ti	-	-	0.029	-	-	0.026	0.029	-	-	-	-	-	-	-	-	-
Al	5.587	6.102	5.578	6.250	6.016	6.346	5.286	5.274	6.381	5.779	5.571	6.394	6.394	6.522	6.342	6.365
Fe^{2+}	0.106	0.086	0.131	0.118	0.131	0.106	0.112	0.128	0.138	0.090	0.125	0.106	0.093	0.128	0.096	0.077
Mg	-	-	-	-	-	-	-	-	-	-	-	-	-	-	-	-
Ca	1.725	2.272	1.728	2.397	2.157	2.368	1.299	1.277	2.403	1.808	1.613	2.406	2.390	2.541	2.378	2.445
Na	2.160	1.734	2.208	1.526	1.792	1.533	2.490	2.496	1.571	2.208	2.272	1.571	1.629	1.472	1.549	1.494
K	0.077	0.035	0.067	0.026	0.051	0.032	0.138	0.125	0.042	0.083	0.090	0.029	0.026	0.032	0.029	0.038
Cations	19.990	20.032	20.032	19.987	20.032	19.997	20.179	19.987	20.077	20.112	20.032	20.054	20.080	20.093	20.006	20.000
End-member compositions																
An	43.5	56.2	43.2	60.7	53.9	60.2	33.1	32.8	59.8	44.1	40.6	60.1	59.1	62.8	60.1	61.5
Ab	54.5	42.9	55.2	38.7	44.8	39.0	63.4	64.0	39.1	53.9	57.2	39.2	40.3	36.4	39.2	37.6
Or	1.9	0.9	1.7	0.6	1.3	0.8	3.5	3.2	1.0	2.0	2.3	0.7	0.6	0.8	0.7	1.0

Table A6.14 Electron microprobe analyses of plagioclase feldspar in group A ol-tholeiitic basalts (continued).

Sample	SAB174										
Analysis	1071-G	1072-G	1073-G	1075-G	1077-G	1081-G	1083-G	1084-G	1097-G	1111-G	1113-G
SiO_2	50.99	52.33	52.36	49.93	52.97	55.83	56.98	53.23	53.07	55.72	59.03
TiO_2	-	-	-	-	-	-	-	-	-	-	-
Al_2O_3	30.07	29.70	29.63	31.24	29.69	27.93	25.98	29.31	29.97	28.12	25.08
FeO_T	0.78	0.63	0.61	0.58	0.95	0.87	0.89	0.51	0.64	1.02	1.07
MgO	-	-	-	-	-	-	-	-	-	-	-
CaO	13.15	12.45	12.49	14.32	12.43	10.18	8.80	12.19	12.51	10.56	7.35
Na_2O	3.91	4.31	4.24	3.22	4.52	5.57	6.41	4.30	4.48	5.50	7.08
K_2O	0.15	0.13	0.14	-	0.14	0.23	0.39	-	0.11	0.25	0.46
Total	99.05	99.55	99.47	99.29	100.70	100.61	99.45	99.54	100.78	101.17	100.07
Number of ions on the basis of 32 oxygen											
Si	9.389	9.552	9.565	9.181	9.574	10.026	10.330	9.680	9.568	9.971	10.592
Ti	-	-	-	-	-	-	-	-	-	-	-
Al	6.528	6.390	6.378	6.771	6.326	5.910	5.549	6.285	6.368	5.933	5.306
Fe^{2+}	0.122	0.096	0.093	0.090	0.144	0.131	0.134	0.077	0.096	0.154	0.160
Mg	-	-	-	-	-	-	-	-	-	-	-
Ca	2.595	2.435	2.445	2.822	2.406	1.958	1.709	2.378	2.416	2.026	1.414
Na	1.398	1.526	1.501	1.146	1.584	1.939	2.253	1.514	1.568	1.907	2.464
K	0.035	0.029	0.035	-	0.032	0.054	0.090	-	0.026	0.058	0.106
Cations	20.067	20.029	20.016	20.010	20.067	20.019	20.064	19.933	20.042	20.048	20.042
End-member compositions											
An	64.4	61.0	61.4	71.1	59.8	49.6	42.2	61.1	60.3	50.8	35.5
Ab	34.7	38.3	37.7	28.9	39.4	49.1	55.6	38.9	39.1	47.8	61.8
Or	0.9	0.7	0.9	0.0	0.8	1.4	2.2	0.0	0.6	1.4	2.7

A6.15 Microprobe analyses of plagioclase feldspar in group A lavas: qz-tholeiitic basalts

Table A6.15 Electron microprobe analyses of plagioclase feldspar in group A qz-tholeiitic baslats.

Sample	SA76															
Analysis	127-C1	128-R1	456-C2	457-R2	460-C3	461-R3	470-C4	471-R4	126-C	136-C	464-C	458-G	459-G	467-G	468-G	469-G
SiO_2	53.23	53.15	53.14	59.14	51.62	53.91	54.46	53.74	52.78	57.15	52.34	58.50	54.54	58.01	53.56	54.43
TiO_2	-	-	0.21	-	-	-	-	-	-	0.19	-	-	-	-	-	-
Al_2O_3	29.54	29.26	29.21	25.12	30.35	29.09	28.38	29.32	29.28	26.75	30.10	25.53	27.93	26.37	28.77	28.51
FeO_T	0.46	0.62	0.59	0.68	0.55	0.66	0.91	0.67	0.47	0.75	0.49	0.86	1.05	0.81	1.00	0.91
MgO	-	-	-	-	-	-	-	-	-	-	-	-	-	-	0.45	-
CaO	12.27	12.13	12.27	7.57	13.77	12.16	11.63	12.33	12.65	9.32	13.51	8.01	11.05	8.84	12.09	11.21
Na_2O	4.56	4.39	4.25	6.78	3.74	4.63	5.04	4.59	4.16	5.84	3.62	6.64	4.91	6.24	4.47	5.22
K_2O	0.15	0.16	-	0.43	-	0.22	0.22	0.15	-	0.32	-	0.40	0.21	0.36	0.21	0.18
Total	100.21	99.71	99.67	99.72	100.03	100.67	100.64	100.80	99.34	100.32	100.06	99.94	99.69	100.63	100.55	100.46
Number of ions on the basis of 32 oxygen																
Si	9.568	9.600	9.661	10.621	9.398	9.722	9.827	9.680	9.565	10.176	9.501	10.509	9.914	10.368	9.690	9.719
Ti	-	-	0.029	-	-	-	-	-	-	0.026	-	-	-	-	-	-
Al	6.259	6.230	6.259	5.315	6.515	6.182	6.035	6.227	6.256	5.616	6.442	5.408	5.984	5.552	6.134	6.000
Fe^{2+}	0.070	0.093	0.090	0.102	0.083	0.099	0.138	0.099	0.070	0.112	0.074	0.128	0.160	0.122	0.150	0.138
Mg	-	-	-	-	-	-	-	-	-	-	-	-	-	-	0.122	-
Ca	2.365	2.346	2.390	1.456	2.688	2.349	2.250	2.381	2.458	1.776	2.627	1.542	2.150	1.693	2.342	2.144
Na	1.590	1.536	1.501	2.358	1.322	1.619	1.763	1.603	1.459	2.016	1.274	2.314	1.728	2.163	1.568	1.805
K	0.035	0.035	-	0.099	-	0.051	0.051	0.035	-	0.074	-	0.090	0.048	0.083	0.048	0.042
Cations	19.888	19.840	19.930	19.952	20.006	20.022	20.064	20.026	19.808	19.795	19.917	19.990	19.984	19.981	20.054	19.847
End-member compositions																
An	59.3	59.9	61.4	37.2	67.0	58.4	55.4	59.2	62.7	45.9	67.4	39.1	54.8	43.0	59.2	53.7
Ab	39.9	39.2	38.6	60.3	33.0	40.3	43.4	39.9	37.3	52.2	32.6	58.6	44.0	54.9	39.6	45.2
Or	0.9	0.9	0.0	2.5	0.0	1.3	1.3	0.9	0.0	1.9	0.0	2.3	1.2	2.1	1.2	1.0

Table A6.15 Electron microprobe analyses of plagioclase feldspar in group A qz-tholeiitic basalts (continued).

Sample	SA77														
Analysis	619-C1	620-R1	623-C2	624-R2	629-C3	630-R3	172-C	173-C	174-C	621-G	622-G	627-G	628-G	631-G	632-G
SiO_2	54.01	53.87	51.14	54.10	51.83	51.53	54.01	54.59	54.72	54.88	55.06	52.79	55.82	54.18	53.83
TiO_2	-	-	-	-	-	-	-	0.20	-	-	-	-	-	-	-
Al_2O_3	28.66	28.88	29.88	29.15	29.70	30.13	27.66	28.60	27.67	28.00	27.65	29.66	27.25	28.66	28.72
FeO_T	0.79	1.11	0.65	0.76	0.88	0.91	1.24	1.02	0.91	0.86	0.84	0.90	0.85	0.86	0.58
MgO	-	-	-	-	-	-	-	-	-	-	-	-	-	-	-
CaO	11.58	11.77	13.62	11.80	13.47	13.63	11.52	11.33	10.85	11.23	10.36	12.56	10.03	11.68	11.93
Na_2O	4.68	4.65	3.50	4.51	3.63	3.54	4.45	4.74	5.20	5.09	5.46	4.40	5.45	4.79	4.72
K_2O	0.18	0.20	0.15	0.18	-	0.13	0.19	0.26	0.30	0.23	0.29	0.18	0.32	0.21	0.20
Total	99.90	100.48	98.94	100.50	99.51	99.87	99.07	100.74	99.65	100.29	99.66	100.49	99.72	100.38	99.98
Number of ions on the basis of 32 oxygen															
Si	9.798	9.741	9.530	9.754	9.485	9.411	9.818	9.754	9.875	9.917	9.994	9.565	10.106	9.792	9.763
Ti	-	-	-	-	-	-	-	0.026	-	-	-	-	-	-	-
Al	6.128	6.157	6.563	6.192	6.406	6.486	5.926	6.022	5.888	5.962	5.917	6.336	5.814	6.106	6.141
Fe^{2+}	0.118	0.166	0.099	0.115	0.134	0.138	0.189	0.154	0.138	0.128	0.128	0.138	0.128	0.128	0.086
Mg	-	-	-	-	-	-	-	-	-	-	-	-	-	-	-
Ca	2.250	2.282	2.720	2.278	2.640	2.666	2.246	2.170	2.099	2.176	2.013	2.438	1.946	2.262	2.317
Na	1.645	1.629	1.267	1.578	1.290	1.251	1.568	1.645	1.821	1.782	1.923	1.549	1.910	1.677	1.661
K	0.042	0.045	0.035	0.042	-	0.032	0.045	0.058	0.067	0.054	0.067	0.042	0.074	0.048	0.048
Cations	19.981	20.019	20.215	19.958	19.955	19.984	19.792	19.827	19.888	20.019	20.042	20.067	19.978	20.013	20.016
End-member compositions															
An	57.2	57.7	67.6	58.5	67.2	67.5	58.2	56.0	52.6	54.2	50.3	60.5	49.5	56.7	57.6
Ab	41.8	41.2	31.5	40.5	32.8	31.7	40.6	42.5	45.7	44.4	48.0	38.4	48.6	42.1	41.3
Or	1.1	1.1	0.9	1.1	0.0	0.8	1.2	1.5	1.7	1.4	1.7	1.0	1.9	1.2	1.2

Table A6.15 Electron microprobe analyses of plagioclase feldspar in group A qz-tholeiitic basalts (continued).

Sample	SAB198								
Analysis	1580-C	1593-C	1586-C	1579-G	1590-G	1591-G	1592-G	1595-G	1596-G
SiO_2	52.18	49.76	52.43	53.90	56.56	57.02	58.92	50.96	53.76
TiO_2	-	-	-	-	0.25	-	-	-	-
Al_2O_3	29.54	30.65	29.24	28.14	25.72	25.83	24.61	30.00	28.21
FeO_T	0.58	0.54	0.73	0.88	0.96	0.77	0.59	0.66	0.85
MgO	0.25	0.33	0.24	-	-	-	-	0.38	0.39
CaO	12.49	13.80	12.01	10.67	8.39	7.89	6.45	13.00	10.85
Na_2O	4.24	3.48	4.61	5.21	6.21	6.59	7.45	3.71	5.27
K_2O	0.17	0.15	0.18	0.30	0.65	0.66	0.84	0.11	0.33
Total	99.45	98.71	99.44	99.10	98.74	98.76	98.86	98.82	99.66
Number of ions on the basis of 32 oxygen									
Si	9.539	9.210	9.587	9.859	10.450	10.450	10.744	9.498	9.795
Ti	-	-	-	-	0.035	-	-	-	-
Al	6.365	6.685	6.304	6.067	5.600	5.581	5.290	6.592	6.058
Fe^{2+}	0.090	0.083	0.112	0.134	0.147	0.118	0.090	0.102	0.131
Mg	0.067	0.093	0.067	-	-	-	-	0.106	0.106
Ca	2.448	2.736	2.355	2.090	1.661	1.549	1.261	2.595	2.118
Na	1.501	1.251	1.632	1.846	2.224	2.342	2.634	1.341	1.862
K	0.038	0.035	0.042	0.070	0.154	0.154	0.195	0.026	0.077
Cations	20.048	20.093	20.099	20.067	20.271	20.194	20.213	20.260	20.147
End-member compositions									
An	61.4	68.0	58.5	52.2	41.1	38.3	30.8	65.5	52.2
Ab	37.6	31.1	40.5	46.1	55.1	57.9	64.4	33.8	45.9
Or	1.0	0.9	1.0	1.8	3.8	3.8	4.8	0.6	1.9

A6.16 Microprobe analyses of alkali feldspar in group A lavas

Table A6.16 Electron microprobe analyses of alkali feldspar in group A lavas.

Rock Type	alkali ol-basalt			hawaiite		ol-tholeiitic basalt			
Sample	SA17		SAB162	SA32	SAB163	SAB152		SAB169	SAB187
Analysis	428-G	431-G	1755-G	1952-G	1971-G	249-G	698-G	15-C1	534-G
SiO_2	63.89	63.81	64.02	64.47	65.20	65.69	64.98	52.27	72.21
TiO_2	-	-	-	0.20	-	0.21	-	-	0.65
Al_2O_3	20.74	21.27	20.72	20.65	20.56	20.11	21.45	29.85	14.02
FeO_T	0.40	0.44	0.39	0.57	0.43	0.63	0.60	0.57	1.34
MgO	-	-	-	-	-	-	-	-	-
CaO	1.68	2.07	1.84	1.35	1.06	1.17	2.21	13.23	0.56
Na_2O	6.14	6.60	7.67	7.10	7.32	8.00	8.50	3.71	4.52
K_2O	5.77	4.90	4.13	5.29	5.75	4.21	2.94	0.12	5.47
Total	98.62	99.09	98.77	99.63	100.32	100.02	100.68	99.75	98.77
Number of ions on the basis of 32 oxygen									
Si	11.603	11.712	11.571	11.594	11.658	11.613	11.432	9.456	13.072
Ti	-	-	-	0.026	-	0.029	-	-	0.090
Al	4.442	4.602	4.416	4.378	4.333	4.189	4.448	6.365	2.992
Fe^{2+}	0.061	0.067	0.058	0.086	0.064	0.093	0.090	0.086	0.202
Mg	-	-	-	-	-	-	-	-	-
Ca	0.326	0.406	0.355	0.259	0.202	0.221	0.416	0.013	0.109
Na	2.163	2.349	2.688	2.477	2.538	2.739	2.899	2.566	1.587
K	1.338	1.149	0.954	1.213	1.312	0.950	0.659	1.302	1.264
Cations	19.933	20.285	20.042	20.032	20.106	19.834	19.944	19.789	19.315
End-member compositions									
Ab	8.5	10.4	8.9	6.6	5.0	5.6	10.5	0.3	3.7
An	56.5	60.2	67.3	62.7	62.6	70.0	72.9	66.1	53.6
Or	34.9	29.4	23.9	30.7	32.4	24.3	16.6	33.6	42.7

A6.17 Microprobe analyses of chromian titanomagnetite and Cr-bearing titanomagnetite in group A lavas

Table A6.17 Microprobe analyses of chromian titanomagmatite and Cr-bearing titanomagnetite in group A lavas.

Rock Type	alkali ol-basalt									transitional basalt						
Sample	SA18			SA19		SAB162				SA07						
Analysis	1775-I	1793-G	1799-G	2000-I	1995-G	1741-I	1744-I	1740-G	1749-G	1892-G	1898-G	1899-G	1900-G	1911-G	1915-G	1916-G
host crystal analysis	ol 1776-C2			ol 2001-C		ol 1815-C	ol 1817-C									
SiO_2	0.53	0.53	0.41	0.33	0.52	0.30	0.43	0.48	0.34	0.96	0.40	0.38	0.52	0.42	0.64	0.81
TiO_2	3.58	25.36	24.38	2.12	24.64	24.09	15.28	27.48	26.79	3.27	3.80	3.90	6.03	1.87	12.35	11.85
Al_2O_3	19.81	1.73	2.02	19.90	3.38	4.26	8.50	2.52	3.04	6.67	5.36	4.64	4.08	4.69	4.22	4.44
Cr_2O_3	26.24	0.32	1.08	29.08	2.54	1.74	3.85	0.47	0.77	23.66	19.09	21.47	10.55	19.28	0.34	0.26
FeO_T	39.94	67.09	67.05	40.07	63.18	62.49	62.71	65.49	64.46	53.58	58.60	57.42	66.76	57.64	74.68	72.98
MnO	-	0.66	0.52	-	0.41	0.37	0.36	0.42	0.46	-	0.51	-	0.44	0.48	-	0.29
MgO	7.80	1.48	1.62	7.88	2.52	4.65	5.21	2.16	2.97	6.81	6.95	6.87	5.63	10.01	2.78	3.03
CaO	-	0.14	-	-	0.38	-	-	-	-	-	0.17	0.27	0.28	-	0.33	0.38
Total	97.90	97.31	97.08	99.38	97.57	97.90	96.34	99.02	98.83	94.95	94.88	94.95	94.29	94.39	95.34	94.04
Number of ions on the basis of 32 oxygen																
Si	0.144	0.166	0.128	0.090	0.157	0.090	0.134	0.144	0.102	0.301	0.128	0.122	0.176	0.138	0.218	0.278
Ti	0.730	6.003	5.792	0.426	5.658	5.456	3.536	6.259	6.061	0.771	0.922	0.950	1.530	0.454	3.126	3.040
Al	6.330	0.643	0.752	6.173	0.611	1.510	3.082	0.899	1.078	5.869	4.877	5.494	2.819	4.938	1.674	1.781
Cr	5.626	0.080	0.272	6.298	1.216	0.413	0.938	0.112	0.182	2.467	2.042	1.773	1.622	1.789	0.090	0.070
Fe^{2+}	9.059	17.661	17.718	8.998	16.138	15.731	16.141	16.589	16.221	14.054	15.827	15.546	18.861	15.610	21.037	20.819
Mn	-	0.176	0.138	-	0.106	0.096	0.096	0.109	0.118	-	0.138	-	0.125	0.131	-	0.083
Mg	3.152	0.694	0.765	3.152	1.146	2.090	2.394	0.976	1.334	3.187	3.344	3.318	2.832	4.832	1.395	1.539
Ca	-	0.048	-	-	0.125	-	-	-	-	-	0.058	0.093	0.102	-	0.118	0.141
Cations	25.040	25.472	25.565	25.136	25.155	25.386	26.320	25.088	25.098	26.650	27.334	27.296	28.067	27.891	27.658	27.754
Recalculated Fe ions and Fe oxides																
Fe^{2+}	6.025	12.942	12.716	5.699	12.457	11.379	9.077	13.094	12.712	6.294	6.089	5.940	6.853	4.503	9.791	9.348
Fe^{3+}	2.658	3.698	3.917	2.892	2.939	3.493	5.641	2.776	2.799	6.363	7.807	7.728	9.274	8.929	8.464	8.656
FeO	27.71	52.18	51.26	26.58	51.12	47.81	38.67	54.04	52.83	26.64	25.68	24.96	28.37	19.32	40.06	37.89
Fe_2O_3	13.59	16.57	17.55	14.99	13.40	16.31	26.71	12.73	12.93	29.93	36.59	36.08	42.66	42.58	38.48	38.99
End-member composition																
mol.% Usp	61.7	77.3	76.4	45.1	82.8	77.8	60.2	84.3	83.0	23.6	18.6	20.8	22.3	6.5	39.3	38.2
Atomic percentages																
$Cr^{\#}$	47.1	11.1	26.6	50.5	66.5	21.5	23.3	11.1	14.5	29.6	29.5	24.4	36.5	26.6	5.1	3.8
$Mg^{\#}$	33.4	4.8	5.3	34.6	8.1	14.8	19.4	6.7	9.1	31.3	32.5	32.9	26.1	48.0	11.0	12.5
$Fe^{\#}$	18.8	84.4	80.3	19.5	62.8	65.8	60.6	74.2	69.9	45.9	56.2	54.7	70.9	60.7	84.7	84.4

Table A6.17 Microprobe analyses of chromian titanomagmatite and Cr-bearing titanomagnetite in group A lavas (continued).

Rock Type	transitional basalt					
Sample	SA10					
Analysis	1816-I	1821-G	1833-G	1835-G	1841-G	1842-G
host crystal analysis	ol 1817-C					
SiO_2	0.68	0.50	0.33	0.41	0.39	0.46
TiO_2	4.56	4.03	4.40	4.72	3.68	4.81
Al_2O_3	17.01	19.23	17.58	16.15	19.30	16.12
Cr_2O_3	27.40	26.77	27.36	26.66	27.44	27.29
FeO_T	40.95	40.48	41.10	41.72	39.13	42.60
MnO	-	0.35	-	-	0.40	0.41
MgO	8.28	7.63	7.76	6.86	8.84	6.73
CaO	-	0.25	0.24	0.29	-	0.19
Total	98.88	99.24	98.77	96.81	99.18	98.61
Number of ions on the basis of 32 oxygen						
Si	0.182	0.134	0.090	0.115	0.106	0.128
Ti	0.931	0.816	0.906	0.998	0.742	1.002
Al	5.446	6.118	5.667	5.350	6.106	5.251
Cr	5.885	5.712	5.917	5.923	5.821	5.968
Fe^{2+}	9.302	9.136	9.398	9.805	8.784	9.850
Mn	-	0.080	-	-	0.093	0.096
Mg	3.350	3.069	3.165	2.874	3.536	2.774
Ca	-	0.070	0.070	0.086	-	0.058
Cations	25.098	25.136	25.213	25.152	25.187	25.126
Recalculated Fe ions and Fe oxides						
Fe^{2+}	6.097	5.831	5.868	6.424	5.353	6.539
Fe^{3+}	2.799	2.892	3.079	2.931	3.017	2.869
FeO	28.07	27.06	26.96	28.65	25.03	29.61
Fe_2O_3	14.32	14.92	15.72	14.53	15.67	14.44
End-member composition						
mol.% Usp	63.5	63.5	62.7	65.1	57.6	65.2
Atomic percentages						
$Cr^{\#}$	51.9	48.3	51.1	52.5	48.8	53.2
$Mg^{\#}$	34.4	33.4	33.9	29.9	38.6	28.8
$Fe^{\#}$	20.5	20.4	21.8	21.4	21.0	21.1

A6.18 Microprobe analyses of titanomagnetite in group A lavas

Table A6.18 Microprobe analyses of titanomagnetite in group A lavas.

Rock Type	alkali ol-basalt										hawaiite							
Sample	SA17						SA18	SA33			SA20				SA32			
Analysis	145-G	149-G	436-G	437-G	440-G	441-G	1787-G	1717-G	1718-G	1730-G	1845-G	1846-G	1847-G	1869-G	1927-G	1928-G	1929-G	1931-G
SiO_2	0.42	0.48	0.38	0.39	0.50	0.48	0.72	0.40	0.45	0.47	0.47	0.85	0.49	0.54	0.41	0.47	0.67	0.72
TiO_2	27.34	28.01	28.06	27.59	27.82	27.76	25.27	25.08	25.55	26.67	25.42	24.29	26.45	25.50	26.17	25.85	22.87	25.31
Al_2O_3	1.61	1.52	1.55	1.58	1.74	1.52	1.47	0.44	0.72	1.28	1.07	0.77	0.43	1.09	1.54	1.47	0.63	1.32
FeO_T	65.03	66.57	64.67	64.90	66.09	65.24	65.43	71.84	70.13	68.19	7-	71.17	70.47	69.88	67.72	67.49	70.17	67.85
MnO	0.49	0.49	0.54	0.53	0.45	0.61	0.51	0.48	0.54	0.34	0.48	0.33	0.46	0.42	0.47	0.45	0.51	0.46
MgO	2.08	2.30	2.26	2.14	2.05	2.19	1.55	0.47	0.50	1.05	0.98	0.60	0.85	0.74	1.57	1.37	0.74	1.33
CaO	-	-	-	0.18	-	-	0.27	-	-	-	-	-	-	-	-	-	0.16	0.32
Total	96.97	99.37	97.46	97.31	98.65	97.80	95.22	98.71	97.89	98.00	98.42	98.01	99.15	98.17	97.88	97.10	95.75	97.31
Number of ions on the basis of 32 oxygen																		
Si	0.134	0.144	0.118	0.122	0.154	0.147	0.230	0.128	0.144	0.147	0.147	0.272	0.154	0.173	0.128	0.150	0.221	0.227
Ti	6.403	6.400	6.518	6.435	6.400	6.438	6.093	6.006	6.122	6.282	6.006	5.827	6.234	6.061	6.138	6.141	5.661	6.013
Al	0.592	0.544	0.563	0.576	0.627	0.554	0.554	0.163	0.269	0.474	-	-	-	-	-	-	-	-
Fe^{2+}	16.938	16.918	16.704	16.832	16.906	16.829	17.546	19.133	18.685	17.856	18.397	18.989	18.470	18.467	17.661	17.830	19.312	17.923
Mn	0.131	0.128	0.141	0.141	0.118	0.160	0.138	0.131	0.147	0.090	0.128	0.090	0.125	0.112	0.125	0.122	0.141	0.125
Mg	0.966	1.043	1.037	0.989	0.931	1.008	0.739	0.224	0.240	0.493	0.461	0.288	0.394	0.349	0.730	0.646	0.365	0.624
Ca	-	-	-	0.061	-	-	0.093	-	-	-	-	-	-	-	-	-	0.058	0.109
Cations	25.165	25.178	25.082	25.155	25.136	25.136	25.392	25.786	25.606	25.341	25.139	25.466	25.376	25.162	24.781	24.890	25.757	25.021
Recalculated Fe ions and Fe oxides																		
Fe^{2+}	13.191	13.134	13.224	13.120	13.249	13.176	13.075	13.376	13.498	13.525	14.663	14.213	13.998	14.660	15.088	14.906	13.630	14.581
Fe^{3+}	2.962	2.993	2.760	2.939	2.892	2.892	3.509	4.432	4.015	3.386	2.900	3.683	3.470	2.955	2.017	2.287	4.365	2.611
FeO	53.10	54.21	53.50	53.02	54.25	53.50	51.59	53.96	54.05	54.54	58.44	56.52	56.47	58.16	59.74	58.51	53.15	57.55
Fe_2O_3	13.25	13.73	12.41	13.20	13.16	13.05	15.38	19.87	17.87	15.17	12.85	16.28	15.56	13.03	8.87	9.98	18.92	11.45
End-member composition																		
mol.% Usp	81.9	81.5	83.2	82.0	82.6	82.3	77.8	71.8	74.8	79.3	74.5	72.0	75.3	75.5	77.8	77.7	68.1	75.9

Table A6.18 Microprobe analyses of in group A lavas (continued).

Rock Type	hawaiite (continued)									ol-tholeiitic basalt							
Sample	SAB151						SAB163			SAB152						SAB181	
Analysis	200-G	204-G	682-G	685-G	687-G	688-G	1962-G	1974-G	1981-G	257-G	262-G	704-G	705-G	709-G	710-G	188-G	196-G
SiO_2	0.58	0.47	0.88	0.56	0.63	0.43	0.41	0.43	0.54	0.58	0.54	0.41	0.48	0.62	0.54	0.94	0.54
TiO_2	25.70	23.31	27.10	25.28	21.97	23.41	30.03	29.02	28.95	24.70	25.94	26.16	20.92	25.07	22.39	18.16	21.64
Al_2O_3	0.42	0.24	0.43	0.77	0.24	0.28	1.26	1.29	1.20	0.63	-	-	1.02	0.41	1.53	1.60	1.40
FeO_T	66.88	69.23	66.24	68.17	71.30	70.10	65.75	66.61	63.77	67.70	69.37	66.96	71.73	68.36	71.71	74.08	72.43
MnO	0.52	0.63	0.58	0.53	0.47	0.61	0.54	0.52	0.66	0.60	0.50	0.51	0.56	0.44	0.49	0.40	0.50
MgO	0.75	-	0.79	0.83	0.52	0.34	1.70	1.42	1.38	0.41	0.50	0.56	0.81	0.25	1.21	0.31	0.67
CaO	0.23	-	0.15	0.15	-	-	-	-	-	-	0.20	-	-	0.23	-	0.58	0.24
Total	95.08	93.88	96.17	96.29	95.13	95.17	99.69	99.29	96.50	94.62	97.05	94.60	95.52	95.38	97.87	96.07	97.42
Number of ions on the basis of 32 oxygen																	
Si	0.189	0.157	0.278	0.179	0.211	0.144	0.125	0.131	0.170	0.189	0.173	0.134	0.160	0.202	0.173	0.317	0.176
Ti	6.291	5.850	6.490	6.122	5.533	5.856	6.803	6.646	6.784	6.118	6.272	6.461	5.219	6.170	5.408	4.579	5.293
Al	0.160	0.093	0.160	0.291	0.096	0.109	-	-	-	0.243	-	-	0.400	0.157	0.579	0.634	0.538
Fe^{2+}	18.208	19.315	17.638	18.362	19.978	19.498	16.570	16.966	16.618	18.646	18.656	18.390	19.910	18.701	19.258	20.771	19.699
Mn	0.144	0.176	0.157	0.144	0.131	0.173	0.138	0.134	0.173	0.166	0.138	0.141	0.160	0.122	0.134	0.115	0.138
Mg	0.365	0.054	0.374	0.397	0.259	0.170	0.765	0.643	0.640	0.202	0.243	0.275	0.400	0.122	0.576	0.157	0.326
Ca	0.080	-	0.051	0.051	-	-	-	-	-	-	0.067	-	-	0.083	-	0.208	0.083
Cations	25.437	25.645	25.149	25.546	26.208	25.949	24.400	24.522	24.384	25.565	25.549	25.402	26.250	25.555	26.128	26.781	26.253
Recalculated Fe ions and Fe oxides																	
Fe^{2+}	13.564	13.972	13.909	13.378	12.903	13.227	15.249	15.244	15.348	13.588	13.645	13.844	12.719	13.668	12.477	11.969	12.517
Fe^{3+}	3.615	4.105	2.924	3.872	5.392	4.807	1.049	1.361	1.008	3.917	3.880	3.531	5.485	3.895	5.212	6.645	5.492
FeO	52.81	53.51	54.74	52.87	50.29	51.42	61.52	61.15	59.84	52.55	54.01	53.35	50.12	53.20	50.58	47.63	50.34
Fe_2O_3	15.64	17.47	12.79	17.01	23.35	20.76	4.70	6.07	4.37	16.84	17.07	15.12	24.02	16.85	23.48	29.39	24.55
End-member composition																	
mol.% Usp	76.7	70.4	81.1	75.3	65.0	69.2	87.2	84.9	87.5	75.1	74.6	77.0	62.7	75.2	66.6	56.4	64.8

Table A6.18 Microprobe analyses of titanomagnetite in group A lavas (continued).

Rock Type	ol-tholeiitic basalt (continued)									transitional basalt								
Sample	SAB187	SAB171	SAB172		SAB173		SA77			SA07			SA10	SA13				
Analysis	276-G	949-G	932-G	936-G	1009-G	1020-G	642-G	644-G	645-G	1893-G	1917-G	1918-G	1822-G	31-G	39-G	573-G	574-G	575-G	576-G
SiO_2	0.60	0.83	0.66	0.73	0.53	1.00	0.64	0.62	0.78	0.61	0.46	0.57	0.93	0.53	0.68	0.46	0.44	0.43	0.63
TiO_2	20.49	20.91	21.73	21.98	22.23	20.72	19.27	19.15	22.06	8.61	12.48	11.95	17.56	25.16	24.82	25.46	19.79	20.90	26.12
Al_2O_3	0.83	1.33	1.34	1.33	1.19	1.42	1.82	1.95	1.34	3.95	3.85	4.08	3.39	1.07	1.16	0.94	1.47	1.67	0.90
FeO_T	72.75	67.04	69.40	69.00	70.62	71.61	72.96	72.84	69.63	73.32	73.97	73.80	69.35	68.80	68.07	66.67	73.34	71.00	65.48
MnO	0.43	0.41	0.54	0.42	0.39	0.34	0.41	0.36	-	0.36	-	-	0.26	0.52	0.44	0.61	0.39	0.43	0.47
MgO	1.00	0.27	0.58	0.62	0.51	0.35	0.70	0.73	0.62	3.87	3.46	3.29	2.14	1.76	1.67	1.64	1.23	1.60	1.70
CaO	0.23	0.22	0.22	0.23	0.14	0.14	-	0.21	0.39	0.29	0.20	0.23	0.31	0.17	-	-	-	0.17	0.33
Total	96.33	91.01	94.47	94.31	95.61	95.58	95.80	95.86	94.82	91.01	94.42	93.92	93.94	98.01	96.84	95.78	96.66	96.20	95.63
Number of ions on the basis of 32 oxygen																			
Si	0.198	0.285	0.221	0.243	0.176	0.333	0.214	0.205	0.256	0.218	0.157	0.195	0.310	0.166	0.218	0.150	0.147	0.141	0.198
Ti	5.110	5.440	5.450	5.504	5.520	5.165	4.835	4.800	5.491	2.333	3.190	3.075	4.400	5.958	5.939	6.150	4.925	5.155	6.275
Al	0.323	0.541	0.528	0.522	0.461	0.557	0.717	0.768	0.522	-	-	-	1.331	0.397	0.435	0.355	0.573	0.646	0.339
Fe^{2+}	20.189	19.395	19.350	19.216	19.507	19.853	20.362	20.301	19.277	22.086	21.034	21.117	19.331	18.122	18.115	17.914	20.288	19.478	17.494
Mn	0.122	0.118	0.154	0.118	0.109	0.093	0.115	0.102	-	0.109	-	-	0.074	0.138	0.118	0.166	0.109	0.118	0.128
Mg	0.493	0.138	0.285	0.310	0.250	0.176	0.346	0.362	0.304	2.077	1.757	1.680	1.066	0.826	0.794	0.787	0.605	0.781	0.810
Ca	0.080	0.083	0.080	0.083	0.048	0.048	-	0.074	0.138	0.112	0.074	0.083	0.109	0.058	-	-	-	0.061	0.112
Cations	26.515	26.000	26.067	25.997	26.070	26.224	26.589	26.611	25.987	26.934	26.211	26.150	26.621	25.664	25.619	25.523	26.646	26.381	25.357
Recalculated Fe ions and Fe oxides																			
Fe^{2+}	12.203	12.980	12.740	12.824	12.875	12.741	12.148	12.029	12.909	12.708	13.860	14.117	11.127	12.797	12.925	13.025	11.917	11.945	13.134
Fe^{3+}	6.071	4.923	5.075	4.916	5.083	5.428	6.231	6.280	4.894	6.973	5.399	5.263	6.301	4.150	4.045	3.819	6.356	5.776	3.425
FeO	48.58	48.61	49.63	49.88	50.63	50.22	48.22	47.86	50.49	47.34	53.23	53.76	44.28	51.95	51.85	51.55	47.83	47.86	51.94
Fe_2O_3	26.86	20.49	21.97	21.25	22.21	23.77	27.49	27.76	21.27	28.87	23.04	22.27	27.86	18.72	18.03	16.80	28.35	25.72	15.05
End-member composition																			
mol.% Usp	60.2	68.7	67.6	68.7	67.8	-	59.9	59.5	68.8	25.9	38.0	37.2	57.6	73.0	73.9	75.5	58.9	62.5	77.9

A6.19 Microprobe analyses of ilmenite in group A lavas

Table A6.19 Electron microprobe analyses of ilmenite in group A lavas.

Rock Type	alkali ol-basalt											hawaiite						
Sample	SA17					SA33			SAB162			SA20			SA32			
Analysis	144-G	151-G	435-G	438-G	439-G	1720-G	1721-G	1724-G	1751-G	1756-G	1766-G	1865-G	1866-G	1870-G	1946-G	1947-G	1948-G	1949-G
SiO_2	0.44	0.79	0.31	0.36	0.49	0.26	0.40	0.38	0.54	0.51	0.41	0.44	0.66	0.45	0.45	0.37	0.39	0.39
TiO_2	51.70	50.02	52.11	51.73	51.35	51.25	51.22	52.07	51.31	51.76	52.43	50.75	50.19	51.09	50.37	50.47	51.36	51.32
Al_2O_3	0.25	0.27	-	-	0.26	-	-	-	0.21	-	0.19	-	-	-	-	-	-	-
FeO_T	44.24	44.07	44.01	44.39	43.78	48.70	48.32	45.85	45.23	44.63	43.79	48.01	48.04	47.12	45.17	45.14	46.42	45.46
MnO	0.67	0.65	0.56	0.58	0.75	0.61	0.58	0.46	0.78	0.75	0.66	0.48	0.52	0.44	0.49	0.52	0.50	0.55
MgO	2.70	2.08	2.77	2.23	2.46	0.50	0.67	1.29	0.70	1.28	1.34	0.60	0.57	0.99	1.22	1.63	1.57	1.78
CaO	0.19	0.26	0.13	-	0.16	-	-	-	-	0.25	0.16	-	-	0.16	0.30	0.21	-	0.29
Na_2O	-	-	-	-	-	-	-	-	-	-	-	-	-	-	-	-	-	-
Total	100.19	98.14	99.89	99.29	99.25	101.32	101.19	100.05	98.77	99.18	98.98	100.28	99.98	100.25	98.00	98.34	100.24	99.79
Number of ions on the basis of 6 oxygen																		
Si	0.022	0.040	0.016	0.018	0.025	0.013	0.020	0.019	0.028	0.026	0.021	0.022	0.034	0.023	0.023	0.019	0.019	0.019
Ti	1.930	1.912	1.951	1.954	1.935	1.934	1.930	1.963	1.960	1.963	1.982	1.930	1.915	1.934	1.942	1.938	1.937	1.939
Al	0.014	0.016	-	-	0.015	-	-	-	0.012	-	0.011	-	-	-	-	-	-	-
Fe^{2+}	1.837	1.873	1.832	1.865	1.834	2.044	2.025	1.922	1.921	1.882	1.841	2.030	2.038	1.984	1.937	1.928	1.948	1.910
Mn	0.028	0.028	0.023	0.025	0.032	0.026	0.025	0.020	0.034	0.032	0.028	0.020	0.022	0.019	0.022	0.023	0.022	0.023
Mg	0.200	0.157	0.206	0.167	0.184	0.037	0.050	0.097	0.053	0.096	0.100	0.046	0.043	0.074	0.094	0.124	0.118	0.133
Ca	0.010	0.014	0.007	-	0.009	-	-	-	-	0.013	0.008	-	-	0.009	0.017	0.012	-	0.016
Na	-	-	-	-	-	-	-	-	-	-	-	-	-	-	-	-	-	-
Cations	4.041	4.040	4.034	4.028	4.033	4.054	4.050	4.019	4.007	4.012	3.992	4.048	4.052	4.043	4.035	4.043	4.043	4.041
Recalculated Fe ions and oxides																		
Fe^{2+}	1.696	1.736	1.714	1.769	1.720	1.858	1.852	1.855	1.897	1.842	1.845	1.865	1.859	1.836	1.817	1.778	1.798	1.769
Fe^{3+}	0.122	0.118	0.102	0.083	0.099	0.159	0.148	0.058	0.020	0.035	-	0.141	0.153	0.127	0.104	0.129	0.129	0.122
FeO	41.28	41.26	41.53	42.40	41.40	44.87	44.74	44.46	44.75	43.80	43.79	44.63	44.38	44.07	42.72	42.09	43.32	42.53
Fe_2O_3	3.29	3.12	2.76	2.21	2.64	4.26	3.98	1.54	0.53	0.92	-	3.75	4.07	3.39	2.72	3.39	3.45	3.25
End-member composition																		
mol.% Ilm	96.7	96.8	-	97.8	97.4	-	96.2	-	-	-	-	-	-	96.7	-	96.7	96.7	96.8

Table A6.19 Electron microprobe analyses of ilmenite in group A lavas (continued).

Rock Type	hawaiite (continued)										ol-tholeiitic basalt							
Sample	SAB151						SAB163				SA80		SAB152					
Analysis	201-G	205-G	681-G	683-G	684-G	686-G	1973-G	1975-G	1978-G	1985-G	108-G	114-G	252-G	254-G	703-G	706-G	707-G	708-G
SiO_2	0.52	0.43	0.43	0.46	0.40	0.44	0.39	0.67	0.56	0.25	0.47	0.38	0.37	0.31	0.33	0.40	0.74	0.40
TiO_2	48.76	49.22	49.40	50.21	50.14	50.21	53.42	52.43	52.55	52.93	48.19	48.23	50.37	50.74	49.89	51.03	50.11	50.87
Al_2O_3	-	-	-	-	-	-	-	-	-	-	-	-	-	-	-	-	-	-
FeO_T	46.63	46.53	47.95	45.81	46.49	47.06	44.75	44.38	45.19	44.58	48.51	48.12	45.44	47.37	47.12	46.23	46.90	46.33
MnO	0.44	0.45	0.51	0.49	0.56	0.47	0.67	0.59	0.71	0.63	0.41	0.45	0.59	0.58	0.63	0.52	0.55	0.55
MgO	0.84	1.64	0.75	1.56	1.67	1.06	1.80	1.78	1.00	1.66	1.02	1.08	2.17	1.45	1.44	1.24	1.01	1.45
CaO	0.21	0.14	-	0.22	-	0.20	0.16	-	0.25	-	0.13	0.15	-	-	-	0.18	-	0.15
Na_2O	-	-	-	-	-	-	-	-	-	-	-	-	-	-	-	-	-	-
Total	97.40	98.41	99.04	98.75	99.26	99.44	101.19	99.85	100.26	100.05	98.73	98.41	98.94	100.45	99.41	99.60	99.31	99.75
Number of ions on the basis of 6 oxygen																		
Si	0.027	0.022	0.022	0.023	0.020	0.022	0.019	0.034	0.028	0.013	0.025	0.020	0.019	0.016	0.017	0.020	0.038	0.020
Ti	1.909	1.901	1.908	1.925	1.916	1.921	1.976	1.964	1.971	1.984	1.874	1.881	1.922	1.921	1.911	1.940	1.915	1.931
Al	-	-	-	-	-	-	-	-	-	-	-	-	-	-	-	-	-	-
Fe^{2+}	2.030	1.999	2.059	1.953	1.976	2.002	1.841	1.849	1.885	1.858	2.098	2.087	1.928	1.994	2.007	1.954	1.993	1.956
Mn	0.019	0.020	0.022	0.021	0.024	0.020	0.028	0.025	0.030	0.026	0.018	0.020	0.025	0.025	0.027	0.022	0.024	0.023
Mg	0.065	0.126	0.058	0.118	0.127	0.080	0.132	0.133	0.074	0.124	0.079	0.083	0.164	0.109	0.110	0.094	0.076	0.109
Ca	0.012	0.007	-	0.012	-	0.011	0.008	-	0.013	-	0.007	0.008	-	-	-	0.010	-	0.008
Na	-	-	-	-	-	-	-	-	-	-	-	-	-	-	-	-	-	-
Cations	4.063	4.076	4.069	4.052	4.064	4.057	4.004	4.003	4.001	4.004	4.101	4.099	4.059	4.063	4.072	4.040	4.046	4.048
Recalculated Fe ions and oxides																		
Fe^{2+}	1.814	1.739	1.820	1.773	1.757	1.807	1.826	1.838	1.882	1.844	1.751	1.746	1.726	1.776	1.761	1.817	1.833	1.790
Fe^{3+}	0.185	0.223	0.204	0.155	0.188	0.167	0.013	0.010	0.002	0.011	0.296	0.290	0.174	0.187	0.211	0.118	0.138	0.143
FeO	42.32	41.24	43.12	42.12	41.99	43.07	44.43	44.15	45.13	44.31	41.50	41.26	41.27	42.87	42.08	43.41	43.62	42.90
Fe_2O_3	4.79	5.88	5.37	4.10	5.00	4.44	0.36	0.26	0.06	0.30	7.78	7.63	4.63	5.01	5.60	3.14	3.64	3.81
End-member composition																		
mol.% Ilm	95.2	-	94.7	-	-	95.7	-	99.8	-	99.7	-	-	-	-	94.5	96.9	96.4	-

Table A6.19 Electron microprobe analyses of ilmenite in group A lavas (continued).

Rock Type	ol-tholeiitic basalt (continued)																	
Sample	SAB181			SAB187			SAB171						SAB172			SAB173		
Analysis	186-G	195-G	517-G	277-G	278-G	524-G	961-G	966-G	969-G	973-G	975-G	617-G	925-G	933-G	935-G	1018-G	1021-G	1022-G
SiO_2	0.58	0.52	0.35	0.39	0.41	0.44	0.44	0.44	0.39	0.64	0.39	1.04	0.61	0.78	0.50	0.42	0.65	0.47
TiO_2	48.60	49.53	49.47	50.06	49.13	50.58	49.66	48.56	47.70	47.88	50.13	48.37	47.97	45.42	48.34	50.82	47.93	50.57
Al_2O_3	0.62	0.25	-	-	-	-	0.30	0.23	-	-	-	0.33	0.28	0.26	0.23	0.20	0.22	-
FeO_T	47.79	48.10	47.56	46.82	47.21	45.32	47.66	47.66	48.72	48.60	46.46	47.99	45.63	48.72	46.81	43.10	47.34	45.53
MnO	0.45	0.45	0.47	0.35	0.39	0.28	0.37	0.32	0.46	0.40	0.43	0.69	0.45	0.56	0.42	0.32	0.36	0.39
MgO	0.89	1.16	1.04	2.21	1.62	2.43	1.33	0.92	0.62	0.72	1.42	0.85	1.04	0.87	0.77	1.17	0.95	0.97
CaO	-	-	0.21	-	-	-	0.13	-	0.14	0.21	-	0.16	0.18	-	0.22	0.14	0.19	-
Na_2O	-	-	-	-	-	-	-	-	-	-	-	-	-	-	-	-	-	-
Total	98.93	100.01	99.10	99.83	98.76	99.05	99.89	98.13	98.03	98.45	98.83	99.43	96.16	96.61	97.29	96.17	97.64	97.93
Number of ions on the basis of 6 oxygen																		
Si	0.029	0.026	0.018	0.020	0.021	0.022	0.022	0.023	0.020	0.033	0.020	0.053	0.032	0.041	0.026	0.022	0.034	0.024
Ti	1.873	1.889	1.907	1.901	1.895	1.922	1.892	1.892	1.876	1.870	1.925	1.856	1.896	1.816	1.897	1.979	1.876	1.953
Al	0.037	0.015	-	-	-	-	0.018	0.014	-	-	-	0.020	0.017	0.016	0.014	0.013	0.014	-
Fe^{2+}	2.049	2.039	2.039	1.977	2.026	1.916	2.020	2.065	2.131	2.110	1.984	2.048	2.006	2.167	2.042	1.867	2.060	1.955
Mn	0.019	0.019	0.020	0.015	0.017	0.012	0.016	0.014	0.020	0.017	0.019	0.030	0.020	0.025	0.019	0.014	0.016	0.017
Mg	0.068	0.088	0.080	0.167	0.124	0.183	0.101	0.071	0.048	0.055	0.108	0.064	0.082	0.069	0.060	0.090	0.074	0.074
Ca	-	-	0.011	-	-	-	0.007	-	0.008	0.012	-	0.008	0.010	-	0.012	0.008	0.011	-
Na	-	-	-	-	-	-	-	-	-	-	-	-	-	-	-	-	-	-
Cations	4.076	4.076	4.075	4.079	4.084	4.055	4.076	4.079	4.103	4.097	4.055	4.080	4.063	4.135	4.070	3.992	4.084	4.023
Recalculated Fe ions and oxides																		
Fe^{2+}	1.786	1.776	1.780	1.705	1.739	1.726	1.757	1.793	1.775	1.775	1.793	1.773	1.788	1.705	1.800	1.871	1.772	1.875
Fe^{3+}	0.225	0.225	0.221	0.234	0.246	0.164	0.225	0.232	0.302	0.285	0.164	0.235	0.187	0.391	0.208	-	0.246	0.069
FeO	42.44	42.69	42.30	41.18	41.37	41.39	42.25	42.20	41.63	41.87	42.57	42.37	41.32	39.64	41.97	43.10	41.58	43.92
Fe_2O_3	5.94	6.01	5.85	6.27	6.49	4.37	6.01	6.06	7.88	7.48	4.32	6.25	4.79	10.09	5.38	-	6.41	1.79
End-member composition																		
mol.% Ilm	94.1	-	94.3	-	93.6	-	-	-	-	-	-	-	95.2	89.9	94.7	-	-	-

Table A6.19 Electron microprobe analyses of ilmenite in group A lavas (continued).

Rock Type	qz-tholeiitic basalt									transitional basalt			
Sample	SA76				SA77				SAB198	SA13			
Analysis	123-G	130-G	171-G	178-G	646-G	647-G	648-G	649-G	1570-G	577-G	578-G	579-G	580-G
SiO_2	0.49	0.61	0.50	0.45	0.49	0.87	0.32	0.58	0.54	0.46	0.76	0.43	0.99
TiO_2	48.52	49.93	48.84	50.27	49.23	47.80	48.40	48.42	50.16	48.72	48.17	48.86	48.61
Al_2O_3	0.21	-	-	-	0.24	-	-	-	-	-	0.25	-	0.22
FeO_T	48.39	47.06	48.64	47.81	46.91	47.61	48.15	48.52	47.34	45.64	46.18	46.20	45.98
MnO	0.42	0.44	0.38	0.34	0.27	0.36	0.29	0.38	0.49	0.60	0.50	0.49	0.46
MgO	0.51	0.76	0.88	1.30	1.62	0.98	0.78	0.86	0.59	2.04	1.64	1.74	2.05
CaO	0.14	0.23	0.22	-	0.16	0.47	-	0.15	0.15	0.35	0.67	0.25	0.42
Na_2O	-	-	-	-	-	-	-	-	-	-	-	-	-
Total	98.68	99.03	99.46	100.17	98.92	98.09	97.94	98.91	99.27	97.81	98.17	97.97	98.73
Number of ions on the basis of 6 oxygen													
Si	0.025	0.031	0.026	0.023	0.025	0.045	0.017	0.030	0.028	0.023	0.039	0.022	0.050
Ti	1.886	1.918	1.883	1.910	1.891	1.854	1.897	1.879	1.925	1.891	1.864	1.897	1.862
Al	0.013	-	-	-	0.014	-	-	-	-	-	0.016	-	0.013
Fe^{2+}	2.092	2.011	2.086	2.020	2.003	2.054	2.099	2.093	2.020	1.969	1.987	1.994	1.958
Mn	0.019	0.019	0.016	0.015	0.011	0.016	0.013	0.016	0.022	0.026	0.022	0.022	0.020
Mg	0.039	0.058	0.067	0.098	0.124	0.075	0.061	0.067	0.045	0.157	0.126	0.134	0.155
Ca	0.008	0.013	0.012	-	0.009	0.026	-	0.008	0.008	0.019	0.037	0.014	0.023
Na	-	-	-	-	-	-	-	-	-	-	-	-	-
Cations	4.081	4.050	4.090	4.067	4.078	4.069	4.086	4.092	4.048	4.085	4.090	4.082	4.082
Recalculated Fe ions and oxides													
Fe^{2+}	1.811	1.838	1.775	1.790	1.737	1.815	1.802	1.776	1.855	1.677	1.680	1.712	1.678
Fe^{3+}	0.239	0.148	0.265	0.197	0.228	0.204	0.253	0.270	0.141	0.251	0.263	0.242	0.240
FeO	42.75	43.55	42.33	43.07	41.46	42.80	42.23	42.12	43.99	39.70	39.93	40.47	40.22
Fe_2O_3	6.26	3.90	7.01	5.27	6.06	5.35	6.58	7.11	3.72	6.60	6.94	6.36	6.40
End-member composition													
mol.% Ilm	-	-	-	-	-	-	93.5	93.1	-	93.3	93.0	93.7	93.6

A6.20 Microprobe analyses of olivine in group B lavas: alkali ol-basalts

Table A6.20 Electron microprobe analyses of olivine for group B alkali ol-basalts

Sample	SA54							SAB188								
Analysis	1669-C1	1670-R1	1691-C2	1692-R2	1700-C3	1701-R3	1695-C	1634-C1	1635-R1	1654-C2	1655-R2	1656-C3	1657-R3	1659-C4	1660-R4	1645-C
SiO_2	39.06	36.92	37.91	36.17	39.70	36.21	36.27	41.35	41.07	39.14	40.45	40.79	41.16	40.22	37.43	41.10
TiO_2	-	-	-	-	-	-	-	-	-	-	-	-	-	-	-	-
Al_2O_3	-	-	-	-	-	-	-	-	-	-	-	-	-	-	-	-
FeO_T	16.21	31.11	23.27	33.28	16.12	32.19	30.07	8.31	8.04	18.09	18.24	7.97	8.81	10.90	24.86	9.28
MnO	-	0.49	0.29	0.59	0.26	0.54	0.49	-	-	-	-	-	-	-	0.36	-
MgO	43.51	31.95	37.73	29.84	43.99	30.13	31.77	50.57	50.31	42.42	40.87	50.41	50.21	48.25	36.19	49.72
CaO	0.23	0.45	0.24	0.50	0.25	0.47	0.40	-	-	0.24	0.22	-	-	-	0.34	-
Total	99.01	100.92	99.44	100.38	100.32	99.54	99.00	100.23	99.42	99.89	99.78	99.17	100.18	99.37	99.18	100.10
Number of ions on the basis of 4 oxygen																
Si	0.990	0.990	0.991	0.988	0.994	0.992	0.988	0.996	0.997	0.993	1.050	0.993	0.995	0.991	0.990	0.996
Ti	-	-	-	-	-	-	-	-	-	-	-	-	-	-	-	-
Al	-	-	-	-	-	-	-	-	-	-	-	-	-	-	-	-
Fe^{2+}	0.344	0.698	0.509	0.760	0.337	0.738	0.685	0.168	0.163	0.384	0.396	0.162	0.178	0.224	0.550	0.188
Mn	-	0.011	0.006	0.014	0.006	0.012	0.011	-	-	-	-	-	-	-	0.008	-
Mg	1.644	1.277	1.471	1.214	1.641	1.231	1.290	1.817	1.820	1.604	1.581	1.829	1.810	1.772	1.428	1.796
Ca	0.006	0.013	0.007	0.014	0.007	0.014	0.012	-	-	0.006	0.006	-	-	-	0.010	-
Cations	2.984	2.988	2.984	2.990	2.984	2.987	2.986	2.981	2.980	2.987	3.033	2.985	2.983	2.987	2.986	2.980
Recalculated Fe ions and oxides																
Fe^{2+}	0.344	0.698	0.509	0.760	0.337	0.738	0.685	0.168	0.163	0.384	0.238	0.162	0.178	0.224	0.550	0.188
Fe^{3+}	-	-	-	-	-	-	-	-	-	-	0.158	-	-	-	-	-
FeO	16.21	31.11	23.27	33.28	16.12	32.19	30.07	8.31	8.04	18.09	10.96	7.97	8.81	10.90	24.86	9.28
Fe_2O_3	-	-	-	-	-	-	-	-	-	-	8.10	-	-	-	-	-
End-member composition																
Fo	82.7	64.3	74.1	61.1	82.7	62.1	64.9	91.6	91.8	80.7	80.0	91.8	91.0	88.8	71.9	90.5

Table A6.20 Electron microprobe analyses of olivine for group B alkali ol-basalts (continued).

Sample	SAB207										
Analysis	1598-C1[1]	1599-R1	1601-C1	1602-C2	1603-R2	1605-C3[1]	1606-R3	1607-C4	1609-C4a[1]	1610-R4	1612-C[1]
SiO_2	37.09	36.76	37.85	39.46	37.58	38.60	37.43	40.38	39.23	38.77	38.21
TiO_2	-	-	-	-	-	-	-	-	-	-	-
Al_2O_3	-	-	-	-	-	-	-	-	-	-	-
FeO_T	26.89	28.46	22.60	14.94	30.72	21.62	31.39	15.89	19.20	27.74	22.17
MnO	0.39	0.42	0.29	-	0.62	0.23	0.44	-	-	0.49	0.33
MgO	33.83	32.86	37.97	44.09	28.70	37.82	29.16	42.34	39.89	31.41	38.85
CaO	0.36	0.53	0.31	0.19	1.20	0.41	0.51	0.17	0.26	0.45	0.32
Total	98.56	99.03	99.02	98.68	98.82	98.68	98.93	98.78	98.58	98.86	99.88
Number of ions on the basis of 4 oxygen											
Si	1.006	0.992	0.992	1.004	1.057	1.030	1.053	1.047	1.025	1.082	0.990
Ti	-	-	-	-	-	-	-	-	-	-	-
Al	-	-	-	-	-	-	-	-	-	-	-
Fe^{2+}	0.610	0.643	0.496	0.318	0.723	0.482	0.738	0.345	0.420	0.647	0.480
Mn	0.009	0.010	0.006	-	0.015	0.005	0.010	-	-	0.012	0.007
Mg	1.367	1.322	1.484	1.672	1.204	1.504	1.223	1.637	1.554	1.306	1.500
Ca	0.010	0.015	0.009	0.005	0.036	0.012	0.016	0.005	0.007	0.014	0.009
Cations	3.002	2.982	2.986	3.000	3.036	3.033	3.040	3.034	3.005	3.061	2.986
Recalculated Fe ions and oxides											
Fe^{2+}	0.571	0.643	0.496	0.318	0.717	0.388	0.652	0.239	0.329	0.633	0.480
Fe^{3+}	0.039	-	-	-	0.006	0.095	0.087	0.106	0.090	0.014	-
FeO	25.18	28.46	22.60	14.94	30.45	17.38	27.71	11.01	15.06	27.13	22.17
Fe_2O_3	1.90	-	-	-	0.30	4.71	4.09	5.43	4.60	0.68	-
End-member composition											
Fo	68.8	67.0	74.7	84.0	62.0	75.5	62.0	82.6	78.7	66.5	75.5

A6.21 Microprobe analyses of olivine in group B lavas: basanites

Table A6.21 Electron microprobe analyses of olivine for group B basanites

Sample	SA12								SA27											
Analysis	1244-C1[1]	1245-R1	1269-C2[1]	1273-R2	1275-C3	1276-R3	1248-C	1267-G	1316-C1	1318-R1	1320-C2	1321-R2	1329-C3	1330-R3	1338-C4	1339-R4	1341-C[1]	1346-C5[1]	1349-R5	1336-C
SiO_2	38.62	36.81	38.94	37.16	39.47	37.78	38.92	33.46	37.21	37.24	38.18	37.15	36.75	36.82	37.59	37.32	37.32	38.18	37.40	36.46
TiO_2	-	-	-	-	-	-	-	-	-	-	-	-	-	-	-	-	-	-	-	-
Al_2O_3	0.33	-	-	-	-	-	0.27	-	-	0.27	-	0.27	-	-	-	0.32	-	0.27	-	0.40
FeO_T	17.06	26.69	16.92	24.40	15.91	22.09	17.01	44.34	24.54	25.08	23.56	24.36	27.85	28.17	23.54	25.70	25.24	22.99	27.08	30.09
MnO	0.21	0.50	0.23	0.43	-	0.42	0.21	1.16	0.36	0.43	0.22	0.44	0.64	0.55	0.28	0.45	0.49	0.29	0.53	0.82
MgO	42.32	34.58	43.00	36.70	43.30	38.41	42.54	19.33	36.15	35.39	36.74	35.93	33.04	33.16	36.90	35.96	35.46	36.95	33.06	30.76
CaO	0.19	0.28	0.29	0.41	0.22	0.32	0.25	0.68	0.25	0.42	0.19	0.36	0.40	0.45	0.26	0.40	0.32	0.17	0.42	0.43
Total	98.73	98.86	99.38	99.10	98.90	99.02	99.20	98.97	98.51	98.83	98.89	98.51	98.68	99.15	98.57	100.15	98.83	98.85	98.49	98.96
Number of ions on the basis of 4 oxygen																				
Si	0.993	0.994	0.994	0.989	1.012	0.994	0.996	0.995	0.996	1.003	1.024	0.994	1.000	0.998	1.000	0.988	1.006	1.021	1.027	1.007
Ti	-	-	-	-	-	-	-	-	-	-	-	-	-	-	-	-	-	-	-	-
Al	0.010	-	-	-	-	-	0.008	-	-	0.008	-	0.009	-	-	-	0.010	-	0.008	-	0.013
Fe^{2+}	0.367	0.602	0.361	0.543	0.341	0.486	0.364	1.103	0.549	0.565	0.528	0.545	0.634	0.639	0.524	0.569	0.569	0.514	0.622	0.695
Mn	0.004	0.011	0.005	0.010	-	0.009	0.005	0.029	0.008	0.010	0.005	0.010	0.015	0.013	0.006	0.010	0.011	0.006	0.012	0.019
Mg	1.622	1.391	1.637	1.457	1.655	1.507	1.622	0.857	1.443	1.421	1.468	1.433	1.340	1.340	1.463	1.419	1.425	1.473	1.354	1.267
Ca	0.005	0.008	0.008	0.012	0.006	0.009	0.007	0.022	0.007	0.012	0.005	0.010	0.012	0.013	0.008	0.012	0.009	0.005	0.012	0.013
Cations	3.002	3.006	3.005	3.010	3.014	3.006	3.001	3.005	3.004	3.019	3.030	3.002	3.000	3.002	3.000	3.007	3.021	3.028	3.027	3.014
Recalculated Fe ions and oxides																				
Fe^{2+}	0.350	0.598	0.347	0.529	0.314	0.450	0.347	1.100	0.543	0.556	0.477	0.465	0.634	0.633	0.486	0.568	0.550	0.459	0.548	0.689
Fe^{3+}	0.017	0.004	0.014	0.014	0.028	0.036	0.017	0.003	0.006	0.010	0.052	0.080	-	0.005	0.038	0.001	0.019	0.056	0.074	0.006
FeO	16.27	26.50	16.27	23.78	14.62	20.45	16.21	44.21	24.25	24.65	21.26	20.77	27.85	27.93	21.84	25.65	24.39	20.49	23.87	29.81
Fe_2O_3	0.88	0.21	0.72	0.69	1.43	1.82	0.88	0.14	0.32	0.47	2.56	3.99	-	0.26	1.89	0.05	0.94	2.77	3.57	0.31
End-member composition																				
Fo	81.4	69.4	81.7	72.5	82.9	75.2	81.5	43.1	72.1	71.2	73.3	72.1	67.4	67.3	73.4	71.0	71.1	73.9	68.1	63.9

Table A6.21 Electron microprobe analyses of olivine for group B basanites (continued).

Sample	SAB102							SAB111									
Analysis	81-C1	82-R1	400-C2	401-R2	404-C3	405-R3	89-C	282-C1	283-R1	284-C2	285-R2	286-C3	287-R3	294-C4	295-R4	296-C5	297-R5
SiO_2	39.43	38.08	39.73	38.14	39.53	37.99	39.15	37.18	37.38	37.64	38.04	38.95	37.74	38.33	37.71	40.01	38.74
TiO_2	-	-	-	-	-	-	-	-	-	-	-	-	-	-	0.20	-	-
Al_2O_3	-	-	-	-	-	-	-	0.31	0.33	-	0.27	0.31	0.29	-	-	0.32	-
FeO_T	16.61	23.18	15.86	26.33	16.54	24.77	18.20	24.82	25.89	25.01	25.48	22.78	26.84	25.89	26.24	15.44	24.66
MnO	-	0.29	-	0.46	0.22	0.44	0.24	0.38	0.46	0.44	0.46	0.32	0.36	0.43	0.51	-	0.46
MgO	42.36	37.58	43.30	34.90	43.26	36.41	41.80	37.03	35.42	36.84	35.14	38.12	33.76	35.51	34.78	44.42	36.51
CaO	0.19	0.37	0.22	0.49	0.27	0.29	0.23	0.32	0.62	0.25	0.54	0.25	0.57	0.39	0.63	0.26	0.46
Total	98.59	99.50	99.11	100.32	99.82	99.90	99.62	100.04	100.10	100.18	99.93	100.73	99.56	100.55	100.07	100.45	100.83
Number of ions on the basis of 4 oxygen																	
Si	1.004	0.994	1.009	1.009	1.002	1.002	0.996	0.955	0.972	0.973	1.000	1.000	1.002	1.002	0.995	0.994	1.004
Ti	-	-	-	-	-	-	-	-	-	-	-	-	-	-	0.004	-	-
Al	-	-	-	-	-	-	-	0.010	0.010	-	0.008	0.009	0.009	-	-	0.010	-
Fe^{2+}	0.354	0.506	0.337	0.582	0.350	0.546	0.387	0.533	0.563	0.541	0.560	0.489	0.596	0.566	0.580	0.321	0.534
Mn	-	0.006	-	0.010	0.005	0.010	0.005	0.008	0.010	0.010	0.010	0.007	0.008	0.010	0.011	-	0.010
Mg	1.608	1.464	1.639	1.376	1.634	1.432	1.585	1.418	1.373	1.420	1.378	1.459	1.337	1.384	1.369	1.646	1.411
Ca	0.005	0.010	0.006	0.014	0.007	0.008	0.006	0.009	0.017	0.007	0.015	0.007	0.016	0.011	0.018	0.007	0.013
Cations	2.972	2.981	2.991	2.992	2.998	2.998	2.980	2.933	2.946	2.951	2.972	2.971	2.969	2.974	2.977	2.977	2.972
Recalculated Fe ions and oxides																	
Fe^{2+}	0.354	0.506	0.337	0.582	0.350	0.546	0.387	0.533	0.563	0.541	0.560	0.489	0.596	0.566	0.580	0.321	0.534
Fe^{3+}	-	-	-	-	-	-	-	-	-	-	-	-	-	-	-	-	-
FeO	16.61	23.18	15.86	26.33	16.54	24.77	18.20	24.82	25.89	25.01	25.48	22.78	26.84	25.89	26.24	15.44	24.66
Fe_2O_3	-	-	-	-	-	-	-	-	-	-	-	-	-	-	-	-	-
End-member composition																	
Fo	82.0	74.1	83.0	69.9	82.1	72.0	80.2	72.4	70.6	72.1	70.7	74.6	68.9	70.6	69.9	83.7	72.2

Table A6.21 Electron microprobe analyses of olivine for group B basanites (continued).

Sample	SAB128								SAB204								SA37			
Analysis	316-C1	317-R1	324-C2	325-R2	329-C3	330-R3	332-C4	333-R4	1352-C1[1]	1353-R1	1354-C2	1355-R2	1367-C3[1]	136R3	1376-C	1377-C	838-C1[1]	839-R1	840-C2	841-R2
SiO_2	39.50	37.94	39.01	38.45	38.56	38.56	39.16	37.67	38.22	37.71	39.18	37.91	38.77	38.34	38.35	39.21	38.53	36.99	39.03	36.86
TiO_2	-	-	-	-	-	-	-	-	-	-	-	-	-	-	-	-	-	-	-	-
Al_2O_3	-	-	-	-	-	0.29	0.27	0.27	0.29	0.29	-	-	-	-	0.37	0.34	0.30	0.57	0.31	-
FeO_T	18.09	24.65	20.35	24.41	24.30	24.61	19.77	25.97	18.73	25.66	14.34	22.84	18.28	19.76	19.03	16.55	18.12	25.70	17.81	26.01
MnO	0.24	0.44	0.27	0.36	0.45	0.36	0.25	0.53	-	0.32	-	0.22	0.23	0.30	0.22	-	0.29	0.49	0.26	0.40
MgO	41.37	37.36	39.87	35.19	36.92	36.63	40.48	33.60	40.97	36.23	45.01	37.93	41.90	40.66	41.63	43.63	41.75	34.17	41.83	34.86
CaO	0.27	0.52	0.28	0.44	0.39	0.48	0.22	0.49	0.32	0.44	0.24	0.38	0.22	0.35	0.27	0.30	0.40	0.65	0.33	0.54
Total	99.47	100.91	99.78	98.85	100.62	100.93	100.15	98.53	98.53	100.65	98.77	99.28	99.40	99.41	99.87	100.03	99.39	98.57	99.57	98.67
Number of ions on the basis of 4 oxygen																				
Si	1.005	0.972	1.001	1.029	1.000	0.998	0.997	1.008	0.992	0.992	0.992	0.997	0.996	0.993	0.985	0.991	0.990	0.996	0.998	0.994
Ti	-	-	-	-	-	-	-	-	-	-	-	-	-	-	-	-	-	-	-	-
Al	-	-	-	-	-	0.009	0.008	0.008	0.009	0.009	-	-	-	-	0.011	0.010	0.009	0.018	0.010	-
Fe^{2+}	0.385	0.528	0.436	0.546	0.527	0.533	0.421	0.581	0.407	0.564	0.304	0.502	0.393	0.428	0.408	0.350	0.389	0.579	0.381	0.586
Mn	0.005	0.010	0.006	0.008	0.010	0.008	0.006	0.012	-	0.007	-	0.005	0.005	0.007	0.005	-	0.006	0.011	0.006	0.009
Mg	1.569	1.428	1.525	1.404	1.428	1.413	1.537	1.340	1.586	1.420	1.699	1.487	1.604	1.570	1.593	1.644	1.599	1.372	1.594	1.401
Ca	0.007	0.014	0.008	0.013	0.011	0.014	0.006	0.014	0.009	0.012	0.007	0.011	0.006	0.010	0.007	0.008	0.011	0.019	0.009	0.016
Cations	2.971	2.952	2.976	3.001	2.976	2.974	2.975	2.964	3.003	3.004	3.001	3.002	3.004	3.007	3.010	3.004	3.005	2.995	2.998	3.006
Recalculated Fe ions and oxides																				
Fe^{2+}	0.385	0.528	0.436	0.544	0.527	0.533	0.421	0.581	0.334	0.557	0.292	0.499	0.386	0.416	0.389	0.324	0.379	0.579	0.381	0.573
Fe^{3+}	-	-	-	0.003	-	-	-	-	0.073	0.007	0.012	0.003	0.006	0.012	0.019	0.026	0.011	-	-	0.014
FeO	18.09	24.65	20.35	24.29	24.30	24.61	19.77	25.97	15.39	25.32	13.79	22.69	17.98	19.22	18.14	15.34	17.62	25.70	17.81	25.40
Fe_2O_3	-	-	-	0.13	-	-	-	-	3.71	0.38	0.61	0.16	0.33	0.60	0.99	1.34	0.55	-	-	0.68
End-member composition																				
Fo	80.1	72.6	77.5	71.7	72.7	72.3	78.3	69.3	79.6	71.3	84.8	74.6	80.1	78.3	79.4	82.5	80.2	69.9	80.5	70.2

Table A6.21 Electron microprobe analyses of olivine for group B basanites (continued).

Sample	SA37 (continued)									SAB175											
Analysis	846-C3	847-R3	910-C4[1]	911-R4	913-C5[1]	914-R5	843-C	844-C	845-C	1026-C1	1027-R1	1028-C2	1029-R2	1030-C3	1031-R3	1204-C4[4]	1205-R4	1035-C[4]	1038-C[4]	1199-C[4]
SiO_2	39.11	37.61	39.85	38.14	39.15	36.95	38.44	38.66	40.03	39.29	37.74	39.66	38.65	38.25	37.94	39.68	38.51	37.51	39.37	37.69
TiO_2	-	-	-	-	-	-	-	-	-	-	-	-	-	-	-	-	-	-	-	-
Al_2O_3	-	-	-	0.31	-	-	-	0.27	0.33	0.31	0.28	0.34	-	-	0.36	0.32	0.39	0.30	0.31	0.34
FeO_T	15.18	22.84	14.84	23.98	15.77	27.69	19.44	18.83	15.32	15.57	23.86	14.09	20.93	22.58	21.67	16.17	31.38	24.43	16.59	21.49
MnO	-	0.46	-	0.43	0.27	0.54	0.28	0.24	0.23	0.26	0.41	-	0.34	0.29	0.37	0.21	0.58	0.45	-	0.31
MgO	44.43	37.53	45.56	37.45	44.23	35.06	40.01	41.30	44.63	44.45	36.72	45.45	40.03	38.17	38.47	43.94	27.18	36.60	44.14	39.95
CaO	0.27	0.47	0.26	0.50	0.26	0.58	0.38	0.36	0.23	0.24	0.42	0.22	0.31	0.17	0.32	0.26	0.78	0.41	0.26	0.34
Total	98.99	98.91	100.51	100.81	99.68	100.82	98.55	99.66	100.77	100.12	99.43	99.76	100.26	99.46	99.13	100.58	98.82	99.70	100.67	100.12
Number of ions on the basis of 4 oxygen																				
Si	0.991	0.995	0.994	0.993	0.992	0.974	1.009	0.993	0.996	0.989	0.997	0.994	0.997	1.002	0.994	0.994	1.102	0.991	0.989	-
Ti	-	-	-	-	-	-	-	-	-	-	-	-	-	-	-	-	-	-	-	-
Al	-	-	-	0.010	-	-	-	0.008	0.010	0.009	0.009	0.010	-	-	0.011	0.009	0.013	0.010	0.009	0.010
Fe^{2+}	0.322	0.505	0.310	0.522	0.334	0.611	0.427	0.404	0.319	0.328	0.527	0.295	0.451	0.495	0.475	0.339	0.751	0.540	0.348	0.460
Mn	-	0.010	-	0.010	0.006	0.012	0.006	0.005	0.005	0.006	0.009	-	0.008	0.006	0.008	0.004	0.014	0.010	-	0.007
Mg	1.678	1.480	1.695	1.454	1.670	1.378	1.565	1.582	1.656	1.668	1.445	1.697	1.539	1.490	1.503	1.641	1.159	1.442	1.653	1.523
Ca	0.008	0.013	0.007	0.014	0.007	0.016	0.011	0.010	0.006	0.006	0.012	0.006	0.008	0.005	0.009	0.007	0.024	0.012	0.007	0.009
Cations	2.999	3.004	3.006	3.002	3.008	2.992	3.018	3.003	2.992	3.006	2.999	3.002	3.003	2.998	3.000	2.994	3.063	3.004	3.006	2.009
Recalculated Fe ions and oxides																				
Fe^{2+}	0.322	0.498	0.306	0.507	0.328	0.611	0.411	0.357	0.319	0.325	0.527	0.278	0.447	0.495	0.467	0.339	0.747	0.539	0.338	0.460
Fe^{3+}	-	0.007	0.003	0.015	0.006	-	0.016	0.048	-	0.003	-	0.017	0.004	-	0.007	-	0.004	0.001	0.011	-
FeO	15.18	22.50	14.69	23.30	15.47	27.69	18.71	16.62	15.32	15.42	23.86	13.28	20.73	22.58	21.33	16.17	31.20	24.38	16.08	21.49
Fe_2O_3	-	0.37	0.17	0.76	0.34	-	0.81	2.46	-	0.17	-	0.90	0.22	-	0.38	-	0.20	0.05	0.56	-
End-member composition																				
Fo	83.9	74.2	84.6	73.2	83.1	68.9	78.3	79.4	83.7	83.3	72.9	85.2	77.0	74.8	75.7	82.7	60.2	72.4	82.6	76.6

Table A6.21 Electron microprobe analyses of olivine for Group B basanites (continued).

Sample	SAB176								SAB177									
Analysis	302-C1	303-R1	308-C2	309-R2	650-C3	651-R3	1221-C[1]	1224-C[1]	1115-C1	1116-R1	1117-C2	1118-R2	1130-C3	1131-R3[1]	1124-C[1]	1127-C[1]	1129-C[1]	1136-C
SiO_2	40.27	38.44	39.75	37.37	39.63	37.18	38.78	38.77	39.51	37.43	39.74	37.76	39.74	39.30	39.15	38.93	38.37	38.98
TiO_2	-	-	-	-	-	-	-	-	-	-	-	-	-	-	-	-	-	-
Al_2O_3	-	-	-	-	-	0.33	0.35	0.33	-	0.36	0.43	-	0.42	-	0.29	0.31	-	-
FeO_T	16.76	21.07	15.82	27.94	2-	31.14	17.55	17.70	14.99	22.56	14.66	24.43	15.91	18.95	17.70	17.23	19.20	18.79
MnO	-	0.39	-	0.57	0.23	0.47	0.22	-	0.21	0.32	-	0.37	0.23	0.33	0.33	0.24	0.23	0.22
MgO	43.17	39.85	43.43	33.50	40.79	30.77	41.84	42.65	44.63	37.55	44.98	36.67	44.17	41.79	42.41	42.63	40.72	41.76
CaO	0.30	0.43	0.26	0.53	0.27	0.56	0.35	0.28	0.27	0.56	0.26	0.44	0.28	0.37	0.31	0.31	0.33	0.34
Total	100.50	100.18	99.26	99.91	100.92	100.45	99.09	99.73	99.61	98.78	100.07	99.67	100.75	100.74	100.19	99.65	98.85	100.09
Number of ions on the basis of 4 oxygen																		
Si	1.006	0.975	1.002	0.997	1.008	1.006	0.996	0.989	0.997	0.990	0.994	0.998	0.994	0.997	0.995	0.992	0.996	0.996
Ti	-	-	-	-	-	-	-	-	-	-	-	-	-	-	-	-	-	-
Al	-	-	-	-	-	0.010	0.010	0.010	-	0.011	0.012	-	0.012	-	0.008	0.010	-	-
Fe^{2+}	0.350	0.447	0.334	0.623	0.426	0.705	0.377	0.378	0.316	0.499	0.307	0.540	0.333	0.402	0.376	0.367	0.417	0.402
Mn	-	0.008	-	0.013	0.005	0.011	0.005	-	0.004	0.007	-	0.008	0.005	0.007	0.007	0.005	0.005	0.005
Mg	1.607	1.508	1.632	1.332	1.546	1.241	1.602	1.622	1.678	1.481	1.678	1.444	1.648	1.580	1.606	1.620	1.576	1.592
Ca	0.008	0.012	0.007	0.015	0.008	0.016	0.010	0.008	0.007	0.016	0.007	0.012	0.008	0.010	0.008	0.008	0.009	0.009
Cations	2.970	2.950	2.974	2.980	2.992	2.989	2.999	3.006	3.003	3.004	2.999	3.002	3.000	2.996	3.001	3.003	3.004	3.004
Recalculated Fe ions and oxides																		
Fe^{2+}	0.350	0.447	0.334	0.623	0.426	0.705	0.377	0.213	0.306	0.491	0.307	0.528	0.333	0.402	0.370	0.364	0.409	0.392
Fe^{3+}	-	-	-	-	-	-	-	0.165	0.011	0.009	-	0.012	-	-	0.006	0.003	0.007	0.010
FeO	16.76	21.07	15.82	27.94	2-	31.14	17.55	9.98	14.49	22.17	14.66	23.90	15.91	18.95	17.40	17.08	18.86	18.34
Fe_2O_3	-	-	-	-	-	-	-	8.58	0.56	0.43	-	0.59	-	-	0.33	0.17	0.38	0.50
End-member composition																		
Fo	82.1	76.8	83.0	67.7	78.2	63.4	80.8	81.1	84.0	74.5	84.5	72.5	83.0	79.4	80.7	81.3	78.9	79.7

Table A6.21 Electron microprobe analyses of olivine for group B basanites (continued).

Sample	SAB178						SAB179							SAB180					
Analysis	1160-C1	1161-R1	1180-C2	1181-R2	1182-C3	1183-R3	217-C1	218-R1	219-C2	220-R2	586-C3	587-R3	1229-C[1]	1287-C1	1289-R1	1301-C2[1]	1303-R2	1313-C3	1315-R3
SiO_2	39.16	38.05	39.46	37.43	39.05	37.81	39.89	36.11	39.75	36.76	38.77	37.14	38.88	39.18	37.36	38.66	37.36	39.34	38.20
TiO_2	-	-	-	-	-	-	-	-	-	-	-	-	-	-	-	-	-	-	-
Al_2O_3	-	-	0.40	0.34	-	-	-	-	-	-	-	-	-	0.30	0.30	-	-	0.31	0.30
FeO_T	17.18	24.39	14.79	25.30	18.16	24.81	15.78	34.42	16.34	33.01	22.51	30.40	18.95	16.10	25.35	16.93	25.86	14.57	20.59
MnO	-	0.49	-	0.47	0.29	0.51	0.22	0.58	0.23	0.59	0.41	0.63	0.30	0.26	0.42	0.28	0.38	-	0.26
MgO	42.46	36.72	44.43	35.28	41.97	35.63	43.80	28.03	42.91	29.20	38.26	31.50	41.06	42.49	35.94	42.48	34.48	44.76	39.23
CaO	0.30	0.58	0.26	0.55	0.30	0.56	0.24	0.57	0.31	0.51	0.25	0.59	0.41	0.28	0.44	0.28	0.45	0.29	0.33
Total	99.10	100.23	99.34	99.37	99.77	99.32	99.93	99.71	99.54	100.07	100.20	100.26	99.60	98.61	99.81	98.63	98.53	99.27	98.91
Number of ions on the basis of 4 oxygen																			
Si	1.002	1.000	0.994	0.997	0.998	1.005	0.999	0.998	1.002	1.003	1.007	1.005	1.000	1.016	0.990	0.994	1.013	0.993	0.997
Ti	-	-	-	-	-	-	-	-	-	-	-	-	-	-	-	-	-	-	-
Al	-	-	0.012	0.010	-	-	-	-	-	-	-	-	-	0.009	0.010	-	-	0.009	0.009
Fe^{2+}	0.368	0.536	0.312	0.564	0.388	0.552	0.330	0.795	0.345	0.753	0.489	0.688	0.408	0.349	0.562	0.364	0.586	0.308	0.450
Mn	-	0.011	-	0.011	0.006	0.012	0.005	0.014	0.005	0.014	0.009	0.014	0.007	0.006	0.010	0.006	0.009	-	0.006
Mg	1.620	1.438	1.668	1.401	1.600	1.412	1.636	1.154	1.613	1.188	1.481	1.271	1.574	1.643	1.420	1.628	1.393	1.684	1.527
Ca	0.008	0.016	0.007	0.016	0.008	0.016	0.006	0.017	0.008	0.015	0.007	0.017	0.011	0.008	0.012	0.008	0.013	0.008	0.009
Cations	2.998	3.000	2.992	2.998	3.002	2.996	2.976	2.978	2.974	2.972	2.993	2.995	3.000	3.031	3.004	2.999	3.014	3.002	2.998
Recalculated Fe ions and oxides																			
Fe^{2+}	0.368	0.526	0.312	0.564	0.387	0.552	0.330	0.795	0.345	0.753	0.489	0.688	0.408	0.333	0.481	0.364	0.575	0.270	0.450
Fe^{3+}	-	0.010	-	-	0.001	-	-	-	-	-	-	-	-	0.016	0.081	-	0.012	0.038	-
FeO	17.18	23.95	14.79	25.30	18.11	24.81	15.78	34.42	16.34	33.01	22.51	30.40	18.95	15.36	21.69	16.93	25.34	12.77	20.59
Fe_2O_3	-	0.49	-	-	0.06	-	-	-	-	-	-	-	-	0.82	4.07	-	0.57	2.01	-
End-member composition																			
Fo	81.5	72.5	84.3	70.9	80.2	71.5	83.0	58.8	82.2	60.8	74.8	64.4	79.2	82.2	71.3	81.5	70.1	84.6	77.0

A6.22 Microprobe analyses of olivine in group B lavas: nephelinites

Table A6.22 Electron microprobe analyses of olivine for group B nephelinites

Sample	SA21								SA28						SA51			
Analysis	1379-C1[1]	1380-R1	1385-C2[1]	1386-R2	1390-C3	1391-R3	1400-C4[1]	1404-R4	1421-C1[1]	1422-R1	1431-C2[1]	1432-R2	1435-C3[1]	1436-R3	1449-C1	1450-R1	1451-C	1453-C2
SiO_2	38.20	37.78	37.67	37.43	37.69	37.96	37.93	37.58	37.45	35.87	37.07	36.26	37.69	35.72	38.07	38.16	38.29	37.85
TiO_2	-	-	-	-	-	-	-	-	-	-	-	-	-	-	-	-	-	-
Al_2O_3	-	1.42	-	-	-	-	-	-	-	-	-	-	-	-	-	-	-	-
FeO_T	21.44	24.84	21.92	24.30	22.81	24.41	23.07	24.81	24.47	31.84	26.00	34.00	24.54	32.32	21.29	22.44	21.71	21.54
MnO	0.34	0.40	0.40	0.43	0.34	0.36	0.42	0.42	0.34	0.86	0.58	0.98	0.32	0.94	0.30	0.29	0.22	0.33
MgO	39.13	33.77	38.16	36.25	37.51	35.48	37.59	35.80	36.36	30.08	34.94	28.74	36.35	29.32	38.90	37.32	38.43	38.83
CaO	0.32	0.61	0.36	0.45	0.21	0.54	0.31	0.54	0.33	0.47	0.27	0.46	0.40	0.61	0.31	0.57	0.30	0.34
Total	99.43	98.82	98.51	98.86	98.56	98.75	99.32	99.15	98.95	99.12	98.86	100.44	99.30	98.91	98.87	98.78	98.95	98.89
Number of ions on the basis of 4 oxygen																		
Si	0.992	1.008	0.991	0.992	0.994	1.020	0.994	0.991	0.992	0.988	0.992	0.994	0.995	0.990	0.993	1.015	1.006	0.989
Ti	-	-	-	-	-	-	-	-	-	-	-	-	-	-	-	-	-	-
Al	-	0.045	-	-	-	-	-	-	-	-	-	-	-	-	-	-	-	-
Fe^{2+}	0.466	0.554	0.482	0.539	0.503	0.548	0.506	0.547	0.542	0.733	0.582	0.780	0.542	0.749	0.464	0.500	0.477	0.470
Mn	0.007	0.009	0.009	0.010	0.008	0.008	0.010	0.009	0.008	0.020	0.013	0.023	0.007	0.022	0.007	0.006	0.005	0.007
Mg	1.514	1.343	1.496	1.433	1.474	1.421	1.468	1.408	1.436	1.234	1.393	1.174	1.430	1.211	1.512	1.480	1.505	1.512
Ca	0.009	0.018	0.010	0.013	0.006	0.016	0.008	0.015	0.009	0.014	0.008	0.014	0.011	0.018	0.008	0.016	0.008	0.010
Cations	2.988	2.977	2.989	2.986	2.984	3.013	2.985	2.970	2.988	2.989	2.987	2.984	2.985	2.990	2.985	3.018	3.001	2.988
Recalculated Fe ions and oxides																		
Fe^{2+}	0.466	0.554	0.482	0.539	0.503	0.538	0.506	0.547	0.542	0.733	0.582	0.780	0.542	0.749	0.464	0.465	0.429	0.470
Fe^{3+}	-	-	-	-	-	0.011	-	-	-	-	-	-	-	-	-	0.034	0.048	-
FeO	21.44	24.84	21.92	24.30	22.81	23.94	23.07	24.81	24.47	31.84	26.00	34.00	24.54	32.32	21.29	20.91	19.51	21.54
Fe_2O_3	-	-	-	-	-	0.53	-	-	-	-	-	-	-	-	-	1.70	2.44	-
End-member composition																		
Fo	76.2	70.4	75.3	72.3	74.3	71.9	74.0	71.7	72.3	62.1	70.1	59.4	72.3	61.1	76.2	74.5	75.7	76.0

Table A6.22 Electron microprobe analyses of olivine for group B nephelinites (continued).

Sample	SA51 (continued)					SAB113							SAB135					
Analysis	1454-R2	1455-C3	1459-R3	1470-C4[1]	1471-R4	232-C1	233-R1	238-C	242-C2	243-R2	751-C3	752-R3	1-C1	2-R1	9-C2	10-R2	12-C3	13-R3
SiO_2	37.55	38.41	37.87	37.78	37.69	38.65	37.45	37.99	39.86	38.17	39.66	38.18	40.16	39.22	40.17	38.55	39.21	38.25
TiO_2	-	-	-	-	-	-	-	-	-	-	-	-	-	-	-	-	-	-
Al_2O_3	-	-	-	-	1.85	-	-	-	-	-	0.45	-	-	-	-	-	0.31	-
FeO_T	22.81	20.34	21.94	22.33	22.23	22.59	25.45	25.49	16.87	25.02	16.81	24.40	15.63	19.82	15.54	20.03	18.52	21.68
MnO	0.44	-	0.30	0.40	0.40	0.25	0.33	0.43	0.21	0.35	0.21	0.38	-	0.37	-	0.32	0.22	0.36
MgO	37.37	39.67	38.25	38.37	36.09	38.38	34.96	35.29	43.09	35.92	41.81	36.37	42.97	38.93	43.16	39.45	41.05	38.73
CaO	0.53	0.19	0.44	0.29	0.51	0.32	0.55	0.52	0.24	0.55	0.20	0.44	0.20	0.44	0.21	0.40	0.27	0.43
Total	98.70	98.61	98.80	99.17	98.77	100.19	98.74	99.72	100.27	100.01	99.14	99.77	98.96	98.78	99.08	98.75	99.58	99.45
Number of ions on the basis of 4 oxygen																		
Si	0.991	1.004	0.993	0.988	0.999	0.998	0.998	1.002	1.000	1.000	1.011	1.006	1.019	1.027	1.012	0.999	0.998	0.993
Ti	-	-	-	-	-	-	-	-	-	-	-	-	-	-	-	-	-	-
Al	-	-	-	-	0.058	-	-	-	-	-	0.014	-	-	-	-	-	0.010	-
Fe^{2+}	0.504	0.444	0.481	0.488	0.493	0.488	0.567	0.562	0.354	0.548	0.358	0.538	0.332	0.434	0.327	0.434	0.394	0.471
Mn	0.010	-	0.007	0.009	0.009	0.006	0.007	0.010	0.004	0.008	0.004	0.008	-	0.008	-	0.007	0.005	0.008
Mg	1.471	1.546	1.495	1.496	1.426	1.478	1.389	1.387	1.611	1.404	1.589	1.429	1.626	1.519	1.620	1.525	1.558	1.499
Ca	0.015	0.006	0.012	0.008	0.014	0.009	0.016	0.015	0.006	0.015	0.005	0.012	0.006	0.012	0.006	0.011	0.007	0.012
Cations	2.991	2.999	2.989	2.990	3.000	2.978	2.977	2.975	2.976	2.975	2.982	2.994	2.982	3.001	2.964	2.977	2.973	2.983
Recalculated Fe ions and oxides																		
Fe^{2+}	0.504	0.444	0.483	0.488	0.493	0.488	0.567	0.562	0.354	0.548	0.358	0.538	0.332	0.431	0.327	0.434	0.394	0.471
Fe^{3+}	-	-	-	-	-	-	-	-	-	-	-	-	-	0.003	-	-	-	-
FeO	22.81	20.34	21.94	22.33	22.23	22.59	25.45	25.49	16.87	25.02	16.81	24.40	15.63	19.70	15.54	20.03	18.52	21.68
Fe_2O_3	-	-	-	-	-	-	-	-	-	-	-	-	-	0.13	-	-	-	-
End-member composition																		
Fo	74.1	77.7	75.4	75.1	74.0	75.0	70.7	70.8	81.8	71.6	81.4	72.4	83.1	77.4	83.2	77.5	79.6	75.8

A6.23 Microprobe analyses of olivine in group B lavas: ne-hawaiites

Table A6.23 Electron microprobe analyses of olivine for group B ne-hawaiites

Sample	SA02				SA25						SA29					
Analysis	1492-C	1493-C	1494-C	1500-C	1523-C1	1524-R1	1527-C2	1528-R2	1525-C	1526-C	152-C1	153-R1	154-C2	155-R2	443-C3	444-R3
SiO_2	38.24	37.96	37.58	37.52	37.53	37.86	37.68	36.48	37.86	37.57	37.68	36.94	38.15	35.30	38.61	36.63
TiO_2	-	-	-	-	-	-	-	-	-	-	-	-	-	-	-	-
Al_2O_3	-	-	-	-	-	-	-	-	-	-	-	-	-	-	-	-
FeO_T	19.73	21.10	23.44	23.10	25.78	25.69	26.16	33.02	25.24	25.49	28.29	32.06	26.16	37.17	24.06	31.25
MnO	0.21	0.34	0.28	0.39	0.36	-	0.26	0.56	0.31	0.33	0.47	0.69	0.46	0.98	0.46	0.71
MgO	40.28	39.15	37.62	37.54	36.28	36.45	36.03	29.60	36.57	36.78	33.72	30.27	35.47	25.71	37.01	30.74
CaO	0.27	0.27	0.14	0.21	0.28	0.20	0.21	0.36	0.23	0.21	0.26	0.44	0.38	0.57	0.22	0.43
Total	98.73	98.82	99.05	98.76	100.23	100.20	100.34	100.02	100.21	100.38	100.42	100.40	100.62	99.73	100.36	99.76
Number of ions on the basis of 4 oxygen																
Si	0.999	0.998	0.996	0.998	0.986	0.992	0.990	0.998	0.992	0.984	0.999	1.000	0.999	0.992	1.008	1.002
Ti	-	-	-	-	-	-	-	-	-	-	-	-	-	-	-	-
Al	-	-	-	-	-	-	-	-	-	-	-	-	-	-	-	-
Fe^{2+}	0.431	0.464	0.520	0.514	0.567	0.564	0.575	0.756	0.553	0.558	0.627	0.726	0.573	0.874	0.526	0.715
Mn	0.005	0.008	0.006	0.009	0.008	-	0.006	0.013	0.007	0.007	0.010	0.016	0.010	0.023	0.010	0.016
Mg	1.569	1.535	1.487	1.488	1.422	1.424	1.412	1.208	1.428	1.437	1.333	1.222	1.384	1.078	1.441	1.253
Ca	0.008	0.008	0.004	0.006	0.008	0.006	0.006	0.011	0.006	0.006	0.008	0.013	0.011	0.017	0.006	0.012
Cations	3.011	3.012	3.014	3.015	2.991	2.986	2.989	2.986	2.986	2.993	2.977	2.976	2.977	2.984	2.991	2.998
Recalculated Fe ions and oxides																
Fe^{2+}	0.428	0.434	0.488	0.477	0.567	0.564	0.575	0.756	0.553	0.558	0.627	0.726	0.573	0.874	0.526	0.715
Fe^{3+}	0.003	0.030	0.031	0.037	-	-	-	-	-	-	-	-	-	-	-	-
FeO	19.59	19.72	22.03	21.46	25.78	25.69	26.16	33.02	25.24	25.49	28.29	32.06	26.16	37.17	24.06	31.25
Fe_2O_3	0.15	1.53	1.57	1.83	-	-	-	-	-	-	-	-	-	-	-	-
End-member composition																
Fo	78.3	76.5	73.9	74.0	71.2	71.6	70.8	61.1	71.8	71.8	67.6	62.2	70.4	54.6	72.9	63.2

Table A6.23 Electron microprobe analyses of olivine for group B ne-hawaiites (continued).

Sample	SA65								
Analysis	1537-C1	1538-R1	1539-C2	1540-R2	1542-C3	1543-R3	1536-C	1562-C[1]	1567-C[1]
SiO_2	36.83	36.68	36.89	35.96	36.79	35.86	37.17	37.04	36.93
TiO_2	-	-	-	-	-	-	-	-	-
Al_2O_3	-	-	-	-	-	-	-	-	-
FeO_T	28.47	30.03	27.85	32.61	28.50	33.34	29.65	28.11	28.65
MnO	0.51	0.66	0.43	0.80	0.47	0.68	0.43	0.39	0.50
MgO	33.24	32.04	33.21	29.80	33.42	29.30	32.88	34.11	33.62
CaO	0.26	0.37	0.23	0.42	0.19	0.44	0.32	0.30	0.35
Total	99.31	99.78	98.61	99.59	99.37	99.62	100.45	99.95	100.05
Number of ions on the basis of 4 oxygen									
Si	0.991	0.991	0.997	0.988	0.990	0.988	0.994	0.988	0.988
Ti	-	-	-	-	-	-	-	-	-
Al	-	-	-	-	-	-	-	-	-
Fe^{2+}	0.641	0.678	0.629	0.749	0.642	0.769	0.663	0.627	0.641
Mn	0.012	0.015	0.010	0.018	0.011	0.016	0.010	0.009	0.011
Mg	1.334	1.291	1.337	1.221	1.341	1.204	1.311	1.356	1.340
Ca	0.007	0.011	0.007	0.012	0.005	0.013	0.009	0.008	0.010
Cations	2.984	2.986	2.980	2.989	2.989	2.990	2.987	2.988	2.990
Recalculated Fe ions and oxides									
Fe^{2+}	0.641	0.678	0.629	0.749	0.642	0.769	0.663	0.627	0.641
Fe^{3+}	-	-	-	-	-	-	-	-	-
FeO	28.47	30.03	27.85	32.61	28.50	33.34	29.65	28.11	28.65
Fe_2O_3	-	-	-	-	-	-	-	-	-
End-member composition									
Fo	67.2	65.0	67.7	61.4	67.3	60.5	66.1	68.1	67.3

A6.24 Microprobe analyses of olivine in group B lavas: mugearite

Table A6.24 Electron microprobe analyses of olivine in group B mugearite

Sample	SA88						
Analysis	52-C1	53-R1	57-C2	58-R2	492-C3	493-R3	65-C
SiO_2	37.11	33.96	36.40	35.40	39.68	39.51	39.60
TiO_2	-	-	-	-	-	-	-
Al_2O_3	-	2.44	-	-	0.28	0.60	-
FeO_T	32.74	42.79	34.36	40.49	17.61	18.99	19.01
MnO	0.43	0.73	0.48	0.60	-	-	0.21
MgO	30.19	17.96	28.76	23.53	42.11	40.89	41.46
CaO	0.25	0.57	0.41	0.41	0.24	0.24	0.23
Total	100.72	98.45	100.41	100.43	99.92	100.23	100.51
Number of ions on the basis of 4 oxygen							
Si	1.002	0.992	0.996	1.000	1.007	1.006	1.001
Ti	-	-	-	-	-	-	-
Al	-	0.084	-	-	0.008	0.018	-
Fe^{2+}	0.740	1.046	0.786	0.957	0.374	0.404	0.402
Mn	0.010	0.018	0.011	0.014	-	-	0.004
Mg	1.216	0.783	1.174	0.992	1.593	1.551	1.562
Ca	0.007	0.018	0.012	0.012	0.006	0.006	0.006
Cations	2.974	2.941	2.980	2.976	2.988	2.986	2.975
Recalculated Fe ions and oxides							
Fe^{2+}	0.740	1.046	0.786	0.957	0.374	0.404	0.402
Fe^{3+}	-	-	-	-	-	-	-
FeO	32.74	42.79	34.36	40.49	17.61	18.99	19.01
Fe_2O_3	-	-	-	-	-	-	-
End-member composition							
Fo	61.9	42.4	59.5	50.5	81.0	79.3	79.4

A6.25 Microprobe analyses of clinopyroxene in group B lavas: alkali ol-basalt

Table A25 Electron microprobe analyses of clinopyroxene in group B alkali ol-basalts.

Sample	SA54													SAB188					
Analysis	1675-C1	1676-R1	1677-C2	1678-R2	1679-C3	1680-R3	1688-C4	1689-R4	1672-G	1681-G	1682-G	1687-G	1690-G	1636-C1	1637-R1	1638-C2	1639-R2	1640-C3	1641-R3
SiO_2	48.11	49.34	48.70	47.87	49.36	47.66	49.92	46.84	49.58	44.18	48.77	46.87	50.27	48.79	45.39	43.37	48.81	48.60	45.96
TiO_2	1.88	1.52	1.42	2.55	2.00	2.90	0.99	2.72	1.96	4.74	2.55	2.81	1.41	1.43	3.57	3.30	2.13	1.55	3.63
Al_2O_3	5.94	4.68	6.70	4.59	3.58	4.98	5.15	6.13	2.91	6.87	3.13	4.89	1.85	5.80	7.00	8.97	4.07	5.46	6.73
Cr_2O_3	0.62	0.43	0.67	-	-	-	0.70	-	-	-	-	-	-	0.54	-	0.52	-	0.67	-
FeO_T	7.46	7.63	7.55	8.81	8.90	9.09	7.04	8.43	9.51	10.92	10.85	10.03	10.79	7.07	8.99	8.77	8.23	6.91	8.71
MnO	-	-	-	-	-	0.22	-	-	-	0.34	0.23	0.26	0.26	-	-	-	-	0.22	-
MgO	13.15	13.84	14.36	12.21	13.16	12.03	15.22	12.22	12.70	9.98	10.84	12.46	11.96	13.58	11.81	11.87	13.53	13.87	11.65
CaO	21.41	21.66	19.48	22.19	22.28	22.46	19.41	22.15	22.03	20.64	21.36	21.72	22.09	21.99	22.79	21.55	22.85	21.78	22.86
Na_2O	1.16	0.93	1.42	1.00	0.89	0.91	1.36	0.91	0.85	1.22	0.92	0.99	1.08	1.19	1.00	1.00	0.91	1.04	0.86
Total	99.73	100.03	100.30	99.22	100.17	100.25	99.79	99.40	99.54	98.89	98.65	100.03	99.71	100.39	100.55	99.35	100.53	100.10	100.40
Number of ions on the basis of 6 oxygen																			
Si	1.802	1.841	1.802	1.818	1.853	1.796	1.850	1.774	1.876	1.719	1.874	1.750	1.912	1.813	1.712	1.655	1.814	1.811	1.732
Ti	0.053	0.043	0.040	0.073	0.056	0.082	0.028	0.077	0.056	0.139	0.074	0.079	0.040	0.040	0.101	0.095	0.059	0.043	0.103
Al	0.262	0.206	0.292	0.206	0.158	0.221	0.225	0.274	0.130	0.315	0.142	0.215	0.083	0.254	0.311	0.404	0.178	0.240	0.299
Cr	0.019	0.013	0.020	-	-	-	0.020	-	-	-	-	-	-	0.016	-	0.016	-	0.020	-
Fe^{2+}	0.233	0.238	0.234	0.280	0.280	0.287	0.218	0.267	0.301	0.355	0.349	0.313	0.343	0.220	0.284	0.280	0.256	0.215	0.274
Mn	-	-	-	-	-	0.007	-	-	-	0.011	0.008	0.008	0.008	-	-	-	-	0.007	-
Mg	0.734	0.769	0.792	0.691	0.736	0.676	0.841	0.689	0.716	0.579	0.621	0.694	0.679	0.752	0.664	0.675	0.749	0.771	0.654
Ca	0.859	0.866	0.772	0.903	0.896	0.907	0.771	0.898	0.893	0.860	0.880	0.869	0.901	0.875	0.921	0.881	0.910	0.870	0.923
Na	0.085	0.067	0.102	0.073	0.065	0.067	0.098	0.067	0.062	0.092	0.068	0.071	0.080	0.085	0.073	0.074	0.065	0.075	0.062
Cations	4.047	4.042	4.054	4.044	4.045	4.044	4.050	4.046	4.034	4.070	4.015	3.999	4.046	4.055	4.067	4.078	4.033	4.053	4.047
Recalculated Al and Fe ions and Fe oxides																			
Al^{IV}	0.198	0.159	0.198	0.182	0.147	0.204	0.150	0.226	0.124	0.281	0.126	0.215	0.083	0.187	0.288	0.345	0.178	0.189	0.268
Al^{VI}	0.064	0.047	0.095	0.024	0.011	0.018	0.075	0.047	0.006	0.034	0.016	-	-	0.067	0.024	0.059	-	0.051	0.030
Fe^{2+}	0.139	0.156	0.128	0.195	0.192	0.199	0.120	0.176	0.232	0.293	0.318	0.184	0.261	0.111	0.150	0.124	0.131	0.109	0.180
Fe^{3+}	0.095	0.082	0.106	0.085	0.088	0.088	0.098	0.091	0.069	0.062	0.030	0.129	0.083	0.109	0.134	0.155	0.124	0.106	0.094
FeO	4.44	5.00	4.13	6.13	6.10	6.30	3.89	5.56	7.33	9.00	9.90	5.89	8.19	3.56	4.74	3.90	4.22	3.51	5.72
Fe_2O_3	3.36	2.92	3.80	2.98	3.11	3.10	3.51	3.19	2.42	2.13	1.05	4.61	2.89	3.90	4.72	5.41	4.45	3.78	3.32
End-member compositions																			
Wo	47.0	46.2	42.9	48.2	46.9	48.3	42.1	48.4	46.8	47.6	47.4	46.1	46.6	47.4	49.3	48.0	47.5	46.7	49.9
En	40.2	41.1	44.0	36.9	38.5	36.0	45.9	37.2	37.5	32.1	33.4	36.8	35.1	40.7	35.5	36.8	39.1	41.4	35.3
Fs	12.8	12.7	13.0	14.9	14.6	15.7	11.9	14.4	15.7	20.3	19.2	17.1	18.2	11.9	15.2	15.2	13.3	11.9	14.8

Table A25 Electron microprobe analyses of clinopyroxene in group B alkali ol-basalts (continued).

Sample	SAB188 (continued)							SAB207								
Analysis	1650-C4	1651-R4	1644-G	1647-G	1665-G	1666-G	1668-G	1613-C1	1614-R1	1615-C2	1616-R2	1617-C3	1618-R3	1620-G	1631-G	1632-G
SiO_2	45.57	47.92	51.57	46.75	46.98	44.34	44.91	46.83	40.89	46.14	46.77	49.23	45.61	47.57	47.27	48.88
TiO_2	3.02	2.70	0.89	2.88	2.86	3.35	3.05	2.26	5.38	2.46	2.82	1.58	3.51	2.60	2.89	2.18
Al_2O_3	7.49	4.80	2.20	6.05	5.34	7.95	5.48	6.33	11.22	8.15	6.06	5.22	7.75	5.28	6.10	4.59
Cr_2O_3	0.40	-	-	-	-	0.31	-	0.40	-	0.63	-	0.52	-	-	-	-
FeO_T	7.91	9.14	7.19	9.63	10.08	8.41	8.34	7.28	8.89	7.17	7.56	6.91	7.97	8.23	7.49	8.18
MnO	-	-	-	-	-	-	-	-	-	-	-	-	-	-	0.26	-
MgO	12.16	11.93	15.29	12.64	11.53	11.96	11.78	13.19	10.42	12.41	12.24	14.36	11.76	12.63	12.45	12.72
CaO	22.65	22.66	22.00	21.87	22.41	22.70	23.80	22.35	22.98	22.24	23.28	21.90	23.05	22.81	23.22	23.19
Na_2O	0.79	1.03	1.11	0.78	1.19	0.89	1.06	0.83	0.86	1.00	0.90	0.82	0.84	0.92	0.76	0.92
Total	99.99	100.18	100.25	100.60	100.39	99.91	98.42	99.47	100.64	100.20	99.63	100.54	100.49	100.04	100.44	100.66
Number of ions on the basis of 6 oxygen																
Si	1.718	1.807	1.900	1.757	1.767	1.682	1.683	1.765	1.542	1.726	1.766	1.822	1.711	1.790	1.769	1.813
Ti	0.086	0.076	0.025	0.081	0.081	0.095	0.086	0.064	0.152	0.069	0.080	0.044	0.099	0.073	0.082	0.061
Al	0.332	0.214	0.095	0.268	0.236	0.356	0.242	0.281	0.499	0.359	0.270	0.227	0.343	0.234	0.269	0.200
Cr	0.012	-	-	-	-	0.009	-	0.012	-	0.019	-	0.016	-	-	-	-
Fe^{2+}	0.250	0.289	0.221	0.303	0.317	0.266	0.262	0.230	0.280	0.224	0.239	0.214	0.250	0.259	0.235	0.254
Mn	-	-	-	-	-	-	-	-	-	-	-	-	-	-	0.008	-
Mg	0.683	0.671	0.840	0.708	0.647	0.676	0.658	0.741	0.586	0.692	0.689	0.792	0.658	0.709	0.694	0.704
Ca	0.915	0.916	0.869	0.881	0.904	0.923	0.955	0.902	0.929	0.892	0.942	0.868	0.927	0.920	0.931	0.922
Na	0.058	0.075	0.079	0.057	0.086	0.065	0.077	0.061	0.062	0.073	0.066	0.059	0.061	0.067	0.055	0.066
Cations	4.054	4.047	4.030	4.055	4.038	4.073	3.963	4.056	4.050	4.052	4.052	4.042	4.049	4.052	4.043	4.020
Recalculated Al and Fe ions and Fe oxides																
Al^{IV}	0.282	0.193	0.095	0.243	0.233	0.318	0.242	0.235	0.458	0.274	0.234	0.178	0.289	0.210	0.231	0.187
Al^{VI}	0.050	0.021	-	0.026	0.004	0.038	-	0.046	0.040	0.084	0.036	0.050	0.054	0.024	0.038	0.014
Fe^{2+}	0.144	0.194	0.097	0.191	0.164	0.120	0.114	0.120	0.105	0.118	0.135	0.130	0.152	0.153	0.150	0.136
Fe^{3+}	0.106	0.095	0.125	0.112	0.153	0.146	0.148	0.110	0.176	0.106	0.104	0.084	0.098	0.106	0.085	0.117
FeO	4.55	6.14	3.14	6.07	5.20	3.79	3.62	3.81	3.32	3.78	4.28	4.20	4.84	4.86	4.78	4.39
Fe_2O_3	3.73	3.33	4.50	3.96	5.42	5.13	5.24	3.86	6.19	3.76	3.64	3.01	3.48	3.74	3.02	4.21
End-member compositions																
Wo	49.5	48.8	45.0	46.6	48.4	49.5	50.9	48.2	51.8	49.3	50.4	46.3	50.5	48.7	49.8	49.0
En	37.0	35.8	43.5	37.4	34.6	36.2	35.1	39.6	32.6	38.3	36.8	42.3	35.8	37.5	37.2	37.5
Fs	13.5	15.4	11.5	16.0	17.0	14.3	14.0	12.3	15.6	12.4	12.8	11.4	13.6	13.7	13.0	13.5

A6.26 Microprobe analyses of clinopyroxene in group B lavas: basanites

Table A26 Electron microprobe analyses of clinopyroxene in group B basanites.

Sample	SA12										SA27							
Analysis	1252-C1	1253-R1	1263-C2	1265-R2	1277-C3	1278-R3	1255-G	1256-G	1258-G	1260-G	1334-C	1335-C	1342-C	1350-C	1322-G	1323-G	1325-G	1326-G
SiO_2	48.78	45.99	46.84	46.66	47.55	43.08	44.32	45.73	48.60	42.60	44.59	47.78	47.51	46.85	45.86	45.40	44.16	47.86
TiO_2	1.60	2.72	2.35	2.89	2.13	4.05	3.55	3.03	1.14	4.46	3.95	2.15	2.69	3.30	3.20	3.51	3.96	2.58
Al_2O_3	4.37	7.17	6.58	6.73	7.35	9.32	7.92	8.02	2.51	9.34	8.35	4.19	5.87	6.79	6.56	7.47	8.24	4.64
Cr_2O_3	0.25	-	0.42	-	0.63	-	-	-	-	-	-	-	-	-	-	-	-	-
FeO_T	7.06	8.08	7.51	8.22	7.01	8.57	8.75	9.30	16.30	8.91	9.04	8.92	8.97	8.55	8.51	8.73	8.79	9.06
MnO	-	-	-	-	-	-	0.22	0.21	0.52	-	-	0.21	-	-	0.25	-	-	-
MgO	13.57	11.88	12.50	11.49	12.13	11.11	10.83	10.21	8.23	10.67	10.47	12.79	11.73	10.91	11.55	11.19	10.90	12.37
CaO	22.60	22.65	22.34	22.69	21.68	22.62	22.45	21.41	19.99	22.51	21.82	22.21	21.64	21.82	22.30	22.32	22.21	21.80
Na_2O	0.47	0.49	0.43	-	0.41	0.54	0.56	1.00	1.23	0.59	0.77	0.40	0.47	0.51	0.54	0.67	0.60	0.42
Total	98.70	98.98	98.97	98.68	98.89	99.29	98.60	98.91	98.52	99.08	98.99	98.65	98.88	98.73	98.77	99.29	98.86	98.73
Number of ions on the basis of 6 oxygen																		
Si	1.855	1.769	1.795	1.796	1.821	1.644	1.702	1.756	1.914	1.633	1.735	1.825	1.838	1.826	1.774	1.745	1.700	1.858
Ti	0.046	0.079	0.068	0.083	0.061	0.116	0.103	0.088	0.034	0.128	0.116	0.062	0.079	0.097	0.093	0.101	0.115	0.075
Al	0.196	0.325	0.297	0.305	0.332	0.419	0.358	0.363	0.116	0.422	0.383	0.189	0.268	0.312	0.299	0.338	0.374	0.212
Cr	0.008	-	0.013	-	0.019	-	-	-	-	-	-	-	-	-	-	-	-	-
Fe^{2+}	0.224	0.260	0.241	0.265	0.224	0.274	0.281	0.299	0.537	0.286	0.295	0.285	0.290	0.278	0.275	0.281	0.283	0.294
Mn	-	-	-	-	-	-	0.007	0.007	0.017	-	-	0.007	-	-	0.008	-	-	-
Mg	0.769	0.681	0.713	0.659	0.692	0.632	0.620	0.584	0.484	0.610	0.607	0.728	0.677	0.634	0.666	0.641	0.626	0.716
Ca	0.921	0.934	0.917	0.936	0.890	0.925	0.924	0.881	0.843	0.925	0.910	0.909	0.897	0.911	0.925	0.919	0.916	0.907
Na	0.035	0.037	0.032	-	0.031	0.040	0.042	0.074	0.094	0.044	0.058	0.029	0.035	0.039	0.040	0.050	0.045	0.032
Cations	4.053	4.084	4.075	4.045	4.071	4.051	4.037	4.051	4.039	4.048	4.104	4.034	4.083	4.096	4.080	4.075	4.060	4.093
Recalculated Al and Fe ions and Fe oxides																		
Al^{IV}	0.145	0.231	0.205	0.204	0.179	0.356	0.298	0.244	0.086	0.367	0.265	0.175	0.162	0.174	0.226	0.255	0.300	0.142
Al^{VI}	0.051	0.095	0.092	0.101	0.153	0.063	0.060	0.119	0.030	0.056	0.118	0.014	0.106	0.138	0.073	0.083	0.075	0.070
Fe^{2+}	0.194	0.245	0.241	0.265	0.224	0.174	0.207	0.274	0.455	0.187	0.295	0.217	0.290	0.278	0.269	0.262	0.243	0.294
Fe^{3+}	0.030	0.015	-	-	-	0.099	0.074	0.025	0.082	0.098	-	0.068	-	-	0.006	0.019	0.040	-
FeO	6.11	7.61	7.51	8.22	7.01	5.46	6.44	8.52	13.81	5.85	9.04	6.80	8.97	8.55	8.31	8.14	7.53	9.06
Fe_2O_3	1.05	0.53	-	-	-	3.46	2.57	0.87	2.77	3.40	-	2.35	-	-	0.22	0.65	1.40	-
End-member compositions																		
Wo	48.1	49.8	49.0	50.3	49.3	50.5	50.4	49.7	44.8	50.8	50.2	47.1	48.1	50.0	49.3	49.9	50.2	47.3
En	40.2	36.3	38.1	35.5	38.3	34.5	33.8	33.0	25.7	33.5	33.5	37.8	36.3	34.8	35.5	34.8	34.3	37.4
Fs	11.7	13.9	12.9	14.2	12.4	14.9	15.7	17.2	29.5	15.7	16.3	15.1	15.6	15.3	15.1	15.3	15.5	15.3

Table A26 Electron microprobe analyses of clinopyroxene in group B basanites (continued).

Sample	SAB102					SAB111									SAB128				
Analysis	408-C1	409-R1	88-C	91-C	86-G	280-C1	281-R1	298-C2	299-R2	763-C3	764-R3	767-C4	768-R4	291-C	318-C1	319-R1	321-C2	322-R2	722-C3
SiO_2	46.33	42.28	44.72	44.28	46.53	49.96	46.55	50.05	43.31	48.77	44.79	47.67	44.37	46.28	44.72	44.99	42.54	45.19	50.34
TiO_2	3.05	4.82	3.41	4.06	3.18	1.77	3.27	1.72	4.33	2.09	3.95	2.80	4.20	3.34	3.28	3.67	4.60	3.67	1.82
Al_2O_3	7.50	10.19	7.66	8.71	5.85	4.83	7.53	4.55	9.30	5.15	9.56	5.52	8.51	6.47	8.61	8.52	10.26	11.41	4.50
Cr_2O_3	-	-	-	-	-	-	-	-	-	-	-	-	-	-	-	-	-	-	-
FeO_T	7.76	8.74	8.50	8.16	8.71	6.89	7.76	6.88	8.10	6.91	8.00	7.86	8.25	8.74	7.70	7.67	8.46	7.98	7.00
MnO	-	-	-	-	-	-	-	-	0.25	-	-	-	-	-	-	-	-	-	-
MgO	12.05	10.07	11.26	10.85	12.11	14.09	11.89	13.63	10.31	13.38	10.39	12.74	10.60	11.88	11.47	10.76	10.62	9.35	13.78
CaO	22.65	22.79	23.19	22.34	22.56	22.40	23.05	22.21	22.55	22.92	22.50	23.18	22.75	22.31	22.37	22.79	22.35	19.47	23.01
Na_2O	0.52	0.45	-	0.71	-	0.39	0.47	-	0.45	-	0.64	-	0.44	-	0.53	0.46	0.53	2.66	0.39
Total	99.86	99.34	98.74	99.11	98.94	100.33	100.52	99.04	98.60	99.22	99.83	99.77	99.12	99.02	98.68	98.86	99.36	99.73	100.84
Number of ions on the basis of 6 oxygen																			
Si	1.741	1.616	1.684	1.668	1.758	1.834	1.726	1.880	1.649	1.828	1.687	1.791	1.689	1.757	1.691	1.709	1.610	1.680	1.855
Ti	0.086	0.139	0.097	0.115	0.091	0.049	0.091	0.049	0.124	0.059	0.112	0.079	0.120	0.095	0.094	0.105	0.131	0.103	0.050
Al	0.332	0.459	0.340	0.387	0.260	0.209	0.329	0.201	0.418	0.227	0.424	0.244	0.382	0.290	0.384	0.382	0.458	0.500	0.196
Cr	-	-	-	-	-	-	-	-	-	-	-	-	-	-	-	-	-	-	-
Fe^{2+}	0.244	0.279	0.268	0.257	0.275	0.211	0.241	0.216	0.258	0.217	0.252	0.247	0.263	0.278	0.244	0.244	0.268	0.248	0.215
Mn	-	-	-	-	-	-	-	-	0.008	-	-	-	-	-	-	-	-	-	-
Mg	0.674	0.574	0.632	0.610	0.682	0.771	0.657	0.763	0.586	0.748	0.583	0.713	0.602	0.672	0.646	0.609	0.599	0.518	0.757
Ca	0.912	0.933	0.936	0.902	0.913	0.881	0.916	0.893	0.920	0.921	0.908	0.933	0.928	0.908	0.907	0.928	0.907	0.776	0.909
Na	0.038	0.034	-	0.052	-	0.028	0.034	-	0.034	-	0.047	-	0.032	-	0.039	0.034	0.039	0.192	0.028
Cations	4.027	4.033	3.957	3.991	3.979	3.983	3.994	4.002	3.995	4.000	4.013	4.008	4.016	3.999	4.004	4.010	4.012	4.016	4.010
Recalculated Al and Fe ions and Fe oxides																			
Al^{IV}	0.259	0.384	0.316	0.332	0.242	0.166	0.274	0.120	0.351	0.172	0.313	0.209	0.311	0.243	0.309	0.291	0.390	0.320	0.145
Al^{VI}	0.072	0.075	0.024	0.055	0.018	0.043	0.056	0.081	0.066	0.056	0.111	0.035	0.071	0.046	0.075	0.091	0.068	0.180	0.051
Fe^{2+}	0.192	0.213	0.169	0.159	0.232	0.157	0.171	0.216	0.188	0.217	0.227	0.232	0.230	0.272	0.157	0.220	0.169	0.121	0.195
Fe^{3+}	0.052	0.066	0.098	0.098	0.042	0.054	0.069	-	0.070	-	0.025	0.015	0.033	0.006	0.086	0.024	0.099	0.126	0.021
FeO	6.10	6.68	5.38	5.05	7.37	5.13	5.52	6.88	5.90	6.91	7.21	7.37	7.22	8.54	4.98	6.93	5.34	3.91	6.32
Fe_2O_3	1.84	2.29	3.47	3.46	1.49	1.95	2.49	-	2.44	-	0.88	0.54	1.14	0.22	3.03	0.83	3.47	4.52	0.75
End-member compositions																			
Wo	49.8	52.3	51.0	51.0	48.8	47.3	50.5	47.7	51.9	48.9	52.1	49.3	51.8	48.9	50.5	52.1	51.1	50.3	48.3
En	36.9	32.1	34.4	34.5	36.5	41.4	36.2	40.8	33.1	39.7	33.5	37.7	33.6	36.2	36.0	34.2	33.8	33.6	40.2
Fs	13.3	15.6	14.6	14.6	14.7	11.3	13.3	11.5	15.0	11.5	14.5	13.1	14.7	15.0	13.6	13.7	15.1	16.1	11.4

Table A26 Electron microprobe analyses of clinopyroxene in group B basanites (continued).

Sample	SAB128 (continued)			SAB204								SA37							
Analysis	723-R3	720-C	320-G	1363-C1	1364-R1	1369-C2	1370-R2	1375-C	1361-C	1362-C	1371-G	854-C1	855-R1	858-C2	859-R2	893-C3	894-R3	852-C	853-C
SiO_2	48.05	48.01	45.08	47.26	42.57	42.40	42.51	48.14	46.99	48.78	44.12	47.33	46.52	45.07	42.56	43.48	47.14	45.28	46.15
TiO_2	2.68	2.60	3.55	1.70	4.42	4.58	4.62	2.15	2.78	2.03	4.09	2.53	3.19	3.41	4.46	3.61	2.79	3.25	2.90
Al_2O_3	6.46	5.86	8.52	6.35	9.37	9.69	9.58	4.50	5.69	4.99	8.71	6.89	6.52	8.90	9.84	8.20	5.78	7.63	6.66
Cr_2O_3	-	-	-	0.40	-	-	-	-	-	0.25	-	-	-	-	-	0.49	-	-	-
FeO_T	7.96	7.81	9.32	7.29	8.97	8.65	8.74	7.83	8.43	7.26	8.45	7.77	9.65	7.97	8.64	7.75	8.41	7.90	7.79
MnO	0.24	-	-	-	-	-	-	-	-	-	-	-	-	-	-	-	-	-	-
MgO	11.98	12.94	10.91	13.31	10.54	10.54	10.49	13.39	12.53	13.54	10.79	11.64	10.74	11.31	10.50	11.66	11.96	11.97	11.95
CaO	22.94	23.32	21.87	22.04	22.72	22.41	22.68	22.79	22.50	22.09	22.58	22.36	22.01	21.81	22.51	23.19	22.80	22.94	22.86
Na_2O	0.61	-	0.77	0.46	0.46	0.52	0.42	-	-	-	-	0.39	0.45	0.46	0.45	0.41	-	-	0.37
Total	100.92	100.54	100.02	98.81	99.05	98.79	99.04	98.80	98.92	98.94	98.74	98.91	99.08	98.93	98.96	98.79	98.88	98.97	98.68
Number of ions on the basis of 6 oxygen																			
Si	1.786	1.788	1.692	1.797	1.633	1.649	1.629	1.835	1.818	1.868	1.707	1.799	1.795	1.730	1.630	1.666	1.790	1.731	1.768
Ti	0.075	0.073	0.100	0.049	0.128	0.134	0.133	0.062	0.081	0.059	0.119	0.073	0.092	0.098	0.128	0.104	0.080	0.094	0.083
Al	0.283	0.257	0.377	0.285	0.424	0.444	0.433	0.202	0.260	0.226	0.397	0.308	0.296	0.403	0.444	0.371	0.259	0.344	0.301
Cr	-	-	-	0.012	-	-	-	-	-	0.008	-	-	-	-	-	0.015	-	-	-
Fe^{2+}	0.247	0.244	0.292	0.232	0.288	0.281	0.280	0.250	0.273	0.232	0.274	0.247	0.311	0.256	0.277	0.248	0.267	0.253	0.250
Mn	0.007	-	-	-	-	-	-	-	-	-	-	-	-	-	-	-	-	-	-
Mg	0.664	0.718	0.610	0.755	0.603	0.611	0.599	0.761	0.723	0.773	0.622	0.660	0.618	0.647	0.599	0.666	0.677	0.682	0.682
Ca	0.914	0.931	0.880	0.898	0.934	0.934	0.931	0.931	0.933	0.906	0.935	0.911	0.910	0.897	0.923	0.952	0.928	0.940	0.938
Na	0.044	-	0.056	0.034	0.034	0.039	0.031	-	-	-	-	0.028	0.034	0.034	0.034	0.031	-	-	0.027
Cations	4.019	4.010	4.007	4.061	4.045	4.092	4.037	4.040	4.088	4.072	4.054	4.026	4.057	4.064	4.036	4.053	4.000	4.043	4.050
Recalculated Al and Fe ions and Fe oxides																			
Al^{IV}	0.214	0.212	0.308	0.203	0.367	0.351	0.371	0.165	0.182	0.132	0.293	0.201	0.205	0.270	0.370	0.334	0.210	0.269	0.232
Al^{VI}	0.069	0.045	0.069	0.082	0.057	0.093	0.062	0.037	0.078	0.094	0.104	0.108	0.092	0.132	0.074	0.037	0.048	0.075	0.069
Fe^{2+}	0.208	0.222	0.198	0.186	0.200	0.251	0.206	0.246	0.273	0.232	0.274	0.247	0.311	0.256	0.204	0.144	0.265	0.245	0.227
Fe^{3+}	0.039	0.021	0.095	0.046	0.088	0.030	0.074	0.004	-	-	-	-	-	-	0.072	0.105	0.002	0.007	0.023
FeO	6.69	7.12	6.30	5.85	6.23	7.73	6.43	7.71	8.43	7.26	8.45	7.77	9.65	7.97	6.38	4.48	8.34	7.68	7.08
Fe_2O_3	1.41	0.76	3.35	1.60	3.05	1.03	2.57	0.13	-	-	-	-	-	-	2.51	3.63	0.08	0.25	0.79
End-member compositions																			
Wo	49.9	49.2	49.4	47.7	51.2	51.1	51.4	47.9	48.4	47.4	51.1	50.1	49.5	49.8	51.3	51.0	49.6	50.1	50.2
En	36.2	38.0	34.2	40.1	33.0	33.5	33.1	39.2	37.5	40.5	34.0	36.3	33.6	35.9	33.3	35.7	36.2	36.4	36.5
Fs	13.9	12.9	16.4	12.3	15.8	15.4	15.5	12.9	14.2	12.1	14.9	13.6	16.9	14.2	15.4	13.3	14.3	13.5	13.3

Table A26 Electron microprobe analyses of clinopyroxene in group B basanites (continued).

Sample	SA37 (continued)								SAB175										
Analysis	850-G	851-G	891-G	892-G	895-G	896-G	897-G	898-G	1040-C1	1041-R1	1042-C2	1043-R2	1045-C3	1047-R3	1054-C4	1055-R4	1060-C4	1061-R4	1044-C
SiO_2	48.76	44.70	47.10	39.38	45.09	44.14	45.34	45.34	49.12	44.17	49.69	42.96	47.30	42.97	47.17	48.01	47.58	45.60	44.26
TiO_2	1.86	3.41	2.54	6.51	3.28	3.92	3.57	3.40	1.73	3.94	1.56	4.15	2.39	3.95	2.09	2.23	2.52	3.21	3.85
Al_2O_3	4.55	8.79	6.07	11.81	7.99	9.00	6.41	7.65	4.56	9.05	4.69	9.60	5.37	9.38	7.24	5.05	6.10	7.78	8.91
Cr_2O_3	0.37	-	-	-	-	-	-	-	0.47	-	0.23	0.23	-	0.36	1.08	-	-	-	-
FeO_T	6.91	9.15	8.24	10.05	8.23	8.13	11.07	8.58	6.58	8.57	7.33	8.25	7.82	8.05	6.23	8.29	8.18	8.16	8.33
MnO	-	-	0.22	-	-	-	0.26	-	-	-	0.20	-	-	-	-	0.28	0.30	-	-
MgO	14.18	10.48	12.01	8.55	11.38	10.77	10.27	11.53	14.22	10.59	14.45	11.12	13.18	11.24	13.22	12.11	12.14	11.38	10.87
CaO	22.91	21.80	22.46	22.24	22.69	22.62	21.80	22.76	23.06	22.98	22.17	22.85	22.65	22.78	22.66	22.91	22.85	22.99	22.67
Na_2O	-	0.63	0.42	0.57	-	0.44	0.46	0.39	-	0.52	0.42	0.52	0.39	-	0.48	0.53	0.64	0.38	0.38
Total	99.54	98.96	99.06	99.11	98.66	99.02	99.18	99.65	99.74	99.82	100.74	99.68	99.10	98.73	100.17	99.41	100.31	99.50	99.27
Number of ions on the basis of 6 oxygen																			
Si	1.825	1.715	1.797	1.525	1.730	1.691	1.736	1.717	1.832	1.673	1.837	1.633	1.790	1.645	1.756	1.816	1.784	1.726	1.682
Ti	0.052	0.098	0.073	0.190	0.095	0.113	0.103	0.097	0.049	0.112	0.043	0.119	0.068	0.114	0.059	0.064	0.071	0.091	0.110
Al	0.201	0.398	0.273	0.539	0.361	0.406	0.289	0.341	0.200	0.404	0.204	0.430	0.239	0.423	0.317	0.226	0.269	0.347	0.399
Cr	0.011	-	-	-	-	-	-	-	0.014	-	0.007	0.007	-	0.011	0.032	-	-	-	-
Fe^{2+}	0.216	0.294	0.263	0.325	0.264	0.260	0.355	0.272	0.205	0.272	0.227	0.262	0.247	0.257	0.194	0.262	0.256	0.258	0.265
Mn	-	-	0.007	-	-	-	0.008	-	-	-	0.007	-	-	-	-	0.009	0.010	-	-
Mg	0.791	0.599	0.683	0.494	0.650	0.615	0.586	0.651	0.791	0.598	0.796	0.630	0.743	0.641	0.734	0.683	0.679	0.642	0.616
Ca	0.919	0.897	0.919	0.923	0.932	0.929	0.895	0.923	0.922	0.933	0.878	0.931	0.919	0.934	0.904	0.929	0.918	0.932	0.923
Na	-	0.047	0.031	0.043	-	0.032	0.034	0.028	-	0.038	0.030	0.038	0.028	-	0.035	0.039	0.046	0.028	0.028
Cations	4.016	4.049	4.046	4.038	4.033	4.047	4.006	4.029	4.012	4.031	4.029	4.049	4.036	4.025	4.030	4.027	4.033	4.023	4.022
Recalculated Al and Fe ions and Fe oxides																			
Al^{IV}	0.175	0.285	0.203	0.475	0.270	0.309	0.264	0.283	0.168	0.327	0.163	0.367	0.210	0.355	0.244	0.184	0.216	0.274	0.318
Al^{VI}	0.026	0.113	0.070	0.063	0.091	0.098	0.026	0.058	0.032	0.078	0.041	0.063	0.030	0.068	0.073	0.042	0.053	0.072	0.081
Fe^{2+}	0.183	0.272	0.247	0.249	0.264	0.243	0.288	0.211	0.180	0.209	0.168	0.163	0.176	0.208	0.137	0.208	0.189	0.211	0.219
Fe^{3+}	0.033	0.022	0.016	0.076	-	0.018	0.067	0.060	0.025	0.063	0.059	0.099	0.071	0.049	0.057	0.054	0.068	0.047	0.046
FeO	5.84	8.46	7.73	7.70	8.23	7.57	8.98	6.67	5.78	6.59	5.44	5.14	5.57	6.52	4.40	6.59	6.02	6.67	6.88
Fe_2O_3	1.19	0.76	0.57	2.61	-	0.62	2.32	2.12	0.89	2.20	2.10	3.45	2.50	1.70	2.03	1.89	2.40	1.66	1.61
End-member compositions																			
Wo	47.7	50.1	49.1	53.0	50.5	51.5	48.5	50.0	48.1	51.7	46.0	51.1	48.1	51.0	49.3	49.3	49.3	50.9	51.2
En	41.1	33.5	36.5	28.3	35.2	34.1	31.8	35.3	41.2	33.2	41.7	34.6	38.9	35.0	40.1	36.3	36.4	35.0	34.1
Fs	11.2	16.4	14.4	18.7	14.3	14.4	19.7	14.7	10.7	15.1	12.2	14.4	12.9	14.0	10.6	14.4	14.3	14.1	14.7

Table A26 Electron microprobe analyses of clinopyroxene in group B basanites (continued).

Sample	SAB175 (continued)					SAB176											
Analysis	1197-C[1]	1053-G	1057-G	1063-G	1194-G	306-C1	307-R1	313-C2	314-R2	652-C3	653-R3	1207-C	315-G	1208-G	1209-G	1210-G	1211-G	1213-G
SiO_2	44.60	44.73	45.57	48.86	47.50	49.27	45.69	44.74	49.95	49.43	46.99	45.64	44.84	47.59	43.83	45.78	43.95	46.77
TiO_2	3.64	3.61	3.16	1.84	2.66	1.91	3.50	3.68	1.71	1.69	3.03	3.03	3.50	2.41	4.04	2.78	3.99	3.00
Al_2O_3	8.75	8.62	7.93	4.55	6.05	4.47	8.51	8.50	4.21	4.34	7.89	7.56	8.58	5.45	9.21	6.99	8.83	7.02
Cr_2O_3	-	-	0.62	0.42	-	-	-	-	-	-	-	-	-	-	-	-	-	-
FeO_T	8.48	8.77	7.24	6.76	8.06	7.13	8.63	8.57	9.17	6.62	8.90	8.02	9.29	7.69	8.59	8.30	8.81	8.51
MnO	-	0.25	-	-	-	-	-	-	-	-	-	-	-	-	-	0.23	-	-
MgO	11.18	10.36	12.42	13.98	12.29	13.81	10.73	10.87	11.96	14.01	11.58	11.75	10.50	13.03	10.48	11.80	11.08	12.05
CaO	23.07	22.25	23.04	23.10	22.96	22.71	22.01	22.93	22.93	22.96	21.29	22.82	22.61	22.44	22.56	22.85	22.75	22.50
Na_2O	0.58	0.66	-	-	0.55	-	0.76	0.43	-	-	0.80	-	0.60	-	-	0.39	0.39	-
Total	100.30	99.25	99.98	99.51	100.07	99.30	99.83	99.72	99.93	99.05	100.48	98.82	99.92	98.61	98.71	99.12	99.80	99.85
Number of ions on the basis of 6 oxygen																		
Si	1.681	1.703	1.710	1.829	1.782	1.832	1.709	1.683	1.859	1.852	1.752	1.757	1.688	1.815	1.697	1.742	1.667	1.758
Ti	0.103	0.103	0.089	0.052	0.075	0.053	0.098	0.104	0.048	0.048	0.085	0.088	0.099	0.069	0.118	0.080	0.114	0.085
Al	0.389	0.386	0.350	0.200	0.268	0.196	0.375	0.377	0.185	0.191	0.347	0.343	0.380	0.245	0.420	0.314	0.395	0.311
Cr	-	-	0.019	0.013	-	-	-	-	-	-	-	-	-	-	-	-	-	-
Fe^{2+}	0.268	0.280	0.227	0.212	0.253	0.222	0.270	0.270	0.286	0.208	0.278	0.258	0.292	0.245	0.278	0.264	0.280	0.268
Mn	-	0.008	-	-	-	-	-	-	-	-	-	-	-	-	-	0.007	-	-
Mg	0.628	0.588	0.695	0.780	0.688	0.766	0.599	0.610	0.664	0.783	0.644	0.674	0.589	0.741	0.605	0.669	0.627	0.675
Ca	0.932	0.908	0.926	0.927	0.923	0.905	0.882	0.925	0.914	0.922	0.851	0.941	0.911	0.917	0.936	0.931	0.925	0.906
Na	0.043	0.049	-	-	0.040	-	0.055	0.031	-	-	0.058	-	0.043	-	-	0.029	0.029	-
Cations	4.043	4.025	4.016	4.013	4.029	3.973	3.989	4.000	3.956	4.004	4.014	4.061	4.003	4.031	4.053	4.036	4.036	4.002
Recalculated Al and Fe ions and Fe oxides																		
Al^{IV}	0.319	0.297	0.290	0.171	0.218	0.168	0.291	0.317	0.141	0.148	0.248	0.243	0.312	0.185	0.303	0.258	0.333	0.242
Al^{VI}	0.070	0.089	0.060	0.030	0.050	0.027	0.084	0.060	0.044	0.044	0.099	0.100	0.068	0.060	0.117	0.056	0.062	0.069
Fe^{2+}	0.183	0.229	0.193	0.187	0.195	0.188	0.205	0.191	0.286	0.199	0.241	0.258	0.203	0.245	0.278	0.192	0.208	0.264
Fe^{3+}	0.085	0.050	0.033	0.025	0.059	0.034	0.065	0.079	-	0.008	0.036	-	0.089	-	-	0.072	0.071	0.004
FeO	5.79	7.20	6.17	5.96	6.19	6.04	6.57	6.06	9.17	6.36	7.73	8.02	6.45	7.69	8.59	6.04	6.57	8.38
Fe_2O_3	2.99	1.75	1.18	0.89	2.07	1.21	2.29	2.79	-	0.29	1.30	-	3.15	-	-	2.51	2.49	0.14
End-member compositions																		
Wo	51.0	50.9	50.1	48.3	49.5	47.8	50.4	51.2	49.1	48.2	48.0	50.3	50.8	48.2	51.5	49.8	50.5	49.0
En	34.4	33.0	37.6	40.7	36.9	40.5	34.2	33.8	35.6	40.9	36.3	36.0	32.9	38.9	33.2	35.7	34.2	36.5
Fs	14.6	16.1	12.3	11.0	13.6	11.7	15.4	15.0	15.3	10.9	15.7	13.8	16.3	12.9	15.3	14.5	15.3	14.5

Table A26 Electron microprobe analyses of clinopyroxene in group B basanites (continued).

Sample	SAB177														SAB178				
Analysis	1119-C1	1120-R1	1142-C2	1143-R2	1144-C3	1145-R3	1146-C4	1147-R4	1135-C	1139-G	1141-G	1148-G	1149-G	1150-G	1174-C1	1175-R1	1176-C2	1177-R2	1178-C3
SiO_2	43.91	42.74	47.14	42.52	48.07	44.67	48.10	43.67	48.81	44.41	46.72	47.10	47.44	44.22	47.42	45.04	47.55	40.90	43.25
TiO_2	3.62	4.49	2.41	4.48	1.76	3.75	2.21	4.01	1.97	4.03	2.86	2.61	2.24	3.92	2.56	3.27	2.40	5.23	3.70
Al_2O_3	9.19	9.61	6.02	10.09	6.04	9.11	5.20	9.21	4.69	8.85	6.48	5.69	5.24	9.02	5.43	8.41	5.03	11.85	9.00
Cr_2O_3	0.41	-	-	-	0.85	-	-	-	0.25	-	-	-	-	-	-	-	-	-	0.63
FeO_T	7.74	8.50	8.74	8.81	6.11	8.26	7.72	8.66	6.77	8.68	8.52	8.29	7.68	8.92	7.99	8.58	8.05	9.30	7.76
MnO	-	-	0.23	-	-	-	-	-	-	-	-	0.23	-	-	-	-	-	0.22	-
MgO	11.06	10.52	12.11	10.20	13.48	11.03	13.37	10.82	13.70	10.26	11.79	12.69	13.44	10.80	13.12	10.93	13.39	9.09	11.36
CaO	22.51	22.64	22.88	22.58	22.81	22.93	22.82	22.84	23.17	22.37	22.55	22.35	22.96	22.58	22.45	22.98	22.79	22.42	23.01
Na_2O	0.48	0.46	0.42	0.53	0.39	0.46	-	0.51	-	0.47	-	-	-	0.63	-	0.49	-	0.50	-
Total	98.92	98.96	99.95	99.21	99.51	100.21	99.42	99.72	99.36	99.07	98.92	98.96	99.00	100.09	98.97	99.70	99.21	99.51	98.71
Number of ions on the basis of 6 oxygen																			
Si	1.683	1.636	1.778	1.626	1.797	1.681	1.808	1.658	1.829	1.713	1.785	1.798	1.795	1.672	1.805	1.706	1.798	1.567	1.655
Ti	0.104	0.129	0.068	0.129	0.050	0.106	0.062	0.115	0.056	0.117	0.082	0.075	0.064	0.112	0.073	0.093	0.068	0.151	0.107
Al	0.415	0.434	0.268	0.455	0.266	0.404	0.230	0.412	0.207	0.403	0.292	0.256	0.234	0.402	0.244	0.375	0.224	0.535	0.406
Cr	0.013	-	-	-	0.025	-	-	-	0.007	-	-	-	-	-	-	-	-	-	0.019
Fe^{2+}	0.248	0.272	0.275	0.282	0.191	0.260	0.242	0.275	0.212	0.280	0.272	0.265	0.243	0.282	0.254	0.272	0.254	0.298	0.248
Mn	-	-	0.007	-	-	-	-	-	-	-	-	0.007	-	-	-	-	-	0.007	-
Mg	0.632	0.601	0.682	0.581	0.751	0.619	0.749	0.613	0.766	0.590	0.671	0.722	0.758	0.609	0.745	0.617	0.754	0.519	0.648
Ca	0.925	0.929	0.925	0.925	0.914	0.925	0.920	0.929	0.931	0.925	0.923	0.914	0.931	0.915	0.916	0.932	0.923	0.920	0.943
Na	0.035	0.034	0.031	0.039	0.029	0.034	-	0.038	-	0.035	-	-	-	0.046	-	0.036	-	0.037	-
Cations	4.055	4.034	4.034	4.037	4.023	4.028	4.013	4.040	4.008	4.063	4.025	4.037	4.024	4.038	4.037	4.031	4.022	4.033	4.026
Recalculated Al and Fe ions and Fe oxides																			
Al^{IV}	0.317	0.364	0.222	0.374	0.203	0.319	0.192	0.342	0.171	0.287	0.215	0.202	0.205	0.328	0.195	0.294	0.202	0.433	0.345
Al^{VI}	0.098	0.070	0.046	0.081	0.063	0.084	0.039	0.071	0.036	0.116	0.077	0.054	0.029	0.074	0.049	0.081	0.022	0.101	0.060
Fe^{2+}	0.216	0.202	0.206	0.208	0.147	0.204	0.214	0.195	0.197	0.280	0.272	0.265	0.195	0.205	0.254	0.208	0.211	0.229	0.196
Fe^{3+}	0.033	0.070	0.069	0.074	0.044	0.056	0.028	0.080	0.015	-	-	-	0.048	0.077	-	0.063	0.044	0.068	0.052
FeO	6.72	6.31	6.54	6.49	4.70	6.47	6.83	6.15	6.28	8.68	8.52	8.29	6.15	6.50	7.99	6.58	6.67	7.17	6.14
Fe_2O_3	1.14	2.43	2.45	2.58	1.57	1.99	0.99	2.79	0.55	-	-	-	1.70	2.69	-	2.22	1.53	2.37	1.81
End-member compositions																			
Wo	51.2	51.6	49.0	51.7	49.2	51.3	48.1	51.2	48.8	51.5	49.5	47.9	48.2	50.7	47.8	51.2	47.8	52.8	51.3
En	35.0	33.3	36.1	32.5	40.5	34.3	39.2	33.7	40.1	32.9	36.0	37.8	39.2	33.7	38.9	33.9	39.0	29.8	35.2
Fs	13.8	15.1	15.0	15.8	10.3	14.4	12.7	15.1	11.1	15.6	14.6	14.2	12.6	15.6	13.3	14.9	13.2	17.5	13.5

Table A26 Electron microprobe analyses of clinopyroxene in group B basanites (continued).

Sample	SAB178 (continued)								SAB179							
Analysis	1179-R3	1163-G	1164-G	1166-G	1168-G	1169-G	1172-G	1193-G	214-C1	215-R1	222-C2	223-R2	593-C3	594-R3	228-G	1231-G
SiO_2	42.95	45.98	46.93	46.10	42.61	46.33	46.92	47.11	49.13	46.38	50.76	46.08	50.38	47.87	49.92	47.33
TiO_2	4.08	2.96	2.62	2.73	4.27	2.93	2.61	2.37	1.57	3.02	1.21	3.07	1.22	1.99	1.97	2.71
Al_2O_3	9.70	6.33	6.46	6.99	9.69	7.07	5.44	6.13	6.20	6.51	4.71	7.54	4.64	6.88	3.65	5.14
Cr_2O_3	-	-	-	-	-	-	-	-	-	-	-	-	-	-	-	-
FeO_T	8.57	8.74	8.31	8.78	8.95	9.47	8.11	8.30	6.09	7.84	6.09	8.11	5.96	6.46	8.45	8.43
MnO	-	-	0.22	-	-	0.30	-	-	-	-	-	-	-	-	-	-
MgO	10.34	11.99	12.13	11.23	10.33	11.11	12.82	12.26	13.29	12.09	14.27	11.40	14.52	13.13	12.52	12.59
CaO	22.82	22.41	22.96	22.45	22.68	22.41	22.77	22.69	22.13	22.60	21.90	22.56	22.07	22.40	22.52	22.66
Na_2O	0.46	0.38	0.41	0.59	0.45	0.39	0.39	0.59	0.64	0.41	-	-	-	-	-	-
Total	98.92	98.79	100.04	98.87	98.98	100.01	99.06	99.45	99.05	98.85	98.94	98.76	98.79	98.73	99.03	98.86
Number of ions on the basis of 6 oxygen																
Si	1.645	1.766	1.766	1.758	1.635	1.751	1.781	1.781	1.843	1.749	1.895	1.748	1.877	1.796	1.880	1.798
Ti	0.118	0.085	0.074	0.078	0.123	0.083	0.074	0.067	0.044	0.086	0.034	0.088	0.034	0.056	0.056	0.077
Al	0.438	0.287	0.287	0.314	0.438	0.315	0.244	0.273	0.274	0.289	0.207	0.337	0.203	0.304	0.162	0.230
Cr	-	-	-	-	-	-	-	-	-	-	-	-	-	-	-	-
Fe^{2+}	0.275	0.281	0.262	0.280	0.287	0.299	0.257	0.262	0.191	0.247	0.190	0.257	0.185	0.203	0.266	0.268
Mn	-	-	0.007	-	-	0.010	-	-	-	-	-	-	-	-	-	-
Mg	0.590	0.686	0.680	0.638	0.590	0.626	0.725	0.691	0.743	0.680	0.794	0.645	0.806	0.734	0.703	0.713
Ca	0.937	0.923	0.926	0.917	0.932	0.908	0.926	0.919	0.889	0.913	0.877	0.917	0.881	0.901	0.909	0.923
Na	0.034	0.029	0.030	0.043	0.034	0.028	0.029	0.043	0.046	0.030	-	-	-	-	-	-
Cations	4.036	4.057	4.031	4.028	4.040	4.021	4.037	4.036	4.031	3.994	3.997	3.993	3.987	3.995	3.976	4.010
Recalculated Al and Fe ions and Fe oxides																
Al^{IV}	0.355	0.234	0.234	0.242	0.365	0.249	0.219	0.219	0.157	0.251	0.105	0.252	0.123	0.204	0.120	0.202
Al^{VI}	0.083	0.053	0.053	0.072	0.073	0.066	0.025	0.054	0.117	0.038	0.102	0.085	0.080	0.101	0.042	0.029
Fe^{2+}	0.203	0.242	0.198	0.223	0.208	0.256	0.184	0.188	0.191	0.176	0.190	0.257	0.185	0.203	0.266	0.250
Fe^{3+}	0.072	0.039	0.064	0.057	0.080	0.044	0.074	0.074	-	0.071	-	-	-	-	-	0.018
FeO	6.33	7.53	6.28	6.98	6.47	8.09	5.79	5.95	6.09	5.58	6.09	8.11	5.96	6.46	8.45	7.85
Fe_2O_3	2.49	1.34	2.26	2.00	2.75	1.53	2.58	2.61	-	2.51	-	-	-	-	-	0.64
End-member compositions																
Wo	52.0	48.8	49.4	50.0	51.5	49.3	48.5	49.1	48.8	49.6	47.1	50.4	47.0	49.0	48.4	48.5
En	32.8	36.3	36.3	34.7	32.6	34.0	38.0	36.9	40.8	36.9	42.7	35.4	43.1	40.0	37.4	37.5
Fs	15.3	14.9	14.3	15.3	15.9	16.8	13.5	14.0	10.5	13.4	10.2	14.1	9.9	11.0	14.2	14.1

Table A26 Electron microprobe analyses of clinopyroxene in group B basanites (continued).

Sample	SAB179 (continued)					SAB180												
Analysis	1233-G	1234-G	1235-G	1240-G	1241-G	1279-C1	1280-R1	1281-C	1282-C2	1283-R2	1309-C3	1310-R3	1284-G	1285-G	1292-G	1293-G	1295-G	1305-G	1306-G
SiO_2	44.20	45.12	45.54	43.21	46.14	48.08	45.53	49.35	47.36	47.88	46.60	48.29	42.25	42.71	48.86	44.54	49.34	45.70	46.49
TiO_2	4.07	3.79	3.78	4.10	3.49	1.79	3.11	1.35	1.92	2.25	2.20	1.87	4.39	4.17	2.33	3.75	2.00	3.66	2.97
Al_2O_3	8.54	7.65	7.54	8.92	6.93	7.28	7.22	5.51	8.74	4.69	7.08	4.08	9.80	10.23	4.20	7.85	3.88	7.10	5.81
Cr_2O_3	-	-	-	-	-	1.00	-	0.70	0.32	-	0.45	-	-	-	-	-	-	-	-
FeO_T	8.52	7.98	8.50	8.94	8.21	6.17	8.05	6.32	6.84	8.33	6.86	9.07	8.70	9.34	9.12	8.46	9.99	9.09	7.96
MnO	0.27	-	-	-	0.28	-	-	-	-	-	-	0.23	-	0.22	0.32	-	0.23	-	0.21
MgO	10.87	11.64	11.81	11.11	11.98	13.07	11.64	13.95	12.39	12.50	12.62	12.07	10.75	9.77	11.70	11.26	11.24	10.67	12.29
CaO	22.79	22.79	22.75	22.54	22.77	21.67	22.74	21.22	20.75	22.56	22.25	22.58	22.49	22.06	22.02	22.26	22.22	22.27	22.68
Na_2O	0.36	0.36	0.54	0.47	0.45	-	0.52	0.48	0.68	0.44	0.54	0.44	0.67	0.56	0.37	0.57	-	0.46	0.52
Total	99.62	99.33	100.46	99.29	100.25	99.06	98.81	98.88	99.00	98.65	98.60	98.63	99.05	99.06	98.92	98.69	98.90	98.95	98.93
Number of ions on the basis of 6 oxygen																			
Si	1.679	1.711	1.711	1.651	1.735	1.828	1.746	1.879	1.792	1.822	1.787	1.845	1.630	1.658	1.892	1.712	1.914	1.766	1.769
Ti	0.116	0.108	0.107	0.118	0.099	0.051	0.090	0.038	0.055	0.064	0.064	0.054	0.127	0.122	0.068	0.109	0.058	0.106	0.085
Al	0.382	0.342	0.334	0.402	0.307	0.326	0.326	0.247	0.390	0.211	0.320	0.184	0.446	0.468	0.192	0.356	0.178	0.323	0.260
Cr	-	-	-	-	-	0.030	-	0.021	0.010	-	0.014	-	-	-	-	-	-	-	-
Fe^{2+}	0.271	0.253	0.267	0.286	0.258	0.196	0.258	0.201	0.217	0.265	0.220	0.290	0.281	0.304	0.296	0.272	0.324	0.294	0.253
Mn	0.009	-	-	-	0.009	-	-	-	-	-	-	0.007	-	0.007	0.010	-	0.008	-	0.007
Mg	0.616	0.658	0.662	0.633	0.671	0.741	0.665	0.792	0.699	0.709	0.721	0.688	0.619	0.566	0.676	0.646	0.650	0.614	0.697
Ca	0.928	0.926	0.916	0.923	0.917	0.883	0.935	0.866	0.842	0.920	0.914	0.925	0.930	0.918	0.914	0.917	0.924	0.922	0.925
Na	0.027	0.027	0.040	0.034	0.033	-	0.038	0.035	0.050	0.032	0.040	0.033	0.050	0.043	0.028	0.042	-	0.034	0.038
Cations	4.027	4.024	4.035	4.047	4.030	4.056	4.059	4.080	4.054	4.024	4.080	4.025	4.082	4.085	4.074	4.053	4.055	4.060	4.034
Recalculated Al and Fe ions and Fe oxides																			
Al^{IV}	0.321	0.289	0.289	0.349	0.265	0.172	0.254	0.121	0.208	0.178	0.213	0.155	0.370	0.342	0.108	0.288	0.086	0.234	0.231
Al^{VI}	0.061	0.053	0.044	0.053	0.042	0.155	0.072	0.127	0.182	0.033	0.107	0.029	0.076	0.126	0.084	0.068	0.092	0.089	0.029
Fe^{2+}	0.216	0.205	0.196	0.191	0.199	0.196	0.218	0.201	0.217	0.216	0.214	0.238	0.192	0.289	0.296	0.227	0.324	0.294	0.183
Fe^{3+}	0.054	0.048	0.071	0.095	0.059	-	0.040	-	-	0.049	0.006	0.051	0.089	0.015	-	0.045	-	-	0.070
FeO	6.81	6.47	6.23	5.98	6.35	6.17	6.80	6.32	6.84	6.79	6.68	7.46	5.94	8.89	9.12	7.07	9.99	9.09	5.76
Fe_2O_3	1.90	1.67	2.52	3.29	2.07	-	1.39	-	-	1.71	0.20	1.79	3.06	0.50	-	1.54	-	-	2.45
End-member compositions																			
Wo	50.9	50.4	49.6	50.1	49.4	48.5	50.3	46.6	47.9	48.6	49.3	48.4	50.8	51.2	48.2	50.0	48.5	50.4	49.1
En	33.8	35.8	35.9	34.4	36.2	40.7	35.8	42.6	39.8	37.4	38.9	36.0	33.8	31.5	35.6	35.2	34.1	33.6	37.1
Fs	15.3	13.8	14.5	15.5	14.4	10.8	13.9	10.8	12.3	14.0	11.9	15.6	15.3	17.3	16.1	14.8	17.4	16.1	13.8

A6.27 Microprobe analyses of clinopyroxene in group B lavas: nephelinites

Table A6.27 Electron microprobe analyses of clinopyroxene in group B nephelinites.

Sample							SA21							
Analysis	1382-C1	1383-R1	1387-C2	1388-R2	1397-C3	1398-R3	1402-C4	1403-R4	1393-G	1394-G	1396-G	1405-G	1406-G	1407-G
SiO_2	48.20	40.93	42.73	43.69	45.13	41.99	40.74	42.78	47.70	42.97	45.00	43.23	46.56	43.32
TiO_2	2.10	5.32	5.11	3.37	3.23	2.83	5.19	4.53	2.57	3.88	3.21	4.35	2.72	4.41
Al_2O_3	4.44	9.88	9.41	8.57	7.65	6.43	10.38	9.50	5.07	8.48	7.40	8.66	6.06	8.85
Cr_2O_3	0.25	0.22	-	-	0.41	-	-	-	-	-	-	-	-	-
FeO_T	6.91	8.47	8.50	8.25	7.32	6.98	8.69	8.17	7.48	9.03	8.23	8.25	7.83	8.48
MnO	-	-	-	-	-	-	-	-	-	-	-	-	-	-
MgO	13.62	10.23	10.45	10.84	11.81	10.62	10.32	10.78	12.55	10.43	11.14	10.86	12.05	10.64
CaO	22.76	22.92	22.65	22.60	22.55	25.31	22.49	22.74	22.67	22.27	22.38	22.62	22.51	22.16
Na_2O	0.77	0.92	0.85	0.95	0.81	0.79	0.84	1.03	0.84	1.05	1.01	0.84	0.96	0.94
Total	99.05	98.89	99.70	98.27	98.91	94.95	98.65	99.53	98.88	98.11	98.37	98.81	98.69	98.80
Number of ions on the basis of 6 oxygen														
Si	1.820	1.576	1.659	1.684	1.738	1.607	1.571	1.575	1.843	1.665	1.729	1.669	1.785	1.676
Ti	0.059	0.154	0.149	0.098	0.094	0.082	0.151	0.151	0.074	0.113	0.092	0.126	0.079	0.128
Al	0.197	0.448	0.431	0.389	0.347	0.290	0.472	0.473	0.231	0.387	0.335	0.394	0.274	0.403
Cr	0.008	0.007	-	-	0.013	-	-	-	-	-	-	-	-	-
Fe^{2+}	0.218	0.273	0.276	0.266	0.236	0.223	0.280	0.281	0.242	0.293	0.265	0.266	0.251	0.274
Mn	-	-	-	-	-	-	0.014	-	-	-	-	-	-	-
Mg	0.767	0.587	0.605	0.623	0.678	0.606	0.593	0.595	0.723	0.602	0.638	0.625	0.689	0.614
Ca	0.920	0.945	0.942	0.934	0.931	1.038	0.956	0.932	0.938	0.924	0.921	0.935	0.925	0.919
Na	0.056	0.069	0.064	0.071	0.061	0.058	0.063	0.063	0.063	0.079	0.076	0.063	0.071	0.071
Cations	4.046	4.058	4.126	4.064	4.096	3.904	4.100	4.069	4.115	4.062	4.057	4.079	4.074	4.085
Recalculated Al and Fe ions and Fe oxides														
Al^{IV}	0.180	0.424	0.341	0.316	0.262	0.290	0.429	0.425	0.157	0.335	0.271	0.331	0.215	0.324
Al^{VI}	0.017	0.024	0.090	0.074	0.085	-	0.043	0.048	0.074	0.052	0.065	0.063	0.059	0.079
Fe^{2+}	0.126	0.117	0.260	0.149	0.198	0.038	0.132	0.142	0.242	0.155	0.168	0.187	0.181	0.216
Fe^{3+}	0.093	0.156	0.016	0.117	0.038	0.185	0.148	0.138	-	0.137	0.097	0.079	0.071	0.059
FeO	3.97	3.64	8.01	4.61	6.14	1.19	4.10	4.14	7.48	4.79	5.21	5.79	5.63	6.67
Fe_2O_3	3.26	5.37	0.54	4.04	1.31	6.44	5.10	4.47	-	4.71	3.35	2.73	2.45	2.01
End-member compositions														
Wo	48.3	52.4	51.7	51.2	50.5	55.6	51.9	51.6	49.3	50.8	50.5	51.2	49.6	50.8
En	40.2	32.5	33.2	34.2	36.8	32.5	32.2	32.9	38.0	33.1	35.0	34.2	36.9	34.0
Fs	11.5	15.1	15.1	14.6	12.8	12.0	16.0	15.5	12.7	16.1	14.5	14.6	13.5	15.2

Table A6.27 Electron microprobe analyses of clinopyroxene in group B nephelinites (continued).

Sample	SA28												SA51							
Analysis	1438-C1	1439-R1	1440-C2	1441-R2	1444-C3	1445-R3	1419-C	1423-G	1424-G	1425-G	1426-G	1417-G	1457-C	1477-C	1462-G	1463-G	1467-G	1468-G	1472-G	1474-G
SiO_2	49.42	45.17	46.74	46.86	46.90	47.23	49.28	46.67	48.59	51.42	48.27	47.35	42.45	43.66	44.46	43.62	40.95	42.35	45.97	48.68
TiO_2	1.63	3.17	2.96	2.63	2.30	2.68	1.61	2.60	1.83	0.74	1.99	2.21	4.96	3.85	3.52	4.04	3.36	4.71	3.06	1.50
Al_2O_3	3.29	6.21	5.88	5.43	5.61	5.49	3.14	6.30	3.39	3.30	3.87	4.99	8.47	8.19	7.32	7.60	6.37	8.94	5.53	5.01
Cr_2O_3	-	-	-	-	-	-	-	-	-	-	-	-	-	-	-	-	-	-	-	-
FeO_T	8.18	8.52	8.45	8.47	8.20	8.56	8.08	9.18	8.25	8.21	8.57	9.26	9.12	8.76	8.83	8.93	14.89	9.11	8.60	10.51
MnO	-	-	-	-	-	-	-	0.21	-	0.22	-	0.23	-	-	-	-	0.22	-	-	0.26
MgO	13.48	11.48	12.12	11.90	12.46	12.30	13.35	11.56	13.15	12.09	12.72	11.86	10.32	10.97	10.88	11.25	14.87	10.44	12.22	10.07
CaO	22.98	23.29	22.89	22.76	22.53	22.92	22.77	22.79	22.73	20.88	23.03	23.01	22.74	22.28	22.79	22.85	17.23	22.53	22.80	21.09
Na_2O	0.97	1.06	1.11	0.98	1.13	1.17	0.89	1.14	0.87	1.57	0.92	1.10	0.93	1.05	0.90	0.96	0.83	0.96	0.81	0.94
Total	99.95	98.90	100.15	99.03	99.13	100.35	99.12	100.45	98.81	98.43	99.37	100.01	98.99	98.76	98.70	99.25	98.72	99.04	98.99	98.06
Number of ions on the basis of 6 oxygen																				
Si	1.858	1.713	1.763	1.786	1.783	1.778	1.866	1.761	1.849	1.938	1.826	1.778	1.647	1.678	1.714	1.673	1.619	1.641	1.769	1.890
Ti	0.046	0.091	0.084	0.076	0.066	0.076	0.046	0.074	0.052	0.021	0.056	0.062	0.145	0.112	0.102	0.116	0.100	0.137	0.088	0.044
Al	0.146	0.277	0.262	0.244	0.251	0.244	0.140	0.280	0.152	0.146	0.172	0.221	0.388	0.371	0.333	0.344	0.296	0.408	0.251	0.229
Cr	-	-	-	-	-	-	-	-	-	-	-	-	-	-	-	-	-	-	-	-
Fe^{2+}	0.257	0.271	0.266	0.270	0.261	0.269	0.256	0.290	0.263	0.259	0.271	0.291	0.296	0.281	0.285	0.287	0.493	0.295	0.277	0.341
Mn	-	-	-	-	-	-	-	0.007	-	0.007	-	0.007	-	-	-	-	0.007	-	-	0.008
Mg	0.755	0.649	0.682	0.676	0.706	0.690	0.754	0.650	0.746	0.679	0.718	0.664	0.597	0.628	0.625	0.643	0.876	0.603	0.701	0.583
Ca	0.926	0.946	0.925	0.929	0.917	0.925	0.924	0.922	0.927	0.844	0.934	0.926	0.946	0.917	0.941	0.939	0.730	0.935	0.940	0.877
Na	0.071	0.078	0.081	0.073	0.083	0.085	0.065	0.083	0.065	0.115	0.068	0.080	0.070	0.079	0.067	0.071	0.064	0.072	0.060	0.071
Cations	4.059	4.025	4.063	4.053	4.067	4.066	4.051	4.067	4.054	4.009	4.045	4.030	4.088	4.066	4.068	4.074	4.184	4.092	4.085	4.043
Recalculated Al and Fe ions and Fe oxides																				
Al^{IV}	0.142	0.277	0.237	0.214	0.217	0.222	0.134	0.239	0.151	0.062	0.172	0.221	0.353	0.322	0.286	0.327	0.296	0.359	0.231	0.110
Al^{VI}	0.003	-	0.025	0.030	0.034	0.021	0.006	0.041	0.002	0.084	-	-	0.035	0.048	0.047	0.017	-	0.049	0.020	0.119
Fe^{2+}	0.140	0.097	0.142	0.164	0.127	0.135	0.154	0.156	0.153	0.208	0.144	0.114	0.197	0.152	0.183	0.139	0.334	0.188	0.181	0.341
Fe^{3+}	0.117	0.174	0.125	0.106	0.134	0.135	0.101	0.134	0.110	0.051	0.127	0.177	0.099	0.129	0.102	0.148	0.159	0.107	0.095	-
FeO	4.45	3.05	4.50	5.14	3.98	4.28	4.88	4.95	4.81	6.60	4.56	3.63	6.07	4.73	5.68	4.32	10.09	5.81	5.64	10.51
Fe_2O_3	4.15	6.07	4.39	3.70	4.69	4.76	3.56	4.70	3.82	1.79	4.45	6.25	3.39	4.48	3.50	5.12	5.33	3.66	3.29	-
End-member compositions																				
Wo	47.8	50.7	49.4	49.6	48.7	49.1	47.8	49.3	47.9	47.2	48.6	49.1	51.4	50.2	50.8	50.2	34.7	51.0	49.0	48.5
En	39.0	34.8	36.4	36.0	37.5	36.6	39.0	34.8	38.5	38.0	37.3	35.1	32.5	34.4	33.8	34.4	41.6	32.9	36.6	32.2
Fs	13.3	14.5	14.2	14.4	13.8	14.3	13.2	15.9	13.6	14.9	14.1	15.8	16.1	15.4	15.4	15.3	23.7	16.1	14.4	19.3

Table A6.27 Electron microprobe analyses of clinopyroxene in group B nephelinites (continued).

Sample	SAB113									SAB135							
Analysis	229-C1	230-R1	236-C2	237-R2	239-C3	240-R3	754-C4	753-R4	234-G	3-C1	4-R1	5-C2	6-R2	756-C3	757-R3	758-R3	11-G
SiO_2	47.59	46.94	45.73	44.83	49.35	45.41	47.51	40.31	47.38	47.87	44.08	42.27	42.79	46.69	43.44	44.85	42.42
TiO_2	2.59	3.11	3.08	3.39	1.61	3.37	2.88	6.50	2.80	2.41	4.09	4.80	4.73	3.24	3.92	3.96	4.83
Al_2O_3	5.67	6.17	8.29	8.37	4.60	7.55	5.74	11.55	6.23	5.04	8.96	9.78	10.09	6.41	14.04	8.06	10.03
Cr_2O_3	-	-	-	-	-	-	-	-	-	-	-	-	-	-	-	-	-
FeO_T	7.74	8.00	7.66	7.53	6.78	7.80	7.97	9.59	8.00	7.37	8.18	8.42	9.41	8.12	8.44	8.58	8.62
MnO	-	-	-	-	0.23	-	-	0.22	-	-	-	-	-	-	-	-	-
MgO	12.46	11.82	11.75	11.64	13.70	11.31	12.69	8.17	11.75	13.05	10.56	10.39	9.27	11.96	6.71	10.93	9.78
CaO	22.67	22.31	22.35	22.75	22.69	22.69	23.11	21.58	22.47	22.86	22.91	23.01	22.35	23.13	18.51	23.09	22.68
Na_2O	-	0.43	0.49	0.49	-	0.50	0.46	0.92	0.40	0.36	0.59	0.36	0.69	-	3.71	0.50	0.69
Total	98.72	98.78	99.35	99.00	98.96	98.63	100.36	98.84	99.03	98.96	99.37	99.03	99.33	99.55	98.77	99.97	99.05
Number of ions on the basis of 6 oxygen																	
Si	1.789	1.780	1.713	1.690	1.838	1.720	1.778	1.558	1.791	1.796	1.664	1.609	1.627	1.762	1.634	1.697	1.615
Ti	0.073	0.089	0.087	0.096	0.045	0.096	0.081	0.189	0.080	0.068	0.116	0.137	0.135	0.092	0.111	0.113	0.138
Al	0.251	0.276	0.366	0.372	0.202	0.337	0.253	0.526	0.278	0.223	0.399	0.439	0.452	0.285	0.622	0.359	0.450
Cr	-	-	-	-	-	-	-	-	-	-	-	-	-	-	-	-	-
Fe^{2+}	0.244	0.254	0.240	0.238	0.211	0.247	0.250	0.310	0.253	0.231	0.259	0.268	0.299	0.256	0.265	0.271	0.274
Mn	-	-	-	-	0.007	-	-	0.007	-	-	-	-	-	-	-	-	-
Mg	0.698	0.668	0.656	0.654	0.761	0.638	0.708	0.471	0.662	0.730	0.594	0.590	0.526	0.673	0.376	0.616	0.555
Ca	0.913	0.907	0.897	0.919	0.906	0.920	0.927	0.893	0.910	0.920	0.927	0.938	0.910	0.935	0.746	0.936	0.925
Na	-	0.031	0.035	0.036	-	0.037	0.034	0.070	0.029	0.026	0.043	0.027	0.051	-	0.271	0.037	0.051
Cations	3.969	4.005	3.994	4.005	3.971	3.994	4.031	4.025	4.002	3.994	4.003	4.009	3.999	4.003	4.025	4.029	4.009
Recalculated Al and Fe ions and Fe oxides																	
Al^{IV}	0.211	0.220	0.287	0.310	0.162	0.280	0.222	0.442	0.209	0.204	0.336	0.391	0.373	0.238	0.366	0.303	0.385
Al^{VI}	0.041	0.056	0.079	0.062	0.041	0.056	0.032	0.084	0.068	0.019	0.063	0.048	0.078	0.047	0.256	0.056	0.065
Fe^{2+}	0.220	0.236	0.171	0.146	0.180	0.178	0.188	0.261	0.242	0.156	0.176	0.174	0.223	0.249	0.106	0.213	0.180
Fe^{3+}	0.024	0.018	0.069	0.092	0.031	0.069	0.062	0.049	0.011	0.075	0.083	0.095	0.076	0.007	0.159	0.058	0.095
FeO	6.98	7.44	5.44	4.63	5.78	5.62	6.00	8.08	7.66	4.98	5.57	5.45	7.02	7.90	3.39	6.75	5.65
Fe_2O_3	0.84	0.62	2.46	3.23	1.11	2.42	2.19	1.68	0.37	2.65	2.90	3.30	2.66	0.25	5.62	2.04	3.30
End-member compositions																	
Wo	49.2	49.6	50.0	50.8	48.1	51.0	49.2	53.1	49.9	48.9	52.1	52.2	52.5	50.2	53.8	51.3	52.7
En	37.6	36.5	36.6	36.1	40.4	35.3	37.6	28.0	36.3	38.8	33.4	32.8	30.3	36.1	27.1	33.8	31.6
Fs	13.1	13.9	13.4	13.1	11.6	13.7	13.2	18.9	13.8	12.3	14.5	14.9	17.2	13.7	19.1	14.9	15.6

A6.28 Microprobe analyses of clinopyroxene in group B lavas: ne-hawaiites

Table A6.28 Electron microprobe analyses of clinopyroxene in group B ne-hawaiites.

Sample	SA02												SA29							
Analysis	1479-C1	1480-R1	1481-C2	1482-R2	1483-C3	1484-R3	1485-C4	1487-R4	1491-G	1495-G	1496-G	1499-G	160-C1	161-R1	162-C2	163-R2	453-C3	454-R3	156-G	167-G
SiO_2	48.49	44.93	48.55	47.92	48.51	48.29	48.59	45.31	49.35	48.73	51.05	47.21	47.02	46.92	48.69	45.94	50.45	47.46	47.15	47.78
TiO_2	1.54	3.35	1.77	1.96	1.79	1.94	1.52	3.12	2.08	2.11	1.62	2.83	2.92	2.85	1.84	3.46	1.41	2.72	2.75	2.35
Al_2O_3	7.09	7.88	4.92	6.34	4.06	4.19	5.35	7.88	6.51	4.73	16.08	4.04	6.06	6.17	3.91	6.66	3.02	6.70	5.93	6.22
Cr_2O_3	0.49	-	-	-	-	-	0.33	-	-	-	0.29	-	-	-	-	-	-	-	-	-
FeO_T	7.36	8.66	7.93	7.93	8.05	8.33	7.55	8.31	7.55	8.03	5.77	10.56	9.21	9.51	9.07	9.46	8.41	9.28	8.98	9.72
MnO	-	-	-	-	-	-	-	-	-	-	-	0.24	0.22	-	-	-	0.22	-	-	-
MgO	12.96	11.66	13.30	11.97	13.38	13.39	13.39	11.44	11.28	12.64	5.96	12.31	11.43	11.24	12.58	11.02	13.27	10.70	11.49	11.13
CaO	20.26	22.27	22.42	21.13	22.35	22.14	21.56	22.09	19.77	21.90	13.26	21.07	22.61	22.57	22.62	22.53	22.31	21.15	22.56	21.66
Na_2O	1.53	1.02	0.93	1.38	0.63	0.86	1.11	0.89	1.51	0.87	2.87	0.91	0.42	0.59	-	0.42	-	0.45	0.39	1.03
Total	99.73	99.76	99.82	98.63	98.76	99.13	99.41	99.02	98.05	99.00	96.91	99.18	99.89	99.85	98.71	99.49	99.09	98.46	99.25	99.89
Number of ions on the basis of 6 oxygen																				
Si	1.820	1.718	1.838	1.824	1.856	1.845	1.840	1.760	1.887	1.880	1.907	1.847	1.765	1.764	1.825	1.735	1.901	1.815	1.777	1.789
Ti	0.044	0.096	0.051	0.056	0.051	0.056	0.044	0.091	0.060	0.061	0.045	0.084	0.082	0.080	0.052	0.098	0.040	0.078	0.078	0.066
Al	0.314	0.355	0.220	0.284	0.183	0.188	0.238	0.361	0.293	0.215	0.708	0.186	0.268	0.274	0.173	0.296	0.134	0.302	0.263	0.275
Cr	0.015	-	-	-	-	-	0.010	-	-	-	0.008	-	-	-	-	-	-	-	-	-
Fe^{2+}	0.231	0.277	0.251	0.252	0.258	0.266	0.239	0.270	0.241	0.259	0.180	0.346	0.289	0.299	0.284	0.299	0.265	0.297	0.283	0.304
Mn	-	-	-	-	-	-	-	-	-	-	-	0.008	0.007	-	-	-	0.007	-	-	-
Mg	0.726	0.664	0.751	0.679	0.764	0.763	0.756	0.663	0.643	0.727	0.332	0.718	0.640	0.630	0.703	0.620	0.745	0.610	0.646	0.621
Ca	0.815	0.912	0.909	0.862	0.916	0.906	0.875	0.919	0.810	0.905	0.531	0.883	0.910	0.909	0.908	0.912	0.901	0.866	0.911	0.869
Na	0.111	0.076	0.068	0.102	0.047	0.064	0.082	0.067	0.112	0.065	0.209	0.069	0.031	0.043	-	0.031	-	0.034	0.028	0.074
Cations	4.075	4.098	4.087	4.059	4.075	4.088	4.084	4.130	4.046	4.111	3.921	4.141	3.992	3.998	3.943	3.992	3.993	4.002	3.986	3.998
Recalculated Al and Fe ions and Fe oxides																				
Al^{IV}	0.180	0.282	0.162	0.176	0.144	0.155	0.160	0.240	0.113	0.120	0.093	0.153	0.235	0.236	0.173	0.265	0.099	0.185	0.223	0.211
Al^{VI}	0.134	0.072	0.057	0.108	0.040	0.033	0.079	0.121	0.180	0.095	0.615	0.034	0.033	0.038	-	0.032	0.035	0.117	0.040	0.063
Fe^{2+}	0.176	0.184	0.180	0.195	0.210	0.192	0.173	0.265	0.241	0.259	0.180	0.324	0.222	0.219	0.214	0.231	0.265	0.297	0.228	0.214
Fe^{3+}	0.055	0.093	0.071	0.057	0.047	0.074	0.066	0.005	-	-	-	0.021	0.068	0.080	0.070	0.068	-	-	0.056	0.090
FeO	5.60	5.76	5.68	6.13	6.57	6.01	5.48	8.17	7.55	8.03	5.77	9.91	7.06	6.96	6.83	7.32	8.41	9.28	7.22	6.83
Fe_2O_3	1.96	3.23	2.49	2.00	1.65	2.58	2.31	0.16	-	-	-	0.72	2.39	2.84	2.49	2.38	-	-	1.96	3.21
End-member compositions																				
Wo	46.0	49.2	47.6	48.1	47.3	46.8	46.8	49.6	47.8	47.9	50.9	45.2	49.3	49.5	47.9	49.8	47.0	48.9	49.5	48.4
En	40.9	35.8	39.3	37.9	39.4	39.4	40.4	35.8	37.9	38.4	31.8	36.7	34.7	34.3	37.1	33.9	38.8	34.4	35.1	34.6
Fs	13.0	15.0	13.1	14.1	13.3	13.8	12.8	14.6	14.3	13.7	17.3	18.1	16.1	16.3	15.0	16.3	14.2	16.8	15.4	17.0

Table A6.28 Electron microprobe analyses of clinopyroxene in group B ne-hawaiites (continued).

Sample	SA25												
Analysis	1507-C1	1508-R1	1510-C2[1]	1512-R2	1513-C3	1514-R3	1515-C4	1516-R4	1519-G	1520-G	1521-G	1532-G	1535-G
SiO_2	50.38	49.86	50.50	47.37	50.52	47.89	47.31	47.64	49.65	49.04	49.93	49.86	50.05
TiO_2	1.19	1.36	1.45	2.58	1.34	2.00	2.30	2.28	1.55	1.59	1.35	1.33	1.04
Al_2O_3	2.86	2.94	2.80	5.57	2.84	5.50	6.08	5.48	2.82	3.38	3.10	3.00	2.23
Cr_2O_3	-	-	-	-	-	-	0.30	-	-	-	-	-	-
FeO_T	8.50	8.37	8.73	9.08	8.46	9.74	9.32	8.78	8.92	14.18	9.64	9.04	11.33
MnO	-	-	-	-	-	-	-	-	-	-	-	-	0.23
MgO	13.72	13.34	13.67	12.24	13.65	11.45	11.95	12.75	13.48	9.16	12.84	13.01	11.19
CaO	22.32	22.84	22.10	23.20	22.41	22.51	21.49	22.56	22.36	20.99	22.49	22.63	22.56
Na_2O	0.84	0.79	0.97	0.86	0.86	0.96	1.17	1.13	1.01	1.53	0.68	0.78	0.97
Total	99.81	99.50	100.22	100.90	100.08	100.05	99.92	100.62	99.79	99.87	100.03	99.65	99.60
Number of ions on the basis of 6 oxygen													
Si	1.891	1.874	1.889	1.777	1.891	1.810	1.786	1.775	1.872	1.886	1.880	1.882	1.912
Ti	0.034	0.038	0.041	0.073	0.038	0.057	0.065	0.064	0.044	0.046	0.038	0.038	0.030
Al	0.127	0.130	0.123	0.246	0.125	0.245	0.271	0.241	0.125	0.153	0.137	0.133	0.101
Cr	-	-	-	-	-	-	0.009	-	-	-	-	-	-
Fe^{2+}	0.267	0.263	0.273	0.285	0.265	0.308	0.294	0.274	0.281	0.456	0.304	0.286	0.362
Mn	-	-	-	-	-	-	-	-	-	-	-	-	0.007
Mg	0.767	0.748	0.762	0.684	0.761	0.645	0.673	0.708	0.758	0.525	0.721	0.732	0.637
Ca	0.898	0.920	0.886	0.932	0.898	0.911	0.869	0.901	0.904	0.865	0.908	0.915	0.923
Na	0.061	0.058	0.070	0.062	0.062	0.070	0.086	0.082	0.074	0.115	0.050	0.057	0.071
Cations	4.044	4.032	4.043	4.058	4.040	4.046	4.052	4.044	4.058	4.045	4.038	4.043	4.043
Recalculated Al and Fe ions and Fe oxides													
Al^{IV}	0.109	0.126	0.111	0.223	0.109	0.190	0.214	0.225	0.125	0.114	0.120	0.118	0.088
Al^{VI}	0.017	0.005	0.012	0.023	0.016	0.054	0.056	0.015	-	0.039	0.018	0.015	0.012
Fe^{2+}	0.181	0.162	0.185	0.167	0.184	0.216	0.190	0.110	0.171	0.358	0.229	0.202	0.274
Fe^{3+}	0.086	0.102	0.088	0.118	0.080	0.092	0.104	0.164	0.111	0.098	0.075	0.084	0.087
FeO	5.76	5.14	5.92	5.32	5.90	6.82	6.02	3.53	5.41	11.14	7.26	6.39	8.59
Fe_2O_3	3.05	3.59	3.13	4.18	2.85	3.24	3.67	5.84	3.90	3.37	2.64	2.95	3.04
End-member compositions													
Wo	46.5	47.7	46.1	49.0	46.7	48.9	47.3	47.8	46.5	46.8	47.0	47.3	47.9
En	39.7	38.7	39.7	36.0	39.6	34.6	36.6	37.6	39.0	28.4	37.3	37.9	33.0
Fs	13.8	13.6	14.2	15.0	13.8	16.5	16.0	14.5	14.5	24.7	15.7	14.8	19.1

Table A6.28 Electron microprobe analyses of clinopyroxene in group B ne-hawaiites (continued).

Sample	SA65										
Analysis	1544-C1	1545-R1	1546-C2	1547-R2	1551-C3	1552-R3	1549-C	1556-G	1557-G	1559-G	1560-G
SiO_2	49.09	45.35	46.72	45.64	49.36	47.14	44.69	45.68	49.88	48.14	49.19
TiO_2	1.57	3.04	2.51	2.73	1.70	2.39	3.43	2.89	1.31	2.04	1.67
Al_2O_3	3.34	6.96	5.72	5.92	3.64	5.46	7.58	6.27	2.99	4.75	3.63
Cr_2O_3	-	-	-	-	-	-	-	-	-	-	-
FeO_T	8.86	9.51	9.73	9.12	10.10	9.68	9.84	9.47	9.10	9.72	9.33
MnO	0.25	-	-	0.24	0.24	0.24	0.27	0.22	0.23	-	-
MgO	13.14	11.26	11.55	11.35	13.05	11.55	11.04	11.44	12.98	12.21	12.99
CaO	22.22	22.18	21.88	23.14	21.56	22.68	21.97	21.83	22.47	21.86	21.98
Na_2O	0.86	1.05	1.08	1.01	0.96	0.91	1.07	1.24	0.87	1.18	0.86
Total	99.33	99.35	99.19	99.15	100.61	100.05	99.89	99.04	99.83	99.90	99.65
Number of ions on the basis of 6 oxygen											
Si	1.861	1.732	1.784	1.721	1.847	1.787	1.703	1.751	1.873	1.821	1.858
Ti	0.044	0.088	0.072	0.077	0.048	0.068	0.098	0.083	0.037	0.058	0.047
Al	0.149	0.313	0.257	0.263	0.160	0.244	0.340	0.283	0.133	0.212	0.161
Cr	-	-	-	-	-	-	-	-	-	-	-
Fe^{2+}	0.281	0.304	0.311	0.287	0.316	0.307	0.314	0.304	0.286	0.308	0.295
Mn	0.008	-	-	0.008	0.007	0.008	0.008	0.007	0.007	-	-
Mg	0.742	0.641	0.657	0.638	0.728	0.653	0.627	0.654	0.727	0.688	0.731
Ca	0.902	0.908	0.895	0.935	0.865	0.922	0.897	0.896	0.904	0.886	0.889
Na	0.064	0.077	0.080	0.074	0.070	0.067	0.079	0.092	0.063	0.086	0.062
Cations	4.051	4.063	4.055	4.005	4.040	4.057	4.067	4.070	4.030	4.059	4.044
Recalculated Al and Fe ions and Fe oxides											
Al^{IV}	0.139	0.268	0.216	0.263	0.153	0.213	0.297	0.249	0.127	0.179	0.142
Al^{VI}	0.010	0.045	0.041	-	0.007	0.032	0.044	0.034	0.006	0.033	0.019
Fe^{2+}	0.177	0.179	0.200	0.106	0.196	0.196	0.178	0.163	0.176	0.192	0.204
Fe^{3+}	0.104	0.125	0.111	0.182	0.120	0.111	0.135	0.140	0.110	0.116	0.091
FeO	5.57	5.61	6.26	3.36	6.27	6.17	5.59	5.10	5.61	6.05	6.45
Fe_2O_3	3.65	4.34	3.85	6.40	4.25	3.90	4.72	4.86	3.88	4.08	3.20
End-member compositions											
Wo	46.7	49.0	48.0	50.0	45.1	48.8	48.6	48.2	47.0	47.1	46.4
En	38.4	34.6	35.3	34.2	38.0	34.6	34.0	35.1	37.8	36.6	38.2
Fs	14.9	16.4	16.7	15.8	16.9	16.7	17.5	16.7	15.2	16.4	15.4

A6.29 Microprobe analyses of clinopyroxene in group B lavas: mugearite

Table A6.29 Electron microprobe analyses of clinopyroxene in group B mugearite.

Sample	SA88						
Analysis	50-C1	51-R1	55-C2	56-R2	501-C3	502-R3	66-C
SiO_2	51.11	51.18	51.32	51.16	50.53	50.34	50.14
TiO_2	1.15	1.37	1.19	1.01	1.02	1.43	1.60
Al_2O_3	2.62	2.26	1.50	1.76	4.51	3.11	3.50
Cr_2O_3	-	-	-	-	-	-	-
FeO_T	8.42	8.83	12.00	11.78	7.03	8.35	8.42
MnO	0.21	0.24	0.22	0.34	0.22	0.24	-
MgO	14.77	14.20	12.98	13.19	14.82	14.02	13.93
CaO	20.81	21.42	20.71	20.49	21.84	21.49	21.43
Na_2O	-	-	-	-	-	-	-
Total	99.09	99.50	99.92	99.73	99.97	98.98	99.02
Number of ions on the basis of 6 oxygen							
Si	1.901	1.903	1.924	1.919	1.870	1.894	1.871
Ti	0.032	0.038	0.034	0.029	0.028	0.040	0.045
Al	0.115	0.099	0.066	0.078	0.197	0.138	0.154
Cr	-	-	-	-	-	-	-
Fe^{2+}	0.262	0.275	0.376	0.370	0.218	0.263	0.263
Mn	0.007	0.008	0.007	0.011	0.007	0.008	-
Mg	0.818	0.787	0.725	0.737	0.818	0.787	0.775
Ca	0.829	0.854	0.832	0.824	0.866	0.866	0.857
Na	-	-	-	-	-	-	-
Cations	3.964	3.964	3.965	3.968	4.003	3.996	3.964
Recalculated Al and Fe ions and Fe oxides							
Al^{IV}	0.099	0.097	0.066	0.078	0.130	0.106	0.129
Al^{VI}	0.015	0.002	-	-	0.067	0.032	0.024
Fe^{2+}	0.243	0.257	0.376	0.349	0.211	0.263	0.248
Fe^{3+}	0.019	0.018	-	0.020	0.006	-	0.015
FeO	7.81	8.26	12.00	11.13	6.82	8.35	7.95
Fe_2O_3	0.68	0.64	-	0.72	0.23	-	0.53
End-member compositions							
Wo	43.3	44.4	42.9	42.4	45.4	45.0	45.2
En	42.7	40.9	37.4	38.0	42.9	40.9	40.9
Fs	14.0	14.7	19.8	19.6	11.8	14.1	13.9

A6.30 Microprobe analyses of plagioclase feldspar in group B lavas: alkali ol-basalt

Table A6.30 Electron microprobe analyses of plagioclase feldspar in group B alkali ol-basalts.

Sample	SA54										SAB188						SAB207		
Analysis	1673-C1	1674-R1	1685-C2	1686-R2	1693-C	1697-C	1698-G	1699-G	1702-G	1703-G	1643-G	1653-G	1661-G	1662-G	1663-G	1664-G	1626-G	1630-G	1633-G
SiO_2	51.76	52.16	52.01	53.17	51.77	52.58	59.51	58.53	50.97	51.07	51.58	51.58	56.90	53.42	60.43	59.40	52.52	51.72	53.96
TiO_2	-	-	0.20	-	0.17	-	0.20	0.20	0.19	-	-	0.45	0.19	0.25	0.19	0.28	0.26	-	-
Al_2O_3	29.93	29.02	29.85	29.10	30.13	29.54	24.24	25.11	30.30	30.33	29.70	28.28	26.89	28.65	24.65	23.90	29.90	31.00	28.94
FeO_T	0.39	0.49	0.50	0.55	0.53	0.85	0.81	0.42	0.72	0.55	1.68	3.44	0.46	0.97	0.42	1.10	0.63	0.74	0.51
MgO	-	0.28	0.27	0.22	0.23	0.35	0.24	-	0.31	0.28	1.21	1.39	-	0.41	0.36	0.71	0.30	0.27	-
CaO	12.59	11.86	12.17	11.41	12.38	11.63	5.43	6.47	12.83	12.55	11.96	1-	8.10	10.05	5.32	4.60	11.99	12.93	10.70
Na_2O	4.12	4.51	4.67	4.90	4.28	4.62	7.61	7.07	3.93	4.29	4.49	5.01	6.40	5.52	7.24	6.77	4.61	4.00	4.95
K_2O	0.31	0.29	0.31	0.32	0.28	0.36	1.24	0.92	0.31	0.30	0.26	0.24	0.79	1.38	2.15	3.12	0.37	0.25	0.44
Total	99.10	98.61	99.98	99.67	99.77	99.93	99.28	98.72	99.56	99.37	100.88	100.39	99.73	100.65	100.76	99.88	100.58	100.91	99.50
Number of ions on the basis of 32 oxygen																			
Si	9.494	9.664	9.472	9.680	9.443	9.571	10.746	10.614	9.341	9.370	9.366	9.459	10.262	9.641	10.762	10.742	9.504	9.341	9.808
Ti	-	-	0.026	-	0.022	-	0.029	0.029	0.026	-	-	0.061	0.026	0.035	0.026	0.038	0.035	-	-
Al	6.470	6.339	6.410	6.243	6.477	6.339	5.158	5.366	6.544	6.560	6.358	6.112	5.718	6.096	5.174	5.094	6.378	6.598	6.202
Fe^{2+}	0.061	0.077	0.077	0.083	0.080	0.128	0.122	0.064	0.109	0.083	0.256	0.528	0.070	0.147	0.064	0.166	0.096	0.112	0.077
Mg	-	0.077	0.074	0.061	0.061	0.093	0.064	-	0.086	0.077	0.326	0.381	-	0.112	0.096	0.192	0.080	0.070	-
Ca	2.474	2.355	2.374	2.227	2.419	2.269	1.050	1.258	2.518	2.467	2.326	1.965	1.565	1.946	1.014	0.893	2.323	2.502	2.083
Na	1.466	1.619	1.651	1.731	1.514	1.629	2.662	2.486	1.395	1.526	1.581	1.782	2.237	1.933	2.499	2.374	1.619	1.402	1.744
K	0.074	0.070	0.070	0.074	0.064	0.083	0.285	0.211	0.070	0.070	0.061	0.058	0.179	0.317	0.486	0.720	0.083	0.058	0.102
Cations	20.038	20.201	20.154	20.099	20.080	20.112	20.115	20.029	20.090	20.154	20.275	20.346	20.058	20.227	20.122	20.221	20.118	20.083	20.016
End-member compositions																			
An	61.6	58.2	58.0	55.2	60.5	57.0	26.3	31.8	63.2	60.7	58.6	51.6	39.3	46.4	25.4	22.4	57.7	63.2	53.0
Ab	36.5	40.0	40.3	42.9	37.9	40.9	66.6	62.9	35.0	37.6	39.8	46.8	56.2	46.1	62.5	59.6	40.2	35.4	44.4
Or	1.8	1.7	1.7	1.8	1.6	2.1	7.1	5.3	1.8	1.7	1.5	1.5	4.5	7.6	12.2	18.1	2.1	1.5	2.6

A6.31 Microprobe analyses of plagioclase feldspar in group B lavas: basanites

Table A6.31 Electron microprobe analyses of plagioclase feldspar in group B basanites.

Sample	SA12		SA27	SAB102						SAB111								
Analysis	1257-G	1259-G	1345-G	83-G	84-G	87-G	406-G	407-G	410-G	762-C	289-G	290-G	293-G	301-G	759-G	760-G	765-G	766-G
SiO_2	58.72	52.19	56.50	54.07	52.82	51.48	53.84	53.91	52.76	55.29	52.34	51.50	51.86	52.63	51.68	51.56	49.53	51.43
TiO_2	0.39	-	0.29	-	0.32	0.79	0.25	0.23	-	0.22	-	0.24	-	0.20	-	-	1.65	0.33
Al_2O_3	23.93	29.40	25.97	28.53	27.67	26.07	28.34	28.73	29.43	28.18	30.14	30.73	30.28	28.78	30.84	30.57	22.15	27.83
FeO_T	0.60	0.53	1.05	0.58	1.25	1.86	0.94	0.41	0.49	0.57	0.68	0.74	0.68	0.74	0.52	0.69	3.56	2.04
MgO	-	-	-	-	0.31	1.71	-	-	-	-	-	-	-	-	-	-	4.33	-
CaO	5.22	11.87	8.18	10.61	10.93	13.09	10.40	10.87	11.75	10.06	12.19	13.18	12.72	12.46	13.42	13.15	16.71	10.16
Na_2O	4.78	4.37	5.88	5.12	5.01	4.03	4.58	4.89	4.48	5.32	3.84	3.88	3.86	4.54	3.65	3.89	2.63	5.29
K_2O	5.00	0.31	0.73	0.44	0.47	0.22	0.34	0.39	0.29	0.52	0.47	0.31	0.40	0.43	0.29	0.29	0.17	1.44
Total	98.64	98.67	98.60	99.35	98.78	99.25	98.69	99.43	99.20	100.16	99.66	100.58	99.80	99.78	100.40	100.15	100.73	98.52
Number of ions on the basis of 32 oxygen																		
Si	10.844	9.657	10.563	9.779	9.677	9.488	9.916	9.805	9.645	9.968	9.469	9.172	9.392	9.504	9.373	9.386	9.286	9.637
Ti	0.054	-	0.042	-	0.045	0.109	0.035	0.032	-	0.029	-	0.032	-	0.029	-	-	0.234	0.048
Al	5.210	6.410	5.722	6.080	5.974	5.664	6.154	6.160	6.339	5.990	6.429	6.451	6.464	6.125	6.592	6.560	4.896	6.147
Fe^{2+}	0.093	0.083	0.163	0.086	0.192	0.285	0.144	0.064	0.074	0.086	0.102	0.109	0.102	0.112	0.080	0.106	0.557	0.320
Mg	-	-	-	-	0.083	0.470	-	-	-	-	-	-	-	-	-	-	1.210	-
Ca	1.034	2.355	1.638	2.054	2.144	2.586	2.054	2.118	2.301	1.942	2.362	2.515	2.470	2.410	2.608	2.563	3.357	2.038
Na	1.712	1.568	2.131	1.795	1.779	1.440	1.635	1.725	1.587	1.859	1.347	1.338	1.357	1.590	1.283	1.373	0.957	1.923
K	1.178	0.074	0.173	0.102	0.109	0.051	0.080	0.090	0.067	0.118	0.109	0.070	0.093	0.099	0.067	0.067	0.042	0.342
Cations	20.124	20.147	20.432	19.898	20.003	20.093	20.018	19.994	20.013	19.994	19.818	19.687	19.878	19.869	20.003	20.054	20.538	20.456
End-member compositions																		
An	26.3	58.9	41.6	52.0	53.2	63.4	54.5	53.9	58.2	49.6	61.9	64.1	63.0	58.8	65.9	64.0	77.1	47.4
Ab	43.6	39.2	54.1	45.4	44.1	35.3	43.4	43.9	40.1	47.4	35.3	34.1	34.6	38.8	32.4	34.3	22.0	44.7
Or	30.0	1.8	4.4	2.6	2.7	1.3	2.1	2.3	1.7	3.0	2.8	1.8	2.4	2.4	1.7	1.7	1.0	8.0

Table A6.31 Electron microprobe analyses of plagioclase feldspar in group B basanites (continued).

Sample	SAB111 (continued)				SAB128												SAB204		
Analysis	769-G	772-G	773-G	775-G	730-C	323-G	327-G	328-G	726-G	727-G	728-G	729-G	735-G	736-G	737-G	738-G	740-G	1356-G	1358-G	1360-G
SiO_2	50.54	51.40	53.37	52.48	52.82	52.81	55.20	52.35	56.23	53.39	52.31	54.74	54.07	59.58	56.84	53.71	52.91	52.10	51.56	51.38
TiO_2	0.22	-	0.31	0.21	-	-	0.27	0.19	0.64	0.23	0.27	0.35	0.26	0.47	0.23	0.31	0.21	0.34	0.19	-
Al_2O_3	31.43	31.19	27.76	29.79	29.56	28.93	27.44	29.24	24.42	29.21	29.64	28.64	29.03	25.41	27.10	29.38	28.04	28.75	29.68	29.71
FeO_T	1.05	0.55	0.97	1.21	0.67	0.65	0.82	0.80	2.36	0.88	0.95	0.92	0.57	0.47	0.80	0.83	1.32	1.16	0.71	0.80
MgO	-	-	-	-	-	-	0.24	-	0.42	-	0.34	-	-	-	-	-	-	-	-	-
CaO	13.69	13.45	10.34	12.07	12.14	11.54	9.17	11.90	6.47	11.49	11.86	9.67	11.32	5.87	8.43	11.71	10.09	11.58	11.79	12.25
Na_2O	3.57	3.69	5.16	4.41	4.27	4.37	5.32	4.38	6.55	4.55	4.75	5.61	4.58	6.92	6.35	4.57	4.63	4.40	4.30	3.91
K_2O	0.26	0.31	0.52	0.37	0.29	0.35	0.76	0.46	1.82	0.61	0.48	0.95	0.39	1.13	0.79	0.41	1.93	0.45	0.48	0.72
Total	100.76	100.59	98.43	100.54	99.75	98.65	99.22	99.32	98.91	100.36	100.60	100.88	100.22	99.85	100.54	100.92	99.13	98.78	98.71	98.77
Number of ions on the basis of 32 oxygen																				
Si	9.078	9.315	9.843	9.465	9.616	9.635	9.971	9.523	10.342	9.674	9.439	9.795	9.766	10.656	10.088	9.613	9.766	9.723	9.504	9.539
Ti	0.029	-	0.042	0.029	-	-	0.038	0.026	0.086	0.032	0.035	0.048	0.035	0.064	0.032	0.042	0.029	0.048	0.026	-
Al	6.656	6.662	6.035	6.333	6.342	6.221	5.843	6.269	5.293	6.237	6.304	6.042	6.182	5.357	5.670	6.198	6.099	6.323	6.451	6.502
Fe^{2+}	0.157	0.083	0.150	0.182	0.102	0.099	0.125	0.122	0.365	0.134	0.144	0.138	0.086	0.070	0.118	0.125	0.205	0.182	0.109	0.125
Mg	-	-	-	-	-	-	0.064	-	0.115	-	0.093	-	-	-	-	-	-	-	-	-
Ca	2.637	2.611	2.045	2.333	2.368	2.256	1.776	2.320	1.274	2.230	2.291	1.853	2.192	1.126	1.603	2.246	1.997	2.317	2.330	2.438
Na	1.242	1.296	1.843	1.542	1.507	1.546	1.866	1.546	2.336	1.600	1.661	1.949	1.603	2.400	2.182	1.587	1.658	1.590	1.539	1.408
K	0.061	0.070	0.122	0.086	0.067	0.080	0.176	0.106	0.429	0.141	0.109	0.218	0.090	0.259	0.179	0.093	0.454	0.106	0.112	0.170
Cations	19.859	20.038	20.080	19.971	20.003	19.837	19.859	19.910	20.239	20.048	20.076	20.042	19.955	19.933	19.874	19.904	20.208	20.289	20.070	20.182
End-member compositions																				
An	66.9	65.6	51.0	58.9	60.1	58.1	46.5	58.4	31.5	56.2	56.4	46.1	56.4	29.8	40.4	57.2	48.6	57.7	58.5	60.7
Ab	31.5	32.6	46.0	38.9	38.2	39.8	48.9	38.9	57.8	40.3	40.9	48.5	41.3	63.4	55.0	40.4	40.3	39.6	38.7	35.1
Or	1.5	1.8	3.0	2.2	1.7	2.1	4.6	2.7	10.6	3.5	2.7	5.4	2.3	6.8	4.5	2.4	11.1	2.6	2.8	4.2

Table A6.31 Electron microprobe analyses of plagioclase feldspar in group B basanites (continued).

Sample	SA37											SAB175							
Analysis	849-G	856-G	857-G	902-G	903-G	905-G	906-G	907-G	908-G	915-G	916-G	1050-G	1058-G	1059-G	1062-G	1064-G	1065-G	1200-G	1201-G
SiO_2	50.52	52.21	56.24	50.68	50.65	52.57	55.05	53.88	54.08	53.72	53.25	51.89	51.46	53.27	49.92	57.65	51.55	52.34	56.70
TiO_2	0.18	0.64	0.24	-	-	0.18	0.19	0.20	0.25	0.20	0.18	-	-	-	-	0.39	-	0.20	0.19
Al_2O_3	30.74	26.99	26.47	31.45	30.83	29.19	28.50	27.81	27.43	29.10	28.67	30.88	30.87	29.14	31.52	24.94	31.33	30.17	26.51
FeO_T	0.66	2.86	1.29	0.65	0.64	0.68	0.54	1.82	1.08	1.14	0.86	0.74	0.57	0.77	0.45	1.14	0.81	0.60	1.07
MgO	-	0.28	-	-	-	-	-	-	-	-	-	-	-	-	-	-	-	-	-
CaO	13.44	8.53	7.64	13.79	13.07	11.03	9.87	9.90	9.52	10.97	11.08	12.56	13.27	10.90	13.84	6.35	13.46	12.26	7.87
Na_2O	3.68	6.23	6.35	3.62	3.72	4.68	5.63	5.44	5.54	5.04	5.00	4.12	3.87	5.06	3.25	6.45	3.73	4.34	6.23
K_2O	0.33	0.99	1.01	0.26	0.29	0.57	0.52	0.77	1.13	0.48	0.57	0.32	0.28	0.43	0.25	2.07	0.24	0.30	0.81
Total	99.55	98.73	99.24	100.45	99.20	98.90	100.30	99.82	99.03	100.65	99.61	100.51	100.32	99.57	99.23	98.99	101.12	100.21	99.38
Number of ions on the basis of 32 oxygen																			
Si	9.270	9.728	10.243	9.216	9.309	9.651	9.920	9.846	9.933	9.709	9.722	9.347	9.350	9.709	9.178	10.525	9.302	9.498	10.285
Ti	0.026	0.090	0.032	-	-	0.026	0.026	0.029	0.035	0.026	0.026	-	-	-	-	0.054	-	0.029	0.026
Al	6.650	5.926	5.683	6.742	6.678	6.317	6.054	5.990	5.939	6.198	6.170	6.557	6.611	6.259	6.829	5.366	6.662	6.451	5.667
Fe^{2+}	0.102	0.445	0.198	0.099	0.099	0.106	0.080	0.278	0.166	0.173	0.131	0.112	0.086	0.118	0.067	0.176	0.122	0.093	0.163
Mg	-	0.080	-	-	-	-	-	-	-	-	-	-	-	-	-	-	-	-	-
Ca	2.643	1.702	1.491	2.688	2.573	2.170	1.907	1.939	1.872	2.125	2.166	2.422	2.582	2.128	2.726	1.242	2.602	2.384	1.530
Na	1.312	2.253	2.240	1.277	1.325	1.667	1.968	1.930	1.974	1.763	1.770	1.440	1.363	1.789	1.158	2.282	1.306	1.526	2.192
K	0.077	0.237	0.234	0.061	0.067	0.134	0.118	0.179	0.262	0.112	0.131	0.074	0.064	0.099	0.058	0.483	0.058	0.070	0.189
Cations	20.080	20.461	20.122	20.083	20.051	20.070	20.074	20.192	20.182	20.106	20.115	19.952	20.058	20.102	20.016	20.128	20.051	20.051	20.051
End-member compositions																			
An	65.6	40.6	37.6	66.8	64.9	54.6	47.8	47.9	45.6	53.1	53.3	61.5	64.4	53.0	69.2	31.0	65.6	59.9	39.1
Ab	32.5	53.7	56.5	31.7	33.4	42.0	49.3	47.7	48.1	44.1	43.5	36.6	34.0	44.5	29.4	56.9	32.9	38.3	56.1
Or	1.9	5.6	5.9	1.5	1.7	3.4	3.0	4.4	6.4	2.8	3.2	1.9	1.6	2.5	1.5	12.1	1.5	1.8	4.8

Table A6.31 Electron microprobe analyses of plagioclase feldspar in group B basanites (continued).

Sample	SAB176											SAB177					SAB178			
Analysis	310-C	312-C	664-C	304-G	654-G	655-G	656-G	657-G	659-G	662-G	663-G	1137-G	1138-G	1151-G	1152-G	1154-G	1170-G	1173-G	1184-G	1185-G
SiO_2	52.02	51.57	51.61	52.12	55.23	52.42	51.07	52.84	51.94	58.59	51.87	51.15	50.94	52.62	56.41	52.01	53.63	55.49	53.33	53.27
TiO_2	0.23	-	-	-	0.37	0.25	0.22	0.24	0.27	0.33	-	-	-	-	0.25	-	0.22	0.20	0.44	-
Al_2O_3	30.38	31.11	30.76	29.74	26.87	30.17	31.32	28.20	30.94	25.31	30.95	31.43	31.40	30.29	27.92	30.41	29.28	28.38	27.17	29.82
FeO_T	0.75	0.44	0.56	0.54	0.96	0.56	0.99	1.10	0.65	0.69	0.70	0.73	0.64	0.62	0.72	0.70	0.52	0.46	2.12	0.53
MgO	-	-	-	-	-	-	-	-	-	-	-	-	-	-	-	-	-	-	0.25	-
CaO	13.08	13.74	13.46	12.43	8.84	12.83	13.39	9.79	13.41	6.30	13.17	13.11	13.18	11.89	8.77	12.05	10.63	9.29	9.96	11.38
Na_2O	4.06	3.67	3.74	4.29	4.68	4.11	3.55	4.85	3.57	6.61	3.83	4.08	3.95	4.65	5.96	4.62	4.97	5.87	5.33	4.60
K_2O	0.27	0.23	0.24	0.28	2.36	0.27	0.24	1.66	0.18	2.55	0.23	0.24	0.20	0.25	0.64	0.34	0.45	0.56	0.78	0.40
Total	100.79	100.76	100.37	99.40	99.31	100.61	100.78	98.68	100.96	100.38	100.75	100.74	100.31	100.32	100.67	100.13	99.70	100.25	99.38	10-
Number of ions on the basis of 32 oxygen																				
Si	9.347	9.261	9.370	9.469	10.109	9.482	9.203	9.827	9.366	10.547	9.376	9.267	9.264	9.530	10.099	9.456	9.734	9.984	9.786	9.651
Ti	0.032	-	-	-	0.051	0.035	0.029	0.035	0.035	0.045	-	-	-	-	0.035	-	0.032	0.029	0.061	-
Al	6.435	6.586	6.582	6.368	5.795	6.432	6.650	6.182	6.576	5.370	6.595	6.710	6.730	6.464	5.891	6.518	6.266	6.019	5.878	6.368
Fe^{2+}	0.112	0.067	0.086	0.083	0.147	0.083	0.150	0.170	0.099	0.106	0.106	0.109	0.096	0.096	0.109	0.106	0.080	0.070	0.326	0.080
Mg	-	-	-	-	-	-	-	-	-	-	-	-	-	-	-	-	-	-	0.070	-
Ca	2.518	2.643	2.618	2.419	1.734	2.486	2.586	1.949	2.589	1.216	2.550	2.544	2.566	2.307	1.683	2.349	2.067	1.792	1.958	2.208
Na	1.414	1.280	1.318	1.510	1.661	1.440	1.238	1.750	1.248	2.307	1.344	1.434	1.392	1.632	2.070	1.629	1.750	2.048	1.898	1.616
K	0.064	0.051	0.058	0.067	0.550	0.061	0.054	0.394	0.042	0.586	0.054	0.054	0.045	0.058	0.144	0.080	0.106	0.131	0.182	0.093
Cations	19.923	19.888	20.032	19.917	20.048	20.019	19.910	20.307	19.955	20.176	20.026	20.118	20.093	20.086	20.032	20.138	20.035	20.074	20.160	20.016
End-member compositions																				
An	63.0	66.5	65.5	60.5	44.0	62.4	66.7	47.6	66.7	29.6	64.6	63.1	64.1	57.7	43.2	57.9	52.7	45.1	48.5	56.4
Ab	35.4	32.2	33.0	37.8	42.1	36.1	31.9	42.8	32.2	56.2	34.0	35.6	34.8	40.8	53.1	40.1	44.6	51.6	47.0	41.3
Or	1.6	1.3	1.4	1.7	13.9	1.5	1.4	9.6	1.1	14.3	1.4	1.3	1.1	1.4	3.7	2.0	2.7	3.3	4.5	2.4

Table A6.31 Electron microprobe analyses of plagioclase feldspar in group B basanites (continued).

Sample	SAB178 (continued)			SAB179										SAB180					
Analysis	1187-G	1188-G	1189-G	226-C	597-C	595-C	596-C	224-G	225-G	585-G	588-G	589-G	1237-G	1290-G	1294-G	1296-G	1298-G	1307-G	1311-G
SiO_2	54.11	52.50	53.14	51.33	55.52	50.89	55.16	50.70	50.70	54.71	51.21	51.24	59.25	54.46	50.35	50.40	57.02	50.98	49.40
TiO_2	0.29	0.22	-	-	-	-	-	-	-	-	-	0.19	0.21	0.18	-	0.22	0.27	-	0.22
Al_2O_3	28.78	29.99	28.96	30.24	28.40	31.19	27.26	30.89	30.94	29.04	31.24	30.85	25.09	27.46	30.73	30.22	26.00	30.40	30.98
FeO_T	0.94	0.64	0.59	0.41	0.50	0.53	0.64	0.79	0.52	0.63	0.65	0.65	0.58	1.30	0.48	0.88	0.73	0.56	0.66
MgO	-	-	-	-	-	-	-	-	-	-	-	-	-	-	-	-	-	-	-
CaO	10.37	11.57	10.87	13.44	10.18	13.77	8.03	12.51	13.70	11.28	13.96	13.51	5.89	8.87	13.61	12.91	8.07	13.23	13.81
Na_2O	5.05	4.72	5.07	3.68	5.43	3.44	5.96	3.62	3.48	4.95	3.53	3.64	7.40	5.85	3.51	3.99	6.13	3.52	3.34
K_2O	0.51	0.38	0.38	0.27	0.49	0.22	2.05	0.42	0.29	0.34	0.26	0.21	1.43	0.68	0.28	0.29	0.63	0.25	0.21
Total	100.05	100.02	99.01	99.37	100.52	100.04	99.10	98.93	99.63	100.95	100.85	100.29	99.85	98.80	98.96	98.91	98.85	98.94	98.62
Number of ions on the basis of 32 oxygen																			
Si	9.802	9.539	9.728	9.341	9.971	9.274	10.102	9.375	9.222	9.814	9.270	9.315	10.646	9.990	9.334	9.367	10.485	9.545	9.158
Ti	0.038	0.032	-	-	-	-	-	-	-	-	-	0.026	0.029	0.026	-	0.032	0.038	-	0.029
Al	6.144	6.422	6.250	6.486	6.013	6.701	5.885	6.733	6.630	6.141	6.669	6.611	5.315	5.936	6.714	6.621	5.635	6.707	6.768
Fe^{2+}	0.141	0.099	0.090	0.061	0.074	0.080	0.099	0.122	0.080	0.096	0.099	0.099	0.086	0.198	0.074	0.138	0.112	0.090	0.102
Mg	-	-	-	-	-	-	-	-	-	-	-	-	-	-	-	-	-	-	-
Ca	2.013	2.253	2.131	2.621	1.958	2.688	1.578	2.480	2.669	2.166	2.707	2.634	1.133	1.744	2.704	2.570	1.590	2.653	2.742
Na	1.773	1.661	1.798	1.299	1.894	1.216	2.115	1.299	1.226	1.722	1.242	1.283	2.579	2.083	1.264	1.437	2.186	1.277	1.203
K	0.118	0.090	0.086	0.061	0.112	0.051	0.480	0.099	0.067	0.077	0.061	0.048	0.330	0.157	0.064	0.070	0.147	0.061	0.051
Cations	20.029	20.096	20.083	19.869	20.022	20.010	20.259	20.108	19.894	20.016	20.048	20.016	20.118	20.134	20.153	20.234	20.193	20.332	20.054
End-member compositions																			
An	51.6	56.3	53.1	65.8	49.4	68.0	37.8	63.9	67.4	54.6	67.5	66.4	28.0	43.8	67.1	63.0	40.5	66.5	68.6
Ab	45.4	41.5	44.8	32.6	47.8	30.7	50.7	33.5	30.9	43.4	31.0	32.4	63.8	52.3	31.3	35.2	55.7	32.0	30.1
Or	3.0	2.2	2.2	1.5	2.8	1.3	11.5	2.6	1.7	1.9	1.5	1.2	8.2	3.9	1.6	1.7	3.8	1.5	1.3

A6.32 Microprobe analyses of plagioclase feldspar in group B lavas: nephelinites

Table A6.32 Electron microprobe analyses of plagioclase feldspar in group B nephelinites.

Sample	SA21			SAB113										
Analysis	1410-G	1413-G	1414-G	231-C	235-C	246-C	245-G	741-G	742-G	743-G	744-G	745-G	746-G	748-G	750-G
SiO_2	51.28	51.76	52.27	49.23	52.14	53.61	53.77	53.14	56.39	54.93	51.13	54.08	52.69	54.00	53.11
TiO_2	0.27	0.21	-	1.66	0.27	0.26	0.41	0.21	0.23	0.20	1.10	0.18	0.19	0.25	0.25
Al_2O_3	29.02	29.30	29.44	23.74	29.31	27.30	27.43	29.28	28.03	28.13	29.04	29.08	29.69	28.48	29.36
FeO_T	0.79	0.68	0.76	3.31	0.61	1.39	1.06	0.63	0.49	0.55	2.79	0.61	0.60	0.54	0.58
MgO	0.56	0.43	-	2.13	-	-	-	-	-	-	-	-	-	-	-
CaO	12.53	11.89	11.87	13.07	12.20	10.03	10.39	11.56	9.43	9.95	11.63	11.18	11.88	10.62	11.69
Na_2O	4.04	4.41	4.25	4.30	3.90	5.44	5.11	4.57	5.44	5.42	4.54	4.77	4.32	4.95	4.35
K_2O	0.30	0.35	0.33	1.22	0.35	1.18	0.60	0.41	0.61	0.48	0.41	0.43	0.42	0.47	0.35
Total	98.79	99.03	98.92	98.66	98.78	99.21	98.77	99.80	100.62	99.66	100.64	100.33	99.79	99.31	99.69
Number of ions on the basis of 32 oxygen															
Si	9.579	9.517	9.709	9.270	9.514	9.715	9.782	9.664	10.090	9.955	9.259	9.763	9.587	9.837	9.658
Ti	0.038	0.029	-	0.237	0.038	0.035	0.058	0.029	0.032	0.029	0.150	0.026	0.026	0.035	0.035
Al	6.390	6.349	6.445	5.270	6.304	5.830	5.885	6.275	5.914	6.010	6.198	6.189	6.368	6.115	6.294
Fe^{2+}	0.125	0.106	0.118	0.522	0.093	0.211	0.160	0.096	0.074	0.083	0.422	0.093	0.093	0.083	0.086
Mg	0.157	0.118	-	0.598	-	-	-	-	-	-	-	-	-	-	-
Ca	2.509	2.342	2.362	2.637	2.384	1.949	2.026	2.253	1.808	1.933	2.256	2.163	2.317	2.074	2.278
Na	1.462	1.574	1.530	1.571	1.382	1.914	1.802	1.610	1.888	1.904	1.594	1.670	1.523	1.750	1.533
K	0.074	0.083	0.077	0.294	0.083	0.272	0.141	0.093	0.138	0.109	0.096	0.099	0.099	0.109	0.083
Cations	20.334	20.118	20.240	20.400	19.798	19.926	19.853	20.019	19.942	20.022	19.976	20.003	20.013	20.003	19.968
End-member compositions															
An	62.0	58.6	59.5	58.6	61.9	47.1	51.0	57.0	47.2	49.0	57.2	55.0	58.8	52.7	58.5
Ab	36.2	39.4	38.5	34.9	35.9	46.3	45.4	40.7	49.2	48.3	40.4	42.5	38.7	44.5	39.4
Or	1.8	2.1	1.9	6.5	2.2	6.6	3.5	2.3	3.6	2.8	2.4	2.5	2.5	2.8	2.1

A6.33 Microprobe analyses of plagioclase feldspar in group B lavas: ne-hawaiites

Table A6.33 Electron microprobe analyses of plagioclase feldspar in group B ne-hawaiites.

Sample	SA02						SA25				SA65	
Analysis	1497-C	1498-G	1501-G	1502-G	1503-G	1504-G	1530-G	1531-G	1533-G	1534-G	1558-G	1565-G
SiO_2	51.45	51.57	52.26	52.24	54.81	52.03	54.96	58.94	58.18	56.38	56.65	56.39
TiO_2	0.22	-	-	0.18	-	-	-	-	-	0.18	-	-
Al_2O_3	29.15	29.47	29.28	29.22	28.00	29.21	26.59	25.74	24.56	26.77	26.71	26.88
FeO_T	0.92	0.66	0.61	0.80	0.80	0.69	2.09	0.71	1.62	0.59	0.58	0.54
MgO	0.38	-	0.32	-	0.22	0.23	0.56	-	0.97	-	-	0.29
CaO	11.98	12.23	12.04	11.83	10.51	11.77	7.76	6.42	5.01	8.22	8.19	8.35
Na_2O	4.21	4.30	4.32	4.42	4.95	4.49	6.60	7.49	6.94	6.54	6.41	6.45
K_2O	0.35	0.35	0.32	0.32	0.45	0.37	0.53	0.68	2.34	0.49	0.62	0.56
Total	98.66	98.58	99.15	99.00	99.74	98.78	99.09	99.98	99.62	99.17	99.16	99.46
Number of ions on the basis of 32 oxygen												
Si	9.585	9.659	9.771	9.788	10.257	9.716	10.077	10.563	10.566	10.234	10.278	10.211
Ti	0.032	-	-	0.026	-	-	-	-	-	0.026	-	-
Al	6.400	6.506	6.454	6.454	6.174	6.429	5.747	5.437	5.258	5.728	5.712	5.734
Fe^{2+}	0.142	0.103	0.094	0.123	0.126	0.106	0.320	0.106	0.246	0.090	0.086	0.080
Mg	0.106	-	0.090	-	0.061	0.065	0.154	-	0.262	-	-	0.080
Ca	2.391	2.456	2.414	2.375	2.107	2.356	1.523	1.232	0.976	1.597	1.594	1.619
Na	1.520	1.559	1.565	1.604	1.798	1.627	2.349	2.602	2.445	2.301	2.256	2.262
K	0.084	0.084	0.077	0.077	0.106	0.087	0.122	0.157	0.544	0.115	0.144	0.128
Cations	20.260	20.367	20.466	20.447	20.629	20.385	20.291	20.096	20.298	20.090	20.070	20.115
End-member compositions												
An	59.9	59.9	59.5	58.6	52.5	57.9	38.1	30.9	24.6	39.8	39.9	40.4
Ab	38.0	38.0	38.6	39.5	44.8	40.0	58.8	65.2	61.7	57.3	56.5	56.4
Or	2.1	2.0	1.9	1.9	2.7	2.1	3.0	3.9	13.7	2.9	3.6	3.2

A6.34 Microprobe analyses of plagioclase feldspar in group B lavas: mugearite

Table A6.34 Electron microprobe analyses of plagioclase feldspar in group B mugearite.

Sample	SA88												
Analysis	59-C1	60-R1	63-C2	64-R2	489-C3	491-R3	54-C	67-C	494-C	486-G	4870G	499-G	500-G
SiO_2	63.18	61.11	53.80	55.49	57.47	53.65	53.39	61.17	57.84	54.17	54.27	57.73	51.98
TiO_2	0.20	0.19	-	-	-	-	-	-	0.20	-	-	0.26	-
Al_2O_3	21.95	23.60	29.37	27.83	26.71	28.78	29.25	23.96	25.76	29.10	28.50	25.33	30.62
FeO_T	0.33	0.39	0.64	0.72	0.52	0.92	0.59	0.43	0.48	0.65	0.99	0.91	0.64
MgO	-	-	-	-	-	-	-	-	-	-	-	-	-
CaO	3.41	5.28	11.92	10.02	8.73	11.71	12.01	5.51	7.85	11.48	11.26	7.46	13.42
Na_2O	8.51	7.54	4.50	5.30	6.21	4.88	4.50	7.86	6.70	4.80	4.95	6.06	3.96
K_2O	1.81	1.20	0.29	0.38	0.58	0.30	0.28	1.01	0.61	0.23	0.21	1.11	0.20
Total	99.39	99.31	100.52	99.74	100.22	100.24	100.02	99.94	99.44	100.43	100.18	98.86	100.82
Number of ions on the basis of 32 oxygen													
Si	11.210	10.880	9.635	9.962	10.310	9.731	9.616	10.835	10.445	9.770	9.827	10.559	9.398
Ti	0.029	0.026	-	-	-	-	-	-	0.026	-	-	0.035	-
Al	4.592	4.954	6.202	5.891	5.648	6.154	6.208	5.002	5.482	6.186	6.080	5.459	6.525
Fe^{2+}	0.048	0.058	0.096	0.109	0.080	0.141	0.090	0.064	0.074	0.096	0.150	0.138	0.096
Mg	-	-	0.003	-	-	-	-	-	-	-	-	-	-
Ca	0.650	1.005	2.288	1.926	1.680	2.275	2.317	1.046	1.517	2.218	2.186	1.462	2.602
Na	2.928	2.602	1.562	1.846	2.160	1.715	1.571	2.701	2.346	1.677	1.738	2.147	1.389
K	0.410	0.272	0.067	0.086	0.131	0.067	0.064	0.227	0.141	0.054	0.048	0.259	0.045
Cations	19.866	19.795	19.853	19.821	20.010	20.083	19.866	19.875	20.029	20.000	20.029	20.059	20.054
End-member compositions													
An	16.3	25.9	58.4	49.9	42.3	56.1	58.6	26.3	37.9	56.2	55.0	37.8	64.5
Ab	73.4	67.1	39.9	47.8	54.4	42.3	39.8	68.0	58.6	42.5	43.8	55.5	34.4
Or	10.3	7.0	1.7	2.2	3.3	1.7	1.6	5.7	3.5	1.4	1.2	6.7	1.1

A6.35 Microprobe analyses of alkali feldspar in group B lavas

Table A6.35 Electron microprobe analyses of alkali feldspar in group B lavas.

Rock Type							basanite						
Sample	SA12	SAB176				SAB177	SAB179						SAB180
Analysis	1272-G	660-G	661-G	1212-G	1215-G	1140-G	591-G	592-G	1236-G	1238-G	1239-G	1242-G	1308-G
SiO_2	63.42	63.58	62.98	63.46	60.12	54.71	61.84	60.83	63.42	63.30	59.53	63.13	62.01
TiO_2	0.69	-	0.43	-	0.32	-	1.36	0.25	-	0.40	0.32	0.25	0.39
Al_2O_3	20.10	19.35	20.25	20.01	21.60	25.10	19.33	23.46	19.90	20.68	22.27	19.84	20.07
FeO_T	0.70	1.38	0.79	0.74	0.98	1.28	1.63	0.47	0.51	0.47	0.70	0.66	0.62
MgO	-	-	-	-	-	-	-	-	-	-	-	-	-
CaO	0.83	0.46	0.91	0.65	0.55	2.03	0.99	2.90	1.08	1.13	0.61	0.88	1.45
Na_2O	4.03	2.05	2.74	2.59	4.78	9.70	3.53	6.70	3.17	4.15	6.11	3.62	4.64
K_2O	9.19	13.15	11.46	12.83	11.32	6.21	10.27	5.96	11.30	9.94	8.99	11.19	9.55
Total	98.96	99.97	99.56	100.28	99.67	99.03	98.95	100.57	99.38	100.07	98.53	99.57	98.73
Number of ions on the basis of 32 oxygen													
Si	11.822	11.734	11.584	11.651	11.174	10.358	11.485	10.979	11.670	11.526	11.088	11.619	11.481
Ti	0.096	-	0.058	-	0.045	-	0.189	0.032	-	0.054	0.045	0.035	0.054
Al	4.419	4.208	4.387	4.330	4.733	5.600	4.234	4.989	4.317	4.438	4.890	4.304	4.381
Fe^{2+}	0.109	0.211	0.122	0.115	0.150	0.202	0.253	0.070	0.077	0.070	0.109	0.102	0.096
Mg	-	-	-	-	-	-	-	-	-	-	-	-	-
Ca	0.166	0.093	0.179	0.128	0.109	0.413	0.195	0.560	0.214	0.221	0.122	0.173	0.288
Na	1.456	0.736	0.979	0.922	1.722	3.558	1.270	2.346	1.130	1.466	2.208	1.293	1.664
K	2.186	3.094	2.688	3.005	2.685	1.498	2.432	1.373	2.653	2.307	2.138	2.627	2.256
Cations	20.254	20.077	19.997	20.150	20.618	21.628	20.058	20.349	20.061	20.083	20.598	20.154	20.221
End-member compositions													
An	4.4	2.4	4.7	3.2	2.4	7.5	5.0	13.1	5.4	5.5	2.7	4.2	6.8
Ab	38.2	18.8	25.5	22.7	38.1	65.1	32.6	54.8	28.3	36.7	49.4	31.6	39.5
Or	57.4	78.9	69.9	74.1	59.5	27.4	62.4	32.1	66.4	57.8	47.9	64.2	53.6

Table A6.35 Electron microprobe analyses of alkali feldspar in group B lavas (continued).

Rock Type	nephelinite	ne-hawaiite					mugearite			
Sample	SA28	SA25	SA29				SA88			
Analysis	1442-G	1529-G	159-G	166-G	442-G	452-G	488-C	497-C	490-G	498-G
SiO_2	63.20	56.94	60.36	64.09	59.46	64.91	67.00	64.40	66.18	65.42
TiO_2	-	-	-	-	0.20	-	-	-	-	0.23
Al_2O_3	21.76	24.13	23.28	18.97	23.87	19.22	19.31	21.22	20.02	20.63
FeO_T	0.52	1.93	0.54	0.67	1.16	0.57	-	0.48	0.81	0.75
MgO	-	0.79	-	-	-	-	-	-	-	-
CaO	2.10	1.40	0.69	0.84	2.79	0.39	0.40	2.31	0.74	1.70
Na_2O	8.75	9.74	8.07	5.24	8.88	4.51	6.94	8.03	7.22	7.81
K_2O	2.45	4.11	6.12	8.99	3.27	9.79	6.69	3.39	5.76	4.21
Total	98.78	99.04	99.06	98.80	99.63	99.39	100.34	99.83	100.73	100.75
Number of ions on the basis of 32 oxygen										
Si	11.454	10.599	11.220	11.749	10.806	11.850	11.939	11.504	11.707	11.606
Ti	-	-	-	-	0.029	-	-	-	-	0.032
Al	4.646	5.296	5.098	4.099	5.114	4.134	4.058	4.467	4.176	4.314
Fe^{2+}	0.080	0.301	0.083	0.102	0.176	0.086	-	0.070	0.122	0.112
Mg	-	0.221	-	-	-	-	-	-	-	-
Ca	0.406	0.282	0.138	0.166	0.544	0.077	0.077	0.442	0.141	0.323
Na	3.072	3.517	2.909	1.862	3.126	1.597	2.400	2.781	2.477	2.688
K	0.566	0.976	1.450	2.102	0.758	2.278	1.520	0.774	1.299	0.954
Cations	20.225	21.191	20.897	20.082	20.554	20.022	19.994	20.038	19.921	20.029
End-member compositions										
An	10.0	5.9	3.1	4.0	12.3	1.9	1.9	11.0	3.6	8.2
Ab	75.9	73.7	64.7	45.1	70.6	40.4	60.0	69.6	63.2	67.8
Or	14.0	20.4	32.2	50.9	17.1	57.7	38.0	19.4	33.2	24.1

A6.36 Microprobe analyses of nepheline in group B lavas

Table A6.36 Electron microprobe analyses of nepheline in group B lavas.

Rock Type	basanite																
Sample	SA12			SA27			SAB102		SAB128	SAB176	SAB177			SAB178	SAB179		SAB180
Analysis	1261-G	1266-G	1271-G	1324-G	1343-G	1344-G	402-G	403-G	725-G	658-G	1114-G	1153-G	1155-G	1191-G	590-G	598-G	1297-G
SiO_2	50.80	49.51	49.76	50.29	46.81	46.07	51.06	50.90	52.21	51.59	50.55	51.13	51.21	50.96	53.01	55.61	49.16
TiO_2	0.21	-	-	-	-	-	-	0.17	0.75	-	-	0.20	-	-	0.22	0.23	-
Al_2O_3	27.86	30.28	29.89	29.38	31.60	31.28	29.51	29.23	21.07	26.51	28.75	27.50	28.29	26.80	29.08	25.52	29.04
FeO_T	1.12	0.64	0.67	0.81	1.44	1.00	0.94	0.84	6.55	2.68	1.34	2.46	1.03	1.83	0.51	0.79	1.72
MgO	0.73	-	-	-	-	-	-	-	1.03	0.40	0.43	0.31	-	0.27	-	-	-
CaO	1.97	0.40	0.43	2.85	1.13	1.09	0.75	0.42	1.44	0.52	0.67	0.42	2.06	2.73	1.65	0.66	0.22
Na_2O	14.79	16.07	16.07	12.65	14.66	15.58	14.47	15.82	10.33	12.63	16.41	14.26	14.14	13.67	14.94	11.68	14.63
K_2O	1.83	2.59	2.33	2.64	3.22	3.51	2.21	2.44	5.44	4.35	2.15	2.50	1.98	2.56	1.37	5.48	3.91
Total	99.31	99.49	99.15	98.62	98.86	98.53	98.94	99.82	98.82	98.68	100.30	98.78	98.71	98.82	100.78	99.97	98.68
Number of ions on the basis of 32 oxygen																	
Si	9.517	9.277	9.341	9.566	9.182	8.893	9.651	9.482	9.994	9.859	9.341	9.705	9.540	9.676	9.677	10.294	9.363
Ti	0.029	-	-	-	-	-	-	0.026	0.109	-	-	0.029	-	-	0.032	0.032	-
Al	6.150	6.688	6.614	6.589	7.306	7.117	6.573	6.416	4.755	5.971	6.262	6.154	6.214	6.000	6.256	5.568	6.518
Fe^{2+}	0.176	0.102	0.106	0.128	0.237	0.163	0.147	0.131	1.046	0.429	0.208	0.390	0.160	0.291	0.080	0.122	0.275
Mg	0.205	-	-	-	-	-	-	-	0.294	0.115	0.118	0.086	-	0.077	-	-	-
Ca	0.394	0.080	0.086	0.582	0.237	0.224	0.150	0.083	0.294	0.106	0.134	0.086	0.413	0.557	0.323	0.131	0.045
Na	5.373	5.840	5.850	4.669	5.574	5.830	5.302	5.715	3.837	4.682	5.882	5.248	5.107	5.034	5.286	4.195	5.402
K	0.438	0.621	0.557	0.640	0.806	0.864	0.534	0.579	1.328	1.062	0.509	0.605	0.470	0.621	0.320	1.296	0.950
Cations	22.282	22.608	22.554	22.174	23.342	23.092	22.359	22.432	21.658	22.224	22.454	22.303	21.905	22.255	21.974	21.638	22.554
End-member compositions																	
Ne ($NaAlSiO_2$)	72.4	75.7	75.9	65.0	72.9	75.6	70.7	74.2	52.2	61.6	76.5	69.6	70.0	67.9	71.9	54.7	69.9
Ks ($KAlSiO_2$)	6.6	8.9	8.1	9.9	11.7	12.5	7.9	8.4	20.1	15.5	7.3	8.9	7.2	9.3	4.8	18.8	13.7
Q (SiO_2)	21.0	15.4	16.0	25.0	15.4	12.0	21.4	17.4	27.7	22.9	16.2	21.5	22.9	22.9	23.3	26.5	16.4

Nepheline in group B lavas (continued)

Table A6.36 Electron microprobe analyses of nepheline in group B lavas (continued).

Rock Type	alkali ol-basalt				ne-hawaiite								
Sample	SA54	SAB207			SA29					SA65			
Analysis	1696-G	1627-G	1628-G	1629-G	157-G	447-G	448-G	450-G	451-G	1554-G	1555-G	1563-G	1564-G
SiO_2	51.62	50.86	50.50	50.99	51.53	53.95	48.96	56.35	55.97	56.91	55.97	55.13	55.74
TiO_2	-	-	-	-	-	0.20	-	-	-	-	-	0.34	-
Al_2O_3	27.86	29.97	30.34	30.20	28.74	27.82	30.45	25.22	25.75	25.54	24.08	24.95	26.10
FeO_T	1.43	0.58	0.62	0.61	0.63	1.05	1.32	0.86	0.58	1.14	2.31	2.03	1.01
MgO	0.34	-	0.30	0.28	-	-	-	-	-	0.31	0.37	0.49	-
CaO	0.48	0.50	0.41	0.43	0.13	0.48	0.14	0.70	0.33	1.71	0.58	1.23	0.68
Na_2O	15.34	15.75	16.37	15.85	16.03	13.84	16.12	10.29	12.39	12.41	11.04	11.62	13.93
K_2O	1.64	2.34	2.45	2.37	2.02	2.75	3.13	5.29	3.93	1.70	5.30	2.91	2.20
Total	98.71	100.00	100.99	100.73	99.08	100.09	100.12	98.71	98.95	99.72	99.65	98.70	99.66
Number of ions on the basis of 32 oxygen													
Si	9.914	9.437	9.210	9.342	9.607	9.923	9.181	10.661	10.423	10.626	10.679	10.272	10.246
Ti	-	-	-	-	-	0.029	-	-	-	-	-	0.048	-
Al	6.307	6.554	6.522	6.522	6.317	6.032	6.730	5.626	5.651	5.622	5.418	5.478	5.654
Fe^{2+}	0.230	0.090	0.093	0.093	0.099	0.160	0.208	0.134	0.090	0.179	0.368	0.317	0.154
Mg	0.096	-	0.080	0.077	-	-	-	-	-	0.086	0.106	0.134	-
Ca	0.099	0.099	0.080	0.083	0.026	0.093	0.029	0.141	0.067	0.342	0.118	0.246	0.134
Na	5.712	5.667	5.786	5.632	5.795	4.938	5.862	3.776	4.474	4.496	4.083	4.198	4.966
K	0.400	0.554	0.570	0.554	0.480	0.646	0.749	1.277	0.934	0.406	1.290	0.691	0.515
Cations	22.759	22.400	22.339	22.302	22.324	21.821	22.758	21.615	21.639	21.759	22.062	21.386	21.670
End-member compositions													
Ne ($NaAlSiO_2$)	73.6	74.2	75.9	74.3	75.0	66.0	75.4	49.9	58.7	61.1	52.7	58.0	65.8
Ks ($KAlSiO_2$)	5.8	8.1	8.3	8.1	6.9	9.6	10.7	18.8	13.6	6.1	18.5	10.6	7.6
Q (SiO_2)	20.6	17.7	15.7	17.5	18.1	24.5	13.9	31.3	27.7	32.8	28.8	31.4	26.6

Table A6.36 Electron microprobe analyses of nepheline in group B lavas (continued).

Rock Type	nephelinite									
Sample	SA21		SA28				SA51			
Analysis	1411-G	1412-G	1415-G	1427-G	1429-G	1446-G	1464-G	1465-G	1466-G	1475-G
SiO_2	50.84	52.16	46.32	49.93	42.94	43.78	5-	50.35	50.93	50.56
TiO_2	0.26	0.43	-	-	-	-	-	-	-	-
Al_2O_3	28.83	26.85	31.90	28.91	35.00	33.05	28.99	28.70	29.20	28.70
FeO_T	1.27	1.29	0.92	0.93	0.97	1.12	1.17	0.93	1.05	1.85
MgO	0.45	0.42	0.41	0.55	0.34	-	0.34	0.27	-	0.25
CaO	1.15	0.55	0.22	0.74	0.17	-	0.49	0.20	0.34	1.04
Na_2O	13.51	14.60	15.87	14.15	16.20	16.85	15.45	15.54	15.86	14.07
K_2O	2.59	2.53	3.25	4.86	4.50	4.46	2.75	2.56	2.56	2.26
Total	98.90	98.83	98.89	100.07	100.12	99.26	99.19	98.55	99.94	98.73
Number of ions on the basis of 32 oxygen										
Si	9.673	9.905	8.870	9.389	8.189	8.435	9.411	9.504	9.488	9.549
Ti	0.038	0.061	-	-	-	-	-	-	-	-
Al	6.464	6.010	7.200	6.406	7.866	7.504	6.432	6.387	6.413	6.387
Fe^{2+}	0.202	0.205	0.147	0.144	0.154	0.182	0.186	0.147	0.163	0.291
Mg	0.128	0.122	0.115	0.154	0.096	-	0.096	0.074	-	0.070
Ca	0.237	0.112	0.045	0.150	0.035	-	0.099	0.038	0.067	0.211
Na	4.986	5.376	5.891	5.162	5.990	6.294	5.638	5.690	5.731	5.152
K	0.630	0.611	0.794	1.165	1.094	1.098	0.659	0.614	0.608	0.544
Cations	22.358	22.401	23.062	22.570	23.424	23.514	22.522	22.454	22.470	22.205
End-member compositions										
Ne ($NaAlSiO_2$)	67.4	69.8	76.6	66.6	78.1	79.2	73.4	73.7	74.1	69.8
Ks ($KAlSiO_2$)	9.5	8.8	11.5	16.7	15.9	15.3	9.6	8.9	8.7	8.2
Q (SiO_2)	23.1	21.4	11.9	16.7	6.0	5.5	17.0	17.4	17.2	22.0

A6.37 Microprobe analyses of chromian titanomagnetite and Cr-bearing titanomagnetite in group B lavas

Table A6.37 Electron microprobe analyses of chromian titanomagnetite and Cr-bearing titanomagnetite in group B lavas.

Rock Type	alkali ol-basalt							ne-hawaiite						basanite					
Sample	SA54	SAB188		SAB207				SA25		SA65				SA12					
Analysis	1694-G	1652-G	1658-G	1597-I	1600-I	1604-I	1608-I	1506-I	1509-I	1541-I	1561-I	1566-I	1568-G	1243-I	1246-I	1247-I	1250-I	1251-I	1268-I
host crystal				ol	ol	ol	ol	cpx	cpx	ol	ol	ol		ol	ol	ol	ol	ol	ol
analysis no.				1598-C1	1601-C	1605-C3	1609-C4a	1507-C1	1510-C2	1542-C	1562-C	1567-C		1244-C1	1248-C	1248-C	1252-C	1252-C	1269-C2
SiO_2	0.86	0.88	0.62	0.48	0.52	0.61	0.37	0.64	0.39	0.50	0.54	0.95	0.50	0.50	0.46	0.61	0.62	0.67	0.47
TiO_2	26.87	28.38	27.24	21.72	17.07	8.74	6.65	18.08	19.64	20.18	14.39	17.69	20.66	24.55	2.01	1.83	7.23	9.12	23.41
Al_2O_3	2.51	1.29	0.95	4.35	7.49	16.68	19.92	4.72	3.95	3.62	5.81	4.41	2.83	4.58	33.66	34.34	13.54	12.04	4.62
Cr_2O_3	0.52	0.24	0.28	5.55	7.31	15.35	15.16	2.41	0.31	1.12	7.47	3.37	0.29	3.36	20.89	20.58	18.57	14.55	3.96
FeO_T	64.87	66.37	66.35	62.50	58.50	46.13	45.67	66.74	67.87	67.86	64.73	67.24	71.31	61.22	28.31	27.18	48.43	52.08	61.33
MnO	0.59	0.75	0.60	0.59	0.38	-	0.30	0.31	0.32	0.67	0.36	0.62	0.74	0.63	-	-	0.37	0.52	0.64
MgO	2.20	1.53	1.98	2.77	5.75	7.24	7.96	3.90	4.50	2.75	4.40	3.49	0.97	2.62	12.80	13.29	6.06	5.56	2.48
CaO	-	0.40	0.36	-	-	0.14	-	0.45	0.50	-	-	-	0.22	0.15	-	-	0.41	0.65	-
Total	98.42	99.84	98.38	97.96	97.02	94.89	96.03	97.25	97.48	96.70	97.70	97.77	97.52	97.61	98.13	97.83	95.23	95.19	96.91
Number of ions on the basis of 32 oxygen																			
Si	0.259	0.266	0.192	0.144	0.157	0.173	0.102	0.202	0.122	0.160	0.166	0.294	0.160	0.150	0.112	0.147	0.186	0.202	0.144
Ti	6.147	6.451	6.330	4.970	3.859	1.878	1.395	4.243	4.621	4.832	3.366	4.147	5.005	5.584	0.368	0.336	1.606	2.058	5.389
Al	0.899	0.461	0.349	1.562	2.656	5.616	6.557	1.734	1.459	1.360	2.131	1.619	1.072	1.632	9.690	9.840	4.710	4.259	1.667
Cr	0.125	0.058	0.067	1.334	1.738	3.469	3.347	0.595	0.077	0.282	1.837	0.832	0.074	0.803	4.035	3.955	4.336	3.453	0.957
Fe^{2+}	16.499	16.774	17.149	15.901	14.707	11.024	10.666	17.421	17.754	18.067	16.842	17.536	19.210	15.485	5.782	5.526	11.958	13.082	15.702
Mn	0.150	0.192	0.157	0.150	0.096	-	0.070	0.080	0.086	0.179	0.096	0.163	0.202	0.160	-	-	0.093	0.131	0.166
Mg	0.998	0.691	0.912	1.254	2.579	3.085	3.315	1.814	2.096	1.306	2.042	1.619	0.467	1.181	4.662	4.816	2.669	2.486	1.130
Ca	-	0.131	0.118	-	-	0.042	-	0.150	0.166	-	-	-	0.077	0.048	-	-	0.128	0.208	-
Cations	25.078	25.024	25.274	25.315	25.792	25.286	25.453	26.240	26.381	26.186	26.480	26.211	26.266	25.043	24.650	24.621	25.686	25.878	25.155
Recalculated Fe ions and Fe oxides																			
Fe^{2+}	13.038	13.469	13.060	11.750	9.239	7.207	6.404	10.470	10.376	11.217	9.270	10.658	12.032	12.174	3.943	3.773	6.971	7.487	12.042
Fe^{3+}	2.752	2.619	3.225	3.325	4.447	3.256	3.653	5.463	5.776	5.342	5.994	5.399	5.520	2.666	1.687	1.614	4.202	4.645	2.939
FeO	53.56	55.57	53.21	48.71	39.49	31.78	29.08	43.86	43.60	45.97	39.31	44.63	48.88	50.22	19.83	19.04	30.22	32.14	49.30
Fe_2O_3	12.56	12.01	14.60	15.32	21.12	15.95	18.44	25.43	26.97	24.33	28.25	25.13	24.92	12.22	9.42	9.05	20.24	22.16	13.37
End-member composition																			
mol.% Usp	84.2	84.0	79.4	80.8	71.0	71.4	61.0	61.0	58.9	65.4	57.4	62.1	65.2	87.1	63.6	62.8	60.8	60.6	85.5
Atomic percentages																			
$Cr^{\#}$	12.2	11.1	16.2	46.1	39.5	38.2	33.8	25.5	5.0	17.2	46.3	33.9	6.4	33.0	29.4	28.7	47.9	44.8	36.5
$Mg^{\#}$	6.8	4.7	6.2	9.2	20.6	28.9	32.8	13.7	15.5	9.6	16.6	12.2	3.4	8.5	53.5	55.4	26.3	23.5	8.2
$Fe^{\#}$	73.7	84.0	89.1	54.8	52.1	27.4	28.1	71.9	80.5	78.0	62.5	70.6	84.1	53.3	11.2	10.7	33.2	39.4	54.0

Table A6.37 Electron microprobe analyses of chromian titanomagnetite and Cr-bearing titanomagnetite in group B lavas (continued).

Rock Type	basanite (continued)																		
Sample	SA27		SAB204		SA37					SAB175						SAB176			
Analysis	1347-I	1348-I	1351-I	1365-I	835-I	912-I	836-G	848-G	899-G	1196-I	1198-I	1032-G	1036-G	1048-G	1052-G	1206-I	1220-I	1222-I	1223-I
host crystal	ol	ol	ol	ol	ol	ol				cpx	ol					cpx	ol	ol	ol
analysis no.	1346-C5	1346-C6	1352-C1	1367-C3	838-C1	913-C5				1197-C	1199-C					1207-C	1221-C	1224-C	1224-C
SiO_2	0.56	0.39	0.54	1.06	0.65	0.80	0.49	0.58	0.57	1.06	0.53	0.47	0.45	0.46	0.47	0.80	0.76	0.49	2.10
TiO_2	14.70	17.22	2.43	2.48	10.14	2.81	20.61	17.03	21.36	5.58	13.16	24.16	24.19	24.56	24.40	8.14	3.65	2.04	2.29
Al_2O_3	6.59	4.13	30.43	30.38	12.52	28.39	6.09	7.26	5.76	17.94	10.40	4.38	4.86	4.28	4.69	13.56	24.07	31.59	32.15
Cr_2O_3	5.21	2.79	20.81	20.41	15.05	21.76	0.22	5.10	0.25	20.17	14.08	0.27	0.26	0.29	0.24	17.18	22.11	22.90	21.55
FeO_T	62.33	66.13	32.48	31.31	49.56	31.14	64.36	61.37	65.83	42.38	53.58	64.99	64.86	66.24	66.22	50.12	36.06	29.04	27.47
MnO	0.33	0.66	-	-	0.53	-	0.54	0.45	0.55	-	0.61	0.76	0.68	0.72	0.83	0.40	-	-	-
MgO	5.42	3.92	11.27	12.58	7.61	12.09	3.15	4.27	2.94	9.23	4.24	1.94	1.98	1.78	2.09	5.46	10.59	12.40	12.80
CaO	-	-	-	-	-	-	0.27	-	0.44	0.66	-	0.34	0.15	0.17	0.18	0.69	0.16	-	0.16
Total	95.14	95.24	97.96	98.22	96.06	96.99	95.73	96.06	97.70	97.02	96.60	97.31	97.43	98.50	99.12	96.35	97.40	98.46	98.52
Number of ions on the basis of 32 oxygen																			
Si	0.176	0.125	0.134	0.262	0.189	0.202	0.150	0.176	0.173	0.294	0.160	0.147	0.138	0.141	0.141	0.234	0.198	0.122	0.509
Ti	3.485	4.186	0.461	0.464	2.221	0.538	4.851	3.952	4.938	1.155	2.944	5.613	5.590	5.651	5.562	1.792	0.720	0.378	0.416
Al	2.448	1.571	9.024	8.902	4.301	8.506	2.246	2.640	2.090	5.830	3.645	1.594	1.763	1.542	1.677	4.678	7.446	9.178	9.168
Cr	1.299	0.714	4.141	4.013	3.469	4.374	0.054	1.245	0.061	4.397	3.312	0.067	0.064	0.070	0.058	3.978	4.589	4.461	4.122
Fe^{2+}	16.429	17.882	6.835	6.512	12.083	6.618	16.842	15.834	16.922	9.773	13.328	16.787	16.672	16.944	16.781	12.269	7.917	5.987	5.558
Mn	0.086	0.179	-	-	0.131	-	0.144	0.118	0.141	-	0.154	0.198	0.176	0.186	0.214	0.099	-	-	-
Mg	2.544	1.888	4.227	4.662	3.309	4.579	1.469	1.962	1.347	3.792	1.878	0.896	0.906	0.813	0.944	2.381	4.147	4.557	4.614
Ca	-	-	-	-	-	-	0.090	-	0.144	0.195	-	0.112	0.048	0.058	0.058	0.214	0.045	-	0.042
Cations	26.467	26.544	24.822	24.816	25.702	24.816	25.846	25.926	25.814	25.437	25.421	25.414	25.357	25.405	25.434	25.645	25.062	24.682	24.429
Recalculated Fe ions and Fe oxides																			
Fe^{2+}	8.931	10.034	4.488	4.193	7.044	4.296	11.066	9.902	11.234	5.606	9.006	12.291	12.355	12.468	12.227	7.377	4.868	4.054	4.337
Fe^{3+}	5.966	6.134	2.120	2.104	4.239	2.104	4.572	4.755	4.498	3.615	3.577	3.562	3.425	3.539	3.607	4.105	2.713	1.767	1.123
FeO	37.37	41.04	22.06	20.85	30.94	20.90	45.54	41.46	47.01	25.76	38.35	50.39	50.78	51.60	51.13	32.20	23.16	20.22	21.82
Fe_2O_3	27.74	27.88	11.58	11.63	20.69	11.38	20.91	22.13	20.92	18.46	16.93	16.23	15.64	16.27	16.77	19.91	14.34	9.80	6.28
End-member composition																			
mol.% Usp	56.7	58.2	60.6	-	64.6	62.5	71.7	69.3	72.2	-	78.4	79.7	81.0	80.0	79.5	64.4	59.5	62.9	-
Atomic percentages																			
$Cr^{\#}$	34.7	31.2	31.5	31.1	44.6	34.0	2.4	32.0	2.8	43.0	47.6	4.0	3.5	4.4	3.3	46.0	38.1	32.7	31.0
$Mg^{\#}$	20.5	14.5	47.7	51.8	30.5	50.8	11.0	15.5	10.0	39.0	16.5	6.4	6.5	5.8	6.8	23.2	44.9	52.2	51.1
$Fe^{\#}$	63.7	74.8	14.3	14.4	36.9	14.5	68.2	56.9	69.2	27.3	35.3	69.4	66.4	69.9	68.8	33.6	19.1	11.8	7.9

Table A6.37 Electron microprobe analyses of chromian titanomagnetite and Cr-bearing titanomagnetite in group B lavas(continued).

Rock Type	basanite (continued)													
Sample	SAB177						SAB178			SAB179			SAB180	
Analysis	1121-I	1122-I	1125-I	1126-I	1128-I	1134-I	1162-G	1165-G	1190-G	1228-I	1227-G	1230-G	1300-I	1299-G
host crystal	ol	ol	ol	ol	ol	ol				ol			ol	ol
analysis no.	1124-C	1124-C	1127-C	1127-C	1129-C	1136-C				1229-C			1301-C2	
SiO_2	0.52	0.70	0.73	0.60	0.59	0.52	0.63	0.51	0.62	0.58	0.45	0.45	0.83	0.46
TiO_2	2.35	2.65	2.28	2.32	2.21	5.42	20.79	19.76	21.04	3.59	26.87	24.01	2.38	25.07
Al_2O_3	30.48	30.90	30.52	30.25	31.18	18.16	6.34	6.59	6.07	29.55	2.77	4.88	32.20	4.11
Cr_2O_3	21.20	19.83	21.50	21.43	21.71	21.83	0.22	0.80	0.43	23.64	0.23	0.27	21.84	0.27
FeO_T	31.37	31.56	29.62	30.04	31.08	44.36	66.15	66.00	66.16	29.03	64.48	62.60	28.28	65.00
MnO	-	-	-	-	-	-	0.60	0.60	0.58	-	0.72	0.58	-	0.64
MgO	12.12	12.37	12.51	12.29	12.15	7.01	2.35	3.17	1.70	11.57	2.36	4.57	11.84	2.22
CaO	-	-	-	-	-	-	0.55	0.15	0.27	0.18	-	0.32	-	-
Total	98.04	98.01	97.16	96.93	98.92	97.30	97.63	97.58	96.87	98.14	97.88	97.68	97.37	97.77
Number of ions on the basis of 32 oxygen														
Si	0.128	0.173	0.182	0.150	0.144	0.144	0.195	0.157	0.192	0.144	0.138	0.138	0.205	0.141
Ti	0.442	0.496	0.429	0.438	0.410	1.136	4.816	4.576	4.925	0.672	6.186	5.453	0.445	5.779
Al	8.989	9.082	9.011	8.982	9.082	5.968	2.301	2.394	2.230	8.669	1.002	1.738	9.389	1.485
Cr	4.195	3.907	4.256	4.269	4.243	4.813	0.051	0.192	0.106	4.653	0.058	0.064	4.272	0.064
Fe^{2+}	6.563	6.579	6.205	6.326	6.422	10.346	17.034	16.992	17.226	6.042	16.506	15.808	5.850	16.656
Mn	-	-	-	-	-	-	0.157	0.157	0.150	-	0.186	0.147	-	0.166
Mg	4.522	4.595	4.669	4.614	4.477	2.915	1.082	1.456	0.790	4.294	1.078	2.058	4.365	1.014
Ca	-	-	-	-	-	-	0.179	0.051	0.090	0.048	-	0.102	-	-
Cations	24.838	24.832	24.752	24.781	24.778	25.322	25.814	25.974	25.709	24.522	25.152	25.507	24.525	25.306
Recalculated Fe ions and Fe oxides														
Fe^{2+}	4.181	4.214	4.072	4.111	4.212	6.465	11.338	10.836	11.827	4.552	12.818	11.092	4.355	12.495
Fe^{3+}	2.160	2.144	1.944	2.017	2.009	3.340	4.498	4.865	4.254	1.361	2.931	3.782	1.370	3.302
FeO	20.68	20.92	20.05	20.15	21.05	29.25	47.36	45.55	48.66	22.35	52.48	46.68	21.51	51.41
Fe_2O_3	11.88	11.83	10.64	10.99	11.15	16.79	20.88	22.73	19.45	7.43	13.34	17.69	7.52	15.10
End-member composition														
mol.% Usp	57.3	59.8	60.6	59.6	59.0	64.6	72.6	69.4	75.1	84.1	83.2	76.6	77.6	81.5
Atomic percentages														
$Cr^{\#}$	31.8	30.1	32.1	32.2	31.8	44.6	2.2	7.4	4.5	34.9	5.4	3.6	31.3	4.1
$Mg^{\#}$	51.1	51.3	52.6	52.1	50.7	29.9	8.1	11.0	5.9	48.0	7.4	14.9	49.5	7.1
$Fe^{\#}$	14.5	14.6	13.1	13.6	13.5	24.6	67.3	67.1	66.1	9.5	74.4	69.0	9.3	69.2

Table A6.37 Electron microprobe analyses of chromian titanomagnetite and Cr-bearing titanomagnetite in group B lavas(continued).

Rock Type	nephelinite													
Sample	SA21						SA28					SA51		
Analysis	1381-I	1384-I	1399-I	1389-G	1395-G	1409-G	1420-I	1430-I	1433-I	1434-I	1428-G	1469-I	1448-G	1460-G
host crystal	ol	ol	ol				ol	ol	ol	ol		ol		
analysis no.	1382-C1	1385-C2	1400-C4				1421-C1	1431-C2	1435-C3	1435-C4		1470-C5		
SiO_2	0.61	0.58	0.51	0.34	0.41	0.54	0.40	0.41	0.57	0.36	0.66	0.75	0.64	0.55
TiO_2	19.10	11.60	4.75	19.97	21.01	20.44	13.02	12.48	11.59	11.85	22.88	10.86	23.67	20.11
Al_2O_3	6.11	11.73	23.31	6.23	5.75	5.76	6.57	6.19	7.89	7.42	0.62	9.35	3.98	5.18
Cr_2O_3	0.59	12.61	18.50	0.74	0.50	0.44	9.00	11.48	12.29	11.23	0.78	11.55	1.15	1.89
FeO_T	62.06	53.09	40.75	63.98	64.44	63.35	61.80	62.85	59.00	60.59	68.30	57.53	65.39	66.03
MnO	-	0.32	-	0.35	0.48	0.45	0.35	0.54	0.31	0.42	0.90	0.41	0.79	0.70
MgO	5.84	6.09	8.90	5.48	3.72	3.67	4.54	4.08	4.93	4.68	2.14	6.23	1.68	1.69
CaO	0.64	-	-	0.14	0.24	0.36	-	-	-	-	-	-	-	0.24
Total	94.95	96.02	96.72	97.23	96.55	95.01	95.68	98.03	96.58	96.55	96.28	96.68	97.30	96.39
Number of ions on the basis of 32 oxygen														
Si	0.192	0.173	0.138	0.106	0.128	0.170	0.125	0.128	0.176	0.112	0.214	0.227	0.198	0.176
Ti	4.474	2.582	0.960	4.589	4.880	4.816	3.078	2.909	2.669	2.768	5.571	2.458	5.523	4.774
Al	2.243	4.096	7.382	2.243	2.093	2.128	2.435	2.259	2.845	2.720	0.237	3.318	1.456	1.930
Cr	0.144	2.954	3.926	0.179	0.122	0.109	2.237	2.813	2.973	2.758	0.198	2.749	0.282	0.474
Fe^{2+}	16.163	13.149	9.155	16.349	16.643	16.598	16.250	16.291	15.104	15.741	18.496	14.490	16.966	17.434
Mn	-	0.080	-	0.090	0.125	0.118	0.093	0.141	0.080	0.112	0.246	0.106	0.208	0.189
Mg	2.710	2.688	3.565	2.496	1.709	1.712	2.128	1.885	2.250	2.170	1.034	2.797	0.778	0.794
Ca	0.214	-	-	0.045	0.077	0.122	-	-	-	-	-	-	-	0.080
Cations	26.141	25.722	25.126	26.096	25.776	25.773	26.346	26.426	26.096	26.381	25.997	26.144	25.411	25.850
Recalculated Fe ions and Fe oxides														
Fe^{2+}	9.598	7.985	5.876	9.895	11.087	11.054	9.105	8.921	8.750	8.544	12.160	8.053	12.470	11.607
Fe^{3+}	5.241	4.284	2.869	5.140	4.410	4.402	5.698	5.875	5.140	5.776	4.916	5.248	3.554	4.579
FeO	40.14	34.55	27.38	42.11	46.10	45.31	38.01	37.90	37.17	36.15	48.64	34.83	50.89	47.35
Fe_2O_3	24.36	20.60	14.86	24.31	20.38	20.05	26.44	27.73	24.26	27.16	21.85	25.23	16.12	20.76
End-member composition														
mol.% Usp	63.5	68.3	62.3	65.4	71.0	70.6	57.1	57.1	59.0	56.7	67.4	55.2	80.0	72.6
Atomic percentages														
$Cr^{\#}$	6.0	41.9	34.7	7.4	5.5	4.9	47.9	55.5	51.1	50.4	45.6	45.3	16.2	19.7
$Mg^{\#}$	20.6	23.9	36.7	18.8	12.5	12.6	17.6	16.1	19.1	18.8	7.3	24.2	5.6	6.0
$Fe^{\#}$	70.5	39.4	21.0	69.8	68.1	67.9	57.2	56.0	49.0	53.7	92.4	48.5	68.4	67.2

A6.38 Microprobe analyses of titanomagnetite in group B lavas

Table A6.38 Electron microprobe analyses of titanomagnetite in group B lavas.

Rock Type	alkali ol-basalt									basanite							
Sample	SA54			SAB188		SAB207				SA12			SA27				
Analysis	1671-G	1683-G	1684-G	1648-G	1649-G	1621-G	1623-G	1624-G	1625-G	1249-G	1254-G	1262-G	1328-G	1331-G	1332-G	1333-G	1337-G
SiO_2	0.39	0.52	0.59	0.39	0.46	0.49	1.02	0.64	0.51	0.61	0.55	0.55	0.54	0.43	0.43	0.49	0.56
TiO_2	27.50	27.91	26.34	27.42	26.84	24.34	25.08	24.51	25.46	22.40	21.67	21.85	18.65	18.67	19.06	19.26	18.83
Al_2O_3	1.83	1.40	1.35	1.16	1.23	2.52	1.94	1.76	2.34	4.26	4.00	4.37	3.74	3.62	3.55	3.58	3.65
FeO_T	66.77	65.69	65.59	66.67	67.50	68.35	66.64	67.98	67.72	66.46	68.32	66.85	67.32	68.29	68.50	68.30	68.34
MnO	0.74	0.54	0.81	0.78	0.66	0.67	0.67	0.62	0.60	0.72	0.92	0.68	0.61	0.64	0.66	0.63	0.73
MgO	1.99	1.79	0.98	1.70	1.79	2.12	2.02	2.10	1.96	1.66	1.06	1.52	3.44	3.40	3.57	3.67	3.31
CaO	0.13	0.17	0.17	0.16	0.13	0.30	0.40	0.29	0.15	0.41	0.15	0.23	-	0.12	-	-	-
Total	99.35	98.02	95.83	98.28	98.61	98.79	97.77	97.90	98.74	96.52	96.67	96.05	94.30	95.17	95.77	95.93	95.42
Number of ions on the basis of 32 oxygen																	
Si	0.118	0.160	0.189	0.122	0.141	0.150	0.317	0.198	0.157	0.192	0.176	0.176	0.176	0.141	0.141	0.157	0.182
Ti	6.282	6.451	6.317	6.371	6.253	5.674	5.843	5.779	5.910	5.309	5.194	5.222	4.595	4.576	4.634	4.662	4.595
Al	0.656	0.509	0.506	0.422	0.451	0.918	0.710	0.650	0.851	1.581	1.504	1.635	1.443	1.392	1.354	1.360	1.398
Fe^{2+}	16.960	16.886	17.488	17.222	17.488	17.715	17.267	17.827	17.482	17.514	18.211	17.766	18.445	18.611	18.522	18.390	18.544
Mn	0.192	0.141	0.218	0.205	0.173	0.176	0.176	0.163	0.157	0.192	0.246	0.186	0.170	0.176	0.179	0.173	0.202
Mg	0.899	0.822	0.467	0.781	0.826	0.982	0.931	0.979	0.902	0.781	0.502	0.723	1.677	1.651	1.722	1.760	1.603
Ca	0.042	0.058	0.058	0.051	0.045	0.099	0.131	0.096	0.051	0.141	0.051	0.080	-	0.042	-	-	-
Cations	25.149	25.027	25.242	25.174	25.376	25.715	25.376	25.693	25.510	25.709	25.885	25.789	26.506	26.589	26.550	26.502	26.525
Recalculated Fe ions and Fe oxides																	
Fe^{2+}	13.262	13.567	13.480	13.433	13.069	12.265	12.861	12.436	12.657	12.096	12.225	12.095	10.651	10.568	10.595	10.611	10.687
Fe^{3+}	2.924	2.627	3.148	2.986	3.470	4.269	3.470	4.217	3.789	4.254	4.660	4.439	6.050	6.231	6.148	6.043	6.092
FeO	54.71	55.03	53.17	54.55	53.34	50.70	52.48	50.77	52.12	49.17	49.46	48.90	42.93	42.96	43.35	43.52	43.53
Fe_2O_3	13.40	11.84	13.80	13.47	15.74	19.61	15.74	19.13	17.34	19.22	20.95	19.95	27.10	28.15	27.95	27.54	27.57
End-member composition																	
mol.% Usp	80.8	82.7	80.7	79.8	78.0	73.1	-	72.8	76.7	74.5	71.7	73.3	59.1	57.9	58.4	59.1	58.9

Table A6.38 Electron microprobe analyses of titanomagnetite in group B lavas(continued).

Rock Type	basanite (continued)																			
Sample	SAB102	SAB111		SAB128	SAB204			SA37		SAB175	SAB176					SAB177				SAB178
Analysis	85-G	292-G	300-G	328-G	1357-G	1359-G	1374-G	900-G	904-G	1195-G	305-G	311-G	1214-G	1217-G	1219-G	1156-G	1157-G	1158-G	1159-G	1167-G
SiO_2	0.47	0.50	0.43	0.42	0.96	0.38	0.44	0.56	0.54	0.55	0.47	0.94	0.51	0.54	0.50	0.69	0.52	0.56	0.65	0.70
TiO_2	23.73	20.57	21.03	19.43	21.62	20.97	21.08	21.13	20.68	24.28	23.32	23.38	23.15	23.87	23.10	22.19	22.73	21.86	22.07	21.19
Al_2O_3	1.71	6.33	5.98	6.37	5.24	5.76	5.93	5.85	6.18	4.00	3.86	2.84	3.75	4.04	3.98	4.37	4.29	4.76	2.90	6.35
FeO_T	69.73	64.07	65.19	64.44	65.91	65.33	65.16	65.22	64.62	66.19	67.86	67.83	66.15	66.08	66.06	67.66	66.42	67.35	67.83	65.99
MnO	0.68	0.45	0.47	0.54	0.52	0.57	0.57	0.51	0.56	0.79	0.84	0.73	0.95	0.84	0.81	0.69	0.90	0.82	0.84	0.72
MgO	1.74	5.35	4.49	4.94	2.38	3.07	3.92	2.83	3.89	1.05	1.02	0.93	1.00	1.63	1.49	1.26	1.39	1.45	1.20	1.68
CaO	0.16	0.15	-	0.14	0.32	0.30	0.32	0.19	0.25	0.18	-	0.43	0.40	0.35	0.45	0.43	0.17	0.33	0.34	0.45
Total	98.22	97.42	97.59	96.28	96.95	96.38	97.42	96.29	96.72	97.04	97.37	97.08	95.91	97.35	96.39	97.29	96.42	97.13	95.83	97.08
Number of ions on the basis of 32 oxygen																				
Si	0.147	0.150	0.134	0.128	0.298	0.118	0.134	0.176	0.166	0.173	0.147	0.298	0.163	0.166	0.157	0.218	0.163	0.176	0.208	0.214
Ti	5.635	4.704	4.835	4.531	5.043	4.925	4.867	4.954	4.800	5.702	5.510	5.555	5.542	5.584	5.478	5.235	5.398	5.158	5.354	4.938
Al	0.637	2.269	2.154	2.326	1.917	2.118	2.147	2.150	2.246	1.472	1.427	1.059	1.408	1.478	1.478	1.616	1.594	1.760	1.104	2.320
Fe^{2+}	18.413	16.288	16.662	16.714	17.101	17.059	16.730	17.005	16.682	17.286	17.834	17.923	17.616	17.187	17.430	17.754	17.536	17.680	18.294	17.101
Mn	0.182	0.118	0.122	0.141	0.138	0.150	0.147	0.134	0.144	0.208	0.224	0.195	0.256	0.221	0.218	0.182	0.240	0.218	0.230	0.189
Mg	0.819	2.426	2.048	2.285	1.101	1.427	1.795	1.315	1.789	0.490	0.477	0.435	0.474	0.755	0.704	0.589	0.653	0.678	0.576	0.774
Ca	0.054	0.048	-	0.048	0.106	0.102	0.102	0.064	0.080	0.058	-	0.147	0.138	0.115	0.154	0.144	0.058	0.109	0.118	0.150
Cations	25.888	26.003	25.955	26.173	25.702	25.901	25.923	25.798	25.907	25.389	25.619	25.613	25.597	25.507	25.619	25.738	25.642	25.779	25.885	25.686
Recalculated Fe ions and Fe oxides																				
Fe^{2+}	12.402	10.103	10.586	10.013	11.729	11.110	10.740	11.358	10.742	12.840	12.662	12.765	12.525	12.390	12.284	12.234	12.316	12.043	12.302	11.776
Fe^{3+}	4.667	4.930	4.821	5.313	4.239	4.697	4.748	4.461	4.711	3.501	4.045	4.030	3.992	3.782	4.045	4.321	4.097	4.417	4.660	4.202
FeO	50.66	43.06	44.79	42.10	48.41	45.92	45.18	46.83	44.92	52.01	51.43	51.55	50.16	50.63	49.70	5-	49.84	49.28	49.19	48.64
Fe_2O_3	21.19	23.35	22.67	24.83	19.44	21.57	22.20	20.44	21.89	15.76	18.26	18.09	17.77	17.17	18.19	19.62	18.43	20.09	20.71	19.29
End-member composition																				
mol.% Usp	69.9	66.9	68.8	64.1	74.1	70.8	69.6	69.8	69.9	80.3	76.3	75.2	76.6	77.8	75.9	74.0	75.8	73.4	70.8	75.4

Table A6.38 Electron microprobe analyses of titanomagnetite in group B lavas(continued).

Rock Type	basanite (continued)								ne-hawaiite										nephelinite		
Sample	SAB179				SAB180				SA02			SA25			SA29		SA65		SA28		
Analysis	216-G	227-G	1225-G	1226-G	1286-G	1291-G	1304-G	1312-G	1488-G	1489-G	1490-G	1517-G	1518-G	1522-G	158-G	164-G	1548-G	1553-G	1416-G	1437-G	1447-G
SiO_2	0.58	0.44	0.51	0.47	0.44	0.63	0.46	0.45	0.38	0.49	0.41	0.44	0.50	0.38	0.50	0.60	0.37	0.47	0.42	0.35	0.65
TiO_2	25.17	25.56	27.32	26.83	25.64	25.58	25.63	25.57	20.91	20.77	20.51	22.27	22.17	22.42	21.71	19.79	20.36	20.25	19.23	21.26	21.53
Al_2O_3	2.83	3.63	1.73	1.03	3.58	3.73	3.61	3.62	3.92	3.98	3.75	1.66	1.24	2.24	2.17	1.82	3.52	2.56	0.63	0.52	0.23
FeO_T	67.13	66.35	66.12	66.76	64.80	64.39	64.88	65.36	65.27	66.47	66.27	71.43	71.83	71.41	70.56	72.18	69.70	71.14	73.40	71.75	66.32
MnO	0.90	0.79	0.71	0.96	0.85	0.83	0.83	0.76	0.51	0.55	0.53	0.65	0.67	0.72	0.77	0.72	0.70	0.70	0.78	0.84	0.80
MgO	1.25	1.97	1.62	1.17	1.84	1.77	1.71	1.91	4.40	3.84	4.14	0.85	0.63	1.09	1.04	0.72	1.92	1.13	1.48	1.14	0.60
CaO	-	0.14	-	0.15	0.19	0.14	-	-	0.13	0.16	0.15	0.30	0.15	-	0.13	0.28	0.45	0.35	0.14	-	0.42
Total	97.86	98.88	98.01	97.37	97.34	97.07	97.12	97.67	95.53	96.27	95.78	97.60	97.19	98.26	96.88	96.11	97.02	96.60	96.08	95.86	90.55
Number of ions on the basis of 32 oxygen																					
Si	0.179	0.134	0.157	0.147	0.134	0.195	0.141	0.138	0.123	0.158	0.132	0.141	0.163	0.122	0.160	0.198	0.118	0.154	0.141	0.115	0.224
Ti	5.891	5.859	6.352	6.352	5.955	5.939	5.968	5.920	5.012	4.980	4.954	5.402	5.430	5.373	5.286	4.931	4.886	4.970	4.858	5.309	5.635
Al	1.037	1.302	0.630	0.384	1.302	1.357	1.315	1.315	1.472	1.494	1.420	0.630	0.477	0.842	0.829	0.710	1.325	0.986	0.250	0.202	0.093
Fe^{2+}	17.478	16.909	17.098	17.574	16.736	16.624	16.800	16.832	17.398	17.724	17.792	19.277	19.562	19.034	19.101	20.006	18.595	19.411	20.618	19.930	19.296
Mn	0.237	0.205	0.186	0.256	0.224	0.218	0.218	0.198	0.139	0.148	0.145	0.179	0.186	0.195	0.211	0.202	0.189	0.192	0.221	0.237	0.237
Mg	0.579	0.896	0.749	0.547	0.845	0.816	0.787	0.877	2.088	1.827	1.982	0.410	0.304	0.515	0.506	0.358	0.912	0.550	0.742	0.566	0.314
Ca	-	0.048	-	0.051	0.064	0.045	-	-	0.042	0.055	0.052	0.102	0.051	-	0.045	0.099	0.154	0.122	0.051	-	0.157
Cations	25.402	25.354	25.171	25.312	25.261	25.194	25.229	25.280	26.273	26.386	26.476	26.141	26.173	26.080	26.138	26.506	26.179	26.384	26.880	26.358	25.955
Recalculated Fe ions and Fe oxides																					
Fe^{2+}	12.983	12.589	13.324	13.346	12.706	12.804	12.865	12.739	10.357	10.335	10.143	12.457	12.625	12.411	12.305	12.065	11.720	11.874	11.551	12.420	13.021
Fe^{3+}	3.531	3.417	2.978	3.317	3.194	3.032	3.117	3.241	5.536	5.786	5.985	5.241	5.313	5.104	5.234	6.050	5.327	5.783	6.857	5.726	4.821
FeO	52.77	52.19	54.04	53.47	51.78	52.06	52.23	52.11	42.53	42.61	41.68	50.28	50.55	50.60	49.50	48.07	47.92	47.84	46.06	49.11	48.40
Fe_2O_3	15.95	15.74	13.42	14.77	14.47	13.70	14.06	14.73	25.27	26.51	27.33	23.51	23.64	23.13	23.40	26.79	24.21	25.89	30.38	25.16	19.91
End-member composition																					
mol.% Usp	79.1	80.3	82.1	79.2	82.0	83.2	82.6	81.6	64.6	64.8	63.0	66.7	66.1	67.9	66.8	60.8	63.8	62.9	54.8	61.3	66.5

Table A6.38 Electron microprobe analyses of titanomagnetite in group B lavas(continued).

Rock Type	nephelinite (continued)						mugearite					
Sample	SA51		SAB113		SAB135		SA88					
Analysis	1461-G	1476-G	241-G	244-G	7-G	8-G	61-G	62-G	476-G	477-G	482-G	484-G
SiO_2	0.58	0.61	0.58	0.49	0.42	0.46	0.47	0.44	0.51	0.45	0.44	0.51
TiO_2	20.41	21.64	20.37	20.42	18.72	19.77	26.46	26.63	26.71	26.92	26.91	26.39
Al_2O_3	4.75	4.18	6.35	6.20	6.55	6.13	0.36	0.75	0.31	0.27	0.82	0.89
FeO_T	67.32	67.16	65.07	65.23	62.31	64.71	69.92	68.07	69.69	69.04	67.92	69.18
MnO	0.71	0.74	0.47	0.58	0.68	0.60	0.64	0.66	0.57	0.69	0.64	0.60
MgO	1.99	0.90	4.15	3.88	5.30	4.17	1.05	1.37	1.03	0.91	1.65	1.49
CaO	0.55	0.24	0.23	-	-	0.19	-	-	-	-	-	-
Total	96.31	95.47	97.22	96.80	93.98	96.03	98.90	97.92	98.82	98.28	98.38	99.06
Number of ions on the basis of 32 oxygen												
Si	0.182	0.198	0.176	0.150	0.134	0.144	0.147	0.138	0.160	0.144	0.138	0.157
Ti	4.877	5.232	4.701	4.749	4.451	4.640	6.243	6.294	6.301	6.381	6.310	6.176
Al	1.779	1.584	2.298	2.259	2.442	2.256	0.134	0.278	0.115	0.102	0.301	0.323
Fe^{2+}	17.888	18.054	16.698	16.864	16.480	16.883	18.349	17.894	18.275	18.192	17.712	17.997
Mn	0.192	0.202	0.122	0.150	0.182	0.160	0.170	0.176	0.154	0.182	0.170	0.157
Mg	0.941	0.432	1.898	1.789	2.496	1.939	0.493	0.643	0.480	0.429	0.768	0.691
Ca	0.189	0.083	0.074	-	-	0.064	-	-	-	-	-	-
Cations	26.048	25.786	25.965	25.962	26.186	26.086	25.536	25.424	25.485	25.430	25.398	25.501
Recalculated Fe ions and Fe oxides												
Fe^{2+}	11.450	12.372	10.591	10.754	9.763	10.414	13.395	13.307	13.482	13.569	13.213	13.171
Fe^{3+}	5.032	4.432	4.843	4.836	5.342	5.119	3.850	3.585	3.729	3.600	3.524	3.767
FeO	46.77	49.45	44.65	45.00	40.27	43.39	54.31	53.63	54.59	54.56	53.62	53.80
Fe_2O_3	22.84	19.68	22.69	22.49	24.49	23.70	17.35	16.05	16.78	16.09	15.89	17.10
End-member composition												
mol.% Usp	68.1	73.6	68.5	68.9	63.3	66.3	75.2	77.0	75.8	76.7	77.4	75.8

A6.39 Microprobe analyses of ilmenite in group B lavas

Table A6.39 Electron microprobe analyses of ilmenite in group B lavas.

Rock Type	mugearite				
Sample	SA88				
Analysis	479-G	480-G	481-G	483-G	485-G
SiO_2	0.44	0.47	0.62	0.37	0.38
TiO_2	51.17	51.35	50.27	51.37	51.18
Al_2O_3	-	-	-	0.27	-
FeO_T	45.63	45.38	44.17	45.10	45.59
MnO	0.61	0.60	0.61	0.68	0.65
MgO	2.28	2.28	2.40	2.22	2.00
CaO	-	0.13	0.54	-	-
Na_2O	-	-	-	-	-
Total	100.13	100.21	98.61	100.01	99.80
Number of ions on the basis of 6 oxygen					
Si	0.022	0.023	0.031	0.019	0.019
Ti	1.925	1.928	1.915	1.930	1.934
Al	-	-	-	0.016	-
Fe^{2+}	1.909	1.895	1.871	1.885	1.916
Mn	0.026	0.025	0.026	0.029	0.028
Mg	0.170	0.170	0.181	0.166	0.150
Ca	-	0.007	0.029	-	-
Na	-	-	-	-	-
Cations	4.052	4.049	4.054	4.044	4.046
Recalculated Fe ions and oxides					
Fe^{2+}	1.729	1.727	1.687	1.734	1.756
Fe^{3+}	0.155	0.145	0.159	0.131	0.138
FeO	41.87	41.87	40.37	41.94	42.28
Fe_2O_3	4.18	3.90	4.22	3.51	3.68
End-member composition					
mol.% Ilm	95.9	96.2	95.7	96.9	96.4

Appendix Seven: Whole-rock Geochemistry

Appendix 7

Whole-rock major and trace element and radiogenic isotope analyses

Whole-rock compositions for 203 SAVF samples were analysed by X-ray fluorescence (XRF) for abundances of the major elements (Si, Ti, Al, Fe, Mn, Mg, Ca, Na, K, and P) and 19 trace elements. Analyses for groups A and B are presented in Tables A7.1 and A7.2 respectively. Each table is organised according to rock type and sample number. Total Fe is reported as Fe_2O_3*. Magnesium numbers (Mg#) were calculated as $100Mg/(Mg + Fe^{2+})$ where the separate oxidation states of iron, FeO and Fe_2O_3, were derived from Fe_2O_3* and Fe_2O_3/FeO is adjusted to 0.20 (Middlemost, 1989).

High-precision whole-rock analyses were conducted on a subset of 34 samples for the abundances of 25 trace elements and each of the rare earth elements (REE), except promethium (Pm), either by spark source mass spectrometry (SSMS) or inductively coupled plasma mass spectrometry (ICP-MS) techniques.

Ratios for the radiogenic isotopes Sr and Nd for 36 samples, and Sm and Pb for a subset of 18 of these samples, were measured by thermal ionisation mass spectrometry (TIMS). Analyses for groups A and B are presented in Tables A7.3 and A7.4 respectively.

Details regarding analytical facilities, procedures, and instrument precision are given in Appendix 5.

Table A7.1 Whole-rock XRF-derived major and trace element data for selected group A samples.

Rock Type	alkali ol-basalt								hawaiite													
Sample	SA17	SA18	SA19	SA33	SA94	SAB159	SAB162	SAB168	SA11	SA14	SA20	SA30	SA32	SA44	SA47	SA52	SA69	SA70	SA74	SA78	SA85	SA87
SiO_2	46.24	47.33	47.87	47.28	47.98	47.10	48.38	47.29	47.74	49.05	48.94	47.18	47.51	47.52	46.87	47.59	48.36	45.68	48.41	48.88	48.39	47.68
TiO_2	2.25	2.29	2.62	2.13	2.41	2.93	3.09	2.94	2.48	1.65	2.17	2.19	1.92	2.00	2.08	2.64	2.31	2.22	2.16	2.16	1.90	2.33
Al_2O_3	13.73	14.02	15.30	13.38	15.43	15.81	16.53	15.83	15.70	14.33	15.01	14.41	13.01	14.04	13.44	15.45	14.07	13.94	14.91	13.75	14.07	14.28
Fe_2O_3*	14.96	13.75	13.34	13.87	13.51	13.68	11.49	13.40	13.67	13.30	13.38	14.73	14.13	13.93	14.05	13.79	13.70	16.77	13.75	13.01	13.78	13.65
MnO	0.18	0.19	0.17	0.18	0.19	0.19	0.16	0.19	0.19	0.18	0.16	0.16	0.16	0.18	0.18	0.18	0.17	0.35	0.18	0.17	0.19	0.17
MgO	10.05	8.76	6.91	10.55	6.31	5.94	5.56	6.12	6.25	9.51	6.81	7.89	10.31	9.43	9.93	6.43	8.32	6.10	7.92	8.89	8.79	8.88
CaO	9.47	9.40	10.04	9.35	10.15	9.45	9.94	9.67	9.59	9.38	9.26	8.58	8.56	9.25	8.50	9.87	8.72	8.53	8.71	9.22	9.47	9.23
Na_2O	3.14	3.31	3.22	3.02	3.33	3.45	3.47	3.30	3.33	2.95	3.23	2.94	2.80	3.01	2.80	3.20	3.10	2.81	3.11	3.12	2.96	3.01
K_2O	0.73	0.91	0.82	0.74	0.71	1.02	1.08	1.01	0.78	0.41	0.76	0.90	0.58	0.61	0.76	0.84	0.83	0.76	0.67	0.81	0.55	0.79
P_2O_5	0.35	0.50	0.36	0.33	0.40	0.48	0.51	0.49	0.41	0.19	0.29	0.38	0.27	0.27	0.31	0.38	0.32	0.32	0.26	0.29	0.26	0.33
Total	101.10	100.46	100.65	100.83	100.42	100.08	100.22	100.23	100.14	100.95	100.01	99.36	99.25	100.24	98.92	100.37	99.90	97.48	100.08	100.30	100.36	100.35
LOI	-0.94	-0.31	-0.51	-0.79	-0.36	-0.71	-0.19	-0.53	0.09	-0.69	0.16	0.43	0.57	-0.21	0.94	-0.19	0.22	2.08	0.02	-0.19	-0.21	-0.21
Mg#	61.1	60.0	54.9	64.1	52.4	50.7	53.3	51.9	51.9	62.6	54.6	56.1	63.6	61.5	62.9	52.4	59.0	47.1	57.7	61.7	60.1	60.5
trace elements (ppm)																						
Sc	24	20	24	23	27	19	24	22	27	27	23	20	19	27	23	24	24	21	24	23	24	25
V	227	228	254	216	248	256	310	263	238	201	224	224	185	228	225	255	220	203	221	222	205	233
Cr	278	242	210	309	222	55	66	78	205	322	244	318	303	351	288	203	296	305	291	332	338	357
Ni	181	173	66	225	71	40	50	44	68	183	103	150	244	217	191	65	183	155	175	216	206	164
Cu	65	70	39	72	60	50	51	46	48	48	62	54	77	62	52	56	66	72	54	69	76	47
Zn	100	118	97	101	94	91	113	86	93	96	96	98	107	98	102	94	96	105	107	105	115	103
Ga	23	24	23	22	24	28	32	29	26	21	22	22	22	22	20	25	24	23	23	22	20	23
As	1.3	2.4	2.8	1.4	0.5	-	-	-	1.7	1.8	2.1	1.3	0.6	1.5	0.7	1.2	0.4	1.3	1.7	1.8	1.6	2.4
Rb	12	15	11	11	9.1	11	11	11	10	7.0	14	17	8.9	10	15	11	14	14	9.2	12	7.5	15
Sr	387	585	450	409	414	534	620	543	400	271	367	469	315	331	328	463	366	376	346	389	338	402
Y	21	23	23	21	30	23	25	22	42	21	26	27	21	25	22	26	52	29	40	27	27	25
Zr	130	177	167	157	171	188	210	189	167	110	138	169	135	130	133	167	156	142	134	146	132	147
Nb	18	29	16	20	19	22	25	22	18	8.7	17	20	15	16	18	19	18	19	12	17	16	19
Ba	120	375	145	124	99	148	385	148	98	76	131	213	89	117	129	168	134	160	141	161	108	145
La	15	30	15	18	18	20	23	21	29	8.4	19	22	14	15	17	18	32	21	38	17	21	19
Pb	2.5	4.0	2.5	3.1	2.6	2.9	4.4	5.0	4.9	5.7	4.9	7.0	3.6	2.1	3.8	5.6	3.6	2.8	1.4	4.8	1.8	2.2
Ce	46	70	47	48	53	49	48	44	48	21	45	61	46	42	49	43	43	54	43	42	41	54
Th	1.3	4.7	3.0	2.7	2.2	2.9	2.6	2.6	1.3	1.1	2.6	4.1	1.6	2.2	2.6	1.2	1.9	2.5	2.5	3.2	2.5	2.9
U	0.1	1.5	0.1	0.1	0.1	1.2	2.1	0.2	0.3	0.25	1.3	0.1	0.3	0.1	1.5	0.4	0.4	0.1	0.1	0.1	0.1	0.2

Table A7.1 continued.

Rock Type	hawaiite															ol-tholeiitic basalt					
Sample	SA90	SA92	SAB133	SAB134	SAB138	SAB140	SAB142	SAB147	SAB151	SAB163	SAB166	SAB167	SAB189	SAB203	SAB208	SA15	SA16	SA34	SA35	SA36	SA43
SiO_2	49.18	47.88	47.86	48.51	48.13	47.59	47.83	48.07	47.73	47.53	47.30	47.15	48.12	48.17	49.04	50.30	49.70	49.96	48.54	49.78	50.47
TiO_2	2.24	2.34	1.97	2.07	2.01	2.65	2.69	2.19	2.15	3.00	2.96	2.93	2.16	2.00	2.18	2.04	1.90	1.65	1.89	1.62	1.84
Al_2O_3	14.73	14.35	13.74	14.07	13.92	15.47	15.40	14.60	14.35	16.02	15.91	15.75	14.68	14.20	14.74	14.57	14.31	14.13	14.80	14.19	14.58
Fe_2O_3*	12.99	13.71	15.34	13.96	13.64	13.57	13.68	13.92	13.58	13.36	13.42	13.99	13.92	14.02	12.82	13.11	13.10	12.94	13.38	12.87	12.11
MnO	0.18	0.17	0.20	0.18	0.18	0.18	0.19	0.19	0.19	0.19	0.18	0.18	0.20	0.19	0.15	0.16	0.16	0.17	0.18	0.16	0.16
MgO	7.47	7.82	8.90	8.73	9.66	6.43	6.35	8.18	8.96	5.92	6.02	5.89	8.42	8.43	7.69	6.66	7.84	8.33	8.53	8.55	8.60
CaO	9.26	9.20	8.80	9.07	9.29	9.92	9.92	9.51	9.49	9.65	9.66	9.63	9.35	9.43	9.44	9.84	9.68	9.02	9.08	9.18	8.98
Na_2O	3.19	3.05	2.83	3.06	2.82	3.17	3.20	3.02	2.95	3.27	3.18	3.15	2.97	3.10	3.14	3.05	2.95	2.75	2.83	2.74	3.07
K_2O	0.76	0.83	0.62	0.68	0.50	0.84	0.86	0.60	0.58	1.02	1.00	0.97	0.59	0.65	0.80	0.51	0.42	0.52	0.37	0.49	0.73
P_2O_5	0.31	0.34	0.30	0.33	0.26	0.39	0.41	0.29	0.28	0.50	0.48	0.48	0.28	0.39	0.34	0.25	0.21	0.19	0.24	0.28	0.27
Total	100.31	99.69	100.55	100.67	100.43	100.21	100.53	100.57	100.25	100.45	100.12	100.12	100.69	100.57	100.36	100.49	100.27	99.66	99.84	99.86	100.81
LOI	-0.26	0.23	-0.48	-0.39	-0.46	-0.43	-0.33	-0.29	-0.63	-0.49	-0.38	-0.13	-0.10	-0.29	-0.04	-0.23	-0.01	0.10	0.57	-0.24	-0.61
Mg#	57.6	57.6	57.8	59.5	62.5	52.8	52.2	58.1	60.9	51.1	51.5	49.9	58.7	58.6	58.6	54.5	58.5	60.5	60.2	61.2	62.5
trace elements (ppm)																					
Sc	24	24	24	23	21	22	23	27	23	23	28	20	26	25	22	25	24	24	25	24	22
V	248	221	215	213	213	251	234	223	215	280	264	268	213	262	222	226	227	193	208	194	204
Cr	254	346	279	251	321	169	163	316	313	67	62	70	321	271	226	221	271	278	324	266	276
Ni	137	158	228	191	219	65	64	181	171	42	44	41	187	197	145	98	143	193	178	184	151
Cu	53	54	38	60	70	54	49	52	61	52	56	54	49	62	92	51	63	72	49	56	38
Zn	112	100	108	108	94	87	87	91	93	96	94	89	108	117	107	105	104	101	101	103	96
Ga	25	23	24	24	22	25	28	23	26	29	30	31	28	22	25	23	21	22	22	21	21
As	2	1.7	-	-	-	-	-	-	-	-	-	-	-	-	-	2.1	3.4	0.7	0.9	1.8	2.4
Rb	11	15	10	10	6	10	10	7	6	10	12	10	7	8	13	7.3	6.4	11	4.6	9.5	16
Sr	378	415	380	373	316	465	470	360	367	592	566	562	360	410	436	281	275	256	315	252	345
Y	23	88	23	46	32	39	56	28	22	25	27	23	43	21	27	26	22	22	26	20	22
Zr	168	157	121	129	122	160	160	132	126	198	192	189	128	121	142	121	110	108	128	103	137
Nb	17	20	15	16	11	18	18	13	13	23	22	22	12	17	19	11	10	9.9	16	10	14
Ba	96	148	142	166	89	142	137	102	109	138	203	168	120	156	170	65	64	77	112	69	153
La	14	74	20	32	20	22	24	16	15	22	24	21	24	19	26	8.4	7.8	9	16	6.1	13
Pb	2.1	2.4	3.7	3.2	1.9	4.3	1.7	1.3	2.1	2.5	2.8	1.3	2.6	3.0	2.2	4.6	4.6	3.5	3.3	2.9	3.9
Ce	51	65	38	44	31	36	42	30	32	48	52	47	37	42	43	32	30	31	43	31	45
Th	2.9	2.9	4.0	1.9	1.2	2.1	2.8	1.4	1.8	1.6	2.6	1.2	2.5	1.3	3.8	2.1	2.2	2.8	2.9	1.8	4.0
U	0.1	1.3	1.9	0.9	0.2	0.9	-	1.0	1.3	0.7	0.3	0.4	-	0.6	2.3	0.1	0.1	0.1	0.2	0.1	0.1

Table A7.1 continued.

Rock Type	ol-tholeiitic basalt																					
Sample	SA53	SA59	SA67	SA68	SA71	SA73	SA79	SA80	SA81	SA89	SA91	SA93	SAB144	SAB149	SAB152	SAB169	SAB170	SAB171	SAB172	SAB173	SAB174	SAB177-2
SiO_2	47.61	49.34	50.31	49.61	49.71	47.01	49.42	49.83	48.76	48.12	49.30	46.59	48.26	47.92	48.07	49.99	50.11	50.00	50.15	49.87	49.90	49.56
TiO_2	2.17	1.85	2.12	2.00	1.80	2.14	1.99	2.07	1.77	1.63	1.89	2.27	2.21	2.13	2.15	2.26	1.67	1.65	1.76	1.67	1.67	1.67
Al_2O_3	13.46	14.51	13.45	13.29	16.04	14.44	13.69	13.96	17.02	14.01	14.20	13.53	14.69	14.26	14.38	15.65	14.26	14.34	14.55	14.34	14.45	14.52
Fe_2O_3*	13.74	12.81	11.89	13.10	11.84	13.51	12.85	12.22	12.03	14.13	12.63	13.85	13.59	13.85	13.57	11.37	12.62	12.91	13.03	13.21	12.87	13.40
MnO	0.18	0.17	0.23	0.17	0.18	0.18	0.16	0.16	0.16	0.22	0.15	0.22	0.17	0.19	0.16	0.17	0.17	0.17	0.18	0.17	0.17	0.16
MgO	9.06	8.20	7.67	9.55	8.11	8.08	9.16	9.11	8.25	7.94	8.32	9.03	8.80	9.41	9.79	6.77	8.73	8.81	8.53	8.90	8.88	8.22
CaO	6.34	8.77	9.85	8.86	9.24	9.30	8.90	8.97	8.66	8.97	9.09	8.41	9.00	9.10	8.95	10.06	9.16	9.22	9.23	9.09	9.15	9.34
Na_2O	3.21	2.92	2.81	2.84	2.72	2.74	2.98	3.07	2.87	2.78	2.88	2.59	2.83	2.68	2.71	3.15	2.74	2.71	2.73	2.73	2.74	2.81
K_2O	0.87	0.54	0.73	0.71	0.62	0.56	0.61	0.82	0.74	0.54	0.45	0.78	0.59	0.56	0.61	0.75	0.52	0.47	0.43	0.40	0.37	0.31
P_2O_5	0.35	0.29	0.26	0.25	0.22	0.32	0.26	0.28	0.27	0.20	0.25	0.33	0.28	0.28	0.28	0.36	0.30	0.30	0.22	0.21	0.22	0.23
Total	96.99	99.40	99.32	100.38	100.48	98.28	100.02	100.49	100.53	98.54	99.16	97.60	100.43	100.38	100.67	100.53	100.28	100.59	100.80	100.60	100.42	100.22
LOI	0.24	0.60	0.95	-0.26	-0.30	1.28	0.01	-0.47	-0.40	1.59	0.43	1.98	-0.01	0.16	-1.13	-0.02	-0.24	-0.22	-0.05	-0.09	-0.14	0.04
Mg#	61.8	60.4	60.6	63.2	61.7	59.1	62.8	63.7	61.7	57.5	61.1	61.4	60.4	61.6	62.9	58.3	62.0	61.6	60.6	61.3	61.9	59.2
trace elements (ppm)																						
Sc	24	23	24	22	26	21	22	21	22	23	22	18	26	25	23	28	24	26	26	17	24	27
V	240	210	202	195	208	216	206	210	204	184	214	210	215	225	209	256	204	192	201	184	196	202
Cr	314	260	288	327	281	289	297	291	275	262	310	274	317	315	303	228	281	264	260	246	272	270
Ni	233	150	163	236	182	124	251	220	147	228	182	194	185	176	184	131	223	199	204	204	217	207
Cu	62	55	65	69	76	64	65	71	52	70	74	44	73	68	70	80	82	70	84	76	81	61
Zn	104	107	106	111	104	101	107	116	99	105	105	97	92	91	98	134	114	105	111	106	109	111
Ga	21	22	23	22	22	23	21	20	24	21	23	23	25	24	27	29	24	25	25	27	24	23
As	1.6	2.5	2.3	2.3	1.8	1.2	2.2	4.3	1.6	1.5	1.1	0.9	-	-	-	-	-	-	-	-	-	-
Rb	17	11	13	14	11	8.1	9.6	14	17	11	7.4	13	8	9	7	12	9	8	7	7	6	5
Sr	413	366	313	316	273	326	340	339	349	251	329	335	347	333	330	393	276	275	266	268	267	263
Y	42	36	25	36	22	22	22	24	24	21	45	24	31	21	21	24	21	21	22	21	21	23
Zr	147	142	139	134	118	145	142	151	138	106	132	148	129	130	131	147	116	111	118	111	114	110
Nb	26	17	13	16	11	17	15	16	15	9.8	16	21	12	13	12	16	9	9	10	9	9	9
Ba	187	200	133	113	75	88	113	122	153	76	96	127	127	114	93	125	95	75	96	105	78	104
La	32	23	12	23	10	14	14	14	18	8.4	26	16	21	14	15	15	9	10	14	13	9	9
Pb	3.8	5.2	3.4	3.7	3.1	1.6	2.6	3.0	4.9	2.5	3.4	3.0	2.1	1.3	1.4	3.6	2.3	2.2	3.5	4.3	1.8	3.8
Ce	58	51	33	54	34	42	41	43	49	34	48	46	32	25	22	32	20	20	25	21	22	16
Th	4.9	3.5	2.8	3.2	3.4	3.1	3.0	3.6	3.7	2.6	4.0	2.8	1.7	1.3	0.9	1.9	1.6	2.0	2.3	2.4	1.2	1.1
U	0.1	1.4	0.8	0.3	0.1	0.2	0.1	0.1	0.1	0.1	0.1	0.2	1.2	1.9	0.7	2.0	0.3	0.7	0.5	1.8	-	-

Table A7.1 continued.

Rock Type	ol-tholeiitic basalt										qz-tholeiitic basalt			
Sample	SAB177-3	SAB178-2	SAB181	SAB184	SAB187	SAB190	SAB191	SAB201	SAB202	SAB205	SA31	SA76	SA77	SAB198
SiO_2	49.88	49.59	49.52	49.17	49.17	48.31	48.30	48.00	48.65	48.07	51.34	51.00	50.93	52.77
TiO_2	1.63	1.63	2.04	1.95	1.91	2.04	2.15	1.97	2.09	1.93	2.09	1.92	2.06	2.47
Al_2O_3	14.36	14.31	13.23	13.47	13.15	14.44	14.66	13.89	14.62	13.86	13.70	13.16	13.52	17.67
Fe_2O_3*	13.15	13.31	13.20	13.20	13.02	14.02	13.90	14.22	14.56	13.96	11.92	12.34	12.09	6.82
MnO	0.16	0.16	0.17	0.18	0.17	0.20	0.19	0.19	0.23	0.20	0.21	0.18	0.19	0.10
MgO	8.69	8.71	9.88	9.48	10.56	8.57	8.76	9.56	7.70	9.66	7.96	7.71	7.76	3.89
CaO	9.27	9.18	8.96	9.14	8.87	9.18	8.96	8.73	8.20	8.74	8.99	9.37	9.23	11.23
Na_2O	2.78	2.80	2.67	2.70	2.63	2.87	2.81	2.74	2.85	2.67	2.81	2.71	2.87	3.80
K_2O	0.44	0.38	0.66	0.65	0.61	0.51	0.58	0.67	0.71	0.64	0.72	0.54	0.67	0.80
P_2O_5	0.29	0.28	0.33	0.37	0.29	0.27	0.28	0.33	0.38	0.33	0.27	0.22	0.27	0.35
Total	100.66	100.36	100.67	100.32	100.40	100.41	100.58	100.29	99.99	100.07	100.01	99.15	99.59	99.90
LOI	-0.24	-0.30	-0.30	-0.07	-0.50	-0.21	-0.35	-1.15	-1.16	-1.66	-0.09	1.07	0.64	0.21
Mg#	60.8	60.7	63.7	62.9	65.6	59.0	59.7	61.4	55.6	62.1	61.2	59.9	60.4	57.4
trace elements (ppm)														
Sc	24	25	22	29	23	23	22	23	25	20	25	23	24	30
V	201	198	219	246	198	235	219	215	232	210	210	196	205	274
Cr	272	276	348	352	368	327	328	242	268	269	316	305	291	315
Ni	193	205	272	276	300	219	205	272	201	434	161	403	183	38
Cu	78	68	60	69	65	90	51	106	46	65	49	78	59	41
Zn	110	106	113	111	108	114	102	116	116	116	108	111	104	170
Ga	22	22	24	24	23	27	26	25	24	22	22	21	23	30
As	-	-	-	-	-	-	-	-	-	-	1.4	1.1	1.6	-
Rb	7	6	10	10	9	7	9	12	11	10	15	10	13	13
Sr	259	251	329	344	321	337	333	365	353	349	321	283	317	445
Y	23	23	22	21	21	32	30	22	25	22	25	23	23	34
Zr	109	107	140	136	130	126	128	126	133	122	141	124	140	149
Nb	9	9	15	15	14	12	12	17	18	17	13	9.6	13	19
Ba	101	101	122	146	120	131	128	152	236	140	115	77	106	235
La	6	12	15	14	13	24	30	21	25	23	13	9.9	11	35
Pb	2.9	3.0	2.5	2.1	2.7	1.4	2.4	2.6	3.1	2.4	6.1	3.8	1.7	2.2
Ce	18	21	31	25	30	39	34	39	59	34	45	25	37	56
Th	0.6	0.9	2.5	2.1	2.4	2.3	1.8	2.9	2.7	2.4	2.4	1.2	2.1	3.4
U	1.1	1.0	0.9	1.8	1.2	1.3	0.4	1.6	1.3	1.0	0.4	0.4	0.6	1.7

Table A7.1 continued.

Rock Type	transitional basalt														
Sample	SA07	SA08	SA09	SA10	SA13	SA39	SA48	SA49	SA72	SA83	SA84	SAB145	SAB150	SAB161	SAB210
SiO_2	45.83	47.26	47.05	46.84	48.63	47.15	46.59	46.81	47.73	47.51	47.69	47.79	47.98	47.07	47.95
TiO_2	2.19	2.04	1.95	1.99	1.69	1.98	2.89	2.03	1.79	1.72	1.75	2.18	2.14	2.92	2.65
Al_2O_3	15.13	14.36	14.74	14.51	14.34	14.53	15.46	13.80	14.03	14.67	14.18	14.61	14.26	15.78	15.27
Fe_2O_3*	14.40	13.76	13.69	13.96	12.91	14.06	14.21	14.17	13.78	14.30	14.42	14.02	13.75	14.19	13.44
MnO	0.20	0.19	0.19	0.18	0.17	0.18	0.18	0.23	0.17	0.19	0.20	0.21	0.17	0.22	0.15
MgO	8.63	8.69	8.94	9.40	9.85	8.68	6.23	9.41	10.04	8.72	9.07	8.45	9.48	6.53	6.97
CaO	9.93	9.77	10.17	9.75	9.40	8.85	9.14	8.80	8.95	9.30	9.48	9.16	9.04	9.15	9.55
Na_2O	2.67	2.84	2.76	2.69	2.87	2.93	3.03	2.69	2.80	2.92	2.83	2.93	2.79	2.89	2.94
K_2O	0.27	0.52	0.26	0.23	0.39	0.50	0.97	0.51	0.53	0.40	0.37	0.58	0.55	0.95	0.84
P_2O_5	0.15	0.26	0.24	0.20	0.21	0.29	0.45	0.24	0.22	0.19	0.18	0.28	0.28	0.48	0.39
Total	99.40	99.69	99.99	99.75	100.46	99.15	99.15	98.69	100.04	99.92	100.17	100.22	100.43	100.18	100.15
LOI	0.93	0.57	0.23	0.41	-0.43	0.80	0.94	1.18	-0.66	0.20	0.04	-1.25	-0.39	-0.94	-0.90
Mg#	58.9	60.0	60.7	61.5	64.2	59.6	51.2	61.5	63.3	59.1	59.8	58.7	61.9	52.1	55.1
trace elements (ppm)															
Sc	27	28	27	29	25	26	23	22	24	27	26	28	25	23	27
V	200	247	273	257	209	209	277	219	195	206	216	223	231	275	253
Cr	336	325	361	340	329	329	81	298	313	349	362	305	298	66	190
Ni	294	173	187	187	196	189	40	214	227	205	213	240	256	50	79
Cu	77	73	64	79	51	49	44	61	42	76	68	53	70	53	57
Zn	117	109	107	113	93	97	92	98	95	98	99	101	110	105	103
Ga	24	22	22	21	21	22	25	23	21	22	23	25	26	31	28
As	2.5	2.6	1.5	1.2	1.2	1.6	1.3	0.4	0.8	0.8	1.1	-	-	-	-
b	5	8.8	2.8	2.4	6.2	6.2	11	5.7	9	4.9	5.2	6	7	9	11
Sr	332	332	345	342	290	311	495	301	305	260	258	327	339	520	444
Y	34	24	23	26	21	25	23	20	26	44	47	22	22	24	23
Zr	150	141	128	134	114	136	192	122	120	104	97	133	132	194	166
Nb	17	19	16	17	9.7	15	23	12	15	13	10	13	13	22	19
Ba	205	111	83	104	93	90	129	74	110	75	65	96	94	142	148
La	24	12	9.8	14	9.1	13	17	11	18	30	18	13	13	21	19
Pb	4.7	3.4	4	4.6	3.4	3.3	3.2	1.9	3.3	1.7	1.5	2.7	2.0	3.1	1.1
Ce	38	44	39	43	31	40	41	35	39	38	30	31	24	43	38
Th	1.8	3.2	2.6	1.9	2.6	3.1	1.5	3.1	2.1	0.7	1.9	1.6	1.7	1.6	1.2
U	0.4	1.1	0.1	0.1	0.6	0.2	0.5	0.1	0.7	0.1	0.3	1.2	-	-	1.1

Table A7.2 Whole-rock, XRF-derived major and trace element data for selected group B samples.

Rock Type	alkali ol-basalt															basanite						
Sample	SA54	SA95	SAB185	SAB188	SAB207	SAB222	SAB224	SAB225	SAB227	SAB229	SAB232	SAB253	SAB270	SAB275	SAB277	SA03	SA05	SA12	SA23	SA26	SA27	SA37
SiO_2	46.18	46.94	45.44	45.71	42.78	47.43	47.53	47.67	45.34	44.89	48.19	47.02	47.41	47.55	47.91	45.15	42.36	43.75	43.92	44.00	42.40	43.21
TiO_2	2.66	2.06	2.68	2.68	3.20	2.49	2.46	2.50	2.97	3.06	2.29	2.47	2.45	2.42	2.35	2.59	3.25	2.83	2.81	3.02	2.98	2.74
Al_2O_3	14.11	13.31	14.09	14.12	12.60	14.62	14.63	14.87	14.17	14.22	15.32	14.50	14.43	14.72	15.57	13.88	12.45	13.70	12.83	12.96	13.11	12.51
Fe_2O_3*	14.37	13.44	13.72	13.81	15.50	13.99	13.89	14.06	14.40	14.77	13.15	13.96	13.78	13.62	13.49	13.34	15.42	14.05	14.38	14.93	15.77	13.76
MnO	0.20	0.20	0.20	0.21	0.20	0.20	0.19	0.20	0.19	0.19	0.19	0.19	0.19	0.19	0.19	0.19	0.20	0.20	0.20	0.19	0.25	0.18
MgO	8.14	10.11	10.07	9.87	11.74	6.74	7.12	6.29	7.73	7.56	6.36	7.36	7.32	6.68	6.30	9.56	10.47	9.34	10.67	10.15	7.17	11.50
CaO	8.49	9.05	8.83	9.06	10.07	8.13	8.08	8.26	10.08	9.45	7.98	7.89	8.06	7.99	7.69	9.10	9.85	9.73	9.59	9.92	8.71	10.45
Na_2O	3.46	3.27	3.01	2.89	2.50	3.63	3.87	3.44	2.83	2.97	3.91	3.90	3.89	3.99	3.44	3.32	4.19	4.29	3.80	3.40	3.96	3.35
K_2O	1.53	1.14	1.45	1.39	0.73	1.74	1.78	1.77	1.53	1.66	2.03	1.80	1.76	1.83	1.91	1.15	1.16	1.61	1.49	1.19	2.08	1.14
P_2O_5	0.61	0.46	0.74	0.74	0.73	0.75	0.77	0.80	0.90	0.85	0.79	0.82	0.78	0.79	0.86	0.62	0.88	0.74	0.72	0.59	1.14	0.61
Total	99.75	99.98	100.25	100.48	100.06	99.72	100.33	99.86	100.16	99.62	100.21	99.91	100.07	99.78	99.72	98.90	100.23	100.24	100.41	100.35	97.57	99.45
LOI	0.38	0.12	-1.04	-1.46	-0.81	0.66	0.36	1.13	2.20	1.62	0.90	-0.02	0.24	0.50	0.93	0.50	-0.07	-0.14	-0.28	-0.23	1.96	0.32
Mg#	57.4	64.0	63.4	62.7	64.2	53.4	54.7	51.5	56.0	54.9	53.3	55.6	55.7	53.8	52.6	63.2	61.6	61.1	63.6	61.6	52.6	66.6
trace elements (ppm)																						
Sc	17	26	20	22	25	17	17	18	15	18	16	14	19	14	12	19	17	19	21	20	15	23
V	210	198	224	228	280	212	206	213	242	254	177	198	203	187	189	232	260	243	254	276	190	277
Cr	239	340	346	319	295	223	222	227	182	201	159	222	228	197	183	263	252	288	308	283	100	342
Ni	135	239	233	235	292	156	156	154	142	145	90	194	181	142	131	289	205	166	237	211	89	268
Cu	67	63	65	65	66	54	59	59	64	64	58	44	46	62	36	64	63	66	66	66	38	71
Zn	104	109	106	112	113	129	127	131	127	134	129	125	127	116	137	98	122	105	115	112	131	112
Ga	26	21	27	27	25	26	26	26	25	25	27	26	26	27	28	24	25	24	23	22	26	23
As	2.9	2	-	-	-	-	-	-	-	-	-	-	-	-	-	3.1	2.6	3.2	3.2	2.7	4.7	2.0
Rb	24	18	22	20	14	26	28	26	21	22	33	27	28	30	29	24	24	27	27	18	40	19
Sr	762	597	784	797	1104	884	855	899	808	824	1300	848	858	896	927	746	932	901	760	632	2193	717
Y	26	28	26	26	22	30	31	31	30	30	32	30	30	31	31	26	27	27	26	24	35	27
Zr	291	242	274	275	238	349	348	356	321	334	410	343	345	364	406	311	311	332	293	225	436	275
Nb	47	40	48	48	45	57	57	58	54	57	65	56	56	58	65	55	56	59	57	43	80	57
Ba	249	187	249	244	256	283	283	301	249	237	548	336	375	719	1089	260	263	299	268	205	383	247
La	41	37	43	40	41	42	48	49	41	46	52	46	50	50	48	44	76	55	48	35	71	49
Pb	4.5	3.9	3.4	3.9	2.3	4.2	4.9	5.0	3.4	5.1	5.5	4.8	6.6	5.0	5.5	5.7	3.8	7.1	6.1	6.4	7.2	3.6
Ce	97	86	81	78	75	90	89	88	88	90	94	87	86	90	90	101	160	121	106	85	149	105
Th	5.6	5.9	4.4	6.3	3.7	5.4	4.9	4.4	5.0	5.5	6.8	5.1	5.7	5.9	6.9	6.8	4.5	8.5	6.9	4.9	8.8	6.6
U	1.0	1.4	0.6	1.1	-	2.5	1.7	2.2	2.5	0.5	4.4	2.6	2.4	2.4	3.3	0.1	1.3	1.4	1.8	-	2.5	-

Table A7.2 continued.

Rock Type	basanite																				
Sample	SA38	SA40	SA41	SA42	SA45	SA55	SA56	SA57	SA58	SA60	SA61	SA75	SA82	SA86	SAB102	SAB107	SAB111	SAB116	SAB128	SAB129	SAB132	SAB173-1
SiO_2	45.06	43.23	43.37	43.36	41.93	44.67	42.77	43.54	43.95	44.16	44.55	43.46	44.62	42.52	42.63	42.42	42.47	42.92	42.40	42.85	42.57	43.36
TiO_2	2.56	2.78	2.82	2.76	3.23	2.67	2.94	2.75	2.81	2.77	2.59	2.66	2.83	2.85	3.23	3.22	3.22	3.13	3.24	2.97	2.98	2.76
Al_2O_3	13.15	12.19	12.35	12.32	12.77	12.83	12.60	13.22	12.88	12.58	13.53	12.83	14.74	13.21	12.62	12.50	12.50	12.57	12.57	13.08	12.96	12.55
Fe_2O_3*	14.49	14.26	14.14	14.32	15.26	13.73	14.53	14.21	14.36	13.48	13.50	14.26	13.66	15.38	15.65	15.56	15.36	15.04	15.43	15.02	15.49	14.36
MnO	0.19	0.20	0.20	0.20	0.20	0.19	0.19	0.20	0.19	0.17	0.20	0.25	0.20	0.23	0.22	0.21	0.20	0.20	0.21	0.23	0.24	0.21
MgO	10.33	11.90	11.69	11.80	9.67	11.65	11.50	10.56	10.60	12.07	10.13	10.04	9.08	9.09	10.70	10.73	11.29	11.52	11.15	9.72	9.81	10.86
CaO	9.51	10.13	10.12	10.03	9.88	10.21	10.22	9.82	9.61	10.38	9.71	9.60	9.38	9.82	9.96	9.86	10.24	9.80	10.08	9.50	9.60	10.31
Na_2O	3.64	3.24	3.59	3.32	4.10	3.00	3.04	3.95	3.53	2.97	4.07	4.12	3.55	4.45	3.59	4.01	3.05	3.30	3.50	4.47	3.92	3.58
K_2O	1.06	1.31	1.41	1.35	1.01	1.17	1.28	1.41	1.42	1.16	1.37	1.31	1.47	1.52	0.97	1.03	1.29	1.31	1.33	1.74	1.64	1.42
P_2O_5	0.64	0.61	0.63	0.61	0.89	0.46	0.64	0.70	0.73	0.48	0.67	0.79	0.57	1.07	0.98	0.96	0.86	0.72	0.86	1.04	1.03	0.69
Total	100.63	99.85	100.32	100.07	98.94	100.58	99.71	100.36	100.08	100.22	100.32	99.32	100.10	100.14	100.55	100.51	100.48	100.51	100.77	100.61	100.24	100.10
LOI	-0.39	-0.06	-0.42	-0.18	0.65	-0.44	0.10	-0.62	-0.01	-0.29	-0.39	0.22	0.12	-0.20	-0.54	0.06	-0.74	-0.19	-0.33	-0.57	0.00	-0.34
Mg#	62.7	66.5	66.1	66.1	60.4	66.6	65.3	63.7	63.6	67.9	63.9	62.7	61.1	58.3	61.7	61.9	63.4	64.4	62.9	60.4	60.0	64.2
trace elements (ppm)																						
Sc	20	21	21	21	17	22	21	20	20	23	21	18	20	17	19	22	25	24	22	19	18	24
V	224	261	268	265	264	276	288	257	249	283	233	233	267	216	262	267	281	275	277	243	247	290
Cr	322	382	380	381	254	392	326	273	314	404	314	283	258	207	243	226	274	288	269	250	258	324
Ni	223	262	259	271	182	263	240	211	234	283	195	203	188	157	230	221	260	277	263	202	205	274
Cu	66	71	67	71	64	69	67	67	65	70	65	65	61	62	64	69	74	71	78	69	67	74
Zn	111	98	103	103	115	91	104	105	114	95	101	111	102	127	121	122	132	123	135	124	128	114
Ga	22	22	21	21	24	22	23	24	23	23	24	24	22	26	26	27	27	26	29	27	27	24
As	2.7	2.1	2.3	3	2.5	2.2	2.6	2.6	2.6	2	4.1	3.7	3.1	3.1	-	-	-	-	-	-	-	-
Rb	17	22	23	22	25	20	20	23	27	19	23	26	20	29	45	29	44	21	26	28	25	23
Sr	673	718	725	702	1026	547	666	802	784	568	774	958	693	1040	1000	960	1255	818	908	1057	1073	741
Y	26	24	25	24	28	23	25	29	26	23	30	29	25	32	24	24	24	23	24	28	28	29
Zr	233	258	264	252	316	194	231	293	293	199	307	330	263	342	302	304	285	251	291	351	354	280
Nb	41	51	54	51	61	38	43	54	57	38	56	65	46	70	58	58	57	48	58	73	73	55
Ba	217	254	256	252	274	200	214	264	263	206	266	321	197	375	285	292	270	245	284	329	333	282
La	41	43	44	44	59	27	37	50	48	36	45	64	35	74	49	51	50	42	52	66	66	44
Pb	3.7	4.5	4.1	4.3	4.5	3.4	4.1	6.3	5.3	3.4	3.7	4.2	2.8	4.7	6.3	4.8	4.1	2.0	5.1	6.0	4.1	4.6
Ce	94	96	102	99	129	61	82	110	106	73	104	131	84	156	93	96	92	78	103	125	124	83
Th	5.5	6.2	6.2	4.7	7.3	3.8	3.8	7.5	7.0	3.8	7.0	7.8	4.1	8.3	6.6	5.8	4.9	3.8	6.0	6.9	7.9	5.0
U	0.1	0.5	0.4	0.4	3.0	0.9	1.1	1.7	1.2	1.0	1.4	2.6	0.8	1.1	0.6	1.8	1.2	1.5	1.5	1.5	1.4	2.5

Table A7.2 continued.

Rock Type	basanite																mugearite
Sample	SAB175	SAB176	SAB176-1	SAB177	SAB177-1	SAB178	SAB178-1	SAB178-2A	SAB179	SAB179D	SAB180	SAB180D	SAB194	SAB196	SAB204	SAB214	SA88
SiO_2	43.20	43.59	43.75	43.17	43.44	42.86	43.44	43.22	43.65	43.73	43.86	43.79	43.46	42.72	42.69	42.65	47.14
TiO_2	2.74	2.75	2.74	2.81	2.74	2.87	2.74	2.76	2.68	2.67	2.76	2.77	2.98	3.09	3.02	2.97	2.96
Al_2O_3	12.41	12.62	12.46	12.46	12.38	12.60	12.52	12.47	12.18	12.13	12.54	12.49	12.86	12.72	12.29	12.25	11.01
Fe_2O_3*	14.23	14.02	14.26	14.49	14.37	14.90	14.34	14.33	14.12	14.30	14.08	14.26	14.95	14.93	15.21	15.02	17.54
MnO	0.21	0.21	0.19	0.22	0.20	0.23	0.20	0.20	0.20	0.19	0.20	0.20	0.21	0.21	0.20	0.20	0.22
MgO	11.30	11.44	11.07	10.96	11.29	10.75	11.15	10.94	12.88	12.48	11.93	11.57	11.07	10.94	12.23	11.05	9.21
CaO	10.46	10.21	10.37	10.35	10.26	10.36	10.67	10.30	10.22	10.28	10.13	10.19	9.68	9.95	10.05	10.24	7.18
Na_2O	3.22	3.44	3.34	3.43	3.29	3.51	3.19	3.56	2.83	2.91	3.02	3.12	3.06	3.22	2.61	3.27	3.32
K_2O	1.45	1.43	1.48	1.48	1.40	1.67	1.40	1.45	1.15	1.17	1.33	1.34	1.44	1.47	1.20	1.36	1.33
P_2O_5	0.64	0.71	0.69	0.73	0.64	0.86	0.64	0.72	0.55	0.52	0.60	0.57	0.75	0.87	0.73	0.70	0.64
Total	99.86	100.42	100.35	100.10	100.00	100.62	100.29	99.94	100.46	100.38	100.47	100.29	100.48	100.13	100.22	99.71	100.55
LOI	0.36	-0.15	-0.04	-0.23	-0.16	-0.40	0.52	-0.23	-0.56	-0.54	-0.40	-0.33	-0.37	-0.10	0.40	-0.32	-0.46
Mg#	65.3	65.8	64.7	64.2	65.1	62.9	64.8	64.4	68.2	67.3	66.6	65.7	63.6	63.4	65.6	63.6	55.4
trace elements (ppm)																	
Sc	20	23	24	19	19	24	22	22	30	23	27	25	25	23	20	19	18
V	284	293	310	275	301	291	280	278	293	288	281	281	267	271	276	284	223
Cr	341	320	346	343	335	312	322	318	363	372	331	337	270	253	376	321	293
Ni	288	302	286	273	290	293	278	266	337	311	318	295	278	271	332	274	203
Cu	78	83	67	80	80	81	86	78	76	78	82	84	75	68	69	79	67
Zn	115	115	115	120	113	138	107	116	101	101	104	109	120	118	126	116	137
Ga	22	27	23	23	24	29	23	23	25	22	25	23	24	25	25	23	26
As	-	-	-	-	-	-	-	-	-	-	-	-	-	-	-	-	2.4
Rb	38	23	25	23	23	45	27	25	17	18	20	21	26	24	20	21	25
Sr	712	751	694	812	700	917	709	812	603	597	631	626	711	817	977	698	317
Y	29	26	28	31	28	28	28	30	22	25	24	27	24	25	22	27	38
Zr	266	268	260	302	260	326	261	293	209	214	231	236	221	242	223	248	253
Nb	53	57	51	60	52	71	51	58	40	40	47	47	46	53	52	48	35
Ba	256	398	593	284	380	373	267	319	230	231	263	267	262	305	384	236	208
La	44	45	36	48	40	62	39	46	34	29	37	34	41	47	40	38	36
Pb	3.0	2.0	5.6	5.0	3.8	5.6	4.3	4.5	4.6	3.9	2.8	3.7	2.6	2.4	2.5	4.5	4.5
Ce	86	90	69	94	75	114	76	86	65	58	69	68	80	89	72	76	90
Th	3.6	6.0	3.8	5.1	4.2	5.4	4.5	5.3	4.5	2.6	5.0	3.6	4.5	4.4	3.1	3.1	4.9
U	0.2	0.6	0.8	1.2	-	0.7	0.5	0.9	0.6	0.4	1.6	0.9	0.7	1.0	0.3	0.9	0.1

Table A7.2 continued.

Rock Type	ne-hawaiite																					
Sample	SA01	SA02	SA22	SA24	SA25	SA29	SA62	SA63	SA64	SA65	SA66	SAB215	SAB217	SAB218	SAB220	SAB221	SAB223	SAB228	SAB231	SAB233	SAB234	SAB235
SiO_2	46.76	46.33	43.84	45.73	44.75	44.90	45.77	46.35	44.46	46.44	42.89	47.64	47.08	46.99	47.34	46.84	47.46	48.32	47.46	47.83	46.91	47.50
TiO_2	2.56	2.52	2.68	2.84	2.60	2.57	2.55	2.69	2.81	2.40	2.77	2.40	2.43	2.41	2.46	2.44	2.51	2.29	2.36	2.38	2.41	2.37
Al_2O_3	15.33	14.71	12.66	14.21	13.62	14.16	14.53	15.02	14.30	14.79	13.05	14.92	14.33	14.39	14.64	14.31	14.81	15.36	14.69	14.87	14.29	14.71
Fe_2O_3*	13.06	12.50	15.49	15.35	15.37	15.26	14.64	14.19	14.59	14.46	15.99	13.24	13.76	13.63	13.83	13.78	14.12	13.18	13.46	13.60	13.61	13.54
MnO	0.19	0.22	0.21	0.19	0.23	0.24	0.23	0.30	0.20	0.27	0.25	0.19	0.19	0.19	0.19	0.19	0.20	0.19	0.19	0.19	0.19	0.19
MgO	7.16	7.31	7.56	6.82	6.86	6.12	5.56	5.70	5.39	5.45	7.48	6.46	7.13	7.30	6.65	7.32	6.66	6.11	6.93	6.70	7.39	6.79
CaO	8.43	9.07	9.41	7.89	8.05	7.87	7.46	7.49	8.69	7.21	9.19	8.06	8.05	7.99	8.26	7.98	8.23	7.65	7.98	7.99	7.96	7.94
Na_2O	4.58	3.77	3.31	4.41	4.20	5.59	5.47	4.70	4.36	5.61	5.24	4.61	4.04	4.61	4.06	4.30	3.56	4.34	4.20	4.17	4.33	4.22
K_2O	1.86	1.70	1.43	1.82	1.74	2.18	2.19	2.05	1.99	2.21	1.93	1.90	1.83	1.88	1.86	1.83	1.76	2.05	1.92	1.91	1.82	1.88
P_2O_5	0.58	0.56	1.19	0.98	1.07	1.23	1.05	0.85	0.97	1.03	1.28	0.77	0.78	0.76	0.77	0.77	0.76	0.82	0.78	0.77	0.78	0.82
Total	100.51	98.69	97.78	100.24	98.49	100.12	99.45	99.34	97.76	99.87	100.07	100.18	99.62	100.16	100.06	99.75	100.06	100.30	99.96	100.43	99.70	99.96
LOI	-0.41	1.13	1.93	-0.16	1.30	-0.57	-0.06	0.29	1.81	-0.01	-0.34	-0.14	0.43	-0.45	0.78	-0.23	0.76	0.54	0.12	0.22	-0.35	0.11
Mg#	56.3	58.4	54.3	51.2	51.9	48.7	47.5	49.0	47.4	47.2	52.6	53.5	55.2	55.9	53.2	55.8	52.8	52.2	54.9	53.7	56.3	54.3
trace elements (ppm)																						
Sc	15	16	17	12	13	12	12	16	14	12	14	15	17	14	16	17	18	18	17	17	17	15
V	218	227	189	163	155	158	159	188	187	147	198	175	205	201	199	202	215	176	189	195	204	189
Cr	195	217	128	111	83	97	75	102	101	61	127	194	223	232	223	226	228	154	225	208	231	221
Ni	118	142	110	100	95	82	69	59	85	61	115	97	151	139	144	149	158	94	128	131	157	146
Cu	55	55	54	46	51	46	57	48	65	44	53	61	48	67	60	45	57	55	59	64	56	53
Zn	103	113	148	123	137	140	132	118	135	140	148	101	120	114	122	119	131	133	117	126	122	119
Ga	26	25	23	26	27	30	28	26	25	29	28	28	25	26	25	26	26	27	27	26	26	26
As	4.1	2.8	2.1	2.8	3.1	4.9	4	3.8	2.8	3.8	3.1	-	-	-	-	-	-	-	-	-	-	-
Rb	30	30	17	24	27	35	38	31	42	38	33	30	32	31	32	29	27	33	32	29	28	29
Sr	816	834	1171	892	1140	1297	1203	948	1202	1253	1517	888	1428	859	978	841	883	905	888	929	829	880
Y	27	29	34	29	36	40	38	31	35	39	40	30	32	30	30	30	30	30	30	30	29	30
Zr	353	338	315	331	420	481	451	399	388	491	404	367	357	349	354	344	350	403	377	379	345	368
Nb	58	56	60	59	77	85	84	66	71	89	78	56	56	56	57	56	58	65	61	62	56	58
Ba	290	284	328	283	372	406	412	301	370	425	478	363	312	301	315	300	288	337	386	528	316	403
La	49	44	76	52	83	99	100	60	77	78	98	53	46	47	48	47	45	54	53	52	47	49
Pb	6.8	6.6	6.9	7.7	7.7	9.5	6.6	6.3	4.9	6.4	7.4	6.6	4.9	3.9	6.0	5.7	4.1	5.0	3.9	6.9	7.0	5.2
Ce	106	100	160	124	165	195	186	129	160	155	210	97	88	97	91	90	91	104	96	92	91	89
Th	8.5	7.2	6.5	5.9	8.5	11	9.9	8	8.2	11	8.3	6.3	4.4	5.3	5.9	5.0	4.7	7.7	6.5	6.1	6.3	5.4
U	1.7	1.3	1.4	-	2.1	3.5	2.4	0.8	2	1.9	2.4	2.2	1.3	1.4	0.2	3.1	0.3	1.8	4.0	1.6	2.7	3.9

Table A7.2 continued.

Rock Type	ne-hawaiite											
Sample	SAB236	SAB237	SAB239	SAB241	SAB245	SAB247	SAB249	SAB259	SAB260	SAB262	SAB266	SAB271
SiO_2	47.26	47.21	47.44	46.95	47.75	47.69	46.73	47.09	47.71	46.97	47.03	47.83
TiO_2	2.44	2.44	2.35	2.44	2.36	2.36	2.45	2.46	2.41	2.45	2.45	2.40
Al_2O_3	14.53	14.47	14.68	14.39	14.73	14.83	14.41	14.46	15.00	14.37	14.35	15.03
Fe_2O_3*	13.75	13.73	13.44	13.82	13.49	13.47	13.83	13.79	13.46	13.75	13.83	13.22
MnO	0.19	0.19	0.19	0.19	0.19	0.19	0.19	0.19	0.19	0.19	0.19	0.19
MgO	7.32	7.40	6.87	7.44	6.84	6.73	7.17	7.33	6.50	7.39	7.31	6.46
CaO	7.99	8.00	7.88	7.95	7.86	7.92	8.00	8.00	8.07	8.10	7.85	8.05
Na_2O	4.25	4.26	4.35	4.27	4.38	4.43	4.24	4.34	4.33	4.17	4.19	4.42
K_2O	1.83	1.82	1.92	1.81	1.93	1.95	1.83	1.82	1.87	1.77	1.86	1.91
P_2O_5	0.78	0.78	0.78	0.79	0.79	0.80	0.88	0.78	0.80	0.77	0.82	0.79
Total	100.36	100.29	99.90	100.05	100.32	100.35	99.72	100.25	100.33	99.93	99.88	100.30
LOI	-0.23	-0.27	-0.20	-0.30	-0.06	-0.11	0.14	-0.31	0.27	-0.17	-0.17	-0.13
Mg#	55.7	56.0	54.8	56.1	54.4	54.1	55.2	55.6	53.2	56.0	55.6	53.5
trace elements (ppm)												
Sc	16	18	15	18	13	14	16	15	15	15	13	14
V	199	202	184	197	193	191	189	197	173	200	201	193
Cr	211	227	206	215	224	225	210	231	206	226	222	208
Ni	152	151	128	149	140	126	160	151	121	173	164	117
Cu	51	61	48	52	43	61	56	42	54	49	53	45
Zn	117	118	116	116	118	123	119	112	113	114	127	108
Ga	26	26	27	27	26	26	25	26	27	26	25	27
As	-	-	-	-	-	-	-	-	-	-	-	-
Rb	28	28	30	28	30	30	28	29	29	28	29	31
Sr	849	845	881	856	878	894	977	850	918	857	828	884
Y	30	29	31	30	30	30	31	29	30	30	30	30
Zr	348	349	377	346	374	382	352	345	369	342	342	373
Nb	56	56	60	56	59	62	56	55	56	54	56	58
Ba	354	360	390	337	399	366	388	343	415	351	301	410
La	47	46	51	46	50	52	46	46	50	47	44	54
Pb	5.1	6.4	4.4	4.8	6.1	4.5	3.4	6.2	5.4	5.4	4.5	6.0
Ce	93	89	97	96	87	93	97	89	95	89	86	102
Th	7.1	5.3	5.5	5.4	6.2	5.9	5.8	6.1	6.1	6.2	6.1	7.2
U	2.0	3.3	3.4	2.7	1.9	2.4	2.0	2.8	3.0	2.5	2.2	2.2

Table A7.2 continued.

Rock Type	nepheline												
Sample	SA06	SA21	SA28	SA46	SA50	SA51	SAB104	SAB105	SAB113	SAB119	SAB127	SAB135	SAB193
SiO_2	41.87	41.56	42.44	41.11	40.31	41.18	42.29	42.56	42.26	42.12	42.05	41.67	41.57
TiO_2	3.21	3.17	2.80	3.09	3.32	3.12	3.23	3.28	3.20	3.23	3.19	3.19	3.17
Al_2O_3	12.35	12.32	12.69	12.34	12.12	12.39	12.65	12.78	12.48	12.47	12.42	12.46	12.42
Fe_2O_3*	15.26	15.37	16.11	15.34	16.14	16.25	15.07	14.73	14.88	15.22	15.23	15.67	15.27
MnO	0.20	0.20	0.25	0.22	0.21	0.24	0.20	0.19	0.20	0.21	0.22	0.22	0.22
MgO	11.06	10.87	7.84	9.71	10.00	8.72	10.78	10.48	11.13	11.03	10.96	10.44	10.74
CaO	10.09	10.04	8.95	10.39	9.74	9.81	9.92	10.07	9.85	9.83	9.82	10.38	10.27
Na_2O	3.65	3.69	5.10	4.95	4.30	4.55	3.97	3.89	3.81	3.90	3.81	3.78	3.99
K_2O	1.29	1.31	2.16	1.72	1.69	1.72	1.63	1.62	1.48	1.59	1.58	1.69	1.61
P_2O_5	0.77	0.81	1.27	1.15	0.95	1.29	0.97	0.97	0.86	0.90	0.90	1.14	1.06
Total	99.75	99.34	99.61	100.02	98.78	99.27	100.71	100.57	100.16	100.48	100.18	100.63	100.32
LOI	0.26	0.35	-0.08	0.00	0.82	0.27	-0.53	-0.07	-0.60	-0.75	-0.59	-0.14	-0.33
Mg#	63.3	62.8	53.7	60.0	59.9	56.3	62.7	62.6	63.9	63.1	63.0	61.1	62.4
trace elements (ppm)													
Sc	18	18	13	19	18	17	16	21	24	18	19	22	28
V	269	262	190	255	263	227	276	286	285	271	271	284	278
Cr	283	271	160	209	191	165	250	254	277	258	253	236	234
Ni	218	216	132	163	171	142	237	238	251	243	243	265	254
Cu	63	61	55	56	55	55	68	70	72	72	74	71	72
Zn	121	122	139	135	135	146	132	135	131	121	127	154	137
Ga	24	24	27	24	25	25	27	29	28	27	28	28	28
As	4	3.1	2.8	5.4	3.8	3.9	-	-	-	-	-	-	-
Rb	38	29	34	29	33	36	23	25	21	22	22	33	32
Sr	901	870	1411	1201	1059	1161	964	1005	869	897	924	1049	1065
Y	28	27	40	32	27	36	25	25	24	24	25	27	26
Zr	290	294	453	358	376	428	314	320	287	291	298	302	281
Nb	56	55	86	74	70	88	60	62	57	56	58	70	63
Ba	241	247	453	358	270	420	319	303	268	288	300	374	359
La	47	51	107	84	64	102	55	54	48	50	54	65	62
Pb	7.8	4.8	8.4	5.2	5.1	5.3	4.7	4.2	5.0	5.5	4.2	4.8	3.3
Ce	114	116	207	174	146	205	99	102	97	91	104	123	108
Th	6.3	5.0	9.4	9.7	5.9	9.4	4.9	5.7	4.8	5.8	4.9	7.3	6.5
U	1.1	1.5	-	2.5	2.2	2.8	0.4	1.6	1.7	0.9	1.9	1.5	0.5

Table A7.3 SSMS and ICP-MS-derived trace element and REE and TIMS-derived radiogenic isotope analyses for selected group A samples.

Rock Type	alkali ol-basalt		hawaiite			
Sample #	SA19[2]	SAB162[2]	SA11[1]	SA14[1]	SA52[1]	SA69[1]
Sc	25	24	27	27	24	24
Ti	15901	18510	15043	9912	15973	14051
V	250	279	238	201	255	220
Cr	218	89	205	322	203	296
Ni	80	51	68	183	65	183
Cu	44	49	48	48	56	66
Zn	112	121	93	96	94	96
Co	78	63	-	-	-	-
Mn	1283	1164	-	-	-	-
Ga	23	32	26	21	25	24
As	2.8	-	1.7	1.8	1.2	0.4
Rb	12	14	10	7.0	11	14
Sr	460	621	400	271	463	366
Y	23	26	42	21	26	52
Zr	178	219	167	110	167	156
Hf	4.8	5.1	4.9	2.7	4.2	4.0
Nb	22	27	18	8.7	19	18
Mo	1.4	1.5	2.4	1.1	1.6	2.1
Sn	1.9	2.3	9.6	8.3	4.7	5.0
Cs	0.31	0.53	0.13	0.26	0.12	0.30
Ta	1.9	2.2	-	-	-	-
Ba	117	397	98	76	168	134
Pb	1.8	2.1	4.9	5.7	5.6	3.6
Th	1.1	1.3	1.3	1.1	1.2	1.9
U	0.53	0.54	0.31	0.25	0.35	0.35
La	15	19	29	8.4	18	32
Ce	35	46	48	21	43	44
Pr	4.9	6.2	7.0	2.5	5.5	7.5
Nd	21	26	32	12	25	34
Sm	5.1	5.9	7.5	3.2	5.2	7.8
Eu	1.7	2.0	2.6	1.2	1.7	2.5
Gd	5.4	6.1	7.6	3.7	5.1	8.3
Tb	0.82	0.90	1.1	0.55	0.75	1.4
Dy	4.3	4.7	6.8	3.3	4.4	7.9
Ho	0.80	0.87	1.4	0.69	0.84	1.7
Er	2.0	2.2	3.6	1.7	2.2	4.6
Tm	0.27	0.29	-	-	-	-
Yb	1.7	1.8	2.6	1.5	1.9	3.5
Lu	0.24	0.26	-	-	-	-
Eu/Eu*	1.01	1.03	1.06	1.03	1.03	0.96
$^{87}Sr/^{86}Sr$	0.703127±20	0.702809±16	0.702949±17	0.703150±17	0.702955±17	0.703069±17
$^{143}Nd/^{144}Nd$	0.51298	0.512971	0.512984	0.512966	0.512962	0.512944
$^{147}Sm/^{144}Nd$	-	-	0.1367±16	0.1630±16	0.1448±12	0.1404±15
ε_{Nd}	6.67	6.50	6.75	6.40	6.32	5.97
$^{206}Pb/^{204}Pb$	19.204	19.226	-	-	-	-
$^{207}Pb/^{204}Pb$	15.587	15.586	-	-	-	-
$^{208}Pb/^{204}Pb$	38.814	38.828	-	-	-	-

[1]Analysed by SSMS
[2]Analysed by ICP-MS

Table A7.3 continued.

Rock Type	ol-tholeiitic basalt					
Sample #	SA15[2]	SA16[2]	SA36[3]	SA93[3]	SAB174[2]	SAB187[2]
Sc	26	26	24	18	25	24
Ti	11536	11364	9850	14190	10116	11762
V	215	218	194	210	192	198
Cr	260	301	266	274	263	385
Ni	127	156	184	194	216	297
Cu	45	67	56	44	74	60
Zn	109	106	103	97	104	110
Co	90	70	-	-	64	75
Mn	1253	1209	-	-	1230	1242
Ga	23	21	21	23	24	23
As	2.1	3.4	1.8	0.9	-	-
Rb	6.6	6.4	9.5	13	7.0	11
Sr	280	270	252	335	255	315
Y	24	23	20	24	22	21
Zr	117	115	103	148	110	132
Hf	4.5	3.5	-		3.0	3.6
Nb	12	11	10	21	10	15
Mo	1.2	1.1	-	-	0.9	1.3
Sn	1.3	1.2	-	-	1.2	1.5
Cs	0.43	0.42	-	-	0.36	0.69
Ta	1.2	1.2	-	-	1.2	1.4
Ba	61	61	69	127	64	104
Pb	1.5	1.5	2.9	3.0	2.3	2.3
Th	0.8	0.8	1.8	2.8	1.1	1.3
U	0.29	0.28	0.10	0.20	0.34	0.42
La	9.6	9.4	6.1	16	8.5	11
Ce	20	19	31	46	20	25
Pr	3.1	3.0	-	-	2.8	3.4
Nd	14	13	-	-	12	14
Sm	3.9	3.8	-	-	3.4	3.9
Eu	1.4	1.3	-	-	1.2	1.4
Gd	4.6	4.6	-	-	4.1	4.4
Tb	0.72	0.72	-	-	0.67	0.70
Dy	4.0	3.9	-	-	3.7	3.7
Ho	0.80	0.80	-	-	0.75	0.73
Er	2.0	2.0	-	-	1.9	1.8
Tm	0.28	0.27	-	-	0.27	0.25
Yb	1.7	1.8	-	-	1.7	1.6
Lu	0.25	0.26	-	-	0.24	0.22
Eu/Eu*	1.02	0.97	-	-	1.01	1.01
$^{87}Sr/^{86}Sr$	0.702987±17	0.703053±14	0.703214±17	0.703099±17	0.703176±19	0.702833±18
$^{143}Nd/^{144}Nd$	0.512965	0.512961	0.512985	0.512949	0.512946	0.51296
$^{147}Sm/^{144}Nd$	-	-	0.1699±16	0.1440±15	-	-
ε_{Nd}	6.38	6.30	6.77	6.07	6.01	6.28
$^{206}Pb/^{204}Pb$	19.075	19.076	-	-	18.95	19.016
$^{207}Pb/^{204}Pb$	15.597	15.592	-	-	15.613	15.608
$^{208}Pb/^{204}Pb$	38.731	38.723	-	-	38.744	38.778

[1]Analysed by SSMS
[2]Analysed by ICP-MS
[3]Analysed by XRF

Table A7.3 continued.

Rock Type	qz-tholeiitic basalt		transitional basalt		
Sample #	SA76[1]	SAB198[2]	SA07[1]	SA48[1]	SAB150[2]
Sc	23	32	27	23	25
Ti	11762	15052	13411	17745	12747
V	196	259	200	277	227
Cr	305	333	336	81	325
Ni	403	40	294	40	245
Cu	78	42	77	44	665
Zn	111	169	117	92	112
Co	-	29	-	-	77
Mn	-	742	-	-	1214
Ga	21	-	24	25	26
As	1.1	-	2.5	1.3	-
Rb	10	16	5.0	11	7
Sr	283	469	332	495	314
Y	23	36	34	23	21
Zr	124	154	150	192	131
Hf	3.4	3.8	4.1	4.9	3.2
Nb	9.6	21	17	23	14
Mo	2.1	1.9	2.3	2.2	1.2
Sn	4.6	1.7	9.1	5.9	1.4
Cs	0.51	0.60	0.21	0.14	0.20
Ta	-	1.6	-	-	1.2
Ba	77	225	205	129	68
Pb	3.8	2.6	4.7	3.2	1.2
Th	1.2	1.9	1.8	1.5	0.7
U	0.39	0.66	0.37	0.49	0.29
La	9.9	28	24	17	10
Ce	25	51	38	41	25
Pr	3.2	6.9	5.8	5.2	3.5
Nd	16	27	26	22	15
Sm	4.3	6.4	6.1	5.5	3.9
Eu	1.5	2.1	2.0	1.8	1.4
Gd	4.7	7.2	6.0	4.9	4.4
Tb	0.74	1.1	0.99	0.78	0.69
Dy	4.4	5.9	6.0	4.5	3.7
Ho	0.88	1.2	1.2	0.80	0.73
Er	2.1	2.9	3.0	1.9	1.8
Tm	-	0.41	-	-	0.25
Yb	1.7	2.5	2.4	1.6	1.6
Lu	-	0.36	-	-	0.23
Eu/Eu*	1.02	0.97	1.01	1.06	1.01
$^{87}Sr/^{86}Sr$	0.703301±17	0.702939±18	0.702876±17	0.703079±17	0.702876±13
$^{143}Nd/^{144}Nd$	0.512991	0.512959	0.512979	0.512956	0.512975
$^{147}Sm/^{144}Nd$	0.1677±15		0.1405±16	0.1462±17	
ε_{Nd}	6.89	6.26	6.65	6.20	6.57
$^{206}Pb/^{204}Pb$	-	19.127	-	-	19.277
$^{207}Pb/^{204}Pb$	-	15.597	-	-	15.596
$^{208}Pb/^{204}Pb$	-	38.823	-	-	38.876

[1]Analysed by SSMS
[2]Analysed by ICP-MS

Table A7.4 SSMS and ICP-MS-derived trace element and REE and TIMS-derived radiogenic isotope analyses for selected group B samples.

Rock Type	alkali ol-basalt			nephelinite		
Sample #	SAB188[2]	SAB224[2]	SAB227[2]	SA28[2]	SA51[1]	SAB135[2]
Sc	21	18	17	17	17	20
Ti	16221	16382	14302	16802	19180	19005
V	208	202	173	172	227	245
Cr	253	172	221	167	165	231
Ni	217	140	159	149	142	225
Cu	61	57	54	57	55	64
Zn	115	121	127	163	146	146
Co	60	62	56	62	-	74
Mn	1443	1395	1431	1909	-	1567
Ga	27	26	25	27	25	28
As	-	-	-	2.8	3.9	-
Rb	23	23	29	37	36	38
Sr	774	726	754	1296	1161	937
Y	26	25	26	37	36	27
Zr	289	310	339	469	428	309
Hf	5.9	6.5	6.5	8.8	10	6.1
Nb	48	57	61	102	88	73
Mo	4.4	4.1	4.7	9.0	7.9	5.1
Sn	2.5	2.5	2.8	3.8	10	2.7
Cs	0.51	0.54	0.52	1.4	1.21	0.95
Ta	4.1	3.9	4.3	7.2	-	5.4
Ba	241	260	277	429	420	364
Pb	3.4	4.0	3.9	5.3	5.3	4.0
Th	3.6	3.9	4.3	6.6	9.4	4.9
U	1.4	1.4	1.6	3.3	2.8	1.8
La	38	41	45	86	102	56
Ce	78	85	90	173	205	115
Pr	9.2	10	11	20	21	14
Nd	35	39	38	71	84	51
Sm	7.1	7.6	7.4	13	14	9.8
Eu	2.2	2.4	2.4	4.1	4.2	3.0
Gd	6.7	7.1	6.9	12	11	9.1
Tb	0.95	0.96	0.94	1.6	1.5	1.2
Dy	4.9	4.8	4.8	7.3	7.5	5.6
Ho	0.89	0.87	0.87	1.3	1.2	0.92
Er	2.2	2.1	2.1	2.9	2.7	2.1
Tm	0.30	0.28	0.29	0.36	-	0.25
Yb	1.9	1.7	1.8	2.1	1.7	1.4
Lu	0.26	0.24	0.26	0.28	-	0.20
Eu/Eu*	1.00	1.00	1.02	0.98	1.05	0.99
$^{87}Sr/^{86}Sr$	0.702843±17	0.702729±19	0.702835±17	0.702788±22	0.702800±17	0.702774±19
$^{143}Nd/^{144}Nd$	0.51298	0.512972	0.512953	0.512978	0.512986	0.512971
$^{147}Sm/^{144}Nd$	-	-	-	-	0.1125±12	
ε_{Nd}	6.67	6.52	6.14	6.63	6.79	6.50
$^{206}Pb/^{204}Pb$	19.237	19.294	19.201	19.285	-	19.323
$^{207}Pb/^{204}Pb$	15.573	15.576	15.589	15.568	-	15.576
$^{208}Pb/^{204}Pb$	38.837	38.887	38.857	38.863	-	38.906

[1]Analysed by SSMS
[2]Analysed by ICP-MS

Table A7.4 continued.

Rock Type	basanite						
Sample #	SA03[3]	SA05[1]	SA27[1]	SA55[1]	SA56[1]	SA60[1]	SAB179[2]
Sc	19	17	15	22	21	23	27
Ti	15932	19732	18688	16115	17941	16783	16922
V	232	260	190	276	288	283	278
Cr	263	252	100	392	326	404	396
Ni	289	205	89	263	240	283	324
Cu	64	63	38	69	67	70	67
Zn	98	122	131	91	104	95	111
Co	-	-	-	-	-	-	79
Mn	-	-	-	-	-	-	1465
Ga	24	25	26	22	23	23	25
As	3.1	2.6	4.7	2.2	2.6	2.0	-
Rb	24	24	40	20	20	19	20
Sr	746	932	2193	547	666	568	581
Y	26	27	35	23	25	23	22
Zr	311	311	436	194	231	199	215
Hf	-	6.9	9.6	5.1	5.4	4.7	4.9
Nb	55	56	80	38	43	38	45
Mo	-	4.9	7.9	2.7	4.0	2.1	2.3
Sn	-	8.9	17.0	5.8	6.2	4.8	1.9
Cs	-	0.35	0.44	0.37	0.40	0.29	0.34
Ta	-	-	-	-	-	-	3.4
Ba	260	263	383	200	214	206	200
Pb	5.7	3.8	7.2	3.4	4.1	3.4	2.8
Th	6.8	4.5	8.8	3.8	3.8	3.8	2.5
U	0.10	1.3	2.5	0.93	1.1	1.0	0.87
La	44	76	71	27	37	36	28
Ce	101	160	149	62	82	73	60
Pr	-	16	16	6.8	9.7	8.3	7.4
Nd	-	56	62	29	40	33	29
Sm	-	11	12	6.1	7.5	6.2	6.1
Eu	-	3.2	3.8	2.0	2.3	1.9	2.0
Gd	-	7.4	8.8	5.3	5.2	5.0	6.1
Tb	-	1.0	1.3	0.84	0.78	0.72	0.85
Dy	-	5.4	7.0	4.5	4.3	4.1	4.2
Ho	-	0.89	1.1	0.81	0.78	0.72	0.77
Er	-	2.1	2.7	2.0	1.7	1.8	1.8
Tm	-	-	-	-	-	-	0.24
Yb	-	1.3	1.9	1.6	1.3	1.4	1.5
Lu	-	-	-	-	-	-	0.21
Eu/Eu*	-	1.08	1.12	1.05	1.13	1.04	0.98
$^{87}Sr/^{86}Sr$	0.702847±17	0.702784±15	0.703228±17	0.702914±17	0.702849±15	0.702829±17	0.702845±18
$^{143}Nd/^{144}Nd$	0.512967	0.512959	0.512963	0.512972	0.512965	0.512975	0.512964
$^{147}Sm/^{144}Nd$	0.1191±16	0.1184±17	0.1146±16	0.1296±17	0.1238±17	0.1289±16	-
ε_{Nd}	6.42	6.26	6.34	6.52	6.38	6.57	6.36
$^{206}Pb/^{204}Pb$	-	-	-	-	-	-	19.221
$^{207}Pb/^{204}Pb$	-	-	-	-	-	-	15.573
$^{208}Pb/^{204}Pb$	-	-	-	-	-	-	38.833

[1]Analysed by SSMS
[2]Analysed by ICP-MS
[3]Analysed by XRF

Table A7.4 continued.

Rock Type	ne-hawaiite					
Sample #	SA02[2]	SA24[2]	SA25[2]	SA65[1]	SA66[1]	SAB218[2]
Sc	20	16	16	12	14	17
Ti	15590	16613	15923	14617	16860	13965
V	211	151	146	147	198	170
Cr	211	112	88	61	127	231
Ni	157	111	102	61	115	153
Cu	59	48	53	44	53	63
Zn	125	146	154	140	148	128
Co	81	71	56	-	-	56
Mn	1426	1430	1707	-	-	1447
Ga	25	26	27	29	28	26
As	2.8	2.8	3.1	3.8	3.1	-
Rb	33	26	31	38	33	32
Sr	783	822	1053	1253	1517	759
Y	27	28	34	39	40	25
Zr	354	352	438	491	404	346
Hf	7.5	7.7	8.4	9.5	8.2	6.8
Nb	61	68	87	89	78	62
Mo	6.1	4.7	5.6	8.2	9.5	5.1
Sn	2.8	3.0	3.6	11	8.7	2.8
Cs	0.81	0.31	0.47	0.25	0.53	0.51
Ta	4.9	4.6	6.5	-	-	4.4
Ba	270	280	355	425	478	281
Pb	4.4	3.3	5.1	6.4	7.4	4.1
Th	4.8	3.7	5.9	10.5	8.3	4.4
U	2.0	1.4	2.0	1.9	2.4	1.8
La	41	45	67	78	98	45
Ce	83	97	137	155	210	92
Pr	9.7	12	16	19	22	10
Nd	35	45	57	75	90	39
Sm	7.1	8.9	11	13	15	7.5
Eu	2.2	2.9	3.4	4.0	4.4	2.4
Gd	6.9	8.6	10	9.4	11	6.9
Tb	0.98	1.1	1.4	1.2	1.5	0.94
Dy	4.9	5.5	6.5	6.4	7.2	4.7
Ho	0.92	0.97	1.2	1.1	1.2	0.87
Er	2.2	2.2	2.6	2.4	2.4	2.1
Tm	0.31	0.28	0.35	-	-	0.29
Yb	1.9	1.7	2.1	1.9	1.4	1.7
Lu	0.28	0.23	0.28	-	-	0.26
Eu/Eu*	0.98	1.00	1.00	1.10	1.07	1.02
$^{87}Sr/^{86}Sr$	0.702834±19	0.702818±14	0.702738±20	0.702782±17	0.702816±17	0.702751±20
$^{143}Nd/^{144}Nd$	0.512978	0.512957	0.512963	0.512989	0.512963	0.512966
$^{147}Sm/^{144}Nd$	-	-	-	0.1076±11	0.1095±15	
ε_{Nd}	6.63	6.22	6.34	6.85	6.34	6.40
$^{206}Pb/^{204}Pb$	19.274	19.296	19.304	-	-	19.293
$^{207}Pb/^{204}Pb$	15.578	15.575	15.572	-	-	15.578
$^{208}Pb/^{204}Pb$	38.873	38.877	38.879	-	-	38.892

[1]Analysed by SSMS
[2]Analysed by ICP-MS

Appendix Eight:
Partial Melting and Source Composition Modelling

Appendix 8

Partial melting and source composition modelling

A8.1 The dynamic melting inversion (DMI) method

The degrees of partial melting for the cogenetic magmas referred to in section 6.4 have been estimated from the dynamic melting inversion method (DMI) of Zou and Zindler (1996) and modified by Zou (1998, 2000). A MATLAB programme has been developed as a substitute for the original FORTRAN programme developed by Zou and Zindler (1996). The modifications described in Zou (1998, 2000) to the original programme have been incorporated into the MATLAB version. Based on the DMI method, the degree of melting required to generate the primary magmas listed in Table 6.1 (p. 175) can be estimated from the concentration ratios of incompatible trace elements (e.g., REE) of two magmas considered to have a common parentage. The following example briefly describes the DMI method and how it was utilised in this investigation.

The garnet peridotite discussed in Green (1973a), 60% ol, 18% opx, 14% cpx, and 8% gt, is the assumed source material for basanite SAB179 and nephelinite SAB135 from group B. The primary compositions for SAB179 and SAB135 (Table 6.3; p. 191) were selected because of their large and contrasting incompatible trace element abundances. The concentration ratio (Q_a) of La of the primary magmas for SAB135 and SAB179 (51 ppm and 28 ppm respectively) is

$Q_a = Q_{La} = 51/28 = 1.84.$

Similarly, the concentration ratio (Q_b) of Ce for primary SAB135 and SAB179 (105 ppm and 59 ppm respectively) is

$Q_b = Q_{Ce} = 105/59 = 1.77$

The concentration ratios Q_a and Q_b are defined in Zou *et al.* (2000) as:

$$Q_a = \frac{C_a^1}{C_a^2} = \frac{X_2\{1-[1-X_1]^{[\Phi+(1-\Phi)D_a]^{-1}}\}}{X_1\{1-[1-X_2]^{[\Phi+(1-\Phi)D_a]^{-1}}\}} \quad (1) \text{ and } Q_b = \frac{C_b^1}{C_b^2} = \frac{X_2\{1-[1-X_1]^{[\Phi+(1-\Phi)D_b]^{-1}}\}}{X_1\{1-[1-X_2]^{[\Phi+(1-\Phi)D_b]^{-1}}\}} \quad (2)$$

where X_1 and X_2 are the melt fractions for SAB135 and SAB179 respectively, extracted from the initial solid, C is the trace element concentration, D is the bulk distribution coefficient. Φ is the mass porosity, which is expressed as

$$\Phi = \frac{\rho_f \phi}{\rho_f \phi + \rho_s (1 - \phi)},$$

where $\Phi = 8.498 \times 10^{-3}$ based on the volume porosity $\phi = 0.01$, the density of the melt $\rho_f = 2.8$ g cm^{-3}, and the density of the solid $\rho_s = 3.3$ g cm^{-3} as defined by Zou and Zindler (1996).

Equations 1 and 2 for Q_a and Q_b have two unknowns, X_1 and X_2, and therefore are solved numerically by Newton's method for a system of nonlinear equations using the MATLAB programme given below (p. 217).

Using the concentration ratios $Q_a = 1.84$ and $Q_b = 1.77$ in the programme generates solutions for X_1 and X_2:

$X_1 = 2.83\%$ and $X_2 = 6.13\%$.

The degree of partial melting required to produce these melt fractions is calculated from

$f = \Phi + (1 - \Phi)X$.

Substituting X_1 and X_2 for X gives

$f_1 = 7.28\%$ for SAB135 and $f_2 = 13.42\%$ for SAB179.

Additional values for X_1, X_2, f_1, and f_2 are calculated by using the initial concentration ratio for La, $Q_a = 1.84$, and new Q_b values for Pr, Sm, Nd, Eu and Tb. Each value (X_1, X_2, f_1, and f_2) derived from these element ratios are summarised in Table A8.1. The mean values $f_1 = 4.46\%$ and $f_2 = 7.97\%$ given in Table A8.1 represent the degree of melting required to produce SAB135 and SAB179 respectively.

The trace element abundances in the source (C_o) given in Table A8.1 and Table 6.3 (p. 191), are calculated using the mean values for X_1 and X_2 in the expression

$$C_O = \frac{C_L X}{\{1 - [1 - X]^{[\Phi + (1-\Phi)D]}\}}$$

where C_L is the element concentration in the liquid, and D is the bulk distribution coefficient.

Table A8.1 Calculated melt fractions, degrees of partial melting, and trace element abundances for the source of the primary magmas of nephelinite SAB135 and basanite SAB179. D = bulk distribution coefficient; C_L = liquid trace element abundance; C_O = source trace element abundance; $(C_O)_N$ = chondrite-normalised source abundance (normalisation values from Nakamura, 1974); X_1 and X_2 = percent melt fractions for SAB135 and SAB179 respectively; f_1 and f_2 = degrees of partial melting for SAB135 and SAB179 respectively; Q = concentration ratio [concentration (ppm) in SAB135/concentration (ppm) in SAB179]. Note that the concentration ratio for La is used as Q_a and the other REE ratios as Q_b.

element	D	C_L SA135	C_L SAB179	Q	X_1 SAB135	X_2 SAB179	f_1 SAB135	f_2 SAB179	C_O SAB135	$(C_O)_N$ SAB135	C_O SAB179	$(C_O)_N$ SAB179
La	0.0033	51	28	1.84	-	-	-	-	1.91	5.81	1.99	6.04
Ce	0.0066	105	59	1.77	7.28	13.42	8.07	14.16	3.93	4.55	4.26	4.93
Pr	0.0259	13	7.32	1.72	5.91	10.93	6.71	11.69	0.48	4.25	0.53	4.70
Nd	0.0153	47	28	1.65	4.68	8.72	5.49	9.50	1.76	2.80	2.04	3.24
Sm	0.0279	8.9	6.0	1.48	2.24	4.67	3.07	5.48	0.34	1.67	0.43	2.14
Eu	0.0350	2.8	1.9	1.42	1.31	3.29	2.15	4.11	0.11	1.37	0.14	1.81
Tb	0.0495	1.1	0.84	1.29	0.4	2.05	1.25	2.88	0.042	0.89	0.061	1.29
mean X					3.64	7.18						
mean *f*							4.46	7.97				

The DMI method works better for LREEs due to their higher Q values. DMI does not always work well for HREEs, in part due to their low Q and larger analytical errors. In addition, when Q is very close to 1.0, a small change in Q can cause large errors in the calculated X and *f* values (Zou, pers. comm., 2001). Ideally, the values X_1 and X_2 should yield very similar source trace element abundances as demonstrated by Zou *et al.* (2000) for basalts in southeastern China. In the case of SAB135 and SAB179, the differences in source concentrations are most likely due to the relatively small Q values.

A8.2 MATLAB programme for the DMI method

The percent melt extraction (X_1 and X_2) and degrees of partial melting (f_1 and f_2) for cogenetic magmas can be approximated by Newton's method for solving a system of nonlinear equations from the following MATLAB programme. The programme is written as separate files (newton10 and fnewt10).

Newton10 calculates the values for X_1 and X_2.

```
% newton10 - Program to solve a system of nonlinear equations
%using Newton's method. Equations defined by fnewt
clear; help newton % Clear memory; print header
x=input ('Enter the initial guess for melt fractions (X1 and X2 values) - ');
% x values are entered as e.g., [0.05 0.07]
a=input ('Enter the parameters for Q - ');
% values for Qa and Qb are entered as e.g., [1.84 1.77]
nstep=n;  %n = the number of iterations before stopping, e.g., n = 10
%%%%% MAIN LOOP %%%%%
for istep=1:nstep
xplot(:,istep) = x(:);  % Save plot variables
[f D]=fnewt10(x,a);  %fnewt returns value of f and D
dx=f/D;  %Find dx by Gaussian elimination
x=x-dx/n; %Newton iteration for new x; e.g., let n = 100
end
xplot(:,nstep+1)=x(:);  %save plot variables
fprintf('After %g iterations the root is\n', nstep);
disp(x);
subplot (121);  %Plot iteration steps, x(1) vs x(2)
plot(xplot(1,:),xplot(2,:),'o',xplot(1,:),xplot(2,:),'-',x(1),x(2),'*');
xlabel('x');  ylabel('y');
```

Fnewt10 contains the equations executed by newton10. The 2 by 2 nonlinear system is solved using Newton's method. Gauss-Jordan's method is used to solve the linear systems directly.

```
function [f,D]=fnewt10 (x,a)
b=85.15; %this parameter is dependent on the most incompatible element
%selected, e.g., La, for the calculation of X values of each element, e.g., Ce, Sm
c=66.90; %this parameter is dependent on the other elements used to determine
%values for X
%Function used by the N-variable Newton's method
%The variable "a" is the Q parameter
%Lorenz model x=[x,y,z], a=r sigma b]
f(1)=(x(2)*(1-(1-x(1))^b))-(a(1)*x(1)*(1-(1-x(2))^b));
f(2)=(x(2)*(1-(1-x(1))^c))-(a(2)*x(1)*(1-(1-x(2))^c));
D(1,1)=(b*x(2)*((1-x(1))^(b-1)))-a(1)+(a(1)*((1-x(2))^b)); %df(1)/dx(1)
D(1,2)=(1-((1-x(1))^b))-(b*a(1)*x(1)*((1-x(2))^(b-1))); %df(2)/dx(1)
D(2,1)=(c*x(2)*((1-x(1))^(c-1)))-a(2)+(a(2)*((1-x(2))^c)); %df(1)/dx(2)
D(2,2)=(1-((1-x(1))^c))-(c*a(2)*x(1)*((1-x(2))^(c-1))); %df(2)/dx(2)
return;
```

Note that the initial value for Q_a is used for all calculations and only Q_b is varied (for each element). The parameters "b" and "c" are the exponents $[\Phi + (1 - \Phi)D_a]^{-1}$ and $[\Phi + (1 - \Phi)D_b]^{-1}$ from equations 1 and 2 respectively. As with the values for Q_a and Q_b, "b" is used for all calculations, whereas "c" is varied for each element. For instance, in the above example $Q_a = Q_{La} = 1.84$ is used in all calculations while Q_b is entered into the

programme for each element Ce, Pr, Sm, Nd, Eu, and Tb. Similarly, b_{La} = 85.15, is used in all calculations while values of "c" for Ce, Pr, Sm, Nd, Eu, and Tb are 66.90, 29.27, 42.44, 27.71, 23.23, and 17.14 respectively, and must be entered into fnewt10 for each new set of calculations. Note also that because Newton's method is a numerical approximation technique the programme may be sensitive to the number of iterations used to determine values for X_1 and X_2. Initially nstep = 10 and x=x-dx/100 are good starting values but may need to be increased depending on the programme's ability to approximate X_1 and X_2.

Procedure:

1. Initiate newton10 by entering "newton10" at the >> prompt.
2. Enter an initial guess for the values of X_1 and X_2 using the format [X_1 X_2], e.g., [0.05 0.07].
3. Enter the concentration ratio values Q_a and Q_b using the format [Q_a Q_b], e.g., [1.84 1.77].
4. Press ENTER.
5. Repeat steps 1 through 3 until values for X_1 and X_2 are determined.
6. Repeat this procedure for each element, e.g., Ce, Pr, Sm, Nd, Eu, and Tb.

Values for X_1 and X_2 are displayed and can be viewed on the graph generated by the programme.